29117

NASA Conference Publication 2434

The 1985 Goddard Space Flight Center Battery Workshop

Proceedings of a workshop held at
NASA Goddard Space Flight Center
Greenbelt, Maryland
November 19-21, 1985

NASA

NASA Conference Publication 2434

The 1985 Goddard Space Flight Center Battery Workshop

G. Morrow, *Editor*
Goddard Space Flight Center
Greenbelt, Maryland

Proceedings of a workshop held at
NASA Goddard Space Flight Center
Greenbelt, Maryland
November 19-21, 1985

NASA
National Aeronautics
and Space Administration

**Scientific and Technical
Information Branch**

1986

PREFACE

This document contains the proceedings of the 18th annual Battery Workshop held at Goddard Space Flight Center, Greenbelt, Maryland on November 19-21, 1985. The Workshop attendees included manufacturers, users, and government representatives interested in the latest developments in battery technology as they relate to high reliability operations and aerospace use. The subjects covered included advanced energy storage, lithium cell technology, nickel-cadmium design evaluation and component testing, simulated orbital cycling and flight experience, and nickel-hydrogen technology.

INTRODUCTION

George W. Morrow
Goddard Space Flight Center

This year the format of the Workshop has remained as it was in the past. Questions and comments from the audience were encouraged and will continue to be encouraged in future Workshops. The discussion periods are no longer included in these proceedings.

The first session, Advanced Energy Storage, dealt with a topic new to the Workshop. It was included to provide attendees with an overview of research and development taking place at NASA and other government agencies in the advanced energy storage field.

The second session, Lithium Cell Technology, filled out the first day. The sessions of the second day addressed Nickel-Cadmium Design Evaluation and Component Testing and Simulated Orbital Cycling and Flight Experience. Nickel-Hydrogen Technology was the topic of the final day.

I hope that the 1985 Battery Workshop was as informative and enlightening as those in the past. I would also like to thank all of the presenters for the time and effort they put in.

PREVIOUS BATTERY WORKSHOP PROCEEDINGS PUBLICATIONS

For your information, we have included a list of the acquisition numbers for all Battery Workshop proceedings since 1970. Copies of previous publications are available upon request. The document numbers and the addresses are as follows:

Year	Contents	Accession Number
1984	Workshop	N85-31371
1983	Workshop	N84-33668
1982	Workshop	N83-35230
1981	Workshop	N82-20402
1980	Workshop	N81-21493
1979	Workshop	N80-20820
1978	Workshop	N79-28669
1977	Workshop	N79-21565
1976	Workshop	N77-21550
1975	Workshop	N76-24704
1974	Workshop	N75-16976
1973	Workshop (1st day)	N75-15152
	Workshop (2nd day)	N75-17808
1972	Workshop (1st day)	N73-21956
	Workshop (2nd day)	N73-21957
1971	Workshop (Volume 1)	N72-27061
	Workshop (Volume 2)	N72-27062
1970	Workshop (1st day)	N71-28569
	Workshop (2nd day)	N71-28672

NASA may contact:

NASA Scientific and Technical Information Facility (STIF)
P. O. Box 8757
BWI Airport
Baltimore, Maryland 21240
(301) 859-5300

All other interested parties contact:

National Technical Information Services (NTIS)
U. S. Department of Commerce
Springfield, Virginia 22161
(703) 487-4600

CONTENTS

1985 GSFC BATTERY WORKSHOP
CO-CHAIRMAN: George W. Morrow
Thomas Y. Yi
Goddard Space Flight Center

Page

PREFACE iii

INTRODUCTION v

PREVIOUS BATTERY WORKSHOP PUBLICATIONS vii

SESSION I

TOPIC: ADVANCED ENERGY STORAGE
Chairman: A. D. Schnyer, NASA/HQ

Presentations:

MECHANICAL ENERGY STORAGE SYSTEMS (NOT RECEIVED FOR PUBLICATION)
G. E. Rodriguez, NASA/GSFC .....

AN OVERVIEW OF SOLAR DYNAMIC SYSTEMS FOR SPACE APPLICATIONS
D. Namkoong, NASA/LERC 3

NASA LEWIS EVALUATION OF REGENERATIVE FUEL CELL SYSTEMS
N. Hagedorn, O. D. Gonzalez-Sanabria, L. L. Kohout, NASA/LERC 13

SODIUM SULPHUR BATTERIES FOR SPACECRAFT ENERGY STORAGE
R. E. Dueber, USAF 19

ENERGY STORAGE SYSTEMS COMPARISON FOR THE SPACE STATION
G. van Ommering, Ford Aerospace 31

SESSION II

TOPIC: LITHIUM CELL TECHNOLOGY
Chairman: G. Halpert, JPL

Presentations:

GALILEO Li/SO_2 BATTERY MODULES
R. A. Smith, Honeywell 43

SESSION II (Continued) Page

DETERMINING THE INFLUENCE AND EFFECTS OF MANUFACTURING VARIABLES ON Li/SO_2 CELLS
W. Zajac, et al., NWSC 67

SAFETY HAZARDS ASSOCIATED WITH THE CHARGING OF Li/SO_2 CELLS
H. Frank, et al., JPL
J. Barnes, et al., NSWC 75

SAFETY CONSIDERATIONS FOR FABRICATING LITHIUM BATTERY PACKS
J. J. Ciesla, Electrochem Industries 93

HEAT DISSIPATION OF HIGH RATE $Li/SOCl_2$ PRIMARY CELLS
Y. Cho, Drexel University
G. Halpert, JPL 107

TEST RESULTS OF $Li/SOCl_2$ CELLS
G. Halpert, et al., JPL 117

A 65 Ah RECHARGEABLE LITHIUM MOLYBDENUM DISULFIDE BATTERY
K. Brandt, Moli Energy Limited 131

EXAMINATION OF DESIGN OPTIONS FOR 35 Ah AMBIENT TEMPERATURE Li/TiS_2 CELLS
D. H. Shen, et al., JPL 145

SESSION III

TOPIC: NICKEL-CADMIUM DESIGN EVALUATION AND COMPONENT TESTING
Chairman: G. W. Morrow, NASA/GSFC

Presentations:

QUALIFICATION TESTING OF GENERAL ELECTRIC 50 Ah NICKEL-CADMIUM CELLS WITH NEW SEPARATOR AND NEW POSITIVE PLATE PROCESSING
G. W. Morrow, NASA/GSFC 159

AIR-FORCE NICKEL-CADMIUM CELL SEPARATOR QUALIFICATION PROGRAM
R. W. Francis, Aerospace Corporation
R. L. Haag, NWSC-Crane 169

A FLOODED-STARVED DESIGN FOR NICKEL-CADMIUM CELLS
L. H. Thaller, NASA/LERC 177

AN ADVANCED Ni-Cd BATTERY CELL DESIGN
L. Miller, Eagle-Picher 185

SELF DISCHARGE CHARACTERISTICS OF NICKEL-CADMIUM CELLS AT ELEVATED TEMPERATURES
S. W. Donley, et al., Aerospace Corporation 195

CONTENTS (Continued)

Page

SESSION IV

TOPIC: SIMULATED ORBITAL CYCLING AND FLIGHT EXPERIENCE
Chairman: T. Y. Yi, NASA/GSFC

Presentations:
MODELING Ni-Cd PERFORMANCE
J. M. Jagielski, NASA/GSFC 217
INVESTIGATION OF LONG-TERM STORAGE EFFECTS ON AEROSPACE NICKEL-CADMIUM CELL PERFORMANCE
T. Y. Yi, NASA/GSFC 249
SATELLITE BATTERY TESTING STATUS
R. Haag and S. Hall, NWSC-Crane 255
VOLTAGE-TEMPERATURE CHARGE VERIFICATION OF 34 Ah NICKEL-CADMIUM CELLS
P. J. Timmerman and D. W. Bondeson, Martin-Marietta 267
NOAA 26.5 Ah LEO CHARACTERIZATION TEST
G. W. Morrow, NASA/GSFC 287
A HIGH RELIABILITY BATTERY MANAGEMENT SYSTEM
M. H. Moody, Canadian Astronautics 305

SESSION V

TOPIC: NICKEL-HYDROGEN TECHNOLOGY
Chairman: L. H. Thaller, NASA/LERC

Presentations:
RECENT ADVANCES IN Hi-H_2 TECHNOLOGY AT NASA LEWIS RESEARCH CENTER
M. A. Reid, et al., NASA/LERC 319
LIGHTWEIGHT, DIRECT-RADIATING NICKEL-HYDROGEN BATTERIES
J. R. Metcalf, Canadian Astronautics 329
INVESTIGATION OF NICKEL-HYDROGEN BATTERY TECHNOLOGY FOR THE RADARSAT SPACECRAFT
D. A. McCoy and J. L. Lackner, Dre-Canada 349
NICKEL-HYDROGEN LOW-EARTH-ORBIT TEST PROGRAM
J. K. Mc Dermott, Martin-Marietta 361
IMPACT OF SHUTTLE ENVIRONMENT ON PRELAUNCH HANDLING OF NICKEL-HYDROGEN BATTERIES
R. S. Green, RCA 373
PARAMETRIC TEST RESULTS OF A 40 Ah BIPOLAR NICKEL-HYDROGEN BATTERY
R. L. Cataldo, NASA/LERC 377
NICKEL-HYDROGEN BATTERIES FROM INTELSAT-V TO SPACE STATION
G. van Ommering and A. Z. Applewhite, Ford Aerospace 387

CONTENTS (Continued)

SESSION V (Continued) Page

NICKEL-HYDROGEN LOW EARTH ORBIT TEST PROGRAM
C. C. Badcock, Aerospace Corporation
R. L. Haag, NWSC-Crane 399

A 4.5" DIAMETER IPV Ni-H_2 CELL DEVELOPMENT PROGRAM
L. Miller, Eagle-Picher Industries 411

LIST OF ATTENDEES 419

SESSION I

TOPIC: ADVANCED ENERGY STORAGE
Chairman: A. D. Schnyer, NASA/HQ

AN OVERVIEW OF SOLAR DYNAMIC SYSTEMS FOR SPACE APPLICATIONS

David Namkoong
Lewis Research Center

Solar dynamic systems are essentially heat engines. Heat is added to a fluid, heat is rejected from the fluid, and the difference is available for producing useful work such as electrical power. The energy source for the conventional heat engine is hydrocarbon fuel. Solar dynamic systems use the sun's energy as the heat source instead of oil combustion.

The current interest in solar dynamics is in its application in the Space Station. Both solar dynamics and photovoltaics are candidates for the initial power system design and for the growth versions. The current design power levels are 75kW and 300 kW for the initial and growth designs respectively. Much of the present thinking for solar dynamics is based on work that NASA-Lewis pursued in the late 1960's. That work was to establish the technology that could be used for extended space flight requiring large power loads. When such missions failed to materialize, the technology was shelved. Today, with little change occurring in the intervening years, that technology is being utilized.

The major change in solar dynamic programs during this interim period has been in applications. DOE developed a number of terrestrial systems as part of its charge to conserve energy. Though this effort did advance the solar dynamic state-of-the-art, the difference in environment largely precluded the use of any such advance for space applications.

The major components of a solar dynamic system are the concentrator, heat receiver, energy converter, and the heat rejection system. Figure 1 shows the concept packaged for space application. The concentrator can be a refractor but is conventionally a reflector surface that focuses solar energy into the heat receiver. The receiver is usually designed integrally with the storage to operate through the shadow part of an orbit. The energy converter is the thermodynamic cycle, the output of which provides useful electrical power. For the Space Station, Brayton and Rankine cycles are being considered. Stirling shows promise for growth or for later space applications. The waste heat is rejected by a radiator.

The advantage of the solar dynamic system over the photovoltaic array in providing power to the Space Station is its higher efficiency in converting solar energy to useful power. The factor is about 4. This means that the photovoltaic field must expose 4 times as much area to the sun as the solar dynamic system. The contrast can be illustrated in Figure 2. The larger area means greater drag even in the rarified environment of the orbiting station. The greater drag means greater expenditure of fuel to keep the solar array in the same orbit as a solar dynamic system.

The drawback to solar dynamics is the paucity of relevant data for such systems. None has been flown in space before. The advanced development program at NASA Lewis is aimed at developing the relevant technologies to maturity.

Though no solar dynamic system has had space experience, there has been data developed for its components and subsystems.

Most of the experience has been accumulated for the Rankine system, more particularly the organic Rankine. Figure 3 shows the schematic of such a system. The Rankine cycle is characterized by the working fluid undergoing phase changes -- liquid boiled to vapor at heat input and returned to liquid in the condenser. Toluene has been used extensively in the past and is the Rankine reference fluid for the Space Station. Maximum temperature is 672°K (750°F).

In thermodynamic cycles, the higher the heat source temperature, the more efficient the system (for constant heat sink temperature). Brayton heat engines are designed to operate as high as 1089°K (1500°F). Brayton systems, however, have not had the experience enjoyed by organic Rankine heat engines. Figure 4 is the schematic of the Brayton cycle. Unlike the Rankine, the working fluid of the Brayton cycle does not undergo any phase change. The Brayton system under consideration uses a He-Xe gas mixture as the working fluid. The higher heat source temperature enables the cycle efficiency to be several points higher than the Rankine.

The foregoing discussion has referred specifically to the Brayton and Rankine heat engines. This is just a part of an overall evaluation when designing solar dynamic systems. Figure 5 lists three typical areas for consideration -- trade-off analysis, developing critical technologies, and assessing the impact on the overall system (the Space Station in this application).

High turbine inlet temperature, as was mentioned previously, is desirable for higher efficiency. The required high operating receiver temperature is also desirable in that a smaller volume, smaller area, and smaller mass is required. On the other hand, high temperatures can cause localized overheating, aperture area becomes more critical to minimize re-radiation loss, and thermal stress problems are exacerbated.

Heat rejection temperature should be low so that in combination with a high heat source temperature, the potential for useful work output is increased. Any decrease in the heat rejection temperature, however, means that the radiator area must be increased to dissipate the required heat.

The Brayton vs. Rankine issue is one comparing a higher efficiency, less data base heat engine with one that has more experience but has a lower cycle efficiency.

These are a few of the principal parameters that are involved in arriving at an optimized system.

Four solar dynamic technologies have been identified as ones that need development to demonstrate operation in orbit. Though this list arises from the Space Station application, these technologies require similar effort in any mission requiring solar dynamics.

The critical technology issues of concentrators include those that affect reflector surface characteristics -- contamination, accuracy, sun/shade thermal distortion, coating performance and durability, and pointing accuracy; and concentrator designs -- Cassegrainian (double reflecting surfaces) vs. single reflectors, fabrication, and space assembly vs. deployable approach.

Critical issues concerning the heat receiver and thermal energy storage include the design affecting integral vs. separate storage; volume change of thermal storage material with phase change; matching the solar flux input with the heat transfer to the working fluid; and structural material to withstand corrosion, to operate in vacuum, and to operate at high temperature.

Fluid stability refers to the organic fluid in the Rankine heat engine. A closed loop where the maximum temperature approaches the decomposition point of the organic needs intensive scrutiny. The other main consideration is operation under zero-gravity where the cycle calls for the fluid to constantly change from liquid to vapor and back again.

The radiator will operate between 200°F and 350°F depending whether the heat engine operates as a Rankine cycle or Brayton cycle. Virtually all experience has been gained by operations at 100°F or less. The higher temperature range calls for different heat rejection fluids and an investigation of the best type of method for the subsystem -- as a heat pipe or as a pumped loop.

Aside from the narrow solar dynamic considerations, there are space station concerns. Stowability is a factor in that the greater compacted package requires fewer shuttle launches -- an increasingly important item because of the cost concerns of the Space Station. The items of extra-vehicular activity and deployability are aimed at making most effective use of the shuttle and crew to minimize the time and effort

prior to power start-up. An important consideration here also is in the safety of astronaut operators. Reliability of deployable mechanisms must be high to avoid a situation where a spring-loaded mechanism can jeopardize the operator.

One of the most critical technologies as mentioned before, and is most appropriate to this audience is the thermal energy storage, Figure 6. The purpose of storage here is to convert the varying heat source associated with the sun-shade cycle of a low earth orbit to a constant energy output required of the power system.

Of the several heat storage mechanisms available, two that have received consideration for the space station are those using sensible heat and latent heat. In sensible heat, energy is stored by an increase in temperature of the material, and returned by temperature decrease. In latent heat, the energy stored by changing the phase of the storage of heat and the energy release occurs at a fixed temperature. This means that the transfer of heat from the storage material to the working fluid would be under constant conditions over the entire sun-shade cycle. The constant energy into the cycle meets the requirement for a constant power output of the heat engine.

The issue of whether heat storage should be integral to or separate from the heat receiver was mentioned previously. An integral design is more complex. It involves combining two separate functions into a single component -- storage and heat transfer to the flowing fluid. A separate storage component is simpler since it can be designed only for storage. However, there will be more of a fluid temperature fluctuation and therefore power fluctuation associated with a separate component. An integral design also contributes to lessening the temperature fluctuations of the heat receiver itself.

The function of thermal energy storage will be enhanced if the storage material had the desirable characteristics of high heat of fusion and high density (for compactness), low volume change with phase change, and no corrosive attack on the container material.

The range of latent storage materials and their properties are listed in figure 7. For Space Station applications, three are being considered -- LiF for the high temperature Brayton system, 46LiF + 44NaF + 10MgF_2 for the lower temperature Brayton, and LiOH for Rankine. These were chosen for the temperatures required for the cycle points of the systems, and for their property characteristics.

Actual fabrication of a heat receiver with integral thermal storage was built in the early 1970's for space applications, though never flown, Figure 8. The design features include many of the concerns expressed thus far. Solar flux reflected from the concentrator enters the heat receiver through the aperture and impinges upon the bank of tubes along the inside surface of the receiver. The gas working fluid flows in parallel through 48 tubes from the inlet to exit manifolds. The receiver was fabricated of columbium (niobium)-zirconium alloy. Because the metal is refractory alloy, the receiver was not tested in atmosphere. Instead, three tubes were tested in a vacuum chamber under simulated solar conditions. Test results indicated that the tube design would operate satisfactorily in application.

Figure 9 shows the detail of the tube design. The diagram indicates that there are really two tubes -- an inner one through which the working gas flows, and an outer convoluted tube. The volume between the tubes is filled with the thermal energy storage material -- LiF salt. This design then is an example of an integrated heat receiver-thermal storage component. The convolutions are designed primarily to maintain the salt distribution along the tube length. Though the tube is initially filled with liquid, the salt shrinks in volume as it solidifies. The convolution is intended to minimize any migration of the salt by early freezing of the material at the neck. The salt then remains distributed along the tube even though the liquid can shrink approximately 30% while freezing. Heat transfer to the gas is, effectively, the same whether in the sun or in the shade.

This is but one design approach to one solar dynamic concept. Within the next few months we expect a decision to be reached on which option, the Rankine or Brayton, shall be carried on, and which power system -- solar dynamic or photovoltaic -- will be the system of choice.

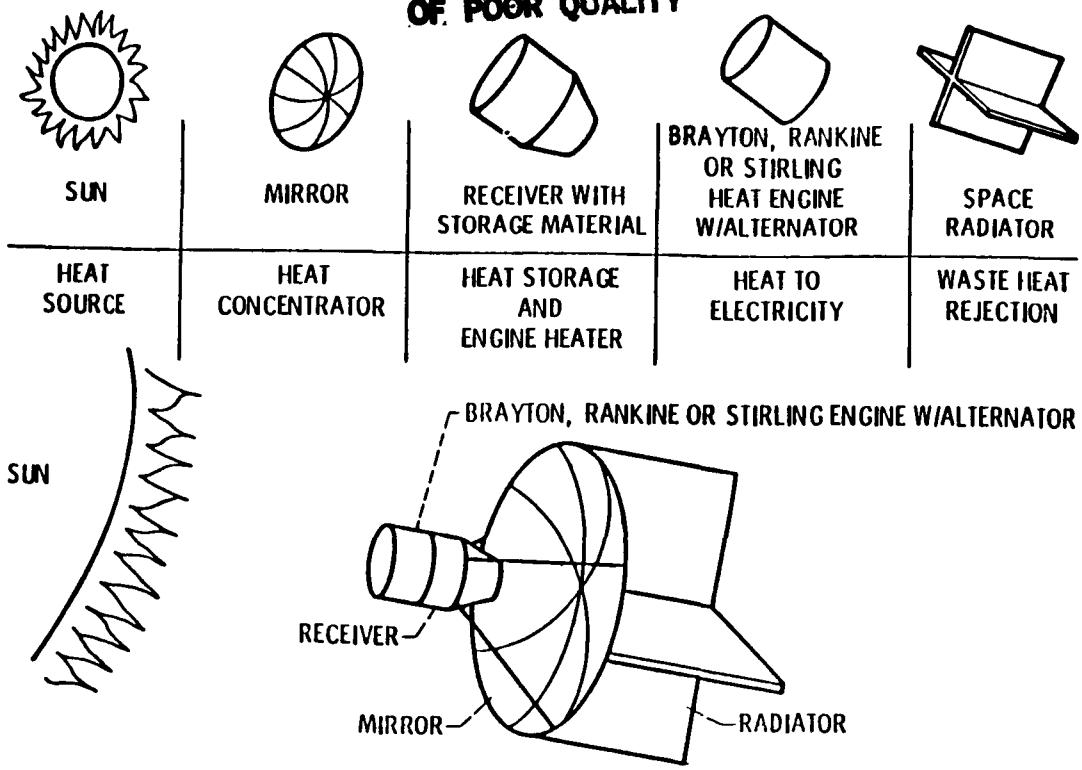

Figure 1. SOLAR DYNAMIC SYSTEM CONCEPT

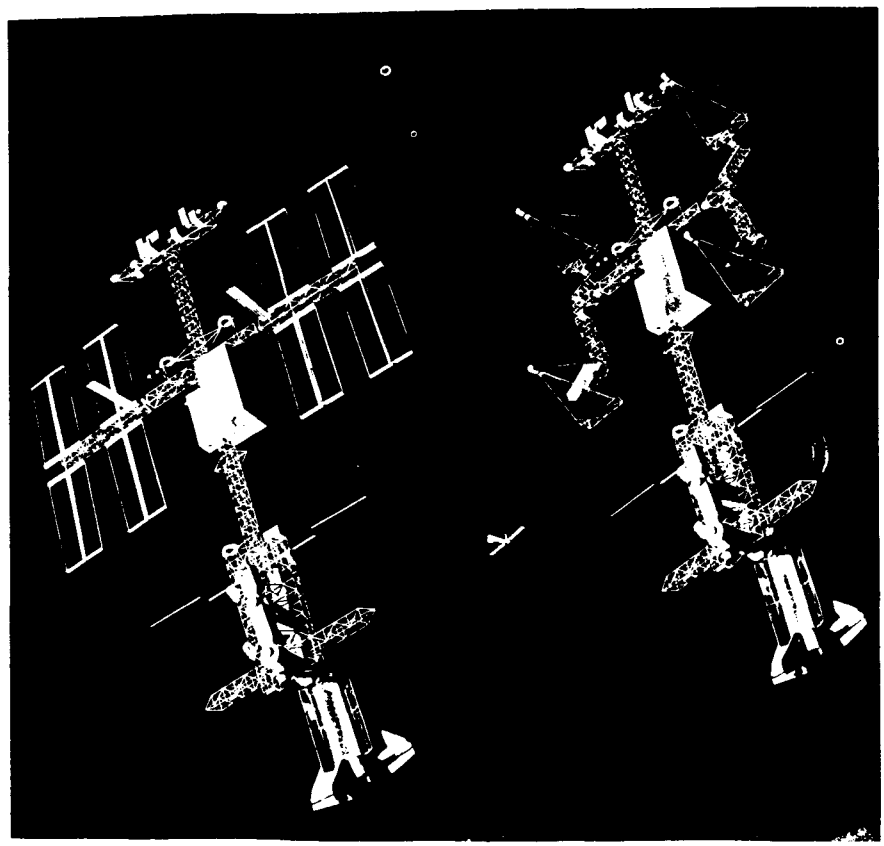

Figure 2. SPACE STATION CONCEPT—PHOTOVOLTAICS ON LEFT, SOLAR DYNAMICS ON RIGHT

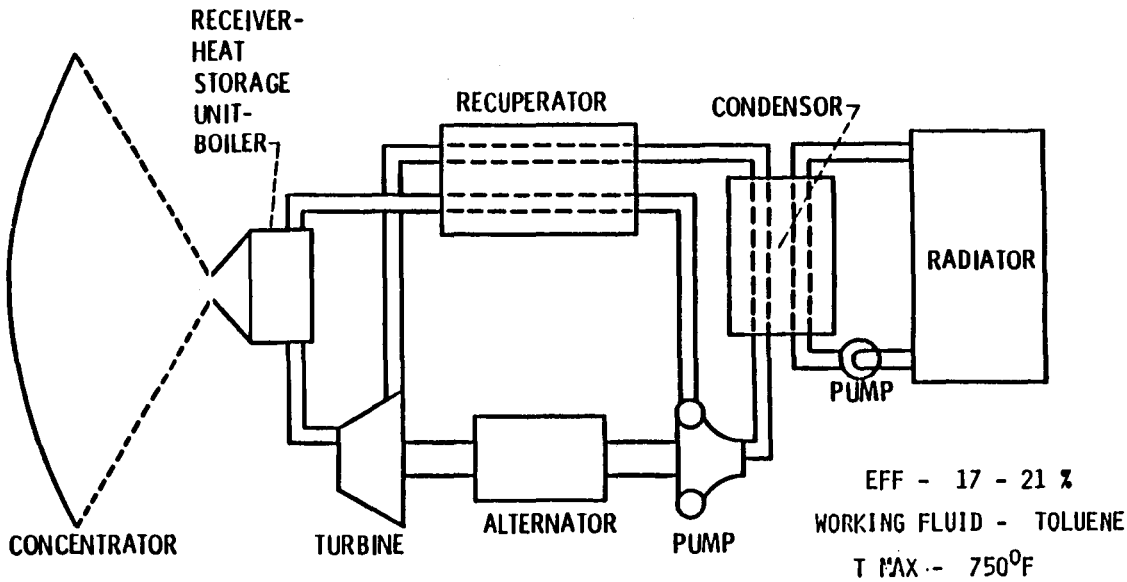

Figure 3. SOLAR RANKINE CYCLE

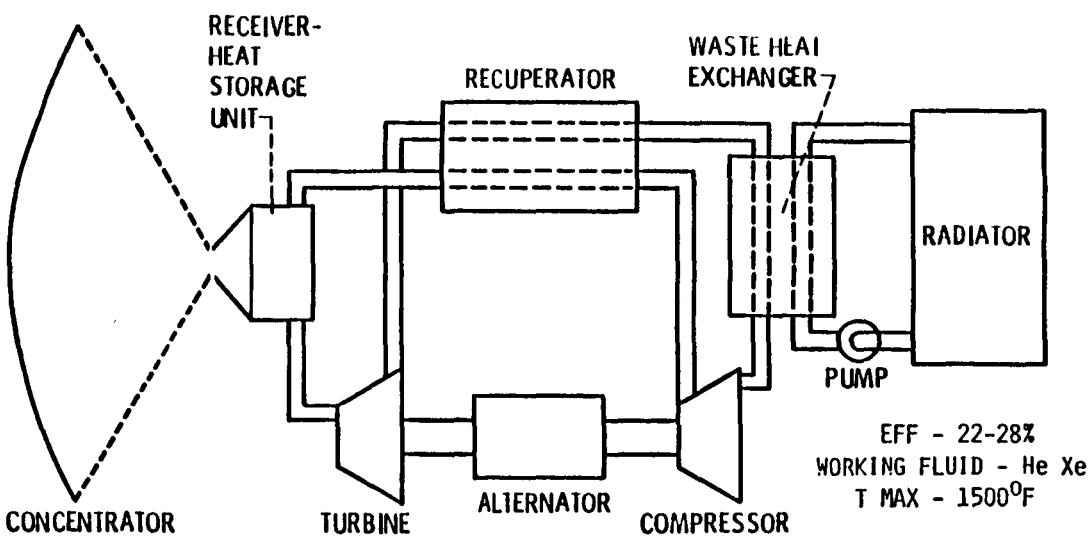

Figure 4. SOLAR BRAYTON CYCLE

CYCLE TRADE-OFFS

- TURBINE INLET TEMPERATURE VS. HEAT RECEIVER
- HEAT REJECTION TEMPERATURE VS. RADIATOR
- BRAYTON VS. RANKINE

CRITICAL SOLAR DYNAMIC TECHNOLOGIES

- CONCENTRATOR
- HEAT RECEIVER AND THERMAL ENERGY STORAGE
- FLUID STABILITY
- RADIATOR

SPACE STATION FACTORS

- SHUTTLE STOWABILITY
- EVA
- DEPLOYABILITY

Figure 5. CONSIDERATIONS IN SOLAR DYNAMIC SYSTEM DESIGN

FUNCTION: LEVEL POWER THROUGHOUT ORBIT

TYPES: SENSIBLE, LATENT

DESIGN: INTEGRAL SEPARATE

DESIRABLE CHARACTERISTICS:

- HIGH HEAT OF FUSION
- HIGH DENSITY
- LOW VOLUME CHANGE
- NON-CORROSIVE TO CONTAINER MATERIAL

Figure 6. SOLAR DYNAMIC THERMAL ENERGY STORAGE

No.	Material	Melt Temp. °K	Heat of Fusion kJ/kg	Density Kg/m³
1	KF	1125	454	2480
2	Na_2CO_3	1125	279	2530
3	Ca	1123	221	1540
4	LiF	1121	1044	2640
5	$LiBO_2$	1108	698	1400
6	75 NaF + 25 MgF_2	1105	649	2680
7	62.5 NaF + 22.5 MgF_2 + 15 KF	1082	607	2630
8	NaCl	1074	484	2180
9	CaI_2	1057	142	3490
10	$CaCl_2$	1046	256	2280
11	KCl	1043	372	1990
12	67 LiF + 33 mgF_2	1019	947	2630
13	65 NaF + 23 CaF_2 + 23 MgF_2	1018	574	2760
14	$Na_2B_4O_7$	1013	523	2370
15	Li_2CO_3	998	605	2200
16	$MgCl_2$	988	454	2240
17	60 KF + 40 NaF	983	479	2510
18	LiH	956	2582	790
19	Al	933	388	2710
20	60 LiF + 40 NaF	925	816	2480
21	Mg	923	372	1740
22	46 LiF + 44 NaF + 10 MgF_2	905	858	2610
23	52 LiF + 35 NaF + 13 CaF_2	888	640	2630
24	LiCl	883	470	2070

No.	Material	Melt Temp. °K	Heat of Fusion kJ/kg	Density kg/m³
25	52 NaCl + 48 $NiCl_2$	843	558	2840
26	$Ca(NO_3)_2$	834	130	2500
27	73 LiCl + 27 NaCl	825	430	2090
28	48 NaCl + 52 $CaCl_2$	773	328	2160
29	49 KF + 51 LiF	765	461	2560
30	80 Li_2CO_3 + 20 K_2CO_3	763	377	2170
31	LiOH	743	930	1460
32	11.5 NaF + 42 KF + 46.5 LiF	727	442	2560
33	NaCl + $MgCl_2$	713	326	2240
34	80 LiOH + 20 LiF	700	1163	1550
35	KOH	673	140	2040
36	LiCl + KCl	623	255	2030
37	KNO_3	613	128	2110
38	NaOH	593	160	2070
39	$Na_2N_2O_2$	588	244	1730
40	93.6 $NaNO_3$ + 6.4 NaCl	568	191	2260
41	95.3 NaOH + 4.7 Na_2SO_4	566	326	—
42	7.8 NaCl + 6.4 $NaCO_3$ + 85.8 NaOH	555	316	2100
43	37 LiCl + 63 LiOH	535	437	1640
44	NaCl + $ZnCl_2$	533	198	2480
45	23 LiOH + 77 NaOH	528	233	1890
46	$LiNO_3$	527	379	2400
47	$AlCl_3$	468	290	2440
48	NaOH + KOH	463	233	2060
49	Li	453	442	530

Figure 7. THERMAL ENERGY STORAGE SALTS

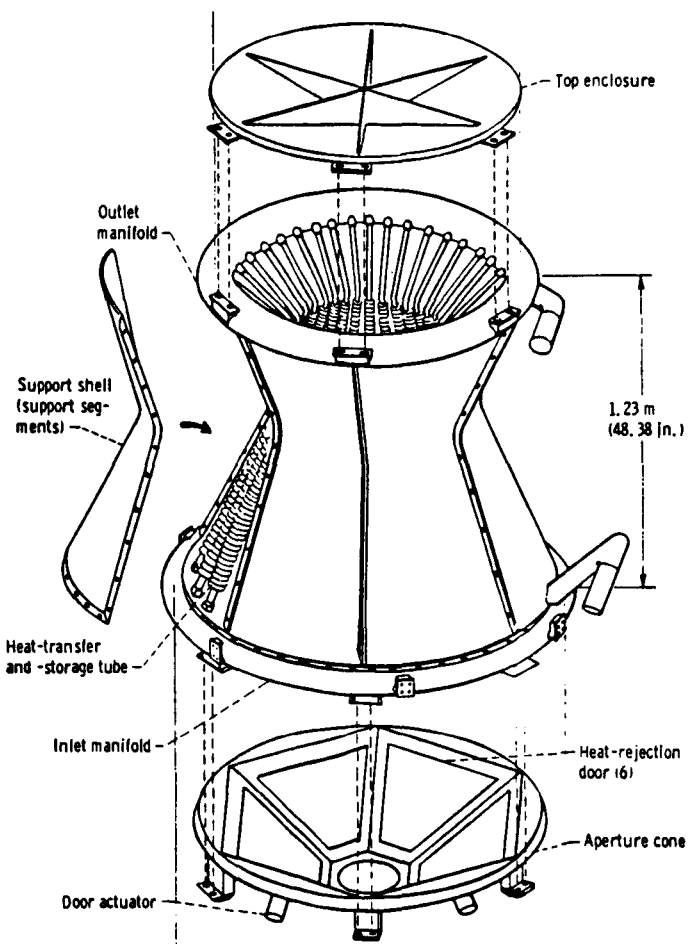

Figure 8. BRAYTON HEAT RECEIVER

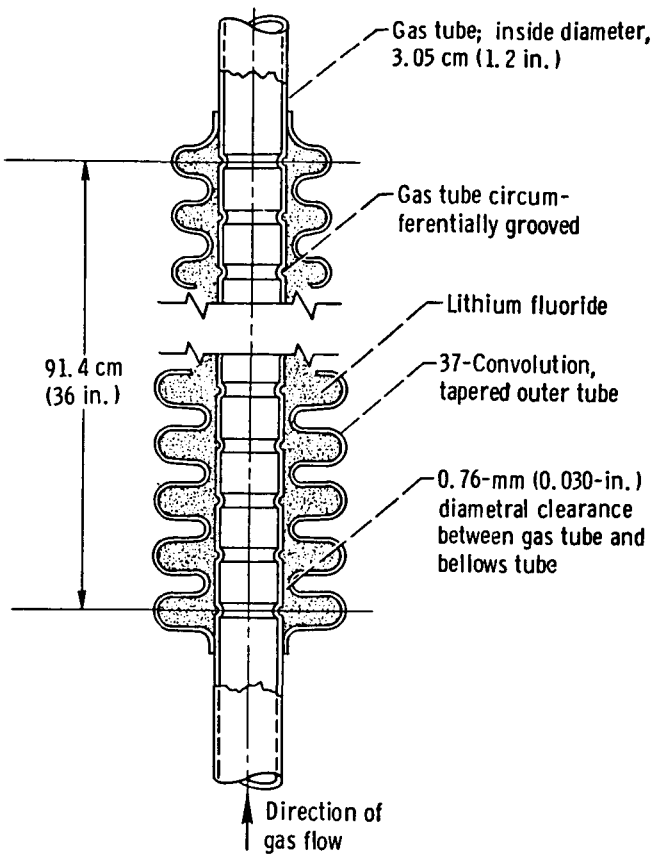

Figure 9. SINGLE TUBE FROM BRAYTON HEAT RECEIVER

NASA LEWIS EVALUATION OF

REGENERATIVE FUEL CELL (RFC) SYSTEMS

N. H. Hagedorn
O. D. Gonzalez-Sanabria
L. L. Kohout
Lewis Research Center
Cleveland, OH 44135

INTRODUCTION

At the present time, the primary focus of the Energy Storage Branch at LeRC is the nickel-hydrogen battery, both IPV and bipolar configurations. However, relatively low-level efforts have been initiated recently on two regenerative fuel cell (RFC) systems. The first of these is the "passive" hydrogen-oxygen RFC, indicating a system capable of operating with no rotating components, such as pumps or compressors. The rationale for considering the development of such a system rests upon the high energy densities projected for hydrogen-oxygen RFC's in GEO orbits, the long life requirements for such orbits, the assumption that components such as pumps and motors would be the life-limiting elements in a conventional hydrogen-oxygen RFC, and the unlikelihood of servicing satellites in GEO orbit. The second RFC being considered is the hydrogen-bromine system. The most promising characteristic of this RFC is that the electrode reactions apparently are reversible, which could result in round-trip energy efficiencies of 75% or more. This would be very significant for LEO missions, since the smaller PV arrays required for the more efficient storage system would cause less atmospheric drag and thus require less reboost fuel over the mission life.

In addition to the advantages which are specific to the respective systems, there are also advantages which are generic to flow batteries. Perhaps the most significant of these is, that since all reactants and products are either liquids or gases, the difficulties associated with solid electrode reactants are avoided. These are related to morphology changes, and include swelling, shedding and dendrite growth. Flow battery systems also are amenable to efficient adaptation to changing mission requirements and growth, because the power-related portions of the system (cell stacks, pumps, etc.) and the energy-related portions (reactants and tanks) can be independently varied. Another characteristic of flow batteries is that they are generally constructed in the bipolar configuration, which results in the cells being electrically in series, but hydraulically in parallel. The effect of this is, that with respect to the concentrations of reactants entering the cells, all cells are always electrochemically in balance with respect to one another. It thus becomes possible to discharge different cells at different rates, or even to charge some cells while discharging others. This allows a great degree of operational flexibility with virtually no attendant penalty. Finally, because the reactants are liquids or gases, they tend to have quite high energy densities.

This paper presents a brief discussion of the significant characteristics of each of the RFC systems under consideration, and indicates what presently is being done to evaluate them.

THE PASSIVE HYDROGEN-OXYGEN RFC

The use of pumps and motors in a conventional hydrogen-oxygen RFC is associated with the removal of waste heat and the storage of product water. Elimination of these dynamic devices will require a system design that provides for an efficient static method of thermal control, and a cell design that can accommodate internal storage of product water. A block diagram of one possible passive RFC configuration is given in figure 1. In this concept, intercell heat pipes would transfer heat to a cold plate for radiation to space. The rate of heat rejection could be controlled by louvers positioned by bimetallic actuators. During the relatively long periods of low-rate charging, conservation of heat would probably be required. The system would therefore be well insulated, and provision probably would be made for parasitic heating of the reactant tanks to prevent condensation of water vapor on the tank walls.

Several options are available with regard to cell and stack configurations for the passive hydrogen-oxygen RFC. The first involves the choice between acid and alkaline electrolytes. Alkaline cells have been used on the Apollo and space shuttle missions. They represent a well-developed technology, and are generally more efficient than the acid electrolyte (SPE) cells. However, acid cells were used on the Gemini mission, and are now considered by some to offer the possibility of invarient performance over very long periods of time. Low power level SPE electrolyzers have been used in space in life-support systems, e.g., for carbon dioxide concentration. Therefore, both the acid and the alkaline technologies have been used in space, both have advantages and disadvantages, and both have their own advocates.

Another configuration issue is whether to incorporate separate cells for the charge (electrolyzer) and discharge (fuel cell) functions, or to use cells which can perform both functions. The latter option, of course, would be lighter and simpler, all things being equal. However, because of the well-known irreversibility of the oxygen electrode, better round-trip efficiencies can be achieved when optimized electrode catalysts are used for the charge and discharge modes, respectively, i.e., when separate cells are incorporated in the system. Such a configuration, though, would require some sort of edge current collection, which well might nullify any potential efficiency advantages.

It can be seen that a careful trade-off analysis must be carried out for the competing cell and stack configuration options for the passive hydrogen-oxygen RFC. Only after this is accomplished can a judgement be made concerning the possible development of the system for GEO missions. International Fuel Cells, Inc. (IFC) is presently starting work on this system analysis. At the same time, considerable effort continues to be expended on the development of oxygen electrode catalysts for fuel cells, electrolyzers

and dual-mode cells. This includes current contracts and grants, supported by LeRC, with Giner, Inc., the Polytechnic Institute of New York and ElTech, Inc. Results of this work naturally will be factored into the trade studies being carried out both at LeRC and at IFC.

THE HYDROGEN-BROMINE RFC

This system has been evaluated in some detail in recent years, for several potential terrestrial applications. In all cases, the cell configuration has been based on the acid, solid polymer electrolyte (SPE) technology. The most attractive characteristic of the hydrogen-bromine cell is the apparent reversibility of the electrodes in both the fuel cell and the electrolyzer modes of operation. As mentioned earlier, this characteristic should be reflected in a stack and system design that is simple, lightweight and quite efficient. A block diagram of a hydrogen-bromine RFC is presented in figure 2, indicating a static hydrogen storage/supply system and a circulating aqueous bromine/HBr positive reactant. The use of such a system in space presents some unique constraints that did not need consideration for terrestrial applications. One of these is the absence of a sufficient gravity field for the separation of multi-phase fluids: Any gas passing through the SPE into the aqueous bromine system, or any liquid passing into the gaseous hydrogen system will tend to remain there and probably interfere with normal system performance. The evaluation of the membrane transport properties with respect to the various operating conditions and the various transportable species is thus of significance. Adding to this is the fact that the hydrogen electrode catalyst, typically platinum, is susceptible to poisoning or dissolution, depending on the electrode potential, in the presence of bromide ions which pass through the membrane.

Another multi-phase fluid situation can arise when the hydrogen-bromine system approaches full charge. As the HBr concentration is depleted, the solubility of bromine in the existing aqueous solution can be exceeded, resulting in a separate, pure bromine phase. The presence of bromine, whether in solution or not, creates a highly corrosive environment for the various cell components. This includes the bromine electrode itself, which may comprise a carbon or graphite structure and therefore be susceptible to intercalation and possible attendant damage.

Membrane transport properties and material compatibilities in the hydrogen-bromine cell environment have been studied by quite a few investigators. At LeRC we are undertaking an experimental program that initially will cover much the same ground as that covered by those investigators. One reason for this repetition is, that because of our interest in orbital missions and their unique characteristics, we bring a different perspective to the studies. Presently, we are carrying out static and electrochemical corrosion tests on candidate materials for cell construction, we are using electrochemical analytical techniques such as cyclic voltammetry for the evaluation of catalysts for the hydrogen and bromine electrodes, and we are evaluating single cells based on membrane and electrode (M&E) assembly technology developed by General Electric (Now Hamilton

Standard Electro-Chem, Inc.). We are also evaluating the transport properties of SPE membranes as functions of reactant concentrations, temperature, electric field intensity and membrane characteristics. In addition, we hope to continue a program with Giner, Inc., for the development of unique electrode catalysts for this system. Under a grant to the University of Akron, a system model is being developed and evaluated against single cell experimental data.

SUMMARY

LeRC has begun the evaluation, both in-house and under contracts and grants, of two regenerative fuel cell (RFC) systems. The passive hydrogen-oxygen RFC offers the possibility of a high-energy density, long-life storage system for GEO missions. The hydrogen-bromine RFC offers the combination of high effficiency and moderate energy density that could ideally suit LEO missions. If successfully developed, either or both of these systems would be attractive additions to the storage options available to designers of future missions.

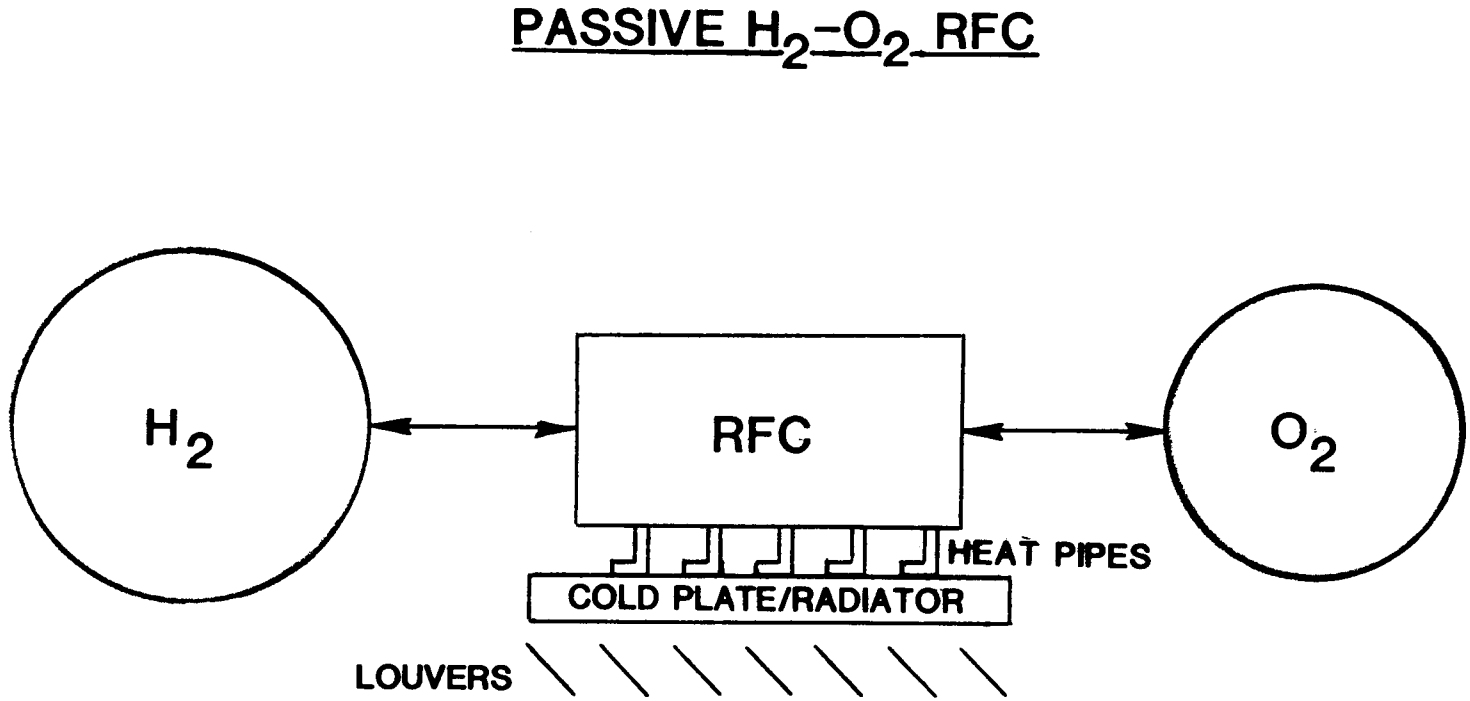

Figure 1. SCHEMATIC OF THE PASSIVE HYDROGEN—OXYGEN RFC

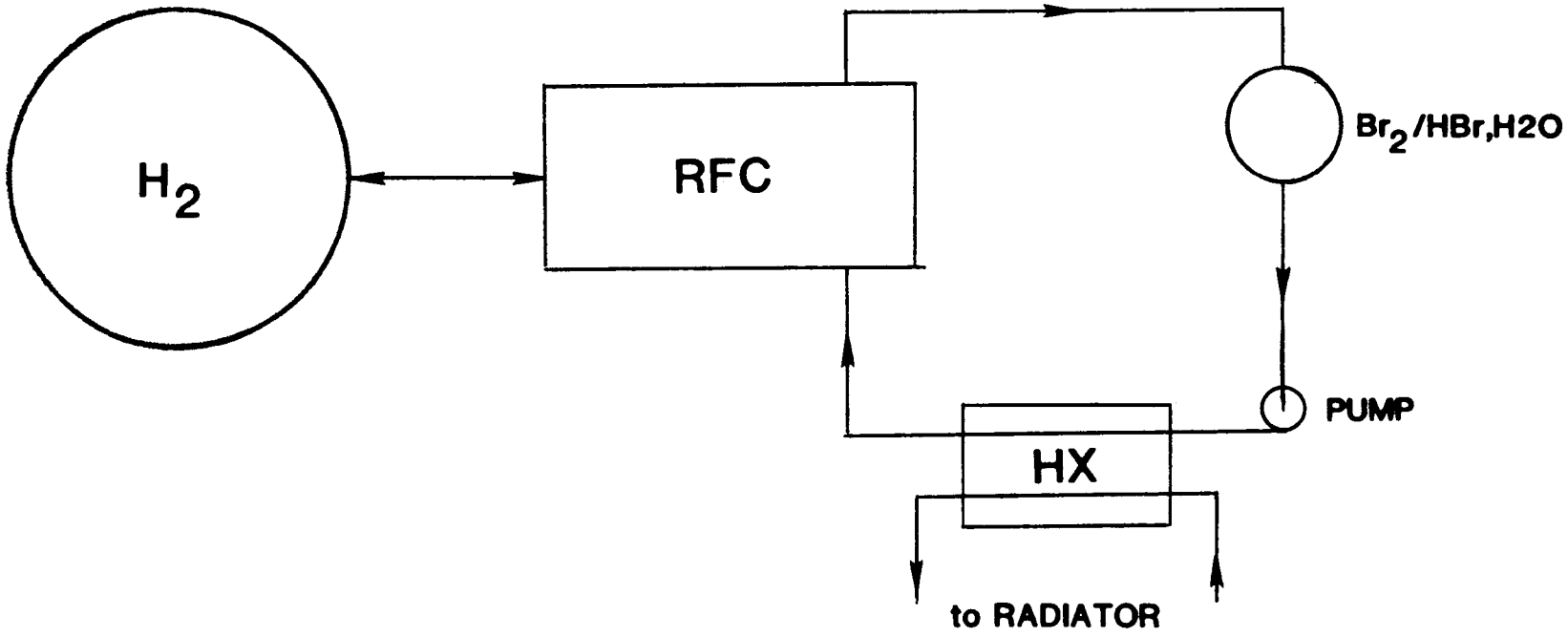

Figure 2. SCHEMATIC OF THE HYDROGEN—BROMINE RFC

Sodium-Sulfur Batteries For Spacecraft Energy Storage

Ross E. Dueber
Aerospace Power Division
Aero Propulsion Laboratory
Wright-Patterson AFB, OH 45433

Abstract

Power levels for future space missions will be much higher than are presently attainable using nickel-cadmium and nickel-hydrogen batteries. Development of a high energy density rechargeable battery is essential in being able to provide these higher power levels without tremendous weight penalties. Studies conducted by both the Air Force and private industry have identified the sodium-sulfur battery as the best candidate for a next generation battery system. A two to three-fold increase in energy density is possible with the sodium-sulfur battery when compared to the nickel-hydrogen battery.

Nickel-cadmium batteries have been a part of our nation's space program since its inception in the 1950's. Their reliability and lifetime have enabled them to endure throughout the years. Development of nickel-hydrogen batteries began in the 1970's and today they are available for use. Lifetime and weight advantages are gained by going to nickel-hydrogen batteries, but the increased capabilities are not enough to meet the requirements of future high power missions.

Future space missions will require much higher power levels than the 0.5 - 5 kW we need today (Figure 1). Directed energy weapons, ultrahigh resolution radar, and direct broadcast communications are three missions that will require multikilowatt to multimegawatt levels of power. Scale up of present battery system technology to these high power levels is not practical due to tremendous weight penalties. A real need exists now for batteries with much higher energy densities capable of achieving these high power levels without unacceptable weight penalties. In this paper, the advantages of the rechargeable sodium-sulfur battery are discussed in light of the shortcomings of current spacecraft battery technology.

The responsibility for providing electrical power aboard spacecraft is shared between the solar array and the battery. During the time a spacecraft is illuminated by the sun, electrical power is provided by the solar array. When an eclipse period occurs, the burden of supplying power to the payload shifts to the battery. The battery recovers its spent energy by recharging from the solar array during the following sunlight periods.

Depending upon the orbit, these sunlight periods may be fairly continual throughout the year or they may occur at certain intervals of the day. A possible cycling regime for low earth orbit (LEO) requires the battery to partially discharge in approximately 30 minutes and fully recharge in 60 minutes. This cycle will be repeated 16 times in a 24 hour day and 5840 times a year. By moving to higher orbits, the number of cycles decreases due to a lessening in the frequency of eclipse periods. When geosynchronous earth orbit (GEO) is reached, the eclipse periods occur only during two 45 day periods per year. Discharge times in this orbit vary from 12 - 72 minutes during each eclipse period, which results in a total battery discharge requirement of 90 cycles a year.

Apparent from the characteristics of the various orbits is the significant decrease in required cycles as the orbit moves from low altitude to high altitude. LEO is much more demanding in terms of the frequency of cycles required from a battery than is GEO. As a result, calendar lives of batteries in the lower orbits are shorter than those in higher orbits. Average lifetimes of nickel-cadmium batteries in LEO run 3-5 years, while lifetimes in GEO average 7-10 years. Nickel-hydrogen batteries are expected to last longer on the average, but still are life-limited by the same nickel electrode used in nickel-cadmium batteries.

The sodium-sulfur battery is different in that both the anode and cathode are liquids instead of solids (Figure 2). As such, they do not experience the fatigue and degradation problems associated with the continuous cycling of solid electrodes. Conceivably, the sodium and sulfur could continue to cycle forever in an ideal cell. The life limiting factor in this case is not the electrode, but the solid ceramic electrolyte and the cathode container. Shaped in the form of a tube, the electrolyte serves as both an ion conductor and a separator in the cell. The cells commonly fail by breakage of the tube resulting from flaws in the ceramic. This allows the sodium and sulfur to mix, causing irreversible failure of the cell. Restriction of the flow of sodium available for reaction is necessary to prevent the occurrence of a large temperature increase when the liquid sodium contacts the liquid sulfur through the crack in the electrolyte. The current Air Force cell design, based upon the Ford Aerospace terrestrial cell, uses a stainless steel protection tube equipped with a restrictive device to limit the sodium flow from the anode compartment. In the event of electrolyte failure, the amount of sodium from the reservoir able to react with the sulfur is limited by the flow rate through the restrictive device.

Corrosion of the cathode container is the other factor presently limiting cell lifetime. Terrestrial cells use chromium coated stainless steel to contain the sulfur/sodium polysulfide catholyte and transport the current. Sodium polysulfides slowly react with the chromium to form corrosion products which deposit on the electrolyte surface (Figure 3). These harmful deposits appear to contribute to cell resistance rise over the life of a cell. Evidence also exists for the corrosion of the electrolyte by the

sodium chromium polysulfides, possibly resulting in strength degradation of the tube's wall.[1]

Still, substantial reduction in flaw sizes in the ceramic electrolyte and the use of corrosion resistant container materials will be necessary before sodium-sulfur cells are ready for space. Development of the components for terrestrial cells has been driven by the need for relatively inexpensive starting materials and low cost fabrication methods. Commercialization goals for terrestrial sodium-sulfur technology set energy storage costs of the battery at between $50 and $100 per kilowatt-hour. Compare these values with the average $50,000 per kilowatt-hour cost for a spacecraft battery and one can see a great deal of improvement can be made. Higher quality starting materials, better fabrication techniques, and higher quality assurance standards will improve the lifetimes of the cell components. Goals of 30,000 cycles and 10 years life should be achievable through advancements in research by the year 2000.

A second factor to consider in regard to spacecraft batteries is efficiency. Efficiency is the amount of energy withdrawn from the battery during discharge divided by the amount of charging energy put into the battery during one typical electrical cycle. The energy storage efficiency directly affects the power level of the accompanying solar array. Increased efficiency of the energy storage system equates to more efficient use of solar array power and a subsequent reduction in the size of the solar array. Efficiency is important in all orbits, but is especially critical in the low altitude orbits where the recharge time is short. Short recharge times imply high solar array power and high battery efficiency can reduce the size of these large solar arrays. Improved energy storage efficiency decreases the energy losses during this stage and results in better utilization of solar array power, as well as reduced thermal management requirements to radiate waste heat. Both nickel-cadmium and nickel-hydrogen batteries have efficiencies of 75%, while sodium-sulfur is 85-90% efficient.

The advantage of switching to more efficient batteries is decreased solar array size, resulting in a weight reduction of up to 10%. A decreased solar array size benefits not only the increased weight allocable to the payload, but also results in reduced drag, smaller radar signature and reduced altitude maintenance propellant requirements. The magnitude of these individual benefits is small, but it becomes significant when they are combined.

A third major factor for spacecraft batteries is the trade-off between power and weight. Missions outlined in the Military Space

[1] J.A. Smaga and J.E. Battles, "Post-Test Examination of Na/S Cell ADA23," Private Correspondence to Air Force Wright Aeronautical Laboratories, 1985.

Systems Technology Plan (MSSTP) project power levels for future spacecraft at 50 kilowatts and above. Present spacecraft batteries supply power up to 5 kilowatts and comprise on the average about 10 - 15 percent of the total satellite weight. As spacecraft power levels rise and spacecraft weights approach the payload limits of boosters and orbital transfer vehicle capabilities, the allowable battery weight will place limits on the power available to the spacecraft (Figure 4). The percentage of spacecraft weight occupied by batteries is determined not only by battery technology, but by the technology of the other subsystems. This percentage can be reduced by improving battery technology through the development of more advanced systems. Increases in the percentage of satellite weight allocated to the batteries at this time must come at the cost of either reduced capabilities of other subsystems or improved technologies in those subsystems or the payload. For spacecraft using advanced nickel-hydrogen batteries, power in mid-altitude orbits will be limited to about 12 kilowatts using the Inertial Upper Stage (IUS) and 22 kilowatts using the High Energy Upper Stage (HEUS). In geosynchronous orbit the power drops to 7 kilowatts with the IUS and 14 kilowatts with the HEUS. When requirements for hardening and autonomy of the entire spacecraft are considered, the available power levels will be reduced further.

In order to achieve the power levels required by the MSSTP and overcome the adverse weight effects of hardening and autonomy, the sodium-sulfur battery must be developed. Present nickel-hydrogen batteries supply approximately 20 watt-hours (Wh) of energy per pound of battery weight in GEO and less than 10 Wh/lb in LEO. Further improvements in nickel-hydrogen will yield only modest increases in these energy density values.

A significant improvement in the energy density can be made through the development of sodium-sulfur batteries. Separate studies performed by AFWAL, Hughes Aircraft and Ford Aerospace predict the energy density of the sodium-sulfur battery to be 50 Wh/lb in GEO and 35 Wh/lb in LEO. These predictions represent over a two-fold increase in energy density when compared to nickel-hydrogen. For GEO using sodium-sulfur batteries with the HEUS, 50 kilowatt power levels will be attainable. This value assumes the battery will still comprise only about 15% of the total satellite weight.

Part of this reduction in weight can be realized when considering the thermal management system of a battery. Hughes Aircraft performed a system design of a mid-altitude orbit radar satellite. The system design called for a 50 kilowatt, 47 kilowatt-hour rechargeable battery. Radiators were sized for both a nickel-hydrogen and a sodium-sulfur battery. Results showed the nickel-hydrogen's radiator having a total area of 490 ft^2 while the radiator for sodium-sulfur was 47 ft^2 (Figure 5). The large disparity is the result of the different operating temperatures of the two batteries. Nickel-hydrogen's low operating temperature (10-20°C) requires a large radiator to dissipate waste heat. Sodium-sulfur, on the other hand, can discharge its waste heat

through a smaller radiator at the battery's operating temperature of 350°C. Reductions in size and complexity would yield a highly reliable thermal management system with greater survivability from future threats in space.

Other lesser factors also deserve consideration when comparing characteristics of spacecraft batteries. Depth-of-discharge (DOD) is expressed as a percentage of the rated energy capacity removed from a battery in a single discharge. Depending on orbit and desired lifetime, nickel-cadmium DOD is limited to about 25% in the lower orbits, while at GEO the value can increase to 60%. The reason for utilizing only a fraction of the rated capacity is to extend the battery's lifetime. Greater than recommended depth-of-discharge results in declining battery performance and premature failure. Advances in nickel-cadmium and nickel-hydrogen batteries may extend DOD to 40% in LEO and 80% in GEO.

Sodium-sulfur cells again will make an improvement over nickel-hydrogen and nickel-cadmium. Cells on test in simulated mid-altitude orbit (MAO) and GEO at the Aero Propulsion Laboratory have been discharged to 80% DOD with no apparent adverse effect on lifetime. The deeper discharge would be a more effective use of available energy for low altitude orbit mission, but consideration will have to be given to the end of life requirements for battery capacity in determining the system's optimum DOD. Since a final cell design has not been selected at this time, performance degradation with time is unknown.

The problem of self-discharge by spacecraft batteries on open circuit will also be eliminated by the use of sodium-sulfur. Charging systems on present satellites are required to perform trickle charging to maintain the batteries at full capacity and account for small differences in charging efficiencies. Also, complicated individual cell controls are required. Sodium-sulfur is unlike present spacecraft batteries in that no self-discharge occurs while it is an open circuit, as Faradaic efficiency is 100%. Transport of sodium ions through the ceramic electrolyte can happen only when a load is placed on the system. Once a battery is charged to a predetermined voltage limit, the capacity will be retained until energy is required.

Problems, however, do exist with the sodium-sulfur battery in its present state. Sufficient lifetime and reliability of the cell for GEO and MAO are questionable. Cells on test at AFWAL have demonstrated the necessary cycle lifes for GEO and are approaching those needed for MAO (Figure 6). Nonetheless, the calendar life goal of 10 years is yet to be attained and will not be known for several years. Cell reliability is also unacceptable due to the percentage (less than 10%) of cell failures still occurring within the first 200 cycles. The keys to solving this particular problem will be improvement of the quality of ceramic electrolyte tubes and cathode containers used in the design.

In the area of battery design, several other problems must be solved before use in spacecraft can begin. Design of the thermal management system will require a lightweight battery container capable of isolating the battery's heat from the rest of the spacecraft. During discharge the battery generates more heat than it requires to remain at the operating temperature. Radiation of excess heat at 350°C could be a significant problem for the spacecraft's delicate instrumentation if the heat is not directed outwards into space. At the same time, sufficient insulation must be used to keep the battery at its operating temperature. Operation of the battery below this temperature would result in decreased efficiency and possible damage to the cells. Internal heaters in batteries for GEO will have to be used to maintain temperature during solstice periods.

Advancements in high temperature cell bypass technology is also necessary for the development of the sodium-sulfur battery. The diodes and relays used for cell bypass in nickel-cadmium and nickel-hydrogen are designed to function in these batteries' operating temperature range of 10-20°C. Placement of the bypass electronics external to the sodium-sulfur battery would result in large thermal losses through the connections to the container. New technology will be needed to withstand the rigors of a 350°C environment with the same reliability as before.

The sodium-sulfur battery is a developing technology with a tremendous potential to expand Air Force operational capabilities in space. This paper has discussed its benefits over existing technology, as well as the genuine need for it in the future. Sodium-sulfur is not just an enhancing technology like nickel-hydrogen, it is an enabling technology which is required for the performance of future high power space missions. Development of the technology must begin now in order for it to be available by the mid 1990's. Several issues concerning the system still must be addressed and technology problems solved before it will be ready for space use. Nonetheless, the advantages this system offers when compared to batteries we have now are so attractive and essential that we cannot afford to delay development any further. Space power is a key enabling technology in the accomplishment of the total space mission. Neglect of it would undoubtedly result in our failure to achieve important future mission objectives in space.

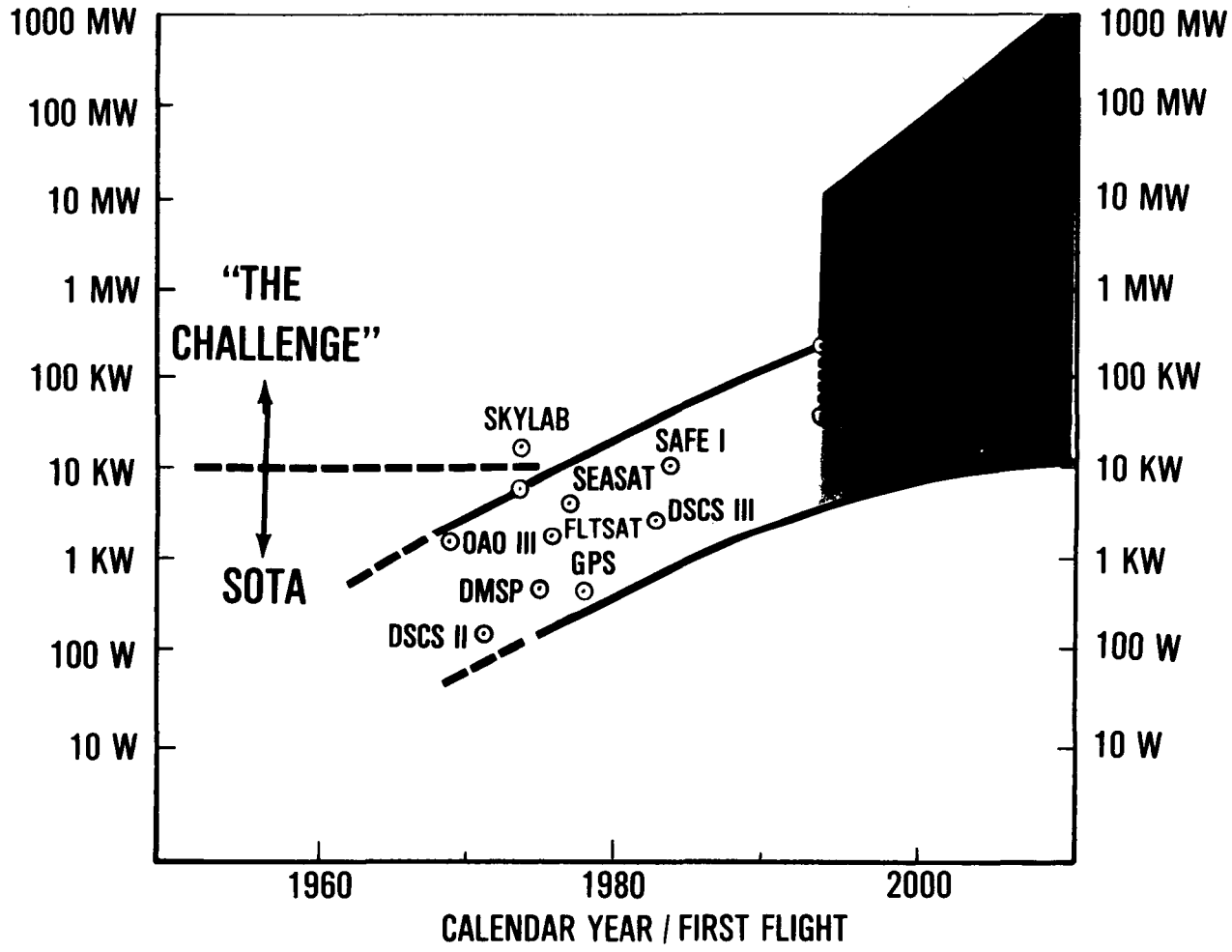

Figure 1. ELECTRICAL POWER TRENDS SPACECRAFT

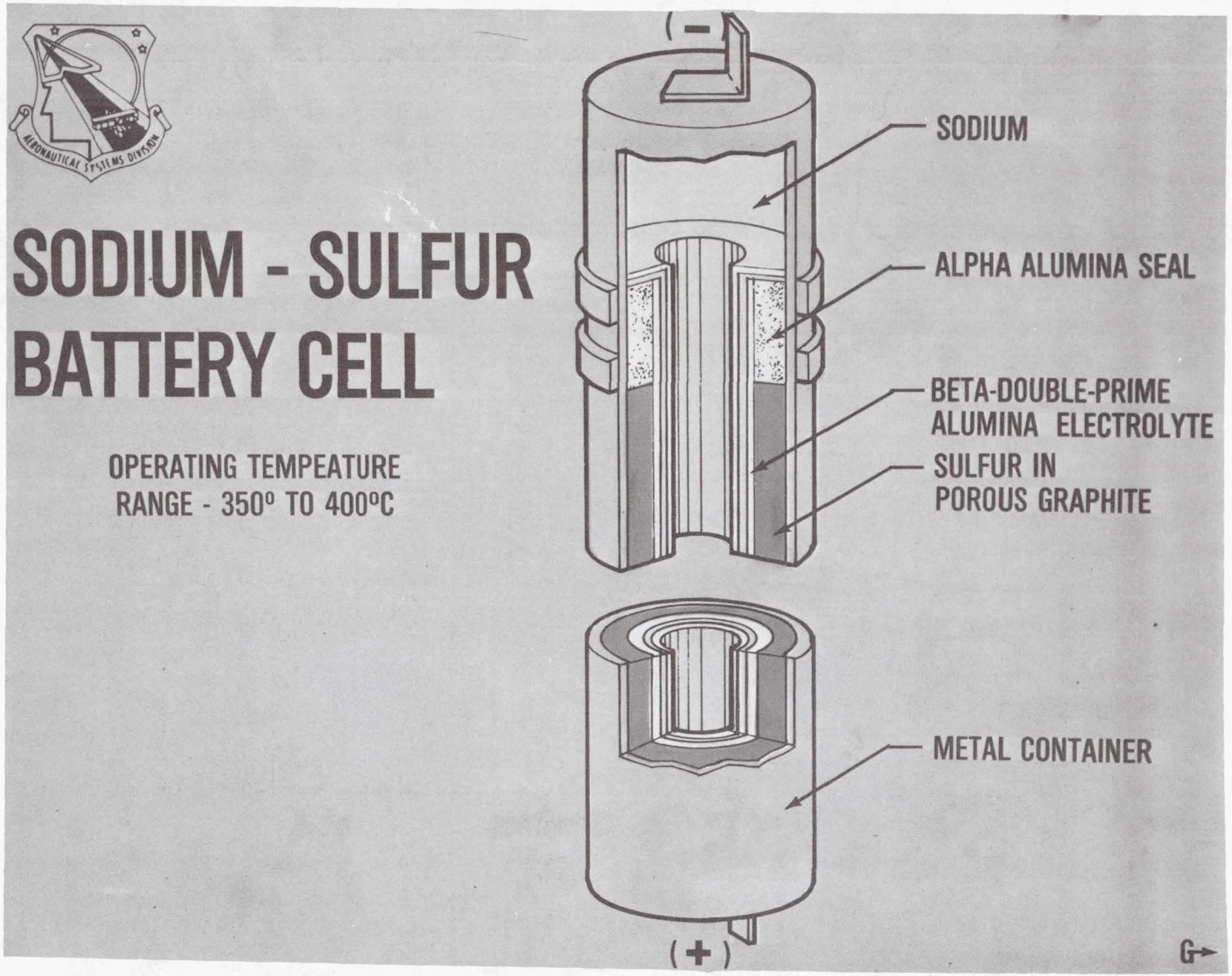

Figure 2. SODIUM—SULFUR BATTERY CELL

Figure 3. $NaCrS_2$ CRYSTALS ATTACHED TO THE ELECTROLYTE SURFACE

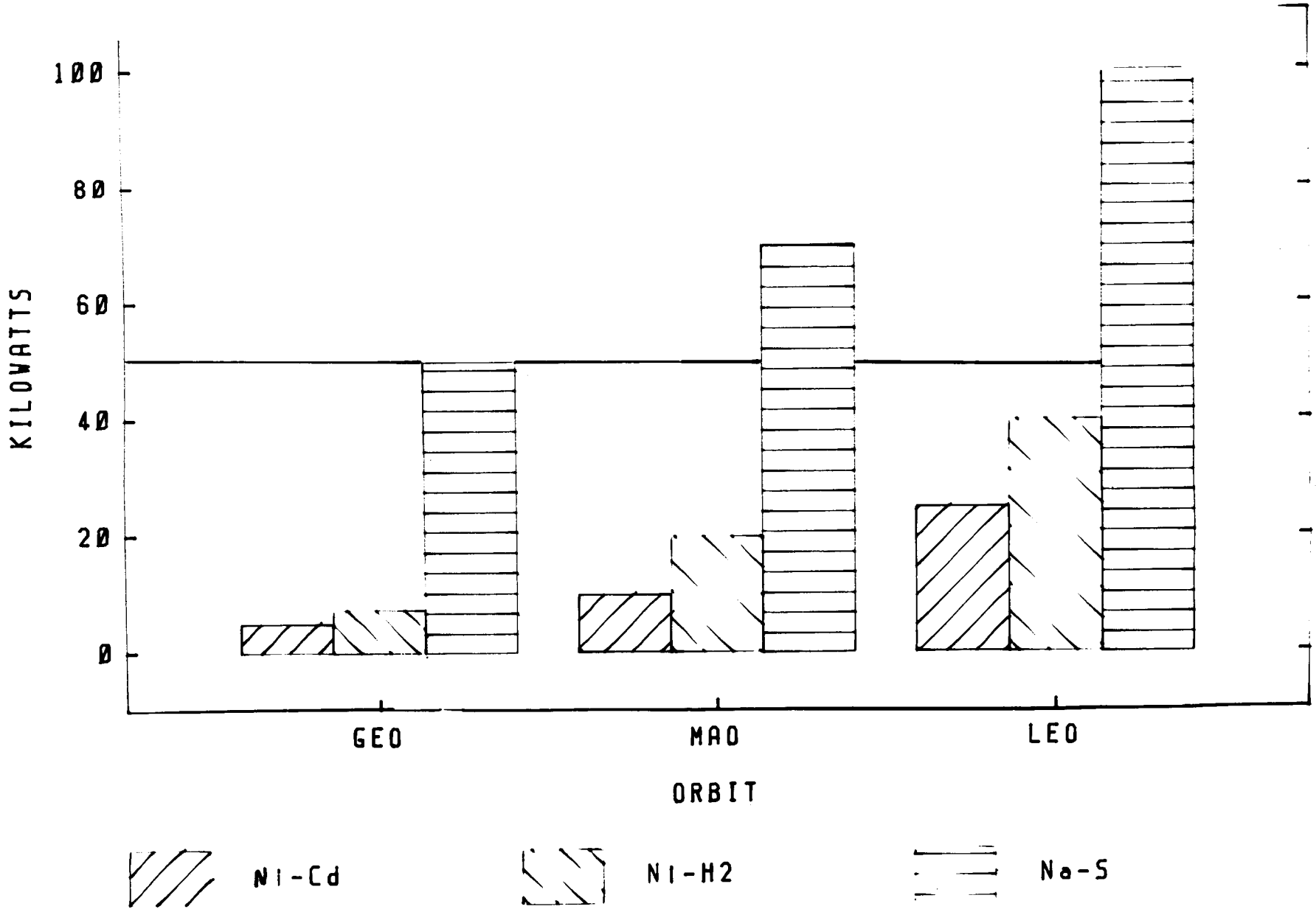

Figure 4. ELECTRICAL POWER SYSTEM OUTPUT CAPABILITY (SHUTTLE-HEUS)

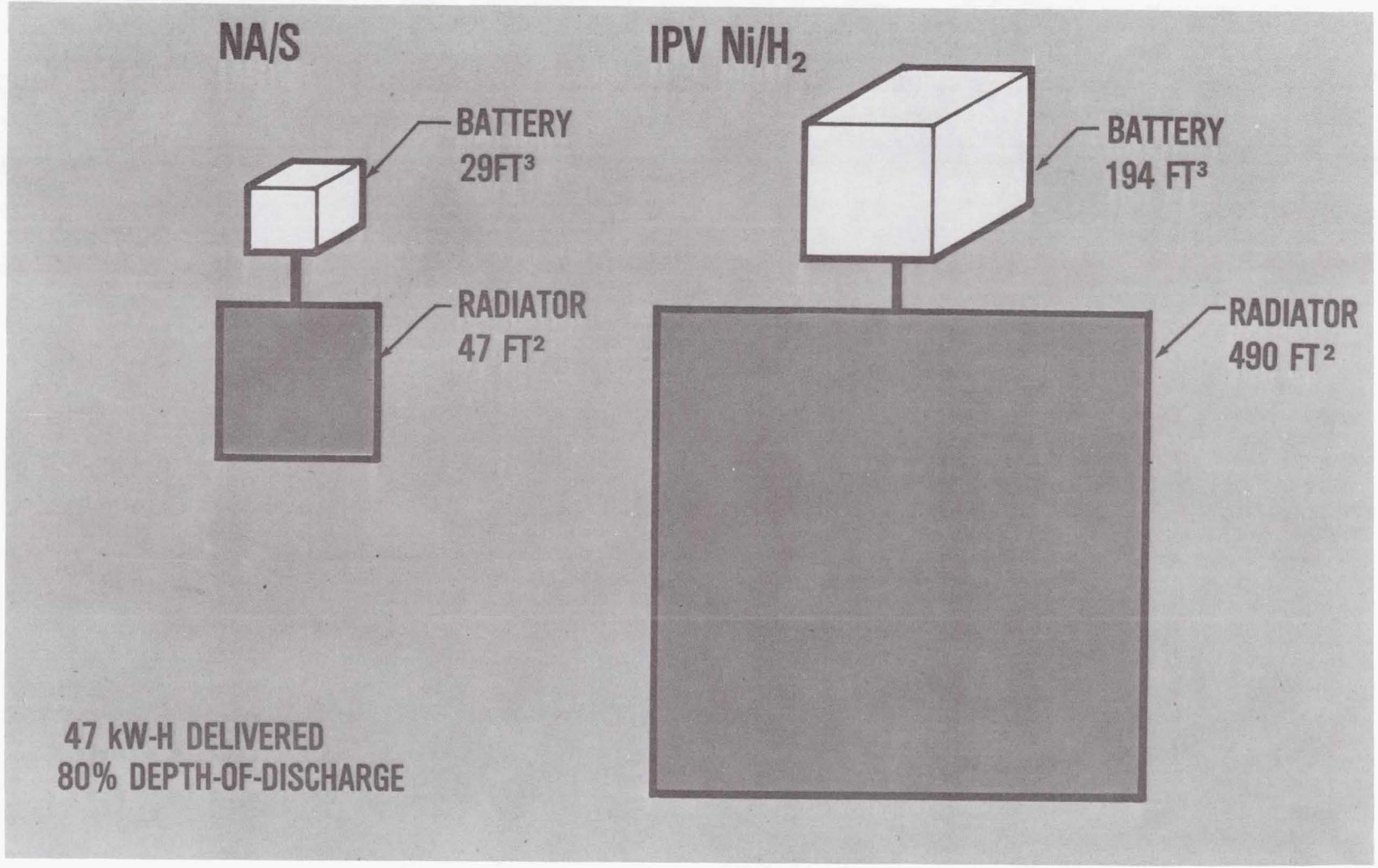

Figure 5. BATTERY SYSTEM SIZE

CELL	CYCLES	DAYS ON TEST
1	2204	601
2	3055	829
*3	2350	650
4	3055	829
5	5407	737
**6	3364	557
7	775	829
8	683	737

* FAILED 25 DECEMBER 1984
** FAILED 4 APRIL 1985

Figure 6. CYCLE LIFE DATA (AS OF 1 OCTOBER 1985)

ENERGY STORAGE SYSTEMS COMPARISON FOR THE SPACE STATION

G. van Ommering

Ford Aerospace & Communications Corporation
Palo Alto, California

INTRODUCTION

The Space Station represents one of the largest space power system applications under serious consideration at this time. Definition and Preliminary Design studies under Phase B of the Space Station Program are in process at most NASA centers and a large group of contractors. In the Work Package 4 Power System studies, NASA Lewis Research Center with contractor teams led by Rocketdyne (with major team members Ford Aerospace, Harris, Garrett, and Sundstrand) and TRW (with General Dynamics and General Electric) is defining the Power System. This effort has progressed through conceptual design of various options, and elimination of some options to a final selection process which is now beginning.

This paper provides an overview of the requirements, options, selection criteria and other considerations, and current status with regard to the energy storage subsystem (ESS) for the photovoltaic power system alternative for the Space Station, presented from the perspective of Ford Aerospace as a member of the Rocketdyne team.

ENERGY STORAGE SYSTEM REQUIREMENTS

Technical Performance Requirements

The current requirements to which the power system is being designed are summarized in Table 1. Significant for the ESS is, beside the 75 kW base load, the contingency requirement which demands the ability to support half the station load for a full orbit after eclipse completion. This limits depth of discharge (DOD) to about 38-40 % for nominal eclipse operation. Peaking support is not very severe in a relative sense, but needs to be factored into DOD and contingency capability for ESS sizing purposes. A design life of five years has been used as a goal. Physical constraints for the ESS derive from the 9 x 9 x 9 foot envelope of the "utility centers" located just outboard of the transverse boom alpha joints, see Figure 1.

Technology Readiness Requirements

Table 2 summarizes the technology readiness and risk implications of the Space Station schedule, which has a goal of a 1992 Initial Operating Capability (IOC) with growth beginning a few years later.

For IOC the desired technology should be scalable to Space Station proportions at low risk, while the growth Station permits more advanced technologies for which both risk and payoff are higher.

IOC Cost Requirements

The cost of the IOC configuration of the Space Station is limited to $ 8B. This must be accommodated by cost-effective design of each subsystem, but in particular by ensuring that the overall system cost is minimized, even if this means choosing a more costly option for a given subsystem. As suggested in Table 3, cost of the ESS should not be minimized in itself, but must be combined with cost impacts on solar arrays, thermal control hardware, power management and distribution (PMAD) equipment, and others as a basis for overall system cost optimization. These cost impacts result from ESS roundtrip efficiency, heat dissipation, and electrical control requirements. Commonality with other subsystems, platforms and free-flyers to save development costs, and modularity and simplicity to save production costs, are desirable to minimize IOC expenses.

Launch and Operations Cost Requirements

Launch cost is a key element of overall cost, and here mass impacts must be accounted for that are caused by ESS selection and design in other subsystems. Volume may in some cases be a stronger launch cost driver than mass, and must be accounted for similarly. As summarized in Table 4, other elements of life cycle cost include operational and maintenance expenses. For the Space Station, operations costs are affected strongly by the need to supply fuel to maintain orbit altitude; this drives the ESS to high efficiency to minimize solar array and radiator size. Replacement costs include considerations of high reliability and wear-out life, and minimal cost of replacement.

SPACE STATION ESS OPTIONS

ESS Options Considered

Within the above framework of requirements, and as quantitatively as possible, a range of ESS options has been evaluated. Table 5 shows the major options considered. The first elimination round involved a global judgement of readiness of each technology and its ability to meet the IOC date. This led to elimination of energy wheels, sodium-sulfur batteries and hydrogen-halogen fuel cells. Bipolar Ni-H_2 batteries were borderline in readiness potential.

For some of the eliminated options an estimate of performance was nevertheless done to estimate the potential for growth. Table 6, discussed in more detail later, gives a comparison of some major representatives of each ESS class. Designs are summarized below.

Overview of ESS Designs

Regenerative Fuel Cell. The alkaline regenerative fuel cell system (RFCS) consists of four identical assemblies. Each includes a fuel cell module (FCM), a water electrolysis module (WEM), a FCM accessory section, and a WEM accessory section. The accessory sections contain the valves, pumps, regulators, heat exchangers, etcetera, required for RFCS operation. A set of hydrogen and oxygen tanks serves two of the assemblies. The electrode areas of the FCM and WEM are sized to provide a relatively high efficiency of 62%, which includes losses associated with accessory section operation. Typical operating voltages of the FCM and WEM stacks are 155 V.

IPV Ni-H_2 Battery. The individual pressure vessel (IPV) Ni-H_2 battery option consists of four batteries of 275 Ah capacity. Each battery has 105 cells of 275 Ah capacity in series, distributed over five identical assemblies. These assemblies hold their 21 cells supported on structural beams that carry heat pipes for efficient heat removal. Twenty assemblies are held in two "oven-rack" type arrangements, one per utility center. Typical discharge voltage is 133 V averaged over the 35-minute, 40% DOD discharge.

Bipolar Ni-H_2 Battery. The bipolar Ni-H_2 battery uses the design concept developed by Ford Aerospace and Yardney under NASA-LeRC sponsorship. It consists of four batteries, each with three assemblies in parallel. The assemblies each consist of a pressure vessel containing two cell stacks of 52 cells in series, with a capacity of 90 Ah. The cells have the long, rectangular configuration: about 12 cm wide by 160 cm long. Each assembly also contains redundant coolant pumps and a heat exchanger interface.

Ni-Cd Battery. The Ni-Cd system consists of 16 batteries of 125 Ah capacity and with 104 series cells. Each battery is divided into four 26-cell battery packs, mounted on a honeycomb panel with embedded heat pipes. The 16 panels are mounted in "oven-rack" type arrangements in the Station utility centers.

Na-S Battery. The sodium-sulfur (Na-S) battery, operating at 300 to 400°C, uses cell sizes close to those being produced currently. The 75-kW system would consist of four batteries each with four 87-kg modules of 70 cells of 65 Ah capacity, delivering about 126 V on discharge. Each module has a variable conductance radiator system on its external surface. The modules are placed on the outside of the utility module.

Energy Wheels. The energy wheel data shown represents a blend of various approaches. This was necessary because of the extremely wide range of characteristics reported for point designs for Space Station flywheels.

ESS OPTIONS COMPARISON

Performance

Table 6 provides a comparison of ESS alternatives described above. The alkaline H_2-O_2 RFCS is used as the baseline in this comparison.

The RFCS has a much lower mass than the other feasible systems, the Ni-Cd, IPV Ni-H_2, and bipolar Ni-H_2 batteries. However, its thermal control equipment is considerably heavier than that of the others, because of the RFCS's relatively low roundtrip efficiency and its resulting high heat rejection rate, albeit at a higher temperature. In the case of the room-temperature systems it is also feasible to use a common thermal control loop for the ESS and PMAD, which is difficult to do with the RFCS. The roundtrip efficiency difference also results in a solar array mass "credit" for the non-RFCS systems. When all the impacts have been included, the RFCS has still the lowest mass, but the other systems become more competitive.

By far the most attractive is the Na-S battery system; however, this technology has not reached the maturity required for serious consideration for the IOC Space Station. It provides low mass, high efficiency, and minimal thermal support requirements due to the high rejection temperature. With sufficient development its benefits may be applicable to the growth station.

Maturity

Table 7 summarizes for the options with initial readiness potential the estimated maturity level using the NASA 1 to 8 rating scale. The levels shown here represent (abbreviated definitions):

4 - Critical function breadboard demonstration
5 - Component or brassboard model tested in relevant environment
6 - Prototype or engineering model tested in relevant environment
7 - Engineering model tested in space
8 - Baselined into production design

The rating for the alkaline/alkaline RFCS is dual: while the fuel cell part has been demonstrated on the STS Orbiters with success, and can be considered a prototype for the Space Station version, the electrolyzer has so far been demonstrated only as a breadboard in the laboratory and rates a 4. The IPV Ni-H_2 battery has a dual rating of 6 for the qualification of smaller LEO cells, and 5 for the slightly lower maturity of the 275-Ah cells. A 220-Ah cell is being demonstrated in December 1985 by Ford Aerospace and Yardney.

In addition to the maturity level, the degree of current development activity, interest, and funding is an important factor in the assessment of potential technology readiness. Qualitative estimates are shown in Table 7.

Combination of the maturity and activity estimates leads to the judgement that only the alkline/alkaline RFCS, the Ni-Cd battery and the IPV Ni-H_2 battery are viable options for Space Station energy storage.

Cost

Costs for the three surviving options are undergoing extensive refinement and therefore quantitative values would be very preliminary. However, a broad qualitative comparison can be made in the different cost categories, and is expected to remain valid. Table 8 summarizes the data. Development costs follow the maturity levels as expected. Production costs are lowest for the Ni-H_2 system due to low complexity, moderate modularity and replication. Ni-Cd batteries are highest because of the large quantity of cells and battery packs. The RFCS is intermediate due to greater complexity and lower modularity. Solar array costs and thermal control system costs are somewhat higher for the RFCS because of the greater heat rejection requirement. Launch costs follow the net mass figures of Table 6. Overall, the IOC costs appear lowest for Ni-H_2 batteries, with the RFCS not very far behind, and Ni-Cd considerably more expensive.

Operations costs for the three options compare as follows. The drag-related fuel costs will be higher for the RFCS due to the larger solar arrays. Random failure occurences will be higher for the RFCS, but the items to be replaced will be generally the accessory sections, which are small and lightweight. While the replaced mass may thus be less than for the batteries, the extravehicular activity repair events are higher in number and therefore more costly.

SUMMARY AND CONCLUSION

Evaluation of ESS options for the Space Station has led to the selection of H_2-O_2 alkaline RFCS, IPV Ni-H_2 batteries, and Ni-Cd batteries, as potentially able to meet requirements. Of these, the Ni-Cd batteries are too heavy and too costly to be a serious contender. Ni-H_2 batteries appear somewhat lower in overall IOC cost and operational costs, and are also favored slightly in non-quantitative criteria, such as maintainability, safety, etcetera. The RFCS has a mass advantage, but has an overall small disadvantage in IOC cost and development risk.

The RFCS versus IPV Ni-H_2 battery decision will be the subject of further sensitivity and trade studies to ascertain the potential effects of evolution of requirements. The final selection is to be made by March 1986 and will involve consideration of all Space Station system impacts.

TABLE 1. SPACE STATION POWER SYSTEM REQUIREMENTS

- IOC - NOMINAL LOAD POWER : 75 kW
  PEAKING : 100 kW FOR 15 min PER ORBIT
  CONTINGENCY : 37.5 kW FOR 1 FULL ORBIT (AFTER ECLIPSE)
- GROWTH - NOMINAL LOAD POWER : 300 kW
  PEAKING : 350 kW FOR 15 min PER ORBIT
  CONTINGENCY : 150 kW FOR 1 FULL ORBIT (AFTER ECLIPSE)
- IOC COST CONSISTENT WITH $ 8 BILLION (1987$) TOTAL STATION COST
- MINIMAL LIFE CYCLE COST

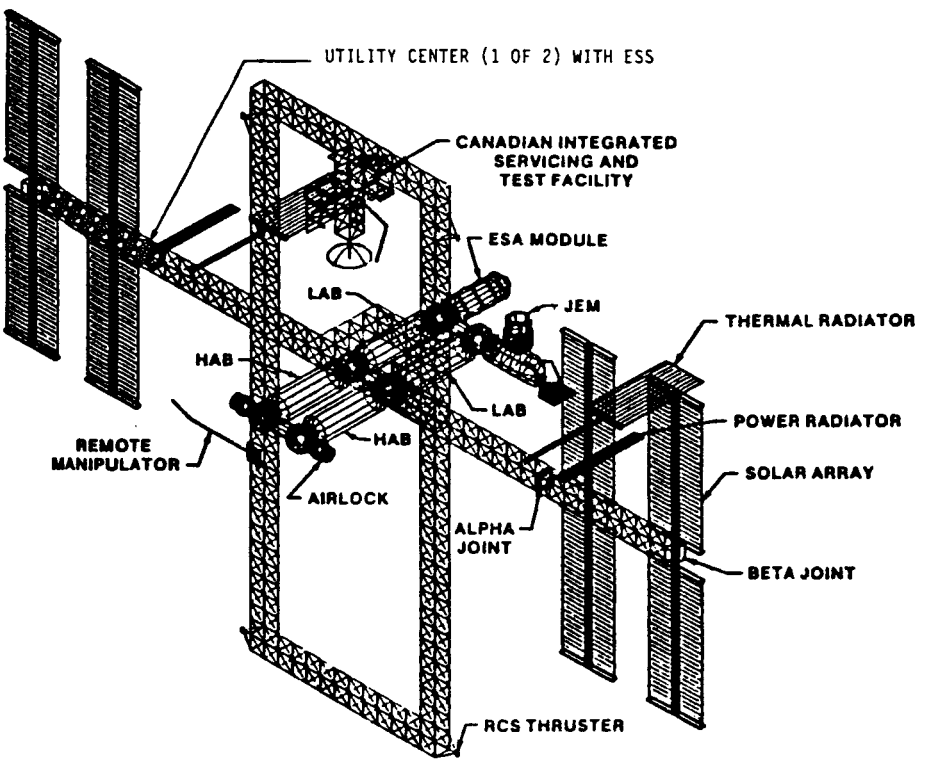

Figure 1. PHOTOVOLTAIC SPACE STATION CONFIGURATION

TABLE 2. SPACE STATION ENERGY STORAGE SUBSYSTEM PERFORMANCE REQUIREMENTS

- IOC : 75 kW + CONTINGENCY + PEAKS
  - LOW RISK SCALE-UP OF CURRENT TECHNOLOGY FEASIBLE
  - TECHNOLOGY READINESS ADEQUATE TO MEET IOC SCHEDULE
  - ABILITY TO MEET PEAK REQUIREMENTS
- GROWTH : 300 kW + CONTINGENCY + PEAKS
  - MEDIUM RISK SCALE-UP OF CURRENT TECHNOLOGY FEASIBLE
    - MORE ADVANCED TECHNOLOGY PERMITTED
  - TECHNOLOGY READINESS ADEQUATE TO MEET GROWTH SCHEDULE
  - ABILITY TO MEET PEAK REQUIREMENTS

TABLE 3. SPACE STATION ENERGY STORAGE SUBSYSTEM IOC COST REQUIREMENTS

- COST CONSISTENT WITH $ 8 BILLION IOC STATION COST

- LOW DEVELOPMENT COST
  - HIGH MATURITY LEVEL
  - HIGH MODULARITY LEVEL
  - LOW COMPLEXITY
- LOW PRODUCTION COST
  - HIGH MODULARITY LEVEL
  - LOW COMPLEXITY
- MINIMAL ADVERSE IMPACT ON OTHER SYSTEMS/SUBSYSTEMS
  - POWER GENERATION SUBSYSTEM
  - POWER MANAGEMENT AND DISTRIBUTION
  - THERMAL CONTROL SUBSYSTEM
  - - ETC -
- HIGH COMMONALITY
  - WITH OTHER SYSTEMS/SUBSYSTEMS
  - WITH PLATFORMS AND FREE-FLYERS

TABLE 4. SPACE STATION ENERGY STORAGE SUBSYSTEM LIFE CYCLE COST REQUIREMENTS

- MINIMAL LIFE CYCLE COST
  - MINIMAL LAUNCH COST
    - LOW MASS
    - LOW VOLUME
  - MINIMAL OPERATIONS COST
    - AUTOMATION
    - MINIMAL IMPACT ON OTHER SUBSYSTEMS
      - POWER GENERATION SUBSYSTEM DRAG
      - THERMAL CONTROL SUBSYSTEM DRAG
  - MINIMAL MAINTENANCE/REPLACEMENT COST
    - HIGH RELIABILITY AND LONG WEAR-OUT LIFE
    - LOW REPLACEMENT COST
      - LOW MEAN-TIME-TO-REPAIR
      - MODULARITY
      - LOW MASS AND VOLUME (LAUNCH COST)
      - LOW PRODUCTION COST

TABLE 5. SPACE STATION ENERGY STORAGE OPTIONS

- BATTERY SYSTEMS
  - NICKEL-CADMIUM
  - NICKEL-HYDROGEN IPV
  - NICKEL-HYDROGEN CPV
  - NICKEL-HYDROGEN BIPOLAR
  - o SODIUM-SULFUR
- REGENERATIVE FUEL CELL SYSTEMS
  - ALKALINE/ALKALINE HYDROGEN-OXYGEN
  - ALKALINE-FC/SPE-EM HYDROGEN-OXYGEN
  - SPE/SPE HYDROGEN-OXYGEN
  - o HYDROGEN-HALOGEN
- 0 ENERGY WHEELS (FLYWHEELS)

● ● COULD BE READY FOR IOC
0 o CANNOT BE READY FOR IOC

TABLE 6. SPACE STATION ENERGY STORAGE OPTIONS CHARACTERISTICS COMPARISON

CHARACTERISTIC	H_2-O_2 RFCS	Ni-H_2 IPV	Ni-H_2 BIPOLAR	Ni-Cd	Na-S	ENERGY WHEELS
ROUND-TRIP EFFICIENCY (%)	62	80	82	80	85	85
DEPTH-OF-DISCHARGE (%)	(40)	40	40	20	40	40
MASS (kg)						
ENERGY STORAGE	2300	4550	3600	9600	1400	6000
THERMAL CONTROL	2100	1100	1100	1100	100	800
SOLAR ARRAY CREDIT	-	(270)	(270)	(270)	(360)	(360)
* TOTAL *	4400	5380	4430	10430	1140	6440
VOLUME (m^3)	19	14	3	11	2	9
ECLIPSE HEAT REJECTION (kW)	55	19	18	19	18	10
TEMPERATURE (^oC)	80	10	10	10	350	30

TABLE 7. SPACE STATION ENERGY STORAGE OPTIONS READINESS AND ACTIVITY ASSESSMENT

ENERGY STORAGE OPTION	MATURITY LEVEL	SPACE DEVELOPMENT ACTIVITY
* ALK/ALK REGENERATIVE FUEL CELL	4/7	HIGH
SPE/SPE REGENERATIVE FUEL CELL	5	LOW
ALK/SPE REGENERATIVE FUEL CELL	5	MED
* NICKEL-CADMIUM BATTERY	8	HIGH
* NICKEL-HYDROGEN IPV BATTERY	5/6	HIGH
NICKEL-HYDROGEN CPV BATTERY	4	LOW
NICKEL-HYDROGEN BIPOLAR BATTERY	4	MED

* = SURVIVOR

TABLE 8. SPACE STATION ENERGY STORAGE OPTIONS QUALITATIVE COST COMPARISON

COST ELEMENT	RFCS	Ni-H2	Ni-Cd
DEVELOPMENT COST	HIGHEST	MEDIUM	LOWEST
PRODUCTION COST	MEDIUM	LOWEST	HIGHEST
SOLAR ARRAY COST	HIGHER	BASIS	BASIS
THERMAL CONTROL COST	HIGHER	BASIS	BASIS
LAUNCH COST	LOWEST	MEDIUM	HIGHEST
OVERALL IOC COST	MEDIUM	LOWEST	HIGHEST

SESSION II

TOPIC: LITHIUM CELL TECHNOLOGY
Chairman: G. Halpert, JPL

GALILEO Li/SO_2 BATTERY MODULES

- PROGRAM UPDATE -

R. A. Smith
Honeywell Power Sources Center
104 Rock Road
Horsham, Pennsylvania

ABSTRACT

In order to meet the unique power needs of NASA's Galileo Probe, the Li/SO_2 high rate "D" cells used in the battery modules have undergone some design changes, an upgrading of hardware quality requirements, and significant testing. A description of the design changes and the cell test data that are of a general nature is presented here. This data includes capacities, open circuit voltages, and internal resistance comparisons. A significant data base has been built up over the years and continues to grow.

INTRODUCTION

Honeywell Power Sources Center (HPSC) has been involved in the development of the Li/SO_2 Galileo Probe Battery with NASA and Hughes Aircraft Company (HAC) since 1978. This program has significantly broadened our experience and capabilities in design and manufacture of hardware to meet space requirements. The terms: performance, quality, and reliability, as regards Galileo high rate "D" cells, have taken on new meaning in this program. Due to the critical nature of this battery's performance, and the lack of previous flight experience with this system, a significant amount of testing has been done in this program. We feel the information gained from these tests has substantially improved the base of knowledge of Li/SO_2 cells and systems, and we would like to present these data for your information, evaluation, and possible use.

BACKGROUND

In a paper presented to this forum in 1982, Dr. L. S. Marcoux and Mr. B. P. Dagarin of Hughes Aircraft Company described the unique requirements for the NASA Galileo Probe power source and explained why the Li/SO_2 system was selected for the application over alternate electrochemistries. The savings in weight and volume were the overriding factors, but low temperature performance and shelf life were also important.

The basic power element, a module of thirteen high rate "D" cells in series, must provide energy after the Galileo probe leaves the orbiter. The requirements of a 150-day coast, seven hours of

pre-entry, and approximately an hour of descent to the planet Jupiter, as well as test requirements, storage losses and contingency dictate a mission energy budget of 19.02 Ahrs for the three modules that comprise the Galileo Probe Battery.

Dr. Marcoux also discussed:

- Mission description and requirements,
- Battery system description,
- Battery safety considerations,
- Description of battery test program.

In a 1984 paper by HPSC and HAC, again at this forum, the test facilities developed and used during this program were discussed by Mr. W. T. Pertuch.

Today, I will present:

- Description of Cell Lots (Design Development),
- Cell Tests
    - Developmental
    - Storage/life tests
    - Environmental,
- Module Tests
    - Developmental
    - Environmental.

DESCRIPTION OF CELL LOTS

The Galileo Probe Battery flight hardware cells are from Lot 6. This cell lot has passed all acceptance criteria, and we have completed a preliminary buy-off of this hardware. Modules have been shipped to Hughes. Previous lots represent the technical evolution of the battery and demonstrate the intense quality assurance demanded for these batteries (See Table 1).

Lot 1 cells were used in:

- Baseline capacity tests
- Simulated battery tests.

Lot 2 cells were used in:

- Life tests
- Corrosion tests.

Alternate cells were used in:

- Baseline capacity tests
- Simulated battery tests
- Life tests
- Corrosion tests
- Vibration tests.

Lot 3 cells were used in:

- Corrosion tests
- Life tests
- Reversibility of Temperature Effect.

Lot 4 cells were used in:

- Cell qualification tests
- Module qualification tests
- Cell life tests.

Lot 5 cells were used in:

- Cell qualification tests
- Storage tests.

Lot 6 cells were used in:

- Cell qualification tests
- Module qualification tests
- Storage tests.

CELL TESTS

Early developmental cell tests indicated that the high rate "D" battery performance level was sufficient to meet the Galileo requirements, but they also showed that there was some design modifications and material and process upgrading required to meet the environmental requirements. Such areas included:

Cathode drying. - Reduced self-discharge reactions.

Increased anode tab widths. - Improved tolerance to vibration.

Grid added to anode. - Improved lithium utilization and added strength.

Lithium-Bromide concentration reduced. - Reduced corrosion.

Glass upgraded. - Reduced cell failure due to corrosion.

Electrolyte mixed in glass vessels. - Reduced contaminants.

Electrolyte reduction. - Increased ullage.

These improvements to the design and the manufacturing processes occurred as a result of data analyses from the extensive environmental, life, and corrosion testing performance on these cells and modules. Environmental tests include:

- o High Temperature Test
- o Sinusoidal Vibration Test
- o Random Vibration Test
- o 150-Day Coast Timer Test (accelerated and real time)
- o Entry Deceleration Test
- o Pressure Thermal Test
- o High Pressure and Condensing Moisture Test
- o Descent Load/Temperature Profile Test
- o DOT Safety Tests
- o Module Venting Test

Cell and modules have passed qualification and acceptance testing(1). The tests were very rigorous and simulated as closely as possible the predicted mission conditions.

While the environmental tests have expanded the baseline performance capabilities in general and specifically for use in space, that baseline is somewhat limited by the fact that it was geared to one specific scenario. The life, storage, and corrosion testing is more general in nature and, therefore, applicable in almost every facet of design where high rate "D" cells are used. I wish to emphasize this group of cell tests due to its universal nature. We obtained considerable data in the following tests:

- o Cell Real Time/Temperature Test -Lot 3
- o Cell Life Tests - Lots 3a, 4, 6
- o Cell Storage Test 0°C - Lot 5
- o Corrosion Tests - Alternate Cells

While I am including some capacity data on Lots 3 and 3a here in Table 2 and 3, I must remind you that this hardware was not to the final configuration, and we did run into corrosion problems with that design. Of much more value is the data from Lot 4, 5, and 6. Figures 1-8 address a comparison of data between Lot 4 and 6.

---

(1) Lot 6 modules still must pass real time descent load/temperataure profile test.

This data includes:

- o Internal resistance (IR) versus time at 20°, 50°, 60°, and 70°,
- o OCV versus time at 20°, 50°, 60°, and 70°.

Figure 9 addresses Internal Resistance versus Capacity in Amp-hours.

As you will note, only limited data are available on Lot 6, but it appears that the lot 6 data follows Lot 4 data except where the chamber was shut down on the Lot 4 cells at 70°C.

Detailed analyses of Lot 4 and Lot 6 data would be premature at this point. This test extends out to the year 1990 and we expect valuable information will be gained by tracking results closely. Some general type trends might legitimately be gleaned now though,

- IR and OCV seem to indicate cell degradation at approximately the same time.
- An internal resistance reading greater than 1.50 ohms is an indication of cell failure.
- 70°C storage will limit life and may add risk to cell integrity.

This information with the additional data that will continue to be obtained will be of significant value in expanding our use of Li/SO_2 cells in future applications especially with what might be called these "pedigreed cells".

MODULE TESTING

The Galileo Probe Module has now passed all environmental test requirements which include:

- Sinusoidal Vibration - See Table 4
- Random Vibration - See Table 5
- Deceleration and Spin -See Table 6
- Temperature/Pressure - See Table 7 and Figure 10

Battery (three modules) capacity is measured on sets of hardware that have experienced accelerated and real time 150-day coast tests. To date, we have completed both Lot 4 discharge tests and the Lot 6 accelerated coast time discharge test. All discharge tests are conducted per the projected mission requirements for

pre-entry (approximately 6 hours) and entry (approximately 1+ hours) time. The data are as follows:

	Lot 4	Lot 6
Accelerated Battery Test	23.9 Ah	23.3 Ah
Real Time Battery Test	21.6 Ah	Nov. 1985 test data

The slight reduction in Lot 6 capacity can be directly attributed to the reduction in cell electrolyte for Lot 6 cells as compared to Lot 4 cells. We also expect a like reduction in real time capacity for Lot 6.

SUMMARY

The test data we have obtained during the Galileo Program has provided us a baseline for further development of power sources for space, both in design and manufacturing processes. The data base gained from this effort for Li/SO_2 cells is not only significant in quantity but due to the quality built in these cells, we hope to be able to deduct new information and hopefully formulate new theories. Limited design variations and tight standard deviations on design characteristics may help define phenomenon previously not understood. Even more valuable will be the review of the relationship between acceptance criteria and the actual battery requirements during the flight to Jupiter. The profusion of applications for power sources in space will be greatly serviced by this program, and we plan to continue our analyses of all data (present and future) to help us meet those needs.

ACKNOWLEDGEMENTS

This work was performed under NASA Contract NAS 2-10000. The program was managed by Hughes Aircraft Company.

The author would like to thank Dr. L. S. Marcoux, Mr. B. P. Dagarin, and Mr. R. Taenaka from HAC for their assistance in testing, organizing, and analyzing the test data during this program; Dr. S. Levy of Sandia National Laboratories for his technical advice; and Mr. J. Van Ess from NASA for his inputs to data analyses. The author would also like to acknowledge the significant support of NASA to the Galileo battery program.

TABLE 1. GALILEO Li/SO_2 CELL EVOLUTION

	Cathode		Anode	GTM		Electrolyte	
Designation	Cathode Drying	Grid	Tab, In.	Glass	Glass Protector	Process	LiBr Conc, %
Lot 1	No	No	0.2	Blue*	Yes	Metal No premix	8
Lot 2	No	No	0.2	Blue*	Yes	Metal No premix	8
Alternate Cells	Yes	Yes	0.2	Fusite 108	No	Glass premix	6.4
Lot 3 Lot 3a	Yes	Yes	0.6	Fusite 108	No	Glass premix	6.4
Lot 4	Yes	Yes	0.6	TA-23 Mo pin	No	Glass premix	6.4
Lot 5	Yes	Yes	0.6	TA-23 Mo pin	No	Glass premix Reduced Electrolyte	6.4
Lot 6	Yes	Yes	0.6	TA-23 Mo pin	No	Glass premix Reduced Electrolyte	6.4

*Glass Seal Products Glass No. 0054-3224

TABLE 2. LOT 3 REAL TIME/TEMPERATURE CAPACITY

Inverted Storage Time (yr.)	Temp. (°C)	Capacity (A-hrs)
0.000	0	5.67
.500	0	5.53
1.417	0	5.66
1.667	30	5.52
1.917	30	5.67
2.167	30	5.67
2.417	30 - 20	5.78
2.713	20	5.57
2.930	20	5.49
3.185	20	5.56
3.407	20	5.57
3.665	20	5.76

TABLE 3. LOT 3a LIFE TEST

Storage Temp. (°C)	Inverted Storage Time							
	6 mos.	12 mos.	18 mos.	24 mos.	27 mos.	30 mos.	33 mos.	36 mos.
10	5.46	5.87	5.78	5.92	5.71	5.77	5.86	5.88
20	5.77	5.54	5.67	5.70	5.48	5.52	5.67	5.58
30	5.43	5.61	5.54	5.51	5.43	5.33	5.46	5.44
40	5.42	5.23	5.35	5.11	4.97	5.12	5.48	5.32
50	5.24	5.52	5.21	4.93[a]	--[a]	--[a]	--[b]	--

Baseline (from fresh cells): 5.80 Ahrs.
Average Capacity in Ahrs to 2.0V cutoff
Discharge Load: 4 amperes constant at 0°C

(a) Cell or cells incapable of sustaining 4-ampere load.
(b) 50°C-stored cells removed from test plan after 31 months per Hughes Aircraft Company

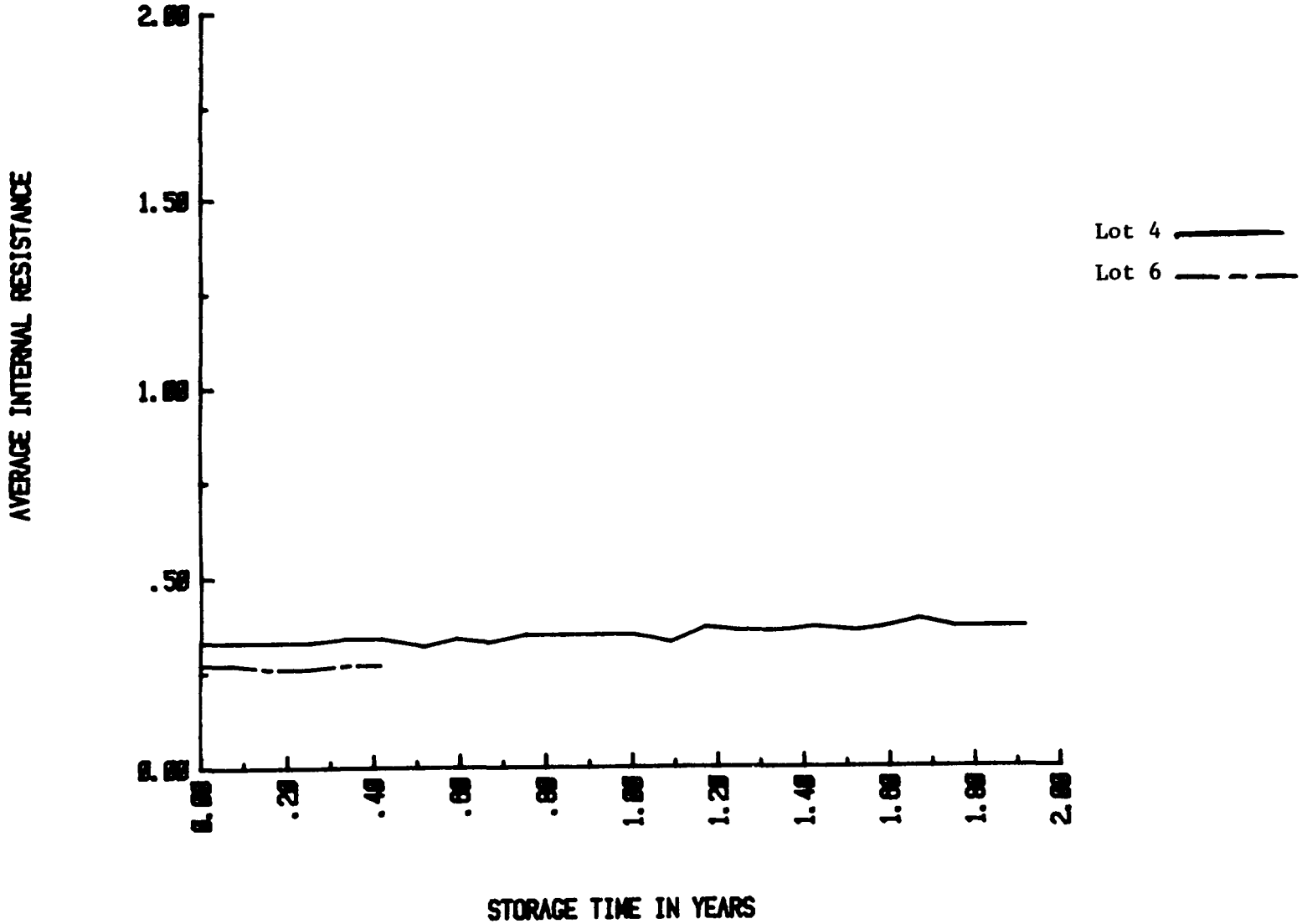

Figure 1. 20°C COMPARISON OF GALILEO LOT 4 & 6 CELL STORAGE RESISTANCE DATA IN OHMS

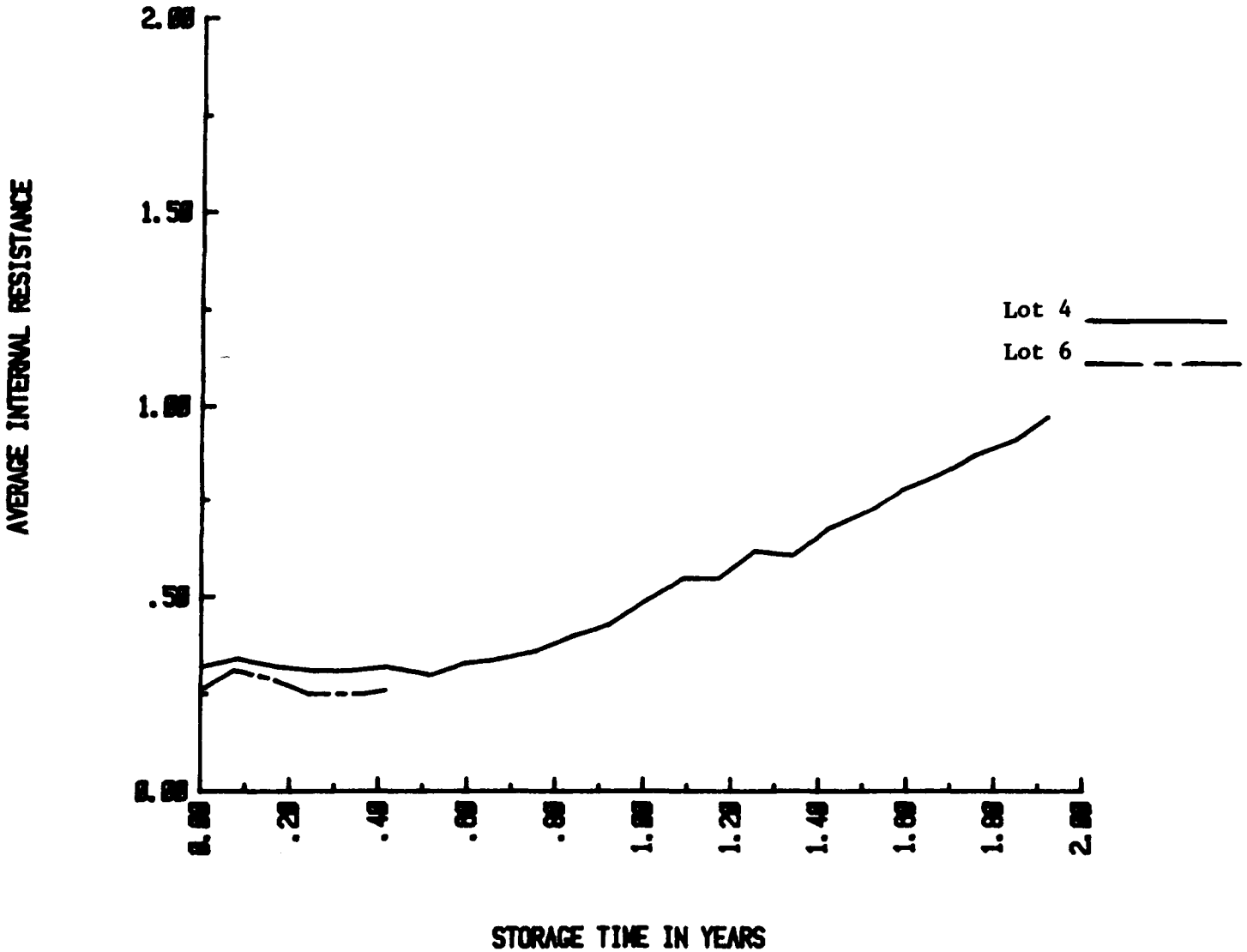

Figure 2. 50°C COMPARISON OF GALILEO LOT 4 & 6 CELL STORAGE RESISTANCE DATA IN OHMS

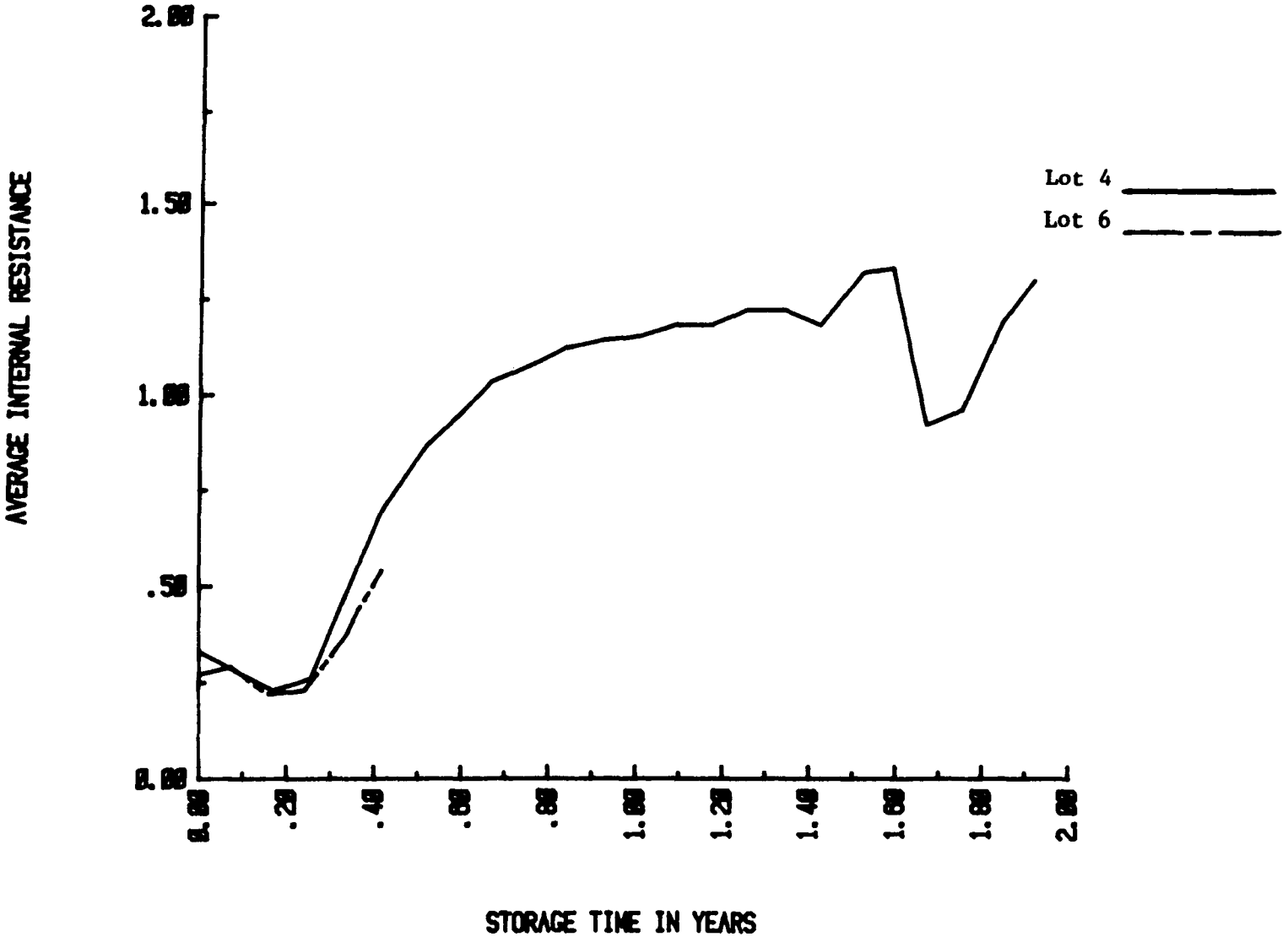

Figure 3. 60°C COMPARISON OF GALILEO LOT 4 & 6 CELL STORAGE RESISTANCE DATA IN OHMS

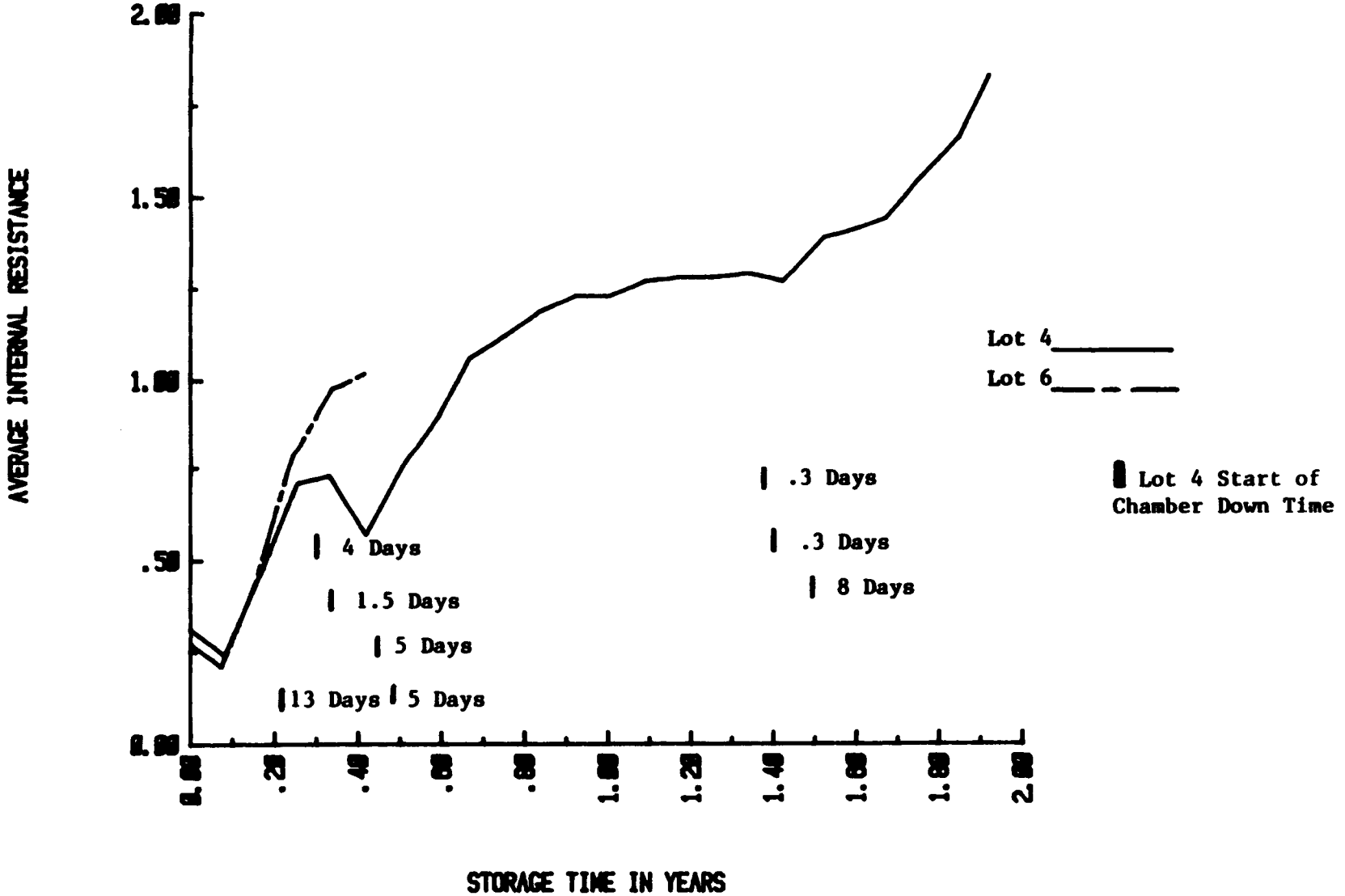

Figure 4. 70°C COMPARISON OF GALILEO LOT 4 & 6 CELL STORAGE RESISTANCE DATA IN OHMS

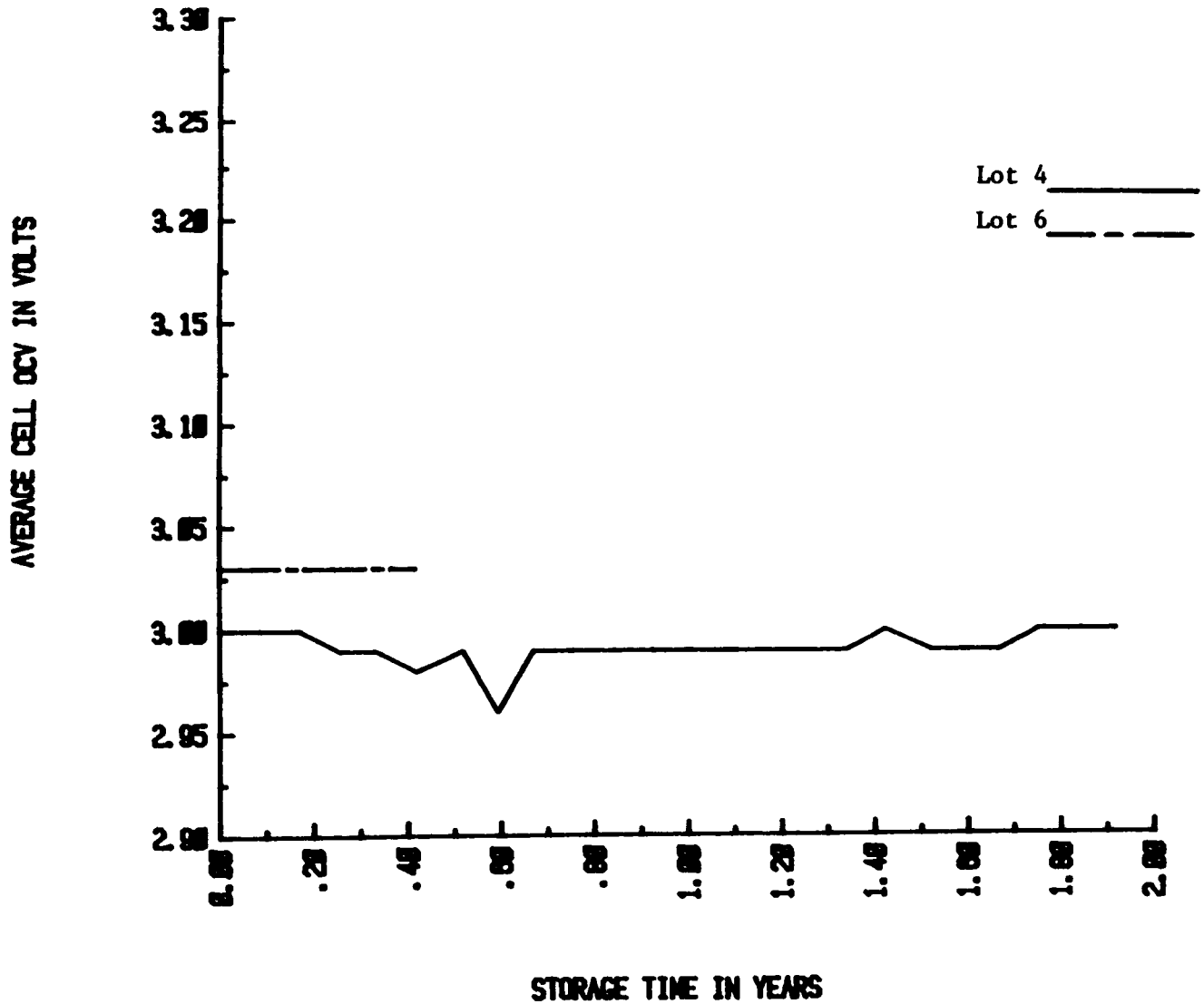

Figure 5. 20°C COMPARISON OF GALILEO LOT 4 & 6 CELL STORAGE OCV DATA

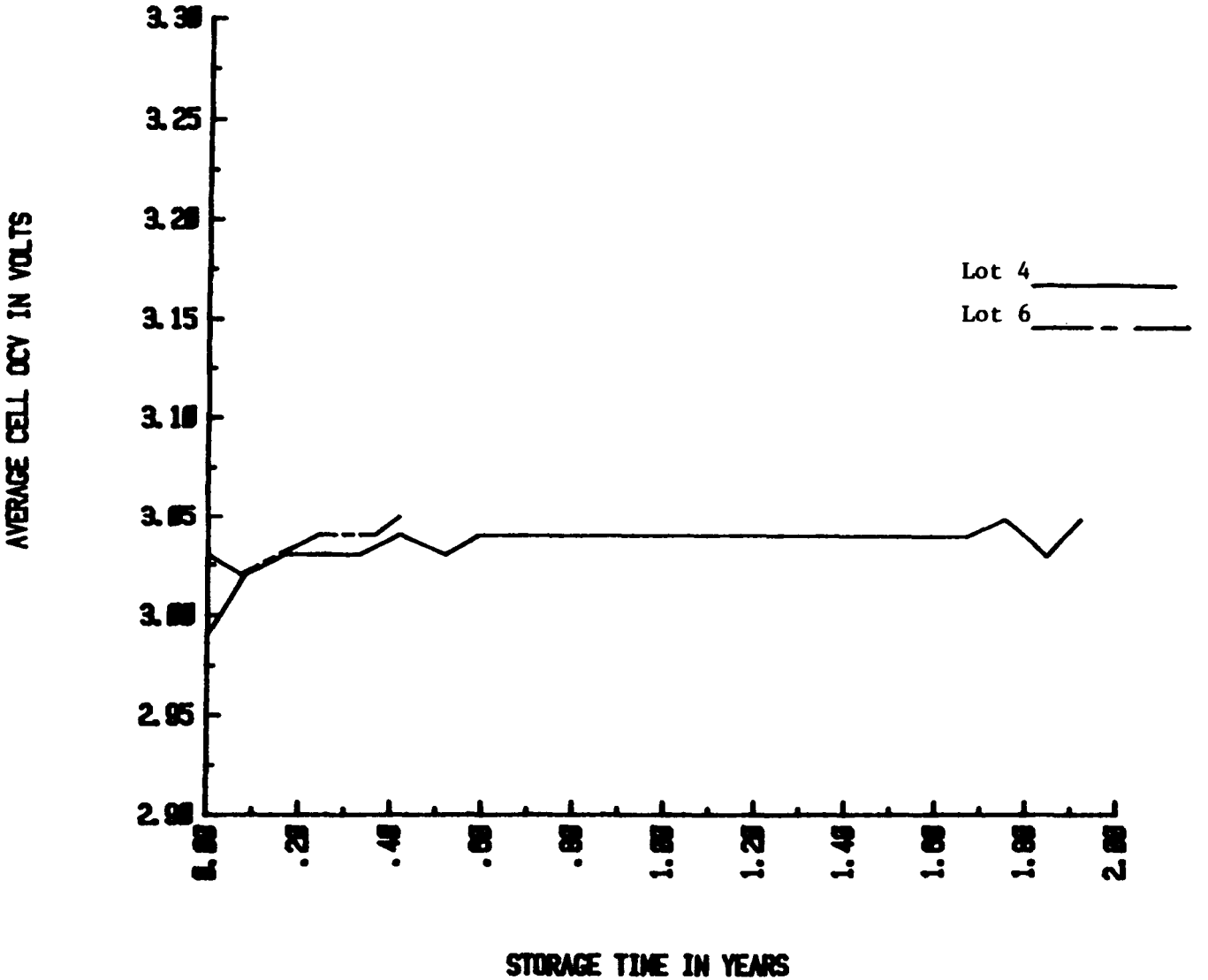

Figure 6. 50°C COMPARISON OF GALILEO LOT 4 & 6 CELL STORAGE OCV DATA

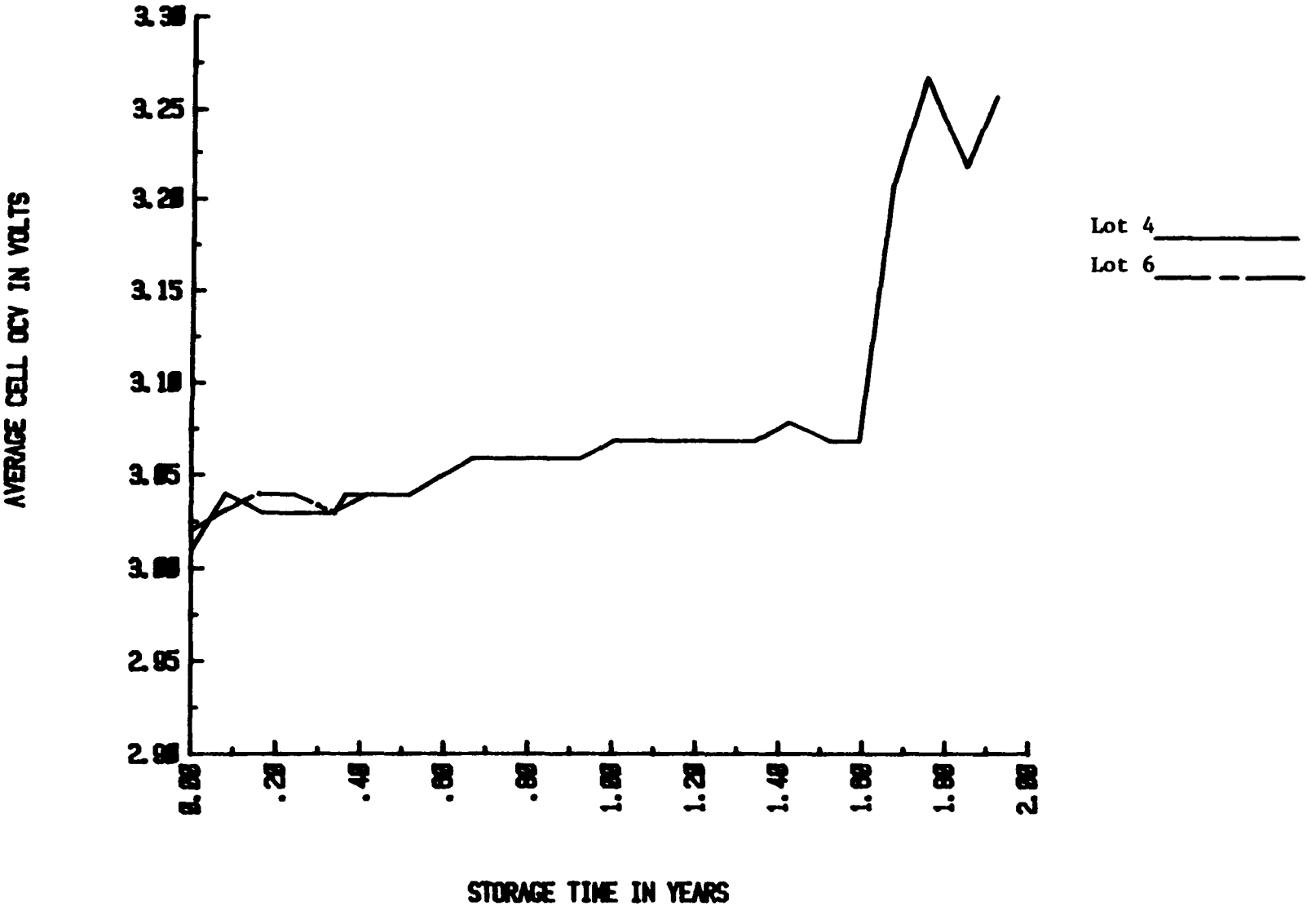

Figure 7. 60°C COMPARISON OF GALILEO LOT 4 & 6 CELL STORAGE OCV DATA

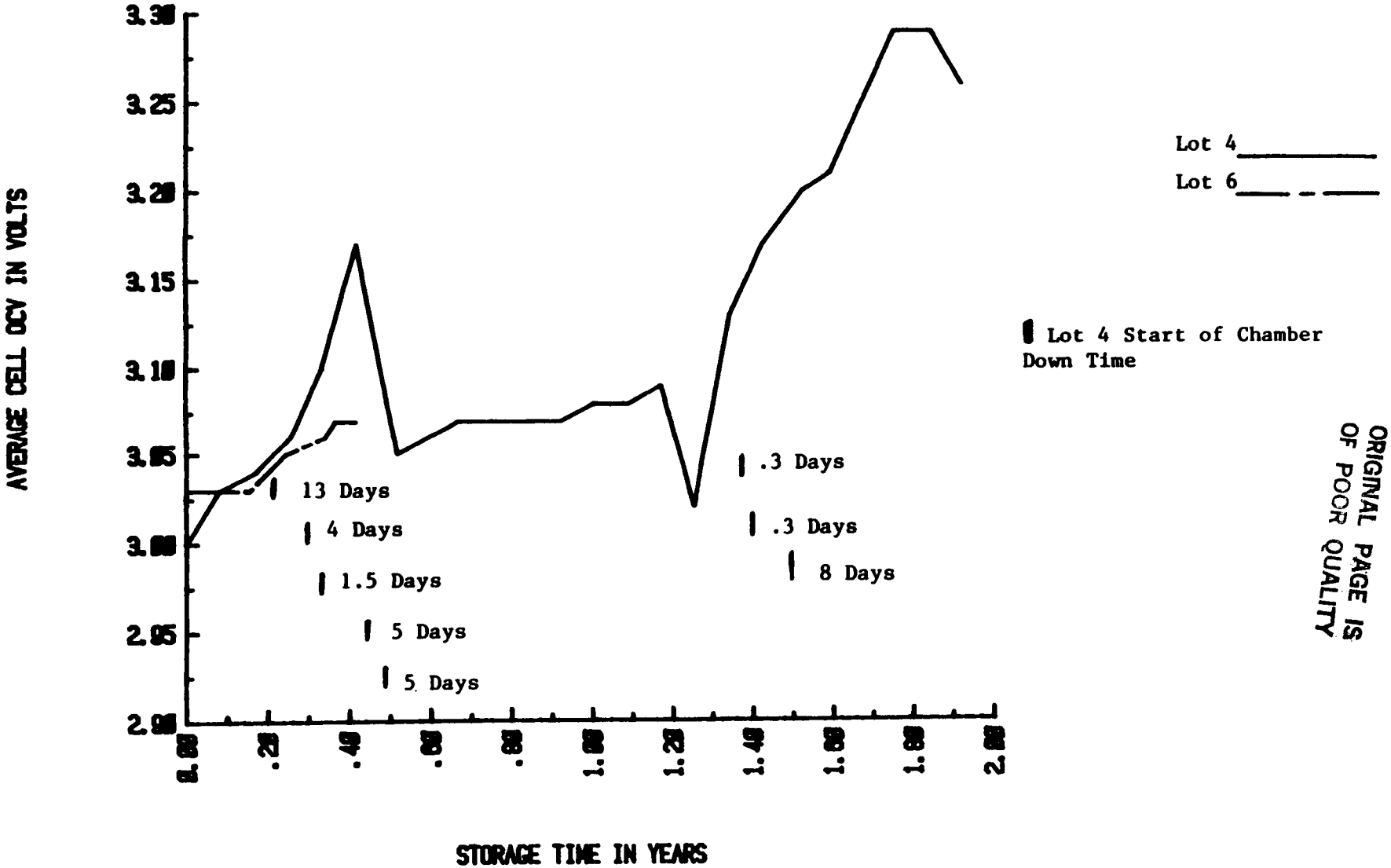

Figure 8. 70°C COMPARISON OF GALILEO LOT 4 & 6 CELL STORAGE OCV DATA

Figure 9. GALILEO LOT 4 COMPARISON OF STORED CELLS AT VARIED TEMPERATURES THEN DISCHARGED (GALILEO DISCHARGE—ALL CELLS AT 0°C, 4 AMPS CONSTANT CURRENT TO 2V CUTOFF)

TABLE 4. SINUSOIDAL VIBRATION INPUT QUALITY LEVELS

AXIS	FREQ, Hz	ACCELERATION, G (0 TO PEAK)	DISPLACEMENT, IN.
X	10 TO 30	–	0.24 (DOUBLE AMPLITUDE)
	30 TO 100	11.0	
	100 TO 170	2.0	
	170 TO 2000	1.0	
Y	10 TO 30	–	0.24 (DOUBLE AMPLITUDE)
	30 TO 70	11.0	
	70 TO 100	2.0	
	100 TO 2000	0.6	
Z	10 TO 46	–	0.047 (DOUBLE AMPLITUDE)
	46 TO 135	5.0	
	135 TO 200	3.0	
	200 TO 450	1.5	
	450 TO 2000	2.0	

NOTE: SWEEP RATE, ALL AXES, IS 2 OCT/MIN, ±10% ON AMPLITUDE.

TABLE 5. RANDOM VIBRATION INPUT QUALITY LEVELS

AXIS	FREQ, Hz	PSD, g^2/Hz	SLOPE, dB/OCT
[g(rms) = 11.54]	20 TO 35 Hz	—	+ 6
	35 TO 80	1.5	-
	80 TO 215	-	-12.0
X	215 TO 500	0.03	-
	500 TO 1000	—	-15.0
	1000 TO 2000	0.001	-
[g(rms) = 8.46]	20 TO 35		+6.0
	35 TO 60	1.5	
	60 TO 123		-21
Y	123 TO 400	0.01	
	400 TO 617		-16.0
	617 TO 2000	0.001	
[g(rms) = 9.05]	20 TO 120	0.1	-
	120 TO 150	—	+15.0
Z	150 TO 280	0.3	-
	280 TO 640	—	-15.0
	640 TO 2000	0.005	-

TABLE 6. DECELERATION AND SPINNING REQUIREMENTS

DESCENT DECELERATION

- **Z-AXIS**
- **PEAK LOAD OF 425 G'S**
- **300 G'S FOR 30 SEC**
- **0.050 IN. MAX STATIC DEFLECTIVITY AT 425 G'S**

SPINNING

RPM	TIME PERIOD
70	1 HR (LAUNCH)
3	30 DAYS (ON ORBITER)
10 TO 11	150 DAYS (ON PROBE)
0.25 TO 40	1 HR
0 TO 120	1 TO 2 MIN (DURING DESCENT; UP TO 425 G)
0	REMAINDER TO MISSION

TABLE 7. MISSION TEMPERATURE PROFILE
(prior to descent)

STEP	t, MONTHS	CUM t, MO	ACTIVITY	TEMP, °C
1	0	0	CELL ACTIVATION	–
2	2.0	2.0	MODULE FABRICATION	30 MAX
3	13.0	15.0	STORAGE DURING QUAL/ACCEPTANCE	0
4	0.5	15.5	SHIPMENT TO SPACECRAFT	30 MAX
5	2.0	17.5	INSTALLATION ON SPACECRAFT	30 MAX
6	0.5	18.0	SHIPMENT TO CAPE	40 MAX
7	4.0	22.0	PRELAUNCH TO CAPE	30 MAX
8	0.1	22.1	LAUNCH	60 MAX
9	19.0	41.1	INTERPLANETARY	20 MAX
10	5.0	46.1	COAST	0 NOMINAL

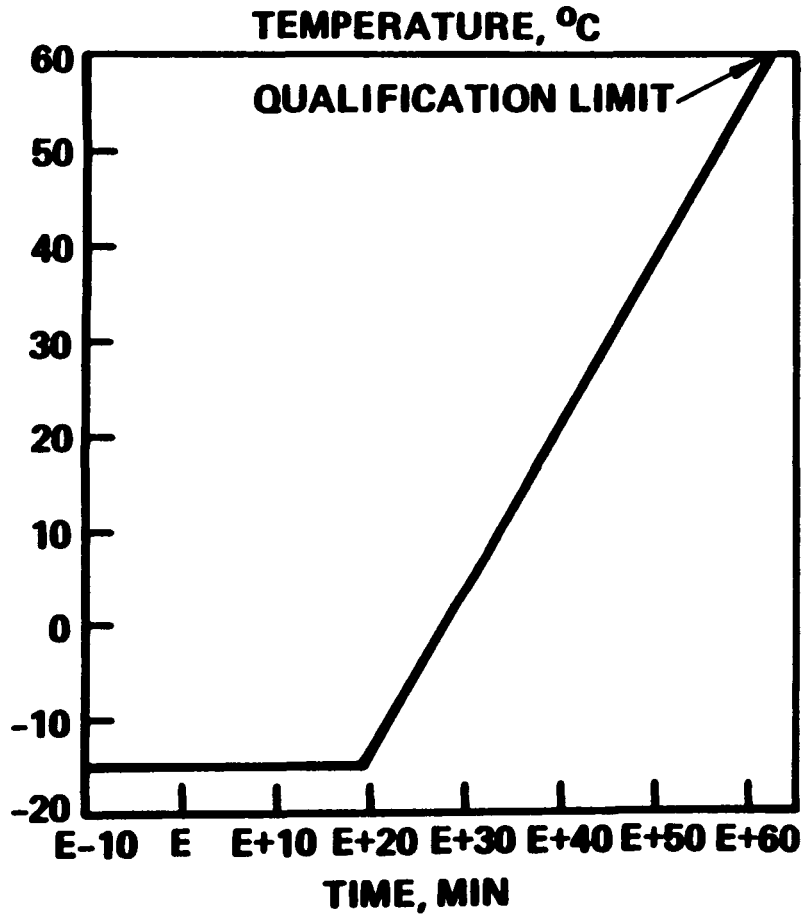

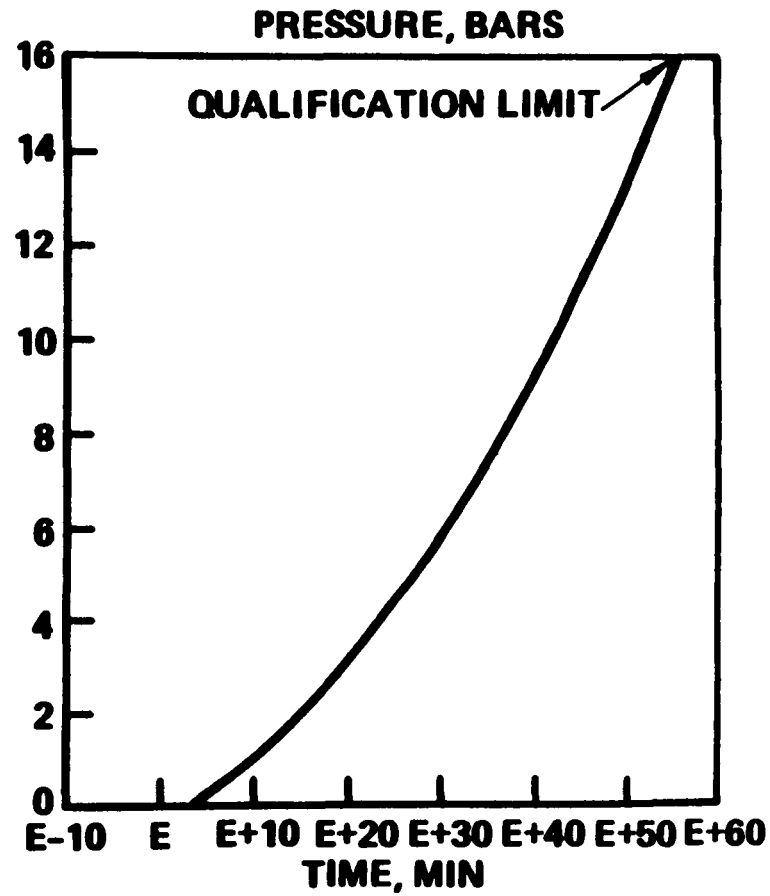

Figure 10. ENTRY TEMPERATURE/PRESSURE PROFILES

Presented at "The 1985 Goddard Space Flight Center Battery Workshop", Nov 1985.

DETERMINING THE INFLUENCE AND EFFECTS OF MANUFACTURING VARIABLES ON SULFUR DIOXIDE CELLS

W. V. Zajac, M. A. Thomas, J. A. Barnes, R. F. Bis,
P. B. Davis, F. C. DeBold, G.W. Gemmill, L. A. Kowalchik

Naval Surface Weapons Center
Silver Spring, Maryland 20903-5000

ABSTRACT

A survey of the Li/SO_2 manufacturing community was conducted to determine where variability exists in processing. The upper and lower limits of these processing variables might, by themselves or by interacting with other variables, influence safety, performance and reliability. A number of important variables were identified and a comprehensive design experiment is being proposed to make the proper determinations.

INTRODUCTION

The Lithium Systems Safety Group at the Naval Surface Weapons Center (NSWC) routinely evaluates lithium power sources for use in Naval applications. Also, in the course of accomplishing this mission and in order to keep abreast of new technology, members of the group actively participate in many research and development programs involving lithium systems. Although many lithium systems are being used and proposed for Naval applications, the Li/SO_2 cell is currently the most widely used and is expected to remain so for at least a decade.

The purpose of this work is to expand the current knowledge about Li/SO_2 cell fabrication which will result in even greater Naval confidence, wider acceptance, and use of this important power source. It is also felt that the information gained in this program will benefit the development and expanded use of other lithium systems as well.

BACKGROUND

A major problem that restricts greater use of Li/SO_2 cells is the lack of standardization among manufacturers and the uncertainty that exists when systems demand energy from these cells outside the regions where they have been previously tested. The regions of safe and reliable use are not just limited to performance capabilities, but performance as a function of environmental and mechanical stress factors such as time (storage) temperature and shock and vibration characteristic of Naval use.

The usual mode of acceptance testing involves simulated worst case evaluations on complete systems and pass/fail judgement can become subjective. In order to maximize confidence, all systems that undergo

evaluation must remain static once approved for fleet use. Even with these safeguards, the Lithium Systems Safety Group occasionally receives disturbing safety or performance information from the scientific community suggesting that something might be different from previously tested and well characterized systems. Tracking down or trying to pinpoint causes for anomalous behavior can be very frustrating because reproducibility is often difficult and is compounded by our limited understanding of the complex chemistry and how it may interplay with unknown or proprietary fabricating techniques.

It was finally decided that in order to gain a full understanding of this system, special cells would need to be fabricated and tested. On the surface, this would appear to be a simple and straightforward task. However, due to the not so obvious subtleties of possible interactions between different variables, and also the fact that what might constitute a defect in one mode of operation might not necessarily be a defect in another, an appreciation for the complexity of this task begins to become apparent.

The need for an organized and unified experiment dictates that the experiment be designed in the classical sense using the powerful techniques referred to collectively as "statistical design of experiment". The rationale for this is simply that whenever the response from an experiment is associated with many variables and/or is subject to appreciable experimental variation, a statistically designed experiment offers the only sound and logical means of drawing valid conclusions. There is no question of any alternative which is equally satisfactory in economy or integrity.

The use of the above approach will require the efforts of statisticians with training and experience in the design and analysis of experiments. But, cooperative efforts in science are not new. Most research problems today have sufficient complexity that many disciplines and fields of specialization can contribute significantly to their solutions. This is certainly true in the area of lithium battery technology where the interdisciplinary efforts of battery scientists and statisticians have the best chance of resolving unanswered questions and uncovering unexpected results. NSWC is one of the few Navy laboratories which has a staff of statisticians available for consulting and analysis. Members of the statistics staff have been associated with the lithium battery problems in the past and have been instrumental in preparing the proposed design of experiment. The library of computer programs maintained by NSWC's staff was utilized in this preparation, and will be invaluable in the analysis of results after the conduct of the experiment.

EXPERIMENTAL DESCRIPTION

The experiment involves eleven compositional variables (referred to as factors) such as the type of carbon in the cathode and the electrolyte dryness. These factors will be considered at two levels each, i.e., two kinds of carbon, two electrolyte drynesses, etc. If it were known that there were no interactions among these factors, the experiment could be conducted on a reasonably small scale. However, since it is believed that the manufacture of safe Li/SO_2 batteries involves the interaction of variables, the experimental design must provide for the calculation of the interaction effects. Here, we define an interaction as a measure of the extent to which the effect (upon battery response) of changing one factor depends on the level of another.

This would be referred to as a two-factor (or first order) interaction. One can analogously define higher order interactions involving more than three factors. However, interactions higher than three-factor interactions are very difficult to interpret. It is generally believed that the interactions involved with the manufacture of Li/SO_2 batteries are not higher than first order (two-factor interactions). Therefore, a minimum design requirement is to provide for the calculation of all two-factor interaction effects. With eleven factors, there are 55 two-factor interactions. One approach to calculating their effects is to conduct an independent experiment with each of the 55 pairs of factors. Each experiment would require two levels of each factor represented in a 2 X 2 table of four different cell configurations. Hence, to proceed in this fashion, one would have to construct 4 X 55 = 220 cells. This would provide measures of the eleven main effects and 55 two-factor interactions. However, it would require 220 different cell configurations and for each response variable one should have at least five "identical" cells of each configuration to measure experimental variation. This is a total of 220 X 5 replicates = 1100 cells per response variable.

One can vastly improve upon the above scheme by employing the powerful technique of fractional factorial experimentation. To employ this technique with eleven factors at two levels each, we consider the $2^{11} = 2048$ different cell combinations formed by crossing each two level factor, for example, see Figure I. However, a 2^{11} experiment would be both wasteful and unrealistic. It would provide information on main effects and two-factor interactions but also on all the other higher order interactions. These high order interactions can be assumed to be negligible, and it is, therefore, not necessary to measure them. One can sacrifice their information by performing only a "fraction" of the full 2^{11} factorial experiment. The degree of fractionation depends upon which interactions one is willing to sacrifice information. Using the previously stated belief that one need not be concerned with interactions beyond first order (two-factor), we need only perform a one-sixteenth fraction of a 2^{11} factorial. This requires 128 different cell configurations (vice the earlier figure of 220). Also, in this design, each two-way interaction is measured with an effective cell replication of 32 (vice the earlier figure of 5). If we allow two replicates per response variable to provide measures of variation in each of the 128 experimental cells, the cost would be 128 X 2 replicates = 256 cells per response variable (vice the earlier figure of 1100). This is a reduction in cost by more than a factor of four. In addition, each main effect and two-factor interaction is measured with much greater precision than before. Also, all information on higher order interactions is not lost. While much has been sacrificed by fractionation, there will still be clean measurements of many three-factor interactions. Hence, by employing "design of experiment" techniques, we actually gain precision and also gain information on some high order interactions with less than one fourth the number of batteries required by treating the experimental process as 55 independent experiments.

VARIABLES

After extensive discussions with all the major Li/SO_2 manufacturers concerning this project, all identifiable variables were grouped into three basic categories: (1) compositional, (2) geometric, and (3) design/process.

Compositional variables refer to major cell components and their purity levels and are universal or common to all cell designs. It is because of this commonality that compositional variables were selected for this study. Geometric and design variables refer to such things as thickness of cathode, vent type, use of anodic current collectors, etc. However, although geometric and design variables are important, it was felt that a strong foundation based upon compositional variables would need to be established before proceeding with a determination of the effects of non-compositional variables. Some examples of geometric and design variables are given in Figure II.

A listing of the eleven compositional variables, each identified alphabetically, can be correlated with the experimental outline (Figure I) showing a one-sixteenth replicate of a 2^{11} factorial experimental design.

A. Carbon Type
B. Carbon Purity
C. Teflon Type
D. Cathode Dryness
E. Sodium in Anode
F. Nitrogen in Anode
G. Passivation of Anode
H. Lithium Bromide Purity
J. Electrolyte Dryness
K. Acetonitrile Purity
L. SO_2: Lithium (Ratio)

An in depth discussion on the relative merits of the selected compositional variables including the proposed two levels for each variable would be too lengthy for this paper. However, they will be discussed in some detail at the oral presentation, time permitting.

MEASUREMENTS AND RESPONSES

Although the Lithium Sulfur Dioxide chemistry is firmly established as a valuable power source for certain Naval applications, NAVSEA NOTE 9310 still mandates that all systems utilizing lithium must be approved for safety prior to use in the fleet. The four basic NAVSEA NOTE 9310 test protocols of forced overdischarge, charge, short circuit and heat tape will form the backbone of the measurement scheme. Preconditioning of cells, i.e., mechanical shock, diurnal and long term storage is planned. A full spectrum of discharge conditions at various rates and temperatures will be made.

Surface responses that will be correlated with the compositional variables will be capacity, power, voltage delay, thermal behavior and time (Δt) to an event (explosion or venting). Several test matrixes are being considered with the emphasis on obtaining maximum information and efficiency. It is currently felt that less than 50 cells at each of the 128 experimental conditions should be more than satisfactory to accomplish this task.

CONCLUSION

There is no question that the project outlined in this paper is an ambitious one. We also feel that a successfully completed project will have no null result because what is really being pursued is the elimination of uncertainty. Furthermore, we strongly believe that valuable clues leading to improvements in other higher energy density lithium systems will be gleaned.

Finally, after many discussions with members of our staff at NSWC, it was decided that the information gained from our survey leading to the development of this design experiment was an important end itself and worthy of presentation to the lithium battery community which would hopefully be appreciative and become stimulated to pursue these and other ideas in a similar fashion on their own.

A ONE-SIXTEENTH REPLICATE OF A 2^{11} FACTORIAL

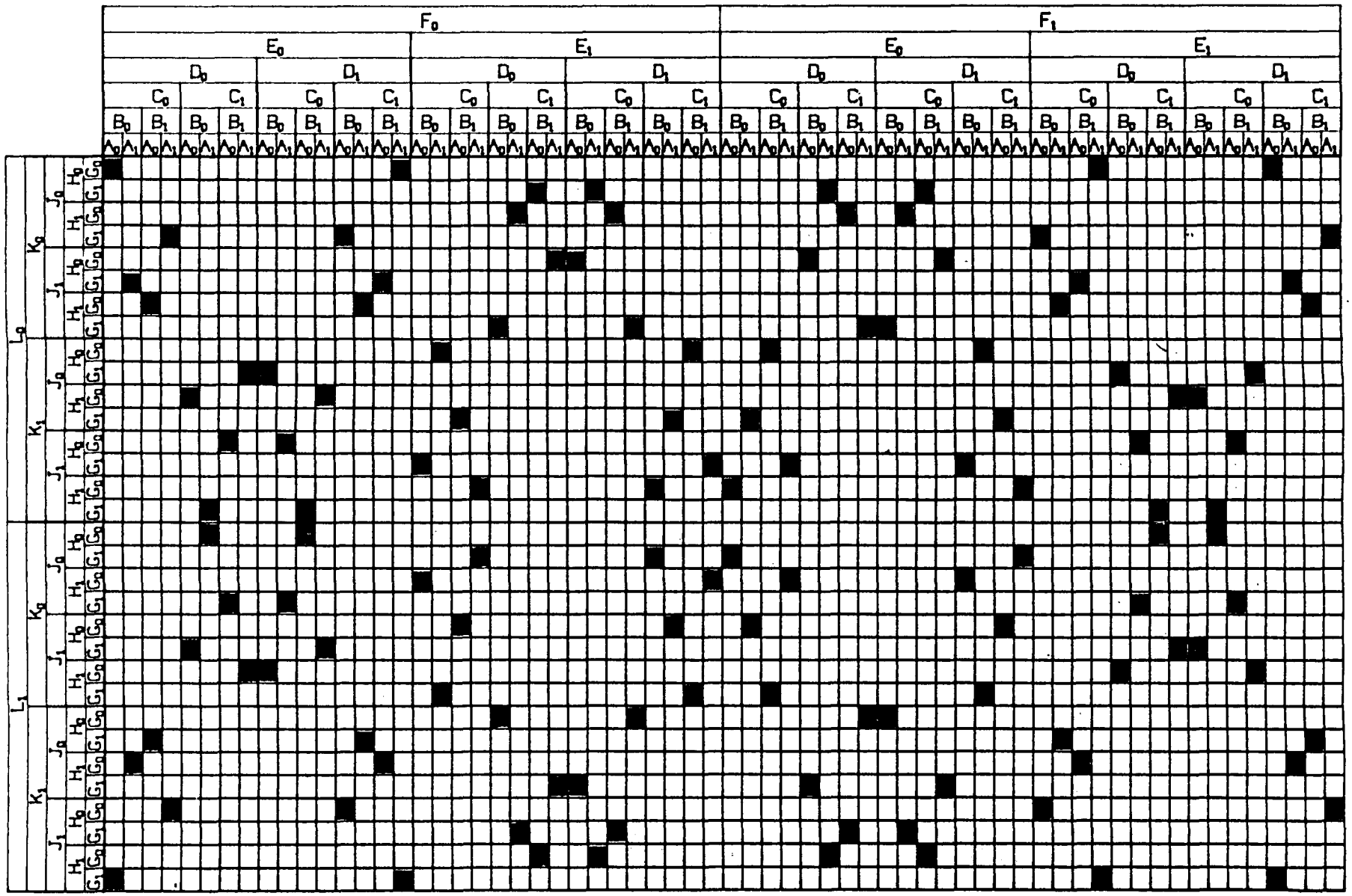

Figure 1. A ONE-SIXTEENTH REPLICATE OF A 2^{11} FACTORIAL

COMPOSITIONAL	GEOMETRIC	DESIGN/PROCESS
CARBON TYPE	VOID VOLUME	GLASS TO METAL SEAL
CARBON PURIFICATION STEP.	TIGHTNESS OF WRAP CONCENTRICITY OF WRAP	CURRENT COLLECTOR TYPE
TEFLON TYPE		TABBED VS. COLD WELDED
CATHODE DRYNESS	REGISTERING	STAINLESS VS. NICKEL PLATED IRON
SODIUM IN ANODE	SEPARATOR THICKNESS	VENT TYPE
NITROGEN IN ANODE	ANODE THICKNESS	CATHODE PROCESSING TECHNIQUES
PASSIVATION OF ANODE	CATHODE THICKNESS	
AN PURITY	MESH GEOMETRY	
ELECTROLYTE DRYNESS		
SO_2:Li		
LiBr PURITY		

Figure 2. EXAMPLES OF VARIABLES

SAFETY HAZARDS ASSOCIATED WITH THE CHARGING OF LITHIUM/SULFUR DIOXIDE CELLS

by

H. Frank, G. Halpert, and D. D. Lawson
Jet Propulsion Laboratory
Pasadena, California

and

J. A. Barnes and R. F. Bis
Naval Surface Weapons Center
Silver Spring, Maryland 20903-5000

ABSTRACT

A continuing research program to assess the responses of spirally wound, lithium/sulfur dioxide cells to charging as functions of charging current, temperature, and cell condition prior to charging is described. Partially discharged cells that are charged at currents greater than one ampere explode with the time to explosion inversely proportional to the charging current. Cells charged at currents of less than one ampere may fail in one of several modes. The data allow an empirical prediction of when certain cells will fail given a constant charging current.

INTRODUCTION

For several years, the Lithium Systems Safety Group at the Naval Surface Weapons Center has been concerned with the behavior of lithium batteries under abusive conditions. In fact, the Navy's safety test program for equipment containing lithium batteries focuses on abusive experiments. (1-4)

At first, these experiments concentrated on physical abuse, internal and external short circuits, and cell voltage reversal. More recently, we have identified the charging of a lithium battery as another potentially hazardous situation which can occur in equipment containing one of the following circuits as shown in Figure 1: (1A) a single series string of cells in parallel with an external source of power, (1B) several equivalent strings of cells in parallel with each other, and 1C) a string of cells in a piece of equipment which contains another source of current.

Blocking diodes should always be installed in the first two situations in order to reduce the hazard. If the diodes function properly, only very low levels of leakage current will be available to charge the cells. If the diodes fail or are omitted from the circuit, significant charging currents can

occur. In the third situation, protective diodes are not normally used because the cells should never be connected to any source of charging current; but wiring errors or equipment failure may allow such a connection with the subsequent charging of a lower voltage string by a higher voltage source. In each of these cases, the charging current obtained will be a function of the difference in the voltages of the charging source and the receiving battery and of the design and condition of the battery.

Because of this concern about the dangers of possible charging, the Lithium Systems Safety Group has funded a joint research program with the Jet Propulsion Laboratory of the California Institute of Technology to characterize the effect of charging on lithium cells. In addition, the program should help to identify the conditions where charging of lithium cells may produce severe safety hazards, and to propose chemical and/or physical mechanisms to explain the effects of charging. Because of limitations on funding and staff, this program has focused on the cells in widest use within the Navy--high rate (lithium rich), spirally wound, lithium/sulfur dioxide cells in "C," "D," and similar sizes. Additional, less extensive work has been done on "balanced" lithium/sulfur dioxide cells and on several lithium/thionyl chloride systems. In all of the systems investigated we have always observed behaviors which are at least qualitatively the same as those reported in this paper.

EXPERIMENTAL

The cells employed in this investigation were obtained by dismantling spare sonobuoy battery packs as shown in Figures 2 and 3. These particular batteries and cells were manufactured by Duracell in 1981 and were kept in storage at room temperature until shipped to JPL by the Navy in 1983. The cells were approximately four years old at the beginning of the current experiments. Except for test loads applied during manufacture, the batteries have not been discharged.

The cells under study are Duracell lithium/sulfur dioxide type L030SH. They are of the spirally wound configuration, are slightly smaller than a standard "D" size, contain excess lithium, and have a rated capacity of 4.3 Ampere hours at the "C/2" discharge rate at 21°C to a 2.0 volt limit.

All charging tests were carried out with power supplies. In each case, the supplies were adjusted to provide a constant current; voltages were allowed to "float." No diodes or other protective devices were included in the circuits. Strain gages mounted to the exterior of the cells were used to estimate the internal cell pressures. The gages were calibrated by pressurizing cell cans with argon gas. This calibration method allows the measurement of pressure changes within the cell relative to the initial pressure when the gage was installed at ambient temperature. The accuracy of long-tern pressure measurements made with this technique may be limited by the calibration procedure which did not include experiments to identify any effects which aging might have on the gages or creep of their bonding agent, ethyl cyanoacrylate; therefore the calculated pressures, after long periods, may not be accurate.

Except where noted, all cells were discharged by 20% (80% of capacity remaining) through a resistive load of 36 ohms (80 mA) before charging. The cells sat on open circuit for at least one week after discharge before being charged. The charging tests were divided into three major groups designated as low, medium, and high rate. These differed from each other in the magnitude of charging current, number of cells, and few other details. A description of each of these is given below.

HIGH RATE CHARGING TESTS

These tests were conducted on single cells inside a large (4 feet x 4 feet x 8 feet), steel lined chamber. Experiments were run at three currents, 1.0, 5.0, and 10.0 Amperes, and at three temperatures, ambient, -20 and +70°C. The low and high temperatures were maintained with a freezer and an oven located inside the large test chamber. In most cases the tests were run three times for each condition of current and temperature. The cells were always instrumented with voltage probes and thermocouples and in some cases with strain gage pressure transducers. Voltages, temperatures, and pressures were recorded with strip chart recorders.

INTERMEDIATE RATE CHARGING TESTS

These tests were carried out on two groups of two series connected cells at currents of 100 and 300 mA. All the tests were run at ambient temperatures inside a steel vessel located in a test area outside a laboratory building. Each of the cells was instrumented with voltage probes, one thermocouple, and a strain gage pressure transducer. Voltages, temperatures, and pressures were recorded with strip chart recorders.

LOW RATE CHARGING TESTS

These experiments were conducted in an isolated laboratory. A matrix of 27 different conditions was established to study the effects of variations in charging rate, temperature, and original cell condition. Each block of the matrix was represented in the experimental program by a single cell. (Duplicate experiments are now being planned.) Nine fresh cells were used as received; nine cells were discharged by 50% through a 36 ohm load; and the remaining nine cells were similarly discharged by 80% (20% of capacity remaining) before beginning the charging experiments. These cells were redivided to yield sets of nine cells containing three cells of each discharged type. These sets were charged at currents of either 0.1, 1.0, or 10.0 mA. The cells were placed in temperature-controlled chambers at -20, +35, or +70°C. One cell of each discharge type and charging rate was tested at each temperature. In order to minimize the number of power supplies required for this long-duration experiment, all of the cells being charged at a given rate were wired in series. A schematic of this experimental matrix is shown in Figure 4. Each of the cells was instrumented with voltage probes and with a strain gage type pressure transducer. Individual cell voltages and pressures were recorded with a Hewlett-Packard data logger. Also the three currents and chamber temperatures were recorded. Data were recorded at half hour intervals for the first several days of the experiment. Then the

recording rate was reduced to once every six hours. When a cell became inoperative, it was manually removed from the temperature chamber and from the circuit; the experiment was restarted on the remaining cells in the affected string. Safety considerations required a "waiting period" of several days after cell failure before conducting the removal and restarting procedures. For this reason, there were several interruptions in this test program.

RESULTS AND DISCUSSION

RESULTS OF HIGH RATE CHARGING

Initial efforts were focused on high rate charging tests at 10 Amperes with the cells at ambient temperature. If the cells were undischarged, they failed with "violent ventings." If they had been partially discharged, they consistently exploded within 5 to 15 minutes after the onset of charging. (If all parameters were carefully controlled, the time before an explosion would not vary more than a few seconds from sample to sample.) These explosions are substantially more severe than the violent ventings normally associated with charging undischarged cells. External cell temperature and internal pressure begin to rise quite rapidly just before cell failure. Strain gage measurements indicate that the explosion is always preceded by a sudden drop in internal cell pressure as would be expected from the cells venting shortly before the explosion. These ventings could be heard from outside the test chamber just prior to the explosions. Typical behavior of the cells during these high rate tests is shown in Figure 5. The explosion typically followed cell venting within half a minute.

Subsequent charging tests at ambient temperature and reduced currents of 5 and 1 Amperes revealed similar behavior. In these cases the cells also consistently exploded. The charging time required to produce the explosion increased as the charging current decreased. These findings suggest at least some correlation between time to explosion and charging current.

The high rate tests were continued by repetition of the runs at ambient temperature and by additional experiments at both high ($+70^{o}C$) and lower ($-20^{o}C$) temperatures. The cells consistently exploded at both the high and low temperatures, and the times to explosion were comparable to those times for cells charged at similar rates; there was no clearcut effect of temperature on the time to explosion. These data are shown in Table 1.

RESULTS OF INTERMEDIATE RATE CHARGING

The purpose of the intermediate rate charging tests was to obtain data for the region between the lowest of the high rate tests at 1.0 Ampere and the highest of the low rate tests at 10 mA. These tests used two groups of two series connected cells at ambient temperature. One group was charged at 100 mA and the other at 300 mA. For safety reasons, the cells were located inside the steel vessel mentioned earlier. The cells have now been on test for almost 100 days. One of the two cells being charged at 100 mA failed after 41 days; the temperature and pressure data indicate that the failure was similar to the explosions observed at higher rates. The failure disconnected

the leads from the other cell in series with the failed one. Because the test chamber contains two cells which are being charged at 300 mA, safety considerations prevent us from entering it to reconnect the circuit or to examine the failed cell. The test on the other two cells was not interrupted by the nearby failure and is still in progress. Data for one of these cells are given in Figure 6. Note that the current has held constant at 300 mA while the voltage has increased from the 3.0 to the 4.0 volt level and the pressure has reached an apparent plateau about 80 pounds per square inch (psi) above the initial cell pressure. This test will be continued.

RESULTS OF LOW RATE CHARGING

Based on early projections from the high rate tests, we anticipated that there would be a period of at least several months before cells charged at low rates would exhibit any type of venting or explosion. For this reason, the low rate charge tests were begun early in the program and are continuing at the present time.

As of October 1985, the cells have been charged at the indicated currents of 0.1 to 10.0 mA for nearly 200 days. During this period, there have been no ventings or explosions of any of the 27 cells. The lack of explosions during the first 200 days of these low current tests is in agreement with the empirical safety map to be discussed later. Although the cells under low rate test have not yet exhibited any explicit safety hazards, the tests have yielded other pertinent data. After a period of one month, the power supply voltages applied across some cells began to rise from the 3 - 4 volt level to nearly 30 volts (the limit of the power supplies) while the current flowing through the string dropped to near zero. This behavior suggested that an open circuit condition had developed within the cells. In each case, the faulty cell was identified and manually removed after a "safety period" of several days. The remaining cells were returned to charging, but the removed cells were not replaced. X-ray examination of these faulty cells revealed the loss of the internal aluminum tab which connects the cathode to the center pin, as shown in Figure 7. So far, five cells have exhibited this open condition and have been removed from the test. All five were at 70°C, and three of these were at the highest current of 10 mA. These observations suggest the occurance of an internal corrosion process. The rate of which increases with temperature and charging current and/or applied voltage.

The internal pressures of the cells and the variation of these pressures with the time on charge are also of interest. The accuracy of the following observations may be limited by the strain gage calibration procedure discussed earlier. After charging began, the cell pressures dropped briefly before increasing to a plateau over a period of several months. These plateaus, or steady state pressures, increase with temperature for a given current; but there does not seem to be any correlation with current for a given temperature. After 180 days, the average pressures of the cells remaining on test are about 300, 10, and -10 psi relative to starting pressures at temperatures of 70, 30, and -20°C respectively. Pressures of two cells at 70°C have reached about 500 psi; these pressures are near (or possibly in excess) of the nominal venting pressure of 450 +/- 50 psig for these cells.

An example of these data is given in Figure 8. This figure shows the current, voltage, and pressure for a cell that was charged at 1.0 mA at 70°C. The indicated interruption in the current was caused by the failure of another cell in the series string and the subsequent bypassing of this "open cell." Note that the pressure of this particular cell has apparently reached a plateau near 500 psi. Even given the limitations on the pressure measurements discussed earlier, the pressure in this cell has been quite high and has approached the pressure at which it would vent.

This program of low rate charging will be continued.

SAFETY ENVELOPE

A tabulation was made of all of the times to explosion for each of the charging currents. These results were plotted both with linear scales and with a logarithmic scale for time and a linear scale for current. The latter curve is given in Figure 9 for currents from 1 to 10 Amperes. This curve indicates that for a given set of conditions--cell type, discharge history, and charging current--there seems to be a specific time threshold which separates "acceptable" and very dangerous charging. The time required to reach a dangerous condition increases as the charging current is reduced. Unfortunately, this threshold is a function of many variables. No model yet exists which will allow the reliable prediction of the dangerous region for a system without first conducting extensive experimental measurements. Therefore, any charging of a lithium/sulfur dioxide cell, even at low currents, must be regarded as potentially hazardous and should always be avoided.

FUTURE EFFORTS

The results which we have reported are part of a continuing program. Future work will be directed towards development and validation of a physical-chemical model to explain the observed phenomena. Experiments will include electrical, thermal, and chemical investigations (including autopsies) on cells of the same type as currently under test. The program will be expanded to other sizes of cells from several manufacturers in order to develop a family of "safety maps" and in an effort to confirm the general nature of the observed behavior.

ACKNOWLEDGEMENT

The research described in this paper was carried out by the Jet Propulsion Laboratory, California Institute of Technology, under a program sponsored by the U. S. Navy through an agreement with the National Aeronautics and Space Administration.

REFERENCES

1. Naval Sea Systems Command, Notice 9310 of 11 June 1985.

2. R. F. Bis and J. A. Barnes, "Policies Governing the Use of Lithium Batteries in the Navy," The 1982 Goddard Space Flight Center Battery Workshop, NASA CP 2263, p. 23 (1983).

3. J. A. Barnes, et al., "Testing of Candidate Batteries for Global Positioning System," The 1983 Goddard Space Flight Center Battery Workshop, NASA CP 2331, p. 159 (1984).

4. J. A. Barnes, et al., "High Rate Discharge Studies of Li/SO_2 Batteries," Ibid.

Table 1. TIMES TO EXPLOSION DURING CHARGING

Current (Amps) / Temp (°C)	1	5	10
Ambient	47 hr 113 hr 27 hr	16 min 48 min 29 min	8 min 14 min 14 min 12 min 7 min 15 min 8 min
-20°C	89 hr	52 min 52 min 51 min 45 min	17 min 11 min
+70°C	104 hr 6 hr 146 hr	63 min	21 min 22 min

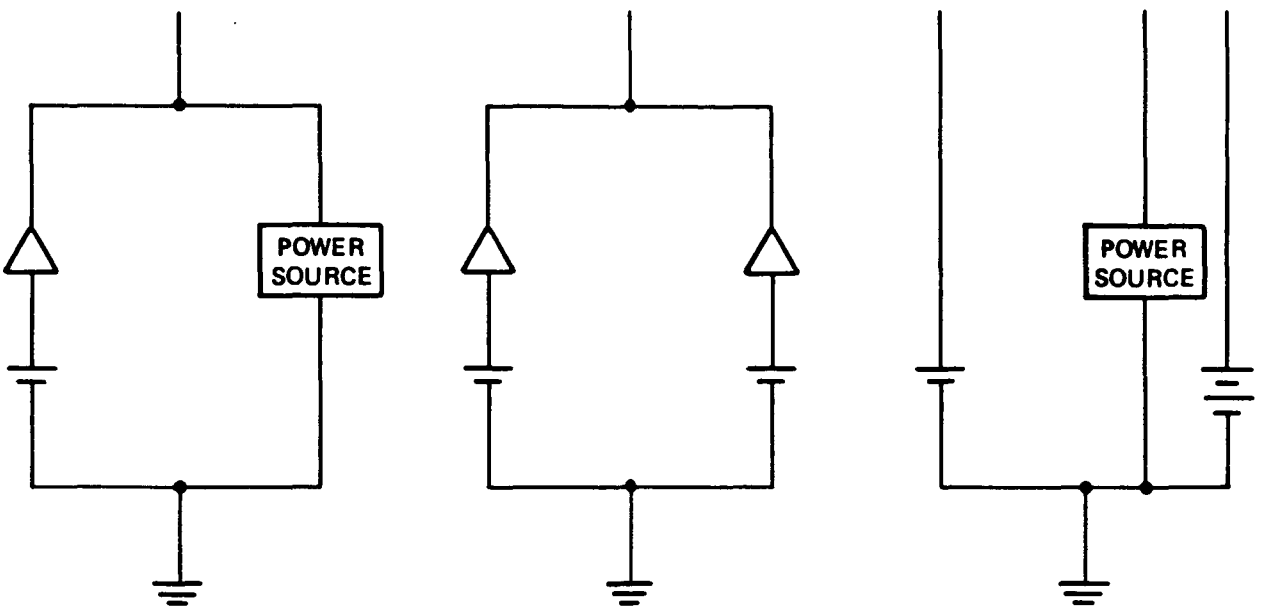

1A. SINGLE SERIES STRING OF CELLS IN PARALLEL WITH AN EXTERNAL POWER SOURCE

1B. SEVERAL STRINGS OF CELLS IN PARALLEL WITH EACH OTHER

1C. A STRING OF CELLS IN EQUIPMENT THAT CONTAINS ANOTHER SOURCE OF CURRENT

Figure 1. CIRCUITS IN WHICH CHARGING CAN TAKE PLACE

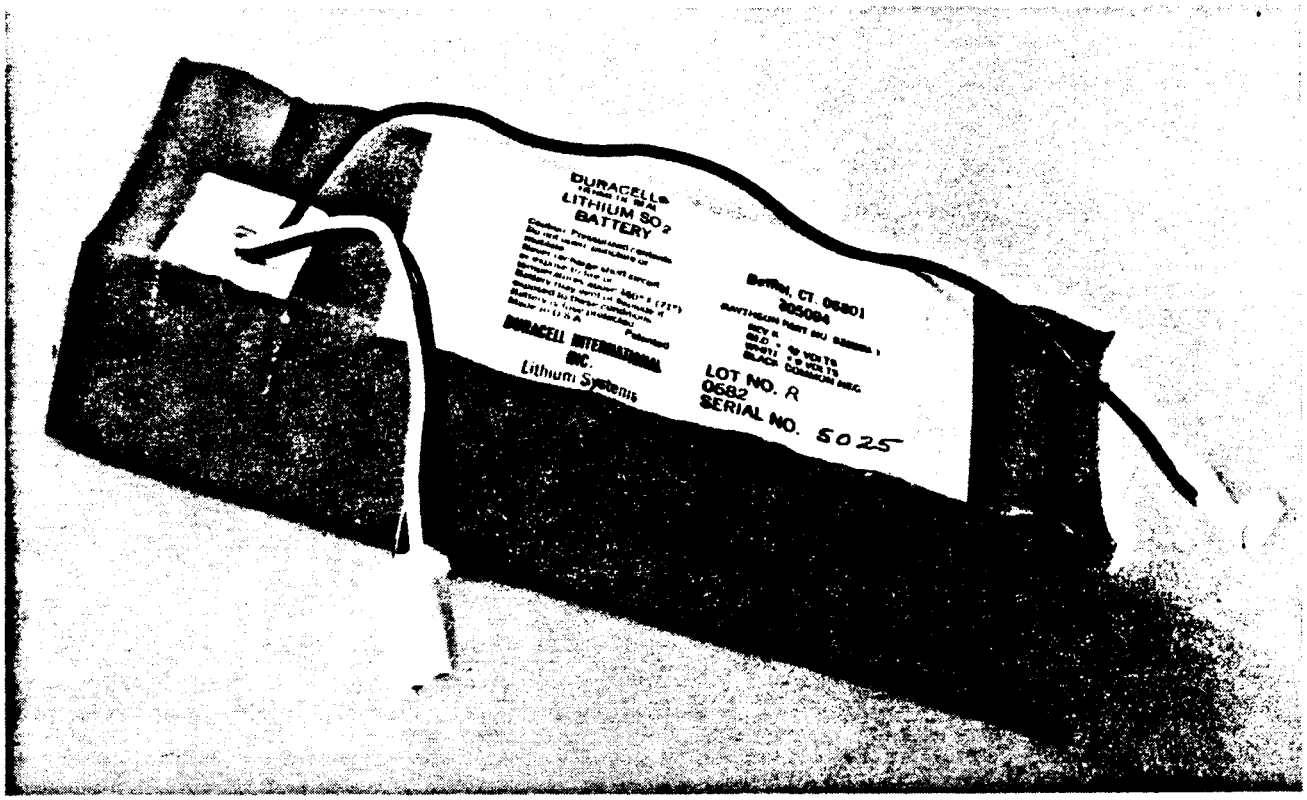

Figure 2. PHOTO OF SONOBUOY BATTERY PACK WITH COVER

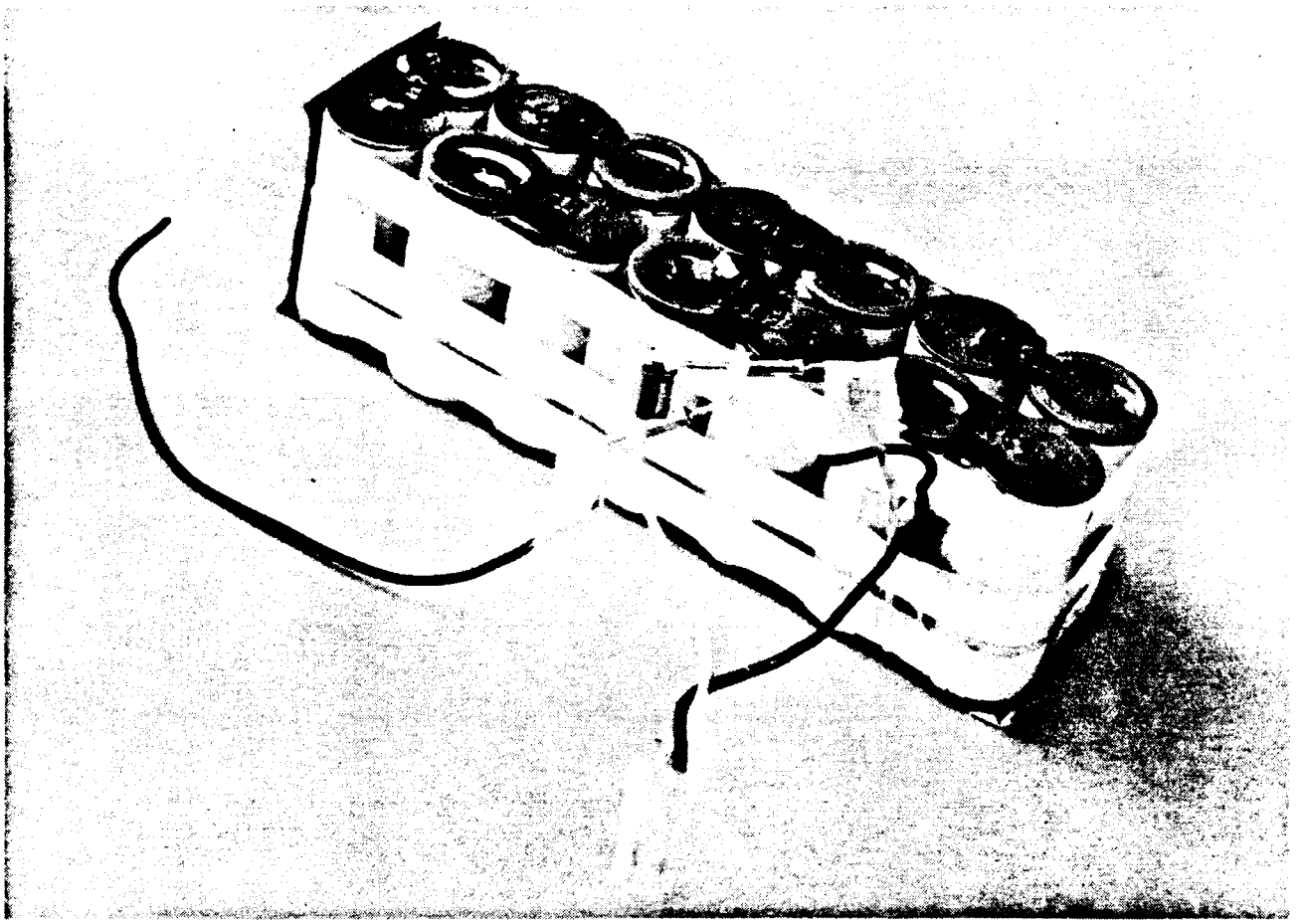

Figure 3. PHOTO OF SONOBUOY BATTERY PACK WITHOUT COVER

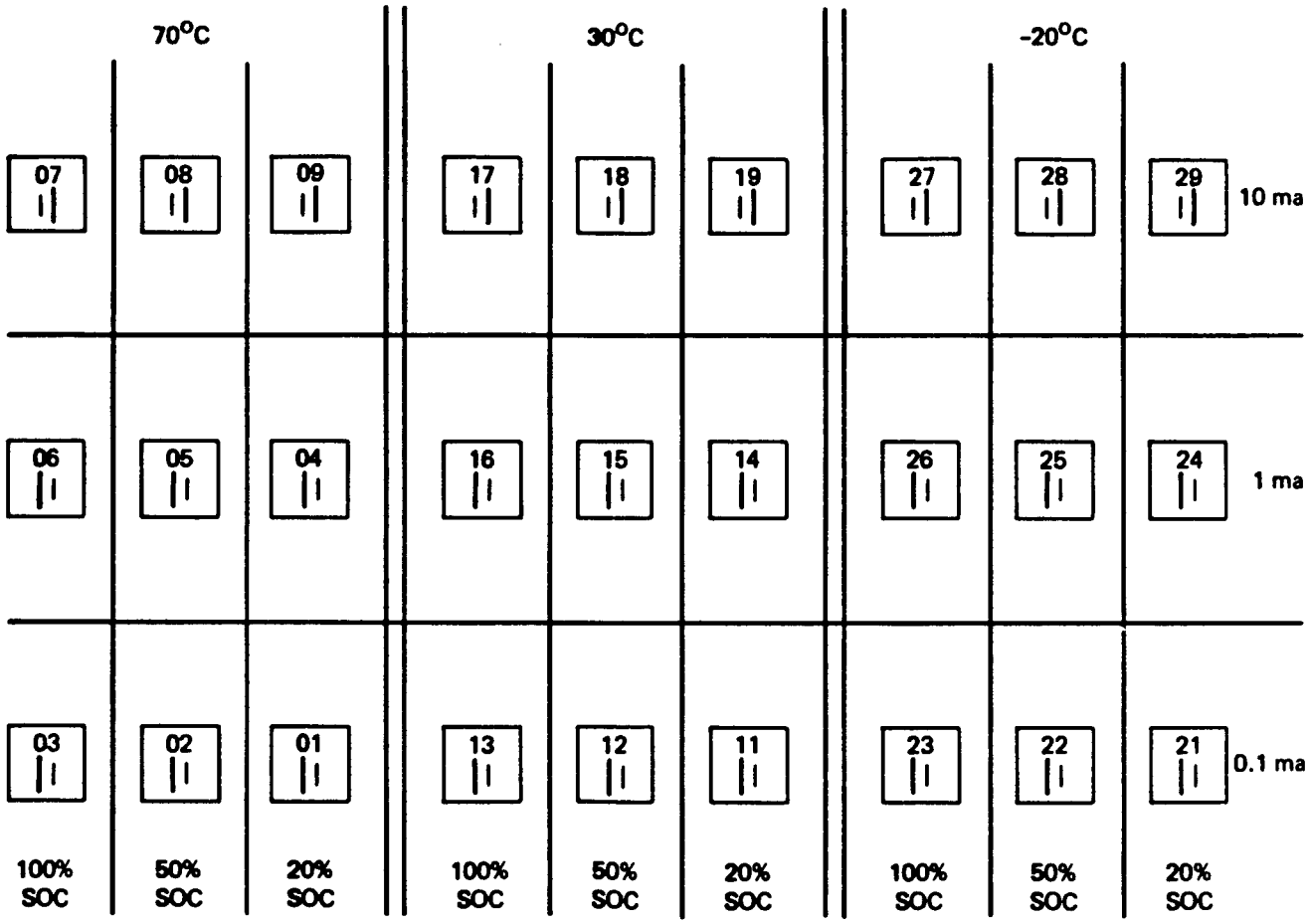

Figure 4. MATRIX FOR LOW RATE CHARGE TESTS

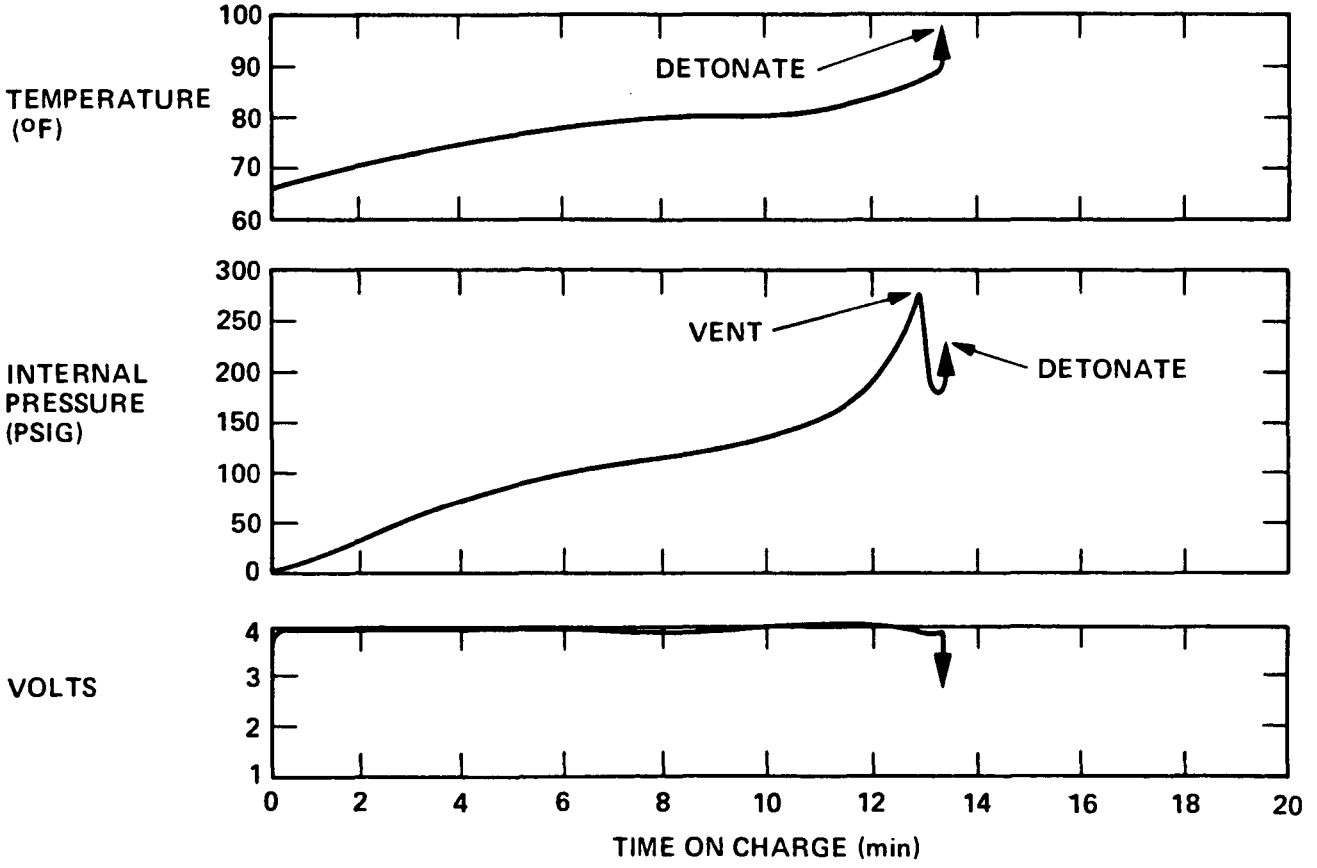

Figure 5. CELL CHARACTERISTICS DURING HIGH RATE CHARGE
I = 10 AMPS, T = AMBIENT

C-2

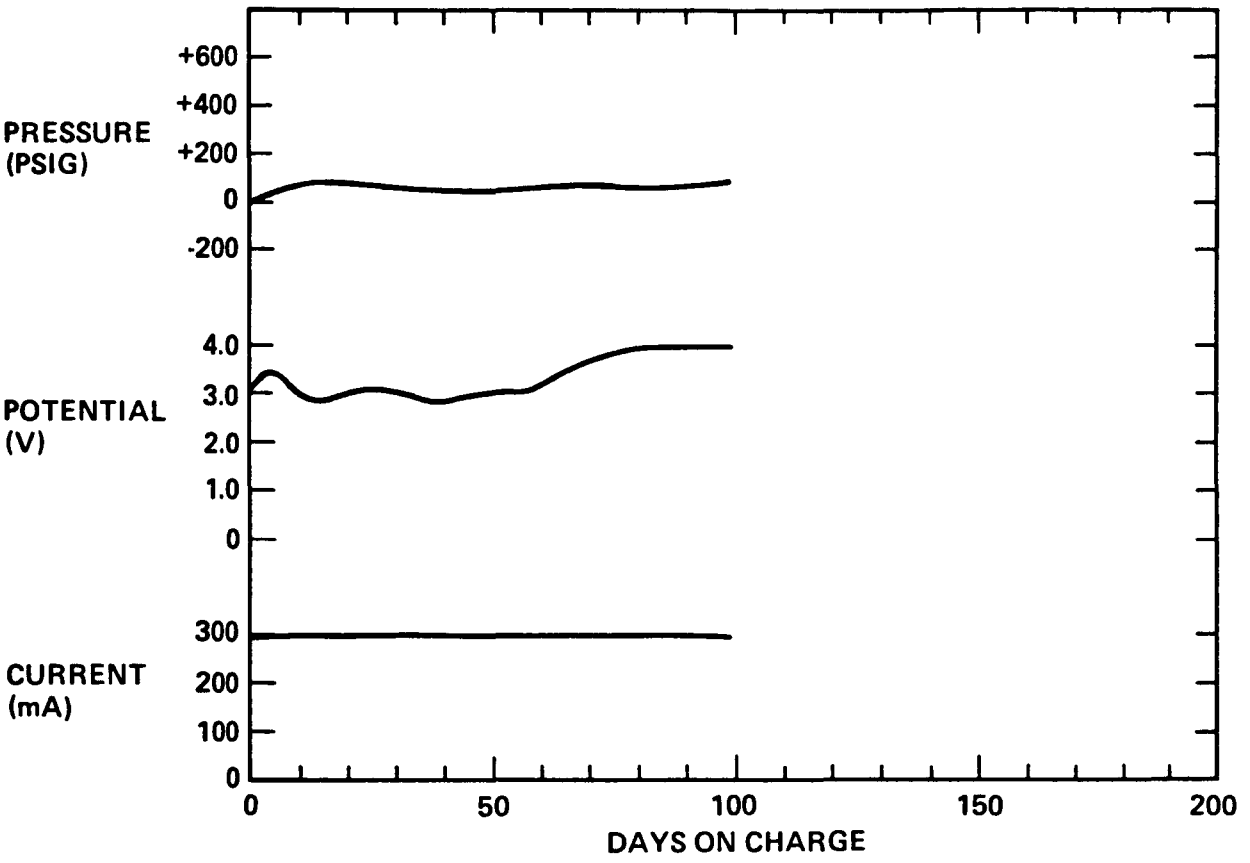

Figure 6. CELL CHARACTERISTICS DURING MEDIUM RATE CHARGE
I = 300 mA, T = AMBIENT

TYPICAL CELL
BEFORE CHARGE

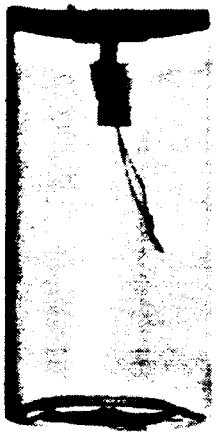

CELL NO. 08 AFTER 34
DAYS AT 10 mA AT 70°C

Figure 7. X-RAY PHOTOGRAPH OF OPENED CELL FROM LOW RATE CHARGE TEST

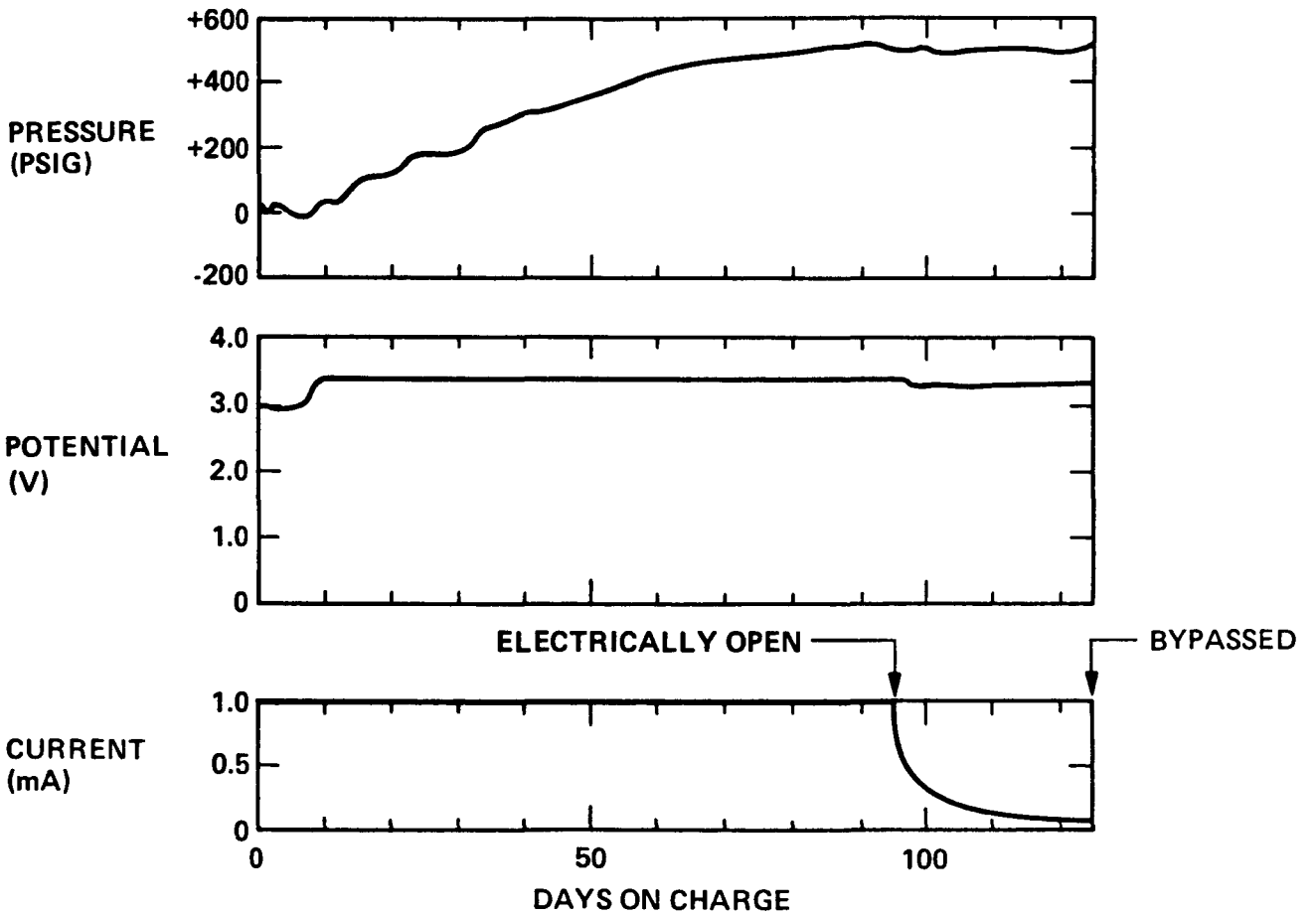

Figure 8. CELL CHARACTERISTICS DURING LOW RATE CHARGE
I = 1.0 mA, T = 70°C

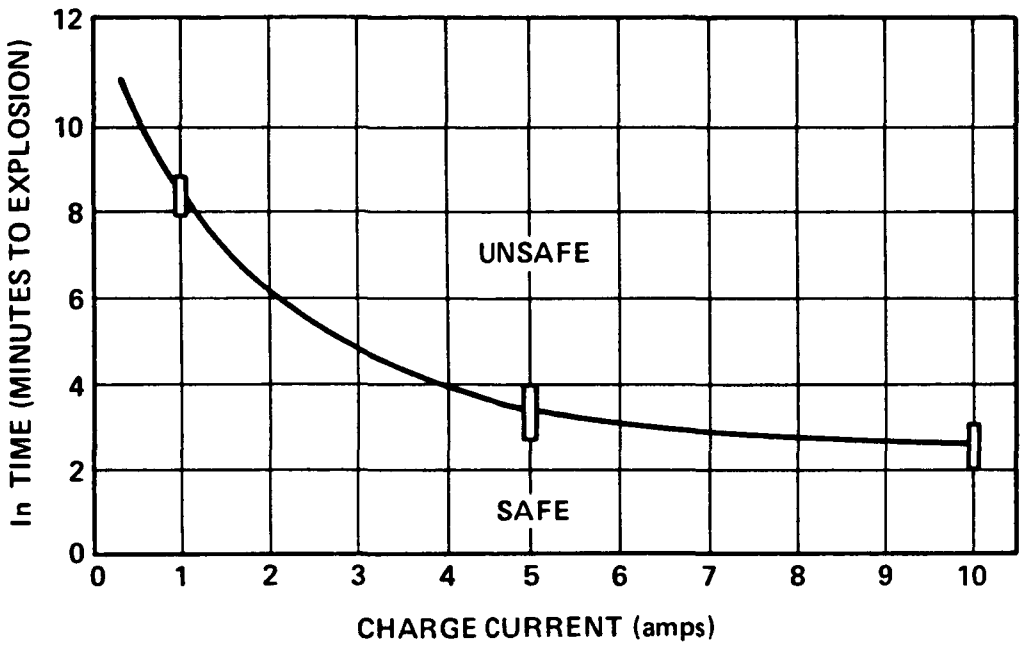

Figure 9. SAFETY ENVELOPE FOR CHARGING (Lo 30SH Li/SO_2 CELLS)

Safety Considerations for Fabricating Lithium Battery Packs

James J. Ciesla
Electrochem Industries, Clarence, New York

ABSTRACT

Lithium cell safety has been a major issue with both manufacturers and end users since first discussed by Brooks (1) and Warburton (2) at the 1974 Power Sources Symposium. Most manufacturers have taken great strides to develop the safest cells possible while still maintaining performance characteristics. The combining of lithium cells for higher voltages, currents, and capacities requires the fabricator of lithium battery packs to be knowledgeable about the specific electrochemical system being used.

The following will refer to relatively high rate, spirally wound (large surface area) sulfur oxychloride cell systems, such as Li/Thionyl or Sulfuryl Chloride. Prior to the start of a design of a battery pack, a review of the characterization studies for the cells should be conducted. The approach for fabricating a battery pack might vary with cell size.

INTRODUCTION

All lithium cell manufacturers recommend limits on the use of a cell for any given application. These limits may or may not have an incorporated safety factor. For the purpose of building a battery pack from any of the cells that are available, it would be prudent to treat the advertised specifications as a working limit. Battery pack designers must look at the same abusive conditions as cell designers. These are high-rate discharge, shorting, forced discharge, charging, overheating, and mechanical abuse. Although single cells may react well under one or more of the above abusive conditions, a battery pack, when subjected to the same conditions, may present a hazard or not function as expected. As an example, a cell discharged at a maximum continuous current of three amperes will dissipate heat at a rate that will keep the cell below its maximum rated temperature. Should a battery be discharged at the same 3 A rate, in a cluster, the internal pack temperature may easily exceed the cell temperature limits. Although the battery pack's intended use may require low current drains at room temperature, the designer must account for all conditions that might compromise battery safety.

The following steps are a precursor to a functional and safe battery design. Knowledge of the performance, storage, environmental, and abuse requirements for the system into which a pack is going will enable the battery pack designer to foresee safety problems about which the system designer may be unaware.

APPLICATION DESCRIPTION

A detailed description of the intended use of a battery will give direction for the successful design of the product. The description may help the designer to move in a more positive manner with respect to the overall safety of the pack design and its fabrication. This method of approach will lead to specific questions that are germane to the application.

GENERAL PERFORMANCE REQUIREMENTS

These will include minimum voltage, maximum voltage, average current, peak current, capacity, minimum temperature, maximum temperature, duty cycles (intermittent or continuous), motion, and orientation.

SPECIFIC REQUIREMENTS

These include available space, weight, method of attachment and termination.

DISCUSSION

With all of the above data taken into account, a preliminary battery pack design should now be analyzed for safety. All precautions should be taken to keep the cells in the pack from cresting the cell's upper temperature limits.

The battery construction should take into account all possible adverse conditions. Some of these scenarios could be venting, shorting, charging, cell reversal, mechanical abuse and overheating. Should a single cell in a battery pack vent, there should be an unrestricted escape path leading away from the cell's venting mechanism - preferably to the pack's exterior or to an absorbent material.

The major protective method for an external short circuit of the pack is through use of fuses. These fuses can be placed internal to the pack or externally in the power supply wires. A replaceable, fast acting fuse will offer the greatest protection and minimize capacity loss. If the fuse is external, it may be replaced after the short is cleared. By far, the highest occurrence of short circuiting in a battery pack is during the installation of a connector. Slow blow fuses are sometimes

used when surge or pulse currents are required. Fuse values should be set at the lowest levels possible for the application.

To protect against cell or series string charging from external power supplies or parallel strings, blocking diodes are used in each series string. Diode placement is usually within a battery pack, but can be external, if standard series packs are assembled into a larger power source. Cells of the same age and history should be used to assemble power sources.

A partially discharged cell in series with a number of fresh cells has been shown to eventually overheat due to forced discharge by the fresher cells. Reversed biased diodes on each cell in a series string may offer some protection against cell voltage reversal. In this case, other factors such as diode leakage current and cell or series string capacity loss must be considered.

Mechanical abuse may happen after the battery pack has been installed in a system or while it is being handled during installation or removal. Each application will dictate the amount of safeguarding necessary during battery design and building.

Overheating cells or battery packs will lead to venting or, in more extreme cases, cell rupture. The following will deal with internally generated heat due to cell discharge.

A current limiting resistor is often used in series with a battery pack, and will, depending on the application, restrict the current level of the battery to a safe level. In most cases a thermally activated device will be utilized to keep the pack from exceeding the safe temperature limit of the cells. Items such as thermal cutoffs (TCO) and polymeric positive temperature coefficent (PTC) resistors are in common use. The PTC can be either temperature or current activated. It will handle transients or brief current overloads. Trip time may typically run from about 0.1 to 1000 seconds dependent upon the degree of overload. Once tripped, the PTC resistor remains in a high resistance state, so long as the source voltage is maintained.

A TCO is primarily a thermal trip device but can be activated due to high current self-heating. A thermal pellet inside the TCO melts when overheated. TCO's are not able to be reset and must be replaced after being tripped. The outer case of the TCO is electrically live, and consideration must be given to this fact when it is being installed in a battery pack. Selection of a TCO to correspond to the maximum recommended temperature of a cell may not offer the protection desired. TCO's are often covered with insulation due to the "electrically live" case.

With this in mind, a series of tests were conducted to characterize the temperature lag between the cell wall and the TCO temperature.

TEST PROCEDURE

A slip fit copper slug with a pencil heater connected to a Variac was inserted into a double D case. Two layers of PVC shrink-wrap were placed on the exterior of the DD case along with two TCO cases. The internal mechanisms of the TCO's were removed (Figure 1). Thermocouples were placed at the inside and outside of the metal can walls, on each layer of shrink-wrap, and in each TCO case. Thermal grease was used between the copper slug and the cell case and in each TCO case to facilitate heat transfer. One TCO case had been covered with one layer of shrinktube. This was done to account for the fact that the TCO case is electrically live in normal use. TCO attachment to the cell was accomplished with cyanoacrylate adhesive. The test setup was covered with a 17cm H x 17cm W x 12cm L box to simulate a dead air environment. All test runs were begun at 24°C. The cell wall temperatures were used to determine the heating rate. Although the heating rate for each test run was not linear, an average heating rate was calculated over the total run time.

44°C/minute	(Figure 2)
23°C/minute	(Figure 3)
1°C/minute	(Figure 4)
10°C/minute	(Figure 5)

In all cases there is an expected lag between the cell wall and TCO temperatures. The thermal cutoff with no shrinktube showed a marked improvement in response to the cell wall temperature, over the thermal cutoff with shrinktube. A closer look at the data for the 1°/minute test run, and the temperature of the non-insulated TCO at the 73°C mark, showed a corresponding cell wall temperature of 82°C. A 68°C TCO temperature had a corresponding 76°C cell wall temperature. These nine and eight degree temperature lags correspond to fourteen and thirteen degrees respectively during the 10°C/minute heating rate.

An increase in heat transfer between the cell and TCO was facilitated by mixing copper metal dust with the cyanoacrylate adhesive. The differential for the 10°C/minute run was now eight degrees. This is a forty-five percent increase in heat transfer for a non-insulated TCO. The increase over the insulated TCO was sixty percent.

Table 1 presents a comparison between an insulated TCO and the cell wall temperature at the various heating rates. The non-insulated TCO with conductive adhesive for the 10°C/minute rate is at the far right. Table 2 presents the temperature lag for the same conditions.

One other non-insulated TCO was attached to the cell wall with the same conductive adhesive. This was a functional TCO. A multimeter was attached to the leads of the TCO and monitored for loss of continuity during a 10°C/minute run. The trip temperature for this TCO was 72°C (+0, -4°C). This TCO tripped 4.4 minutes after the cell wall temperature hit 72°C. The thermocouple in the non-insulated TCO case with conductive adhesive indicated a temperature of 100°C. The cell wall temperature at that time was 111°C.

TEST SUMMARY

Conductive adhesive will greatly improve the heat transfer for thermal cutoffs. Appreciable temperature lag can result if a thermal cutoff is insulated prior to installation. Careful consideration must be given to the trip temperature of a TCO if it is to act as a protection device in the event of cell self-heating.

CONCLUSION

The design and construction of a lithium battery pack must be accomplished methodically if it is to function in a safe manner. Devices which are added to a cluster of cells have their own distinctive characteristics and these should be understood if they are to be relied upon as a safety item.

The reaction time of a thermal cutoff will be different than the above test if it is in a cluster of cells, in a colder or hotter environment, has air movement by it, or is from a different manufacturer. A battery pack becomes a system in itself that must be looked at from every perspective. Overall safety depends on it!

REFERENCES

1. Brooks, E.S., Proc. 26th Power Sources Conf., p. 31, 1974

2. Warburton, D.L., Proc. 26th Power Sources Conf., p. 34, 1974

Table 1. CELL WALL AND TCO TEMPERATURE COMPARISON

CELL WALL vs INSULATED TCO TEMPERATURE					Conductive Adhesive
Cell Wall (°C)	TCO (°C)				
	Heating Rate (°C/Min)				
	1	10	23	44	10
55	47	45	40	31	49
75	63	55	50	43	67
85	72	60	55	49	76
95	80	70	64	55	85
105	87	79	69	60	95
115	-	85	79	-	103

Table 2. TCO TEMPERATURE LAG

CELL WALL vs INSULATED TCO (TEMPERATURE LAG)					Conductive Adhesive
Cell Wall (°C)	TCO (°C)				
	Heating Rate (°C/Min)				
	1	10	23	44	10
55	8	10	15	24	6
75	12	20	25	32	8
85	13	25	30	36	9
95	15	25	31	40	10
105	18	26	36	45	10
115	-	30	36	-	12

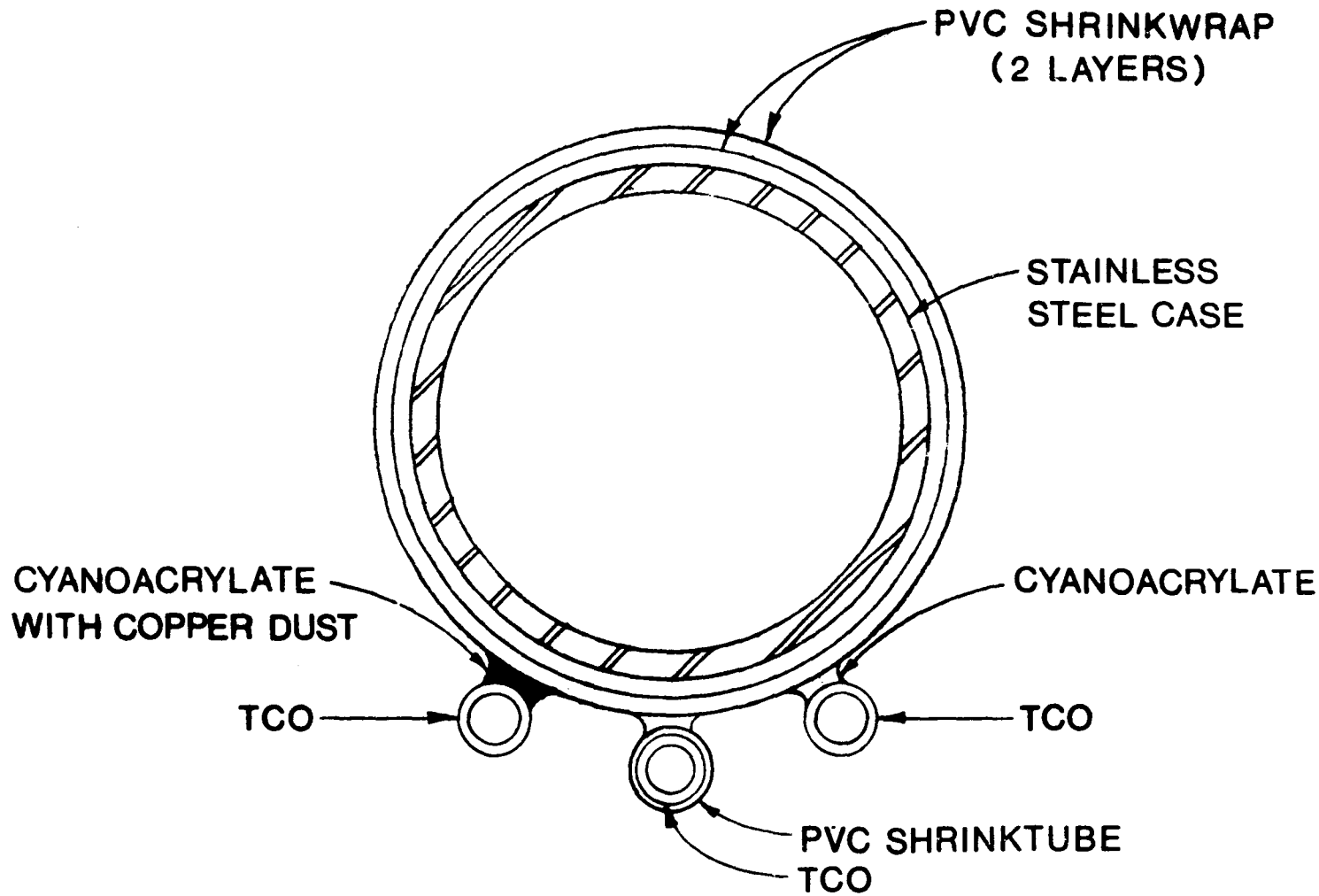

Figure 1. TEST SETUP

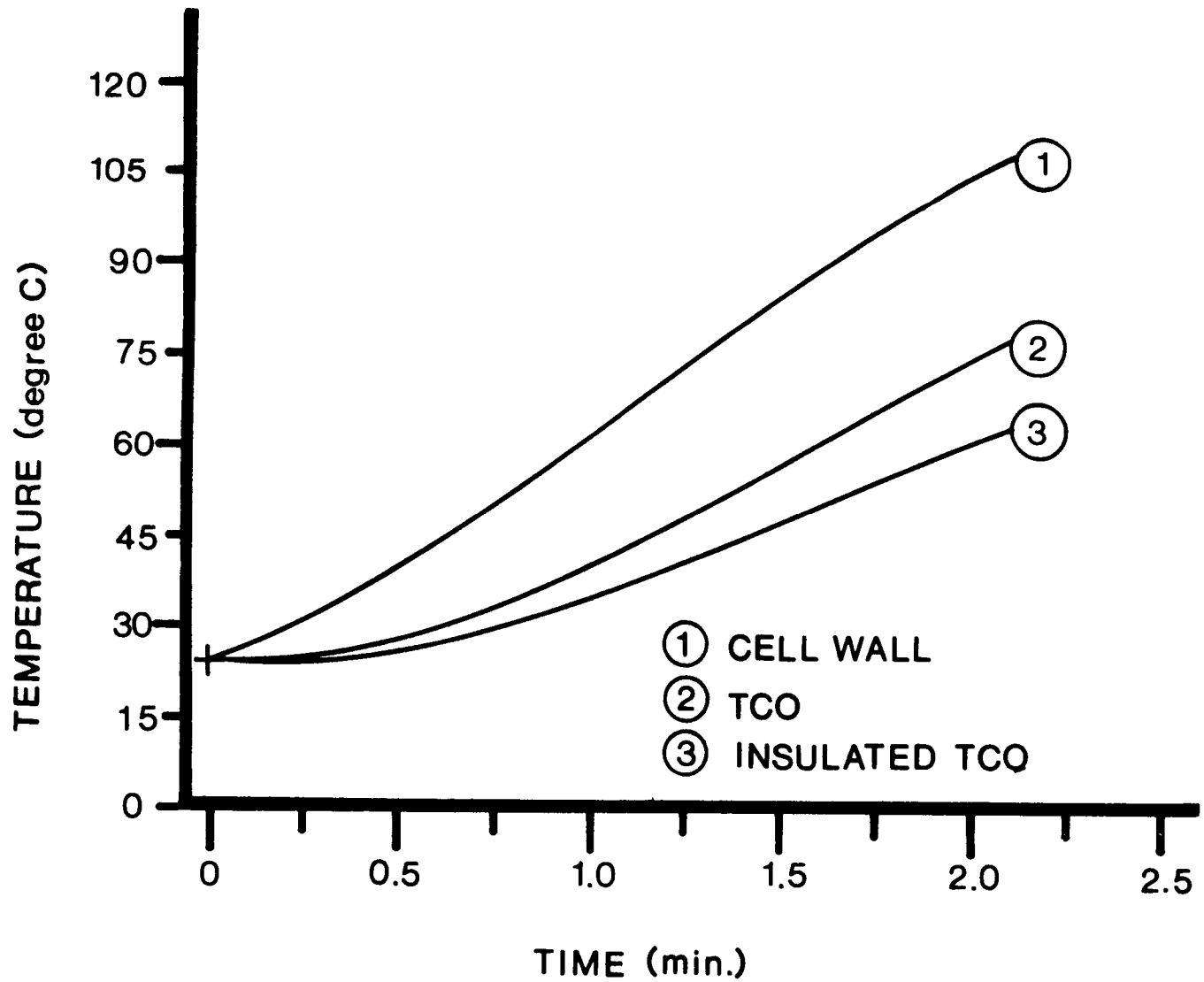

Figure 2. 44 DEG. C PER MIN.

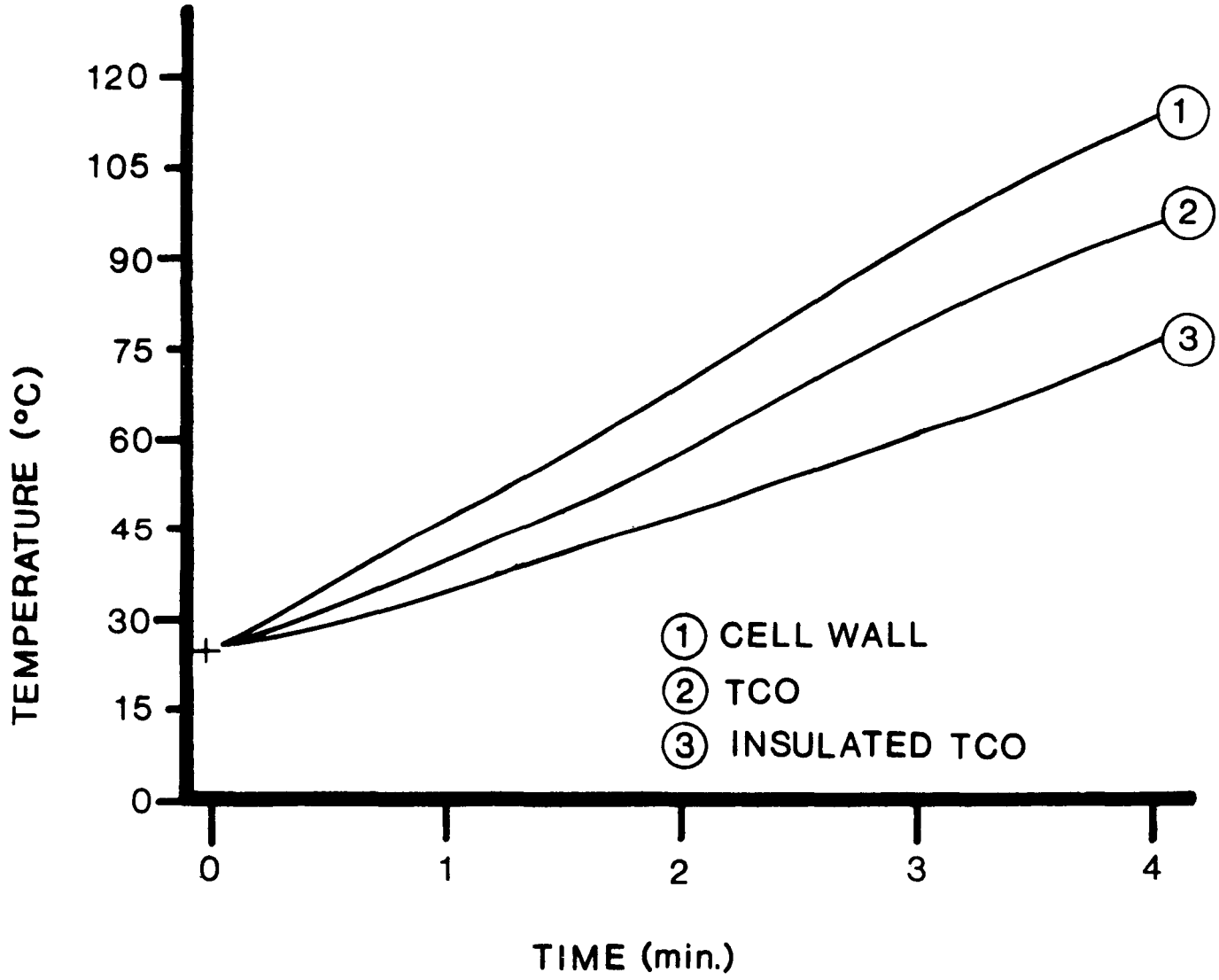

Figure 3. 23 DEG. C PER MIN.

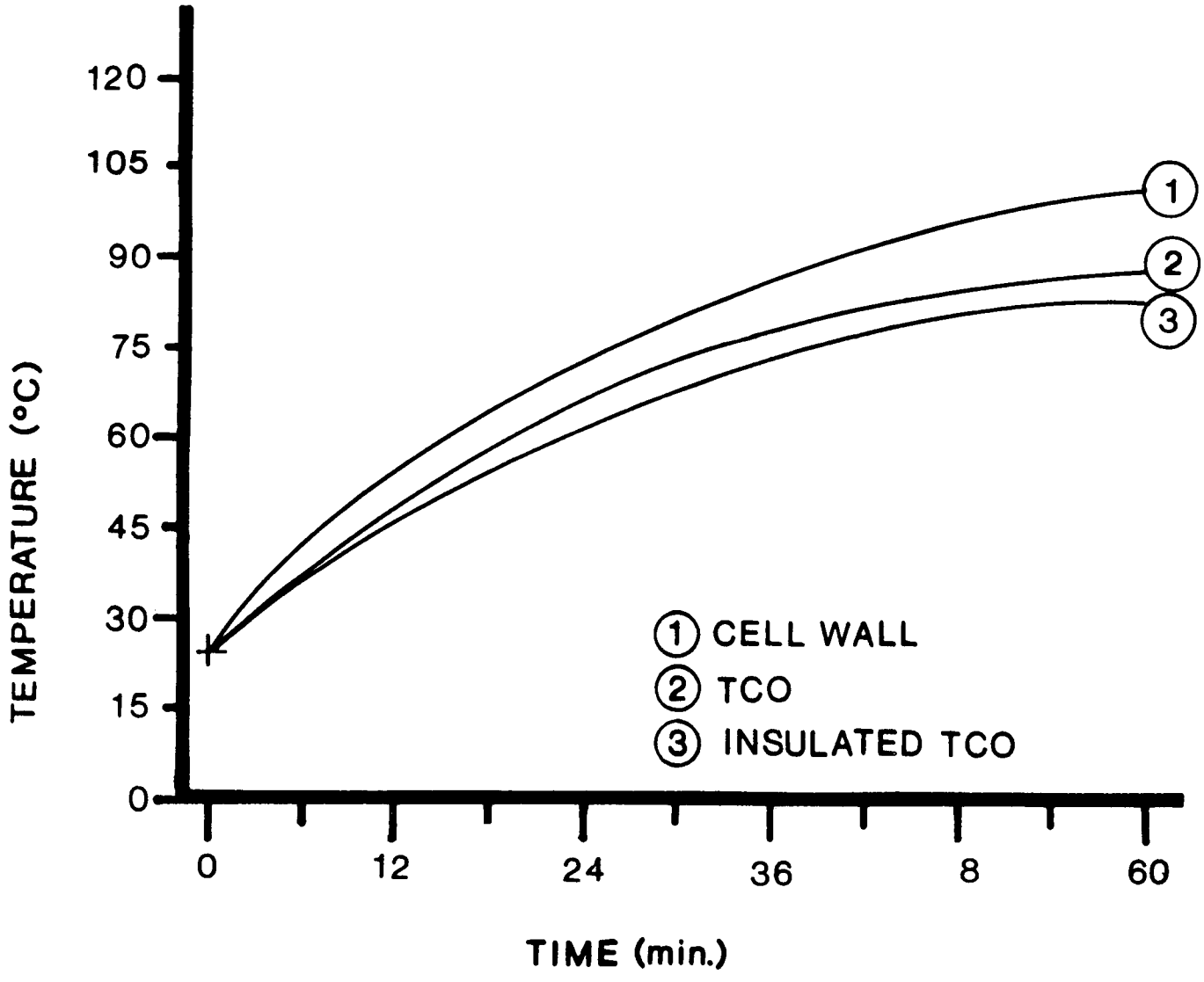

Figure 4. 1 DEG. C PER MIN.

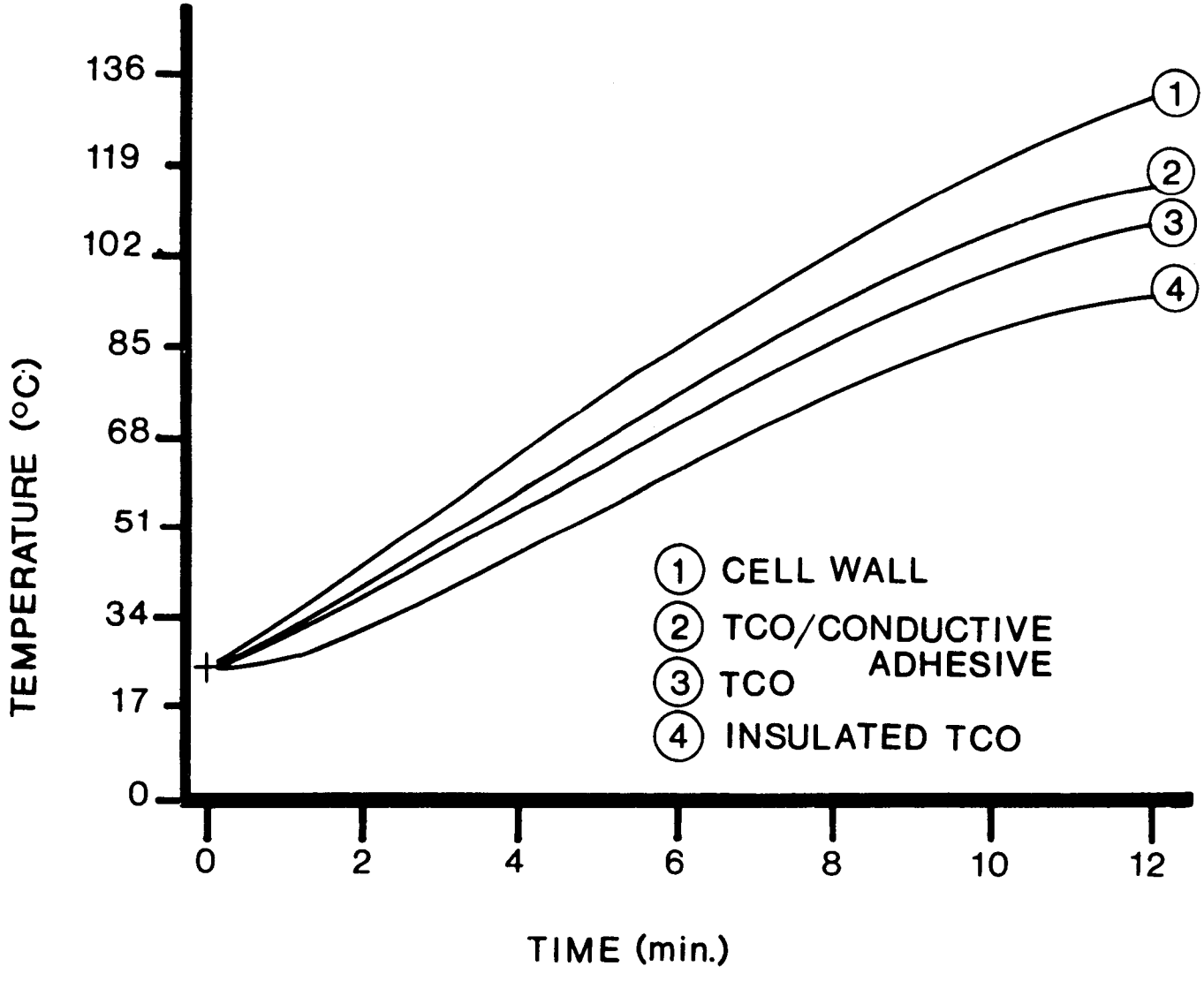

Figure 5. 10 DEG. C PER MIN.

HEAT DISSIPATION OF HIGH RATE Li-$SOCl_2$ PRIMARY CELLS

Young I. Cho and Gerald Halpert
Drexel University Jet Propulsion Laboratory
Philadelphia PA 19104 Pasadena CA 91109

INTRODUCTION

The present investigation is a part of a series of investigation being carried out at JPL and Drexel University to better understand the heat dissipation problem occurring in the lithium thionyl chloride cells discharged at relatively high rates under normal discharge conditions. The earlier work presented at the 168th Electrochemical Society Meeting at Las Vegas[1] identified four heat flow paths, and the thermal resistances of the relating cell components along each flow path were accordingly calculated. From the thermal resistance network analysis, it was demonstrated that about 90 percent of the total heat produced within the cell should be dissipated along the radial direction in a spirally wound cell.

In addition, the threshold value of the heat generation rate at which cell internal temperature could be maintained below 100°C, was calculated from total thermal resistance and found to be 2.8 W. However, these calculatons were made only at the cell components' level, and the transient nature of the heat accumulation and dissipation was not considered. In the present study, a simple transient model based on the lumped-heat-capacity concept has been developed to predict the time-dependent cell temperature at different discharge rates. The overall objectives of the study was to examine the influence of cell design variables from the heat removal point of view under normal discharge conditions and to make recommendations to build more efficient lithium cells.

TRANSIENT ANALYSIS OF HEAT DISSIPATION FROM THE CELL

In the present investigation, the co-called lumped-heat-capacity method has been used instead of solving the energy equation in the cylindrical coordinates system. As demonstrated in our previous study[1], approximately 90 percent of thermal resistance particularly along the radial direction occurs from the outer wall of the case can to the environment, where heat is removed from the cell by natural convection. In other words, the thermal resistances of cell components along the radial as well as axial direction within the cell are so small that heat will be diffused out quickly throughout the cell, reaching the case can without much delay. This also implies that the internal temperature of the cell may be assumed uniform radially and axially and equal to the cell wall temperature as a first-order approximation. Hence, it is an ideal problem to apply the lumped-heat-capacity concept to estimate the transient temperature of the cell. Of note is that a more complicated modelling work to take

into account radial and axial temperature variation is being developed and will be reported in the future.

The governing transient heat balance equation becomes

$$\dot{q} = \rho VC \frac{dT(t)}{dt} + hA\,[T(t) - T_\infty] \tag{1}$$

where h is the heat transfer coefficient from the cell surface to the environment and ρVC is the so-called thermal mass of the cell. Physically, the first term in the right hand side represents the amount of heat stored within the cell and the second term that dissipated into the environment. Since the amount of heat to be dissipated out by natural convection depends on the temperature difference between the wall and the environment, the heat transfer coefficient h is a function of the cell temperature accordingly. However, in the present study, h is assumed to be constant for the mathematical simplicity.

Using the initial boundary condition, $T = T_\infty$ at $t = 0$, the solution of the above equation becomes

$$T(t) - T_\infty = \frac{\dot{q}}{hA}\left[1 - e^{\frac{hA}{\rho VC}t}\right] \tag{2}$$

where $\dot{q}$ is the heat generation rate to be determined by the discharge rate of the cell. Since hA is the inverse of the thermal resistance R_{SV} between the case can and the environment, it becomes

$$hA = \frac{1}{R_{SV}} = 0.0352 \quad W/°C \tag{3}$$

Note that the heat transfer coefficient h for the present D-size cell becomes 4.4 $W/m^2°C$, which is a typical value[2] for the case of heat dissipation to the room temperature by natural convection. Also note that for the adiabatic boundary condition which occurs in many military applications of the lithium cells, the second term of the right hand side in Eq. (1) disappears and the corresponding solution becomes

$$T(t) - T_\infty = \frac{\dot{q}}{\rho VC}t \tag{4}$$

As shown in Eqs. (2) and (4), the thermal mass of the cell PVC is an important parameter in the calculation of the transient cell temperature T. Therefore, the thermal mass of each cell component was calculated based on the JPL's first generation D-size cell specification and shown in Table 1. Values of mass of each cell component, ρV, are the data experimentally measured at JPL and the

specific heats of lithium, nickel and stainless steel were taken from Ref. (3). The specific heat of the electrolyte (i.e., 1.8 M $LiAlCl_4$ in $SOCl_2$, received from Lithium Corporation of America, Lithcoa) was estimated from the work by Venkatasetty[4] and founded to be 1215 J/KgK.

Table 1 shows that about 54 percent of the total thermal mass can be attributed to the electrolyte at the beginning of the discharge. Of note is that near the end of normal discharge, i.e., 80 percent DOD, approximately half of the electrolyte is consumed, thus reducing the thermal mass of the cell correspondingly. In this regard, of note is that a flooded cell may be safer than a starved cell from the heat transfer point of view since the percentage loss of thermal mass in the flooded cell due to the electrolyte consumption is relatively small compared to the case of the starved cell. However, in the present study, the time-dependent effect of the electrolyte consumption was not considered. A complete model to take into account the transient nature of the thermal mass of the electrolyte as well as the heat transfer coefficient h will be developed and reported in the future.

The cell temperature was predicted from Eq. (2) in which the heat generation rate, $\dot{q}$, was calculated from the discharge characteristics curve experimentally obtained at C/2, i.e., see Fig. 1. The resulting cell temperature vs. time is shown in Fig. 2, which also gives the percentage depth of discharge along the abscissa. This figure clearly demonstrates that the cell temperature increases gradually to 100°C for the first 95 min and then suddenly jumps to about 200 250°C within the next 15 min. The horizontal dashed line indicates the maximum allowable cell temperature of 100°C, which is below the melting points of cell components such as sulfur (112°C) and lithium (179°C). The corresponding DOD to the cell temperature of 100°C was approximately 80 percent with the discharge rate of C/2. This indicates that the present cell may be discharged safely at C/2 rate up to 80 percent DOD. Although the time-dependent temperature prediction with the lumped-heat-capacity method was carried out with the constant values of the heat transfer coefficient h and the initial thermal mass ρVC, the resulting temperature showed the actual trend observed in the test of the lithium cell. An IBM-PC based computer code to calculate thermal resistance of cell components and to predict the transient cell temperature including the effect of electrolyte consumption and the temperature-dependent heat transfer coefficient h will be developed and reported accordingly with a detail comparison with experimental data.

FIN ANALYSIS

When the lithium cells are in contact with the environment during the normal discharge, one way to improve heat dissipation from the cell is to add fins around the cell. In so doing, it is important to recognize the conditions for which the finned surface has advantages over the unfinned surfaces. Particularly for aerospace applications, the weight

added, the space needed and the cost of adding fins are of the greatest importance. Also note that the installation of fins on a heat transfer surface will not necessarily increase the heat transfer rate. In general, if the value of 2k/ht is larger than 5, it is advantageous to use fins around the heat transfer surface. Here, k is the thermal conductivity of a fin material, h is the heat transfer coefficient between the fin surface and the environment, and t is the fin thickness. For the present application, h is relatively small, being approximately 4 7 $W/m^2°C$ and k is large, being 16.3 W/m°C for stainless steel and 204 W/m°C for aluminum. Hence, it is clearly advantageous to install fins around the cell.

The proposed fin dimensions in the present study as shown in Fig. 3 are as follows; t(thickness) = 0.04 cm, L(length) = 0.44 cm and H(height) = 5.69 cm same as the height of the D-size cell. The proposed total number of fins is 32. Therefore, the value of 2k/ht for stainless steel fins becomes 18,500, which demonstrates the usefulness of installation of these types of fins. A valid method of evaluating fin performance is to compare heat transfer with the fin to that which would be obtained without the fin. The ratio of the two for a single fin becomes

$$\frac{\langle \dot{q} \rangle \text{ with fin}}{\langle \dot{q} \rangle \text{ without fin}} = \frac{\tanh mL}{\sqrt{hA/kP}} \qquad (5)$$

where < > indicates a value for a single fin and m is $\sqrt{hP/kA}$. Of note is that when the value of L/(t/2) is equal to or larger than unity, the fin is considered long, in which the heat loss from the fin end surface is negligibly small. In the present study, the value of L/(t/2) becomes 285, which is far beyond the threshold value of one. Hence, the simple solution, Eq. (5), which was derived for the case with an insulated fin end, is valid for the present analysis. Applying the proposed fin dimensions, the ratio in Eq. (5) for a single fin was calculated to be

$$\frac{\langle \dot{q} \rangle \text{ with fin}}{\langle \dot{q} \rangle \text{ without fin}} = 21.65 \text{ for a stainless steel fin} \qquad (6)$$

Next, the total heat dissipated from the cell with 32 fins was calculated and compared with that without fins. The ratio of the two becomes

$$\frac{\text{total heat dissipated from the cell with 32 fins}}{\text{total heat dissipated without fins}} = 3.4 \qquad (7)$$

This indicates that the heat transfer from the cell could be enhanced by a factor of 3.4 when compared with that without fins. This implies that the thermal resistance will be decreased to the one-third of the

present value of 28.4 °C/W. This is a considerable improvement in the heat dissipation from the lithium cell when heat is removed from the cell to the environment by natural convection.

Use of aluminum (k = 204 W/m°C) or copper (k = 385 W/m°C) as a fin material was also examined to see if those materials may further increase the heat dissipation from the cell. However, the fins considered in the present study are too short to show any improvement over the fins made with stainless steel (k = 16.3 W/m°C). For reference, the ratio in Eq. (6) for copper fins was found to be 21.96. Also, when the thickness of fins is doubled to 0.08 cm, the corresponding ratio in Eq. (7) was calculated to be 3.35. Therefore, the heat transfer enhancement with thicker fins (i.e., t = 0.08 cm) is essentially the same that with thinner fins (i.e., t = 0.04 cm).

SUMMARY AND CONCLUSIONS

A simple transient model to predict the time-dependent cell temperature was developed based on the lumped-heat-capacity method. The transient cell temperature predicted from the model for the case of C/2 discharge rate with the JPL's D-size cell indicated a gradual increase of the cell temperature for the first 95 min. Then, for the next 15 min, there was a sharp increase of the cell temperature to about 200~250°C, as was observed in many of experimental test results. This suggests that the present cell may be discharged safely at C/2 discharge rate up to 80 percent DOD while the cell temperature remains below 100°C.

As a practical way of the heat transfer enhancement, the feasibility of installing fins was considered. With the proposed fins in the present study, it was demonstrated that about three times more heat could be removed from the cell. Additionally, the use of aluminum or copper fins, and thicker fins than the present ones was also discussed.

As a final remark, the present analysis is based on the assumption that the cell is in contact with air. Therefore, in some of aerospace applictions of these cells where there is no air, the heat dissipation analysis based on the radiation heat transfer should be carried out.

REFERENCES

1. Y. Cho, S. Subbarao, J.J. Rowlette and G. Halpert, Thermal assessment of high rate Li-$SOCl_2$ primary cells, presented at the 168th Electrochemical Society Meeting, Las Vegas, Oct. 1985. (Extended Abstracts, ,Vol. 85-2, pp. 169-170).

2. J.P Holman, "Heat Transfer," McGraw-Hill, New York (1981).

3. Handbook of Tables for Applied Engineering Science, R.E Bolz and G.L. Tuve, Editors, CRC, Cleveland (1970).

4. H.V. Venkatasetty, Final Report to Naval Ocean Systems Center, E47992, Dec. (1982).

Table 1. THERMAL MASS OF CELL COMPONENTS

	ρVC (W·S/°C)	%
Lithium	19.5	20
Nickel	6.7	6.8
Stainless Steel	19.2	20
Electrolyte	53.0	54
Others	0	0
Total	98.4	100%

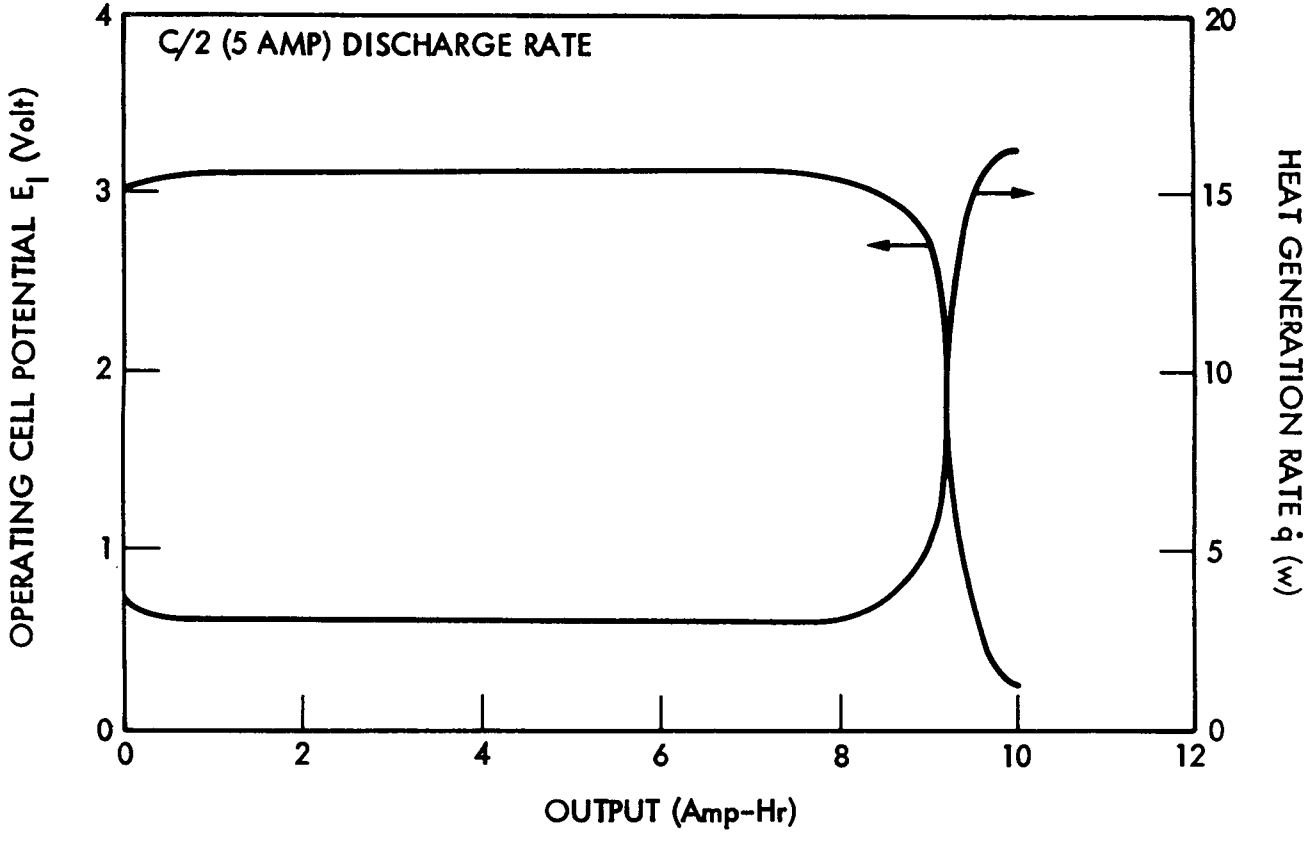

Figure 1. DISCHARGE CHARACTERISTICS OF JPL'S D-SIZE CELL AT C/2 RATE AND THE CORRESPONDING HEAT GENERATION RATE CALCULATED BASED ON $q = I(E_H - E_I)$, WHERE E_H IS THE THERMONEUTRAL POTENTIAL, 3.72 VOLT

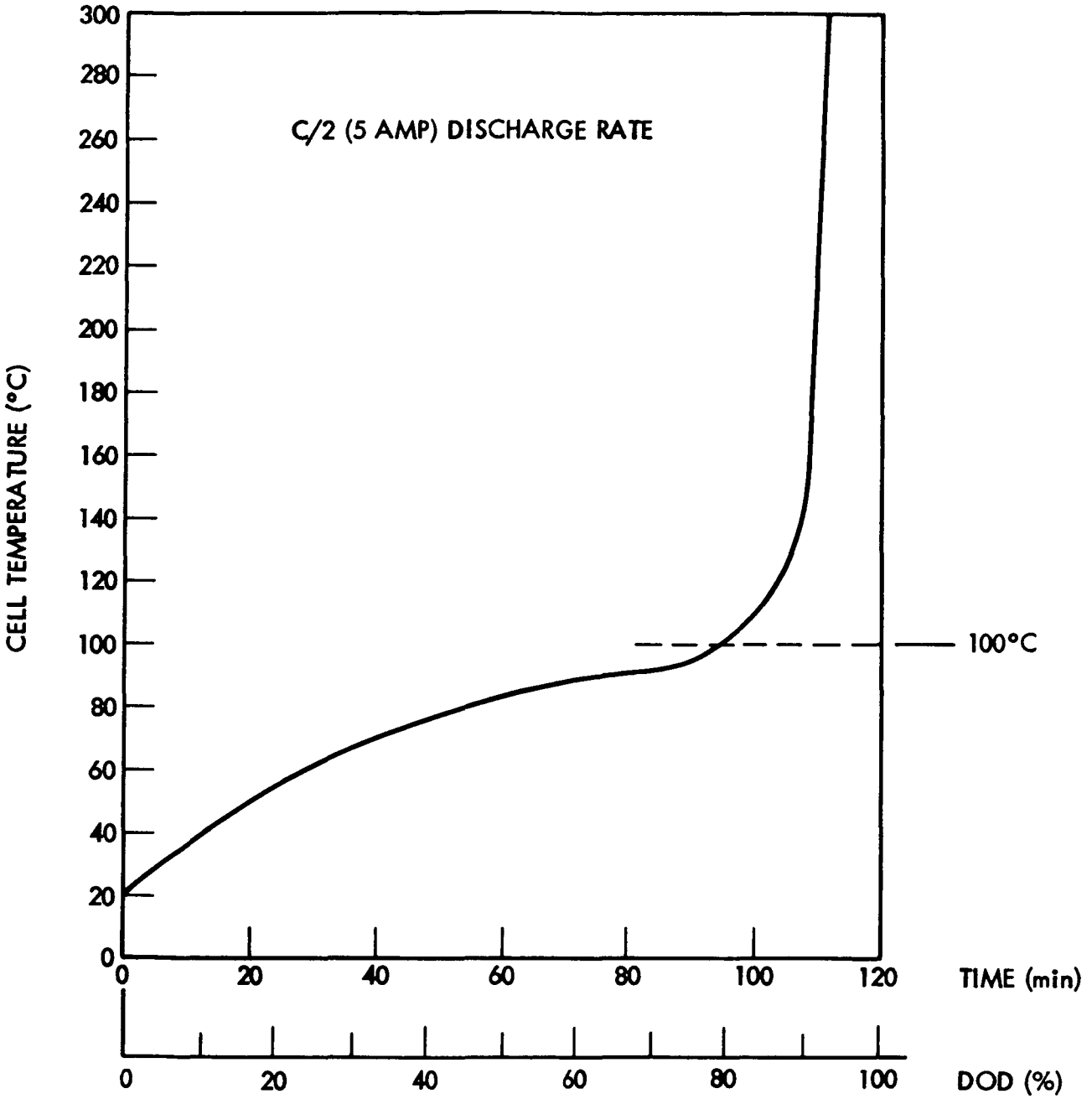

Figure 2. CELL TEMPERATURE PREDICTION FROM THE TRANSIENT MODEL, EQ. (1)

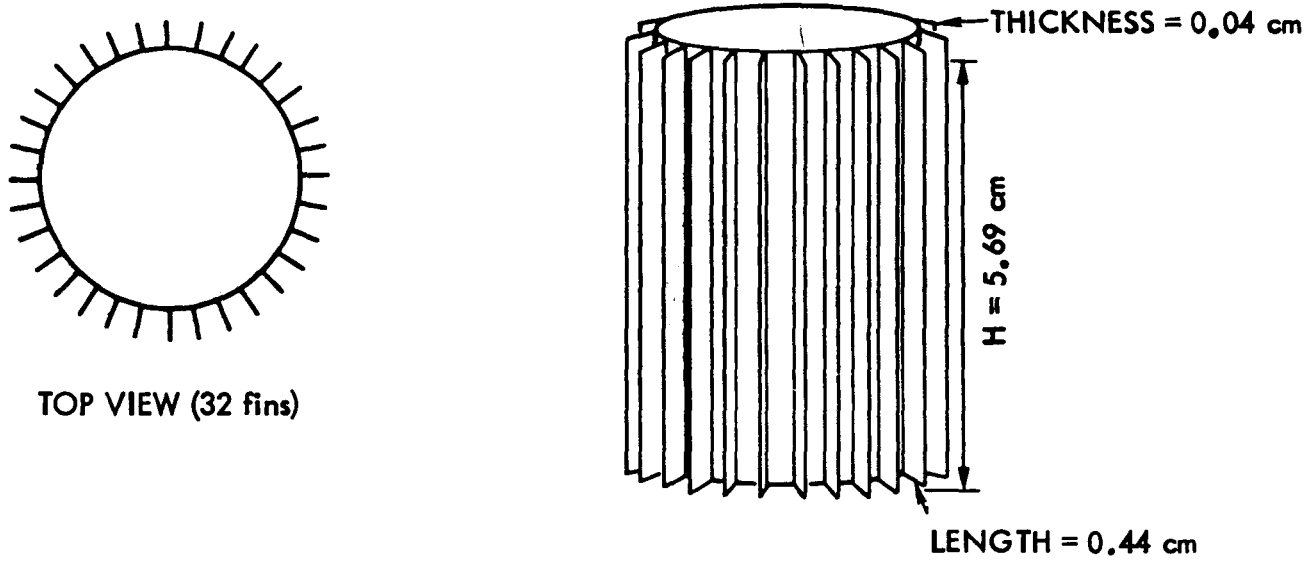

Figure 3. TOP VIEW AND SKETCH OF 32 FIN ARRANGEMENTS

TEST RESULTS OF JPL $LiSOCl_2$ CELLS

G. HALPERT, S. SUBBARAO, S. DAWSON, V. ANG, E. DELIGIANNIS

JPL has been involved in the development of high rate Li-$SOCl_2$ cells for various applications. The goal is to achieve 300 watt-hours per kilogram at the C/2 (5 amp) rate in a "D" cell configuration. The JPL role is to develop the understanding of the performance, life, and safety limiting characteristics in the cell and to transfer the technology to a manufacturer to produce a safe, high quality product in a reproducible manner.

The approach taken to achieve the goals is divided into four subject areas:

Cathode processes and characteristics
Chemical reactions and safety
Cell design and assembly
Performance and abuse testing

Last year, I described the results of what was termed a "first generation" design. In this initial work, the goal was to evaluate positive versus negative limited and case positive versus case negative designs. The cell was not optimized for anode, cathode, or thionyl chloride capacities.

To fabricate these cells required an evaluation of the cathode processing steps. There are several steps included in the preparation of cathode including mixing order and speed, composition of the mix, rolling/pressing method, and curing procedure. These steps were evaluated by characterization of the cathode. The final product utilized Shawingan Acetylene Block (SAB) carbon, comprising 10% PTFE on an Exmet current collector. There were no known additives. The cathode thicknesses varied between 20 and 27 mils depending on the program stage.

The assembly process included developing a technique for handling the electrode pack including separator. The lithium anode consisted of two layers of lithium film mechanically pressed on opposite sides of nickel screen. The separator is a Meade fiberglass material. The cathode, anode, and separator pack were rolled on a mandrel and placed in the stainless steel case. After welding the cover containing a single glass for metal seal, the cell was vacuum-filled with electrolyte to ($LiAlCl_4$ in $SOCl_2$).

The results of testing these first generation cells is given in figure 1. The surprising results showed that at the 0.2 and 1 amp rate the 300 Wh/Kg (10.7 Ah) was achievable. At the 5 amp discharge rate, this goal was not quite met. The V-I power characteristic curves presented at last year's workshop are given in figure 2. The ability of producing 50 watts at full charge and 30 watts at 90% discharge was also impressive.

The goal of this past year's effort was to optimize the design for a high rate application (see figure 3). This included characterization of the carbons and the electrodes, evaluation of electrolyte concentration, anode/cathode ratio, effect of reversal, inside/outside carbon, among others.

The second generation design is given in figure 4 [1]. Note that the lithium electrode capacity is minimized. The reason for this is that at the high rate the carbon electrode will limit the capacity so it is unnecessary to add the additional lithium. There is an important point to be made here. In order to design a safe cell to meet a specific application, the anode, cathode, and electrolyte balance must be designed with the applications in mind; a high rate design will result in different performance than a low rate design.

From a safety standpoint, it has been shown [2] that a $SOCl_2$-limited cell can lead to safety hazards. Thus, its capacity must be maximized so that there is adequate electrolyte to provide conductivity throughout and at the end of discharge.

The work on the cathode characterization has led to some interesting results. The work performed on this subject included determining particle size, surface area, and structure of several carbons (SAB, Ketjen Black, Vulcan, and Black Pearls) and the surface area and pore-size distribution (PSD) of the carbons as electrodes measured using the BET and mercury porosimetry methods [3]. Although no definitive statement can be made at this time, some of these characteristics appear to more relevant than others. For example, the mercury porosimetry provided some insight into the PSD of the cathode. An example is shown in figure 5 in which the SAB electrode characteristic is compared before and after discharge. More work is continuing in this area to better understand the controlling physical processes.

Experimental work on the safety of Li-$SOCl_2$ during reversal [4] especially the carbon-limited cells of interest for this application. This work indicates that during carbon-limited reversal lithium forms on the carbon. However, if there is adequate electrolyte, the lithium will quickly dissolve removing the potential for dendrite formation - a condition that has been reported on hazards. The innovative experimental setup of his work is given in figure 6. The results given in figure 7 indicate that there is plating of lithium on carbon during reversal as can be seen by the potential of the reference carbon (C2) versus the reversed carbon (C1). The 3.5 volts is typical of the Li-$SOCl_2$ cell potential. The reversal lasted for 200 mah. However, after a 1-hour stand, only 24 mah of lithium capacity was available indicating there was a reaction between the Li and the $SOCl_2$ solution.

The test results all done at ambient temperatures are given in the next few figures [5]. The 1 amp discharge is given in figure 8. The voltage was level at 3.3V. The temperature increased only slightly in the forced air circulation chamber until close to failure. The capacity to 2 volts was greater than 12 Ah (340 Wh/Kg). At 2 amp in figure 9, the results were similar with a minor difference in capacity of 11.2 Ah (318 Wh/Kg). The 5 amp discharge resulted in higher temperature (162°F) - less than the 212°F predicted and required for safe operation. The capacity of 11.1 Ah at 3.3 (316 Wh/Kg) was surprisingly high and exceeded beyond the 300 Wh/Kg goal.

The design considerations described earlier were evaluated and the results given in figure 11. Three cells of each type were included in the evaluation. The results are the average of the three. There was not much difference in the placement of the carbon or in the electrolyte concentration. However, the 1.8 mah electrolyte has greater conductivity and the need to maximize the carbon electrode by placing it on the outside makes the selection of design more appropriate.

Additional tests were conducted in which the cells were reversed for 2 hours at 5 amps. There were no incidents reported during this revised test. Summarizing the work on the JPL design cells. A goal of 300 Wh/Kg at the ship rate has been exceeded. And thus, design of the cell appears to be adequate to meet the requirements. The thermal analysis discussed by Cho [6] at this conference further verifies that the cells are capable of meeting the mission goal.

REFERENCES

1. V. Ang, Internal Memorandum of October 1985

2. S. Subbarao, G. Halpert, and I. Stein, "Safety Considerations of Lithium Thionyl Chloride Cells" (JPL Document soon to be released)

3. S. Dawson, Fall Meeting, Electrochemical Society, Las Vegas, Nevada, October 1985

4. S. Subbarao, Fall Meeting, Electrochemical Society, Las Vegas, Nevada, October 1985

5. F. Deligiannis, Paper to be presented at the IECEC Meeting in San Diego, California, August 1986

6. Y. Cho, The 1985 NASA/GSFC Battery Workshop

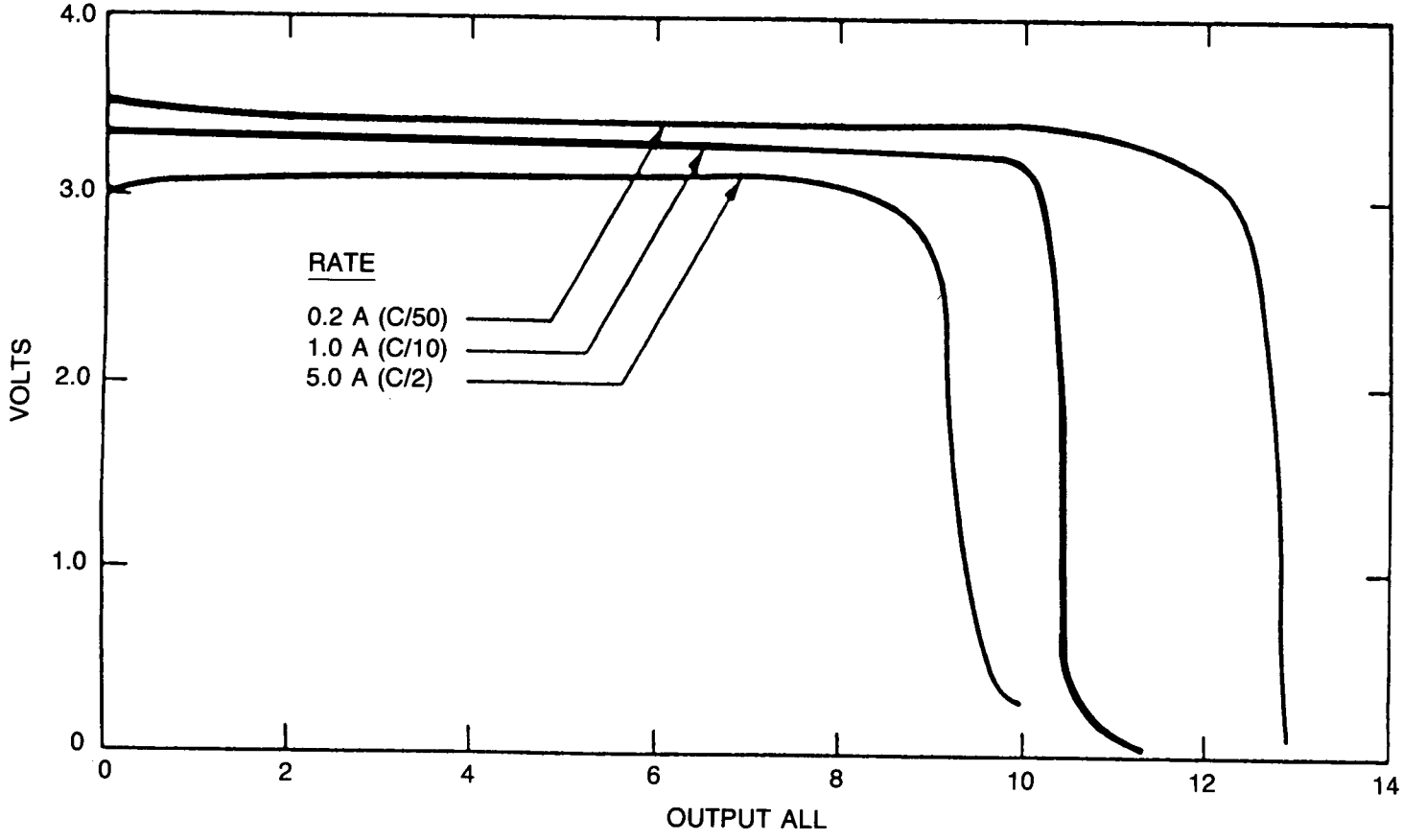

Figure 1. EFFECT OF DISCHARGE RATE ON Li-$SOCl_2$ CELL PERFORMANCE

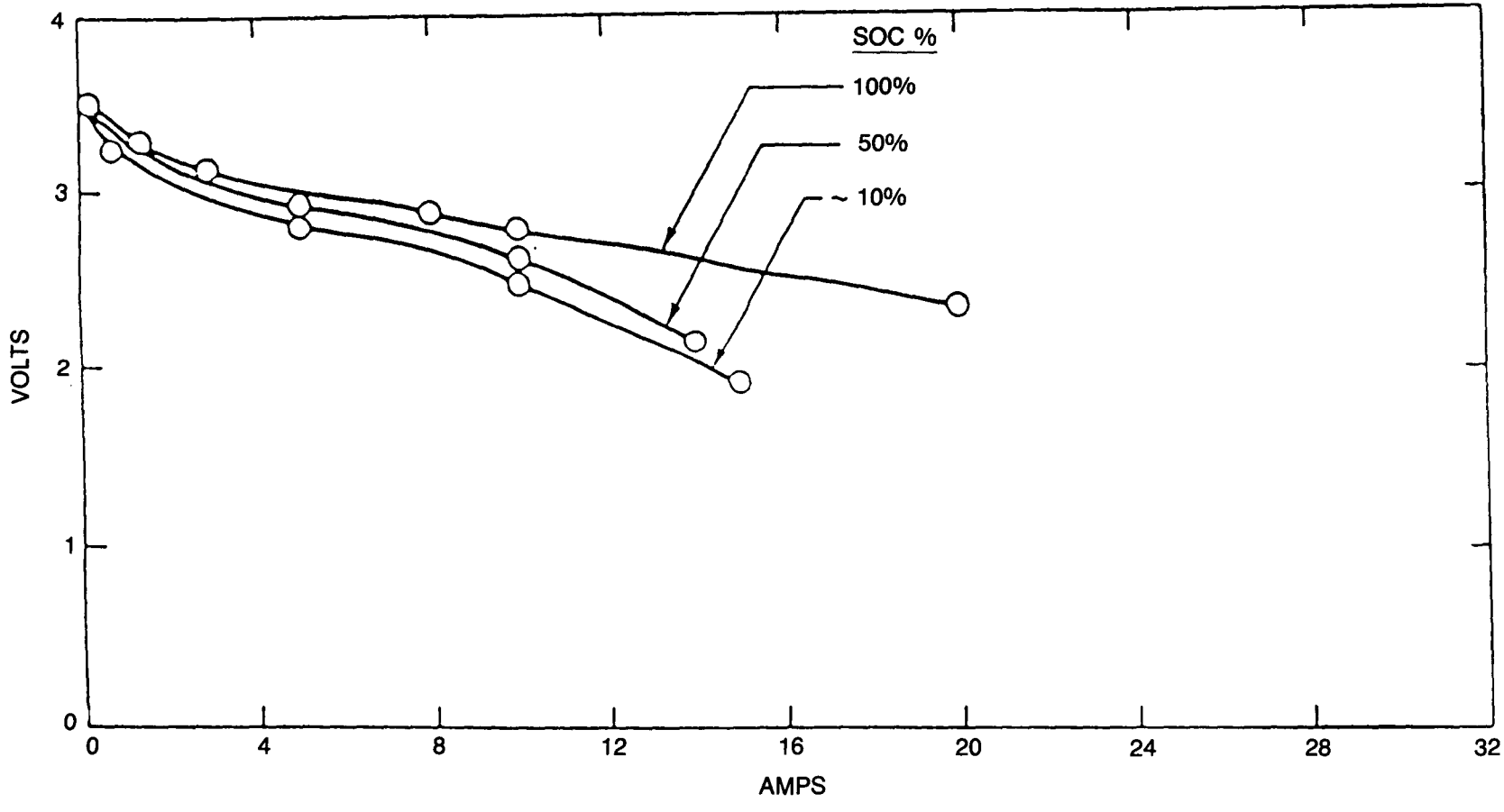

Figure 2. EFFECT OF STATE OF CHARGE ON VOLTAGE—CURRENT CHARACTERISTICS

JPL

OPTIONS	1ST GEN	2ND GEN
POS/NEG LIMITED	X	
CASE +/ CASE –	X	
ELECTROLYTE CONC		X
ELECTRODE CONFIGURATION		X
ELECTRODE CAP RATIO		X
INSIDE/OUTSIDE CARBON		X
TAB DESIGN		X
LINER MATERIALS		X

Figure 3. CELL DESIGN CONSIDERATIONS

JPL

Li	14.8 ± 0.2 Ah
$SOCl_2$	18.5 ± 0.5 Ah
CARBON (LIMITING)	13 ± 1 Ah
ELECTROLYTE	1.8 M $LiAlCl_4$ TN $SOCl_2$
SEPARATOR	MEAD 934-S FIBERGLASS SEPARATOR
CASE	304L STAINLESS STEEL CYLINDRICAL 1.36″ DIAM × 2.60″ TALL
COVER/SEAL	FUZITE
CELL WEIGHT	116 ± 1 GM

Figure 4. THE SECOND GENERATION CELL DESIGN

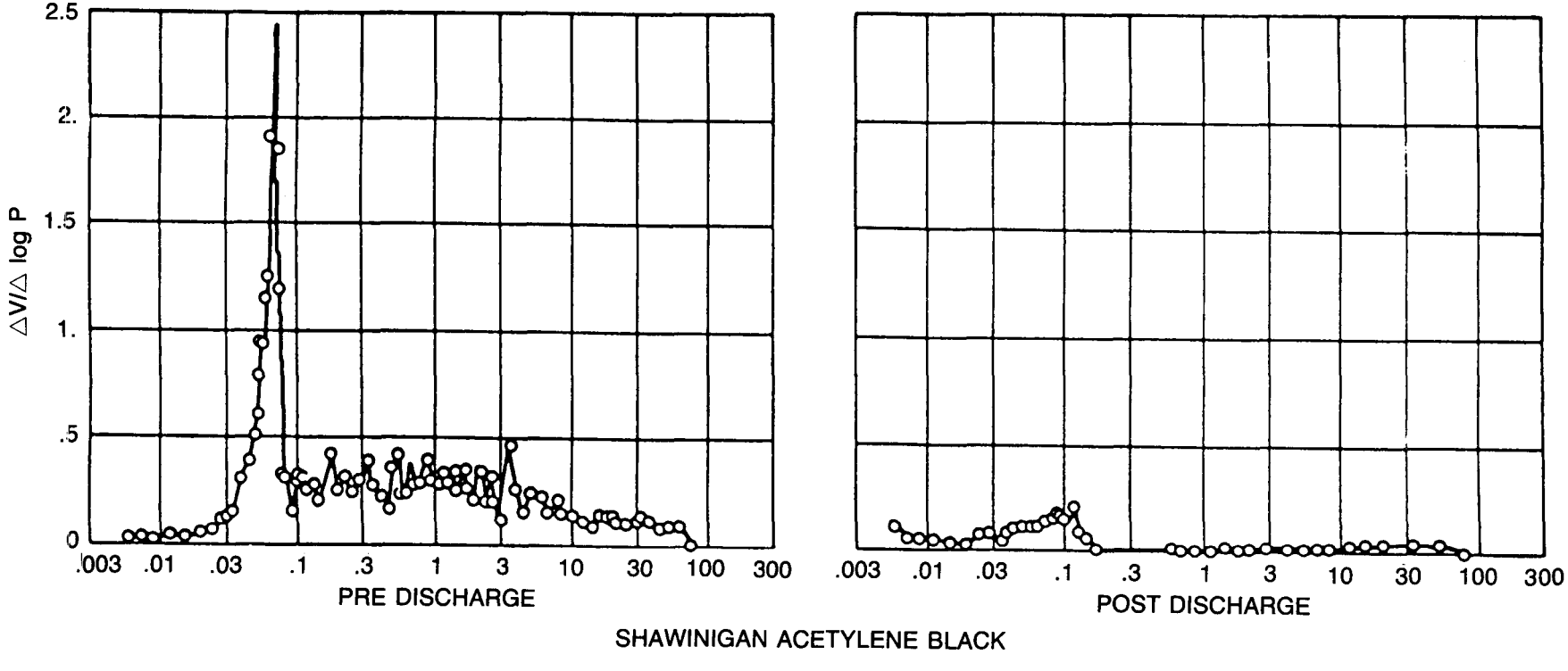

Figure 5. PORE DISTRIBUTION VS PORE DIAMETER PRE/POST LABORATORY CELL DISCHARGE

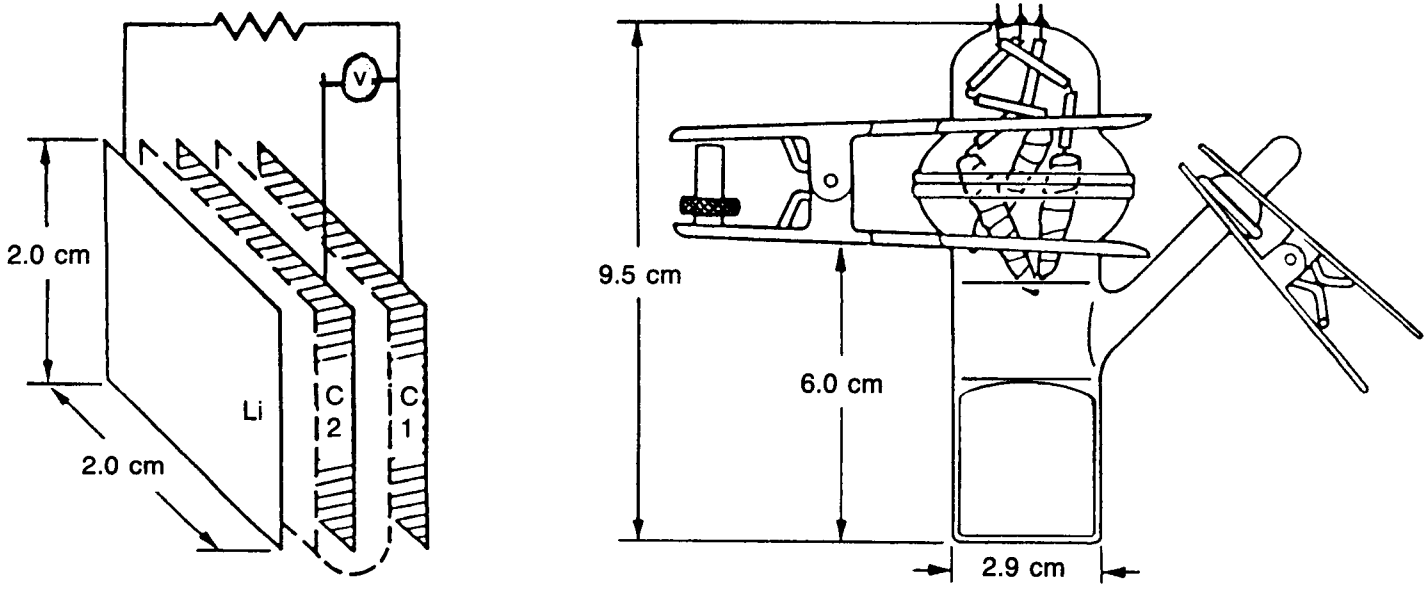

CELL DETAILS

ELECTROLYTE COMPOSITION	1.5 M $LiAlCl_4/SOCl_2$ ELECTROLYTE
ELECTROLYTE QUANTITY	3CC (FLOODED)
CARBON ELECTRODE CAPACITY (10 mA/cm^2)	~0.12 AH
LITHIUM ELECTRODE CAPACITY	~1.5 AH

Figure 6. EXPERIMENTAL CELL FOR CATHODE REVERSAL STUDIES

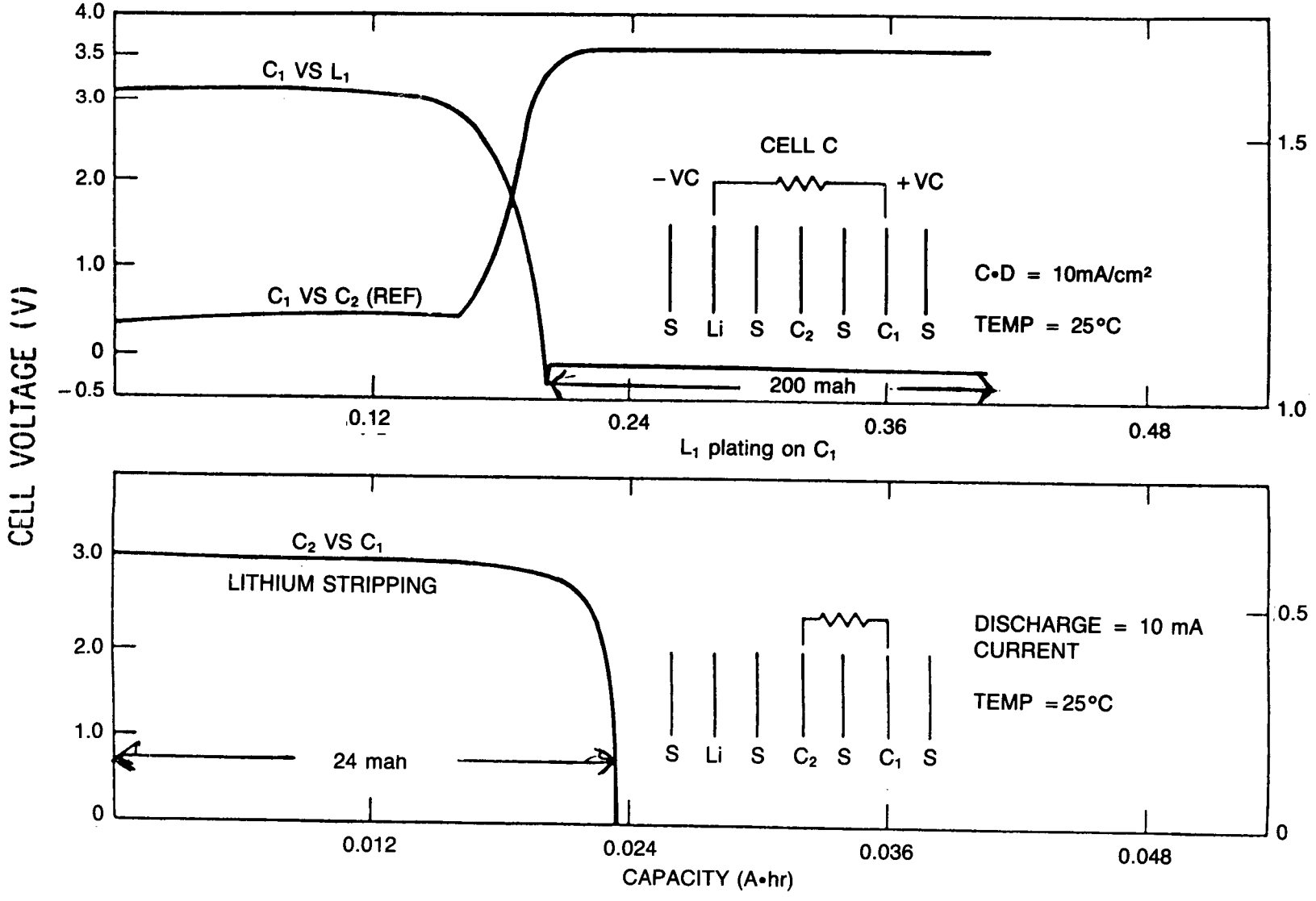

Figure 7. DISCHARGE CHARACTERISTICS OF SPECIAL CELLS

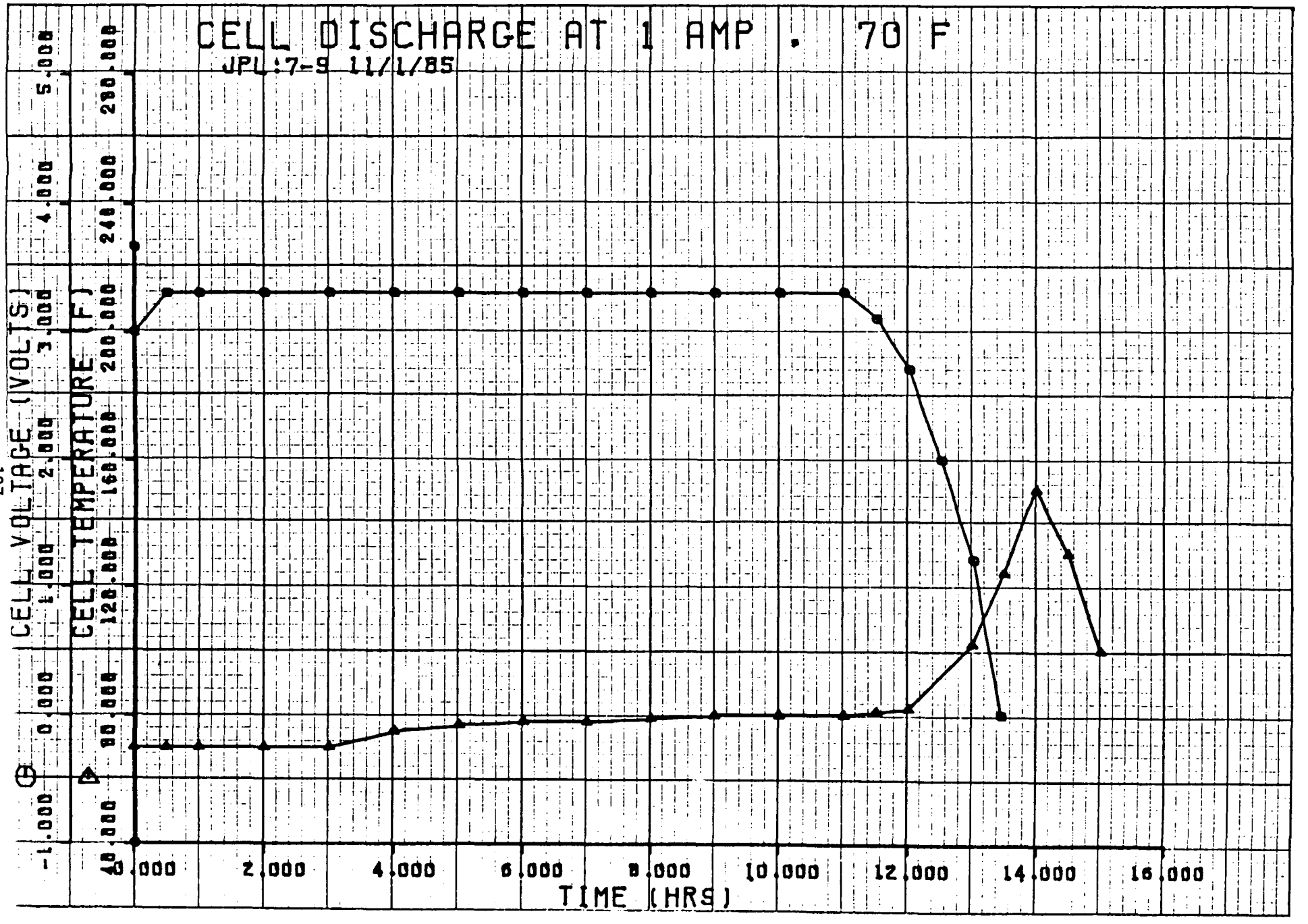

Figure 8. DISCHARGE OF JPL Li-$SOCl_2$ CELL AT 1 AMP

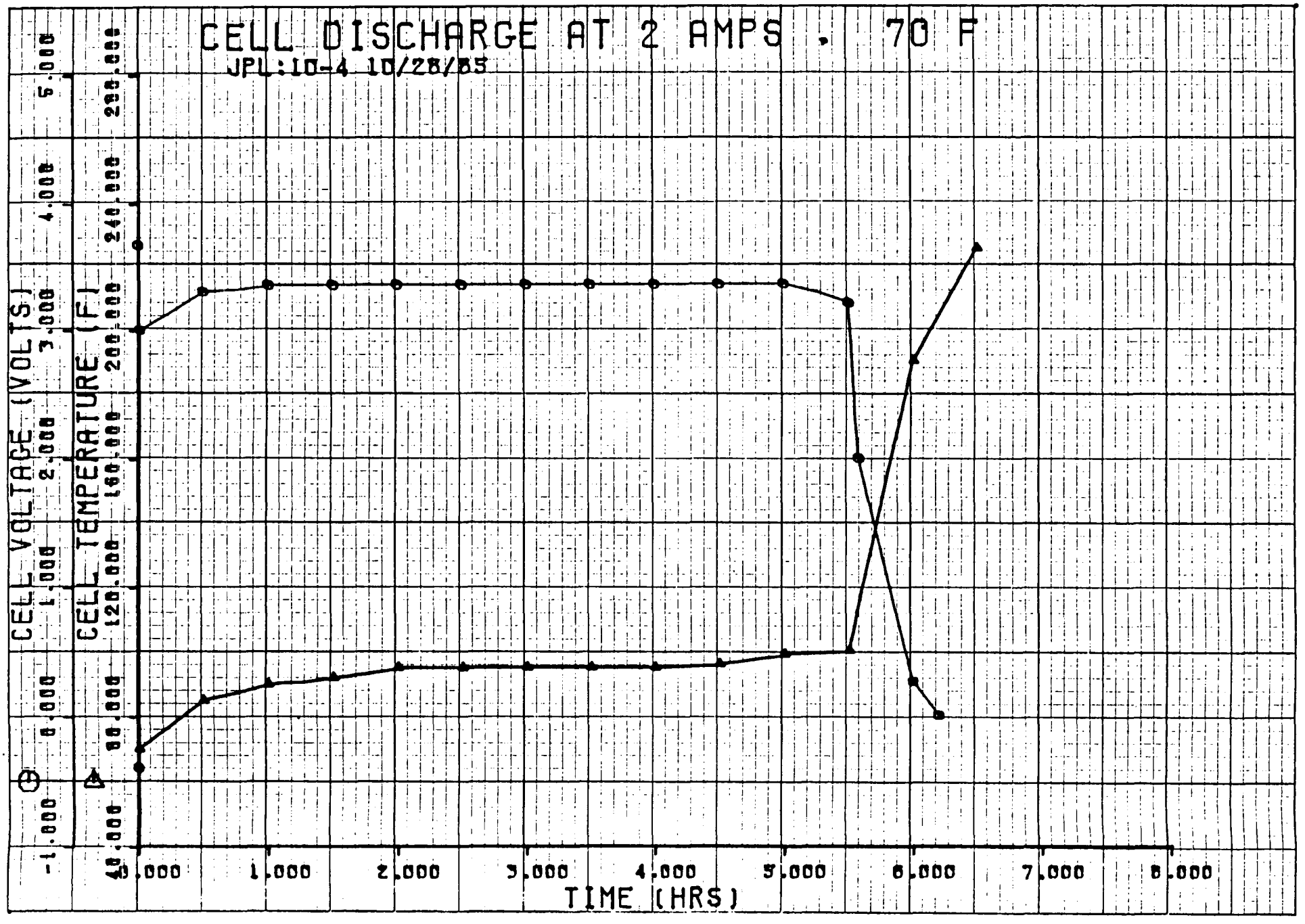

Figure 9. DISCHARGE OF JPL Li-$SOCl_2$ CELL AT 2 AMPS

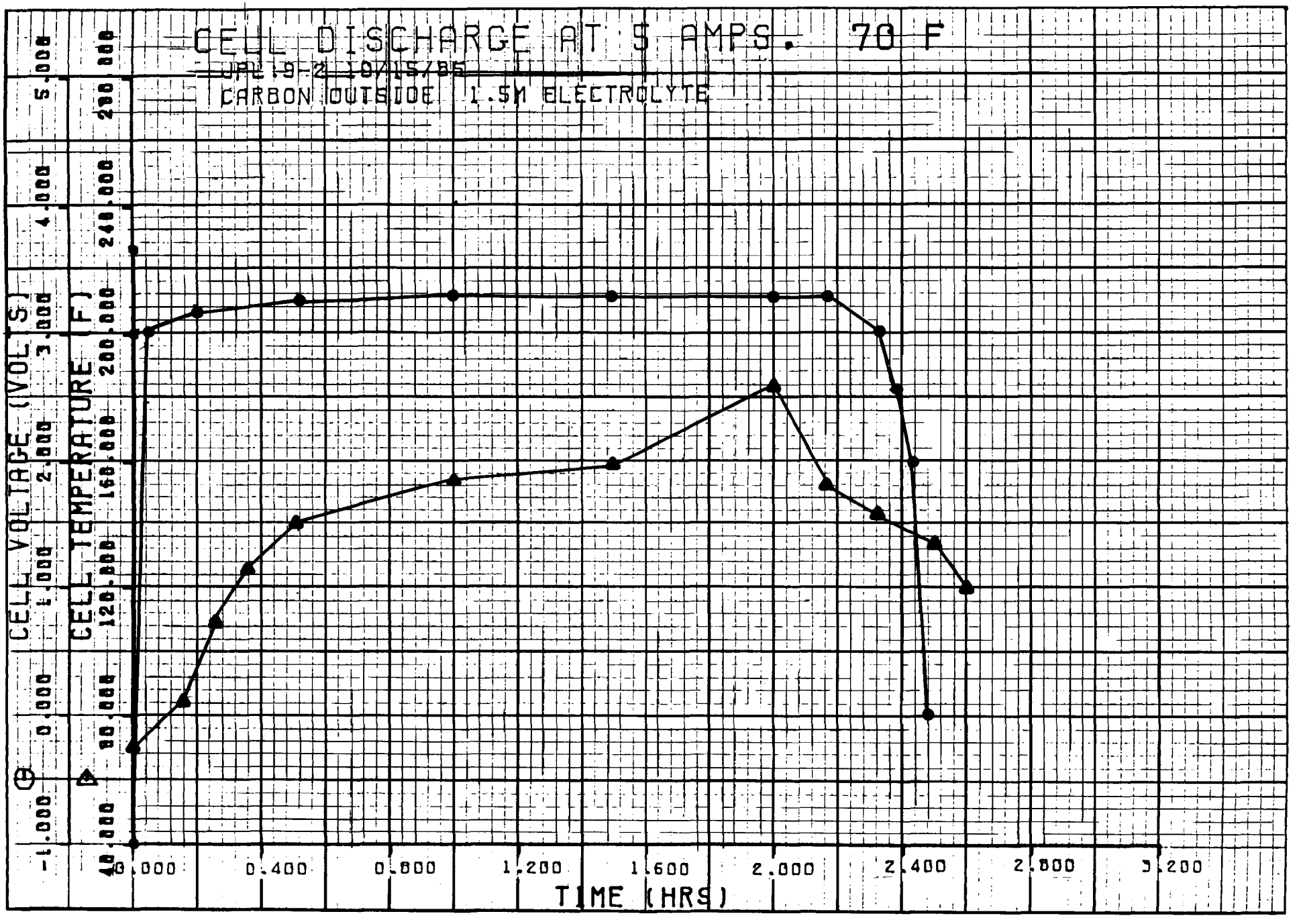

Figure 10. DISCHARGE OF JPL Li-$SOCl_2$ CELLS AT 5 AMPS

JPL

JPL CELL TEST DATA

DESIGN NO	PARAMETER	CAPACITY AH TO 2.0V		$E_{1/2}$	$T_{1/2}$ .F	$T_{2.0}$ F
6	LITHIUM OUTSIDE	5A	10.7	3.10	150	200
	1.8M	2A	11.5	3.15	90	135
	ELECTROLYTE	1A	11.8	3.40	82	95
7	CARBON OUTSIDE	5A	12.1	---	150	210
	1.8M	2A	11.7	3.25	90	125
	ELECTROLYTE	1A	12.5	3.35	78	95
8	CARBON OUTSIDE	5A	10.0	3.20	160	180
	1.0M	2A	11.4	3.20	90	125
	ELECTROLYTE	1A	12.4	3.35	78	105
9	CARBON OUTSIDE	5A	11.7	3.20	155	205
	1.5M	2A	12.0	3.25	95	142
	ELECTROLYTE	1A	12.5	3.37	78	100
10	CARBON OUTSIDE	5A	11.6	3.20	160	240
	1.8M	2A	11.1	3.28	95	150
	ELECTROLYTE	1A	12.0	3.35	78	100

Figure 11. SUMMARY OF DISCHARGE DATA OF JPL Li-$SOCl_2$ "D" CELLS

A 65 Ah RECHARGEABLE LITHIUM MOLYBDENUM DISULFIDE BATTERY

K. Brandt
Moli Energy Limited
3958 Myrtle Street
Burnaby, B.C.
Canada V5C 4G2

1. INTRODUCTION

Moli Energy Limited has, during the past seven years, developed rechargeable lithium molybdenum disulfide batteries which have a number of superior performance characteristics which include a high energy density, a high power density, and a long charge retention time. The first cell sizes developed include a "C" size cell and an "AA" size cell, whose performance characteristics have been discussed elsewhere[1].

Over the last two years, a project to demonstrate the feasibility of the scale up of this technology to a "BC" size cell with 65 Ah capacity has been undertaken. The objective of the project was to develop, build, and test a .6 kWh storage battery consisting of 6 "BC" cells in series.

2. BATTERY DESIGN

The design of the "BC" cell was based on concepts developed for "C" size cells. Both cell sizes were of a jelly roll type construction and the scale up was achieved by increasing the electrode area by a factor of 22 to a total of 16,700 cm^2 without changing the thickness of the electrodes. The capacity was calculated to 65 Ah using a linear scale factor.

Figure 1 shows an exploded view of the "BC" cell design. The anode was a 125 μm thick lithium foil connected with six nickel tabs to the negative terminal. These tabs were positioned along the anode strip at equidistant intervals. The cathode consisted of the cathode powder bonded to a metal foil current collector which was connected to the positive terminal with six nickel tabs. A glass-to-metal seal was used to insulate the positive terminal from the case. The two electrodes were separated by a microporous polypropylene separator. The separator and the porous cathode were impregnated with an electrolyte consisting of a 1 molar solution of $LiAsF_6$ in a mixture of organic solvents. The cell case was hermetic with a safety vent in the cell bottom.

The .6 kWh battery consisted of six cells connected in series and held together by two rigid plated tied together with bolts. The battery hardware was not optimized with respect to weight or volume. Table 1 gives the specifications for this battery.

3. SINGLE CELL PERFORMANCE TESTING

Tests on single cells were performed after recharging at 21°C with a constant current of 5 A to a cell voltage of 2.4 V. For some tests, cells were charged to a voltage of 2.6 V, a condition which will be referred to as "supercharged". The discharges were performed at constant current and the cell voltage was used to determine the endpoint. Figure 2 shows the voltage profile for a single cell cycle consisting of a charge half cycle followed by a discharge at 15 A to a cell voltage of 1.3 V. The shape of the voltage profiles is characteristic of the Li_xMoS_2 intercalation compound used in these batteries[2].

Figure 3 shows the capacity as a function of cycle number for two cells cycled under different conditions. Cell #001 was supercharged and then discharged to 1.1 V, Cell #002 was charged under standard conditions and then discharged to 1.3 V. The first cell achieved a first cycle capacity of 66 Ah, at 15 A. This capacity is slightly higher than the nominal capacity. The second cell achieved a first cycle capacity of 42 Ah. These capacities are approximately equal to the values expected from a linear scale-up of the "C" cell performance. Both tests were terminated voluntarily, Cell #002 after achieving 107 cycles at an average capacity of 32.5 Ah.

The impedance of the "BC" cell was determined over a wide frequency range using a frequency response analyzer. The results are displayed in Figure 4 in the form of a Cole-Cole Plot. The impedance at a frequency of 1 kHz is approximately 4.6 m Ω. This measured value is approximately double the value calculated from "C" cell measurements using the linear scale factor of 22. This discrepancy is due to the relatively large resistance of the electrode terminals and the connections of the electrodes to the terminals. For frequencies higher than 1 kHz the cell impedance is dominated by an inductance which is due to the wound nature of the electrode assembly. For frequencies below 1 kHz, the impedance of the electrochemical interfaces and the mass transport of ions in the electrolyte determine the shape of the plot[3].

4. BATTERY PERFORMANCE TESTING

Performance testing of the 6 cell battery was conducted under conditions similar to the cell performance testing with the battery voltage being used to determine the endpoints of charge and discharge. No attempt was made to equalize the state of charge between individual cells once the testing began. Figure 5 gives the realized battery capacity as a

function of cycle number. With exemption of the special tests performed around cycle 30, the battery was cycled between 14.4 V and 7.8 V. These voltages correspond to a single cell voltage ranging from 2.4 V to 1.3 V. The average energy delivered by the battery was 360 Wh per cycle with an average capacity of 33.5 Ah. The test was terminated voluntarily at cycle 110. A comparison with the single cell cycle test (Figure 3) shows no difference between single cell cycle life and battery cycle life under these conditions.

The sustained power capability of the battery was assessed by discharging the battery to a fixed voltage limit at various currents.

Figure 6 shows the realized capacity as a function of the drain current for three different temperatures. Prior to the discharges, the battery was given a standard charge at 21°C. Cutoff voltage or discharge was 1.3 V per cell. At 20°C and 0°C the battery delivered about 50% of its low current capacity at a 50 A rate. At -10°C, the rate capability is reduced significantly. The average power delivered during the 50 A discharge at room temperature was 510 W.

The realized capacity of the battery can be increased for all drain rates by supercharging and by using a discharge cutoff of 1.1 V per cell. Figure 7 shows the realized capacity for the battery at a temperature of 20°C under these conditions. The capacity increase is about 58% compared to the condition represented in Figure 6. The energy delivered by the battery at the lowest rate was 686 Wh corresponding to a gravimetric energy density of 94 Wh/kg.

The results presented in Figures 6 and 7 are a measure of the sustained power capability of the battery. The peak power capability of a supercharged battery was determined by discharging the batteries at various rates for a duration of 5s. After each discharge, the battery was rested on open circuit for about 1 minute. Figure 8 shows the power output at the end of each discharge pulse as a function of the discharge current. The peak power was 932 W which corresponds to a peak power density of 128 W/kg.

5. SUMMARY AND CONCLUSION

The results of the "BC" battery performance testing can be best summarized in a Ragone Plot which shows the relationship between power density and energy density (Figure 9). A comparison with the Ragone Plot for a "C" cell shows the effects in scaling. At lower power densities, the larger cells show an increased energy density due to a reduction of the fraction of the non-active material of the total cell

weight. However, the relatively large resistive losses in the current carrying elements of the "BC" cells cause a significant reduction in the power capability.

The cycle life of this battery is in excess of 100 cycles. No reduction in battery performance relative to cell performance which might be caused by capacity mismatch or charge imbalance between cells was observed.

This analysis shows that substantial improvements to the battery performance in the area of power density are possible by improvements to the cell design. Peak power densities of the order of 200 Wkg^{-1} should be obtainable. Initial tests of a new generation of "BC" cells presently under development that incorporates improved current collectors support this extrapolation.

Improvements in energy density, however, will only be minor unless the lithium insertive capacity of the cathode can be improved. The maximum energy density of batteries using current cathode technology is 100 Wh/kg. Improved cathodes will be used in the future to break this barrier.

REFERENCES

(1) K. Brandt, J.A.R. Stiles, The 1984 Goddard Space Flight Center Workshop, NASA CP, 1985

(2) R.R. Haering, J.A.R. Stiles, K. Brandt, U.S. Patent 4,224,390, September 23, 1980

(3) F.C. Laman, J.A.R. Stiles, R.J. Shank, K. Brandt, J. Power Sources, 14, p.p. 201-217, 1984

TABLE 1: Specifications for 6 Cell "BC" Battery

Battery Dimension	:	25 cm x 16 cm x 21 cm
Battery Weight	:	7.3 kg
Nominal Battery Voltage	:	10.8 V
Nominal Battery Capacity	:	65 Ah
Charging	:	5 A Constant Current
Voltage Cut-off on Charging (Standard Charge)	:	14.4 V

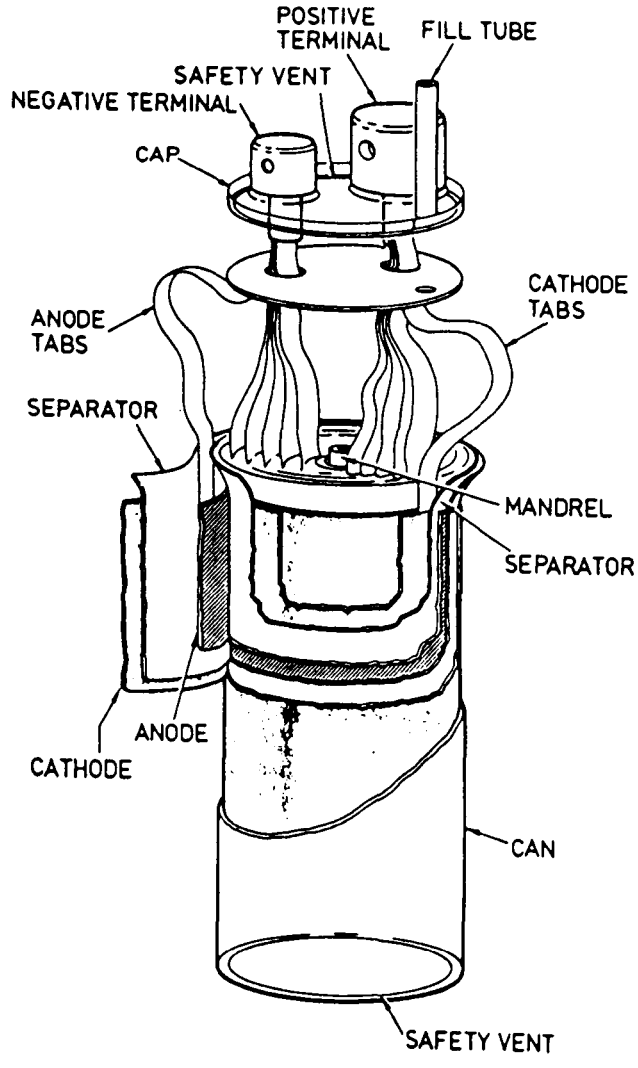

Figure 1. EXPLODED VIEW OF A "BC" CELL

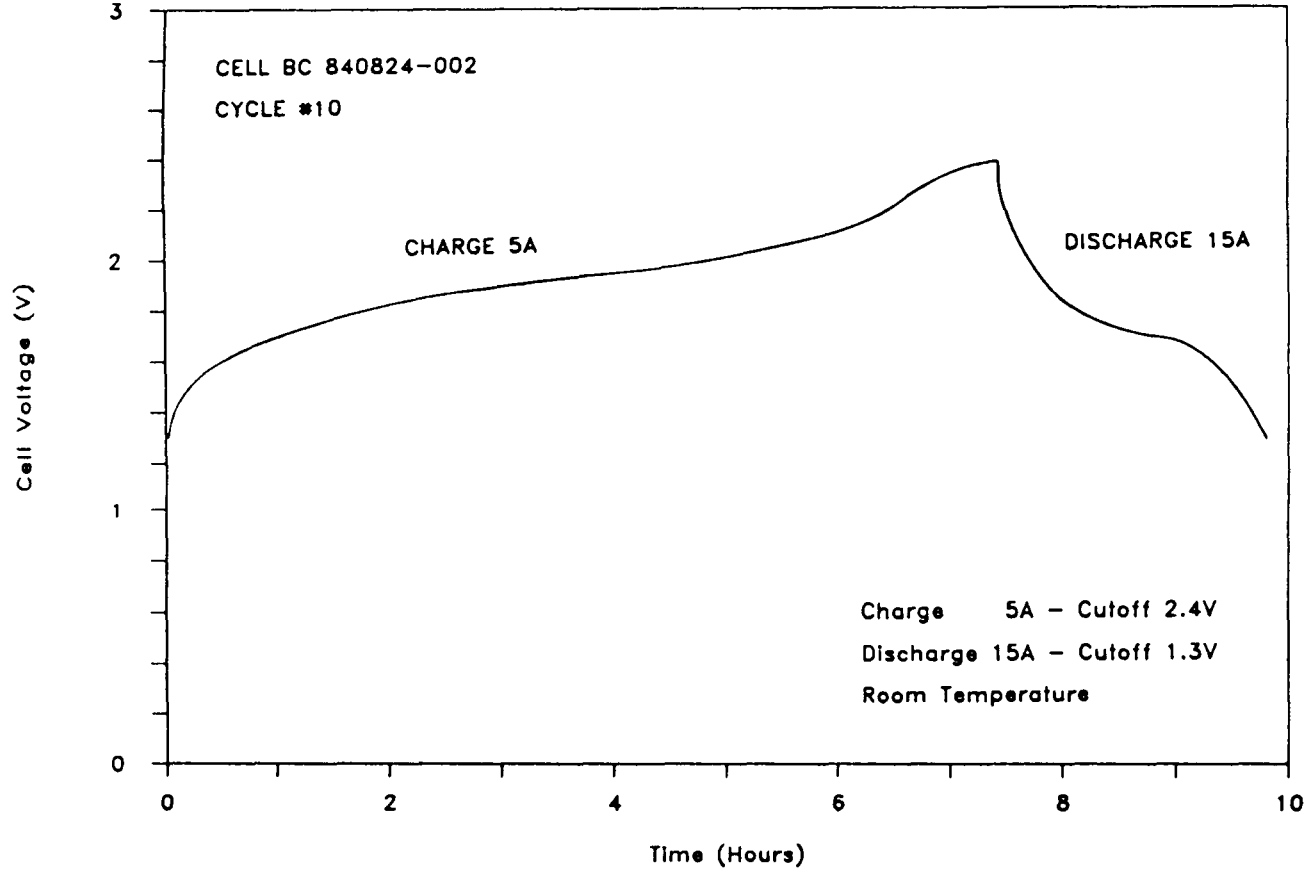

Figure 2. CHARGE AND DISCHARGE VOLTAGE PROFILE OF A "BC" CELL
CHARGE 5 A, CUTOFF 2.4 V
DISCHARGE 15 A, CUTOFF 1.3 V

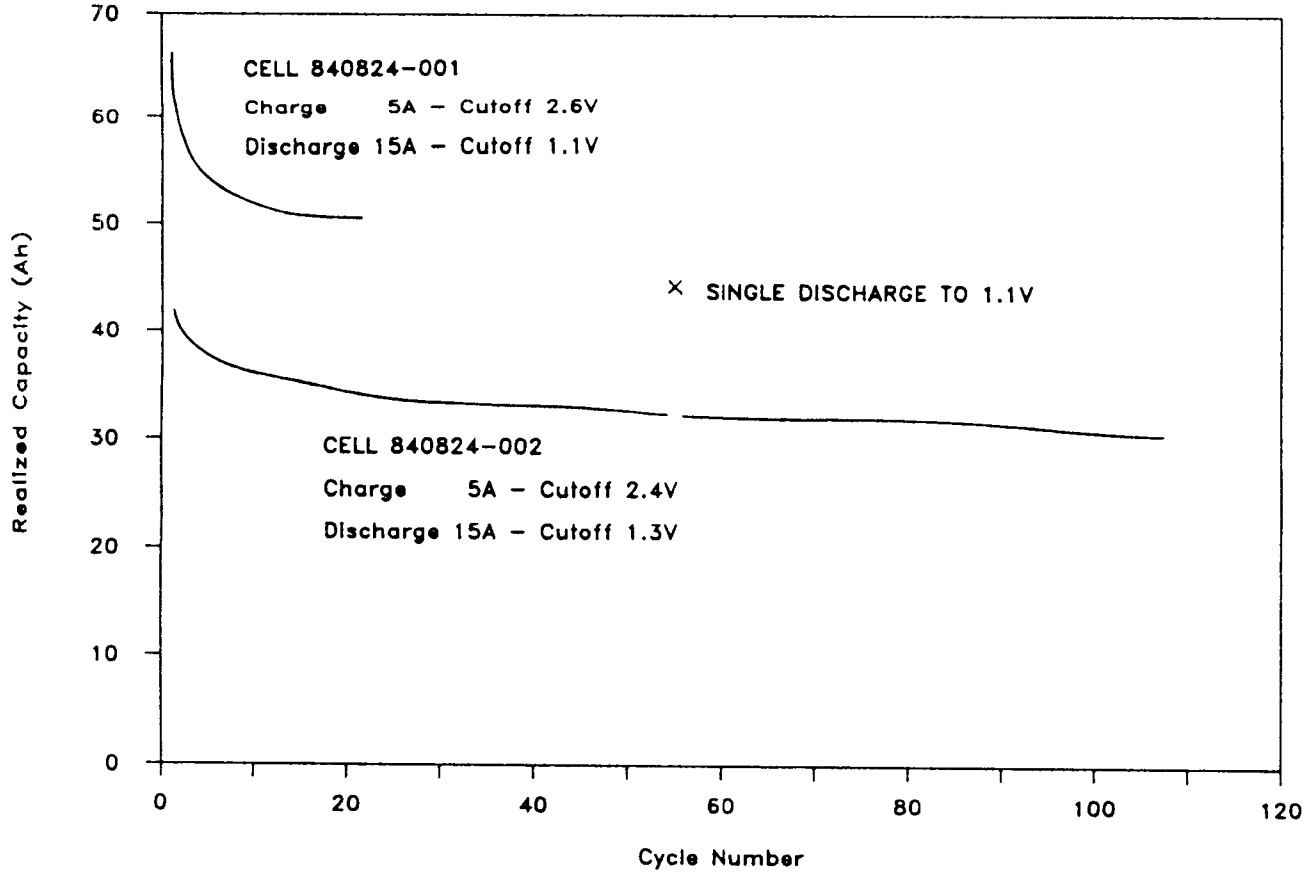

Figure 3. CYCLE LIFE PLOTS FOR TWO "BC" CELLS
CELL 001: CHARGE 5 A, CUTOFF 2.6 V
DISCHARGE 15A, CUTOFF 1.1 V
CELL 002: CHARGE 5 A, CUTOFF 2.4 V
DISCHARGE 15 A, CUTOFF 1.3 V

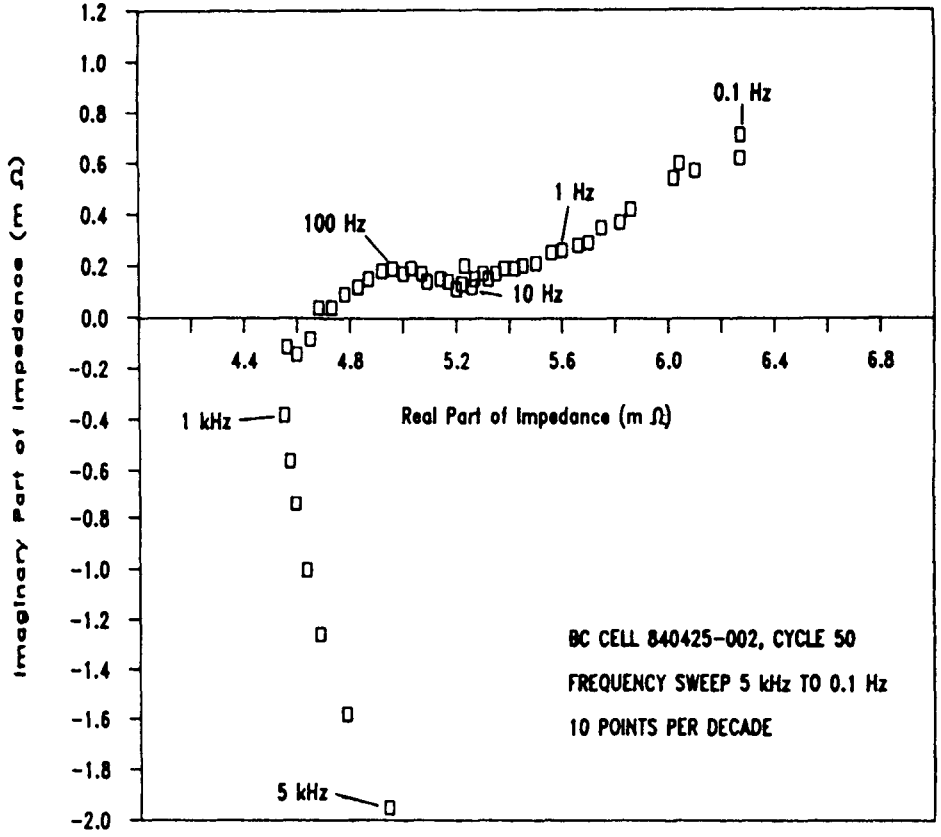

Figure 4. COLE-COLE PLOT OF THE IMPEDANCE OF A "BC" CELL

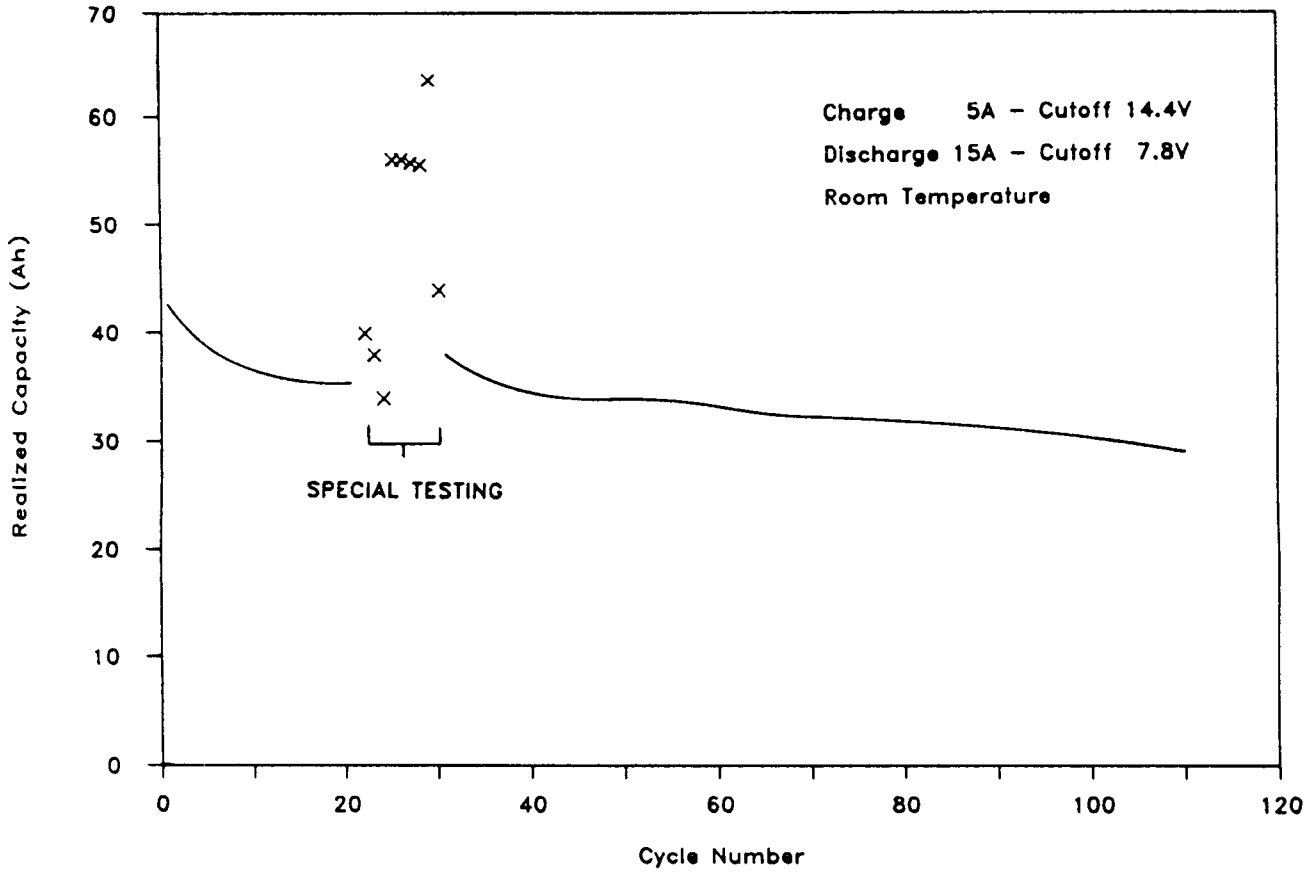

Figure 5. CYCLE LIFE PLOT FOR A 6 CELL "BC" BATTERY. CONDITIONS FOR ALL CYCLES EXCEPT THOSE MARKED SPECIAL TESTING:
CHARGE 5 A, CUTOFF 14.4 V
DISCHARGE 15 A, CUTOFF 7.8 V

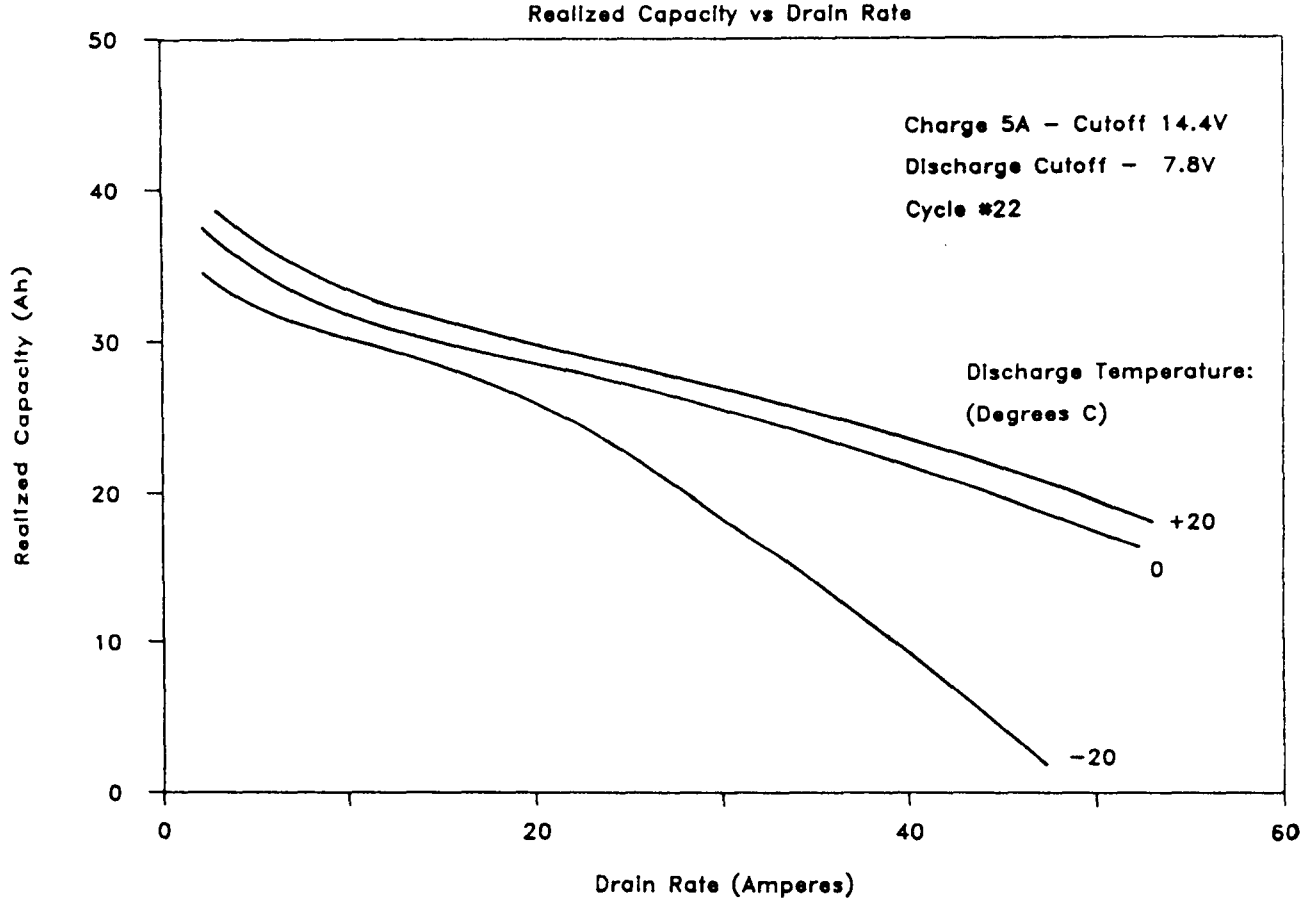

Figure 6. REALIZED CAPACITY AS A FUNCTION OF DRAIN RATE FOR A 6 CELL "BC" BATTERY:
CHARGE 5 A, CUTOFF 14.4 V
DISCHARGE 15 A, CUTOFF 7.8 V

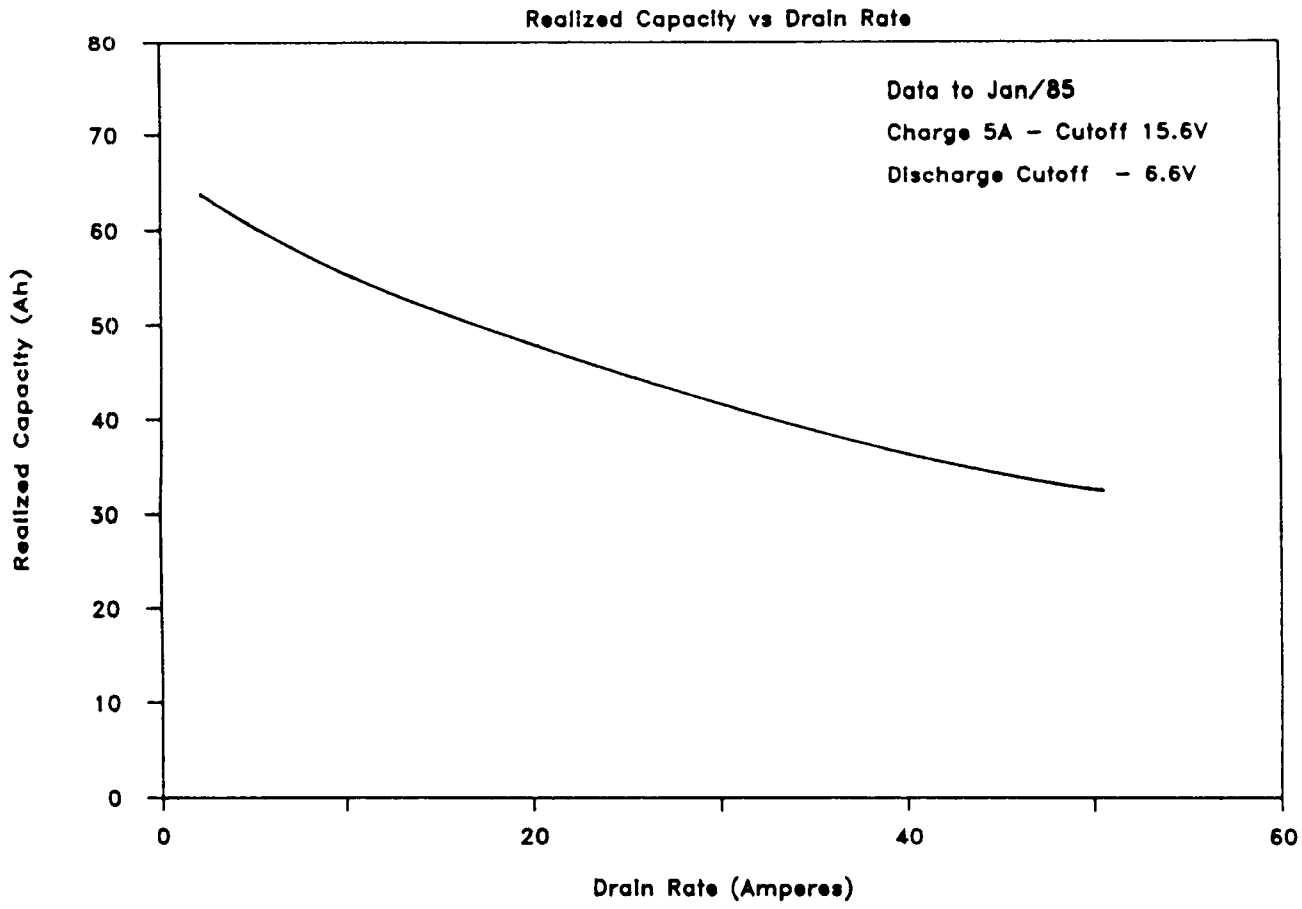

Figure 7. REALIZED CAPACITY AS A FUNCTION OF DRAIN RATE FOR A SUPERCHARGED 6 CELL "BC" BATTERY.

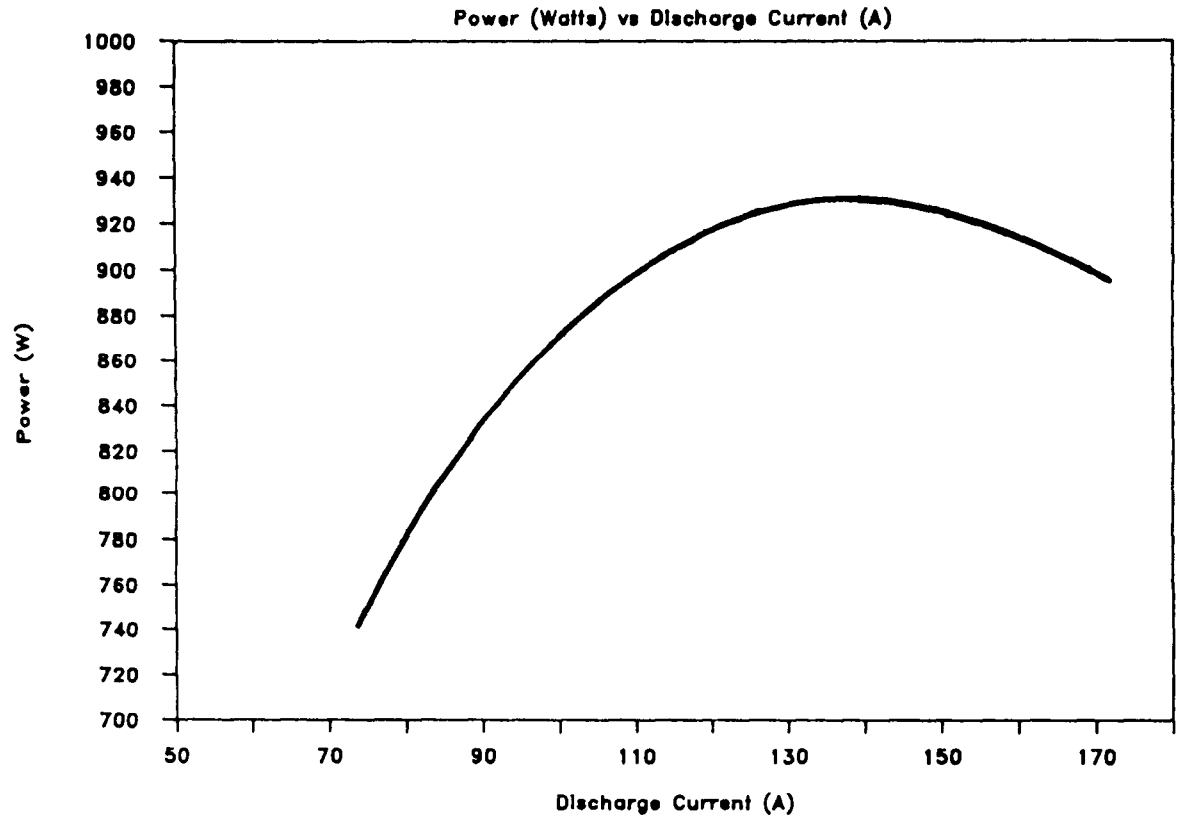

Figure 8. POWER OUTPUT OF A 6 CELL "BC" BATTERY FOR VARIOUS PULSE CURRENTS. PULSE DURATION 5 SEC.

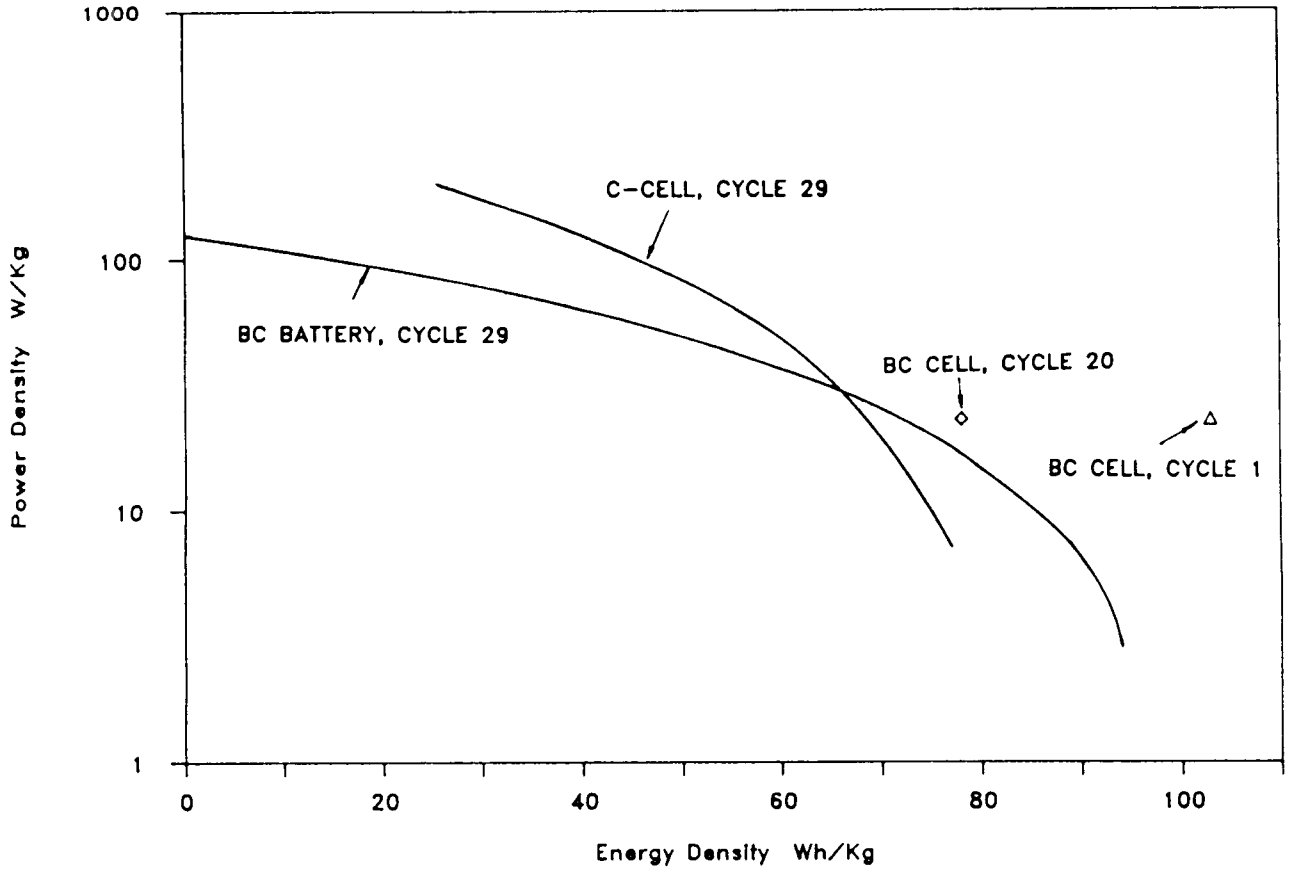

Figure 9. RAGONE PLOT FOR A 6 CELL "BC" BATTERY, SINGLE "BC" CELLS, AND "C" CELLS

EXAMINATION OF DESIGN OPTIONS FOR 35 Ah AMBIENT TEMPERATURE Li-TiS_2 CELLS

D.H. Shen, S. Subba Rao, S.P.S. Yen, and R.B. Somoano

Jet Propulsion Laboratory
California Institute of Technology
Pasadena, California

The Jet Propulsion Laboratory is actively engaged in the development of ambient temperature rechargeable lithium cells for future NASA GEO missions. The Program goals are given in the Figure 1.

To achieve these ambitious goals, we have examined Li-TiS_2, Li-MoS_3 and Li-V_6O_{13} systems in detail. Among these three, the Li-TiS_2 system has shown the longest life cycle and highest rate capability. Experimental Li-TiS_2 batteries (10.5V, 0.4Ah) developed in-house have completed eight simulated and accelerated GEO seasons successfully. Evaluation of these batteries is being carried out at Rockwell International, and some of these results were reported by B. Otzinger in the 1984 Battery Workshop at GSFC. In view of these encouraging results, we have examined the design options for a scaled-up Li-TiS_2 cell. It is hoped that the results of these studies will provide guidelines for prioritizing the research efforts and guiding the selection of optimized materials. In our present study, we have examined designs for 35 Ah Li-TiS_2 cells because present day GEO synchronous satellites are powered by batteries of 35 Ah capacity. We have developed a computer program to evaluate the influence of various design parameters on the specific energy and the rate capability of the cells.

Figure 2 summarizes the important design parameters that have been considered in the present study. Some of the issues that have not been considered are thermal design parameters, utilization of the lithium

electrode, and the degradation of the electrolyte. We have also restricted ourselves to the prismatic cell configuration.

The program details are summarized in Figure 3. To date, no engineering database exists in the literature for the utilization of TiS_2 cathodes of different thicknesses and porosities at various current densities. We have created a database for the execution of the program, based on the limited published, and in-house, experimental results. Since the cells are required to operate at the C/2 rate, we considered cathodes in the thickness range of 20 to 40 mil. An anode to cathode capacity ratio of 6:1 has been used in the present studies, as excess of lithium has minimum influence on cell energy density. The various materials that have been considered for the cell case and cover are stainless steel (SS), titanium (Ti), carbon composite (C) and polypropylyne (PP). A thickness of 30 mil is considered for stainless steel, titanium, and carbon composite and 120 mil is considered for polypropylyne.

Figure 4 shows the dependence of specific energy on the cathode thickness. Cathodes of 25 mil thickness provide highest energy density for cells that are required to operate at C/2 rate. All further analysis is based on cathodes of 25 mil thickness.

Figure 5 gives the number of cathodes required for different R ratios (R represents the height to width ratio of the electrode). As can be seen, the number of cathodes required increases with decreasing plate width and R ratio. Current distribution, heat management and ease of fabrication are key issues in selecting the plate width, height-to-width ratio, and the plate number. One needs to make a judicious choice of these parameters, keeping in view the performance requirements and fabrication limitations. For our further analysis, we have chosen a cathode width of 12 cm and height-to-width ratio of 1.5.

Figure 6 gives the specific energies that can be achieved, with different can and grid materials. Aluminum grids are also considered for cathodes current collectors. They are not considered for anodes because of the reactivity of Al with Li. Ti/Al, C/Al, and PP/Al materials all look promising in terms of energy density. While Ti cans are lighter than S.S, they are more expensive. Also, C cases are strong and lightweight, but their chemical and electrochemical stability with the active components needs to be determined. Polypropylene cans are cheap, but in view of their poor mechanical properties, thicknesses of greater than 100 mil are needed for cell cans. In view of their poor thermal characteristics, it may not be the material of choice for space applications.

The details of the cell weight budget (cells with stainless steel can) are given in Figure 7. The can contributes the dominant fraction to the weight budget. Among the active materials, the contribution of the anode active material is the lowest. Grid contribution is more than lithium itself (with respect to weight).

In summary, a specific energy of 80 to 100 Wh/kg at C/2 for 35 Ah Li-TiS_2 cells is feasible. This calls for the use of advanced hardware materials. Cathode widths greater than 10 cm width at 25 mil thickness are needed for 35 Ah cells operating at C/2. Development of an engineering database for the utilization of lithium and TiS_2 electrodes is needed to verify, and make further improvements in cell design. Other cell configurations and active materials will be considered in the future.

ACKNOWLEDGEMENTS

One of the authors, S. Subba Rao, acknowledges the National Research Council for providing him the Research Associateship during this work.

The research described in this paper was performed by the Jet Propulsion Laboratory, California Institute of Technology, under contract with the National Aeronautics and Space Administration.

JPL

- DEMONSTRATE FEASIBILITY OF AMBIENT TEMPERATURE SECONDARY LITHIUM CELLS FOR GEO APPLICATIONS BY FY'89
- TARGETS
  - ≥ 100 WH/KG
  - 10 YEAR LIFE
  - 1000 CYCLES
  - SAFE

Figure 1. NASA SECONDARY LITHIUM BATTERY PROGRAM GOAL

JPL

CATHODE	ANODE	ELECTROLYTE	SEPARATOR	GRID	CAN
• CURRENT DENSITY	• NEGATIVE TO POSITIVE RATIO	• COMPOSITION	• MATERIAL	• MATERIAL	• MATERIAL
• THICKNESS	• NUMBER	• DENSITY	• POROSITY	• TYPE	• THICKNESS
• WIDTH	• Li FOIL THICKNESS	• QUANTITY	• INTER-ELECTRODE SPACING		• SEAL
• HEIGHT TO WIDTH RATIO			• THICKNESS		• OVERHEAD SPACE
• NUMBER			• WEIGHT		
• POROSITY					
• WEIGHT					
• CAPACITY					

Figure 2. DESIGN PARAMETERS

JPL

INPUTS

- CAPACITY
- OVER RATING
- DISCHARGE CURRENT

CONSTANTS/VARIBLES

- ANODE TO CATHODE CAPACITY RATIO: 6 TO 1
- NO. OF ANODE = NO. OF CATHODE + 1
- PLATE WIDTH: 7 TO 14 CM
- HEIGHT TO WIDTH RATIO: 0.8 TO 2
- CATHODE THICKNESS: 20 TO 40 MIL
- GRID MATERIAL: NI, AL
- CASE MATERIAL: S.S. TI, C, PP
- SEAL: CERAMIC/ZIGLER

DATA BASE

CURRENT DENSITY (mA/cm^2)	UTILIZATION*
1	0.85
2	0.85
3	0.76
4	0.53

*FOR 25 MIL CATHODE THICKNESS

OUTPUT

- DESIGN CAPACITY
- ENERGY DENSITY
- CATHODE NO. AND DIMENSION
- ANODE NO. AND DIMENSION
- GRID DETAILS
- ELECTROLYTE QUANTITY
- SEPARATOR DETAILS
- CAN DIMENSIONS
- COMPONENTS WEIGHT BUDGET

Figure 3. PROGRAM DETAILS

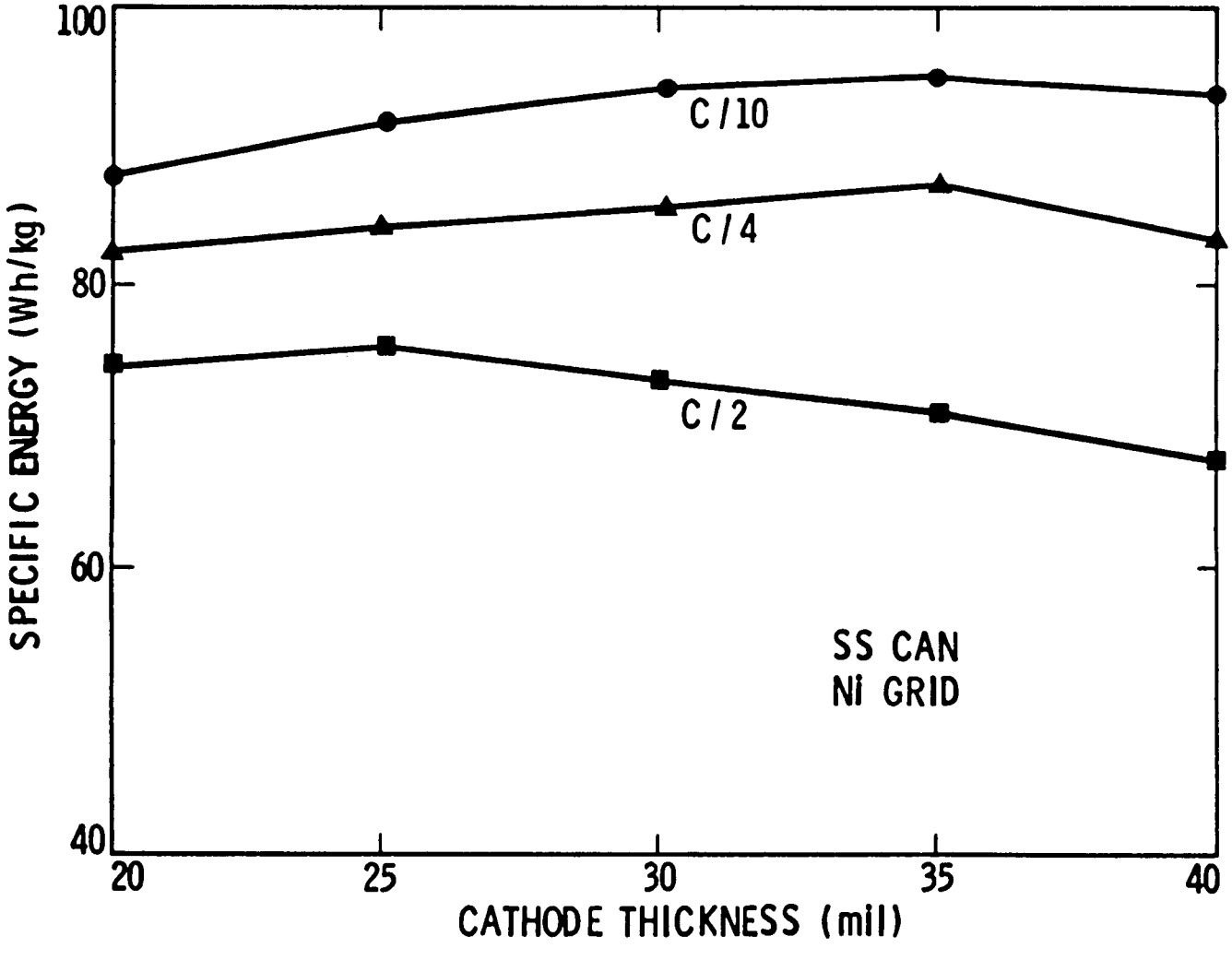

Figure 4. DEPENDENCE OF SPECIFIC ENERGY ON CATHODE THICKNESS OF A Li-TiS_2 CELL FOR VARIOUS DISCHARGE RATES

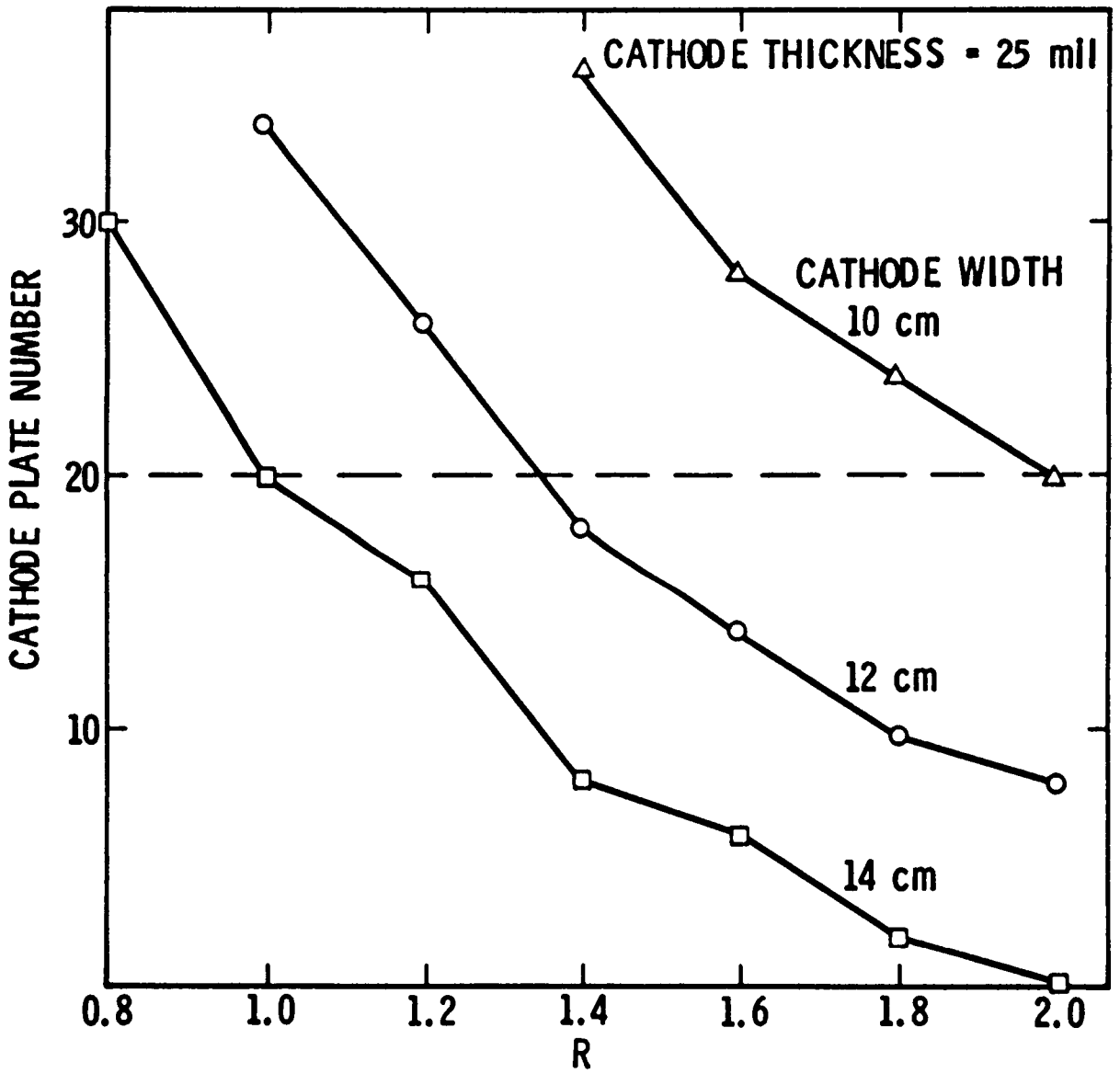

Figure 5. DEPENDENCE OF CATHODE PLATE NUMBER ON CATHODE HEIGHT TO WIDTH RATIO, R

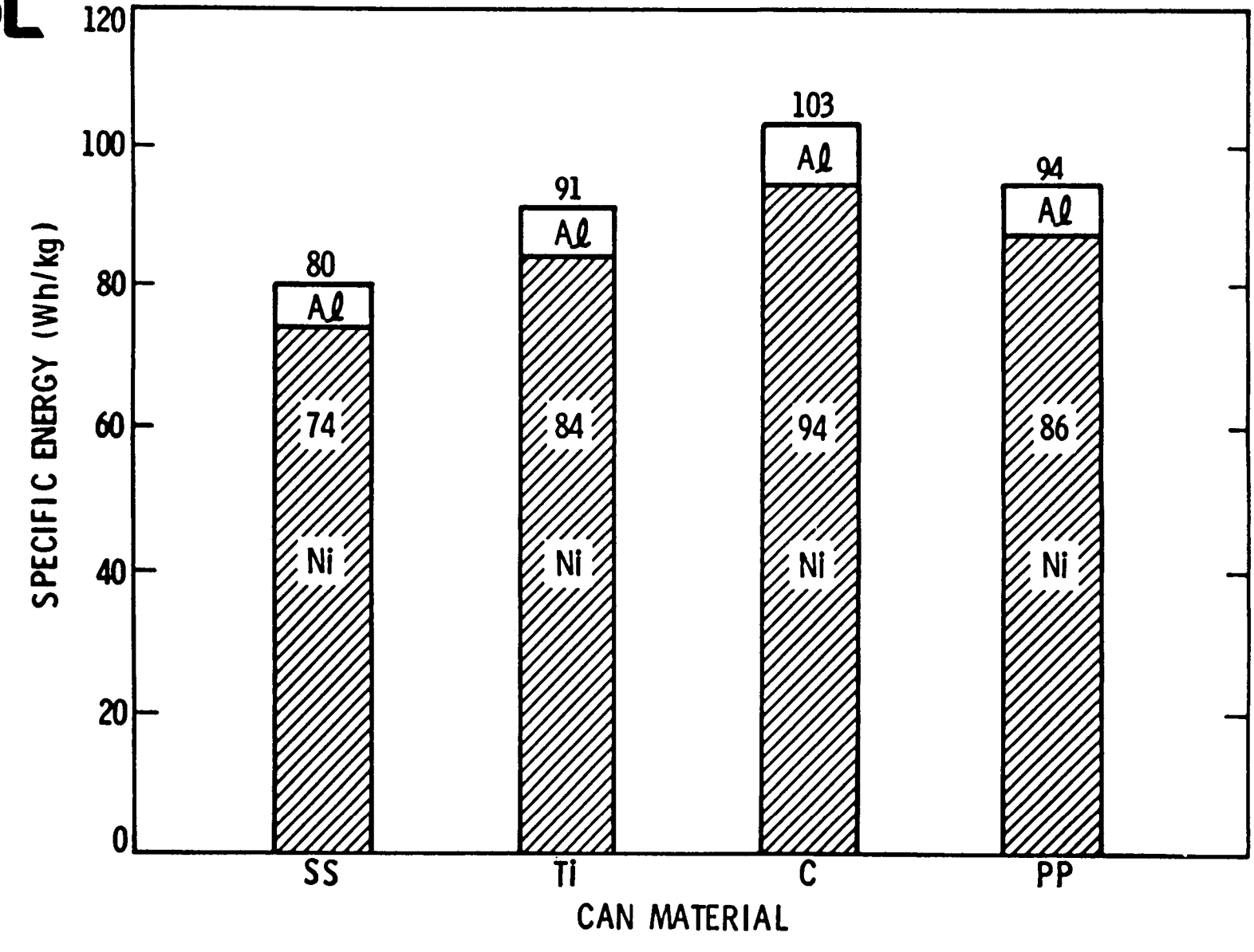

Figure 6. DEPENDENCE OF SPECIFIC ENERGY ON HARDWARE MATERIALS FOR A 35 Ah Li-TiS_2 CELL

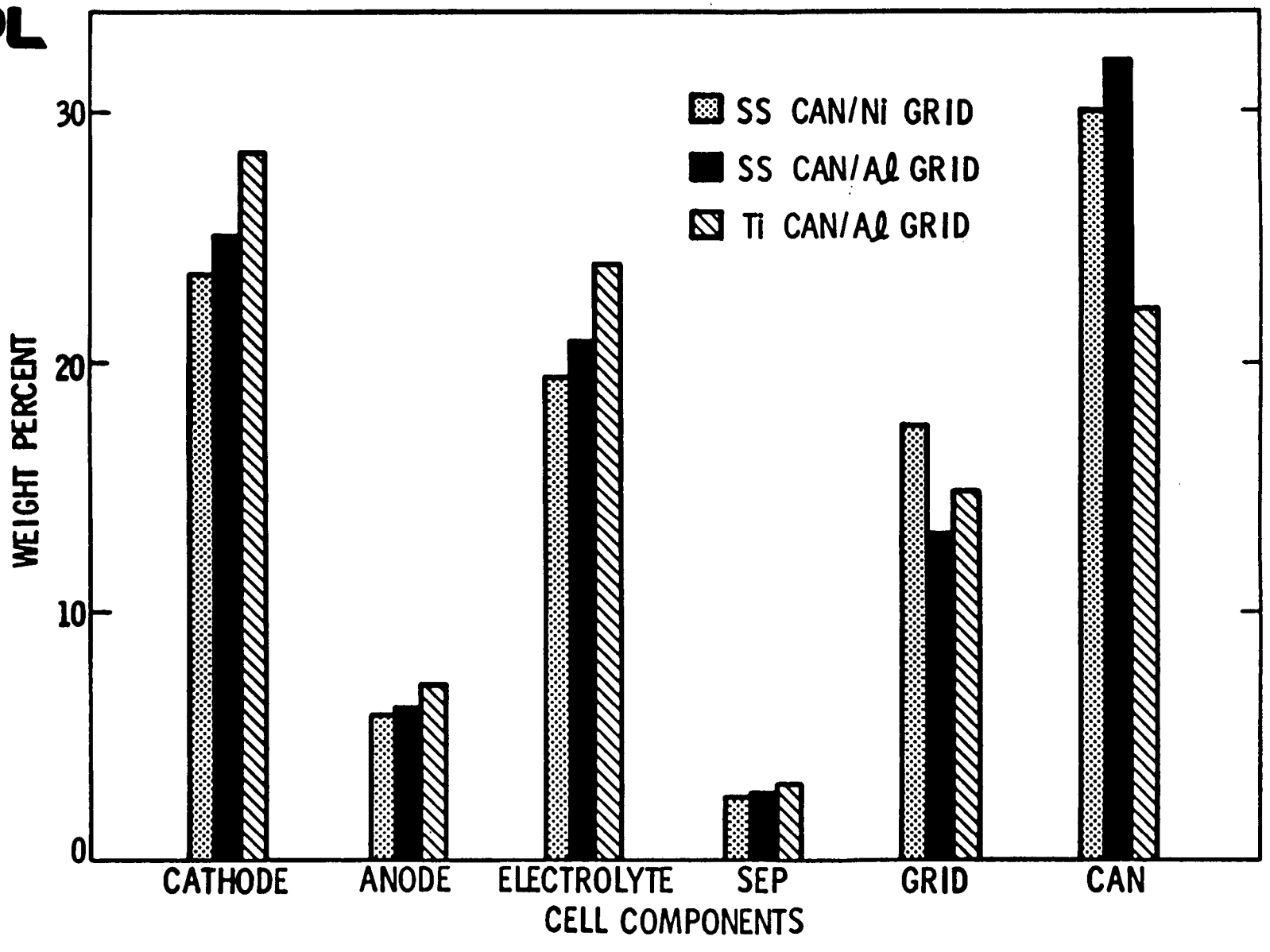

Figure 7. Li-TiS_2 CELL WEIGHT BUDGET

SESSION III

TOPIC: NICKEL-CADMIUM DESIGN EVALUATION
AND COMPONENT TESTING
Chairman: G. W. Morrow, NASA/GSFC

QUALIFICATION TESTING OF GENERAL ELECTRIC 50 Ah NICKEL-CADMIUM CELLS WITH NEW SEPARATOR AND NEW POSITIVE PLATE PROCESSING

George W. Morrow
Goddard Space Flight Center
Greenbelt, MD 20771

ABSTRACT

Forty-two 50 Ah aerospace nickel-cadmium cells were delivered to Goddard Space Flight Center (GSFC) by General Electric (GE) in February, 1985 for the purpose of evaluating and qualifying a new nylon separator material, Pellon 2536, and the new GE Positive Plate Nickel Attack Control Passivation process. Testing began in May, 1985 at the Naval Weapons Support Center (NWSC) in Crane, Indiana with standard initial evaluation tests. Life cycling in both Low Earth Orbit (LEO) and Geosynchronous Orbit (GEO) began in July, 1985 with approximately 1200 LEO cycles complete at this writing. Early test results show that cells with positive plate passivation exhibit higher than normal charge voltage characteristics. Other aspects of performance have been nominal.

INTRODUCTION

In the early 1980s, Pellon Corporation announced that it would discontinue the manufacture of aerospace nickel-cadmium separator material, Pellon 2505 ml. That announcement meant that a new separator material would have to be found and qualified for aerospace use. Pellon 2536, very similar to 2505 ml, was chosen in 1984 as the new aerospace separator. In the meantime, GE had developed a new positive plate process to reduce the amount of attack on the nickel sintered structure during the active material impregnation. This process would also need to be qualified. Therefore, a test program was put together by the GSFC to evaluate and qualify both the separator and positive plate process. Cell fabrication for this program was initiated in early 1984 and the cells were delivered in February, 1985.

CELL DESCRIPTION

The 50 Ah nickel-cadmium cells undergoing test were activated with electrolyte during the 37th week of 1984. All cells have dual, nickel-braze, ceramic-to-metal seals and welded prismatic cases with a nominal case wall thickness of 0.0265 inch. The test group is made up of 4 cell designs: 1) NASA standard (42B050AB20), 2) old positive, new separator (42B050AB25), 3) new positive, old separator (42B050AB26), and 4) new positive, new separator (42B050AB27). Cell design data is provided in Table 1. The cells were manufactured to GE Manufacturing Control Document (MCD) 232A2222AA-84 and acceptance tested at GE to Acceptance Test Procedure P24A-PB-222 prior to delivery.

TEST OBJECTIVES

The objectives of this test program are: (1) to evaluate the effects of the new separator material, Pellon 2536, and the new GE Positive Plate Nickel Attack Control Passivation process on cell performance and life, and (2) to qualify these changes for use in NASA/GSFC spacecraft applications.

Initial Evaluation Test Results

The standard initial evaluation test used by the GSFC is outlined in Figure 1. During these tests, the cells were placed in packs of ten and set up so that each pack utilized the same charge and discharge power supplies. This set-up allowed data to be compared across the packs as must be done in a test of this nature.

Tables 2 and 3 provide an overview of data from all 3 capacity tests, 2 overcharge tests, and a charge efficiency test. Review of this data reveals that groups with positive plate passivation exhibited slightly higher peak and end-of-charge (EOC) voltages during the 35°C overcharge. Voltages were as much as 19 mV higher. Also capacity test data shows that all groups began the test with approximately the same capacity. This will allow capacity degradation to be compared directly throughout life. The highest average capacity experienced was 63.7 Ah while the lowest was 58.7 Ah.

From data not included here, it was observed that groups with positive plate passivation recovered to a lower voltage during internal short testing. These voltages were as much as 35 mV lower than expected while still well above the requirement of 1.17 v/cell after 24 hours of open circuit stand. It was also observed that data from internal resistance, charge retention, and pressure versus capacity tests compared well between all groups.

Life Cycling Evaluation Test Description

The identification of each test group and the test matrix outline is detailed in Figure 2. There are 3 cycling regimes in this test: LEO 40% DOD and 20°C (L4020), LEO 40% DOD and 0°C (L4000), and GEO 80% DOD and 20°C (G8020). All 4 cell designs are being tested in the L4020 regime while only the old positive – new separator and new positive – new separator designs are tested in the G8020 regime and only the new positive – new separator design is tested under the L4000 regime.

In the L4020 and L4000 regimes, the cells are discharged at a 0.8C rate (40 amps) for 30 minutes and charged at a 0.8C rate to a voltage clamp at which point the current is allowed to taper for the remainder of the 60 minute charge period. The voltage clamp is selected to allow a percent recharge (C/D) of 112 $\pm$ 2 percent. The G8020 regime is a real-time GEO regime with a 42-day eclipse period occurring twice per year. During shadow periods the cells are discharged at a 0.667C rate (33 amps). Figure 3 shows the daily discharge times for each eclipse season. Following each shadow the packs are charged at a 0.1C rate (5 amps) to 115 percent recharge (C/D) or 1.48 volts any cell, whichever occurs first. At that time the rate is reduced to a 0.17C rate (0.83 amp). During periods of continuous charge (full sun periods), the packs are trickle charged at the 0.17C rate. The packs are reconditioned to 0.75 v/cell before each eclipse season. All test packs contain 5 cells.

Life Cycle Results

At this time the L4020 packs have experienced approximately 1200 cycles while the L4000 pack has seen 800 cycles and the G8020 packs have not yet had the first eclipse season. Problems had been encountered early in cycling in controlling the pack temperatures of the L4020 packs. Pack temperatures rose to as high as 28°C. This was corrected by increasing air circulation in the environmental chambers.

As a whole, the LEO groups have exhibited slightly higher voltages than expected. Voltage clamp levels were expected to be set at GSFC level 7 or below to maintain 112% recharge at the 40% DOD. This, however, has not been the case as levels have had to be raised to 7.5 after about 800 cycles. Also, all packs are exhibiting charge voltage divergence of as much as 20 mV after the voltage is clamped. This can be seen on the typical cycle plots of Figures 3-7.

CONCLUSIONS

Slightly higher charge voltages as well as increased voltage divergence has been observed of all new positive plate test packs. This is observed most clearly in overcharge tests and LEO cycling test voltage level settings. Apart from this, all packs are performing nominally. Life cycle testing will continue to failure.

Table 1: CELL DESIGN DATA

	NASA STANDARD		OLD POSITIVE NEW SEPARATOR		NEW POSITIVE OLD SEPARATOR		NEW POSITIVE NEW SEPARATOR	
	Pos.	Neg.	Pos.	Neg.	Pos.	Neg.	Pos.	Neg.
	31069	45008	31069	45008	45046	45008	45046	45008
	59.23	130.06	59.23	130.06	60.62	130.06	60.62	130.06
Ah	78.50	149.71	78.50	149.71	74.86	149.71	74.86	149.71
	76	87	76	87	81	87	81	87
	16	17	16	17	16	17	16	17
	1.422	1.422	1.422	1.422	1.422	1.422	1.422	1.422
in.)	0.027	0.031	0.027	0.031	0.027	0.031	0.027	0.031
	12.21	15.86	12.21	15.86	12.12	15.86	12.12	15.86
	166		157		162		155	
	Pellon 2505		Pellon 2536		Pellon 2505		Pellon 2536	
	20.83		21.25		21.40		20.97	

Table 2. INITIAL EVALUATION CAPACITY TEST RESULTS

	C/20 Chr., 48 hrs., 25°C			C/10 Chr., 24 hrs., 25°C			C/10 Chg., 24 hrs., 20°C		
	Ave.	Low	High	Ave.	Low	High	Ave.	Low	High
	63.2	62.8	63.8	56.8	56.5	57.3	56.3	55.8	57.0
ew Sep.	62.7	61.8	63.8	56.6	55.3	57.3	56.1	55.3	57.8
ld Sep.	60.1	59.5	61.3	55.9	55.3	56.8	57.8	56.5	58.8
lew Sep.	59.4	58.8	60.3	55.0	54.0	58.0	56.4	54.8	58.8
ew Sep.	63.7	62.1	64.3	58.9	57.8	59.6	60.6	60.3	61.3
New Sep.	58.7	57.8	59.1	54.3	53.1	54.9	58.4	57.8	58.8
New Sep.	59.2	58.5	59.6	54.6	53.4	55.6	58.8	57.8	59.3

Table 3. INITIAL EVALUATION OVERCHARGE TEST AND CHARGE EFFICIENCY TEST RESULTS

	Overcharge #1 C/20 Chg., 60 hrs., 0°C		Overcharge #2 C/10 Chg., 24 hrs., 35°C		Charge Efficiency C/40 Chg., 20 hrs., 20°C		
Group	Ave. EOCV	Peak V	Ave. EOCV	Peak V	Ah In	Ah Out	Eff.
NASA Std. (Grp. 1)	1.512	1.538	1.406	1.407	29.9	17.2	69.1
Old Pos., New Sep. (Grp. 2)	1.516	1.542	1.404	1.408	24.9	16.7	67.1
New Pos., Old. Sep. (Grp. 3)	1.513	1.541	1.419	1.424	24.9	15.1	60.6
New Pos., New Sep. (Grp. 4)	1.512	1.541	1.412	1.423	25.7	16.5	64.2
Old Pos., New Sep. (Grp. 7)	1.514	1.536	1.406	1.408	24.5	16.6	67.8
New Pos., New Sep. (Grp. 8)	1.512	1.543	1.418	1.427	25.0	16.6	66.5
New Pos., New Sep. (Grp. 9)	1.511	1.545	1.418	1.425	25.0	16.5	66.0

- PHENOLPHTHALEIN LEAK TEST
- THREE CAPACITY TESTS
- INTERNAL RESISTANCE TEST
- CHARGE RETENTION TEST, 20°C
- INTERNAL SHORT TEST
- CHARGE EFFICIENCY TEST, 20°C
- OVERCHARGE TESTS, 0° and 35°C
- PRESSURE VERSUS CAPACITY TEST
- PHENOLPHTHALEIN LEAK TEST

Figure 1. INITIAL EVALUATION TEST REGIME

ORBIT	DOD	TEMP (°C)	NASA STD. CELLS	OLD POS. NEW SEP.	NEW POS. OLD SEP.	NEW POS. NEW SEP.
LEO	40	20	Group 1 42B050AB20 S/N 2-7	Group 2 42B050AB25 S/N 2-7	Group 3 42B060AB26 S/N 2-8	Group 4 42B060AB27 S/N 3-6, 11, 12
GEO	80	20		Group 7 42B050AB25 S/N 1, 8-12		Group 8 42B050AB27 S/N 1, 7-10
LEO	40	0				Group 9 42B050AB27 S/N 2, 13-16

Figure 2: LIFE CYCLING TEST MATRIX

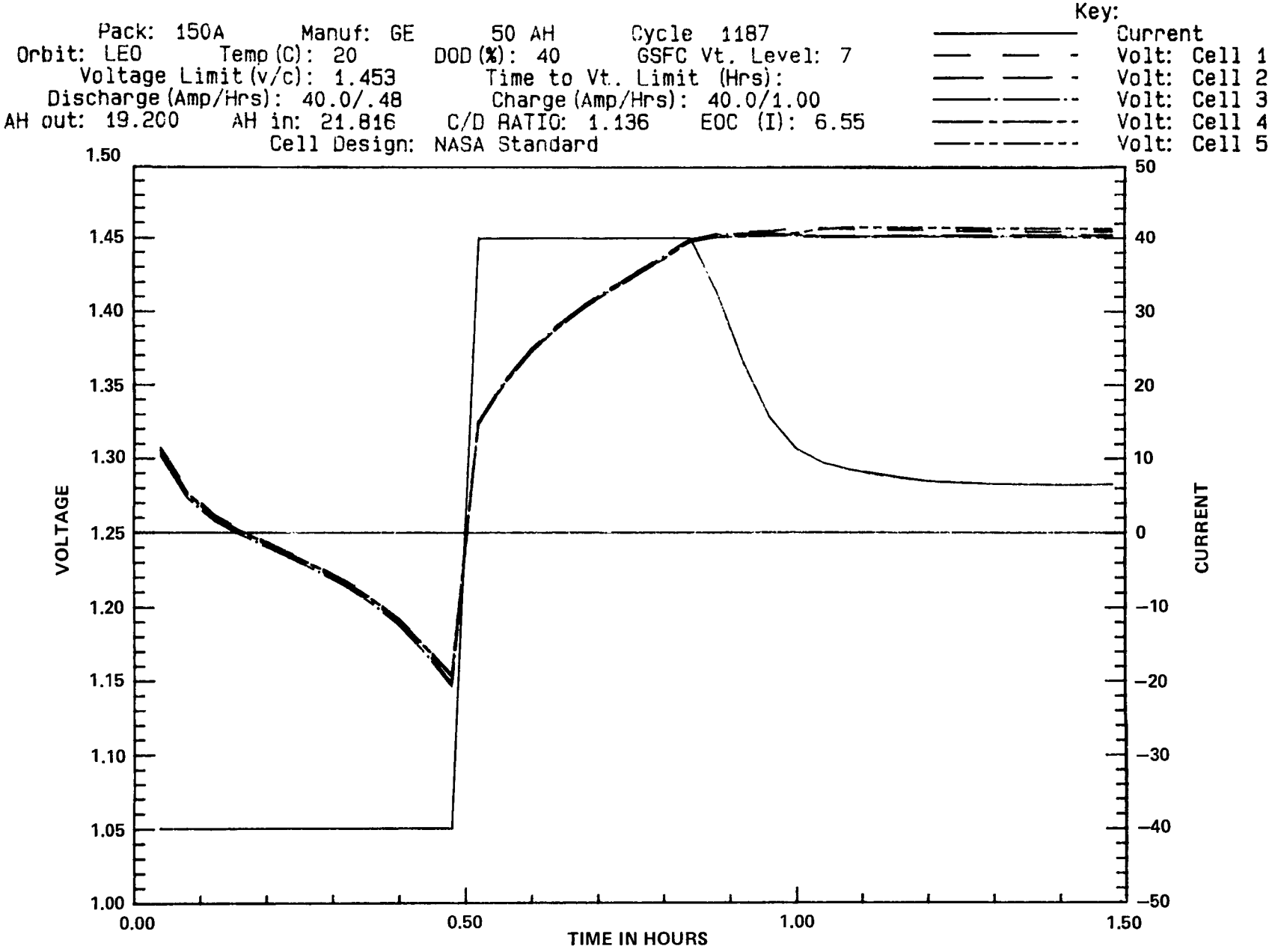

Figure 3. REQUALIFICATION-LIFE CYCLING

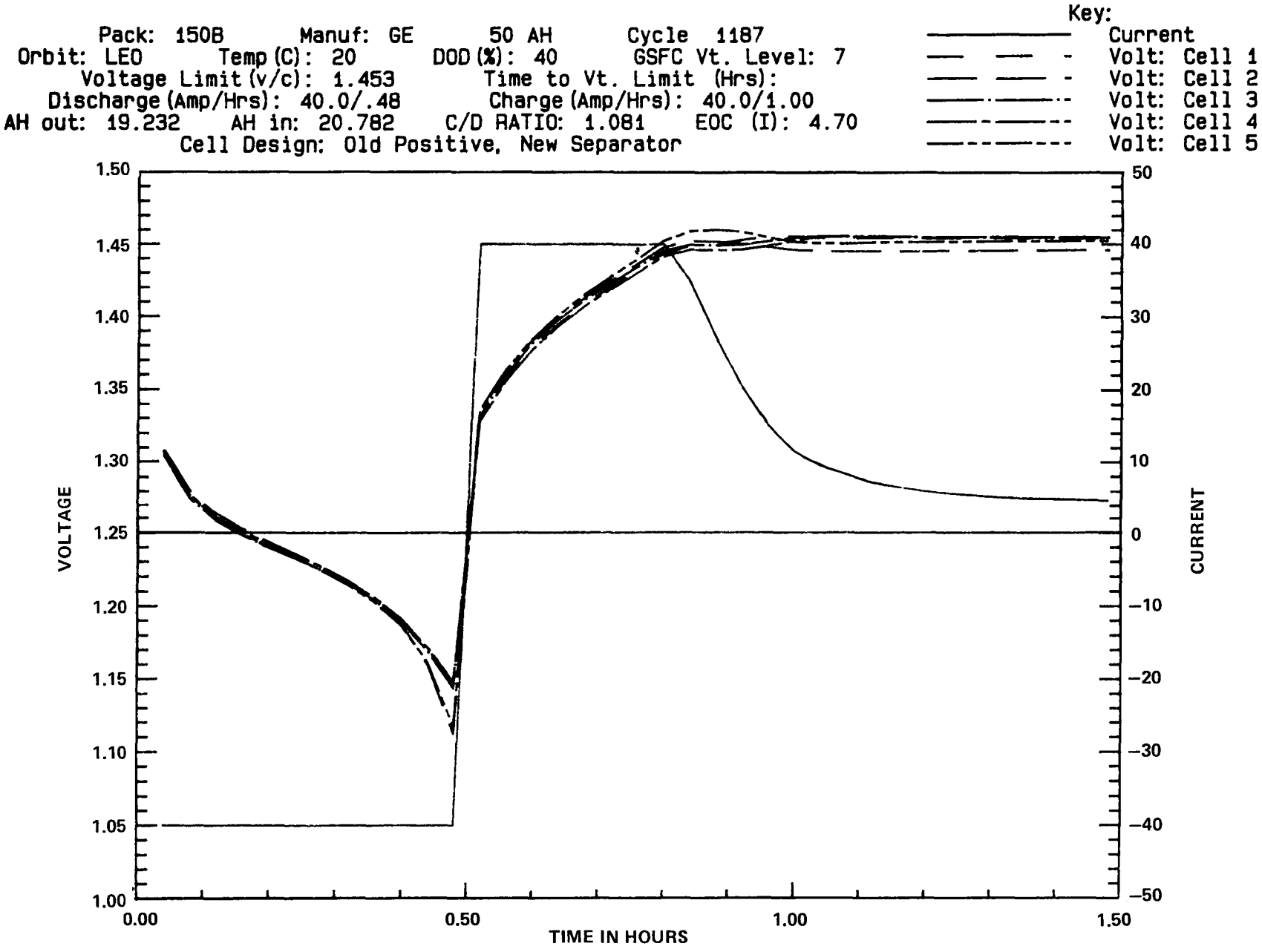

Figure 4. REQUALIFICATION-LIFE CYCLING

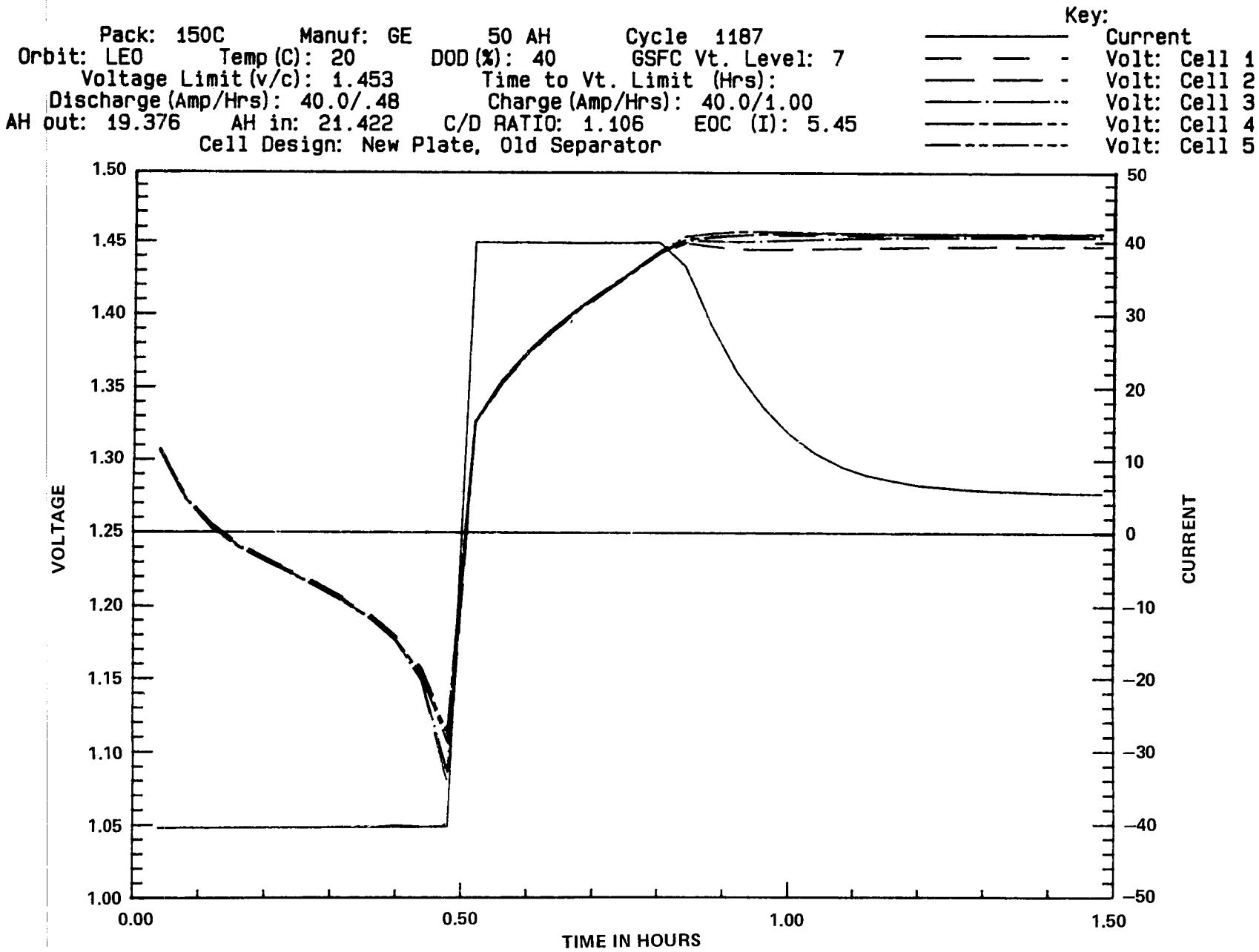

Figure 5. REQUALIFICATION-LIFE CYCLING

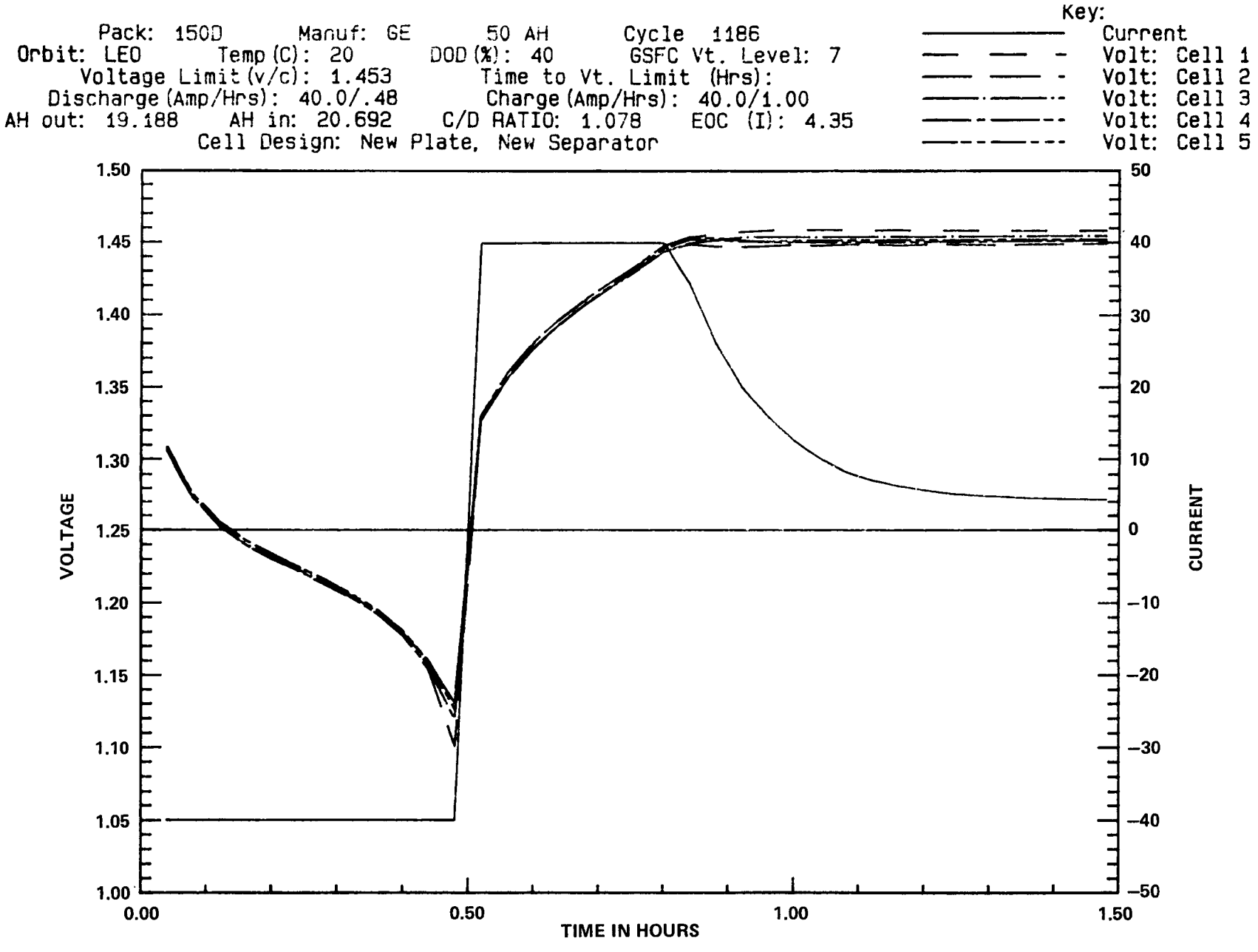

Figure 6. REQUALIFICATION-LIFE CYCLING

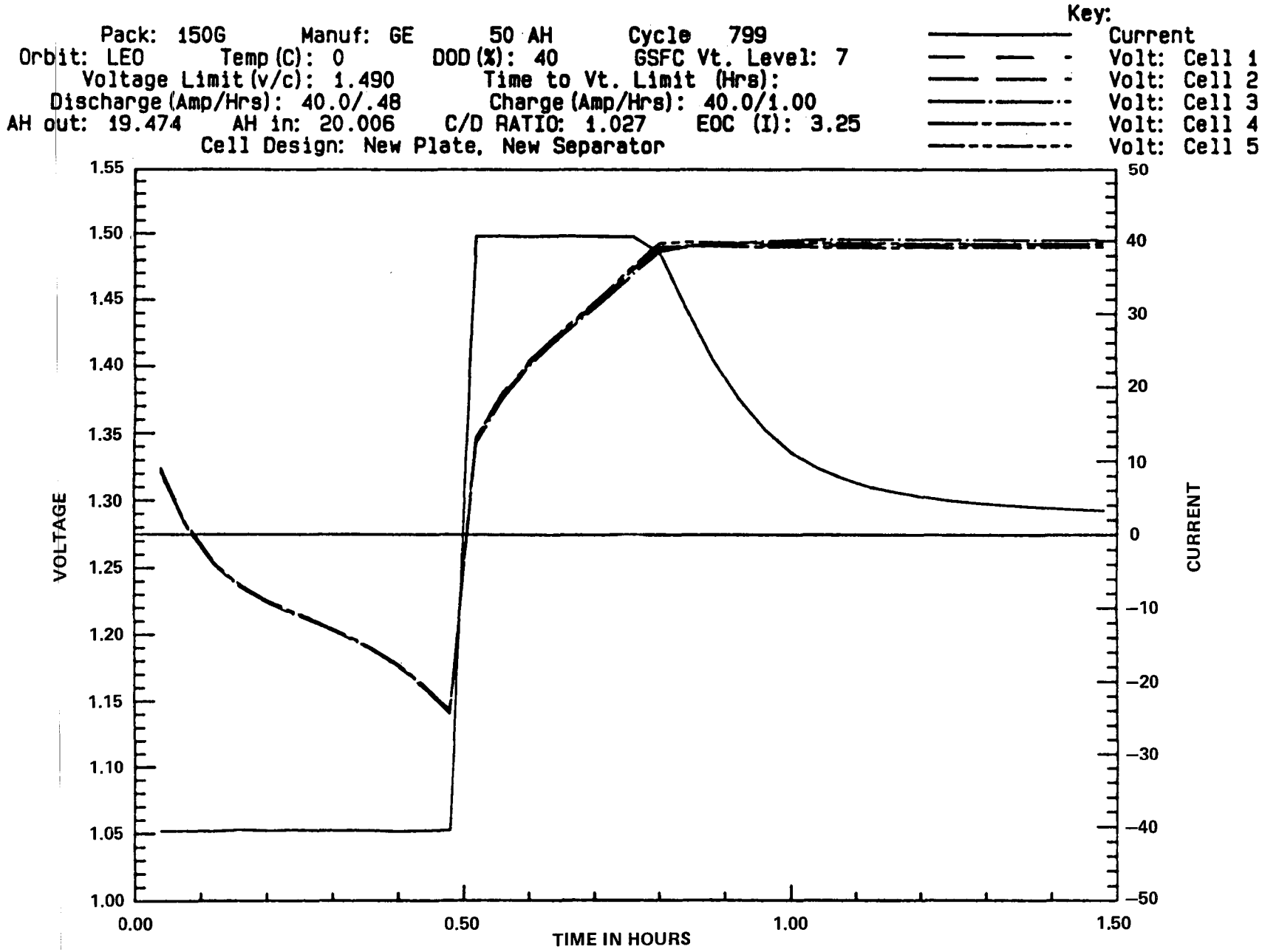

Figure 7. REQUALIFICATION-LIFE CYCLING

AEROSPACE NICKEL-CADMIUM CELL SEPARATOR QUALIFICATIONS PROGRAM

R. W. Francis
The Aerospace Corporation
El Segundo, California

R. L. Haag
Naval Weapons Support Center
Crane, Indiana

ABSTRACT

The present space qualified nylon separator, Pellon 2505 ML, is no longer available for Aerospace nickel-cadmium (NiCd) cells. As a result of this anticipated unavailability, a joint Government program between the Air Force Space Division and the Naval Research Laboratory has been established. Four cell types have been procured with both the old qualified and the new unqualified separators. Acceptance, characterization, and life cycling tests are to be performed at the Naval Weapons Support Center, Crane, IN (NWSC/Crane). The scheduling and current status of this program are discussed and the progress of testing and available results are projected.

BACKGROUND

The qualified separator material for Aerospace hermetically sealed NiCd cells has been Pellon 2505 ML, produced by the Pellon Corporation. Pellon 2505 ML is a non-woven nylon fabric used for 15 years in the Aerospace industry. In 1976 Pellon Corporation discontinued manufacture of the 2505 ML separator material. The fabrication process incorporated zinc chloride in the bonding of fibers into structures and the process effluent removal required costly treatment. In 1981 General Electric Battery Business Division (GEBBD) informed all users of this separator that continued supply would be unavailable. GEBBD had stored enough of the 2505 ML separator to satisfy cell lot commitments to the end of 1984. Concern over this issue encouraged Pellon to reactivate their 2505 ML production line. In the interim, however, enough changes in the raw nylon fibers and processing equipment were made that product characteristics were variable. During this period, GEBBD was coordinating their separator physical, mechanical and chemical parameter needs with Pellon Corporation. A new nonpolluting process, similar to that used in their German manufacturing plant for 10 years, was introduced and installed into the U.S. Pellon plant to manufacture separator material. GEBBD and Pellon claimed that the new separator, 2536, was superior from a uniformity, durability, and performance standpoint. Comparative characteristics and evaluations between the 2505 ML and 2536 separator types appeared encouraging. This preliminary data along

with the new separator qualification program definition and structure were published by M. Milden at the Intersociety Energy Conversion Engineering Conference in 1984 (Ref. 1). The essential elements of this program have been updated and are listed below:

- o Air Force Space Division and Naval Research Laboratory procurement of typical military cells from GEBBD.
- o Coordinate with spacecraft battery contractors to insure test plan validity and performance acceptability.
- o NWSC/Crane to perform acceptance, characterization and life cycle testing.
- o Generate a consolidated data base for the military customer and the battery contractors/users.
- o Eliminate duplication of effort and qualification costs.

More recent analysis (Ref. 2) of the Pellon 2536 separator, which was performed at the Aerospace Corp. Laboratories, shows characteristics apparently equivalent, if not superior, to that of the standard Pellon 2505 ML. Table 1 illustrates and compares these pertinent component parameters.

PROGRAM STRUCTURE

The Air Force and Navy have similar NiCd cell requirements and needs. Program efficiency to provide overall benefit was attained through joint military funding for a single and common cell buy. A coordinated program management function is established at NWSC/Crane. Technical support, component testing, military and program office interface, and data analysis are being conducted by The Aerospace Corporation. The Air Force Space Division Product Assurance Division AFSD/PDP coordinates, monitors and transfers funds to NWSC/Crane; whereas, the Naval Research Laboratory provides the same function for the Navy. Prior to 1985 the Air Force and Navy had already allocated the necessary money to purchase a total of 173 cells. The division of cells for test and evaluation are shown in Table 2. Negative electrodes are all silver treated except the 26.5 A-Hr cells which have teflon treatment. Positive electrodes consist of the current and standard process design. Half of each cell type is constructed with Pellon 2505 ML and half with the proposed new Pellon separator 2536.

Cell specification is not program specific but performance oriented. The specification establishes requirements for manufacturing methods and procedures and defines processes and fabrication methods at a point in time for a NiCd cell type.

CELL TESTING AND EVALUATION

After cells are received at NWSC/Crane, they undergo three separate but consecutive tests. These are:

- o Acceptance
- o Characterization
- o Life Cycling

1) Acceptance testing at Crane enables performance comparison to acceptance test data from GEBBD and provides a basis for cell matching and pack fabricaton.

2) Characterization testing is performed on all cell types after being subjected to random vibration to simulate the launch environment. Following vibration the cells will be placed in restraining plates with temperature monitoring. Following a conditioning cycle and ten capacity stabilization cycles the cells will undergo voltage characterization at various charge current rates (C/2 to C/80) and temperatures (30° to -10°C). These characterization tests will differentiate between the two separator types according to the electrochemical mass transport capabilities. In other words, the existing voltage-temperature charge curves will be requalified for the Pellon 2536 separator in relation to the existing Pellon 2505 ML.

   As seen in Table 2, cell types will also be stored in both the activated (wet storage) and unactivated (dry storage) state as elapsed test time controls for comparative analysis.

3) The life cycling test matrix consists of 135 cells and is illustrated in Table 3 with the test details shown in Table 4.

   The cells are assembled into five- and ten-cell packs following a pack fabrication procedure which is weighted with eleven parameters from the NWSC/Crane acceptance tests. For both orbits, two test levels are imposed to simulate both actual and accelerated performance behavior. For the low earth orbit (LEO) only, the higher temperature and greater depth of discharge is used to enhance any performance level limitations for either separator. The geostationary orbit (GEO) is considered accelerated, since no trickle charging, simulating conditions between eclipse seasons, is imposed. The two GEO temperature levels will bracket actual use environments. The LEO orbital simulation consists of a 33.6-minute (0.56 Hr.) eclipse and a 67.2-minute (1.12 Hr.) sunlight period. The cycling is continuous with no scheduled capacity measurements or reconditioning. The preselected temperature-compensated voltage limit (V/T-limit) is chosen to maintain a charge-to-discharge ratio of 1.00-1.08, including the taper current. The GEO orbital simulation consists of a typical 42-day eclipse season, and following each season the packs are trickle charged at C/60 for two days. Each pack is to be reconditioned to 0.75-volt average pack voltage for approximately ten days following the trickle charge. Recharge prior to

the next season is at the C/4 rate. Within an eclipse season, cell packs are charged at the C/10 rate to a V/T-limit followed by a taper current charge for the remainder of the eclipse day.

STATUS AND SCHEDULE

The joint Air Force/Navy separator qualification program has been funded up to and including FY 90. A chronological list of key program milestones are listed below:

o Procurement Specification	Sep 1983
o Contract with GEBBD for Procurement of 154 NiCd Cells	Mar 1984
o Amend Contract to Add 19 Additional 50 A-Hr Cells	Aug 1984
o Contract Modifications and Material Review	Jun 1985
o 30 and 34 A-Hr Cells Consigned to NWSC/Crane	Jun 1985
o Detailed Test Plan	Sep 1985
o 35 and 50 A-Hr Cells Consigned to NWSC/Crane	Nov 1985

The current status and projected test schedule at NWSC/Crane is illustrated in Table 5 on a time-line diagram.

At the time of this writing, as can be seen in Table 5, the first of the four cell types, 42B034AB02 and 03 (34 A-Hr cells), has completed acceptance testing at Crane. The raw data demonstrates comparable and nominal capacities for both the Pellon 2505 ML and 2536 separator types in the 25°, 10°, and 0°C capacity and overcharge acceptance tests. In addition, the typical roll-over in charge voltage was observed for both cell types, indicating good negative plate electrochemical behavior. Maximum charge voltage for the Pellon 2536 cells, however, is attained earlier in the alloted time for charge than for the Pellon 2505 ML. The significance of this will not be known until the characterization tests are completed and the life cycling initiated.

FUNDING

Not including cell procurement costs, which have been appropriated, the funding level allocated by the Air Force and Navy for the qualification test program alone is approximately $150K per year up to FY 91. These funds represent the required support to conduct the acceptance, characterization, and life cycle tests. Thus, life cycle testing is ensured for almost five

years, since all cell types are projected to have completed their acceptance tests at NWSC/Crane by February 1986.

The structure of the separator test program was designed to provide a high degree of confidence based on long term testing exposing any subtle differences far in advance of actual flight usage. As a result of an accelerated schedule in the military which forces utilization of the new Pellon 2536 separator for near-term cell lot buys, the separator qualification test program has received the support and encouragement of many spacecraft program offices. Preliminary test evaluation data to demonstrate comparable performance and acceptability of the new material to that of the Pellon 2505 ML will not be available, however, with any degree of confidence and reliability until the end of 1986. This will obviously impact decisions to purchase NiCd cells with the new Pellon 2536 separator for spacecraft flight use.

CONCLUSION

The NiCd cell separator qualification program will provide a common data base for the comparison of performance characteristics of cells with Pellon 2505 ML and identical cells with Pellon 2536 in concurrent tests. Preliminary life cycle data at more severe temperatures and discharge depths will be available by the end of 1986 to verify cell performance with the new Pellon 2536. Close to five years of long-term real-time cell cycling is funded to verify cell performance and acceptability of the Pellon 2536 separator. Joint Air Force and Navy funding to one centralized facility, NWSC/Crane, will produce a statistically more valid data base at an overall lower cost by minimizing individual spacecraft program office evaluation, management, coordination, and testing. This will enhance the value of the data base by enabling direct comparison of the two cell types with different separator components.

Test reports will be issued after each cell type acceptance test and after each characterization test. In addition, NWSC/Crane will distribute annual cycle life test reports and trends analysis at selected times throughout the year. These reports will be made available on request to NWSC/Crane and will be distributed in normal fashion subject to approval from the Air Force and Navy.

REFERENCES

1. Milden, M. J. and Harkness, J., Proceedings of the Nineteenth Intersociety Energy Conversion Engineering Conference 1, 108 (1984).

2. Badcock, The Aerospace Corp., Private Communication, Oct. 31, 1985, to be published.

TABLE 1. SEPARATOR PARAMETRIC COMPARISON

Parameter	2505 ML	2536
Process	$ZnCl_2$ Stabilized Bonded Nylon	High temperature Inert Gas Bonded Nylon
Fiber Diameter	13 m	13 m
Density		1.25 (2505 ML)
Electrolyte Retention	400%	300%
Hydrolysis Rate (70°-100°C) *31% KOH		0.5 (2505 ML)
*Cd^{+2} Added		0.5 (2505 ML)

TABLE 2 CELL TEST DISTRIBUTION

A-Hr Capacity	Cell Type Designation	Test Matrix	GE Destruct	Quantity/End Use Wet Storage	Quantity/End Use Dry Storage	Characterization
26.5	42B030AB10/14	30	1	2	2	4
34	42B034AB02/03	30	1	2	2	2
35	42B035AB02/13	30	1	2	2	4
50	42B050AB24/28	45	1	5	3	4
		135	4	11	9	14

TABLE 3. TEST MATRIX

Orbit	DoD % Actual	Charge Control	Test Temp °C	2505 ML Separator 50AH	34AH	35AH	26.5AH	2536 Separator 50AH	34AH	35AH	26.5AH
LEO	25	V-T Taper	0		5		5	5	5		5
LEO	40	V-T Taper	20		10		10	10	10		10
GEO Accel	75	V-T Taper	0	5		5		5		5	
GEO Accel	75	V-T Taper	20	10		10		10		10	

TABLE 4. LIFE CYCLE DETAILS

Test	Capacity Nameplate	Est. Actual	Current Discharge	Charge	V/T Curve	C/D Range
LEO, 25%, 0°C	26.5AH	30AH	13.4A	c/3	5	1.00-1.08
	34	41	18.3	c/2	5	1.00-1.08
	50	50	22.3	c/3	5	1.00-1.08
LEO, 40%, 20°C	26.5	30	21.4	c/2	5	1.00-1.08
	34	41	29.3	c/2	5	1.00-1.08
	50	50	35.7	c/2	5	1.00-1.08
						Taper Current
GEO, 75%, 0°C	35AH	37AH	23.1A	c/10	5	0.5 -0.3A
	50	50	31.3	c/10	5	0.75-0.5A
GEO, 75%, 20°C	35	37	23.1	c/10	5	0.5 -0.3A
	50	50	31.3	c/10	5	0.75-0.5A

TABLE 5. CURRENT AND PROJECTED SCHEDULE

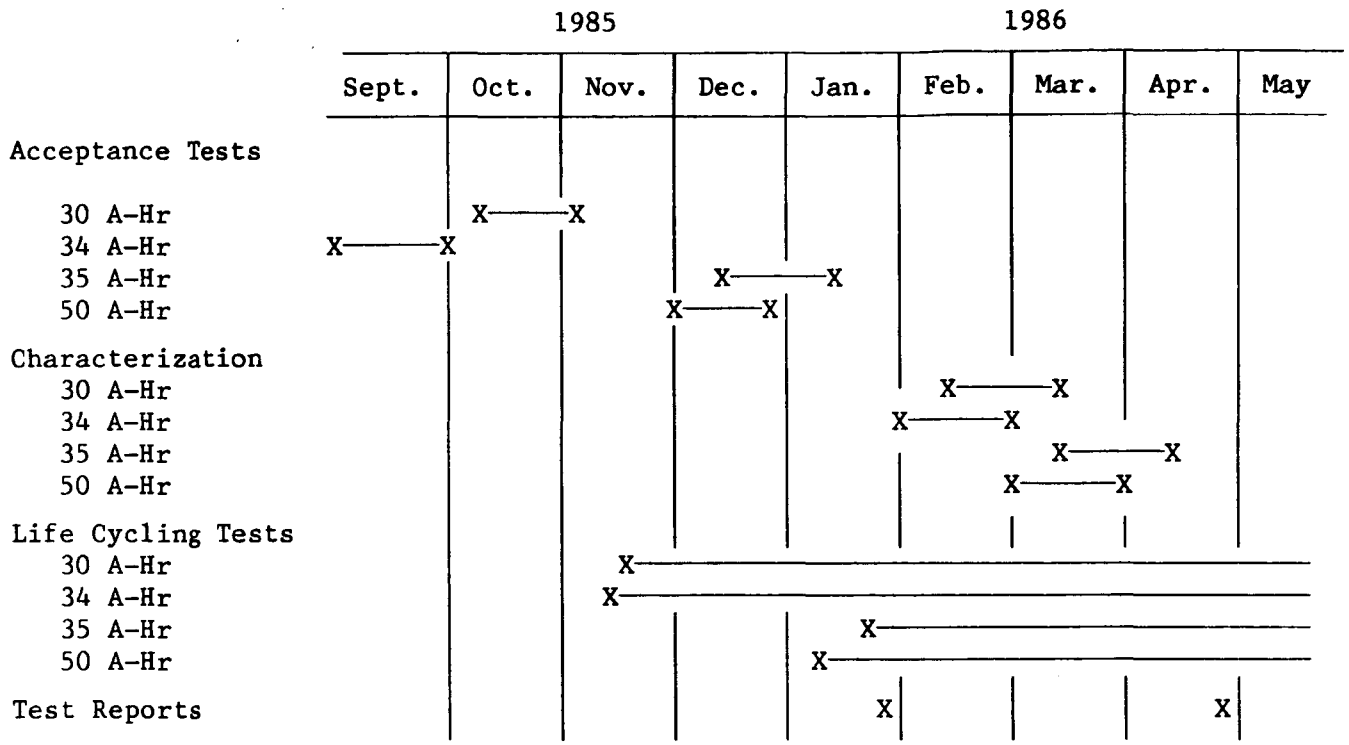

N87-11086

A FLOODED-STARVED DESIGN FOR NICKEL-CADMIUM CELLS

Lawrence H. Thaller
National Aeronautics and Space Administration
Lewis Research Center
Cleveland, OH 44135

INTRODUCTION

Sealed nickel-cadmium cells for aerospace applications have been made for several decades by a variety of manufacturers. Although each manufacturer has his own set of processes, procedures, and design techniques, these cells owe much of their long cycle life to the electrochemical couples employed and the physical properties of the separator material used. This material has the combination of pore size distribution and wetting characteristics which permits the oxygen evolved at the positive electrode during the latter stages of charge to have access to the metallic cadmium on the negative electrode while at the same time holds enough electrolyte to maintain good ionic conductivity between the electrode pairs. This condition is usually referred to as being "starved" in terms of the amount of electrolyte. Depending on the particular separator type and number of layers, the characteristics of the electrodes, and the compression on the plate pack, an electrolyte loading value (X cm^3/Ahr) will yield the proper balance in terms of gas permeability and electrolyte conductivity. A particular manufacturer will aim for a certain cell pressure on overcharge based on the experience gained from past performance.

There are several possible difficulties associated with this general procedure which may well result is substandard performance of the cell. This results in part from the statistical aspects among groupings of plate packs and/or cell sets and in part from the growth with cycling characteristics of the electrodes used in these cells.

It is the purpose of this paper to describe in detail a somewhat analogous situation among groupings of alkaline fuel cells where the stochastic aspects have been much more accurately documented and then illustrate how this problem was eliminated using straight forward principles of pore size engineering (Ref. 1). This is followed by a suggested method of adapting these same design principles to nickel-cadmium cells. It must be kept in mind that when cells are cycled to typically twenty percent depth of discharge that eighty percent of the weight of the cell is simply dead weight. Some of this dead weight might be put to better use by trading it for a scheme that would increase the time during which the cell would be working more closely to its optimum set of operating parameters.

BACKGROUND

In the early stages of the development of alkaline fuel cell technology at

what is now called International Fuel Cells, a cell was made up as shown in figure 1. These cells employed a fixed, trapped amount of electrolyte within each cell. The oxygen electrode was a thin screen onto which was placed a mixture of catalyst powder and Teflon. The Teflon content was such as to render the electrode wet proof. The separator was an asbestos mat fully filled with electrolyte and the hydrogen electrode was a thick (~0.060 in.) sheet of sintered nickel which was catalyzed more or less uniformly throughout. The pore sizes of the individual components were selected so that the separator would at all times be filled with electrolyte. The electrolyte-gas interface would be set up somewhere within the thick nickel sinter. As conditions arose that resulted in temporary changes in the volume of the electrolyte, this interface simply moved slightly to the right or left.

OPTIMUM VOLUME

Optimum volume is a term that is used to describe the effect of electrolyte volume on cell performance and in particular that volume which results in the peak performance of the cell. The reason for a change in performance with cell electrolyte volume (interface position) and an optimum volume can be readily seen with the help of this diagram. If the electrolyte-gas interface is very close to the gas cavity (right hand edge of the hydrogen electrode) then most of the catalytic surface is covered over with electrolyte. The slow diffusion of hydrogen through the bulk electrolyte along with the relatively high ionic IR drop across this thick electrode will result is poor cell performance. As the interface recedes into the sintered electrode, there will be a greater degree of electrolyte film-catalyst surface-gas interface, and performance will increase. As this interface apporaches the matrix, the diffusion of gas into and water vapor out of this sinter becomes the controlling factor and again performance falls off. This discussion is not meant to imply any similarity between a nickel-cadmium cell and a hydrogen-oxygen fuel cell. It is only meant to illustrate how a cell can have a preferred amount of electrolyte for optimum operation. An interesting series of experiments were carried out on a group of 36 individual cells of this type which illustrates several characteristics of groupings. Using a technique which is peculiar to the fuel cell industry and is not particularly germane to the discussion at hand, the optimum volumes of each one of these cells was determined. Figure 2 shows the histogram of these results. The results, of course, show a considerable standard deviation or spread in the values of the optimum volume. These results are particularly significant in that fuel cells are filled as a group that are stacked together in a manner that results in each cell receiving approximately the same volume. This, of course, would result in some cells receiving more than their optimum amount and some cells receiving less than their optimum amount. Before being able to discern whether this would result in acceptable or unacceptable performance of this particular grouping of cells, a second characteristic called volume tolerance, must be known. As the name implies, volume tolerance describes the cell performance as a function of the electrolyte volume. In essence, the shape of the electrolyte volume vs. cell

performance curve is a measure of the volume tolerance of the cell. Without going into the details of the matter, it can be stated (and it should be obvious) that if the grouping of cells as shown in figure 2 were all filled with 13 cm^3 of electrolyte, then three of the cells would be over filled where as eight cells would be under filled.

The answer to this problem in the fuel cell industry was the invention of what was called the electrolyte reservoir (Ref. 2). The thick nickel sinter electrode (figure 3) was replaced with a thin screen-Teflon-catalyst type gas electrode similar to the oxygen electrode. Placed behind the hydrogen electrode was a porous nickel sinter with a waffled pattern on it so that reactant gas could flow on the back side of the electrode while the sinter would also be in contact with it. Here again, the pore size and pore size distribution of each component is carefully selected so as to maintain proper electrolyte placement. The electrolyte reservoir has the largest pore size of wettable material so that is will freely accept and give up electrolyte as the cell undergoes temporary wetting or drying conditions. The electrodes themselves under normal conditions do not undergo any changes in their electrolyte volume; only changes in the electrolyte concentration as the water content temporarily is in excess of or is less than that value about which the control point is fixed. Figure 4 is a plot of the volume tolerance characteristics of three different cell constructions that have been used over the years by IFC. The slanted straight line depicts the characteristics of the cells that employ the electrolyte reservoir behind the screen hydrogen electrode. The curve showing the intermediate degree of volume tolerance was the configuration described earlier with the thick sintered electrode. The cell construction showing a very minimal amount of volume tolerance was of yet an earlier level of technology. Cells with the widest degree of volume tolerance are the type used aboard the space shuttle. Groupings of these cells are much less affected by the stochastic aspects associated with groupings of individual cells.

FLOODED STARVED DESIGN FOR NICKEL-CADMIUM CELLS

It would not be incorrect to say that a nickel-cadmium cell has an optimum electrolyte volume associated with it. The optimum electrolyte volume in this case is related to the balance required between the cell ionic resistance and the gas recombination characteristics. Further, it probably would not be incorrect to say that among a grouping of cells there would be a certain distribution associated with the optimum volume values. It is however conjectural at this point to state that when a group of cells are filled, some are overly filled while others are under filled. Likewise, it would probably be dangerous to state that the growth characteristics of the nickel electrode, coupled with the chemical degradation of the nylon separator material in the KOH and oxidative environment, would result in adverse effects on the cell optimum volume, but it certainly can't do it any good. What is suggested is to adopt, where feasible, some of the techniques used in the alkaline fuel cell field into the nickel-cadmium technology. Figure 5 shows a simplistic diagram of a nickel-cadmium cell that employs an electrolyte reservoir

consisting of a wettable material with a pore size intermediate between the large gas filled pores and the small electrolyte filled pores of the separator. Even in well behaved nickel electrodes, there is an increase in the fine pore structure of the active material which would tend to draw electrolyte out of the separator (Ref. 1). If a reservoir were present it could yield up electrolyte as needed to replace the amount lost to the electrodes. The placement of the reservoir at the bottom is just meant to be illustrative. Depending on the pore size characteristics of the separator, the reservoir function could be performed by the separator itself. It should be noted here that there are driving forces other than capillary pressure (pore size) that come into play in these cells and need to be taken into account when doing an overall cell design. They include diffusional forces and migrational forces and possibly some electro-osmotic effects. In nickel-cadmium cells in contrast to nickel-hydrogen cells, there is a greater amount of electrolyte volume change due to the water associated with the electrochemical reaction.

The steps involved in designing a flooded-starved cell might proceed as follows:

1) Investigate the electrolyte volume tolerance characteristics of nickel-cadmium cells. This should be done both from an optimum volume point of view as well as a volume tolerance point of view.

2) Investigate the stochastic aspects of the optimum volume characteristics so the degree of variance within a cell population can be estimated.

3) Establish the net plate expansion characteristics (while under the pack compression) of both the nickel and cadmium electrodes.

4) Establish the pore size and pore size distribution characteristics of the cell plates as a function of cycling, electrolyte composition, plate additive, etc.

5) Establish the pertinent physical characteristics of chemically stable oxidation resistant separator materials. These would include their compressibility-pore size distribution characteristics.

6) Calculate the reservoir requirements so as to keep the cell(s) within proper electrolyte tolerance bounds over the expected lifetime of the cell(s).

SUMMARY

A methodology for increasing or extending useful lives of nickel-cadmium cells and batteries is suggested based on a somewhat analogous situation that was present in early technology trapped electrolyte alkaline fuel cells. The

fuel cell industry was able to document and quantize the problem. The solution came when the volume tolerance characteristics of the cells were widened. This same approach is suggested for first quantifying the problem and then gathering the required data to develop a modified nickel-cadmium cell design.

REFERENCES

1. Abbey, K. M. and Thaller, L. H.: Proc. 17th IECEC, Vol. 2, pp 757-764, 1982.

2. U. S. Patent No. 3,779,811 (1973); "Matrix-Type Fuel Cell;" Stedman, J. K. and Bushnell, C. L.

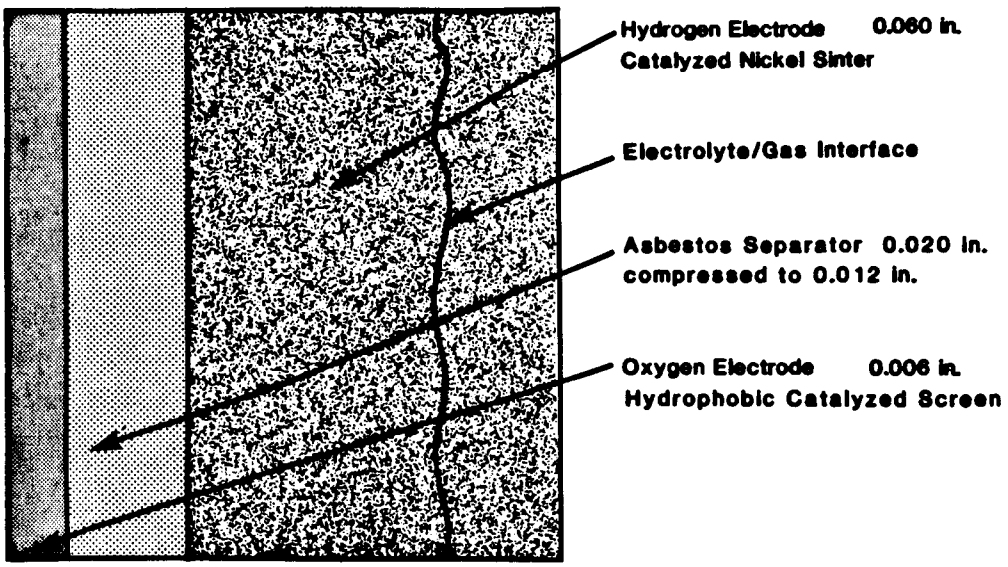

Figure 1. SCHEMATIC OF A SINTER-SCREEN FUEL CELL

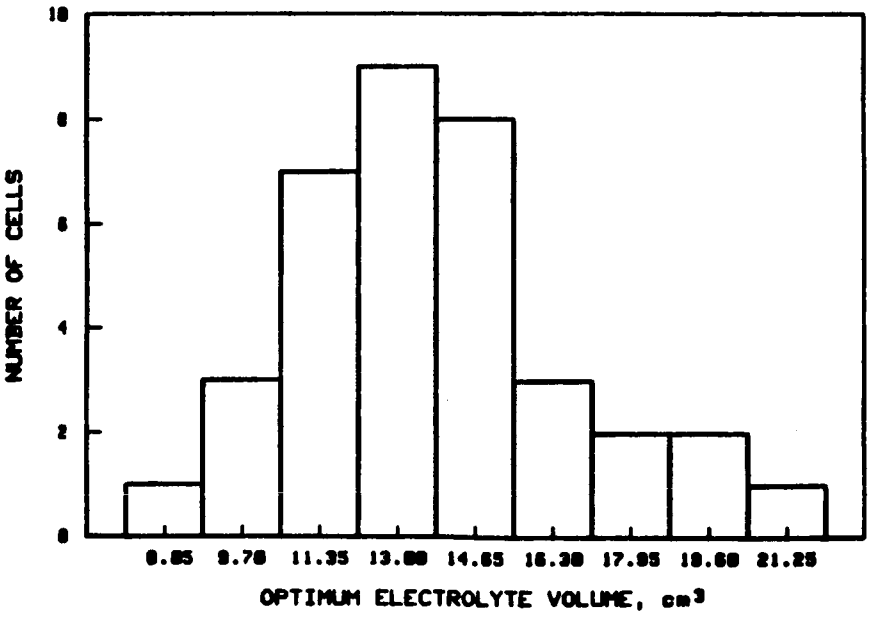

Figure 2. DISTRIBUTION OF OPTIMUM ELECTROLYTE VOLUMES

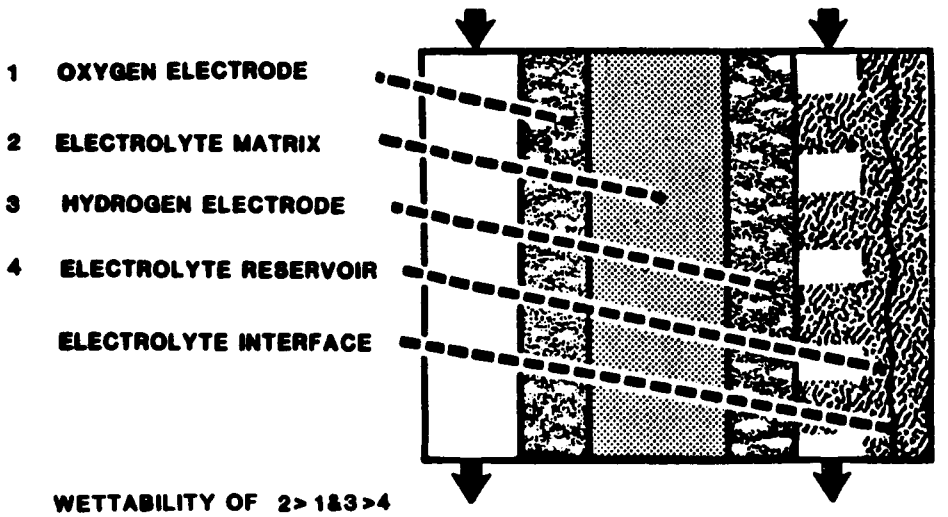

Figure 3. FUEL CELL EMPLOYING ELECTROLYTE RESERVOIR

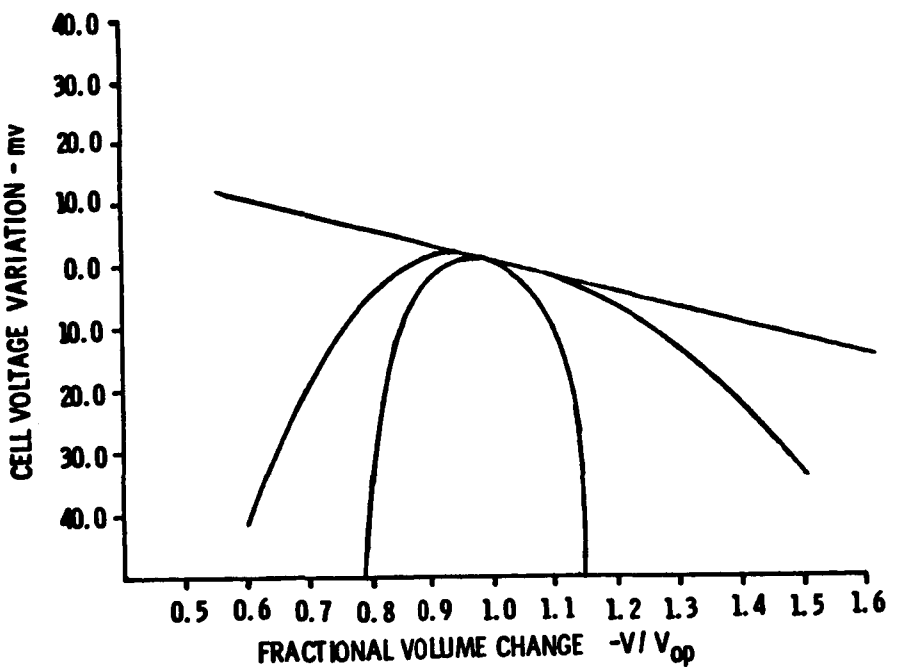

Figure 4. CELLS CAN BE CONSTRUCTED WITH DIFFERENT DEGREES OF VOLUME TOLERANCE

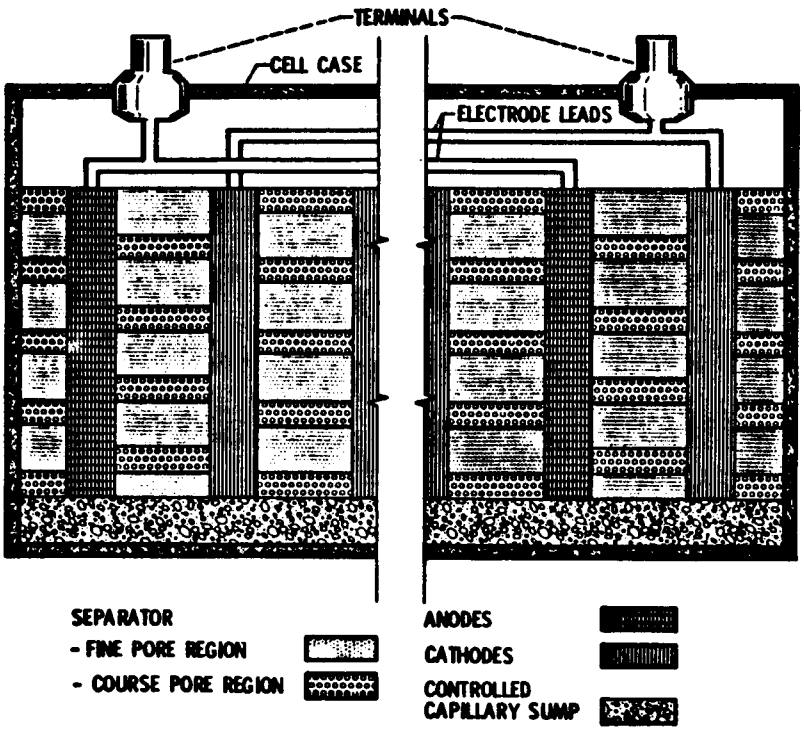

Figure 5. A FLOODED-STARVED DESIGN FOR NICKEL-CADMIUM CELLS

AN ADVANCED NI-CD BATTERY CELL DESIGN

Lee Miller

Eagle-Picher Industries, Inc.

Introduction

An advanced Ni-Cd space battery cell design is evolving as the result of the incorporation of Ni-H_2 battery cell design technology. High rate oxygen and hydrogen gas recombination capability with higher levels of electrolyte activation have been demonstrated. Increased performance and life are projected via extended operational range and the use of inorganic separator materials.

Electrode Stack Design

The advanced electrode stack configuration is shown in Figure 1. The first major design feature involves the use of two (2), half thickness negative electrodes in a "back-to-back" configuration. Enhanced oxygen gas recombination is achieved by the application of a hydrophobic (to prevent electrolyte flooding), gas permeable membrane to their inter surfaces which are separated by a gas accessibility spacer material (Ni-H_2 design technology).

Recombination performance dependency upon an intra electrode couple, specific porosity, organic separator material is eliminated. Various more stable materials of inorganic compositions should be accommodated extending system life. In addition, intra couple separator flooding concerns are eliminated allowing higher electrolyte activation levels also extending life.

The second major design feature involves the incorporation of a catalyzed gas electrode. The gas electrode interfaces the electrode stack edge surfaces and is connected electrically to the cell positive terminal. Design intent is to offer a mechanism for rapid hydrogen gas recombination.

If a cell is subjected to sufficient operational or environmental stress to promote hydrogen gas generation (either by design to increase system performance or inadvertently), the gas would be rapidly recombined by the Ni-H_2 reaction defined in Figure 2.

Testing

Testing of the above design concepts has been reported in a previous Battery Workshop [1].

The results of this effort may be summarized as follows.

A group of 6 AH rated cells were constructed in three (3) design versions.

1) Standard space cell design.

2) Same as 1) except incorporated gas electrode.

3) Same as 1) except incorporated "back-to-back" negative electrodes (split negative).

Figure 3 graphically presents the results of a test designed to evaluate electrolyte activation level sensitivity. Clearly the "back-to-back" negative electrode design version demonstrates a significantly improved tolerance to electrolyte activation level.

Figure 4 graphically presents the results of a test designed to measure hydrogen gas recombination ability. The test temperature and charge rate were chosen to assure the hydrogen overvoltage potential would be achieved. Again, clearly proper functioning of the gas electrode design version was demonstrated.

More recent testing was initiated with a small group (3 each) of current production 50 AH rated cells. All three (3) cells incorporated the same gas electrode design version configured as depicted in Figure 5. To assure hydrogen gas generation, discharged excess negative electrode capacity or overcharge protection was not incorporated in these cells.

Figure 6 graphically presents the results of a test designed to assess hydrogen gas recombination rate capabilities. Surprisingly doubling the charge rate (from C/10 to C/5) did not increase the maximum pressure achieved. It would appear a relatively small catalytic gas electrode area is capable of managing high gas generation rates.

Conclusion

The evolution of an advanced Ni-Cd space battery cell design continues to prove very promising. High oxygen/hydrogen gas recombination rates (currently up to a C/5 charge rate) and increased electrolyte activation level tolerance (currently up to 5.6 grams/AH of positive capacity) have been demonstrated by test.

A superior performance, extended life battery cell offering the advantages listed in Figure 7 should soon be available for mission applications.

References

1. Miller, L. (Eagle-Picher Industries): Advanced Sealed Nickel-Cadmium Design. Proc. 1976 Goddard Space Flight Center Battery Workshop, X-711-77-28, GSFC Greenbelt, Maryland, November 1976.

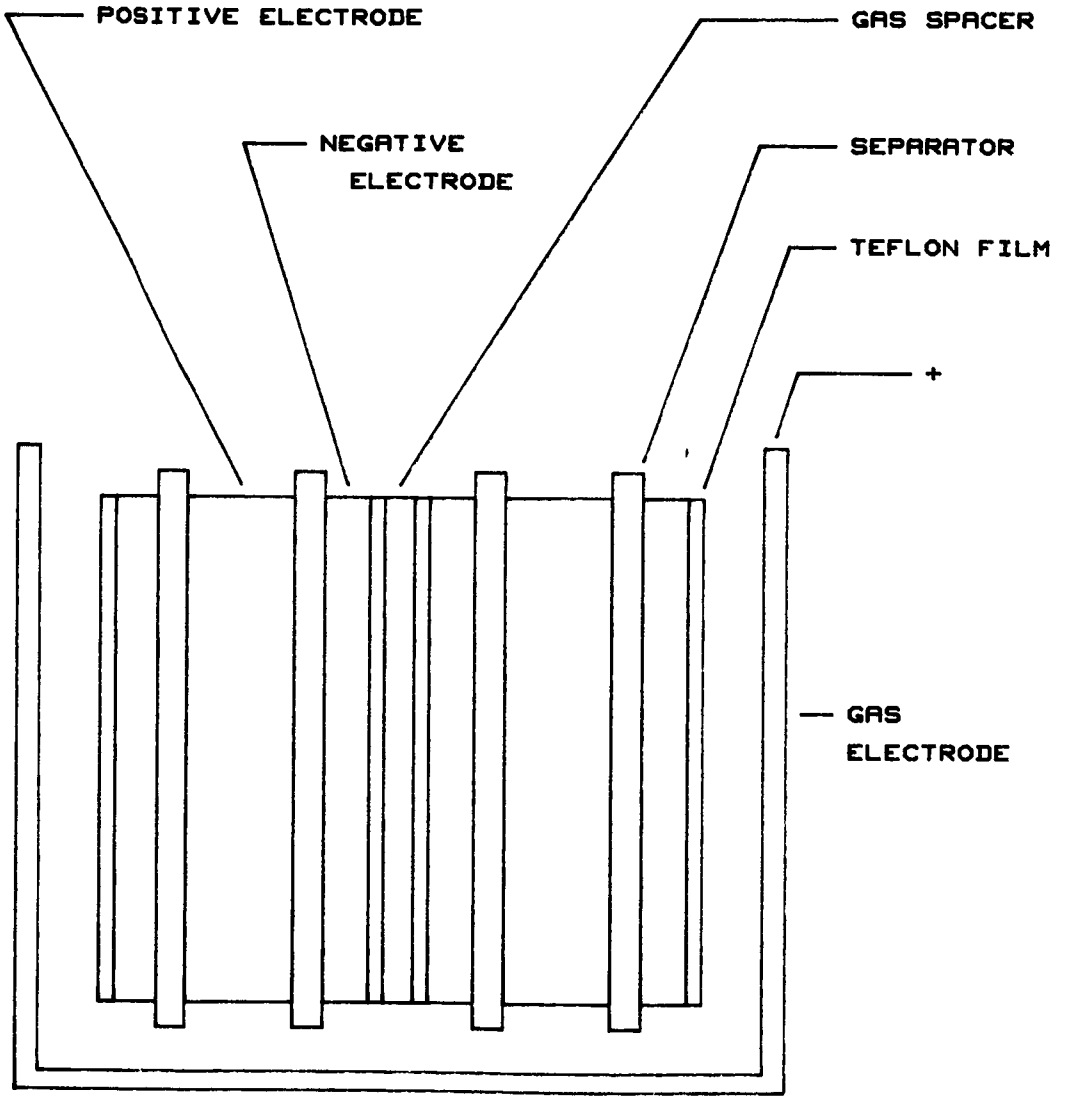

Figure 1. SEALED NICKEL-CADMIUM ADVANCED ELECTRODE STACK DESIGN

1. $H_2 + 2\ OH^- \rightarrow [2\ H_2O + 2e^-]$

2. $2\ NiOOH + [2\ H_2O + 2e^-] \rightarrow 2\ Ni(OH)_2 + 2\ OH^-$

COMBINED REACTION

3. $2\ NiOOH + H_2 \rightarrow 2\ Ni(OH)_2$

Figure 2. SEALED NICKEL-CADMIUM GAS ELECTRODE REACTION

EAGLE PICHER

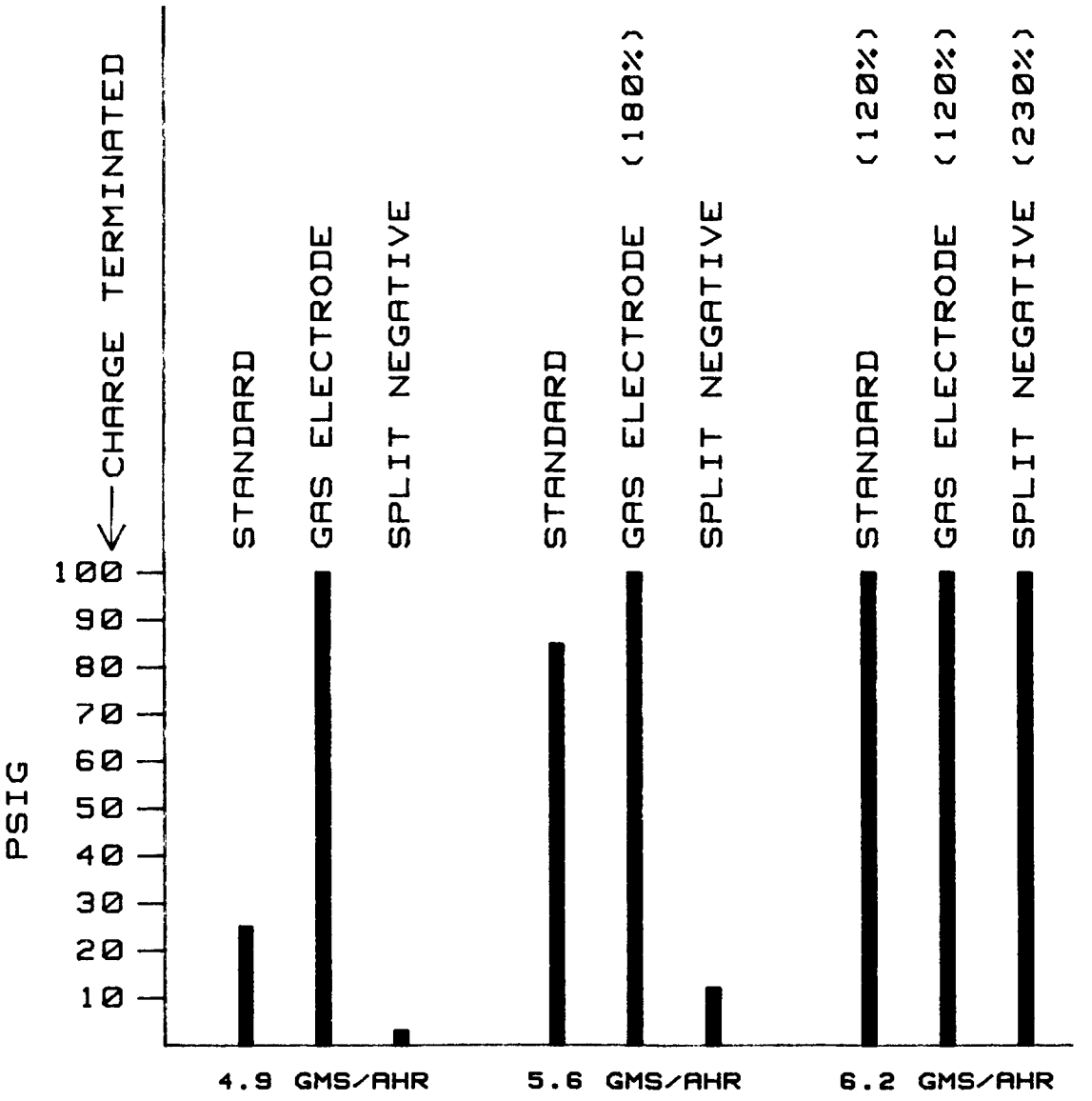

Figure 3. OVERCHARGE PRESSURE (O_2) VERSUS ELECTROLYTE QUANTITY CHARGE 250%, RATE C/10, TEMPERATURE 20°C

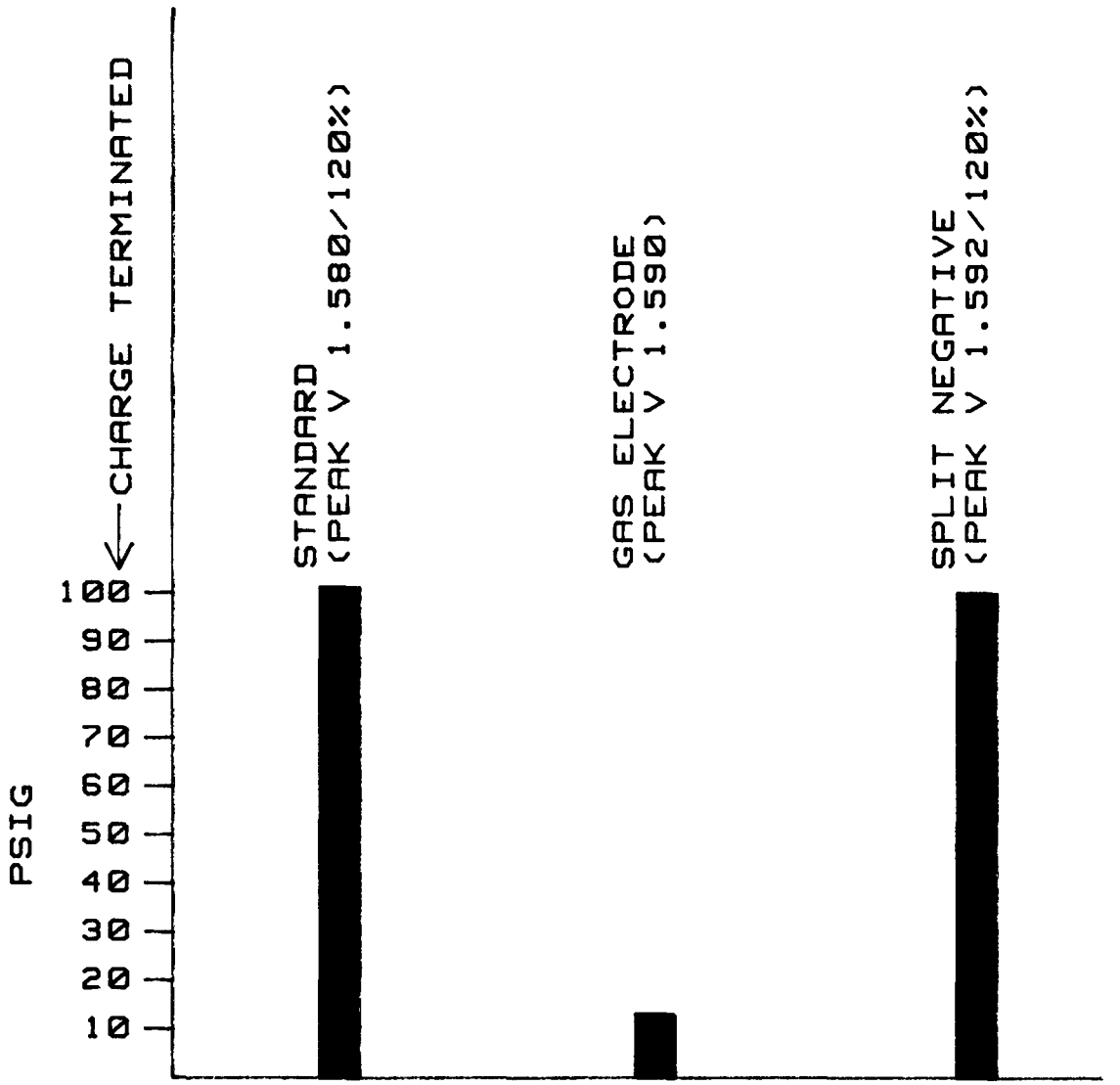

Figure 4. OVERCHARGE PRESSURE (H_2) VERSUS STACK DESIGN
CHARGE 200%, RATE C/10, TEMPERATURE 0°C

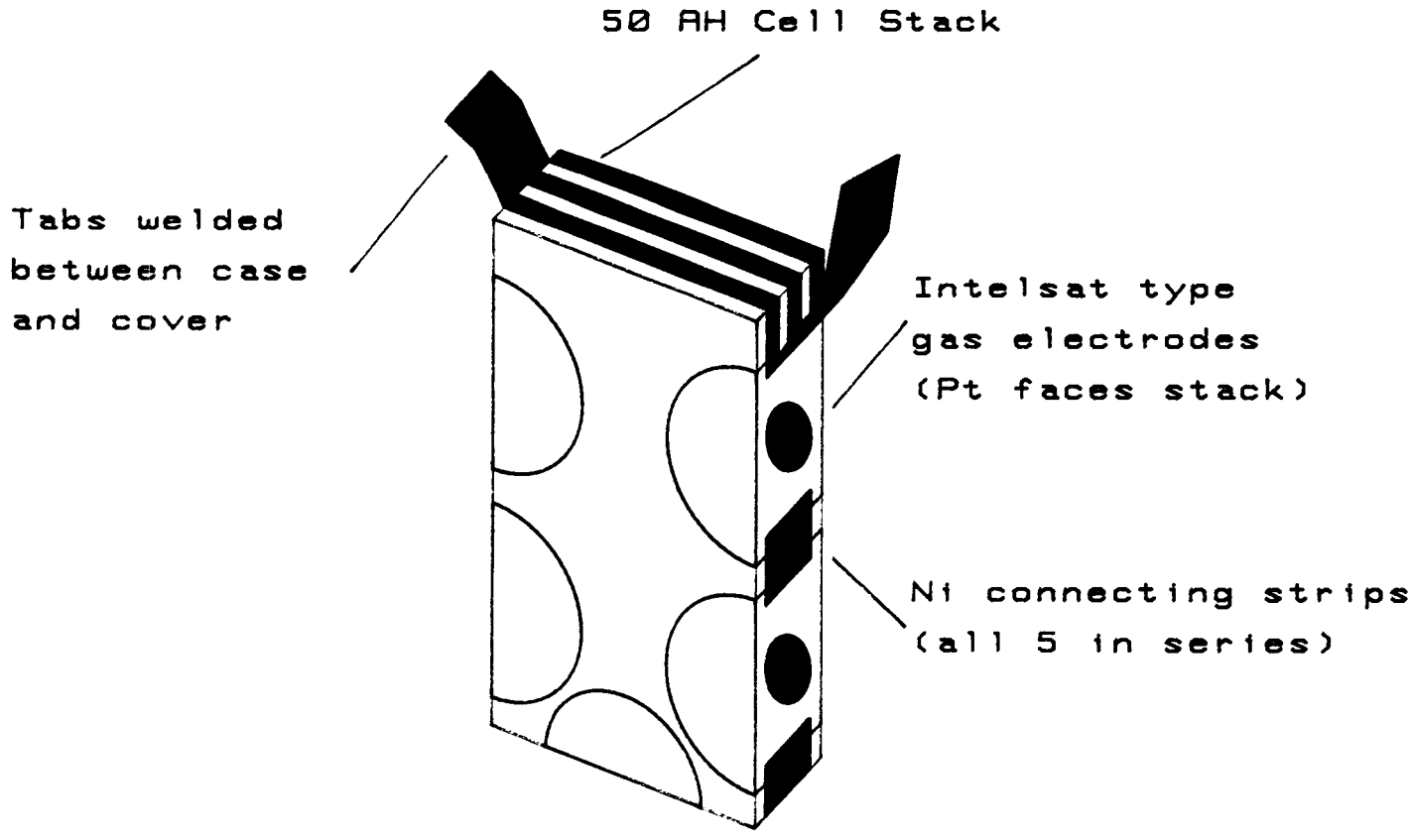

Figure 5. ADVANCED Ni-Cd TEST CELL ASSEMBLY SKETCH

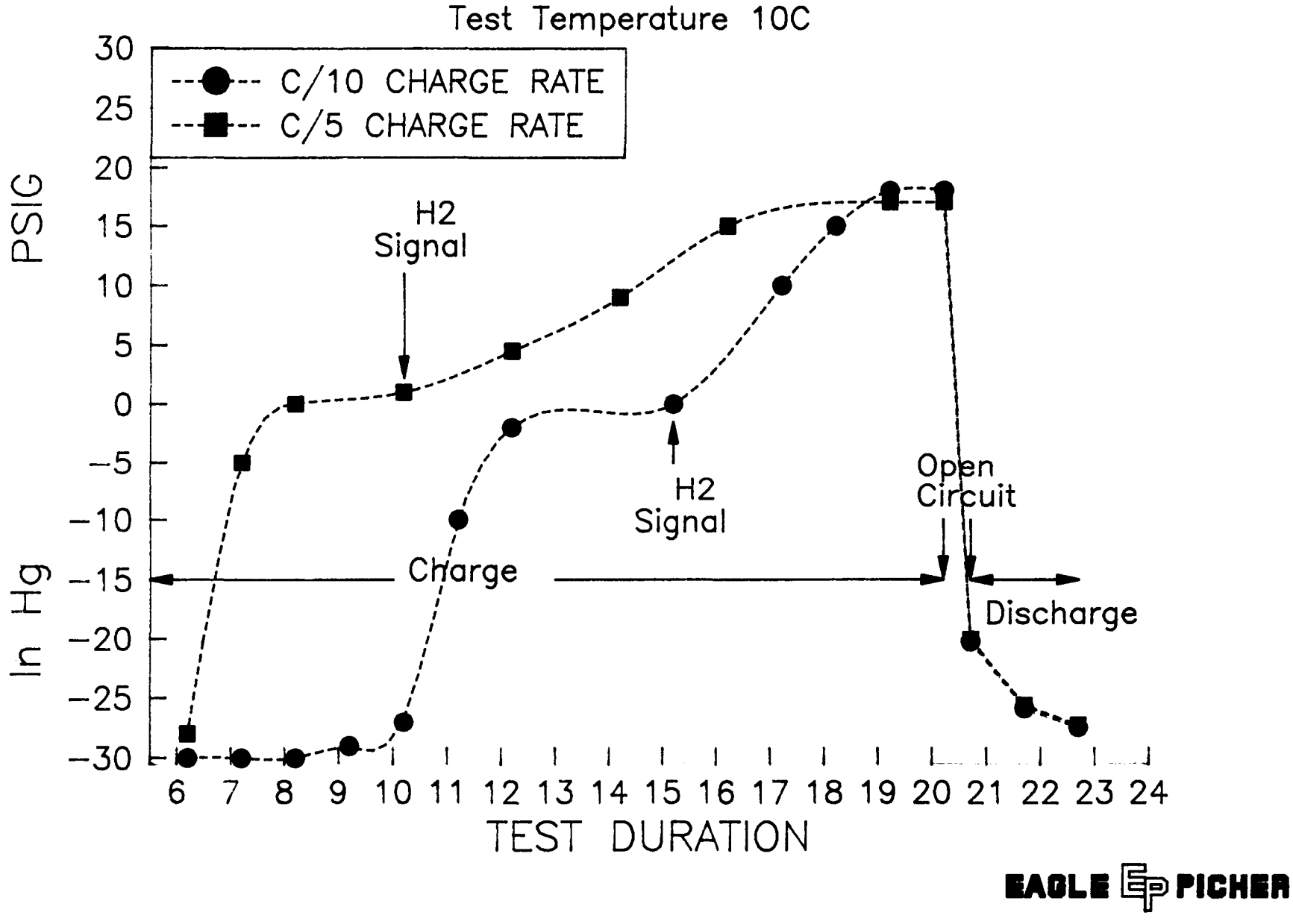

Figure 6. 50 Ah RATED Ni-Cd CELLS

1. GREATER OVERCHARGE TOLERANCE RELATIVE TO BOTH O_2 AND H_2 GAS EVOLUTION.

2. SIGNIFICANTLY DECREASED MAXIMUM ELECTROLYTE QUANTITY SENSITIVITY PROMOTING LONGER CYCLE LIFE.

3. IMPROVED CELL PERFORMANCE VIA EXTENDED OPERATIONAL RANGE.

4. ALLOWS CONSIDERATION OF MORE STABLE, LONGER LIFE INORGANIC SEPARATOR MATERIALS.

5. ENHANCED CELL REVERSAL TOLERANCE.

Figure 7. SEALED NICKEL-CADMIUM ADVANCED ELECTRODE STACK DESIGN ADVANTAGES

EAGLE PICHER

Self-Discharge Characteristics of Spacecraft Nickel-Cadmium Cells at Elevated Temperatures

Paper to be Presented at the
1985 NASA/GSFC Battery Workshop

November 19-21, 1985

by

S. W. Donley, J. H. Matsumoto, and W. C. Hwang
The Aerospace Corporation
P. O. Box 92957
Los Angeles, CA 90009

VUEGRAPH 1

Little is known concerning the self-discharge and heat generation in nickel-cadmium cells when they are subjected to temperatures far in excess of ambient. It is known that in general the rate of chemical energy loss from the cells in the form of heat increases with temperature and that thermal runaway is a likely result at sufficiently high temperatures, even with cells on open circuit. Actual conditions promoting thermal runaway have heretofore not been established. The work reported here provides such data in tests performed on open-circuited NiCd cells, fully charged, when such cells were heated externally to temperatures from 40°C to 120°C.

VUEGRAPH 2

The objective of this paper is to relate the effects of heat generation in spacecraft nickel-cadmium (NiCd) cells during high temperature storage on open circuit. When nickel cadmium batteries are open circuited in the charged state, chemical reaction(s) provide a means of self-discharge and heat-generation. The rates of self-discharge and heat-generation are relatively low at normal spacecraft operation temperatures (-5 to 30°C); however, the rates and possibly the complexity of the reactions increase with temperature. There is little data available concerning capacity losses via self-discharging in NiCd cells due to elevated temperature (above 40°C) exposure. Such data could be useful in space programs, as temperatures in the range 80-100°C may cause the batteries to become thermally unstable. Additional heating generated by battery self discharge may drive the batteries into catastrophic failure with consequence for the integrity of the spacecraft and its contents. The testing described here was designed to

determine the extent to which battery thermal stability is a valid concern, at temperature of exposure (externally effected) between 40°C and 120°C.

VUEGRAPH 3

The NiCd cells selected for testing are General Electric catalog number 35AB11, 35 Ah nominal capacity. It is expected that the results obtained with these cells can readily be extended to other NiCd spacecraft batteries.

The cells were enclosed in an insulating container (Fibrothal (Reg.), Kanthal Furnace Products Co.) prior to test. The cell test apparatus is shown in vuegraph 3, which is not drawn to exact scale in order to show some of the details. The large faces of the cell were supported by 1/4 inch aluminum restraints which were held together by 4 screws (not shown in drawing). The cell and restraints were designed to slip into the aluminum liner along with the heater and aluminum shims to provide a snug fit. All sliding pieces were coated with silicon heat conducting compound. The liner was bonded to the glass foam insulation with a high thermal conductivity RTV compound. Empty spaces within the glass foam insulator (top, bottom, and small faces of cell) were filled with glass wool. Thermistors were mounted at the top and bottom of the cell, on the outside of the cell restraint opposite the heater, on the inside of a small face of the liner, on two outside surfaces of the foam insulator, and at the bottom of the foam insulator. A strain gauge was placed on either the cell top or bottom in order to monitor any possible bulging of the cell case.

VUEGRAPH 4

The insulated test assembly was operated inside an environmental chamber. The seven thermistors and the strain gauge measurements were monitored by a computer which also controlled the heater, the insulator, and the temperature of the environmental chamber. Calibrations of the thermistors, specific heat of a cell, specific heat of the test apparatus, and thermal conduction through the test apparatus were made with a solid aluminum "dummy cell" of known specific heat. At a given environmental chamber temperature, the heater inside the assembly provided sufficient heat for particular initial internal temperatures.

VUEGRAPH 5

Measurements of temperature after heating provided the necessary calibration data. While the initial external (environmental chamber) temperature was to be 60°C, the internal temperatures for the determination were 60, 80, 100, 120, 140, and 160°C. The thermal processes operating in the experimental

test fixture during the calibration runs with a dummy cell of known heat capacity (b') are described by the equation:

$$(1) \quad a\int_{\tau_1}^{\tau_2} [T(t)-T'(t)]dt + \frac{c}{2}[T(\tau_2)-T(\tau_1) + T'(\tau_2)-T'(\tau_1)] = b'[T(\tau_1)-T(\tau_2)]$$

where a is the constant for heat loss through the insulator to the environment, and c is the heat capacity of the insulator, and where T(t) = temperature of cell as a function of time, and T'(t) = temperature of chamber as a function of time.

VUEGRAPH 6

VUEGRAPH 6 is a computer plot of actual data for selected thermistors from one of the "dummy cell" runs, which were performed in order to determine the heat dissipation rate through the walls of the cell insulating container at various temperatures of the container/contents and the surrounding thermal chamber. In this case both the dummy cell and the chamber were brought initially to 60°C, then the cell heaters were disconnected and the dummy cell surface temperatures were monitored for one hour. In this way the dummy cell was heated to successively higher temperatures, and the temperatures with no cell heating were monitored. The chamber temperature, nominally constant, demonstrated a small upward drift throughout the test, in addition to a significant ripple associated with each cell heating and cooling cycle.

VUEGRAPH 7

The values of the insulator heat capacity, c, and the rate of heat dissipation through the walls of the insulator, a, were determined from analysis of the thermistor data during the periods of active heating and by determining the cooling rates (heaters off) respectively.

The heat capacity (b) of the actual 35 Ah cells that are the subject of this paper were determined by calculation from the materials of construction of the cells. The value obtained for a fully discharged cell was then adjusted by calculation to account for the differences in the heat capacition between the charged and discharged active cell materials. A value of ΔH (cell) of 0.235 Wh/°C (202 cal/°C) was derived from this calculation, in good agreement with data found in the literature.[1]

VUEGRAPH 8

In the cell testing, fully charged cells were fastened between restraining plates, fitted with thermistors, etc., and inserted into the insulating housing in the same way that the dummy cells were treated

earlier. The experiments were performed with fully charged cells at initial internal and external temperatures of 44, 64, 82, 85, and 118°C. The temperatures following the initial heating were monitored for up to 48 hours and provided the data necessary for calculating the self-heat generation of these NiCd cells in this temperature range. The same two cells were used for the 60° tests that were tested at 40°, after recharge. Otherwise, fresh cells were used in each cell temperature test. The testing procedure was to heat the test chamber to the preset test temperature, then to heat the cells to approximately the same temperature via timed resistance heaters contained inside the insulators, in contact with the cell surface, at the rate of ~ 2°C/min. In vuegraph 8 are shown the actual cell wall temperatures achieved at the completion of the heating period, and also the maximum temperatures achieved.

VUEGRAPHS 9, 10, 11

Example cell and chamber actual temperature data (for simplicity not all thermistor outputs are shown) appear in vuegraph 9-11. In all these plots the chamber temperature was subjected to a periodic perturbation, arising from an idiosyncrisy in the test computer database that caused the chamber heaters to activate at 8 hr intervals. One hour after the Tenney chamber reached the setpoint temperature the cell heaters were fed a predetermined amount of energy, calculated from the cell constant, and sufficient to bring the cells and other contents of the insulating containers to the setpoint temperature. Thereafter the chamber temperature was maintained and both chamber and cell temperatures were monitored. As in the earlier calibration runs each cell had five thermistors attached to it, and three thermistors were attached to the outside surface of the insulator. The thermistor readings were monitored at intervals throughout the test and the data stored on floppy disks. Values of all the cell surface temperatures were averaged prior to the succeeding calculation of self discharge rates, as were chamber temperatures.

The calculation of cell self discharge rates assumed that all cell capacity and energy losses were converted entirely to heat, and that the heat dissipation rate through the walls of the insulator and the cell thermal capacity derived earlier are valid at all temperatures of the testing. The cell discharge rates, q, at various temperatures were calculated from actual time/temperature data and the calculated slopes of the time/temperature plots with the following equation:

$$(2) \qquad q(\tau) = \left(b + \frac{c}{2}\right) \frac{dT(\tau)}{d\tau} + \frac{c}{2} \frac{dT'(\tau)}{d\tau} + a \left[T(\tau) - \tau'(T)\right].$$

VUEGRAPH 12

The calculated cell heat generation data are plotted (as log q v. T^{-1} in vuegraph 12 together with error bars. The errors are greater at the lower temperatures because at these temperatures the derived heating rates are dominated by the term in the equation requiring the determination of small temperature differences. Previous 40°C data are shown for comparison reference 2 (Scott, et al., shown in Vuegraph 12). These data can now be used to evaluate thermal runaway conditions for any battery system with a known thermal control properties. The data should be scalable to other cell sizes.

VUEGRAPH 13

We earlier described a cell as having "exploded" at cell surface temperature in excess of 230°C. At the calculated rate of heat generation (> 500W) at a few minute before the catastrophic event occurred it is likely that the actual temperature at points within this cell were well in excess of that measured at the cell surface. At these temperatures the separator material fused, allowing the electrode materials to come into intimate contact. Although we do not have information adequate to judge whether an explosion indeed occurred or merely a forceful venting, a decided odor of organic combustion was detected in the surrounding laboratory area after the event. Photographs of the cell chamber and its environmental chamber are shown in vuegraph 13. The heavy stainless steel walls of the environmental chamber were bowed outward and the door hinges were bent, in spite of a 4 inch diameter hole having been provided for pressure dissipation. As can be seen in the photos, the 1/4 inch aluminum restraining plates over the cell faces were bent but held, while all four side panels of the cell were blown free. The electrode sinter was covered by black frangible dust which was all that was left of the active material

VUEGRAPH 14

The conclusions of this study are that thermal runaway can occur from elevated temperature self-discharge of NiCd batteries. Thermal runaway can be fast enough to rupture cells in batteries and cause physical damage in the surrounding area. In our particular case battery temperatures above about 80 deg. C cannot be allowed without adequate provision for heat dissipation.

References

1. A. Laursen and P. H. Jacobsen, "Analysis and Testing of the Thermal Properties of Space Battery Cells," European Space Agency Contract No. 498/82/NL/JS(SC), January 1983.

2. W. R. Scott and D. W. Rusta, "Sealed-Cell Nickel-Cadmium Battery Applications Manual," NASA Reference Publication 1052, December 1979, p. 101.

VUEGRAPH 1

HEAT GENERATION FROM SELF-DISCHARGE OF NICKEL-CADMIUM CELLS AT ELEVATED TEMPERATURES

BY

S. W. DONLEY, J. H. MATSUMOTO, AND W. C. HWANG
THE AEROSPACE CORPORATION
P. O. BOX 92957
LOS ANGELES, CA 90009

NOVEMBER 20, 1985

VUEGRAPH 2

OBJECTIVE

* TO DETERMINE THE HEAT GENERATION IN SPACECRAFT NiCd CELLS DURING OPEN CIRCUIT STAND AT ELEVATED TEMPERATURES

METHOD

* ENCLOSE CELLS (AT 100% S.O.C.) IN INSULATIVE CONTAINERS AT ~ADIABATIC CONDITIONS AT T: 40° to 120°C

* FOLLOW TEMPERATURE PROFILES OF CELLS AND SURROUNDINGS

* CALCULATE CELL HEAT GENERATION RATES VERSUS TEMPERATURE

VUEGRAPH 3

Thermal Test Assembly

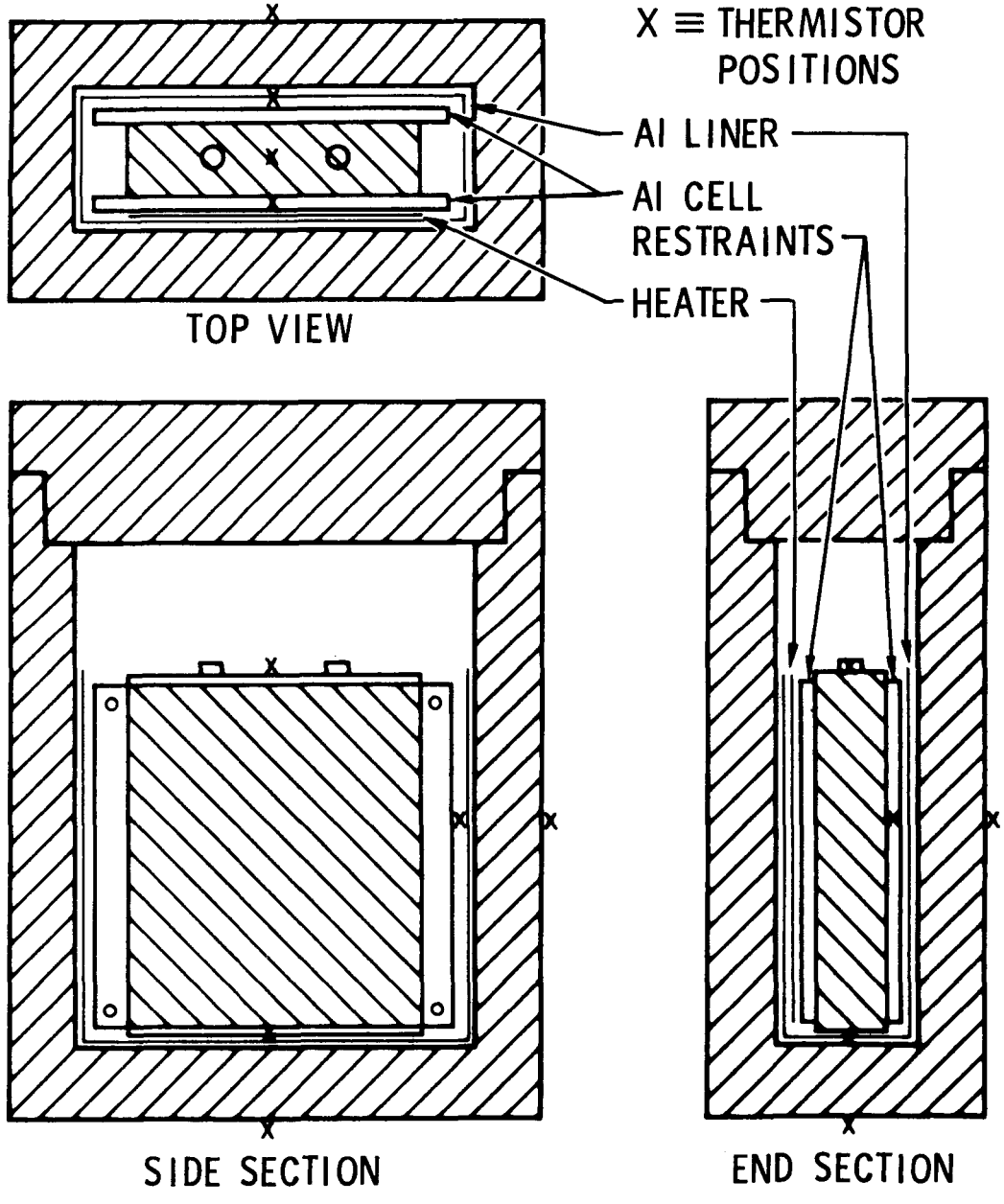

NOT TO EXACT SCALE

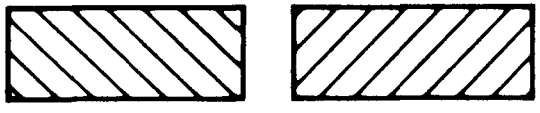

VUEGRAPH 4

Block Diagram of Test Apparatus

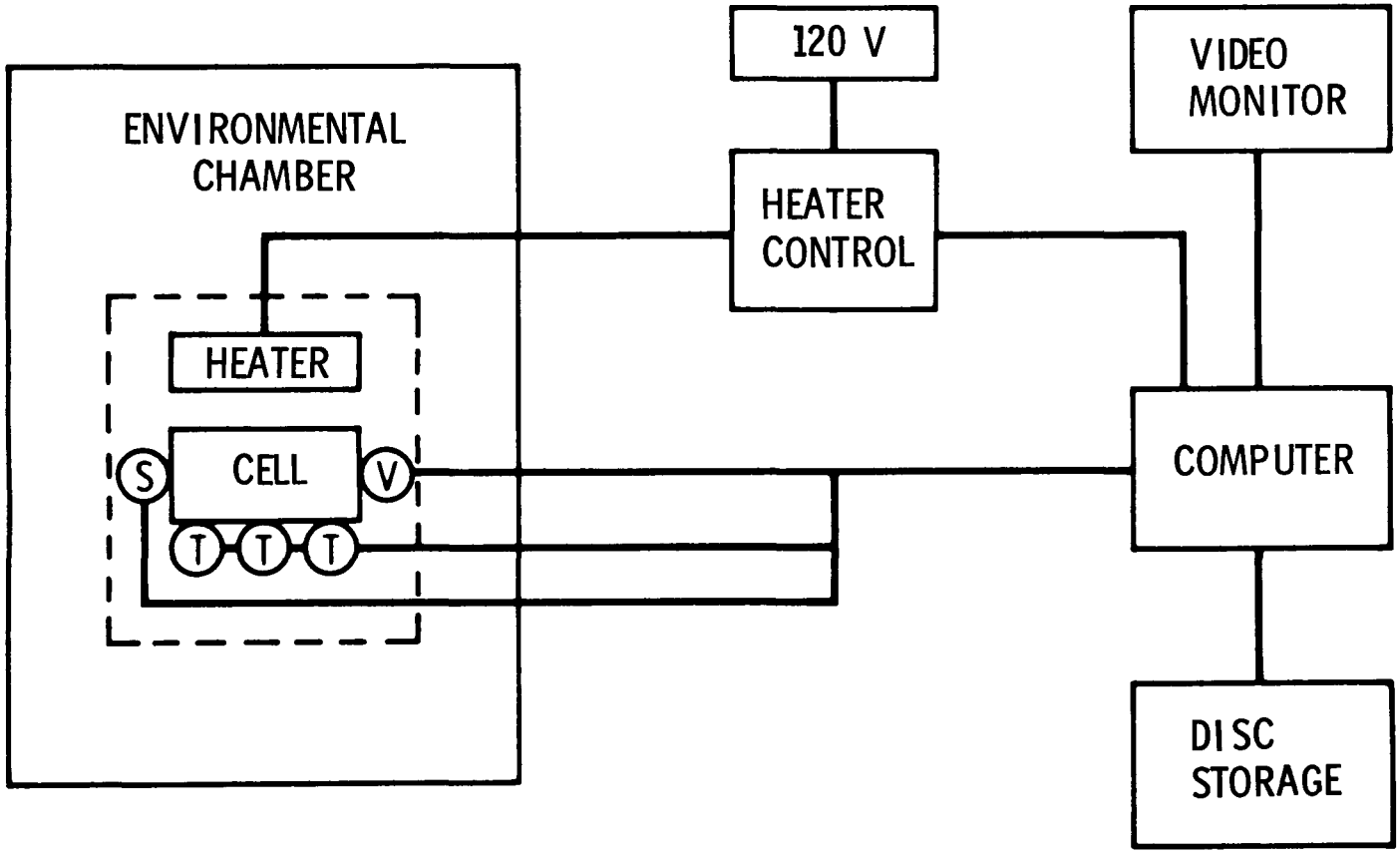

VUEGRAPH 5

CALIBRATION OF TEST APPARATUS

* INSULATOR CONSTANTS DETERMINED WITH "DUMMY" CELL OF KNOWN HEAT CAPACITY:
  * CONSTANT FOR HEAT LOSS RATE THROUGH INSULATOR (W/DEG)
  * CONSTANT FOR HEAT CAPACITY OF INSULATOR (Wh/DEG)
* CELL CONSTANT FOR A 35 Ah NiCd CELL
  * HEAT CAPACITY OF DISCHARGED CELL (Wh/DEG), CALCULATED AND VERIFIED EXPERIMENTALLY
  * CORRECTION FOR FULLY CHARGED CELL, BY CALCULATION

$$a\int_{t_1}^{t_2}\left[T(t) - T'(t)\right]dt + c/2\left[T(t_2) - T(t_1) + T'(t_2) - T'(t_1)\right] = b'\left[T(t_2) - T(t_2)\right]$$

where a is constant for heat loss through insulator
c is heat capacity of insulator
b' is heat capacity of "dummy" cell
T(t) is the cell temperature as a function of time
T'(t) is chamber temperature as function of time

VUEGRAPH 6

Temperature vs Time

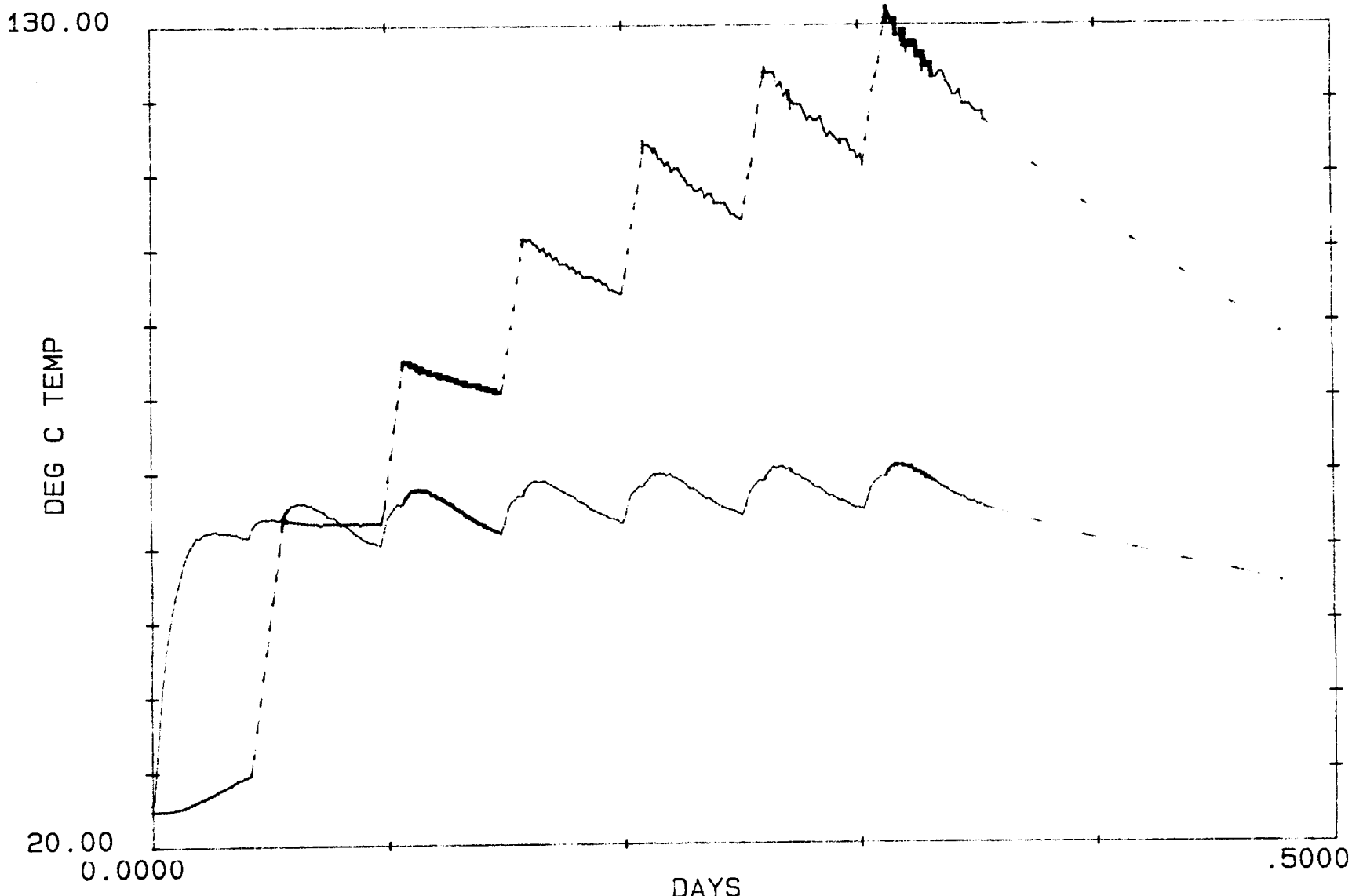

VUEGRAPH 7

THERMAL PARAMETERS

Heat Dissipation Rate:	**0.126 W/deg C**
Cell Heat Capacity:	**0.235 Wh/deg C**
Cell Restraints Heat Capacity:	**0.216 Wh/deg C**
Insulation Heat Capacity:	**0.156 Wh/deg C**

VUEGRAPH 8

CELL TEMPERATURE DATA SUMMARY

NUMBER OF CELLS TESTED	INITIAL TEMP DEGREES C	CELL TEMP. ACHIEVED AT END OF TEST, ° C	ENVIRONMENTAL CHAMBER TEMP DEGREES C
2	~44	42	36 - 38
(2)[1]	~64	64	58 - 59
2	~82	85	70 - 72
2	~85	>166[2]	72 - 79
1	~118	230	121 - 129

1. SAME CELLS AS 40°C TEST
2. CELLS WERE FULLY DISCHARGED

VUEGRAPH 9

Temperature vs Time

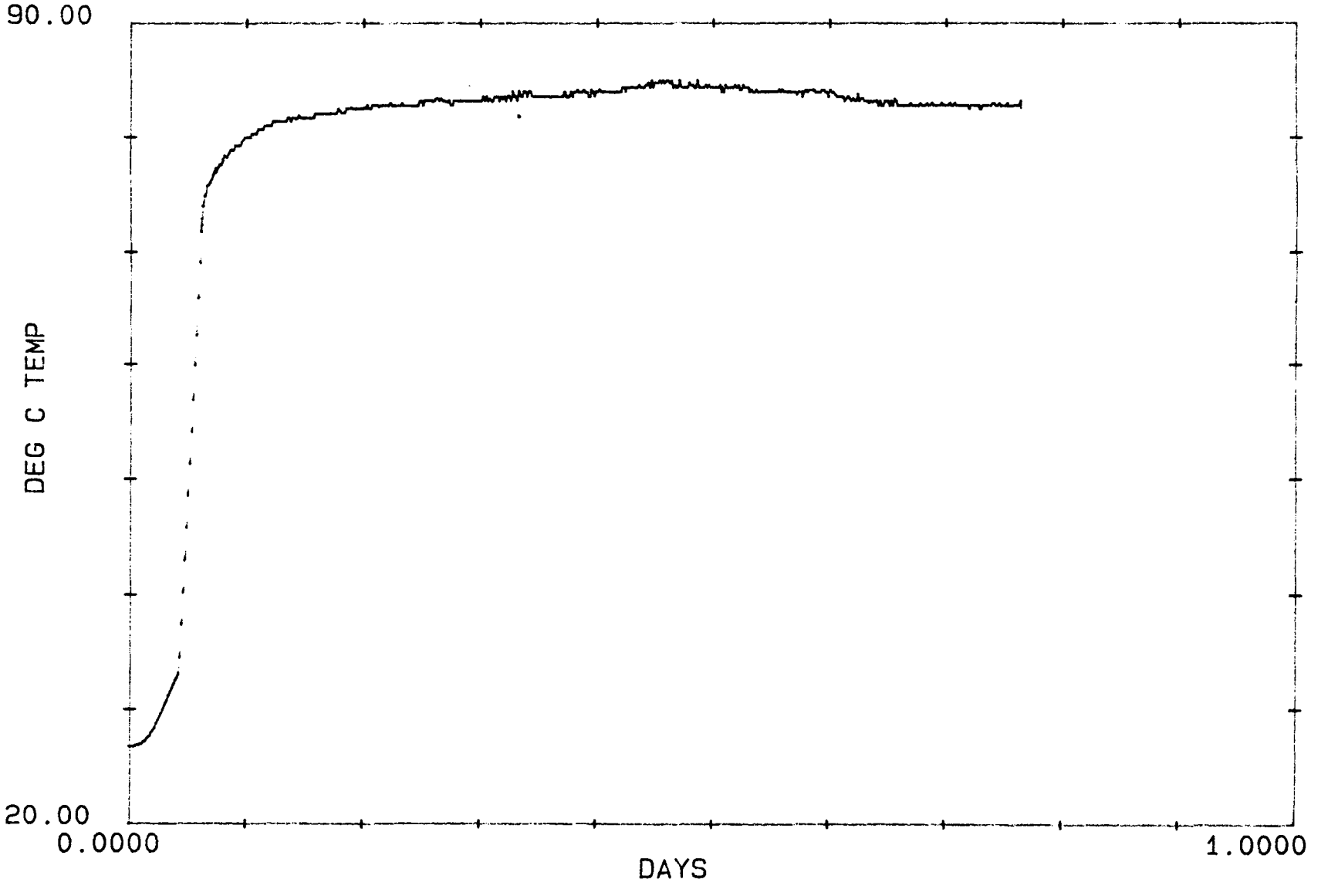

VUEGRAPH 10

Temperature vs Time

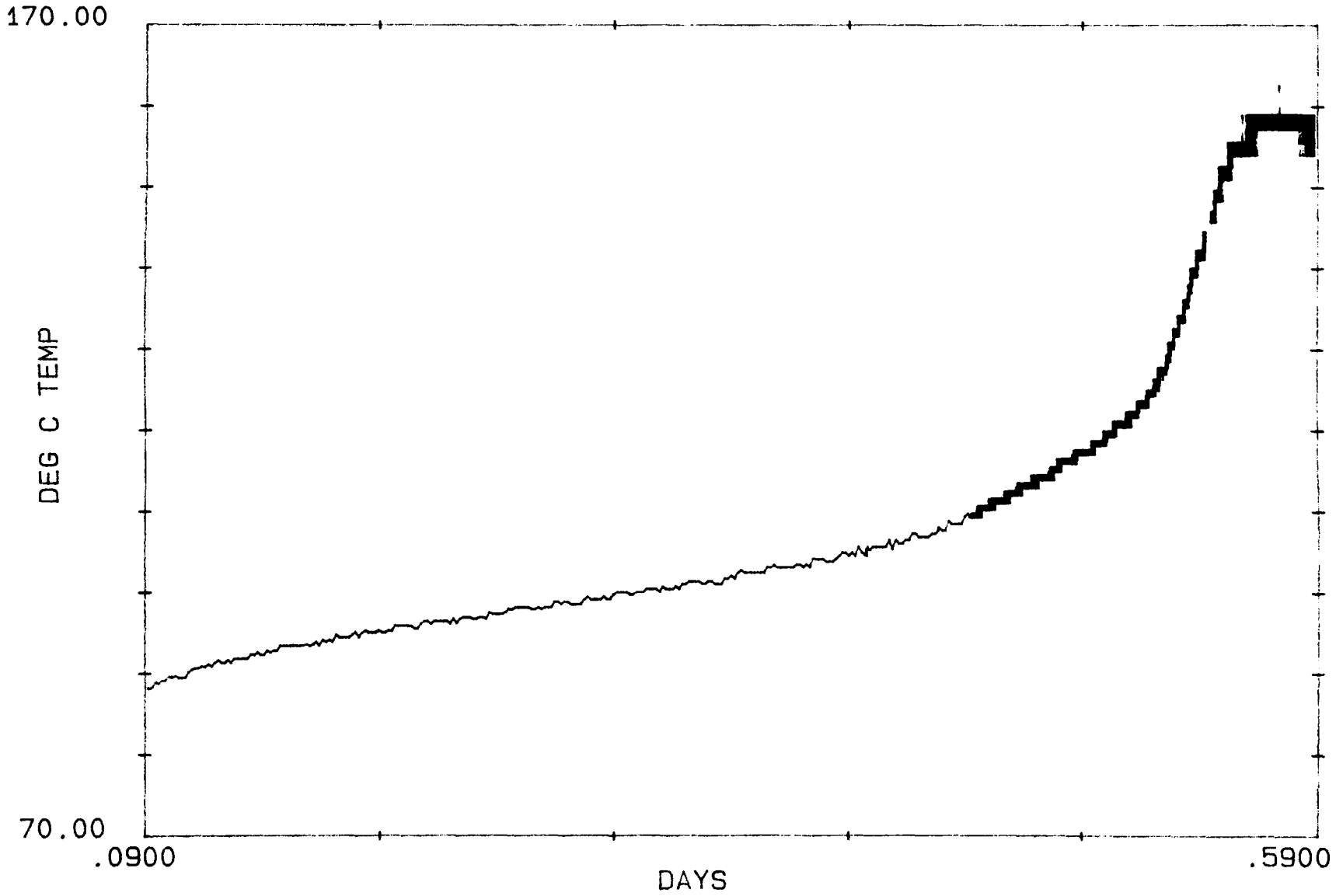

VUEGRAPH 11

Temperature vs Time

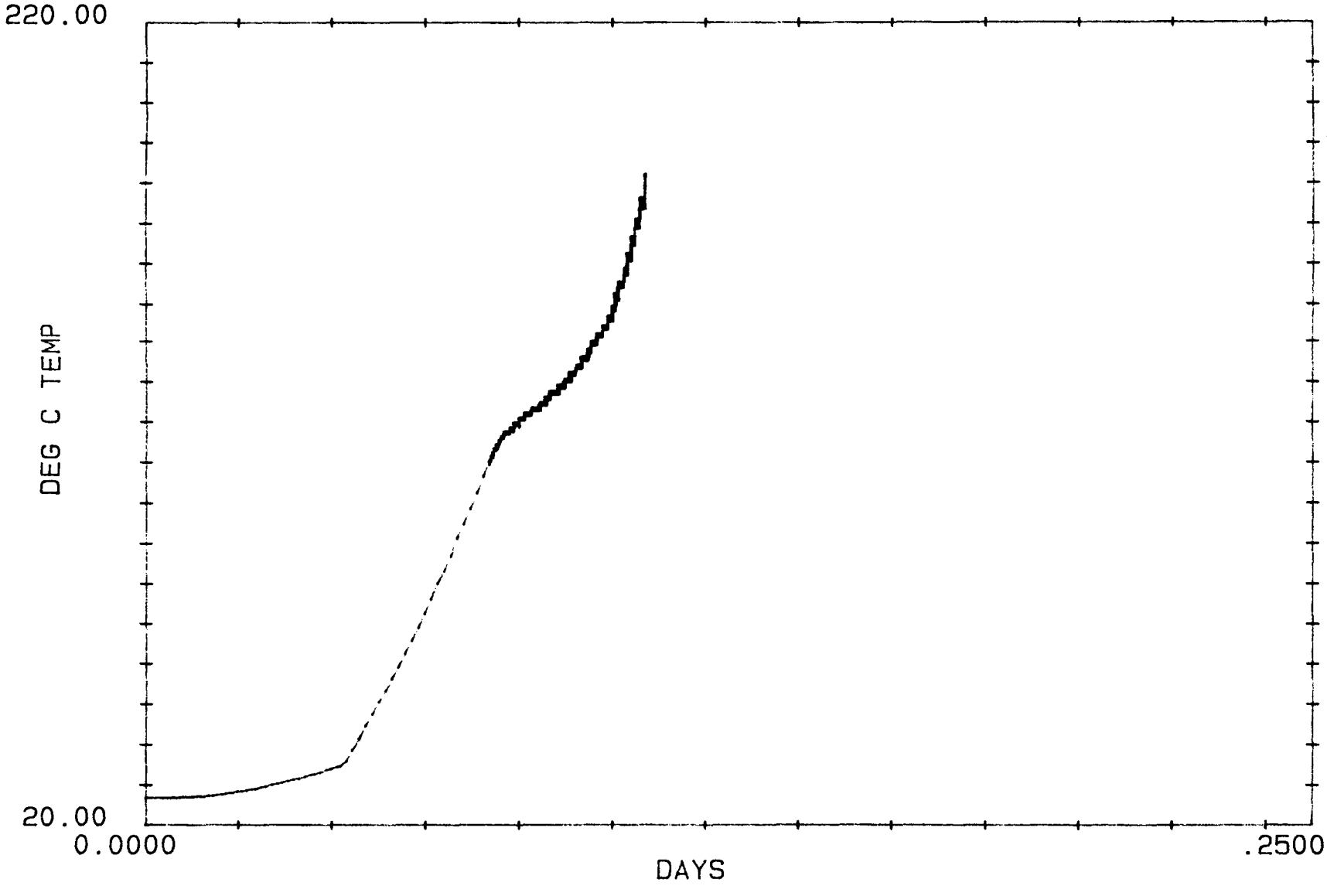

VUEGRAPH 12

Post–Explosion Photographs

A. CHAMBER INTERIOR

B. REMAINS OF 35 Ah CELL

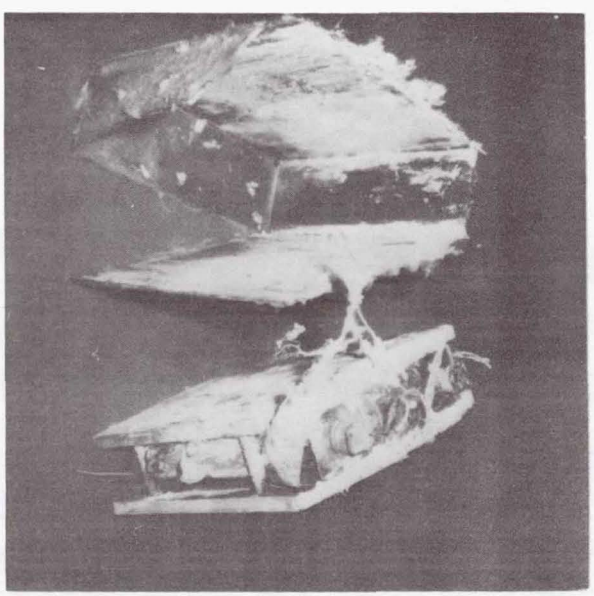

VUEGRAPH 13

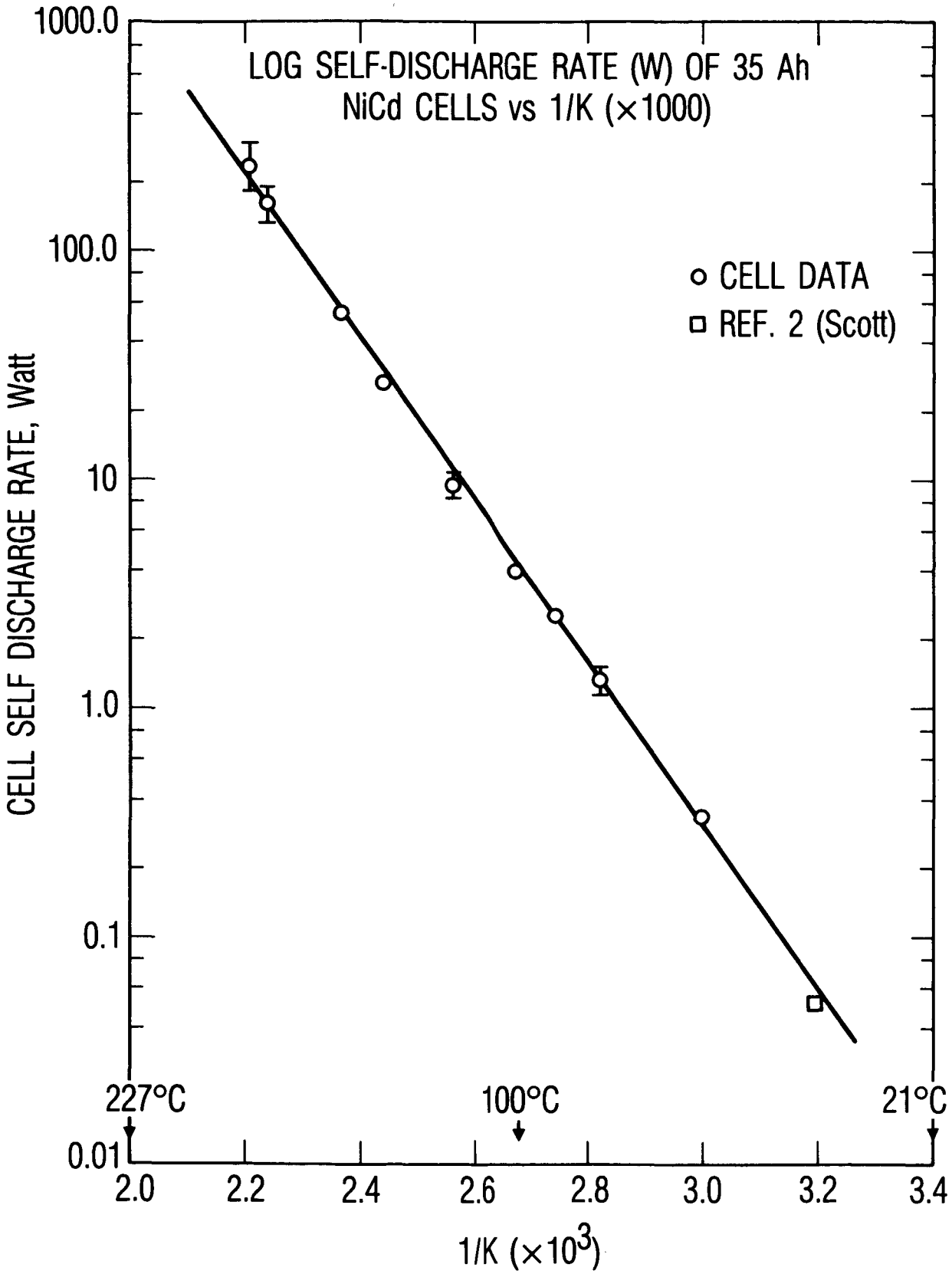
LOG SELF-DISCHARGE RATE (W) OF 35 Ah
NiCd CELLS vs 1/K (×1000)
CELL DATA
REF. 2 (Scott)
CELL SELF DISCHARGE RATE, Watt
1000.0
100.0
10
1.0
0.1
0.01
227°C
100°C
21°C
2.0
2.2
2.4
2.6
2.8
3.0
3.2
3.4
1/K (×10³)

VUEGRAPH 14

CONCLUSIONS

* THE HEAT GENERATED FROM SELF-DISCHARGE HAS NOW BEEN DETERMINED OVER A WIDE RANGE OF TEMPERATURES

* THERMAL RUNAWAY CAN OCCUR FROM ELEVATED TEMPERATURE SELF-DISCHARGE

* THERMAL RUNAWAY CAN BE FAST ENOUGH TO RUPTURE CELLS IN BATTERIES AND CAUSE PHYSICAL DAMAGE IN THE SURROUNDING AREA

* TEMPERATURES OF A CHARGED BATTERY MUST BE LIMITED FOR SAFETY MEASURES EVEN ON OPEN CIRCUIT. THE MAXIMUM ALLOWABLE TEMPERATURE DEPENDS ON THERMAL MANAGEMENT. IN OUR CASE 80° C WAS THE UPPER LIMIT.

SESSION IV

TOPIC: SIMULATED ORBITAL CYCLING AND FLIGHT EXPERIENCE
Chairman: T. Y. Yi, NASA/GSFC

MODELING NI-CD PERFORMANCE

Planned alterations to the Goddard Battery Model

James M. Jagielski

NASA/Goddard Space Flight Center

ABSTRACT

The Goddard Space Flight Center (GSFC) currently has a preliminary computer model to simulate Nickel Cadmium (Ni-Cd) performance. The basic methodology of the model was described in the paper entitled "Fundamental Algorithms of the Goddard Battery Model" (reference 1) submitted to the 1984 GSFC Battery Workshop. At present, the model is undergoing alterations to increase its efficiency, accuracy, and generality. This paper will give a review of the present battery model, and describe the planned changes to the model.

INTRODUCTION

Ni-Cd batteries have been, are, and will be the energy storage devices for the vast majority of photovoltaic-based spacecraft power systems. As the complexity, size, and cost of these spacecraft increase, however, it becomes less desirable (or even possible) to test and verify the performance of the power system by actual land-based testing. Therefore, another method of power system "testing" must be made available to the power system engineer. The method that has arisen is computer modeling and simulation.

By creating an accurate computer model of the system, the engineer can simulate various situations and scenarios that the system may encounter. As long as the model is accurate, and the simulation meaningful, the engineer can be confident of the results.

Ni-Cd batteries have long been difficult components to model. This is due, in part, to their being electro-chemical devices, and not purely electrical. Various approaches have been used to model Ni-Cd cells including The Equivalent Electrical Circuit approach (reference 2 and others), The Chemical Reaction approach (reference 3), The Parametric Fit

approach (reference 4), and The Data Base Manipulation approach (reference 1, 5 and others). The Goddard Battery Model is of the last type.

THE PRESENT BATTERY MODEL

The Data Base

The data base for the present battery model is a family of charge and discharge matrices for various temperatures, voltage-temperature (V/T) charge limits, and depths of discharge (DODs). A typical charge/discharge matrix is shown in figure 1.

As can be seen, the matrix itself relates cell voltage with cell current and a variable called Instantaneous Proportional Capacity (IPCAP). IPCAP is a variable which keeps track of the throughput capacity of the cell. For example, consider a 50 ampere hour cell. If 20 amp-hrs were discharged from the cell, the value of IPCAP would be 0.60. If 30 amp-hrs were returned to the cell, the value of IPCAP would increase to 1.20. The actual formula for IPCAP is given in equation 1.

$$1)\quad IPCAP_{T+t} = IPCAP_{T} + \frac{\text{Amp-Hr to/from Battery}}{\text{Cell Rated Capacity}}$$

The value of "Amp-Hr to/from Battery" is positive if the cell is being charged, and negative if being discharged. Therefore, discharging the cell results in a decrease in the value of IPCAP while charging results in an increase. As can be seen from the equation, IPCAP is very similar to cell State Of Charge (SOC) and can be thought of as a "tracking" SOC variable. (In many charts and graphs, the variables SOC and IPCAP are used interchangeably.)

Using these matrices, it is possible to generate two battery performance curves: Voltage versus Current with IPCAP as the third variable or Voltage versus IPCAP with Current as the third variable. (Of course, cell temperature, DOD and V/T limit are also variables, but do not vary within the matrices themselves, but from one matrix to the other.)

Methodology

The approach currently used by the model is to have the data from the corresponding DOD, temperature, and V/T limit matrix represented as two families of curves relating cell voltage to current with IPCAP is the third variable. One family of curves represents the charge data, while the other characterises the discharge data. The curves themselves are stored as polynomial equations with cell voltage being the dependant variable and current being the independant variable. Each different curve (or equation) corresponds to a different IPCAP. Figure 2 shows a typical family of curves.

The model has two major modes or functions. The first is known as the **Normal Mode** and is used to determine the cell voltage when the charge/discharge current is known. The second mode is called the **Taper Mode** and is used to predict the current needed to maintain a constant cell voltage. This mode is used whenever a V/T-type charge control is used.

Normal Mode Operation

In calculating cell voltage, the values of normalized cell current (charge or discharge) and the IPCAP of the cell are known. The model proceeds to find the closest upper and lower bounding curves relative to the cell's actual IPCAP. For example, if the data base has curves for the IPCAP's of 100, 97, 90, 85, and 80% and the cell IPCAP is 95%, the model determines that the 97% curve is the closest upper bounding curve whereas the 90% curve is the closest lower bounding curve. This process is accomplished by using a standard binary search algorithm. The model then calculates the cell voltage relating to the (known) cell current for the upper and lower IPCAP curves. This, in essence, provides the model with two cell voltages at a particular cell current: one voltage refers to a cell slightly more fully charged than the simulated cell, the other voltage refers to a cell slightly less charged. The cell voltage for the simulated cell is then determined through a linear interpolation of the two bounding voltages. The linear interpolation introduces little error if the number of IPCAP curves is large.

Figure 3 is a graph comparing the model predicted voltage curve actual cycling data. The cell temperature was 20 deg C, 40% DOD, 20 ampere-hour rated capacity, 16 amp discharge (30 minutes), 16 amp charge (60 minutes), with a GSFC V/T limit of 7. As can be seen, the discharge voltage

correlates very highly. The charge voltage also correlates but not as well. It should be noted that the cycling data being compared was not the data used to generate the data base. Also, it should be noted on figure 3 that the actual cycling data does not hit a hard voltage clamp, but "creeps" up to it. This makes the model appear to be more in error than it actually is.

Taper Mode Operation

This mode of operation calculates the amount of charge current needed to maintain a cell at a constant voltage. Since, as is the case in voltage clamping charge control schemes, the current exhibits an exponential-like downward taper as the voltage remains clamped and the IPCAP increases, this charge current is generally known as the Taper Charge Current. The approach used by this method is somewhat different than the previous mode, although, as it will be seen, it actually uses the methodology of the Normal Mode Operation.

In calculating cell current, the cell voltage is known as is the cell IPCAP. However, the structure of the data base curves does not directly allow the model to calculate cell current. To circumvent this problem, the model uses a search approach to determine the taper charge current. The search approach is based on the Binary Search Algorithm.

The model begins by setting up two bounds for the taper charge current. These bounds represent the upper and lower limits of the possible values for the current. Since these values are initially unknown, they are set to reflect a wide range. (At present, the lower bound is set at 0 amps, the upper at 60 amps.) In essence, this means that the model assumes that the value for taper charge current needed to maintain the voltage clamp falls between these two bounds. The model then proceeds to calculate the median value between the two bounds. This median value is the Taper Charge Estimate (TCH). Using this value, the model, using the exact same method as the Normal Operation Mode, calculates the cell voltage corresponding to the TCE and compares this with the voltage clamp. If the calculated voltage is greater than the voltage clamp, the TCE was too high. In this case the model resets the upper bound to the TCE since it is now known that the actual taper charge current must be less than the TCE and does not fall between the TCE and upper bound (the taper current is no greater than TCE). Conversely, if the calculated voltage is less than the voltage clamp, the TCE was

too small (the current was insufficient to maintain the cell at the voltage clamp). In this case the model resets the lower bound to the TCE since it is now known that the actual taper charge current must be greater than the TCE. The process then continues by calculating a new TCE with the adjusted bounds. In this way, as the bounds are constantly being adjusted, the model "zeroes in" on the actual taper charge current. Figure 4 shows a comparision between actual cycling data and model predicted data for the taper charge current. Once again it should be noted that the cycling data depicted is not the data used in the data base.

THE PLANNED MODIFICATIONS TO THE BATTERY MODEL

As mentioned in reference 1, the data base used in the battery model is of questionable accuracy. Also, the data form itself is non-standard. It was determined that the majority of cell performance data is in the form of cycling tests. In standard LEO cycling V/T limited tests, the data does not result in the same type as depicted in figure 1. This is due to the fact that the present data base extrapolates data **beyond** the V/T clamp, and it is this extrapolation which results in the suspected inaccuracy of the data. However, the model at present requires data in this format. It was therefore determined that the model be altered to accept data in the standard cycling format. This will result in not only a model modification, but also an alteration in the way the data is used, as will be seen below.

The New Data Base

The new data base was generated by cycling 5 NASA standard 50 ampere-hour cells under various V/T limits, DODs, temperatures, and charge/discharge rates as defined in the following table.

Data Base Voltage-Temperature (V/T) Limits (GSFC):	3, 5, 7
Cell Operating Temperatures (degrees C):	0, 10, 20
Charge Rates (Amps):	10, 25, 30, 40
Discharge Rates (Amps):	5, 10, 25, 40
Discharge Time (minutes):	30
Charge Time (minutes):	60

Since the discharge time is 30 minutes, the discharge rates of 5, 10, 25, and 40 amps correspond to a DOD of 5, 10, 25, and 40% respectively. Additionally, cases where the cell would not be recharged after a cycle (for example, a discharge rate of 40 amps for 30 minutes and a charge rate of 10 amps for 60 minutes) were not run. Therefore, the data base has data according to the table below.

5 Amp Discharge Rate		36 test cases
V/T	3, 5, 7	(3)
Temp	0,10,20	(3)
Charge	10,25,30,40	(4)
10 Amp Discharge Rate		36 test cases
V/T	3, 5, 7	(3)
Temp	0,10,20	(3)
Charge	10,25,30,40	(4)
25 Amp Discharge Rate		27 test cases
V/T	3, 5, 7	(3)
Temp	0,10,20	(3)
Charge	25,30,40	(3)
40 Amp Discharge Rate		18 test cases
V/T	3, 5, 7	(3)
Temp	0,10,20	(3)
Charge	30,40	(2)

The Data Curves

As was mentioned above, the present model uses a family of curves in which cell voltage is related to current with IPCAP as a third variable. For the new model, the data will be in the form of a family of curves relating cell **power** to IPCAP, with the cell power being defined as the charge/discharge current multiplied by the cell voltage measured at the same instant in time. In this technique, each curve represents a different cycling scheme. To make it easier for the model to differentiate between curves, a identifying code is used for each curve. The code used is defined below.

TTVCD

where "TT" is the temperature of the cell in degrees C, "V" is the GSFC V/T limit, "C" is the charge C-rate of the cell multiplied by 10, and "D" is the discharge C-rate of the cell multiplied by 10. Therefore, an identity code of "10356" distinguishes a data curve taken from cell data run at 10

degrees C, at V/T 3, with a 0.5 C charge rate and a 0.6 C discharge rate. Figures 5A to 5F are typical data curve plots.

Data Curve Relationships

Upon investigating the data curves, a few interesting relationships were uncovered. These relationships describe how the curve shapes alter with varying cycling parameters. In all cases, only one parameter was allowed to vary while the rest were held constant. The actual relationships will be described below.

Varying V/T Limit

As shown in figure 6, when varying V/T limits, the curves alter in two aspects. The first is in the discharge portion of the curve. It appears that discharge power varies linearly with V/T limit. A higher V/T limit results in a higher (or larger) power output from the battery. The second change is in the taper charge portion of the curve. Again, it appears that taper power varies linearly with V/T limit. The higher the V/T limit, the higher power input during taper. A higher V/T limit also extends the taper power curve, although the actual relationship is not known at this time.

Varying Charge Current

As shown in figure 7, varying charge current seems to affect only the charge power portion of the curve. The taper and discharge curves seem totally unaffected. It should be noted that the upper curve in the figure is skewed towards the y-axis due to an error in the data acquisition system. If the curve is readjusted to superimpose the charge/discharge continuities of all three curves, it will be seen that only the charge curves are changed. Again, the relationship appears linear since the curves are for 0.5C, 0.6C, and 0.8C charge rates.

Varying Other Parameters

The effects of varying the other cycling parameters have not been investigated as of this date.

Future Work

The effects of varying the remaining cycling parameters will be investigated in the near future. At present it is planned that the model will use the entire data base and not take into account the relationships found between the cycling parameters and the power curves. Later versions of the model will incorporate the relationships to reduce the data base size, however.

CONCLUSIONS

The GSFC Battery Model is currently being modified. Its modification will greatly enhance its accuracy and generality. The data base generated for the model has been investigated as well as a new data format. The data format relates battery power to the tracking variable IPCAP. Various relationships have been discovered linking cycling parameters to the data curves and initial investigations reveal the relationships to be linear. Further work is underway to complete the battery model modification and more thoroughly analyse the data curve relationships.

ENCLOSURES

A copy of the view-graphs presented at the 1985 workshop are included with this paper.

REFERENCES

1. J. Jagielski, "Fundamental Algorithms of the Goddard Battery Model," Proc. The 1984 GSFC Battery Workshop, November 1984, p. 255-268.

2. H. Zimmerman, R. Peterson, "An Electrochemical Cell Equivalent Circuit for Storage Battery/Power System Calculations by Digital Computer," IECEC Transactions, 1970, p. 533-539.

3. M. Spritzer, "Fitting Voltage Curves with an Electrochemically Derived Equation," Proc. The 1982 GSFC Battery Workshop, November 1982, p. 164-177.

4. P. McDermott, "Prediction of Battery Life and Behavior from Analysis of Voltage Data," Proc. The 1983 GSFC Battery Workshop, November 1983, p. 245-258.

5. P. Bauer, "Battery Mathematical Computer Model," TRW/Power Subsystem Engineering Department, an unpublished work.

20 AH GE 20 DEG C LEO 25%DOD

IPCAP --> / URIV	0.60	0.65	0.70	0.75	0.80	0.85	0.90	0.95	1.00
-40.0				1.186	1.194	1.211	1.235	1.264	1.294
-20.0				1.228	1.237	1.252	1.278	1.305	1.335
-16.0				1.238	1.247	1.262	1.286	1.314	1.344
-10.0				1.252	1.262	1.275	1.298	1.330	1.360
- 4.0				1.273	1.283	1.300	1.325	1.350	1.380
- 2.0				1.278	1.286	1.303	1.328	1.355	1.385
- 1.0				1.281	1.289	1.306	1.331	1.358	1.388
- 0.5				1.284	1.292	1.309	1.334	1.361	1.391
0.0				1.289	1.302	1.323	1.349	1.374	1.401
0.5				1.294	1.311	1.338	1.364	1.387	1.412
1.0				1.297	1.314	1.342	1.369	1.393	1.416
2.0				1.303	1.320	1.349	1.376	1.400	1.423
4.0				1.310	1.327	1.357	1.385	1.410	1.434
10.0				1.332	1.350	1.379	1.407	1.433	1.458
16.0				1.349	1.368	1.398	1.427	1.453	1.478
20.0				1.361	1.380	1.411	1.440	1.467	1.492
40.0				1.407	1.426	1.458	1.487	1.513	1.538

Figure 1. LEO TEST DATA AT BEGINNING OF LIFE [CYCLE 12]

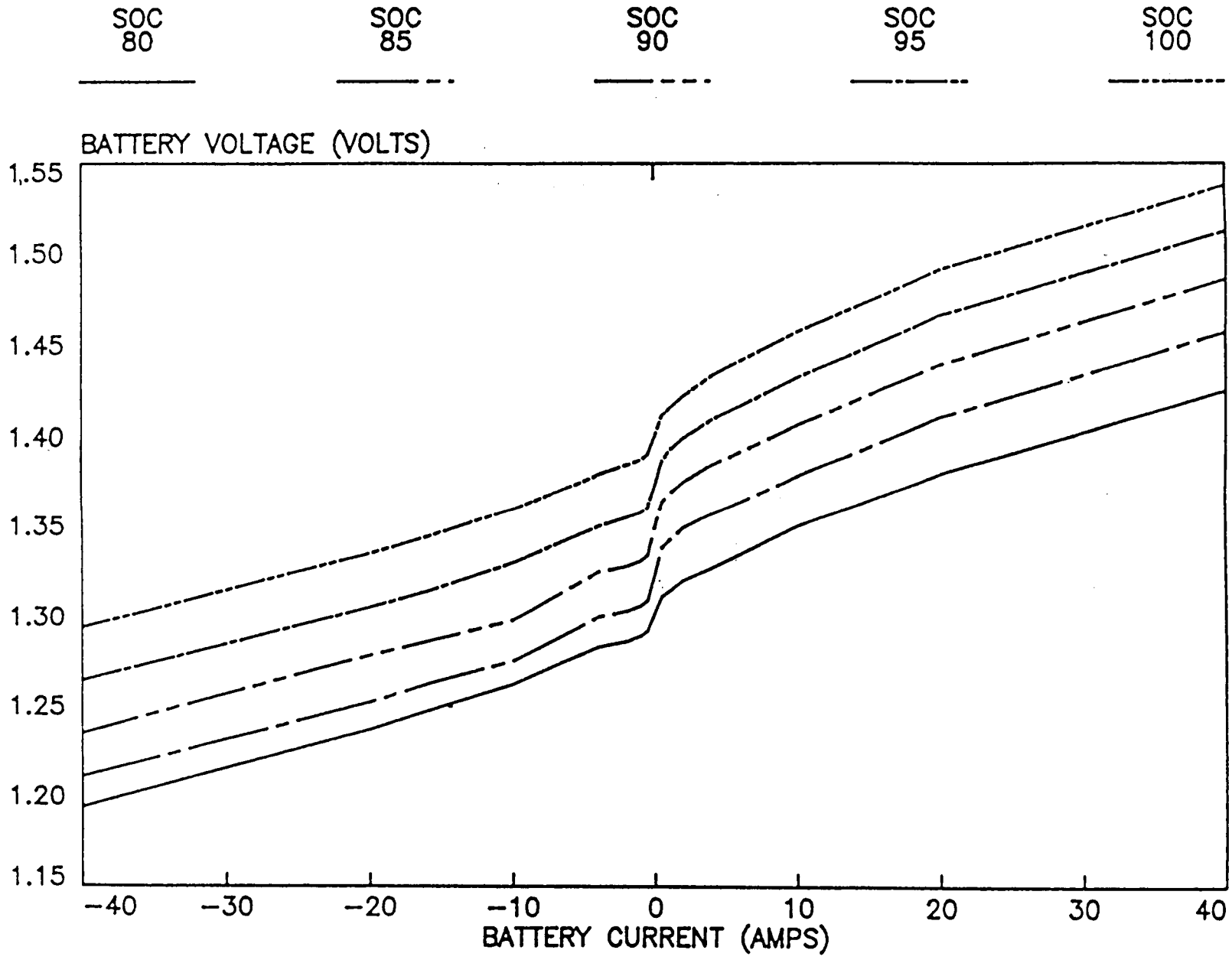

Figure 2. BATTERY CURRENT VS VOLTAGE WITH SOC AS 3RD VARIABLE

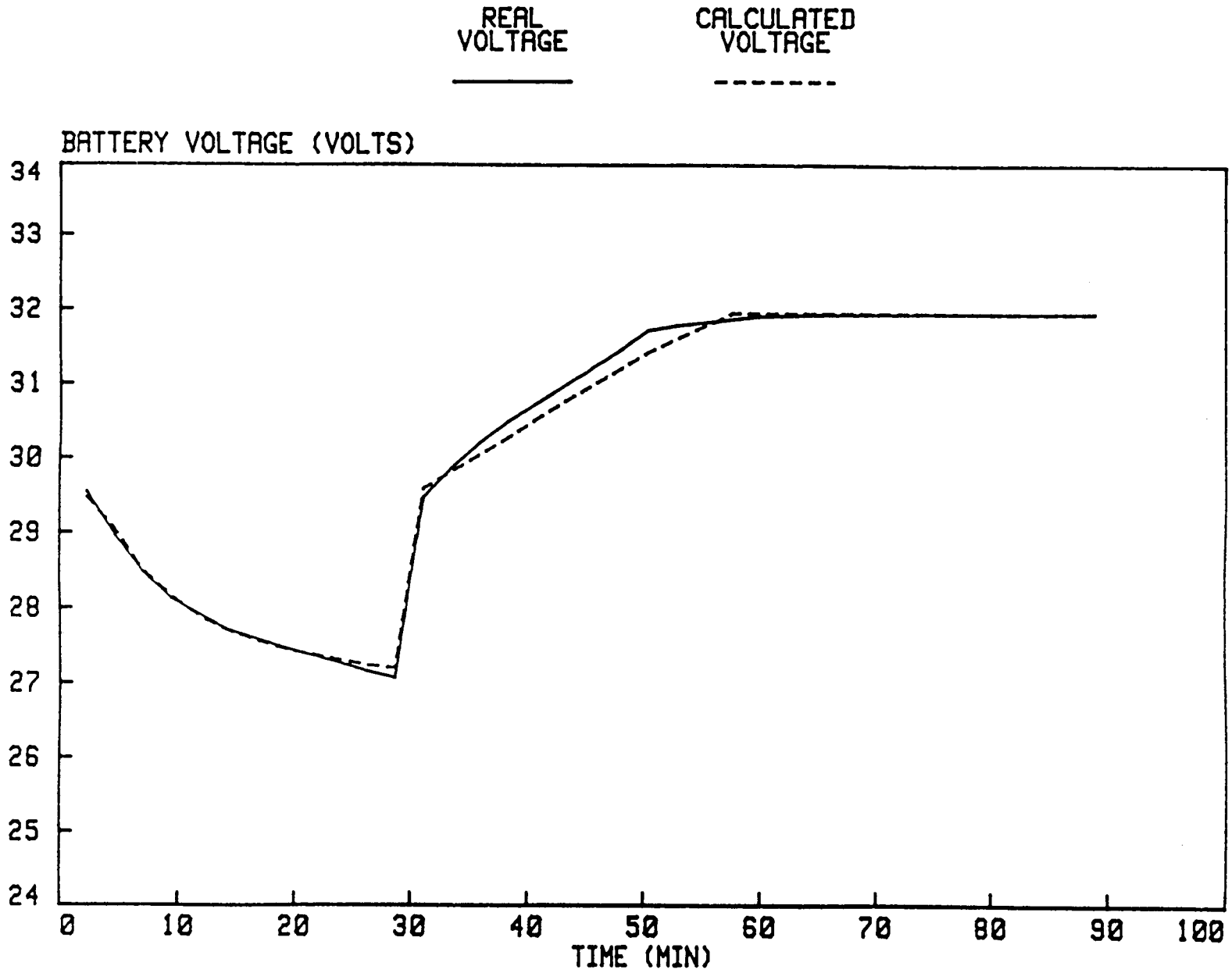

Figure 3. MODELING STUDY USING PACK 12H
CYCLE 15, 20 C, 40% DOD, 16A CHG, 16A DISCHG

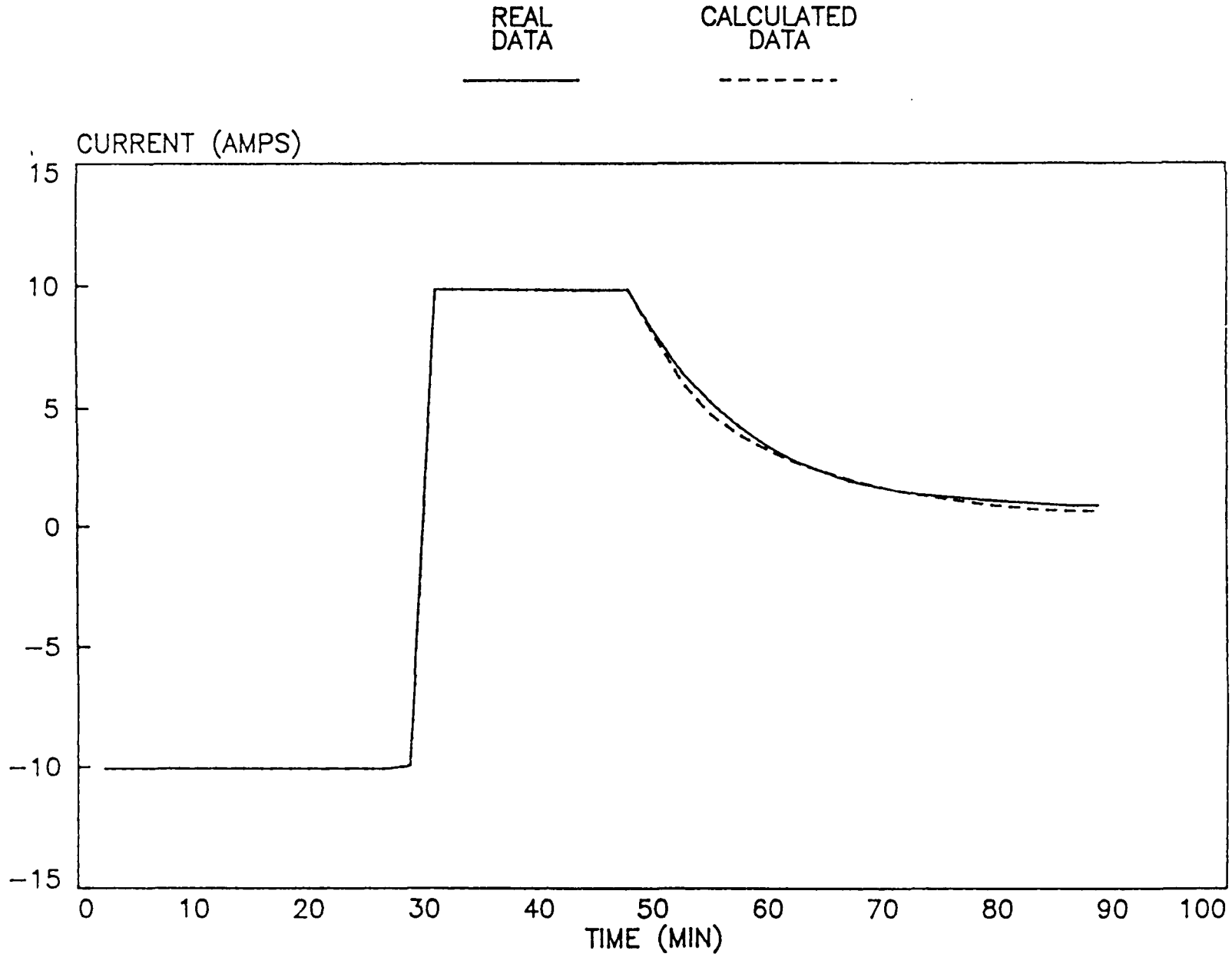

Figure 4. MODELING STUDY USING PACK 12G
COMPARISON—REAL AND CALCULATED CURRENT DATA

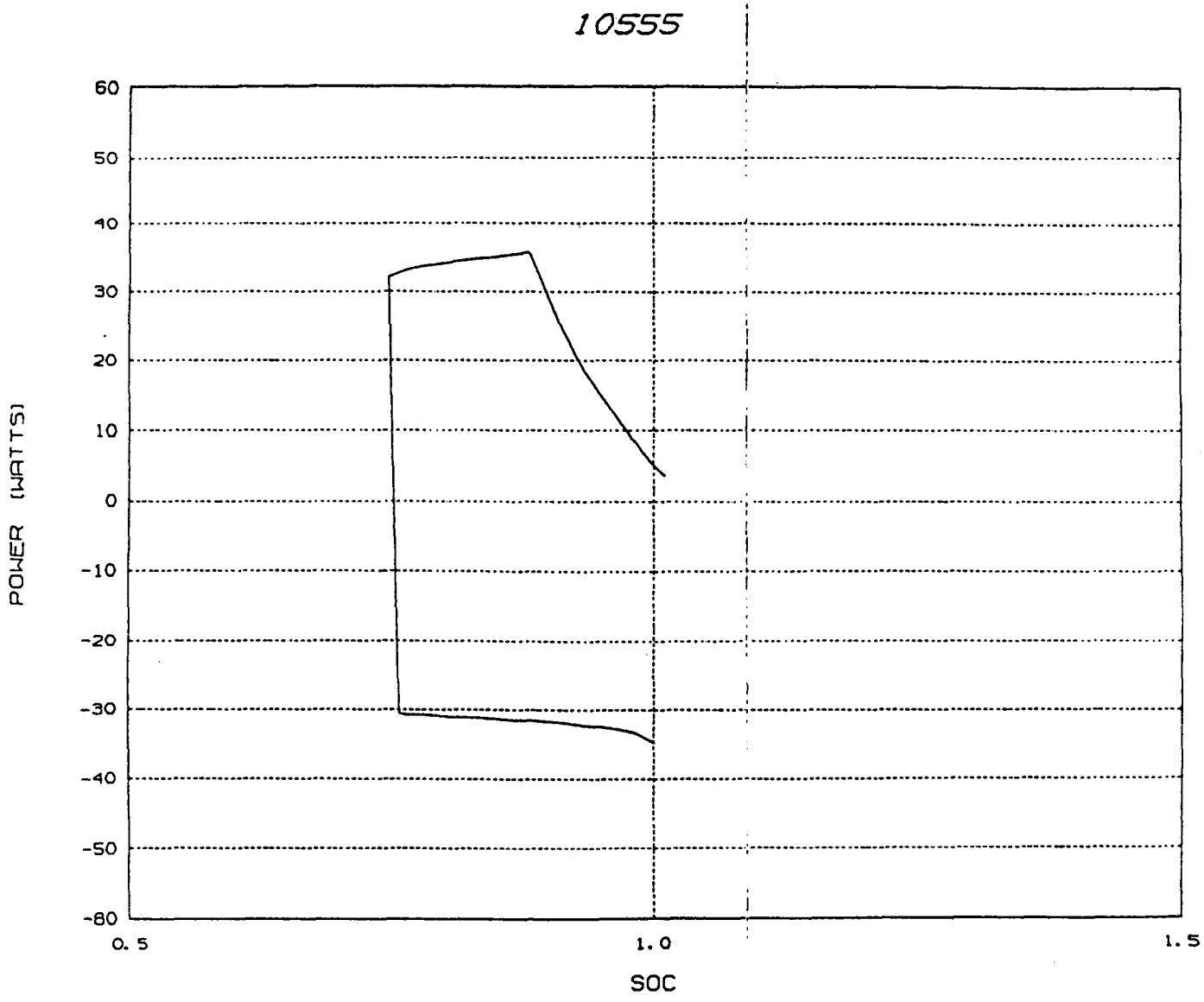

Figure 5A

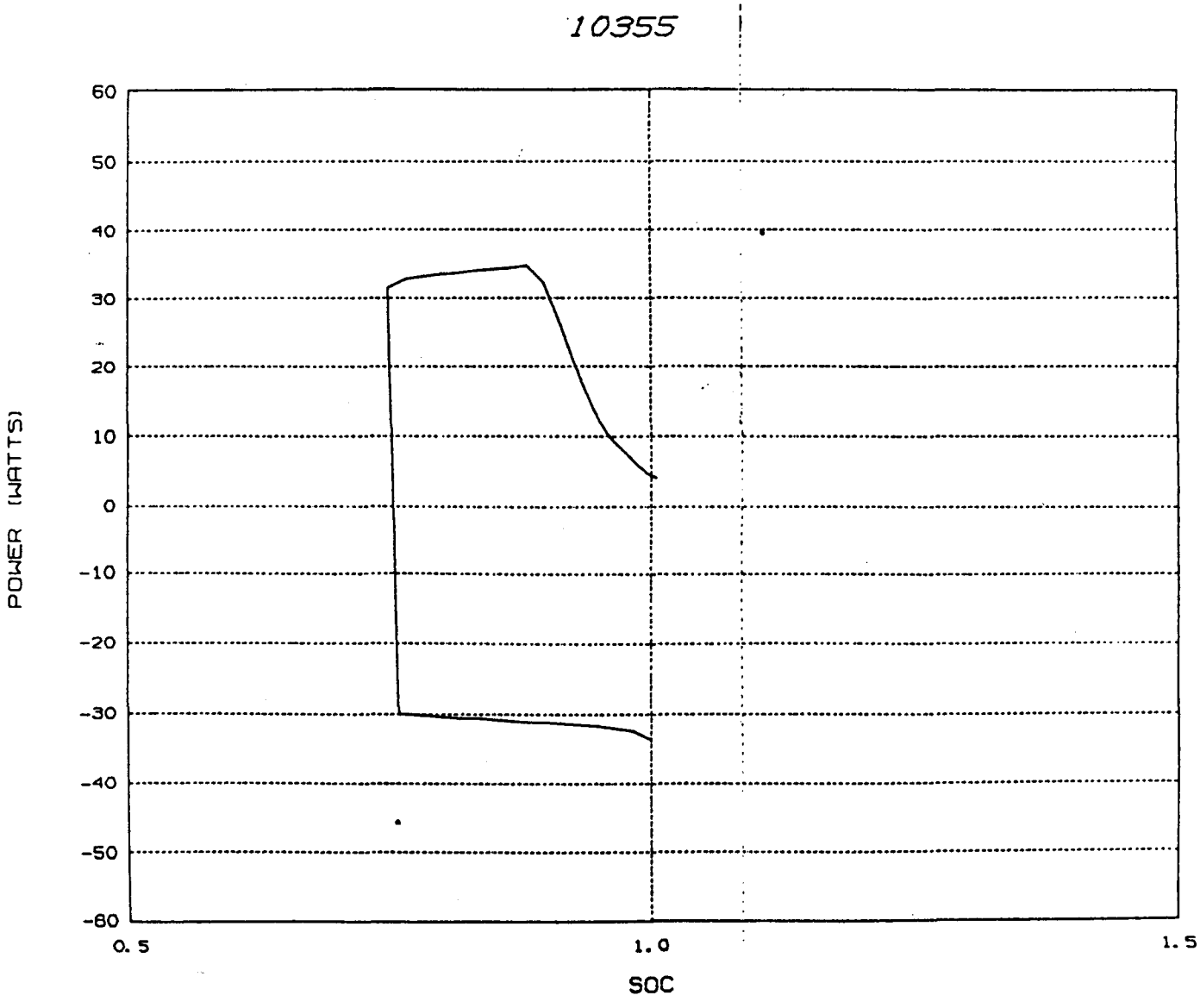

Figure 5B

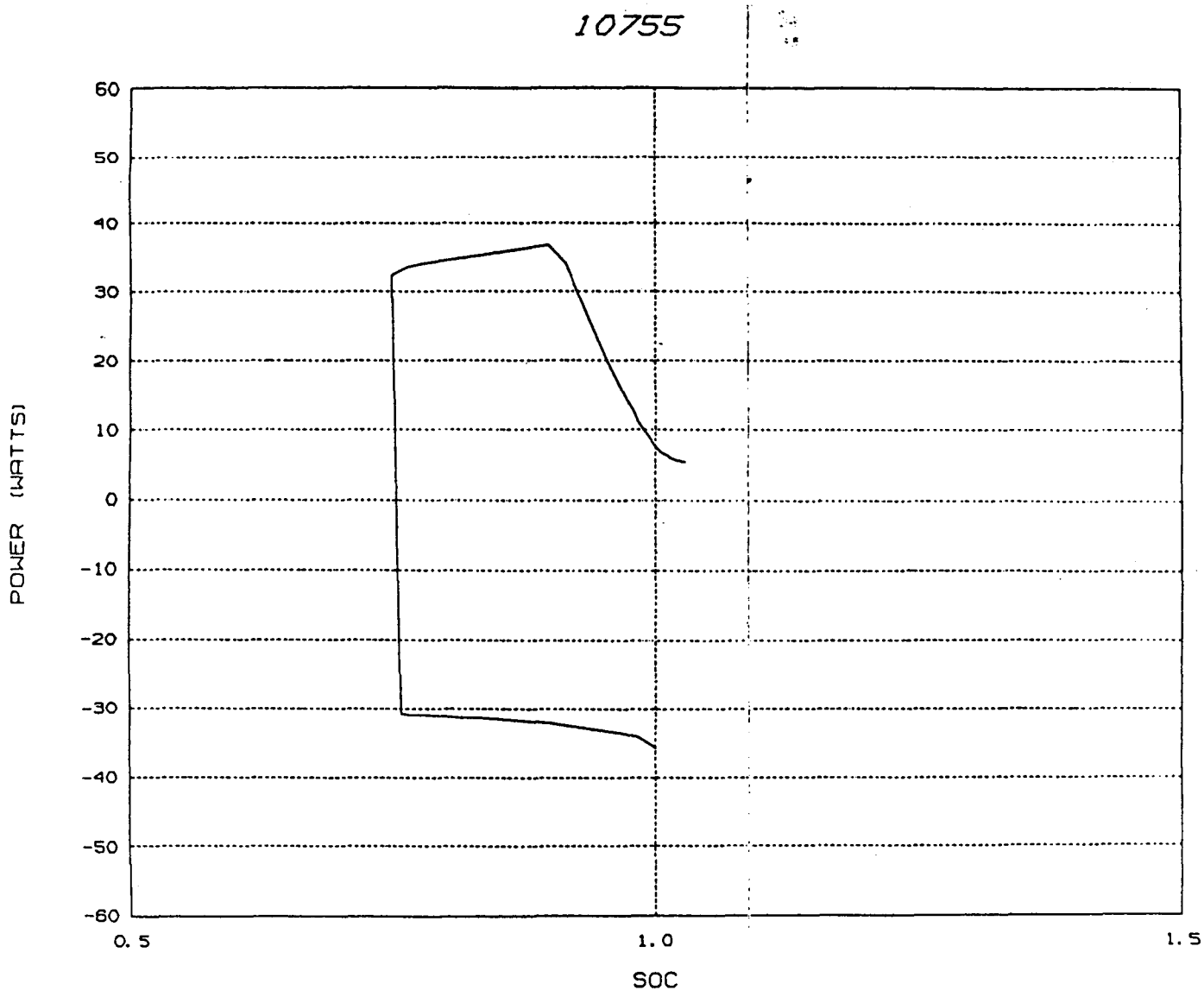

Figure 5C

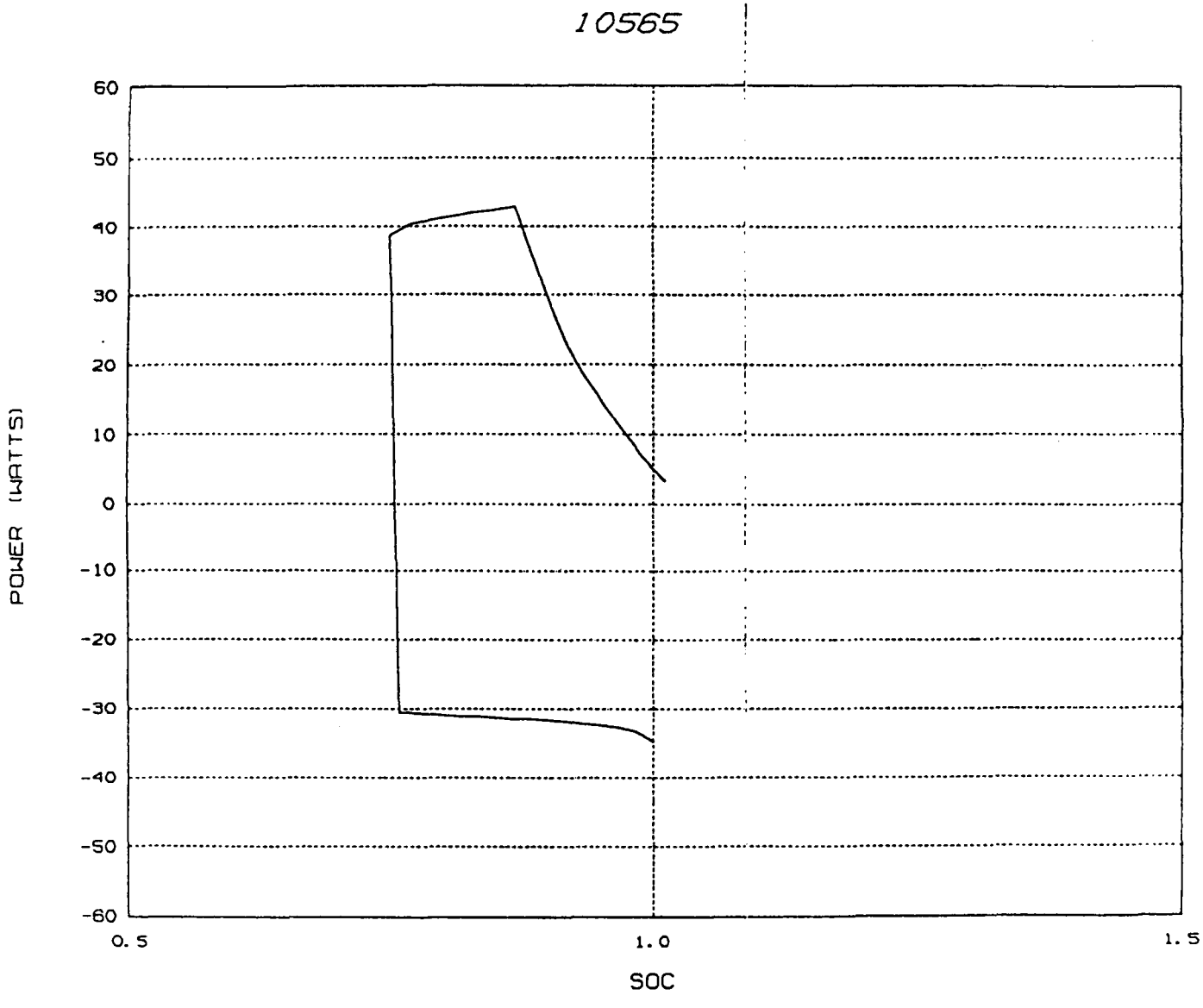

Figure 5D

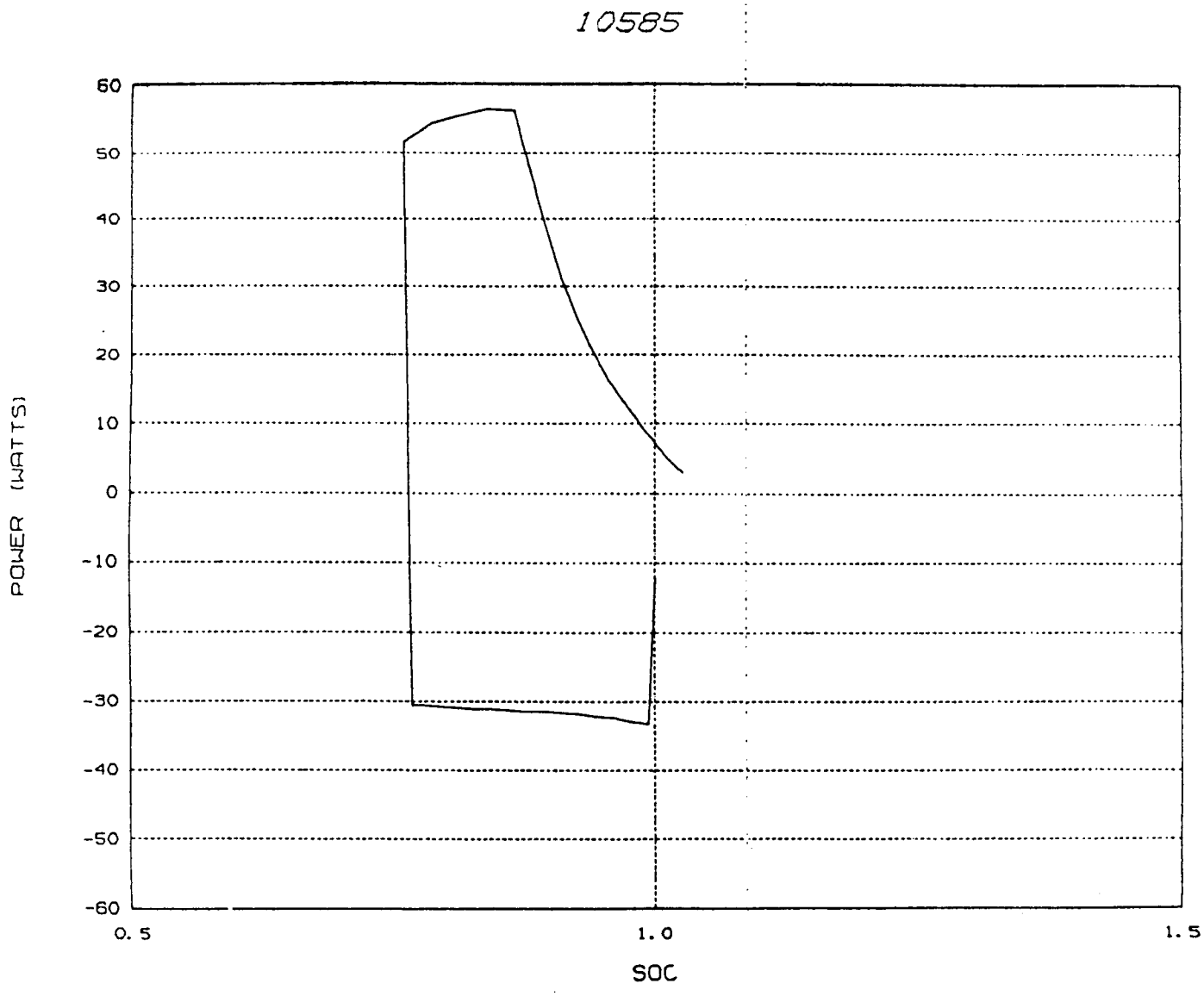

Figure 5E

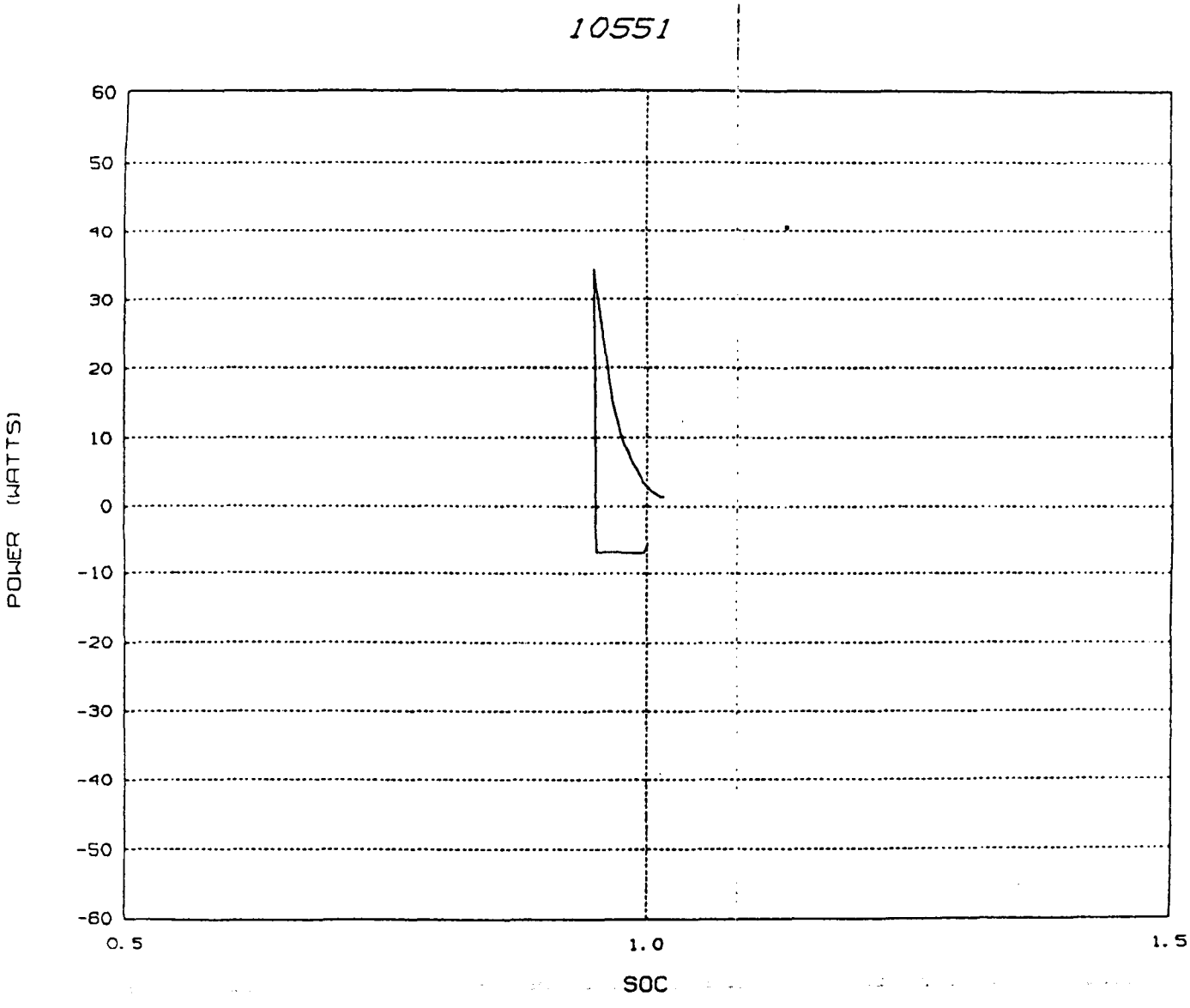

Figure 5F

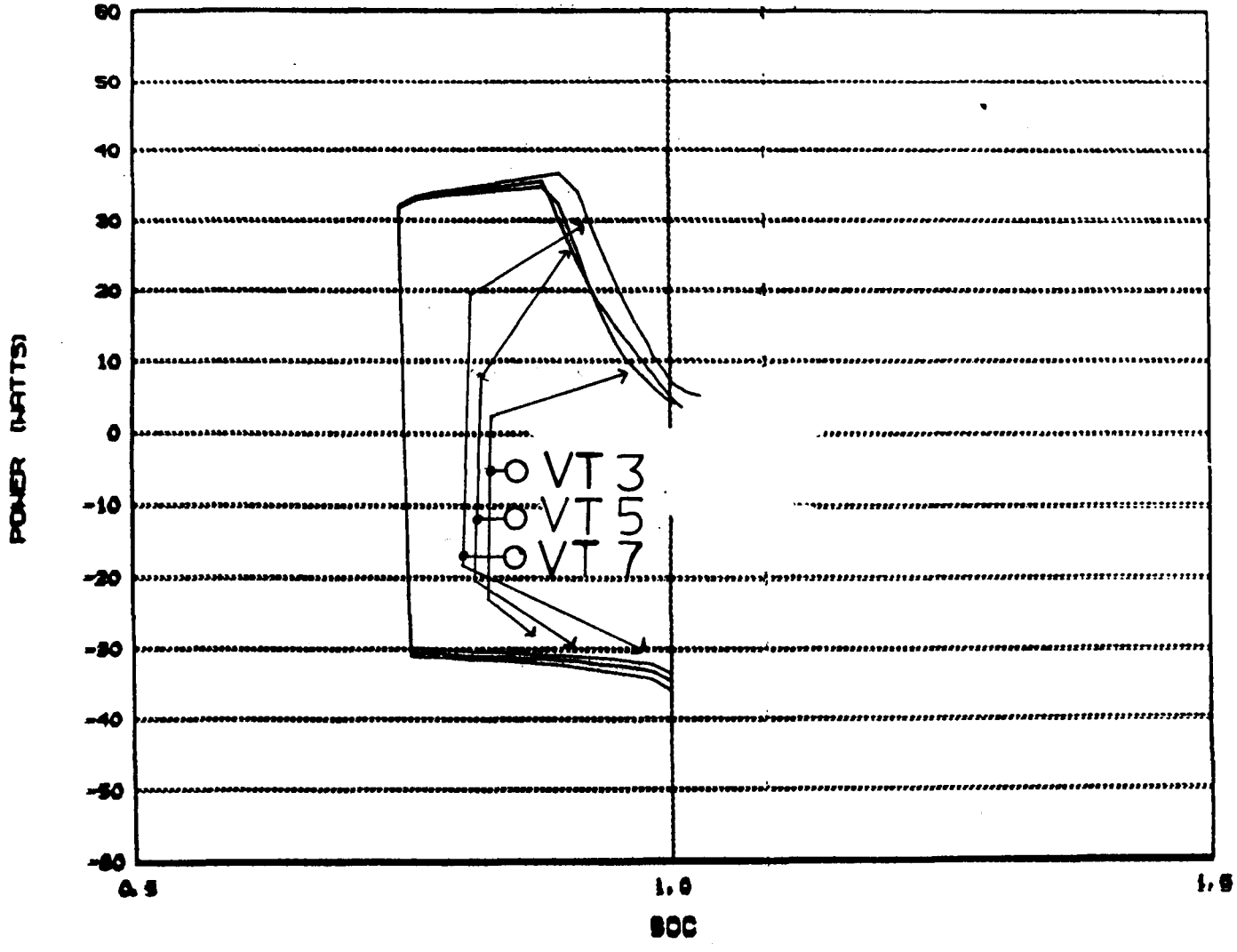
60
50
40
30
20
10
0
-10
-20
-30
-40
-50
-60
POWER (WATTS)
VT 3
VT 5
VT 7
0.5
1.0
1.5
SOC

Figure 6

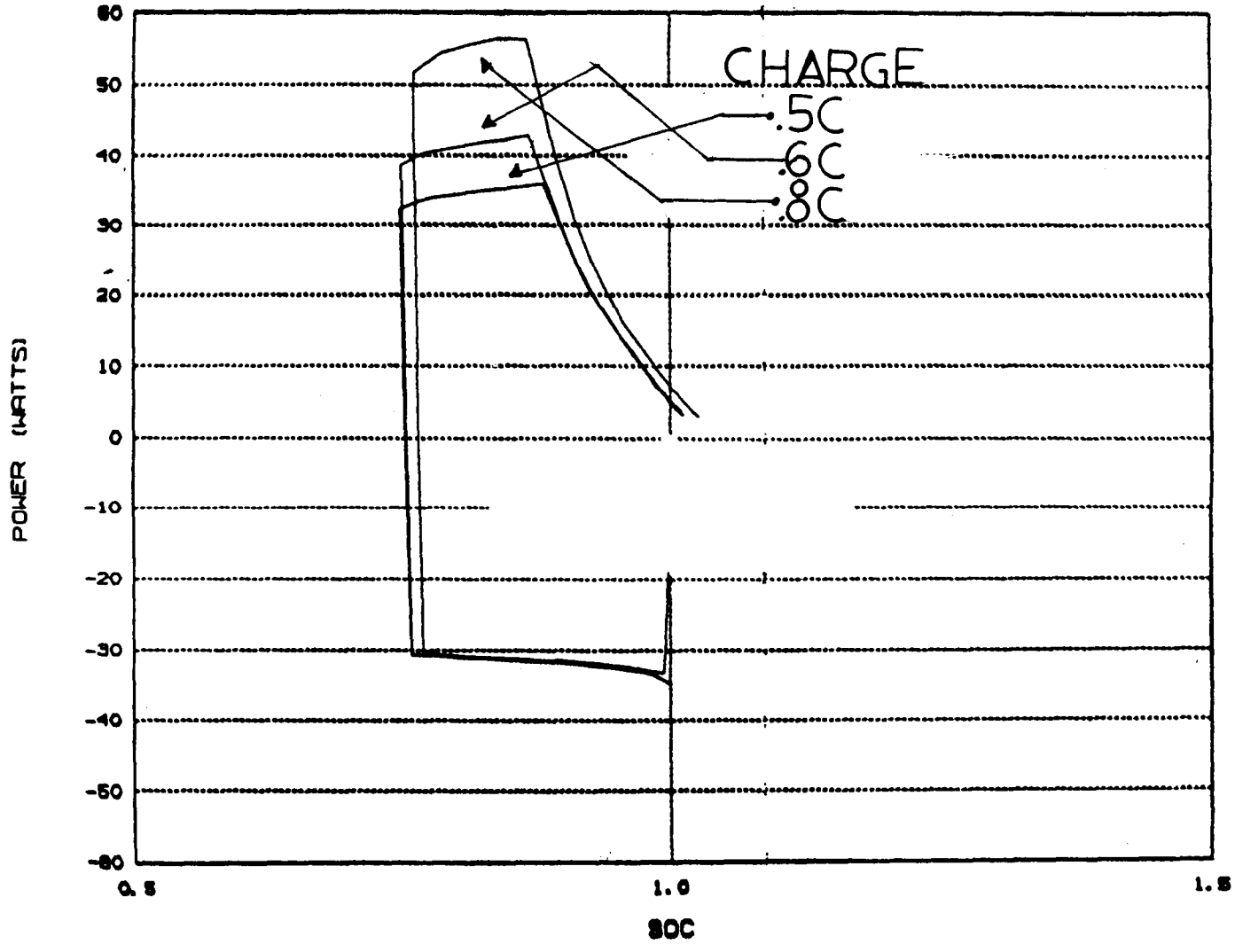
CHARGE
.5C
.6C
.8C
POWER (WATTS)
60
50
40
30
20
10
0
-10
-20
-30
-40
-50
-60
0.5
1.0
1.5
SOC

Figure 7

MODELING NI-CD PERFORMANCE

Planned Alterations to the Goddard Battery Model

James M. Jagielski

NASA/Goddard Space Flight Center

The Goddard Battery Model

- The Present Model
  - The Data Base
  - Methodology
- Planned Modifications
  - The New Data Format

The Present Battery Model

- Data curves: Vc vs. Ic with IPCAP third variable
- 2 modes: NORMAL and TAPER

BATTERY CURRENT VS VOLTAGE WITH SOC AS 3RD VARIABLE

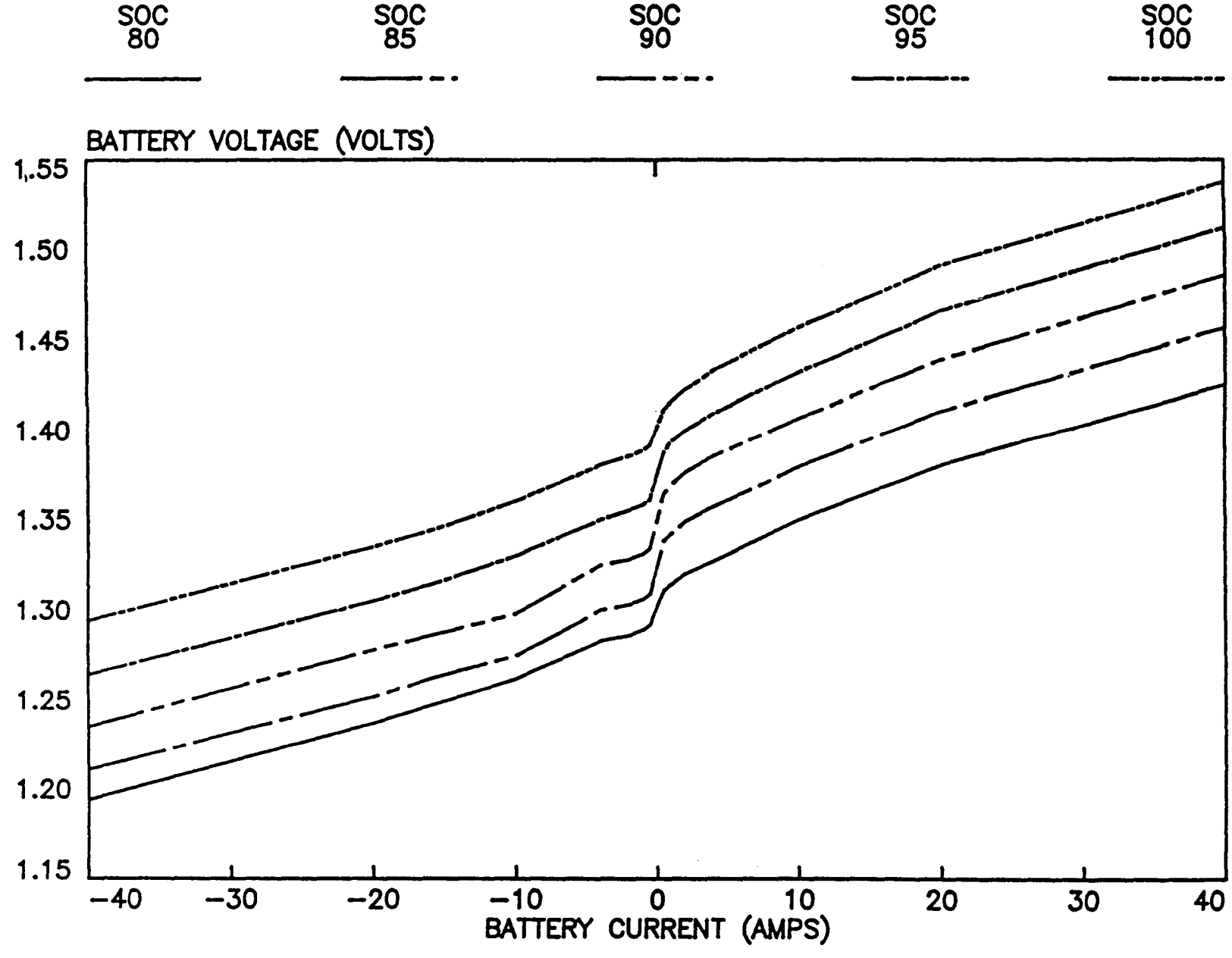

GETIBATT FLOWCHART

CALCULATE TAPER CURRENT

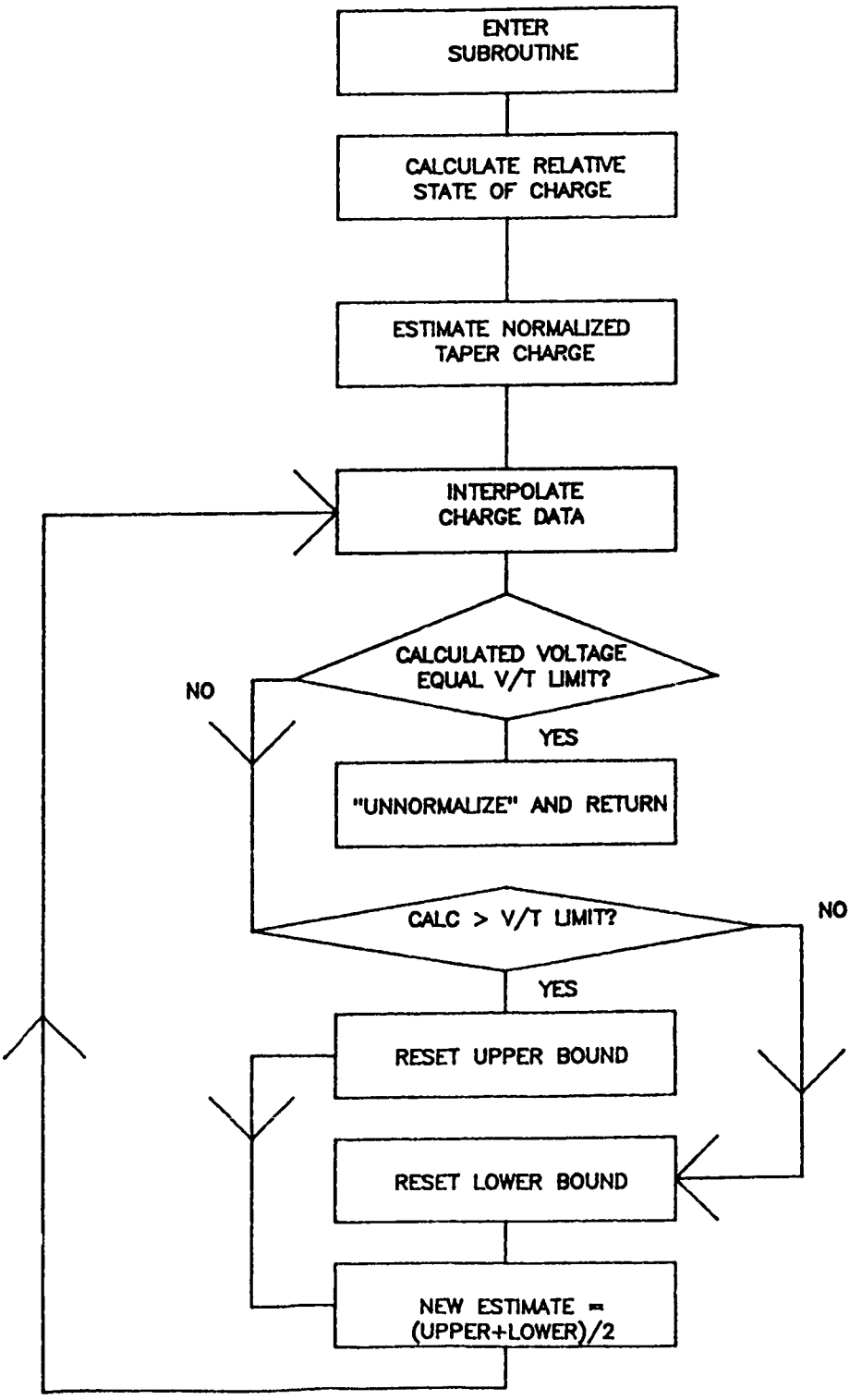

GETVSYS FLOWCHART

CALCULATE BATTERY VOLTAGE

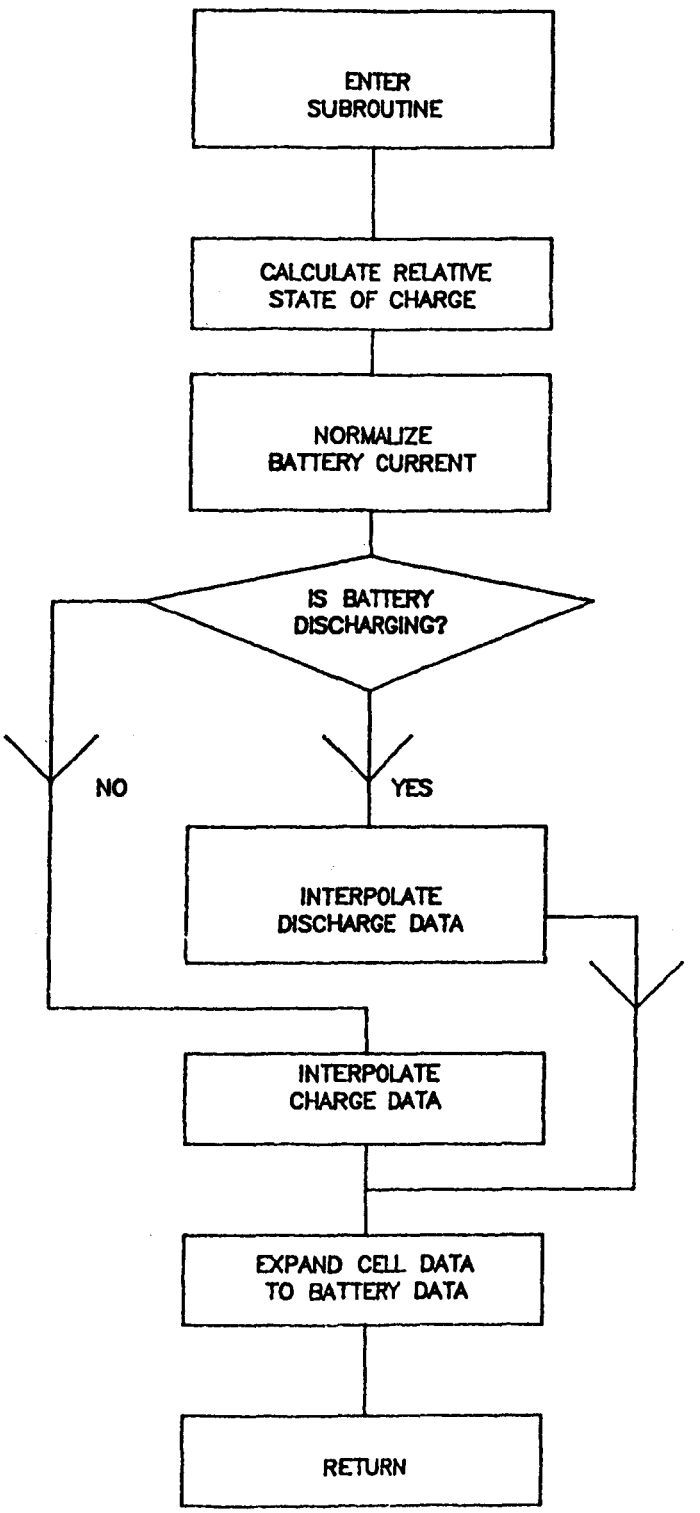

MODELING STUDY USING PACK 12H
CYCLE 15, 20 C, 40% DOD, 16A CHG, 16A DISCHG

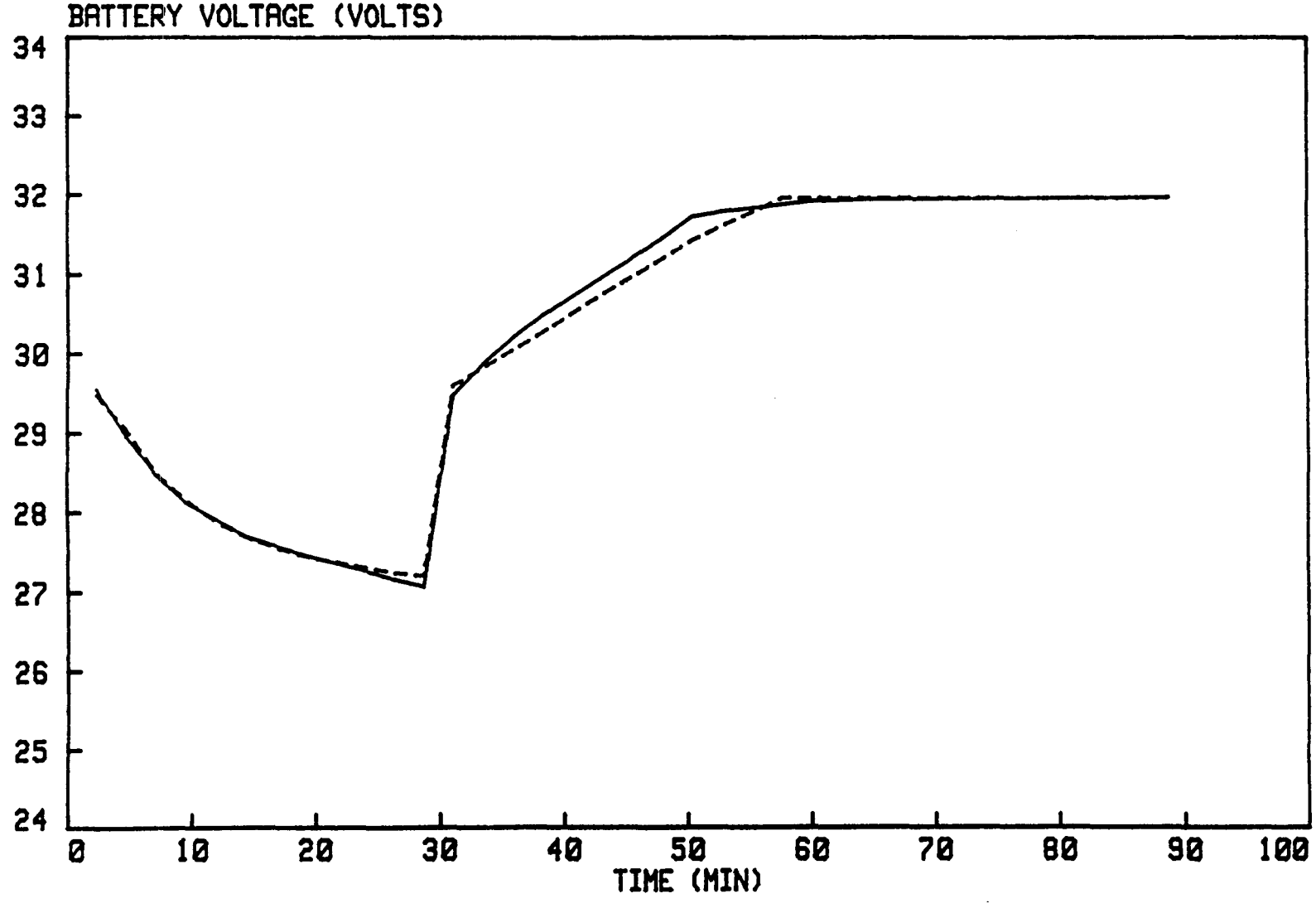

MODELING STUDY USING PACK 12G

COMPARISON – REAL AND CALCULATED CURRENT DATA

REAL DATA ——— CALCULATED DATA - - - - - - -

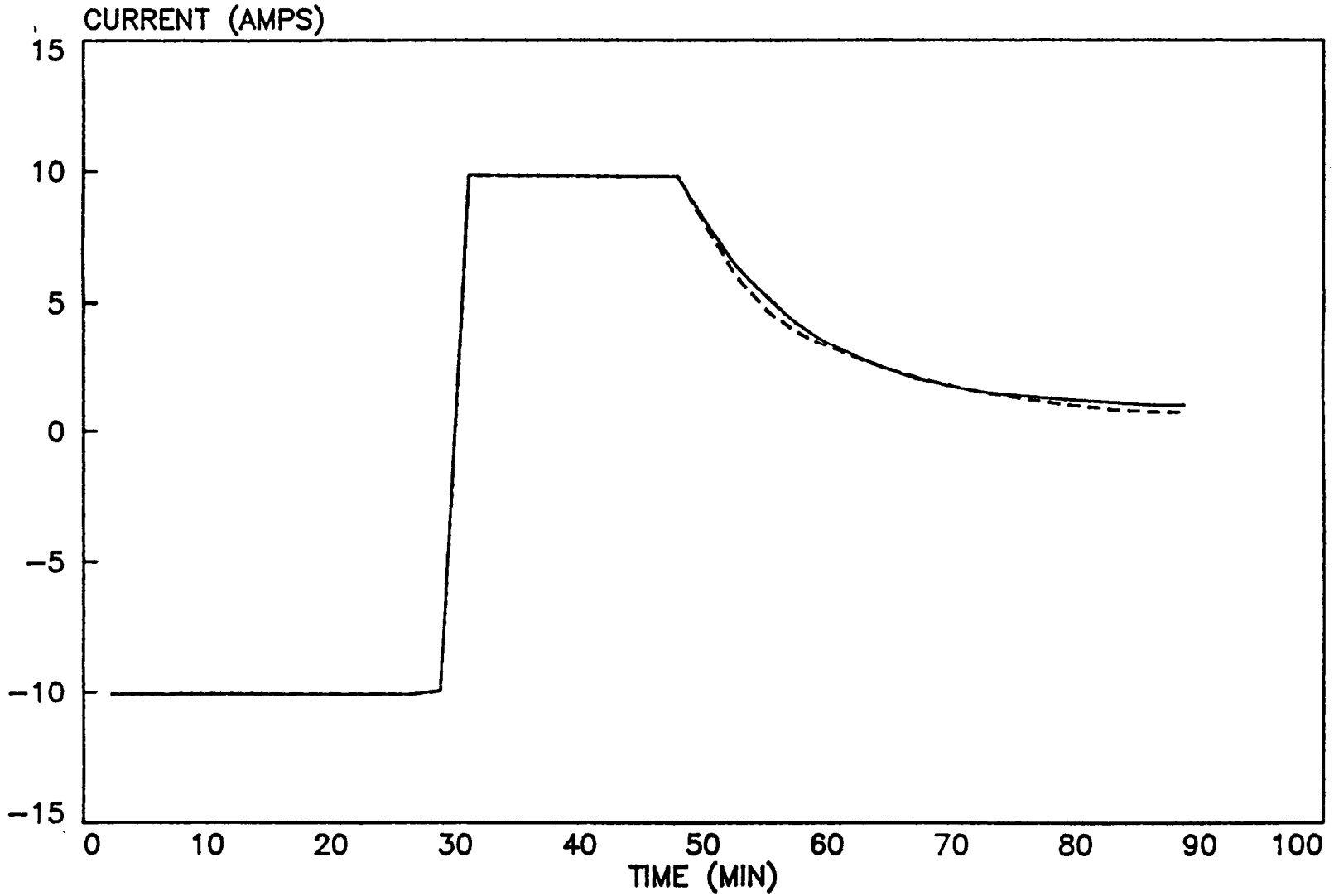

Planned Modifications to the Model

- Uses new data base
- Uses different data format
- Methodology

The New Data Base

- VT limits: 3, 5, 7
- Temperatures: 0, 10, 20 (deg C)
- Charge Rates: .2C, .5C, .6C, .8C
- Discharge Rates: .1C, .2, .5C, .8C
- Tests run on 50 Amp-Hr cells

The New Data Format

- Data curves: Cell Power vs. IPCAP
- Advantages
  - Uses all LEO cycling data
  - Battery is a "power" device
  - Allows for inclusion of other data

INVESTIGATION OF LONG TERM STORAGE EFFECTS ON AEROSPACE NICKEL-CADMIUM CELL PERFORMANCE

BY

THOMAS Y. YI
SPACE POWER APPLICATIONS BRANCH
CODE 711
NASA/GODDARD SPACE FLIGHT CENTER
GREENBELT, MD 20771

ABSTRACT

A study on evaluation of the long term storage effects on aerospace nickel-cadmium cells currently being performed at NASA/Goddard Space Flight Center (GSFC) is described. A number of cells of 6AH and 12AH capacities which have been stored in shorted condition for 8 to 9 years at the GSFC have been selected for this study. These cells will undergo electrical acceptance testing at the GSFC, and life cycling at the NASA Battery Test Facility at the Naval Weapons Support Center (NWSC) in Crane, Indiana; in addition, some cells from the study will undergo destructive analyses.

INTRODUCTION

Investigation of long term storage effects on aerospace nickel-cadmium cell performance is an important topic that has received relatively few interests because of the long time that is required. Although at the GSFC as well as at other facilities, there are many spare and test nickel-cadmium cells held in storage, uncertainties in the cell capabilities after years of storage have hindered their present usage. Another dilemma we face at the GSFC is the reliability of the cells at the time of launch. Cells for a flight project are procured and tested, and battery made well ahead of the launch date. Inevitably because launch delays arise, the question of battery capability with age is often asked. In the few studies done in this area of storage effects on nickel-cadmium cells [1-3], Thierfelder et al. recommends the maximum cell age of 3-1/2 years for maximum reliability in a 7-1/2 year mission [3]. In the above studies, tests that were performed were either accelerated tests or electrical characterization tests after certain periods of storage. Although these techniques may be useful because of the short duration needed in the cell age study, we find that these are not dependable. It has been our experience that the best way to gain a high degree of confidence with the cells is to perform real time testing on them.

The objective of this study is to investigate the effects of long term storage on aerospace nickel-cadmium cells through electrical acceptance testing, real time testing, and destructive analyses. The results from the study will be compared with previous data on these cells, namely from the initial acceptance data at the GSFC, and from the life cycling data at the

NWSC on the cells from the same lot. The study will use 12 General Electric (G.E.) 6AH nickel-cadmium cells (G.E. 42B006AB55/56) and 12 G.E. 12AH nickel-cadmium cells (G.E. 42B012AB20/21). These cells have been chosen because of their relative abundance in the Battery Lab at the GSFC, and also because of availability of the GSFC acceptance data and the NWSC life cycling data on them. These cells were stored shorted in the Battery Lab since 1976 and 1977. They were purchased for the International Ultraviolet Explorer (I.U.E.) Project, and are presently held as reserve cells for the mission. Specific information on these cells, the assembled battery, as well as the performance of the I.U.E. spacecraft is mentioned elsewhere [4-12].

TEST DESCRIPTION

Twelve cells have been selected from each of the I.U.E. 6AH and 12AH cell lots at the Battery Lab at the GSFC. Of the 12 cells within the lot, 2 cells will undergo destructive analysis per NASA Document X-711-74-279 [13]. The remaining 10 cells will be fabricated into two 5-cell packs, 1 of which will be tested at the GSFC/Battery Lab, and the other at the NWSC. Upon completion of the tests, 2 cells from each pack will go through destructive analysis. In all, 12 cells will undergo destructive analysis.

From each lot, one 5-cell pack will be subjected to the cell electrical characterization test at the GSFC that is similar to the acceptance test these cells underwent when they were first procured 8 to 9 years ago [14]. Table 1 shows the outline of the present electrical test. Direct comparisons between the original acceptance test data and the present characterization data from after storage will be made.

The remaining 5-cell packs from each lot will go through an acceptance test at the NWSC, and then a life test. The 6AH test pack will undergo geosynchronous orbit cycling (GEO), whereas the 12AH pack will operate at low-earth orbit cycling (LEO). The operating parameters for these orbits are shown in Table 2. These test parameters were deliberately chosen to operate under similar operating conditions as pack 231A for the 6AH pack and pack 8G for the 12AH pack at the NWSC [5-13]. These two I.U.E. packs, 231A and 8G, which are from the same lot as the cells being tested for this study, have been life cycled at the NWSC since 1978.

Prior to the start of life test, 2 preconditioning cycles will be performed on all cells. The first preconditioning cycle of C/10 charge for 24 hours at 20 C and a C/1.25 discharge with a cutout voltage of 0.75V for each cell will be followed by a second cycle of C/10 charge for 24 hours at 10 C and the same discharge profile as in the first preconditioning discharge.

In the LEO cycling, duration of the test is planned for 1 year. Capacity check will be performed on the 12AH pack at the C/1.25 rate to a voltage limit of 0.75 V/cell on one of the cells at 6 months, and on two of the cells at 12 months. These cell(s) will be recharged at the C/1.25 rate to the voltage limit and tapered until 115% recharge is reached. Other cells will remain open-circuited during the check.

Like the LEO pack, the 6AH GEO pack will be cycled for 1 year. During every other solstice period, each period lasting 2 weeks, the packs will be reconditioned. In the first reconditioning cycle, the pack will be recharged at a float rate of C/60, followed by a discharge at C/1.5 rate until any cell reaches 0.75V, and then open-circuited for 5 days. Thereafter each reconditioning cycle will go through a 3-step charge.

REFERENCES

1. Braham, R. W., et al., Power Sources, 1977, v6, p. 129-159.

2. Hobbs, B. S., et al., J. Appl. Electrochem., 8(1978) p. 305-311.

3. Thierfelder, H. E., et al., Proc. Intersoc. Eng. Conf., 1984, v1, p. 319-323.

4. Tiller, S. E., Battery Fabrication and Acceptance Test Plan for International Ultraviolet Explorer (IUE) 6AH Batteries. NASA X-711-78-5, 1978.

5. Naval Weapons Support Center. Evaluation Program for Secondary Spacecraft Cells: Synchronous Orbit Testing of Sealed Nickel-Cadmium Cells. Contract S-53742-AG, WQEC/C 81-120A, 1981, p. 114-133.

6. Naval Weapons Support Center. Evaluation Program for Secondary Spacecraft Cells: Synchronous Orbit Testing of Sealed Nickel-Cadmium Cells. Contract S-53742-AG, WQEC/C 81-120B, 1981, p. 76-90.

7. Naval Weapons Support Center. Evaluation Program for Secondary Spacecraft Cells: 16th Annual Report of Cycle Life Test. Contract C-13105-D, WQEC/C 80-34, 1980. p. 28-32.

8. Naval Weapons Support Center. Evaluation Program for Secondary Spacecraft Cells: 17th Annual Report of Cycle Life Test. Contract C-13105-D, WQEC/C 81-1, 1981, p. 28-32.

9. Naval Weapons Support Center. Evaluation Program for Secondary Spacecraft Cells: 18th Annual Report of Cycle Life Test. Contract C-13105-D, WQEC/C 82-23, 1982, p. 29-32.

10. Naval Weapons Support Center. Evaluation Program for Secondary Spacecraft Cells: 19th Annual Report of Cycle Life Test. Contract C-13105-D, WQEC/C 83-1, 1983, p. 29-33.

11. Naval Weapons Support Center. Evaluation Program for Secondary Spacecraft Cells: 20th Annual Report of Cycle Life Test. Contract C-13105-D, WQEC/C 84-5, 1984, p. 15-19.

12. Naval Weapons Support Center. Evaluation Program for Secondary Spacecraft Cells: 21st Annual Report of Cycle Life Test. Contract C-13105-D, WQEC/C 85-52, 1985, p. 36.

13. Halpert, G., and Kunigahalli, V., Procedure for Analysis of Nickel-Cadmium Cell Materials. NASA X-711-74-279, Rev. A., 1980.

14. Tiller, S. E., Cell Acceptance Test Plan for Nickel-Cadmium Cells. NASA X-711-76-143, 1976, p. 17-19.

Table 1. TEST OUTLINE/SCHEDULE

Sequence Number	Test Condition Number	Test Description	Temperature (°c)	Current	Voltage Limits		Test Duration (hours)	
					Upper Limit (V)	Lower Limit (V)	Specified	Estimated
1	1	Conditioning Charge	25	C/20	1.51	0.80	48	—
2	2	Conditioning Discharge	25	C/2	1.51	0.80	—	3
		Resistive Drain	25	—	—	—	—	2
3	3	Conditioning Charge	25	C/10	1.51	0.80	24	—
4	2	Conditioning Discharge	25	C-2	1.51	0.80	—	3
		Resistive Drain/Temperature Stabilization	20	—		—	—	2
5	4	Capacity Charge	20	C/10	1.51	0.80	24	—
6	5	Capacity Discharge	20	C/2	1.51	0.80	—	3
		Resistive Drain	20	—	—	—	16	—
7	6	Charge Retention — Open Circuit	20	—	—	—	24	—
		Resistive Drain/Temperature Stabilization	10	—	—	—	—	2
8	7	Capacity Charge	10	C/20	1.53	0.80	48	—
9	8	Capacity Discharge	10	C/2	1.53	0.80	—	3
		Resistive Drain/Temperature Stabilization	0	—	—	—	—	2
10	9	Overcharge Charge	0	C/20	1.53	0.80	72	—
11	10	Overcharge Discharge	0	C/2	1.53	0.80	—	3
		Resistive Drain/Temperature Stabilization	10	—	—	—	—	2
12	11	Burn-in Charge #1	10	C/20	1.53	0.80	23	—
13	12	Burn-in Discharge #1	10	C/2	1.53	0.80	1	—
14	11	Burn-in Charge #2	10	C/20	1.53	0.80	23	—
15	12	Burn-in Charge #2	10	C/2	1.53	0.80	1	—
16	11	Burn-in Charge #3	10	C/20	1.53	0.80	23	—
17	12	Burn-in Discharge #3	10	C/2	1.53	0.80	1	—
18	11	Burn-in Charge #4	10	C/20	1.53	0.80	23	—
19	12	Burn-in Discharge #4	10	C/2	1.53	0.80	1	—
20	11	Burn-in Charge #5	10	C/20	1.53	0.80	23	—
21	12	Burn-in Discharge #5	10	C/2	1.53	0.80	1	—
22	11	Burn-in Charge #6	10	C/20	1.53	0.80	23	—
23	12	Burn-in Discharge #6	10	C/2	1.53	0.80	1	—
24	11	Burn-in Charge #7	10	C/20	1.53	0.80	23	—
25	12	Burn-in Discharge #7	10	C/20	1.53	0.80	1	—
26	11	Burn-in Charge #8	10	C/20	1.53	0.80	23	—
27	13	Burn-in Capacity Discharge	10	C/2	1.53	0.80	1	—
		Resistive Drain/Temperature Stabilization	20	—	—	—	—	2
28	4	Capacity Charge	20	C/10	1.51	0.80	24	—
29	5	Capacity Discharge	20	C/2	1.51	0.80	—	3
		Resistive Drain	20	—	—	—	—	2

Table 2. OPERATING PARAMETERS OF THE 6AH AND 12AH NICKEL CADMIUM CELL PACKS SCHEDULED TO BE LIFE CYCLED AT NWSC, CRANE, IN.

	6AH Pack	12AH Pack
Life cycling regime	GEO	LEO
Duration (year)	1	1
Temperature (°C)	10	0
Depth-of-Discharge (%)	80	40
Orbit	25 day Eclipse	90 min.
Charge	C/10	C/1.25
Discharge	Eclipse	C/1.25

Satellite Battery Testing Status
Naval Weapons Support Center
Crane, Indiana

by

Randy Haag and Steve Hall
Naval Weapons Support Center

ABSTRACT

Because of the large numbers of satellite cells currently being tested and anticipated at the Naval Weapons Support Center (NAVWPNSUPPCEN) Crane, Indiana, satellite cell testing is being integrated into the Battery Test Automation Project (BTAP). The BTAP, designed to meet the growing needs for battery testing at the NAVWPNSUPPCEN Crane, will consist of several Automated Test Stations (ATSs) which monitor batteries under test. Each ATS will interface with an Automation Network Controller (ANC) which will collect test data for reduction.

DISCUSSION

FIGURE 1

Aircraft battery testing has been conducted at the NAVWPNSUPPCEN Crane since 1960. Over the years battery testing has expanded to include many test programs (manned 24 hours a day, 365 days of the year) including the National Aeronautics and Space Administration (NASA) Satellite Program. This test program has produced data from over 1800 satellite cells of various chemistries.

FIGURE 2

In discussions of NASA Satellite Battery Programs, acronyms are frequently used. Figure 2 clarifies these acronyms.

FIGURE 3

NASA currently supports testing of 140 cells (28 battery packs). All cells were manufactured by General Electric and range in sizes from four to 50 ampere-hours. LEO and GEO cycling are the primary test scenarios with one pack currently undergoing Power Profile Cycling. The favorable performance of some of these cells is exemplified by the successful completion of over 52,800 LEO cycles and 20 GEO cycles since 1976.

FIGURE 4

NASA has indicated the need to add two additional battery packs to the NAVWPNSUPPCEN Crane Satellite Battery Test Program in fiscal year 1986.

FIGURE 5

Other major satellite cell test programs being conducted at the NAVWPNSUPPCEN Crane consist of 173 cells for Air Force and Navy qualification testing of a new separator material proposed for future use in nickel-cadmium cells, and an Air Force Nickel-Hydrogen Data Base Program consisting of 57 cells to date. It is anticipated that more cells will be added to this test program later.

FIGURE 6

The BTAP currently being inplemented at the NAVWPNSUPPCEN Crane is designed to meet the growing need for a sophisticated automated test facility capable of rapid data accumulation and reduction. Dynamic (real-time) control of power supplies to follow arbitrary voltage, current, and power time-varying profiles is scheduled for implementation this fiscal year.

FIGURE 7

The BTAP will consist of a network of existing data acquisition systems and newly procured systems used to monitor batteries under test and acquire data on voltage, current, temperature, pressure and other performance factors. An ATS also controls charge, discharge, open circuit, and short circuit times and events in accordance with a sponsor's test plan. Progress of the test can be examined at any time on a CRT terminal at each ATS. The CRT terminal also can be used to change some aspect of the on-going test, such as, the number of batteries under test (add new batteries, remove failed ones). In addition to analog voltage data acquisition, each ATS will have relays and D/A converters to enable the ATS to connect and disconnect strings of batteries from one or more power supplies automatically. An ANC will collect test data from each of the ATSs for storage on disc drives, and for both on-site and off-site archiving on magnetic tape to provide data backup and data security. Test procedures, data analysis, graphing, and report preparation using standard software packages will be provided via CRT terminals in engineering offices.

FIGURE 8

To date, those who have contributed to the BTAP system are the Navy, Air Force, and NASA.

FIGURE 9

With the existing data acquisition systems at the NAVWPNSUPPCEN Crane and those currently on order, the BTAP will begin operation shortly after the delivery of the ANC computer in December 1985.

CLOSING REMARKS

Through NASA support the NAVWPNSUPPCEN Crane has published many reports on satellite cell test projects. With continued NASA support and with the addition of new sponsors to the NAVWPNSUPPCEN Crane Satellite Cell Test Program (such as the Navy and the Air Force), test project data will continue to be published. Interested parties are encouraged to acquire clearance from the appropriate test program sponsor to be included on test report distribution lists.

- BATTERY/CELL TESTING SINCE 1960
- LARGE VARIETY OF CHEMISTRIES
- NASA SATELLITE BATTERY/CELL TESTING SINCE 1963
  - OVER 1800 CELLS
    - NICKEL-CADMIUM
    - SILVER-CADMIUM
    - SILVER-ZINC
    - LEAD-ACID

Figure 1

AMPTE:	ACTIVE MAGNETIC PARTICLE TRACER EXPLORER
ERBS:	EARTH RADIATION BUDGET SATELLITE
IUE:	INTERNATIONAL ULTRAVIOLET EXPLORER
NOAA:	NATIONAL OCEANIC ATMOSPHERIC ADMINISTRATION
TDRSS:	TRACKING DATA RELAY SATELLITE SYSTEM
GOES:	GEOSTATIONARY OPERATIONAL ENVIRONMENTAL SATELLITE
UARS:	UPPER ATMOSPHERE RESEARCH SATELLITE
COBE:	COSMIC BACKGROUND EXPLORER
REQUAL:	PELLON SEPARATOR REQUALIFICATION

Figure 2. CLARIFICATION OF ACRONYMS

FLIGHT PROGRAM	NUMBER OF CELLS	RATED CAPACITY (A-H)	MANUFACTURER	SIMULATED ORBIT	CYCLES OR SHADOW PERIODS TO DATE	DATE TEST BEGAN
AMPTE	5	4	GENERAL ELECTRIC	LEO	765	10-83
ERBS	4	50	GENERAL ELECTRIC	POWER PROFILE	4,228	4-84
IUE	10	12	GENERAL ELECTRIC	GEO	18	8-77
IUE	5	12	GENERAL ELECTRIC	LEO	52,800	8,77
IUE	5	12	GENERAL ELECTRIC	LEO	10	10-85
IUE	5	6	GENERAL ELECTRIC	GEO	10	10-85
IUE	5	12	GENERAL ELECTRIC	GEO	20	4-76
NOAA	5	26.5	GENREAL ELECTRIC	LEO	14,000	7-82
NOAA	5	26.5	GENERAL ELECTRIC	LEO	900	8-85
TIROS-N	5	26.5	GENERAL ELECTRIC	LEO	52,800	1-78

Figure 3. CURRENT NASA TEST STATUS

FLIGHT PROGRAM	NUMBER OF CELLS	RATED CAPACITY (A-H)	MANUFACTURER	SIMULATED ORBIT	CYCLES OR SHADOW PERIODS TO DATE	DATE TEST BEGAN
TIROS-N	5	26.5	GENERAL ELECTRIC	LEO	52,800	1-78
TDRSS	5	40	GENERAL ELECTRIC	GEO	15	12-78
TDRSS	5	40	GENERAL ELECTRIC	GEO	12	3-80
GOES	5	6	GENERAL ELECTRIC	GEO	13	8-79
GOES	5	6	GENERAL ELECTRIC	GEO	9	9-82
GOES	5	6	GENERAL ELECTRIC	GEO	13	3-84
GOES	5	6	GENERAL ELECTRIC	GEO	4	3-84
GOES	3	6	GENERAL ELECTRIC	GEO	8	3-84
UARS	4	50	GENERAL ELECTRIC	LEO	500	10-85
REQUAL	34	50	GENERAL ELECTRIC	LEO	1,800	4-85
REQUAL	10	50	GENERAL ELECTRIC	GEO	--	4-85

Figure 3. (cont.) CURRENT NASA TEST STATUS

- COBE - 50 A-H, LEO
- UARS - 50 A-H, POWER PROFILE

Figure 4. FUTURE PLANNING (NASA)

- AIR FORCE/NAVY NICKEL CADMIUM SEPERATOR REQUALIFICATION - 173 CELLS
- AIR FORCE NICKEL-HYDROGEN - 57 CELLS TO DATE

Figure 5. OTHER TESTING

BATTERY TEST AUTOMATION PROGRAM (BTAP)

Figure 6.

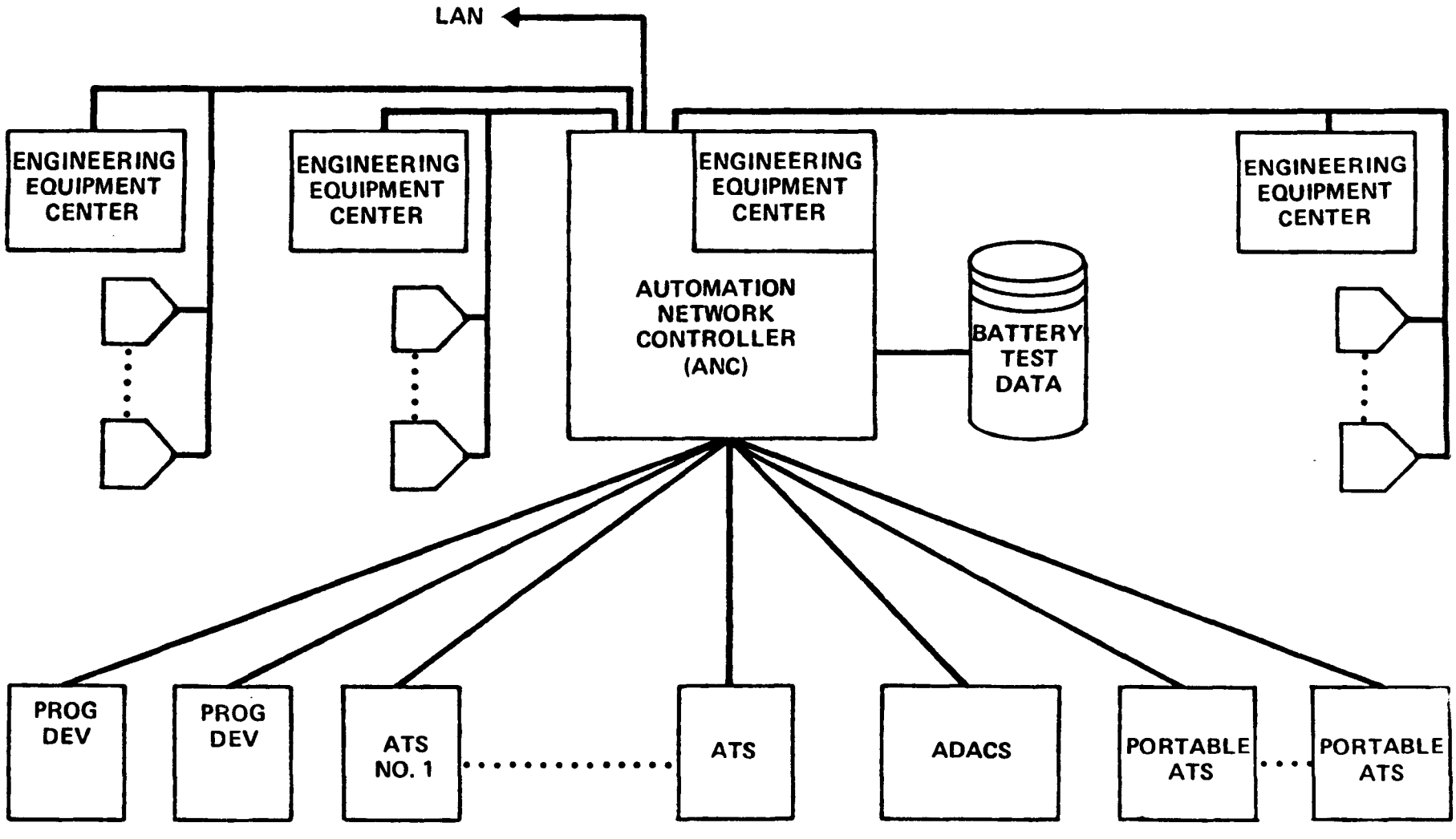

Figure 7. Battery Test Automation System

- NAVY
- AIR FORCE
- NASA

Figure 8. BTAP Participants

- EQUIPMENT DELIVERY - DECEMBER 1985
- DATA REDUCTION CENTER OPERATIONAL - FEBRUARY 1986

Figure 9. Automated Network Controller Progress

VOLTAGE-TEMPERATURE CHARGE VERIFICATION TESTING OF 34 AMPERE-HOUR NICKEL-CADMIUM CELLS

Paul J. Timmerman
and
Donald W. Bondeson
Martin Marietta Denver Aerospace
Denver, Colorado

ABSTRACT

This testing was designed to evaluate various voltage-temperature (V-T) charge curves for use in low-earth-orbit (LEO) applications of nickel-cadmium battery cells. The trends established relating V-T level to utilizable capacity were unexpected. The trends toward lower capacity at higher V-T levels was predominant in this testing. This effect was a function of the V-T level, the temperature, and the cell history. This effect was attributed to changes occurring in the positive plate. The results imply that for some applications, the use of even lower V-T levels may be warranted. The need to limit overcharge, especially in the early phases of missions, is underlined by this test program.

INTRODUCTION

V-T compensated charge control is the primary method of battery charging in low-earth-orbit (LEO) spacecraft. The careful selection of V-T levels is crucial for mission longevity. The ability to change V-T levels during operation gives the necessary flexibility to adapt to changing cell electrical characteristics. To evaluate the three most likely curves available in this spacecraft, a matrix of nine V-T combinations was selected. For each of these points, a series of tests was performed. The test series allowed for the evaluation of utilizable capacity as well as cyclic parameters. Based upon the results of this testing, implications regarding cell and system operation can be made.

TEST ARTICLES

The testing was performed concurrently on two (2) separate six (6) cell-packs of thirty-four ampere-hour (34 AH) sealed nickel-cadmium cells. The two cell packs have different test histories, although both were manufactured from the same plate lot. The group referred to as the "new cells" had no previous testing aside from pre-ATP, ATP, and cell receiving and matching. The "old cells" had been in test for approximately one and one-half years prior to this testing. The testing performed on the old cells includes minimum trickle charge evaluation (1), various characterization cycles, and a small amount of hot case testing. In all, approximately sixty 100% depth-of-discharge (DOD) cycles were performed. Each of the cell-packs was mounted in a restraining fixture to provide physical support and electrical isolation. The cells are series wired. The cell-packs were instrumented for battery and cell voltages and skin temperature. All tests were performed in an environmental temperature chamber.

TEST OPERATIONS

Prior to the start of any test series, the cells were shorted with one-quarter (0.25) ohm resistors. The testing was performed at 0°C, 15°C, and 30°C. At each of these three temperatures, three V-T levels were evaluated. Each of the V-T levels was evaluated using the following sequence:

Initial Capacity Check

A capacity check is performed following temperature stabilization. This test is performed once per temperature for each cell pack. The test uses a C/20 charge rate (1.70 amperes) for forty (40) hours. Discharge is performed immediately, at a C/2 (-17.0 amperes) rate, until a pack voltage of 6.0 volts (1.0 volt/cell) is reached. The recorded discharge capacities are then interpolated to the exact voltage cut-off level. Cell shorts are then installed, bringing the cells to less than twenty millivolts (20 mV) before continuing.

Pre-Charge

The cells are then charged at a C/20 rate (1.70 amperes) for forty (40) hours.

V-T Cycling

Following the pre-charge test, the simulated LEO cycling was initiated. Each of the cycles is one-hundred and eight (108) minutes long, with a seventy-two (72) minute charge phase, and a thirty-six (36) minute discharge phase. The charge current is limited to fourteen amperes (14 A) and tapers

at the assigned voltage limit. The discharge current is a constant eight and one-half amperes (-8.5A). This results in a consistent fifteen percent (15%) DOD. Operation of the simulated LEO cycing is continued until the cyclic parameters have stabilized, as determined through the use of specialized software routines.

Upon stabilization of recharge fraction, end-of-charge current, and end-of-discharge voltage, the test is stopped. This test halt is executed at the end of the charge phase. The set-up and test start of the next test is performed immediately. See Figure 1 for the V-T levels tested.

Post-Cyclic Capacity Check

This discharge test is very similar to the last half of the capacity check. It uses the same C/2 discharge rate and cell short-down procedure. At this time the testing proceeds to the next V-T series. Either a temperature stabilization or a pre-charge is performed, depending upon whether a change in temperature is required.

TEST RESULTS

To preface the discussion of the effects of V-T levels on cell performance, it is important to first look at the constant current testing performed. Both of the cell-packs displayed normal performance, considering the respective histories. Figure 2 displays the results of the capacity check tests for both cell packs at a range of temperatures. As would be expected, the old cells showed marginally lower capacities, with extreme temperatures perturbing the difference. The general shape of the curves fits very well with classical capacity curves (2). Figure 3 depicts the maximum charge voltage for the respective cell-pack as a function of temperature. The effect of test history on the old cells manifests itself again as higher charge voltage. This effect is most pronounced at low temperature. The formation of large crystals of active material, and the resulting reduction in the oxygen recombination rate is considered the primary cause of this phenomenon (2, 3, 4).

The cyclic testing can be evaluated by a number of electrical parameters. The parameters of greatest interest in this testing are recharge fraction, end-of-charge current (EOCI), end-of-discharge voltage (EODV) and temperature. The raw data from these parameters would constitute a large volume. For this reason, only the most representative data was presented. Figures 4 and 5 depict the data presented in Table 1. Figure 4 depicts the effect of V-T level on the EOCI of the two cell-packs as function of temperature. Figure 5 depicts the effect of V-T level on the recharge fraction of the two cell-packs as a function of temperature. This data represents values for the cycling just prior to the discharge.

The strong correlation between Figures 4 and 5 would be anticipated. Note that the plots for adjacent V-T levels of different cell-packs are very similar. This is another indicator of the general state of health of the respective cell-packs. The trends shown toward higher values at higher temperatures and/or V-T levels is normal. The fact that the new cells have consistently higher values is witness to the inherently lower charge voltages, as seen earlier.

The data presented thus far fit well into the expected trend for LEO applications of sealed nickel-cadmium battery cells. The results of the post-cyclic capacity checks do not fall into the range of anticipated values. Figures 6 and 7 present the ampere-hour capacities for the two cell-packs, as functions of the V-T level and the temperature. The most notable trend in these figures is that of decreased capacity with increased V-T level. Note also that this effect is a function of temperature as well. There are notable exceptions to this trend, as seen in Figure 6, "Effect of V-T Levels on Capacities of New Cells." While the 30°C data show clear and consistent trends, the 15°C and 0°C regions are less clear. The differences in the values at 15°C are quite minimal, considering the range of capacities recorded. The unexpected low value for the 0°C measurement for V-T curve number two can be attributed to an excessive number of cycles needed to achieve stabilization.

Figure 8 represents the general trends for capacities achieved by the new cells. The curves generated are interpretations of the data in Figure 6. Modification to the trends are based upon aforementioned factors.

Figure 7, "Effect of V-T Levels on Capacities of Old Cells", gave clear values for the 0°C and 30°C regions, with the 15°C region showing an excessively low capacity for V-T curve 2. This resulted from improper charge control and an excessive number of cycles being performed. Figure 9 is an expression of the trends established in Figure 7.

There are two major differences between Figures 8 and 9. First is the reversal in the general trend for the old cells at low temperature. An increase in discharged capacity correlated with increased V-T level for this one case. The exact temperature at which the crossover in trend occurs is beyond the scope of this testing. This testing lacks the necessary precision to identify that point. Second is the smaller reduction in utilizable capacity in the old cells. The presence of this reduction in utilizable capacity, and the magnitude of this effect, can be related to the data presented earlier in this paper.

DISCUSSION

The results of this testing represent a deviation from the traditional effects ascribed to V-T levels with respect to capacities. This paper does not, however, contradict reports which show increases in capacity with increased V-T level where only one cycle was performed (4). Earlier reports showed instances of phenomonon similar to that seen here (5). The presence of such an effect was attributed to a high self-discharge rate, as a result of elevated plate temperatures. This explanation is not feasible in light of the test method used in this testing. The self discharge rate would have to be in the C rate range (-34 A) for this to be the cause, based on maximum residual capacity and the average set-up time for the post-cyclic discharge test.

The phenomenon of lower capacities upon discharge can be attributed to many causes. A simple approach is to look at the individual components and analyze them separately. First is the separator. Degradation and drying out of the separator are gradual and primarily irreversible trends (6). Since the effect observed in this report is reversible, the separator is not a likely cause. The negative plate is a likely candidate to have the effect ascribed to it. The trend toward a decrease in surface area, and thus effective excess negative active material, is well known. Reconditioning of cells increases the surface area by decreasing the cadmium crystal size. Thus, the effects of the negative electrode can be considered somewhat reversible, like the effect reported herein. The fact that the decrease in utilizable capacity was most dramatic in the new cells, as seen by comparing Figures 8 and 9, is an indication that the negative plate is not the cause. It has long been known that overcharging of nickel-hydroxide electrodes results in the formation of charged active material of higher valence states, gamma-nickel-oxy-hydroxide (NiOOH) (7). Additionally, it has been noted that electrodes with high concentrations of the Gamma-NiOOH experience poor efficiency upon discharge (8, 9). The capacity unavailable at high rate is referred to as the residual capacity. Further evidence and explanations of the residual capacity effect were presented in a recent study of charge and discharge efficiencies (10). This paper shows a significant inefficiency for discharging at states-of-charge less than twenty-five percent (25%). In addition, the level of inefficiency is related to both the charge and discharge profiles used. These parameters affect the existence of depletion and defect layers in the positive electrode.

These previous studies do not address all of the intricacies of the data reported here. One example is the variation in the magnitude of residual capacity for the cell-pack with different levels of degradation. This phenomenon is simply an artifact of the higher charge efficiency of the new cells, and the resulting overcharge level. Consistent with the above theories, the higher level of overcharge results in a lower charge utilization. It is, however, unanticipated that the C/2 rate would result in residual capacity of the magnitudes seen. Another example is the lack of the manifestation of the residual capacity loss at low temperatures for the old

cells. It is common knowledge that cold temperature oxygen recombination, especially in cells with an extensive history, can be a problem, due to the morphological changes in the negative plate. A simple explanation would be to attribute the rise in capacity with V-T level to the increase in temperature of the electrodes. Another possible influence may be the effect of intra-cell oxygen pressure upon the equilibrium of the cell reactions. The effect of a reduction of charged excess negative active material may also play a role in this phenomenon.

CONCLUSIONS

This report presents data which supports the most modern theories on charge and discharge efficiencies and the related cell electro-chemistry. In addition it gives indications of the conditions under which the residual capacity effect will manifest itself. Applying these principles to system operation, several things become apparent. Primarily, the adverse effect of overcharging cells is highlighted. At the other extreme, the lower threshold for V-T charge effectiveness was not firmly established. These test results do indicate that effective charging at low temperature can be accomplished with extremely low recharge fractions. It becomes apparent that to some extent lower V-T curves are better for most cases. In conclusion, an approach of maintaining a minimum recharge fraction is a good approach toward monitoring the state-of-charge of a spacecraft electrical power system. Maximum life and higher operating efficiency may be obtained at recharge fractions lower than currently being used. In addition, the use of non-linear V-T curves might give more accurate charge control, especially in highly variable thermal environments.

BIBLIOGRAPHY

1. P. Timmerman, "Minimum Trickle Charge Testing of 34 Ampere-Hour Nickel-Cadmium Cells", 1984 GSFC Battery Workshop Proceedings, 1984, pp. 369-386.

2. W. R. Scott and D. W. Rusta, "Sealed Cell Nickel-Cadmium Battery Applications Manual", NASA NAS5-23514, Ref. Publ. 1052, 1979, p. 96.

3. "Nickel-Cadmium Battery Application Engineering Manual", Second Edition, Ed. by J. C. Grant, General Electric Company Publication Number GET-3148A, 1975, para. 6.5.5.

4. W. R. Scott and D. W. Rusta, Ibid, p. 94.

5. W. R. Scott and D. W. Rusta, Ibid, p. 97.

6. W. R. Scott and D. W. Rusta, Ibid, p. 213.

7. S. U. Falk and A. J. Salkind, "Alkaline Storage Batteries", John Wiley and Sons, Inc., New York, NY, 1969, p. 50.

8. R. Banard, G. T. Crickmore, J. A. Lee and F. L. Tye, "The Cause of Residual Capacity in Nickel Oxyhydroxide Electrodes", Journal of Applied Electro-Chemistry, 10-1, January, 1980, pp. 61-70.

9. R. Banard and C. F. Randall, "Studies Concerning Charged Nickel-Hydroxide Electrodes. VIII. The Relative Potentials of the Beta-Nickel-Oxyhydroxide Reduction Process", The Journal of Applied Electro-Chemistry, 12-1, January, 1982, p. 121.

10. A. H. Zimmerman and P. K. Effa, "Charge Efficiency and Charge Utilization in the Sealed Nickel-Cadmium Cell", Report SD-TR-82-91, The Aerospace Corporation, 20 December 1982.

Table 1. DISCHARGE CAPACITIES

Test / Temperature	Baseline Capacity Test, Ah	V-T Level One, Ah	V-T Level Two, Ah	V-T Level Three, Ah
0°C	(41.18, 40.93)	1.45 (V/Cell) (37.73, 38.03)	1.47 (V/Cell) (34.82, 38.40)	1.49 (V/Cell) (35.10, 39.01)
15°C	(41.83, 41.72)	1.42 (V/Cell) (38.37, 38.77)	1.44 (V/Cell) (38.90, 36.73)	1.46 (V/Cell) (37.58, 38.73)
30°C	(40.03, 39.21)	1.38 (V/Cell) (37.39, 37.46)	1.40 (V/Cell) (35.73, 34.71)	1.42 (V/Cell) (33.06, 36.20)
	Note: All capacities are given as new cells & old cells.			

Table 2. CYCLIC DATA MATRIX

Test Temperature		Cell Pack	0°C			15°C			30°C		
Test Parameter			Recharge Fraction	EOD Voltage	EOC Current	Recharge Fraction	EOD Voltage	EOC Current	Recharge Fraction	EOD Voltage	EOC Current
(Units)			N/A	Volts	Amps	N/A	Volts	Amps	N/A	Volts	Amps
V-T Level 1	0°C = 1.45 15°C = 1.42 30°C = 1.38	New	1.003	1.257	0.44	1.055	1.252	0.69	1.078	1.235	0.74
		Old	1.005	1.248	0.46	1.035	1.259	0.5	1.045	1.238	0.60
V-T Level 2	0°C = 1.47 15°C = 1.44 30°C = 1.40	New	1.025	1.254	0.57	1.162	1.256	1.264	1.230	1.244	1.67
		Old	1.015	1.265	0.52	1.086	1.251	0.711	1.12	1.247	1.00
V-T Level 3	0°C = 1.49 15°C = 1.46 30°C = 1.42	New	1.03	1.259	0.60	1.464	1.248	1.461	1.562	1.231	3.50
		Old	1.04	1.265	0.56	1.18	1.248	1.16	1.31	1.251	1.42

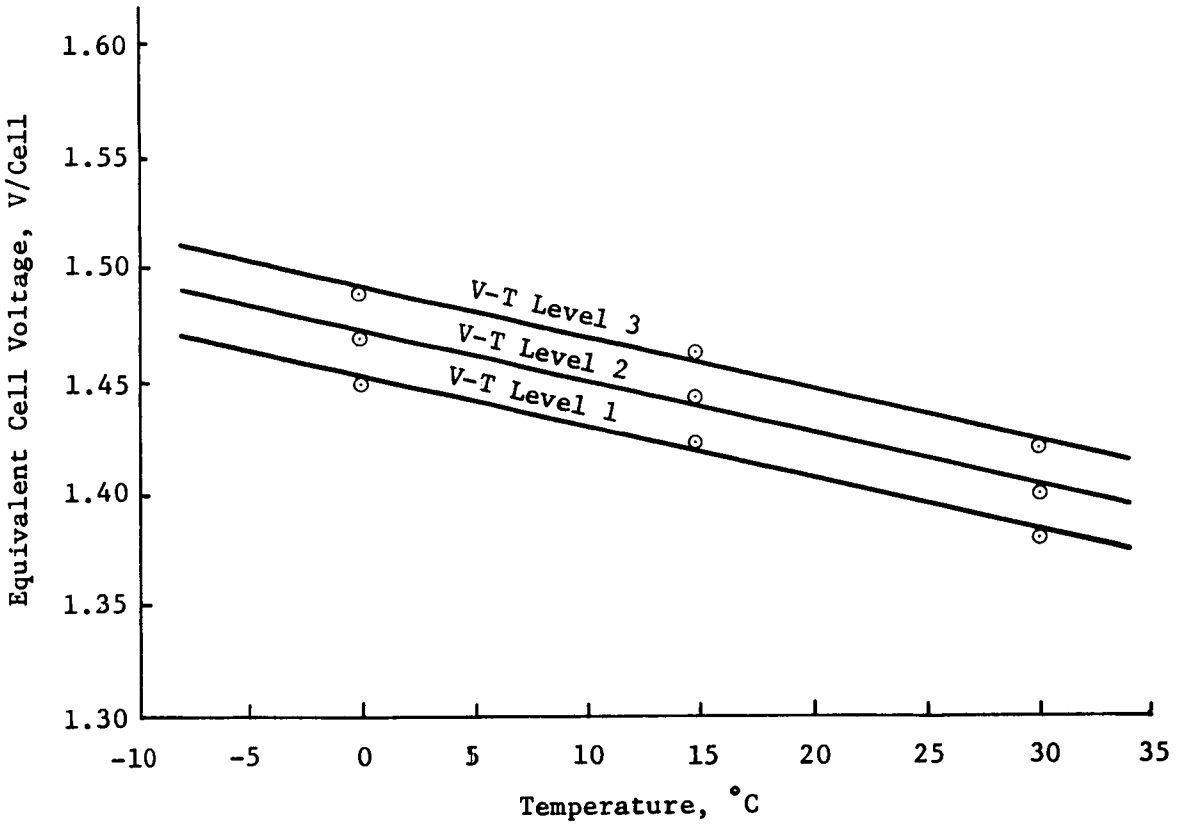

Figure 1. V-T LEVELS TESTED

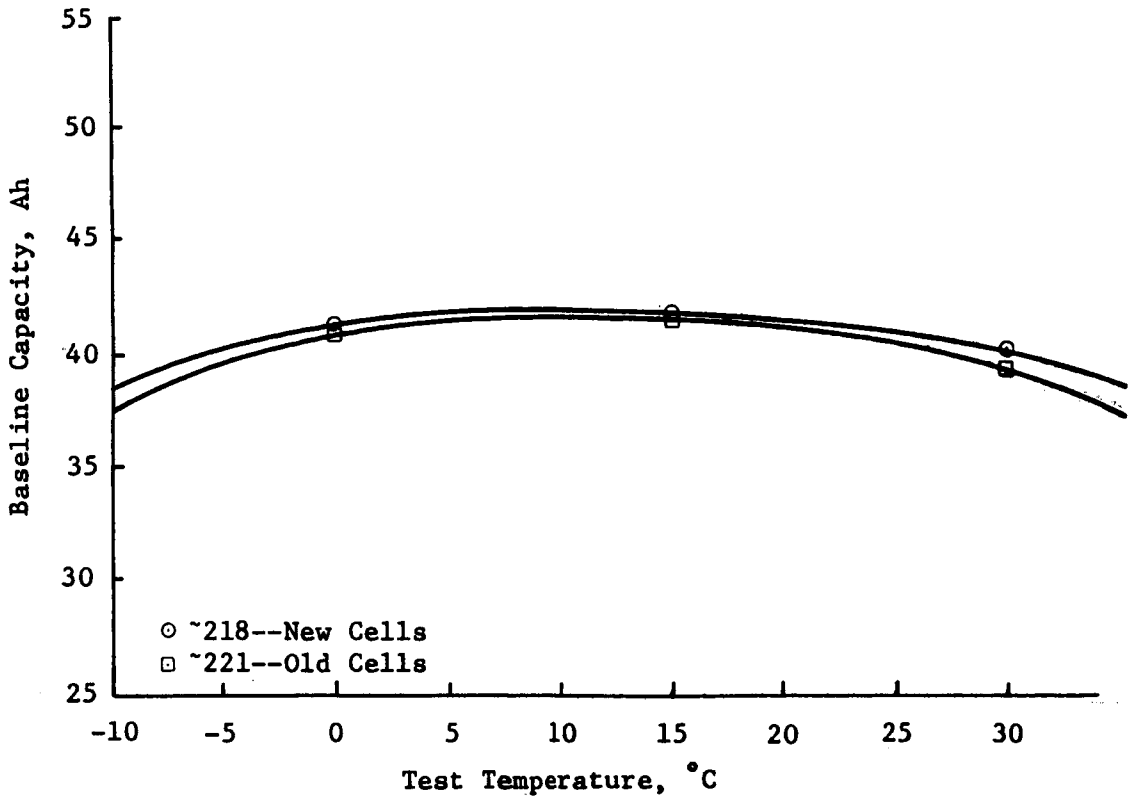

Figure 2. BASELINE CAPACITIES VERSUS TEMPERATURE

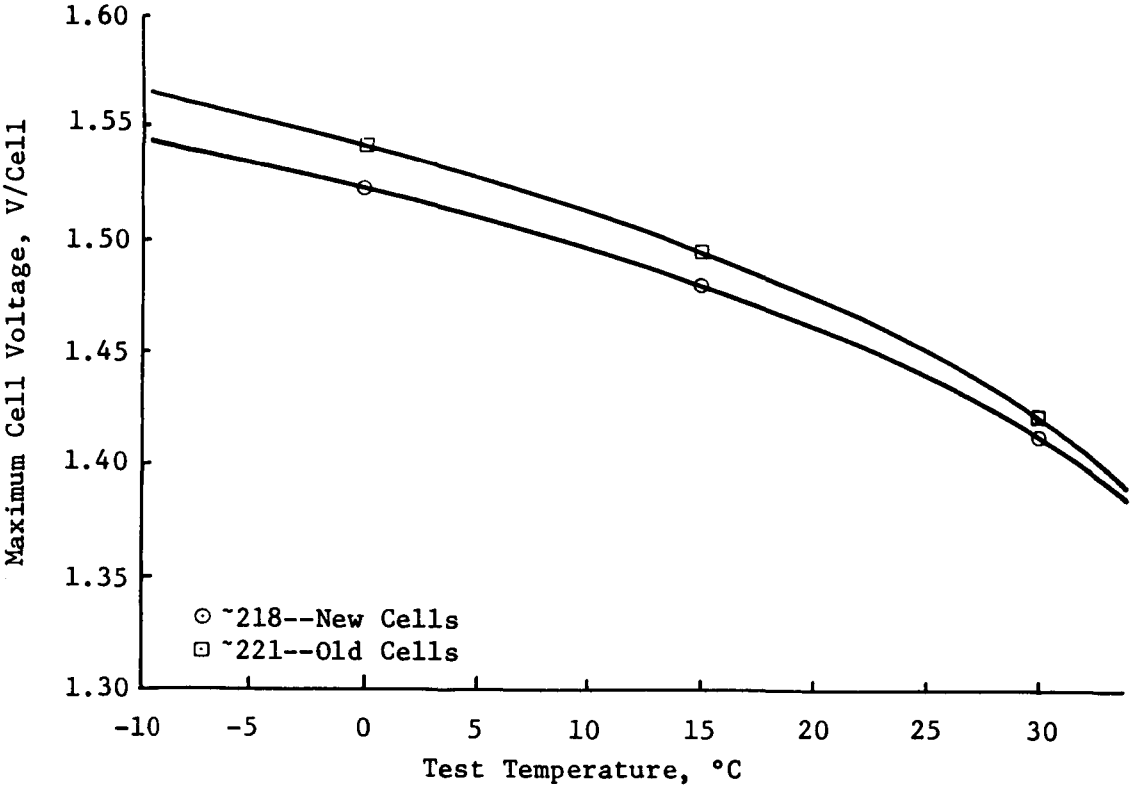

Figure 3. MAXIMUM CELL VOLTAGE FOR C/20 CHARGE RATE

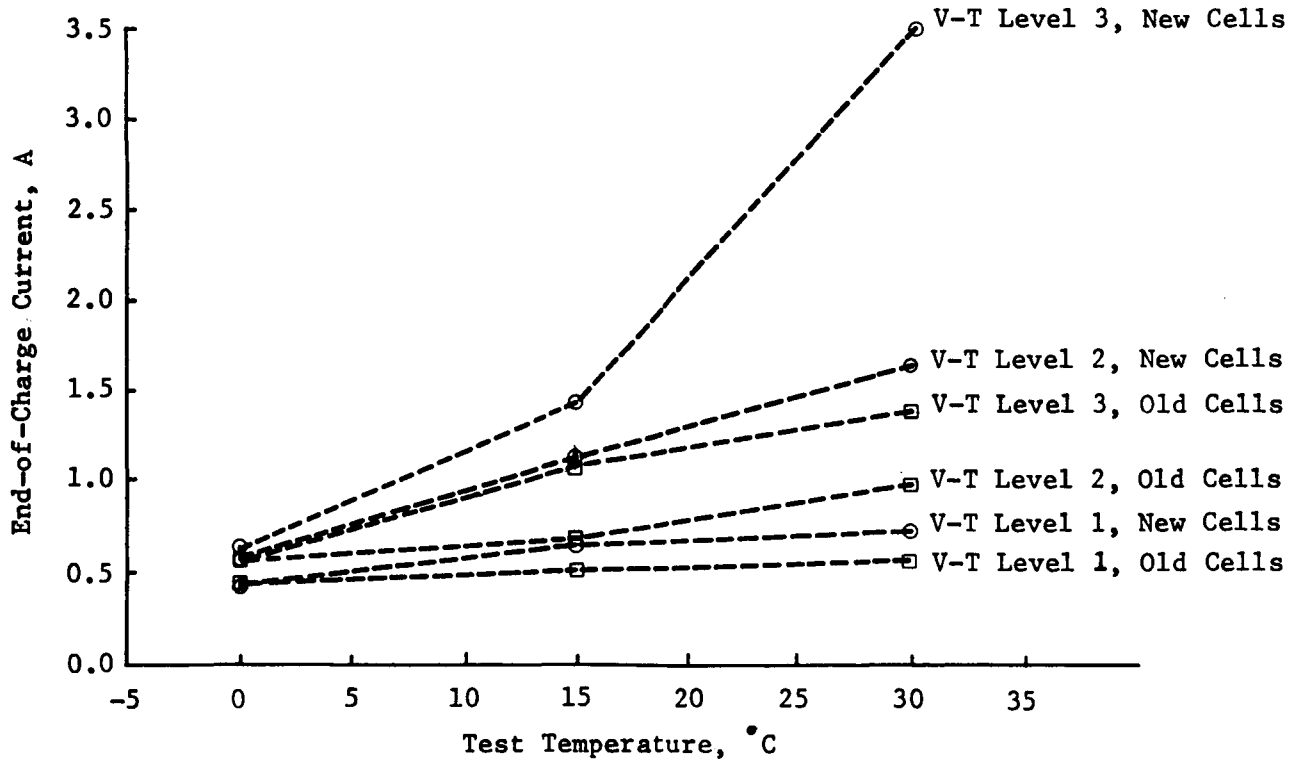

Figure 4. EFFECT OF V-T LEVEL ON END-OF-CHARGE CURRENT (EOCI)

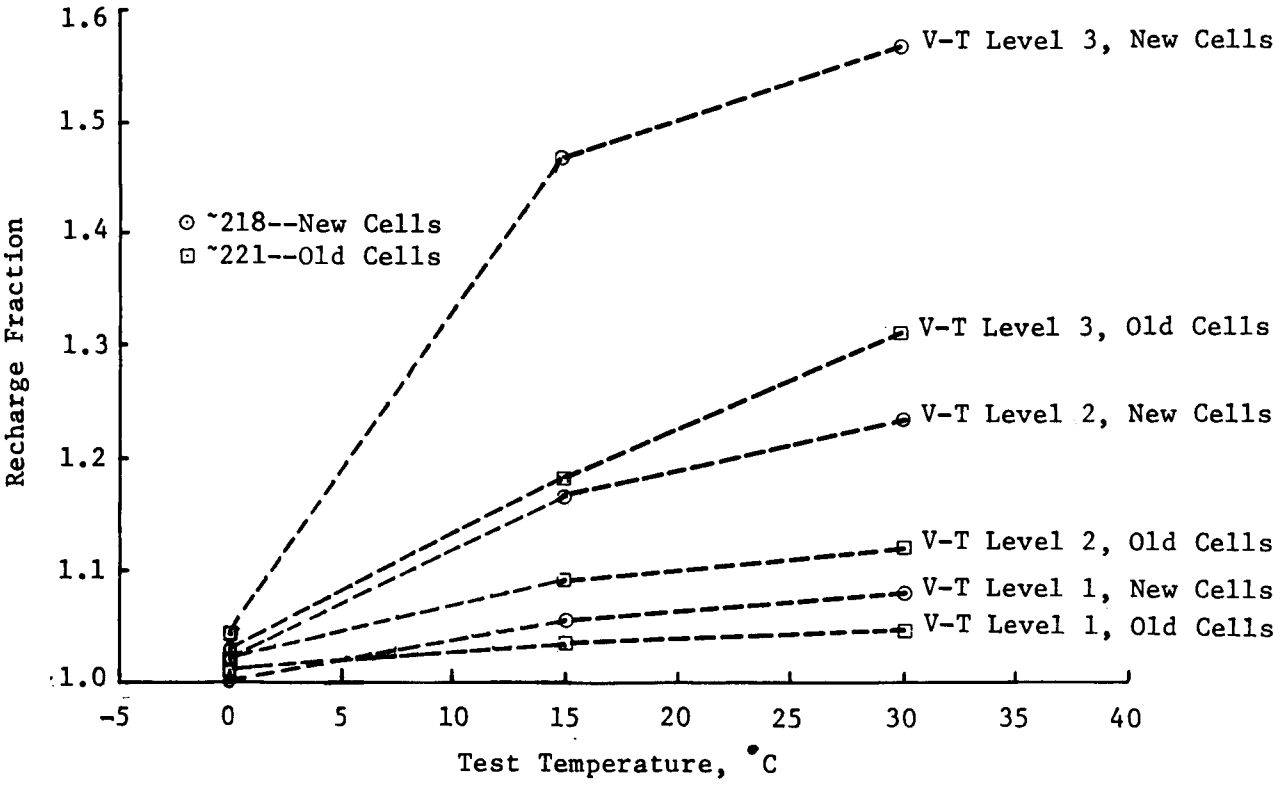

Figure 5. EFFECT OF V-T LEVEL ON RECHARGE FRACTION (RF)

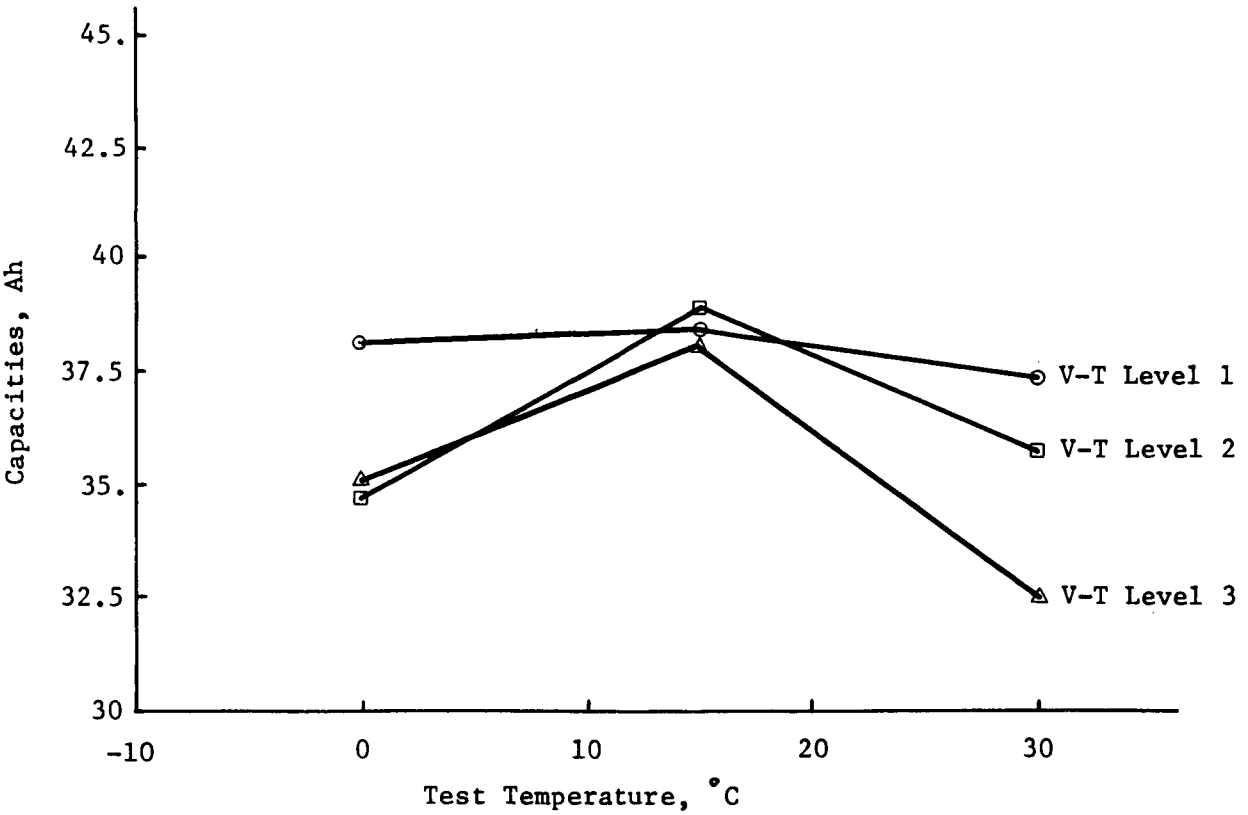

Figure 6. EFFECT OF V-T LEVELS ON CAPACITIES OF NEW CELLS

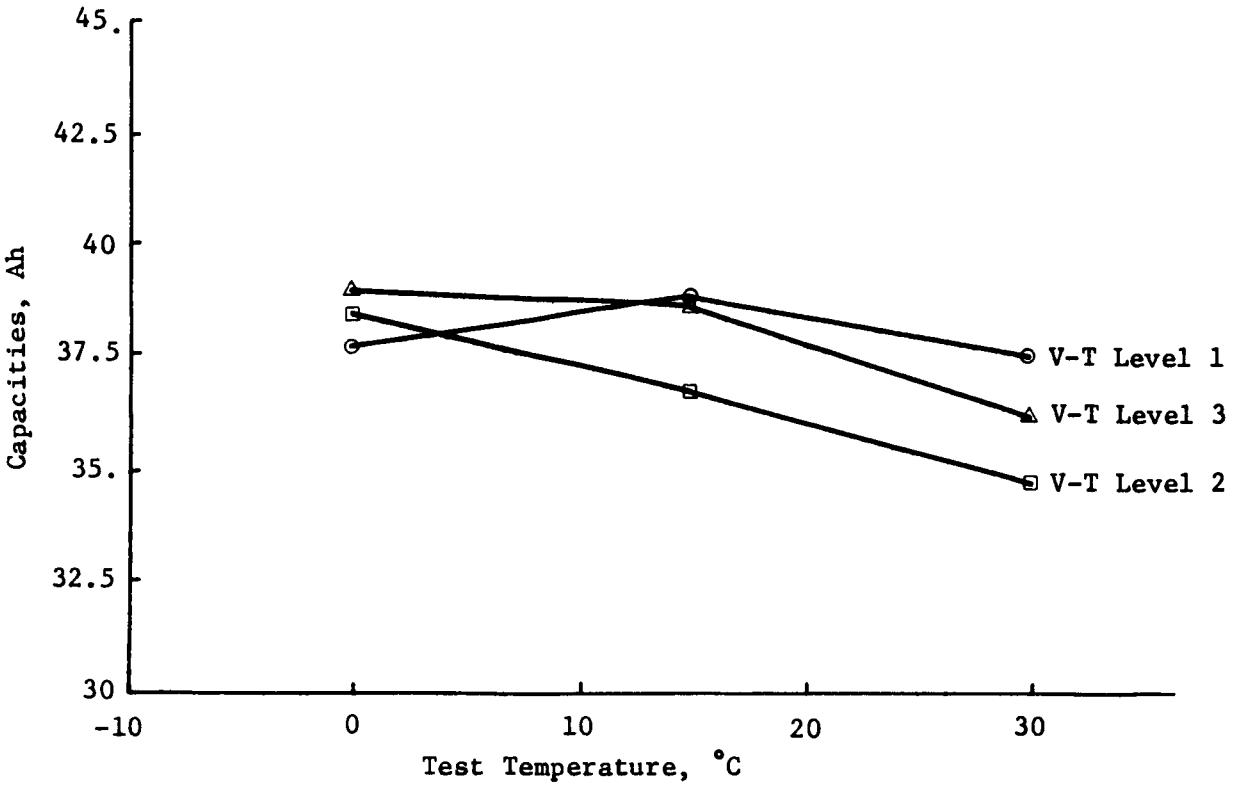

Figure 7. EFFECT OF V-T LEVELS ON CAPACITIES OF OLD CELLS

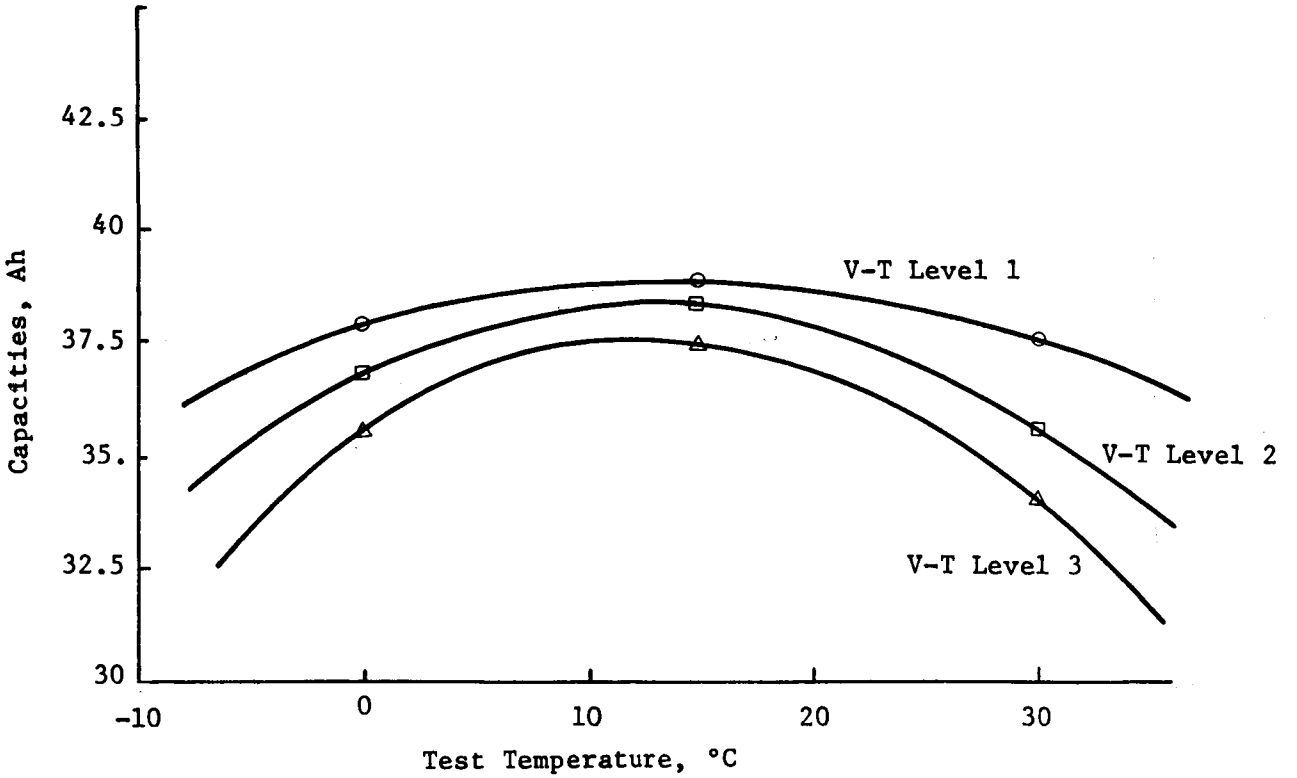

Figure 8. EFFECT OF V-T LEVELS ON CAPACITIES OF CELLS NEAR BEGINNING-OF-LIFE

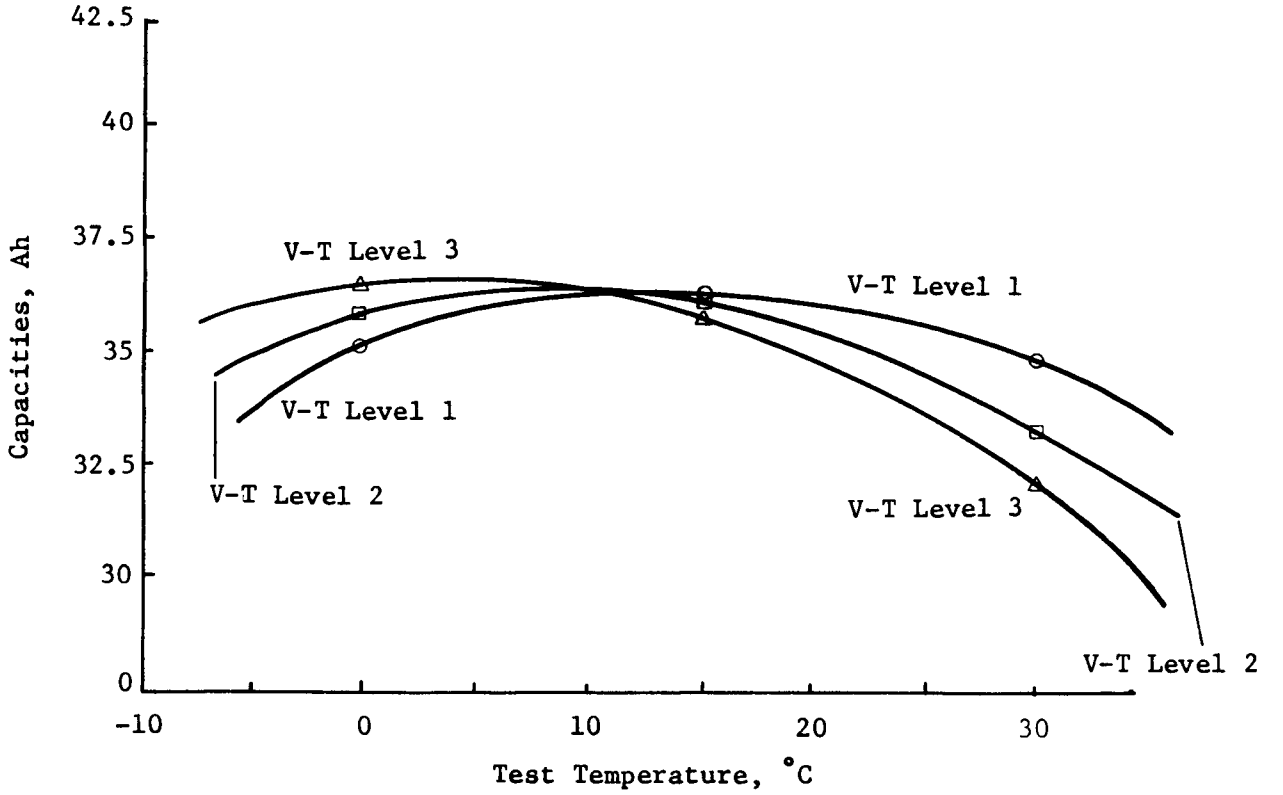

Figure 9. EFFECT OF V-T LEVELS ON CAPACITIES OF CELLS NEAR MIDDLE-OF-LIFE

NOAA 26.5 Ah LEO CHARACTERIZATION TEST

George W. Morrow
Goddard Space Flight Center
Greenbelt, MD 20771

ABSTRACT

Five General Electric (GE) 26.5 Ah NOAA-G flight nickel-cadmium cells were obtained from RCA-Astro Electronics to undergo performance characterization testing at the Goddard Space Flight Center (GSFC). This lot of cells was manufactured with passivated positive plate, to control nickel structure attack during active material impregnation, and less electrolyte than normal (< 3cc/Ah). The cells were tested in a parametric Low Earth Orbit (LEO) cycling regime that had previously been used to test and characterize GSFC standard 50 Ah cells. Life cycle testing at the Naval Weapons Support Center (NWSC) in Crane, Indiana followed. The results of the test showed nominal performance in comparison with previous test data on the standard 50. Life cycle testing in the NOAA orbital regime is continuing at NWSC.

INTRODUCTION

The NOAA-G spacecraft battery cell flight lot was manufactured by GE in Gainesville, Florida. GE fabricated these cells using a new positive electrode processing step designed to increase the strength of the electrode by reducing attack on the nickel sintered structure by active material impregnation solutions. This passivation process reduces the void volume of the cell, thus reducing the amount of electrolyte that can be added. Questions about the reliability of cells with this new processing step and less electrolyte brought about characterization testing by the GSFC.

Characterization was accomplished by subjecting 5 cells to a parametric LEO cycling regime developed to characterize GSFC standard 50 Ah cells. Data was then compared between the cell designs. Following the characterization test, the cells were shipped to NWSC for life cycle evaluation.

TEST OBJECTIVES

The objectives of this test program were: (1) to study the behavior of aerospace cells manufactured with GE positive trode nickel attack control passivation, (2) to compare this behavior to that of cells without passivation, and (3) to char-rize the performance of these cells in a typical NOAA orbit with the same charge voltage levels as the NOAA-F spacecraft.

Description

The cells tested are GE 26.5 Ah aerospace nickel-cadmium cells containing third (signal) electrodes. They were manufac-l with teflonated negative electrodes, cadmium treated positive electrodes, and positive electrode nickel attack control vation. The cells were manufactured to GE Manufacturing Control Document (MCD) 232A2222AA-80 and are desig-l Catalog Number 42B030AB10/11. The cells are from NOAA lot 11 activated in February 1984 and acceptance tested E Acceptance Test Procedure P24A-PB-222 prior to shipment to RCA.

Performance Characterization Test Description

he cells were tested in a series connected 5-cell pack separated and isolated by 3/8-inch aluminum plates followed by -inch PVC sheets. The pack was held by 3/8-inch stainless steel bolts torqued to 30 lb/in^2. The cell bottoms were filled RTV to provide a flat, thermally conductive surface. The pack was wired with individual cell voltage monitors and 5 ocouples. The thermocouples were located on the tops of cells 1, 3, and 5 and on the broadface center of cells 2 and

4. For the test, the pack bottom was coated with thermal grease and placed on an active thermal cooling plate in a Tenney environmental chamber.

The parametric test regime is shown in Figure 1. Four charge rates (0.2C, 0.3C, 0.5C, 0.8C) and 4 discharge rates (0.1C, 0.2C, 0.5C, 0.8C) were chosen for the test. The discharge rates coupled with a discharge time of 30 minutes resulted in depths of discharge (DOD) of 5, 10, 25, and 40 percent. Three charge voltage levels were chosen (GSFC 3, 5, 7) as were 3 temperatures (0, 10, 20°C). The charge voltages corresponding to each temperature are shown in Figure 2.

During the test, 8 cycles of each of the 13 charge-discharge combinations, shown in Figure 1, were completed at each temperature and voltage level. Before each temperature or voltage level change, 16 stabilization cycles were run. A stabilization cycle consisted of one 30-minute discharge at 0.5C followed by a 60-minute voltage limit taper charge at 0.5C to GSFC voltage level 6 at 20°C. Eight hundred stabilization cycles were also run prior to test startup to stabilize pack characteristics. The entire parametric test consisted of approximately 1900 cycles.

RESULTS

Throughout the test each set of 16 stabilization cycles was compared to chart the state of the pack. End-of-discharge (EOD) voltage remained constant throughout the test as did the end-of-charge (EOC) taper current level and C/D recharge ratio. This is shown on Figure 3. Capacity performance was also very good considering the varying conditions experienced. A precycling capacity measurement provided 33.2 Ah from the cells at an average plateau voltage of 1.24 v/cell, while a post-cycling capacity check yielded 30.1 Ah capacity at an average plateau voltage of 1.22 v/cell. Capacity test data is provided in Figure 4.

Parametric test data was plotted in the form of percent recharge (C/D) versus voltage level and C/D versus charge current level. This data was plotted against data from the standard 50 Ah cells under the same conditions. The trends of these plots compare very well as can be seen in the sample plots of Figures 5 – 13. Actual numerical data cannot be directly compared because of differences in cell design. Trend data is expected to compare very well for all aerospace nickel-cadmium cells regardless of design as is the case here. Poor correlation of trend data between cell designs may indicate problems related to manufacture and fabrication of the cells.

Data from this test also indicates that the cells exhibit slightly lower voltage characteristics than the 50 Ah cells to which they were compared. Full recharge was reached in almost all cases at both voltage levels 5 and 7. There was, therefore, no indication of slightly higher voltages as might have been expected from cells with low amounts of electrolyte.

NOAA Regime Test Results

Following the LEO performance characterization test, the cells were cycled in a parametric regime with characteristics similar to those experienced on the NOAA-F spacecraft. The pack was discharged for 35 minutes at 0.42C and charged for 69 minutes to RCA voltage levels 1, 2, 3, and 4 at 10°C. Eight cycles at each voltage level were performed with 16 stabilization cycles between each voltage level change. Full recharge ($>$106% C/D) was reached at RCA levels 3 and 4. In all other aspects, the cells performed nominally.

Life Cycle Test at NWSC

In June 1985 following all testing at the GSFC, the cells were sent to NWSC to undergo life cycle testing. The life cycle regime is detailed in Figure 14. The cells have performed nominally since the start of testing and have undergone approximately 1200 cycles at the time of this writing. The initial voltage level of 1.47 v/cell has provided approximately 106% C/D as is shown in the typical cycle plots of Figures 15 – 18.

CONCLUSIONS

LEO performance characterization tests have shown that the capacity and voltage performance of these cells is nominal. Also, parametric test data trend plots show that these cells react in a manner consistent with other aerospace nickel-cadmium cells when subjected to various charge-discharge currents, charge voltage levels, and temperatures. Further, these tests have shown that these cells obtain full recharge with the same range of charge voltage levels as experience predicts.

Parametric tests using the voltage levels and charge-discharge currents of the NOAA-F spacecraft indicate that these cells will perform satisfactorily under those conditions. Lastly, life cycle data during the first 1200 cycles of simulated LEO operation shows no abnormal or unexpected behavior. In light of the above findings, the cells should perform nominally in orbit. No problems are foreseen and no concern exists with regard to the low electrolyte levels or the positive plate nickel attack control passivation.

		DISCHARGE RATE			
		0.1C	0.2C	0.5C	0.8C
CHARGE RATE	0.2C	X	X		
	0.3C	X	X	X	
	0.5C	X	X	X	X
	0.8C	X	X	X	X

- 8 CYCLES AT EACH CONDITION
- DISCHARGE TIME: 30 MINUTES
  CHARGE TIME: 60 MINUTES
- VOLTAGE LIMITS: GSFC 3, 5, 7
- TEMPERATURES: 0, 10, 20°C

NOTE: 16 BASELINE CYCLES RUN BETWEEN EACH VOLTAGE LIMIT/TEMPERATURE TEST TO STABILIZE PACK

Figure 1. LEO PERFORMANCE CHARACTERIZATION REGIME

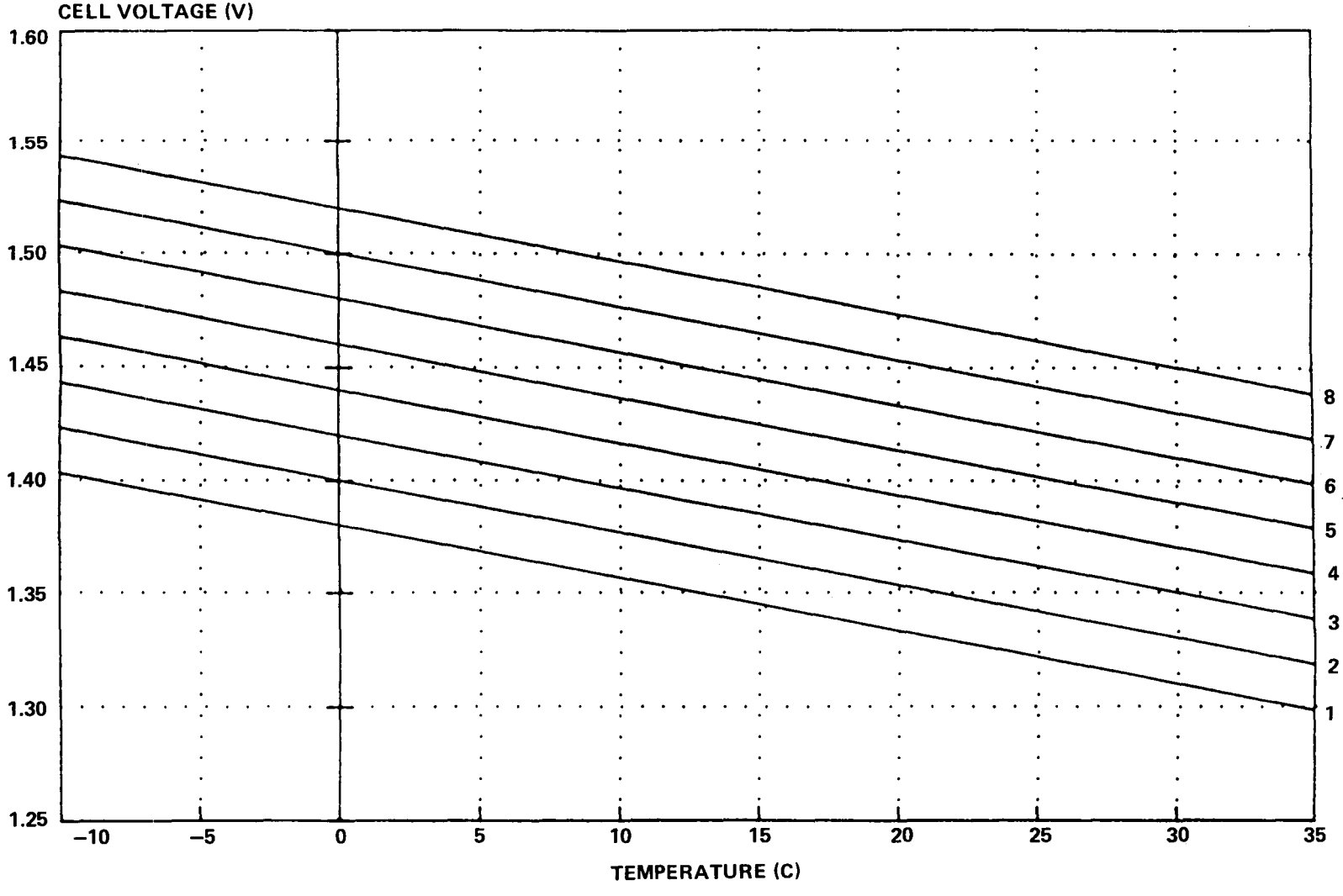

Figure 2. NASA/GSFC STANDARD Ni-Cd VOLTAGE/TEMPERATURE CHARGE CHARACTERISTICS ON A CELL BASIS

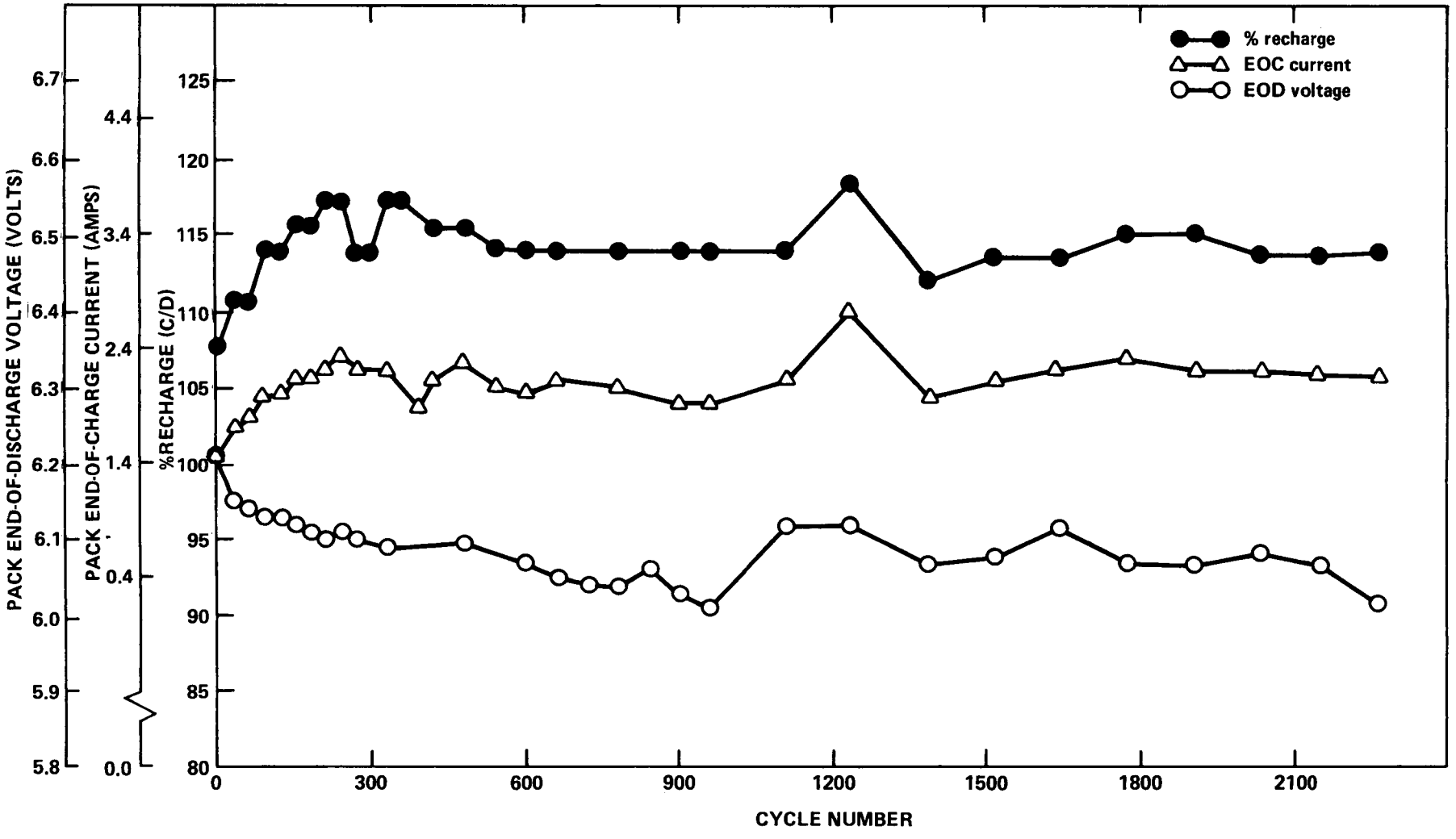

Figure 3. NOAA 26.5 Ah PARAMETRIC LEO CYCLING TEST
% RECHARGE, EOD VOLTAGE, EOC CURRENT, VS CYCLE
25% DOD, GSFC V_T6=1.433 V/CELL, 20°C
CYCLES 0 TO 965 BURN-IN, 966-2300 TEST

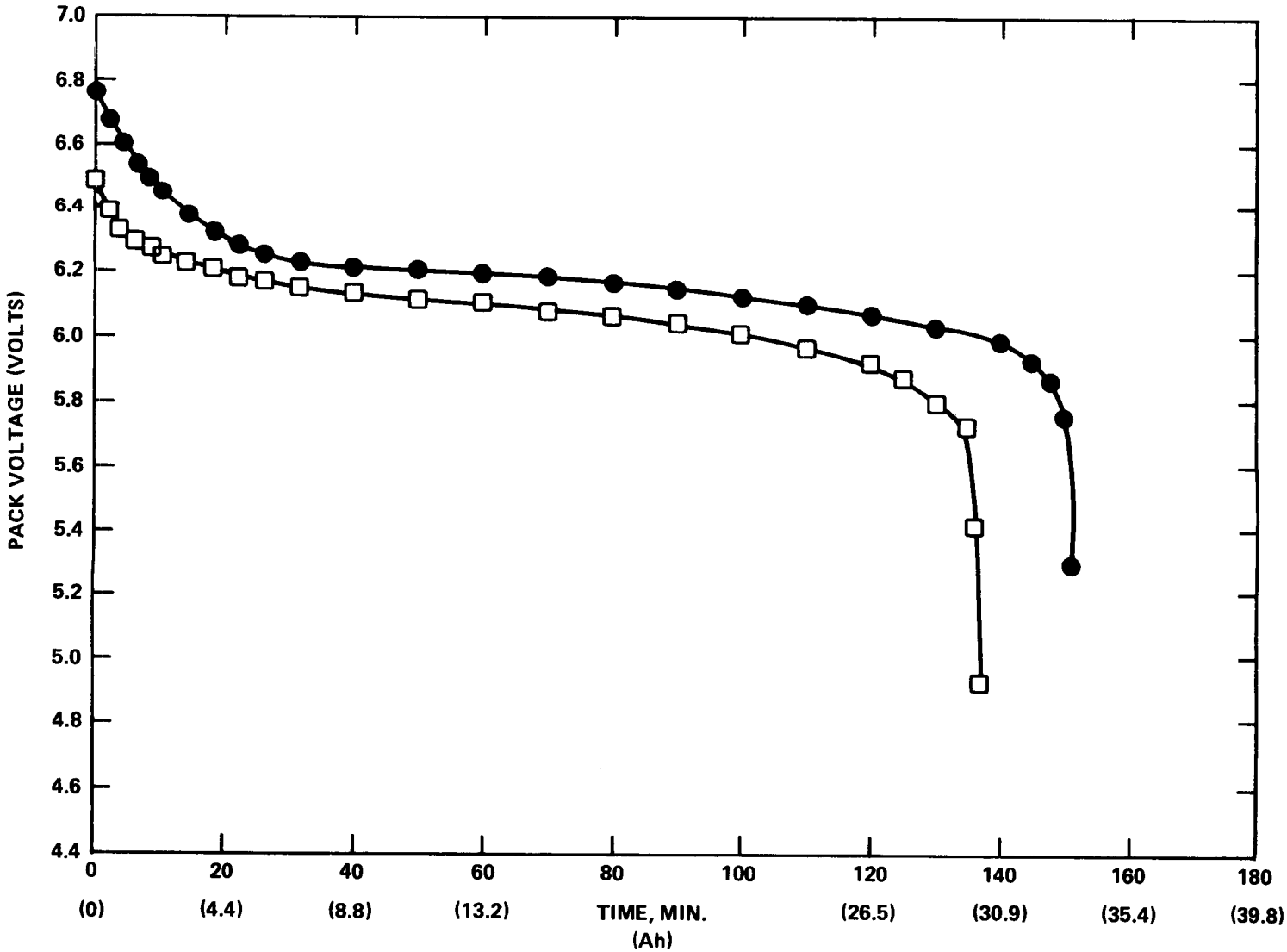

Figure 4. NOAA 26.5 Ah LEO CYCLING TEST
PRECYCLING CAPACITY VS POSTCYCLING CAPACITY
0.5C DCH TO 0.75V FIRST CELL
TEMPERATURE: 23 °C

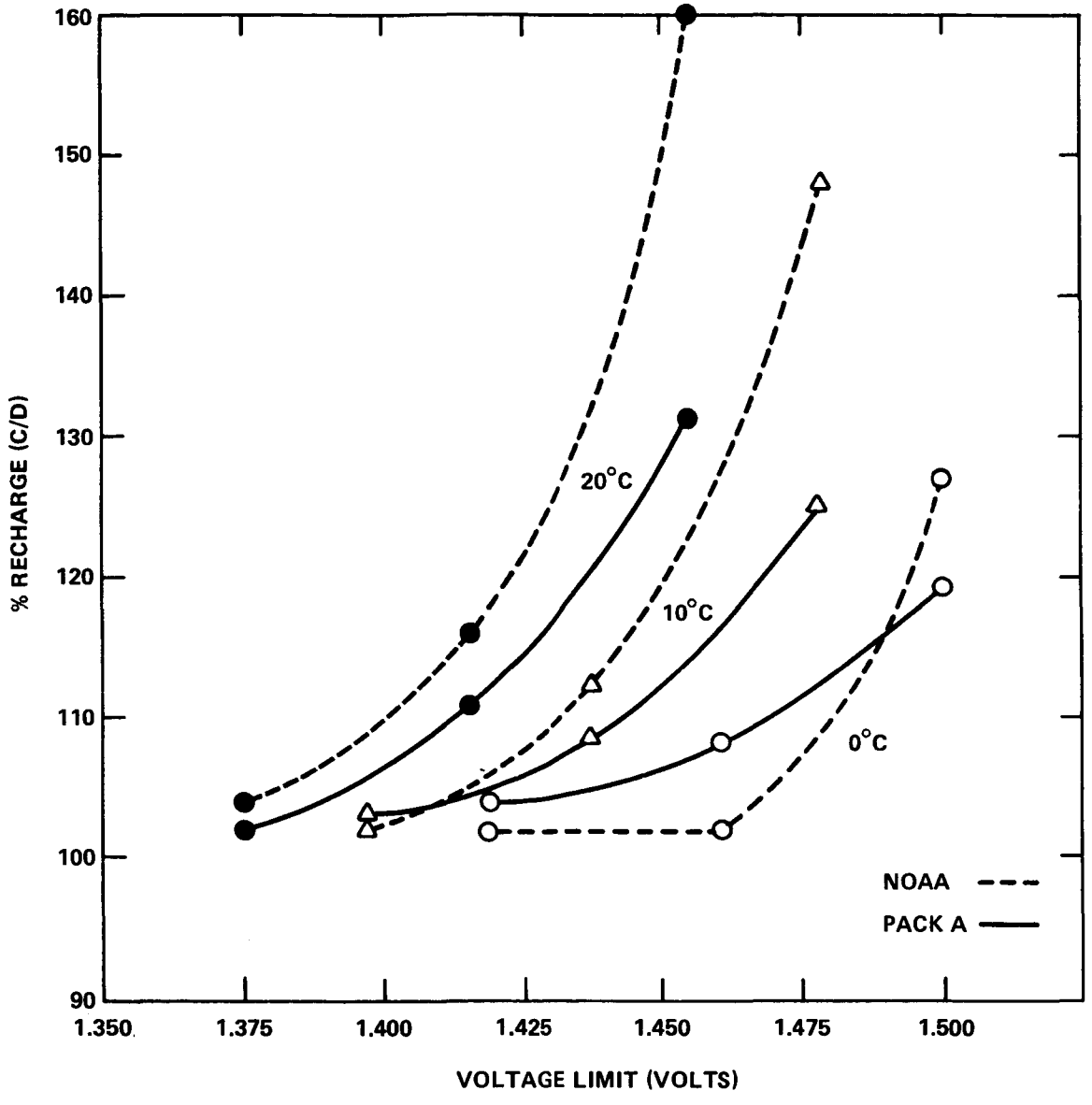

Figure 5. NOAA 26.5 Ah VS PACK A 50 Ah
CHARGE CURRENT: 0.2C
10% DEPTH OF DCH

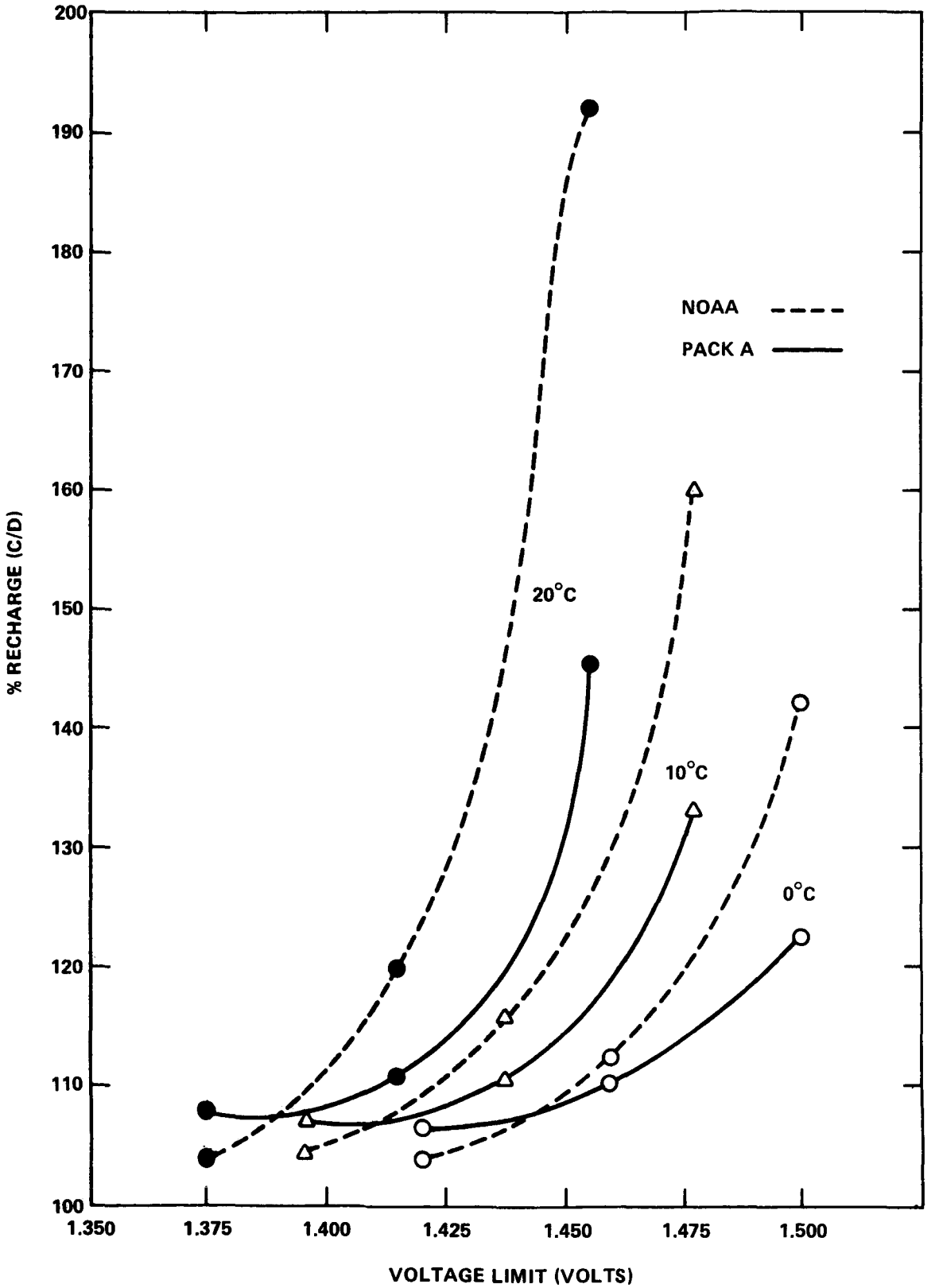

Figure 6. NOAA 26.5 Ah VS PACK A 50 Ah
CHARGE CURRENT: 0.5C
10% DEPTH OF DCH

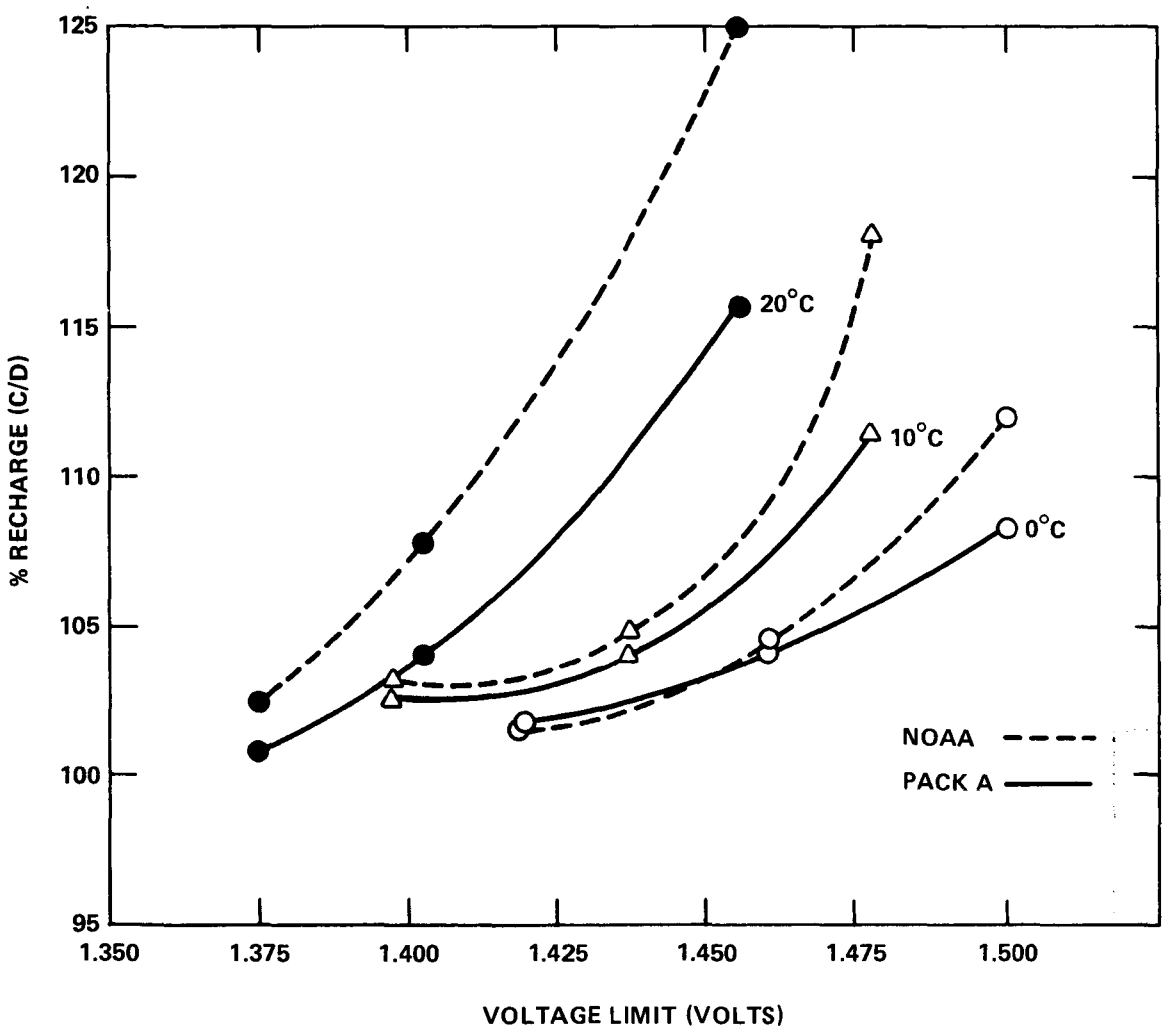

Figure 7. NOAA 26.5 Ah VS PACK A 50 Ah CYCLING TEST
% RECHARGE VS VOLTAGE LIMIT
CHARGE CURRENT: 0.5C
25% DEPTH OF DISCHARGE

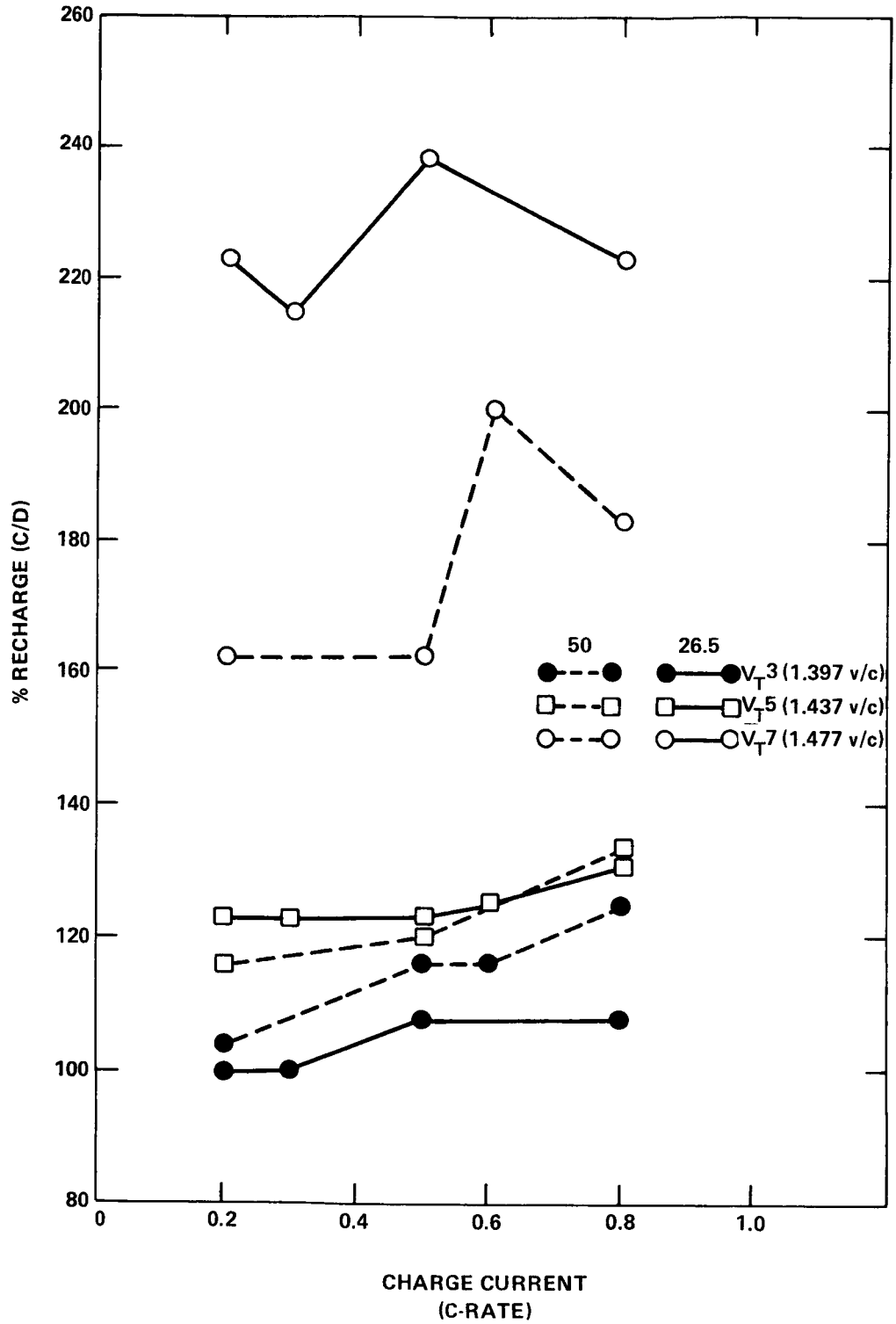

Figure 8. PACK A 50 Ah VS NOAA 26.5 Ah LEO CYCLING TEST
% RECHARGE VS CHARGE CURRENT
5% DEPTH OF DCH
TEMPERATURE: 10°C

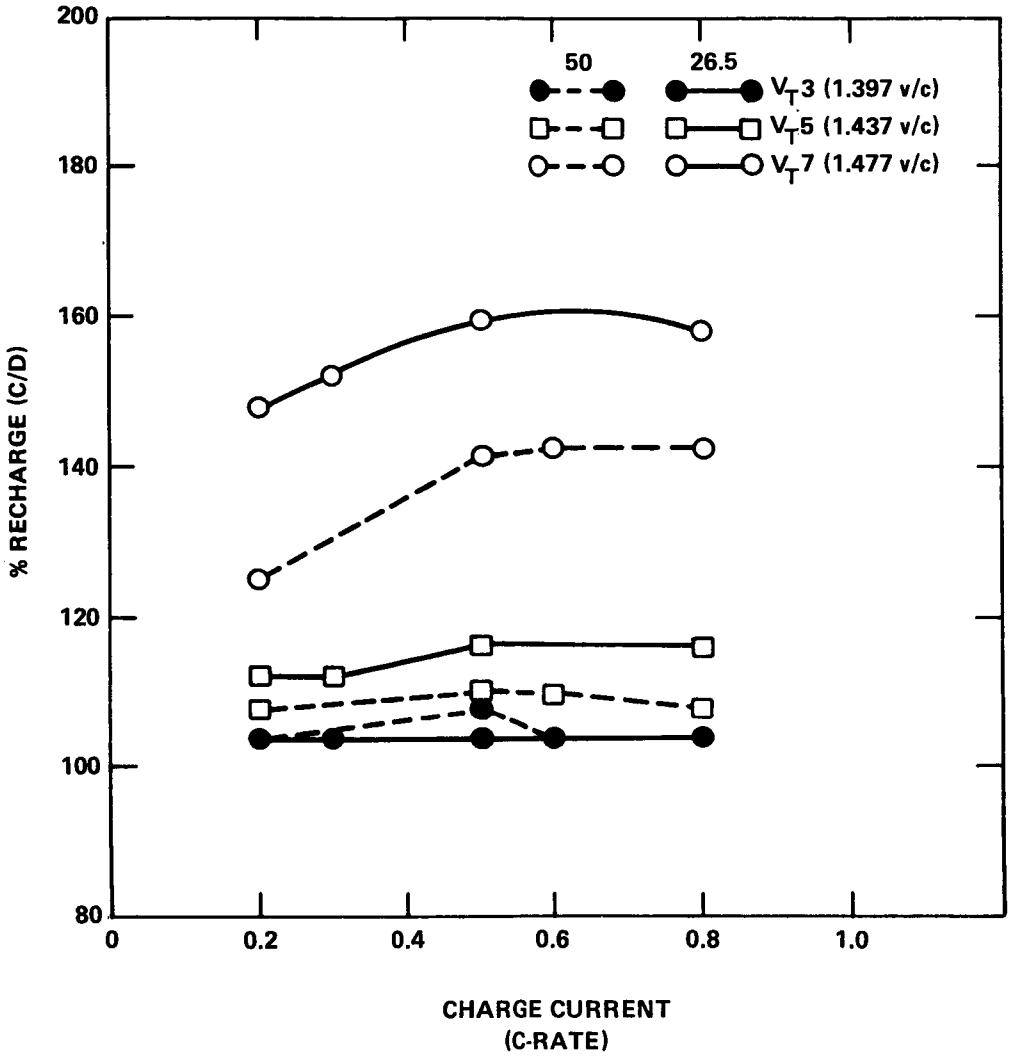

Figure 9. PACK A 50 Ah VS NOAA 26.5 Ah LEO CYCLING TEST
% RECHARGE VS CHARGE CURRENT
10% DEPTH OF DISCHARGE
TEMPERATURE: 10 °C

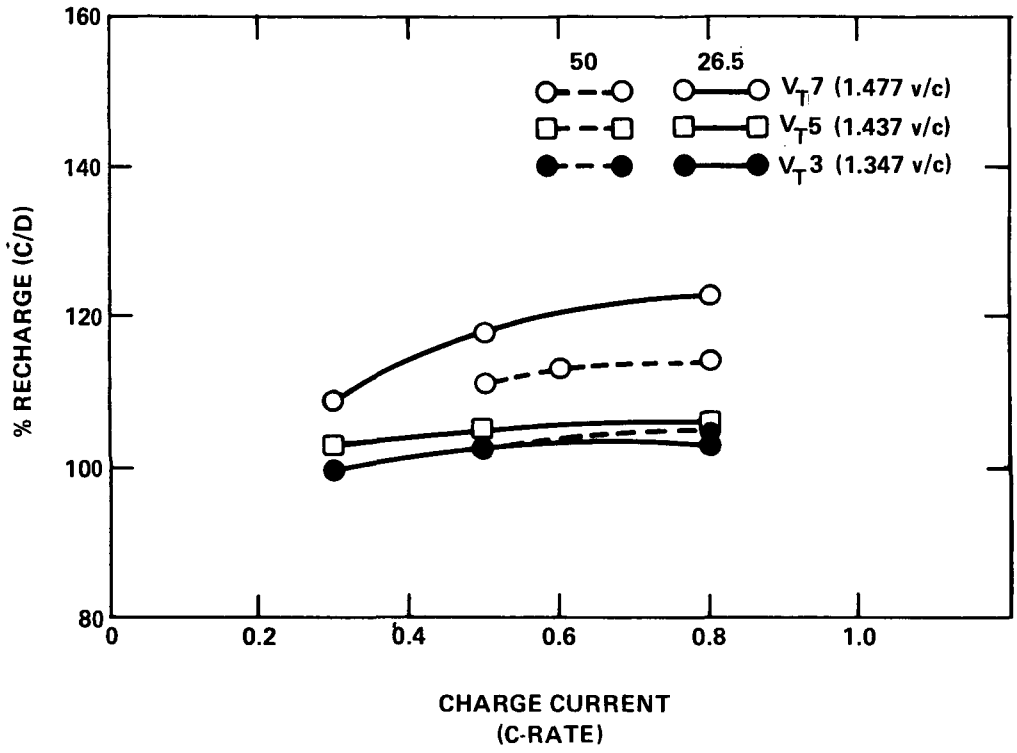

Figure 10. PACK A 50 Ah VS NOAA 26.5 Ah LEO CYCLING TEST
% RECHARGE VS CHARGE CURRENT
25% DEPTH OF DISCHARGE
TEMPERATURE: 10°C

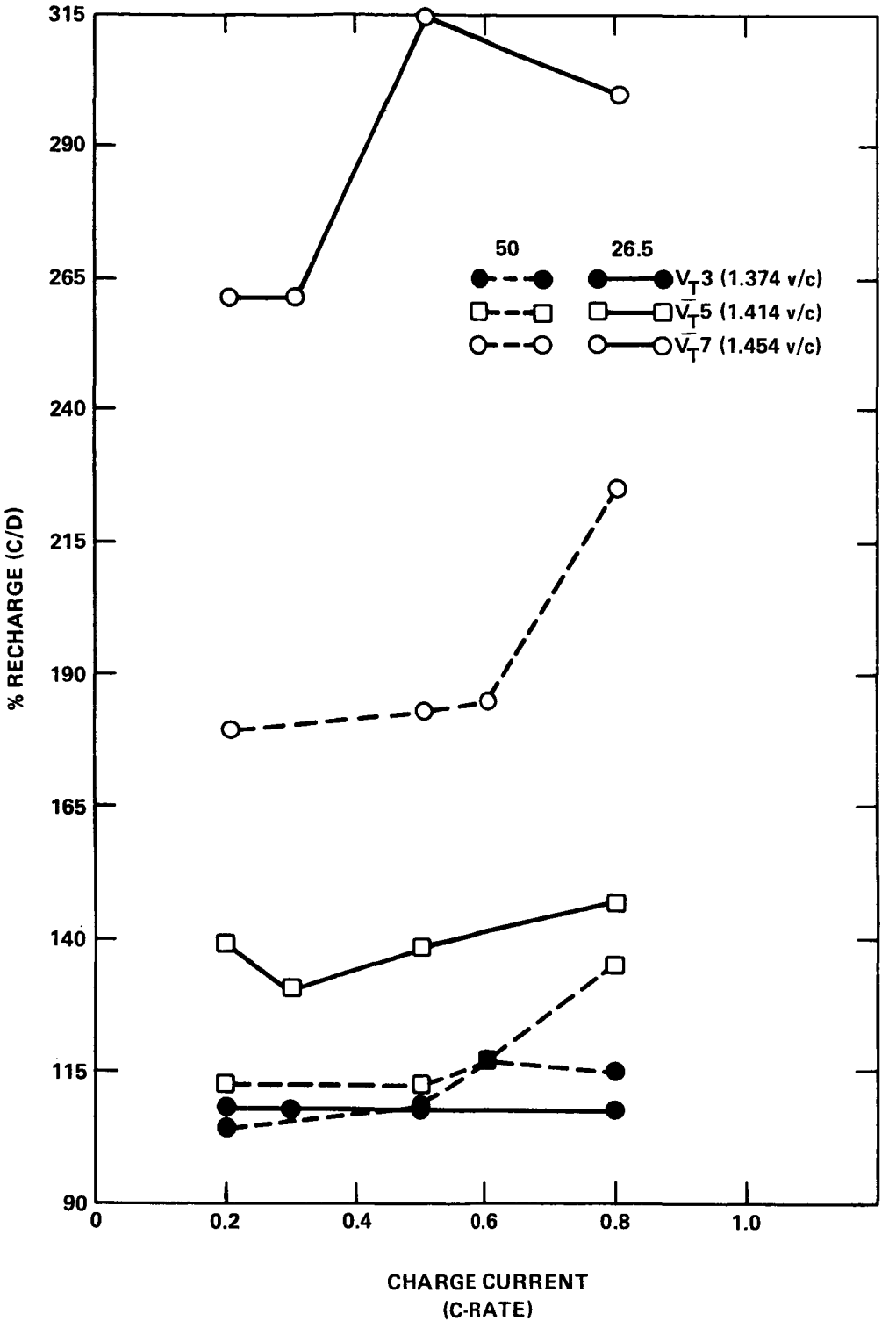

Figure 11. PACK A 50 Ah VS NOAA 26.5 Ah LEO CYCLING TEST
% RECHARGE VS CHARGE CURRENT
5% DEPTH OF DISCHARGE
TEMPERATURE: 20°C

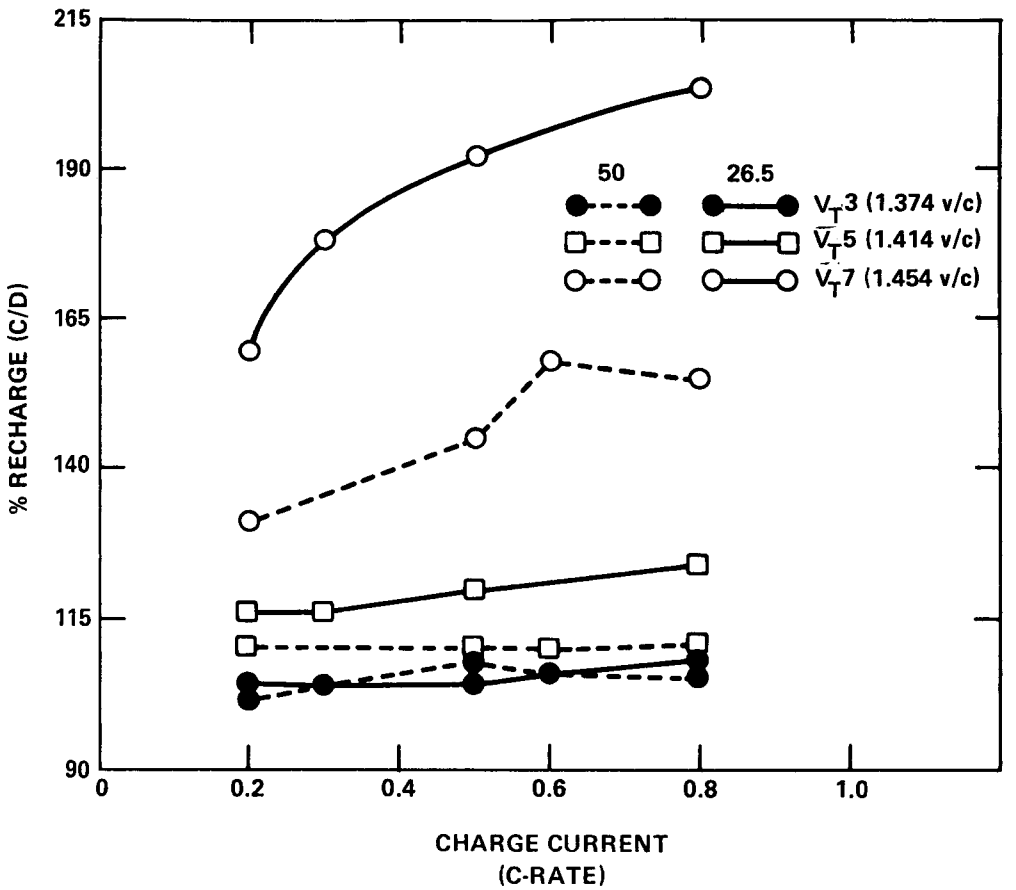

Figure 12. PACK A 50 Ah VS NOAA 26.5 Ah LEO CYCLING TEST
% RECHARGE VS CHARGE CURRENT
10% DEPTH OF DISCHARGE
TEMPERATURE: 20°C

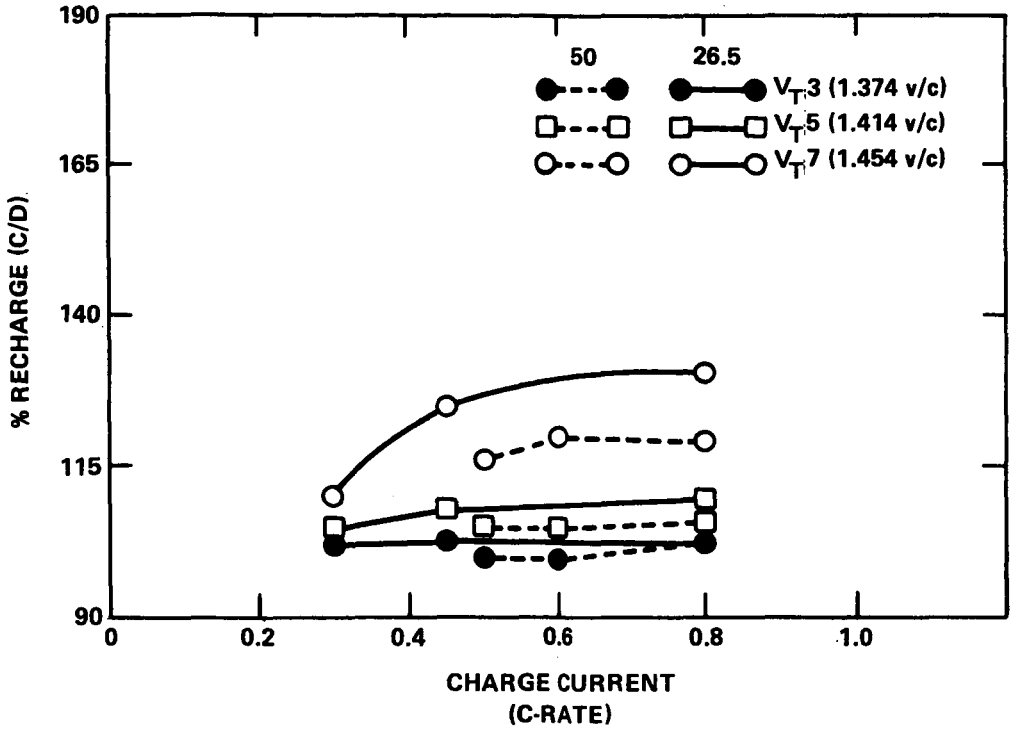

Figure 13. PACK A 50 Ah VS NOAA 26.5 Ah LEO CYCLING TEST
% RECHARGE VS CHARGE CURRENT
25% DEPTH OF DISCHARGE
TEMPERATURE: 20°C

TEMPERATURE: 10°C

ORBIT: 104 minutes – 69 minutes charge
35 minutes discharge

DEPTH OF DISCHARGE: 25 percent (11.35A Constant I)

CHARGE: 7.5A Constant I
to a voltage limit and taper

VOLTAGE LIMIT: 1.47 V/Cell (initially)

Figure 14. LIFE CYCLING REGIME

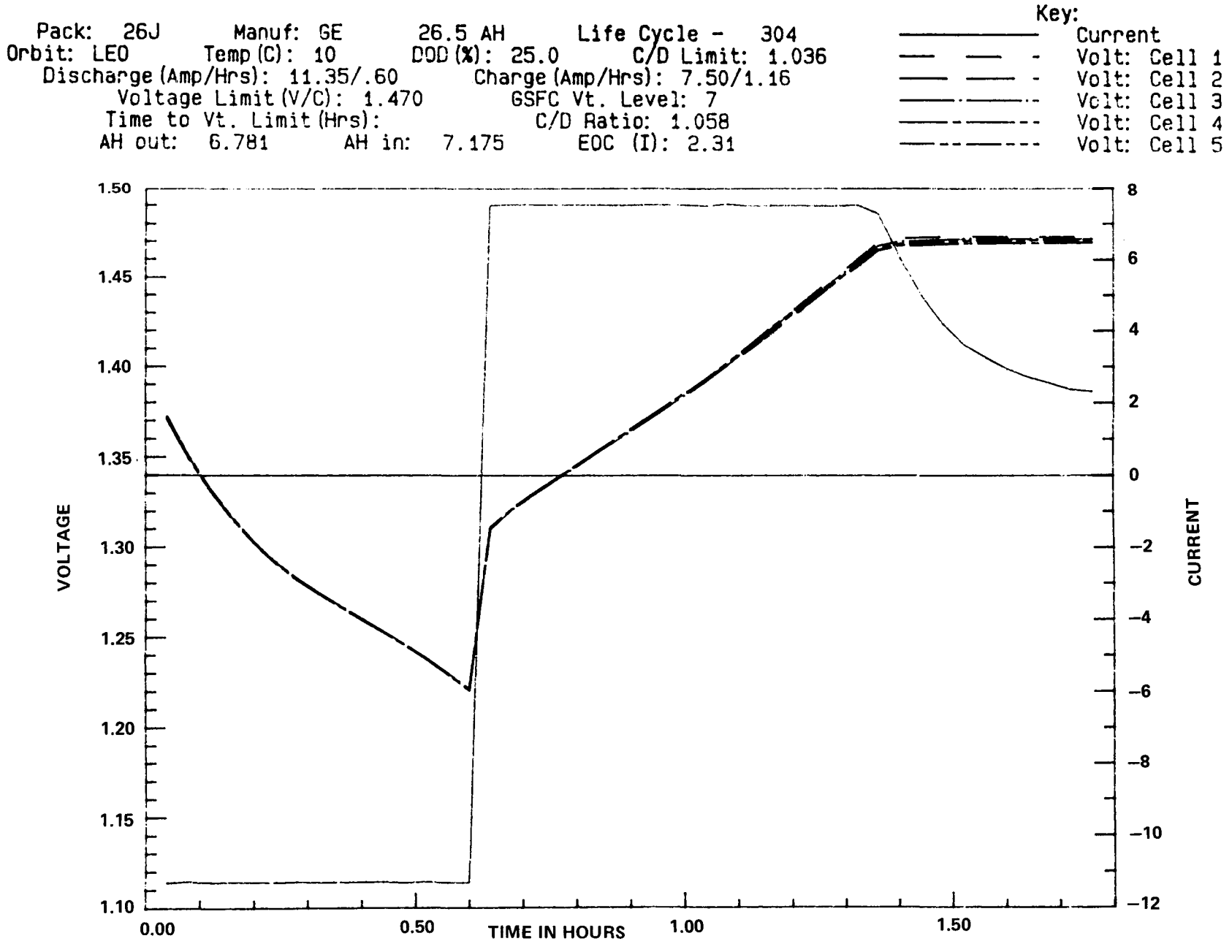

Figure 15. NWSC CRANE LIFE CYCLE 304 PLOT

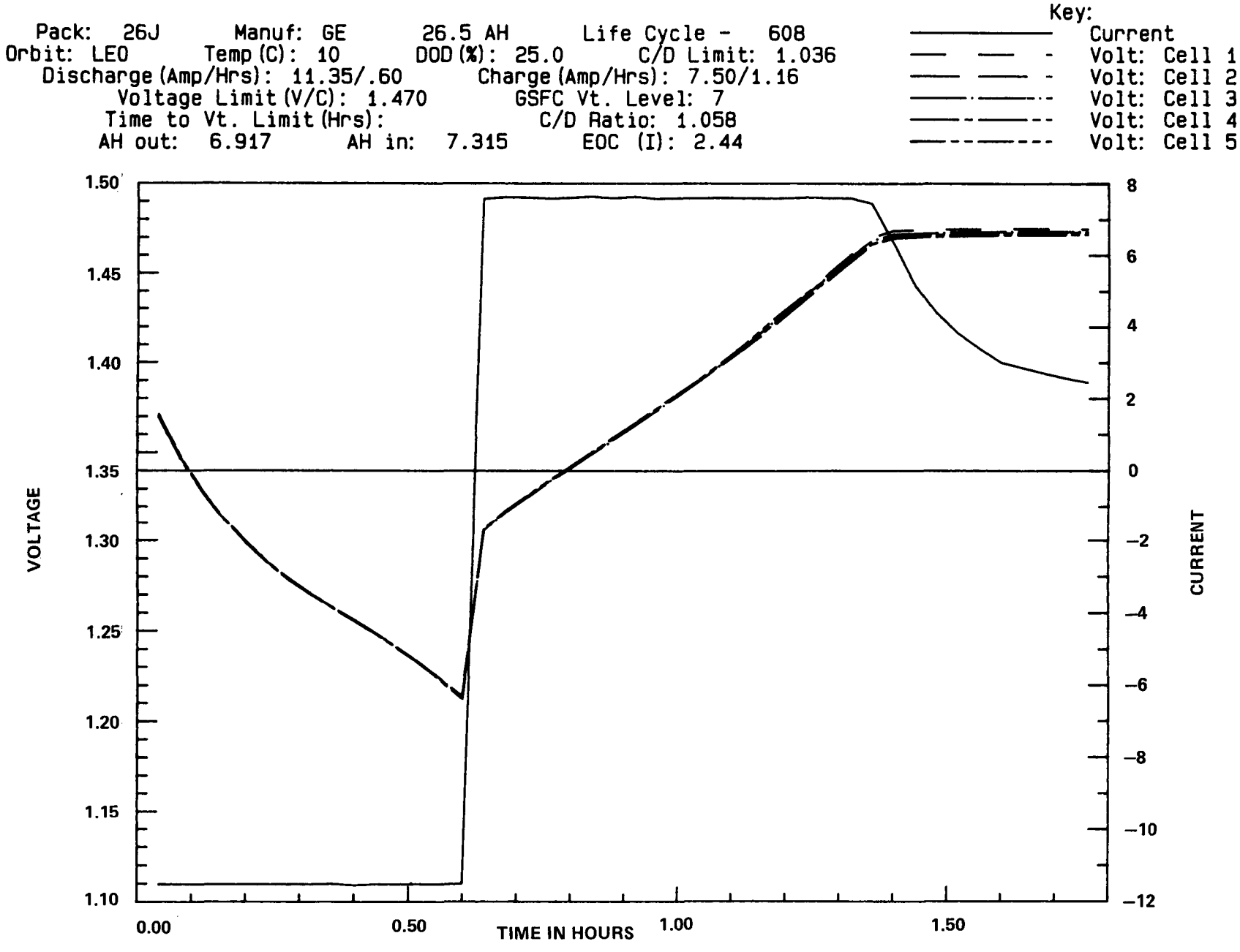

Figure 16. NWSC CRANE LIFE CYCLE 608 PLOT

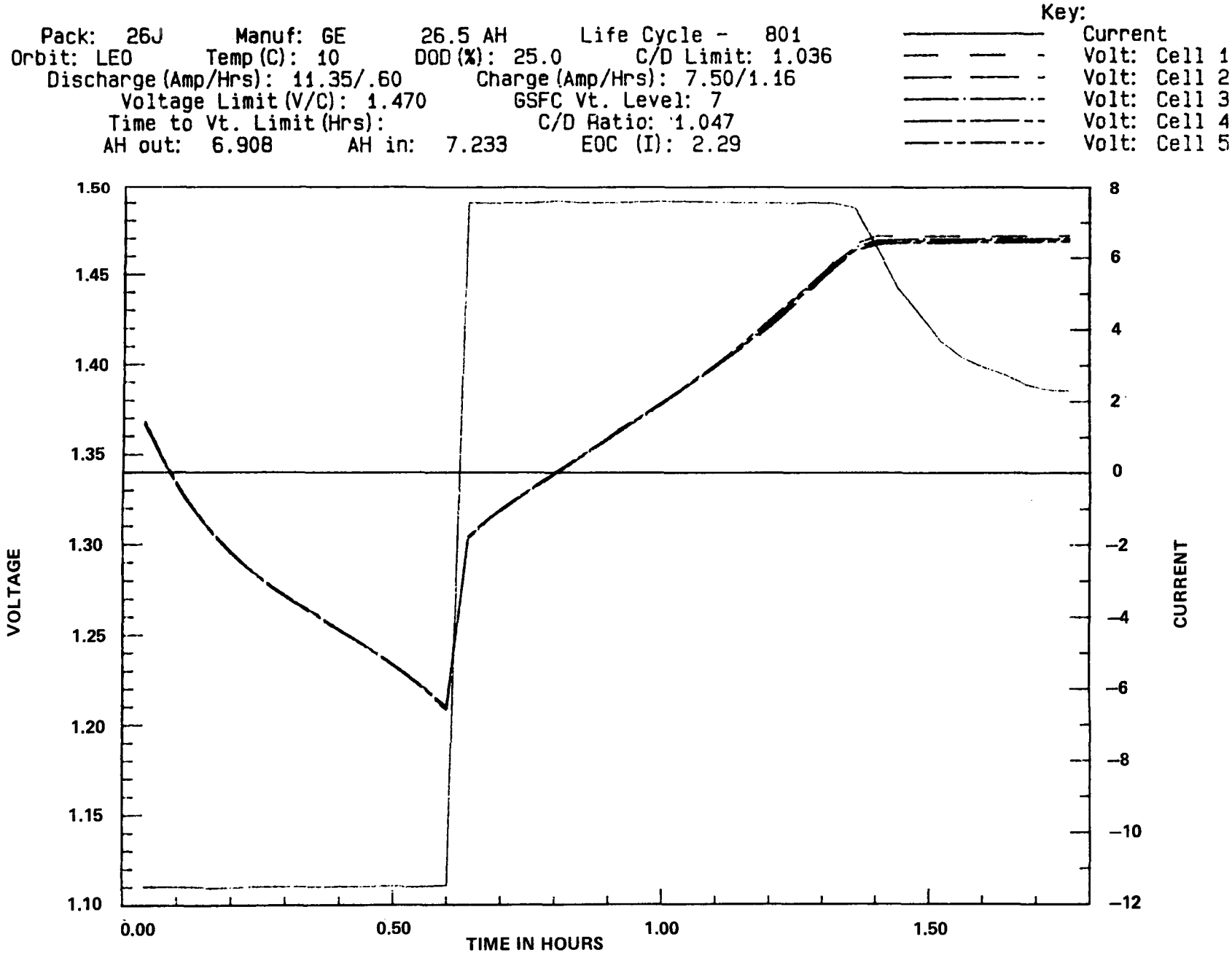

Figure 17. NWSC CRANE LIFE CYCLE 801 PLOT

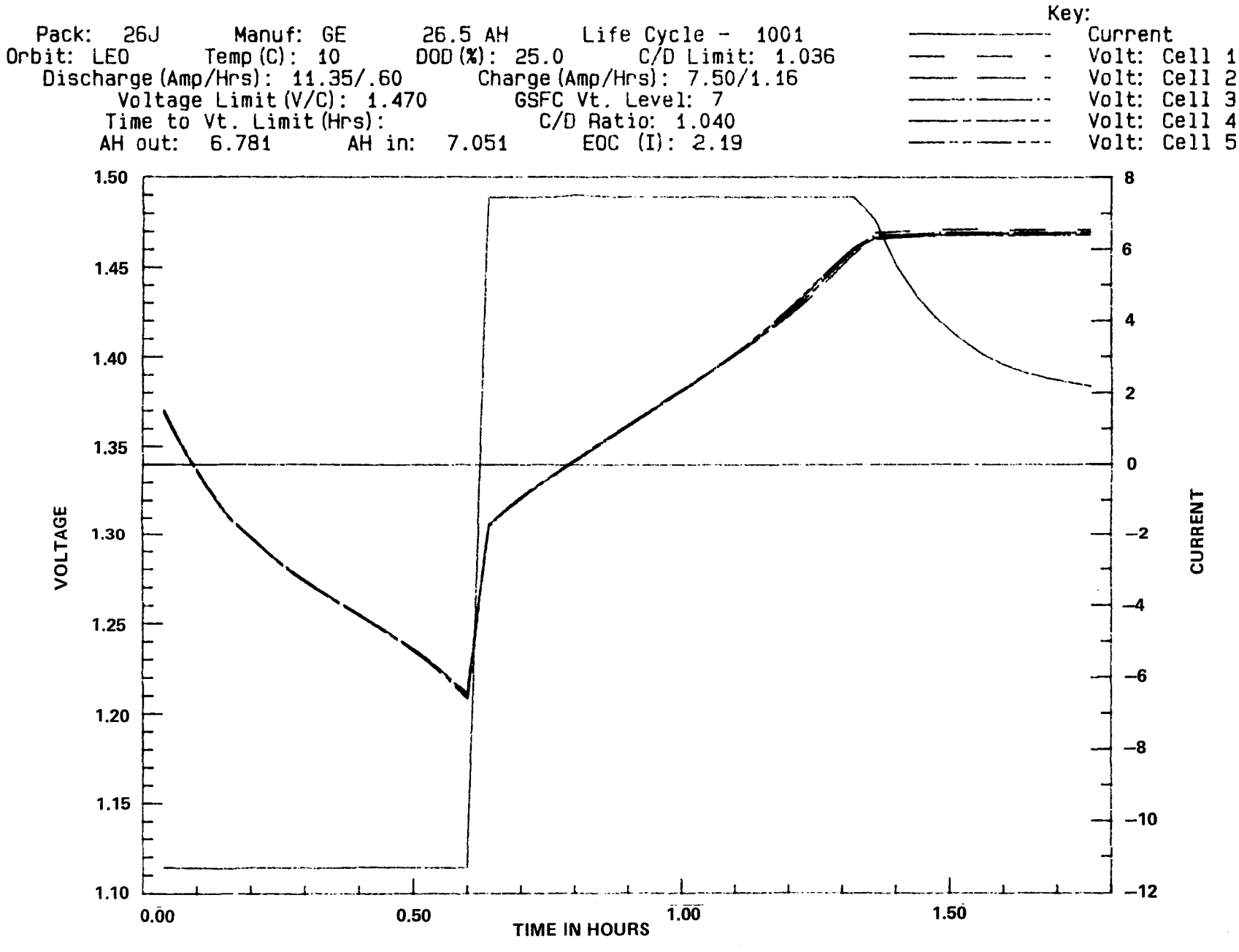

Figure 18. NWSC CRANE LIFE CYCLE 1001 PLOT

A HIGH RELIABILITY BATTERY MANAGEMENT SYSTEM

By Malcolm H Moody
of Canadian Astronautics Limited, Ottawa, Canada

SUMMARY

Over a period of some 5 years Canadian Astronautics Limited (CAL) has developed a system to autonomously manage, and thus prolong the life of, secondary storage batteries. During the development, the system has been aimed at the space vehicle application using nickel cadmium batteries, but is expected to be able to enhance the life and performance of any rechargeable electro-chemical couple.

The system handles the cells of a battery individually and thus avoids the problems of over, and under, drive that inevitably occur in a battery of cells managed by an averaging system. This individual handling also allows cells to be totally bypassed in the event of failure, thus avoiding the losses associated with low capacity, partial short circuit, and the catastrophe of open circuit. The system has an optional capability of managing redundant batteries simultaneously, adding the advantage of on line reconditioning of one battery ,while the other maintains the energy storage capability of the overall system.

As developed, the system contains a dedicated, redundant, microprocessor, but the capability exists to have this computing capability time shared, or remote, and operating through a data link. As adjuncts to the basic management system CAL has developed high efficiency, poly phase, power regulators for charge and discharge power conditioning.

A number of the units comprizing the system were developed to the level of qualification hardware, including a fully redundant discharge converter.

BASIC CONCEPT

CAL undertook a series of contracts under the sponsorship of the Canadian Department of Communications, to design, develop, manufacture and test a concept for the improvement of life expectancy of spacecraft nickel cadmium batteries. It was clear from the body of work carried out to determine the life limiting factors of nickel-cadmium cells and batteries, and was well summarized in the NASA 'Sealed-Cell

Nickel-Cadmium Battery Applications Manual', that good control of a small number of key operating modes should bring about a significant improvement in useable life and capacity.

These controls are:-

- Prevention of voltage reversal.
- Minimise overcharging.
- Eliminate secondary effects of open, or short, circuiting a cell.
- Provide facility for reconditioning cells.

On developing this short list it is clear that all these parameters relate to single cells rather than to complete batteries and that the secret to the improvement needed was to be able to control individual cells, rather than entire batteries.

The basic concept,then, was fairly simple, to provide each cell with a controllable by-pass system, and this was made feasible by the introduction of the high current, vertical D-MOS power MOSFET transistor.

The basic circuit for a cell by-pass circuit is shown here (Fig 1). It consists of a relay controlled shorting switch and a logic operated, controlled current, by-pass transistor. The logic operating the bypass transistor includes a d.c. isolator, such that the control logic can operate at a common reference level. Providing a logical ON command to a by-pass input, enables a multivibrator oscillator. The output of the oscillator is transformer coupled, providing d.c. isolation, and rectified into a preset voltage divider to provide the controlled gating voltage to operate the by-pass transistor.

The shorting switch actually consists of two sets of relay contacts in series so the the accidental closure of one relay will not cause a catastrophic short circuit across the cell.

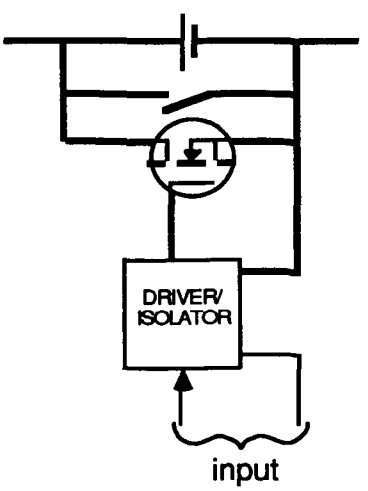

Figure 1. BASIC CIRCUIT

The MOSFET transistor contains an inherent diode between the source and drain which tends to prevent a cell from being driven too far into voltage reversal during a deep discharge. In normal operation this feature is not required since, as soon as it is determined that the cell has been drained of energy, the shorting switch is closed. This prevents any voltage inversion occurring within the cell, and prevents the depleted cell's internal impedance causing unnecessary power loss.

The by-pass transistor is set up such that when it is operated only the normal trickle charge current flows in the cell. Consequently, when an individual cell is adjudged to have reached its 'top of charge', its current can be reduced to a maintaining level while the cells in series with it continue to accumulate charge to their individual full capacity.

IMPLEMENTATION

The figure below (Fig. 2) represents a implementation of the basic system outlined above, expanded to the level of a power sub-system, having a solar array source, and providing a coarsely stabilised output.

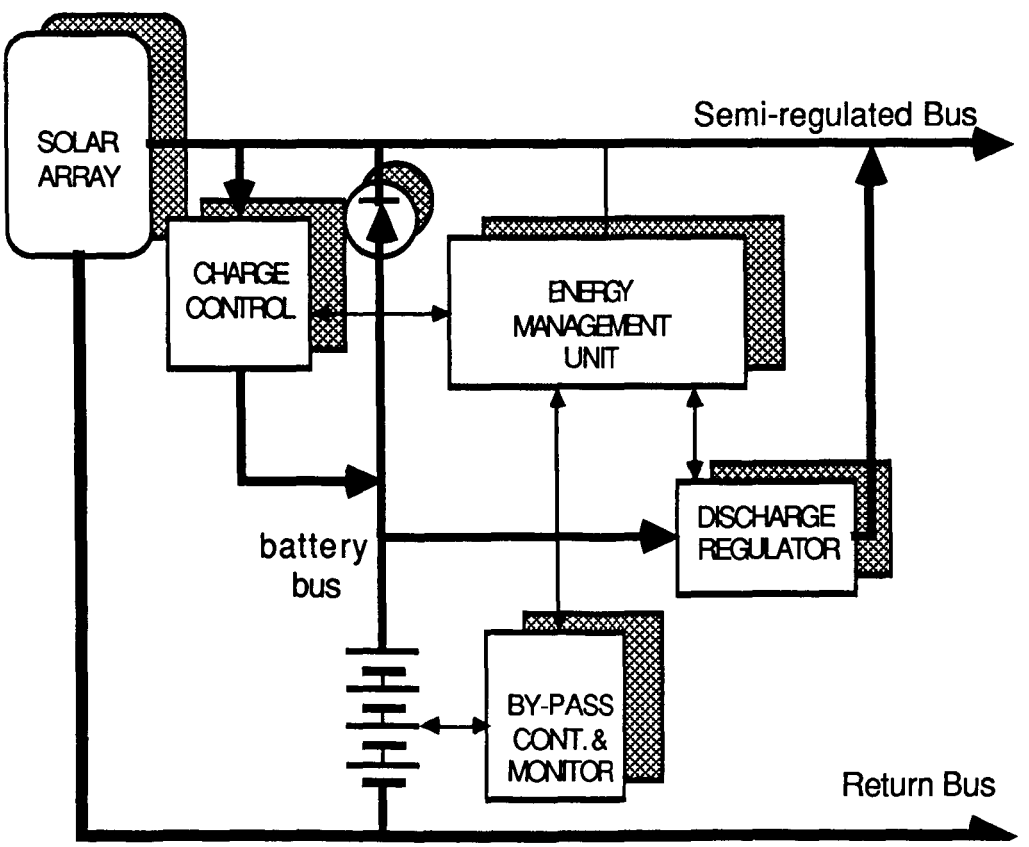

Figure 2. BASIC SYSTEM BLOCK DIAGRAM

It is assumed that the solar array is provided with a shunt regulator, and that during insolation periods, the solar array will maintain the semi-regulated bus. The energy management unit monitors the voltage of this bus, and , providing its voltage is high enough, it directs the charge control regulator to provide power to the battery for the storage or maintenance of charge. The energy management unit is also monitoring the state of charge of the cells in the battery and so knows if the charge current required is for a full charge or for a maintaining (trickle) mode. When the demand on the semi-regulated bus exceeds the capacity of the solar array to the point where the bus voltage falls below some predetermined level, the management unit disables the charge control regulator, switches off any active by-pass circuits, except those around permanently failed cells, and enables the discharge regulator. So as the semi-regulated bus voltage falls to the predetermined output level of the discharge regulator the loading transfers gracefully from the solar array to the battery. A similar, but reverse, process is followed at eclipse emergence.

This graceful change-over is possible because eclipse entry and emergence are slow compared with the processing speed of a computer. There exists, however the possibility of a sudden demand on the bus; either by design, or as a fault clearing pulse. In this case the energy management unit requires some milli-seconds of grace, and this is provided by connecting the 'top' of the battery to the semi-regulated bus through a high current diode.

Within the system designed and implemented at CAL, the energy management unit played a purely passive role during battery discharge.This was because the aim was to demonstrate life improvement on a battery, but the capability is present to monitor the discharge against a predetermined profile and to take interventionary action, in the form of load shedding, if required. In the system as implemented, however, the management unit maintained a count, per cell, of the energy being removed, and if any cell became fully discharged, shorted it out, and stopped incrementing the AHr count on that cell.

This bypassing of a cell is considered, by the system, to be an acceptable part of normal operation and, assuming the cell continues to fully discharge prior to the end of discharge, the cell will continue to be used in each successive charge/ discharge cycle, finishing each discharge in a shorted state.

The reasoning behind this is that while the cell is capable of storing some useful energy it might as well continue to be used. This cannot be

allowed in a system which manages a battery as a whole, because the low capacity cell becomes a power waster and a hot spot.

There is a manual overide, via. telecommand, which allows the operator to make the short circuit permanent after the next time the shorting switch closes. The exception to this is in the rare case of an open circuit cell, where the management unit immediately closes the shorting switch, and will only reopen it on telecommand.

Eclipse emergence is detected by a rise in the semi-regulated bus voltage, and at some predetermined voltage, the charge control regulator is turned on and the discharge regulator turned off. The management unit now opens all non-permanent shorting switches and sets up conditions for a full charge current to be applied to the battery, counting AHrs into each cell. As this process continues, the management unit monitors each cell for any indication of a fault condition by checking for; (a)falling cell voltage,(b) rapidly rising temperature, or (c) a voltage in excess of 1.6V, which would indicate gassing within the cell. The occurrence of any of these malfunctions causes that cell to be immediately put into the maintaining mode (by-passed), and the monitoring algorithm to lower the point at which this cell is adjudged to have reached top of charge.

The point at which each cell has reached top of charge (TOC) is determined by its voltage. At fixed intervals the charge current is turned off momentarily and the terminal voltage of all cells is read. These voltages are compared with a list of calculated TOC voltages and consequently the cell is either by-passed or returned to full charge for a further period. The calculated TOC voltage is automatically reviewed, by a control algorithm, at the completion of each charge cycle, and revised to maximise cell voltage at TOC, and charge efficiency, simultaneously.

CONTROL ALGORITHM

As mentioned earlier, the management of the battery is based on operating each cell in its most efficient mode, and this requires an algorithm which is tailored to the cell and can adapt to changes as the cell ages. The algorithm is structured to attempt to maximise cell voltage and charge efficiency simultaneously. This is an impossible task, but it will lead to the cell being operated in its optimum range. An explanation of this is best understood after examining the typical curves of charge input vs. cell voltage, and charge efficiency, shown in Fig.3.

It should be noted that the normal definition of charge efficiency is; the ratio of total charge input to total charge extractable, at any instant,

but that CAL uses a modified definition, i.e. charge last input divided by charge previously extracted, starting from, and finishing at TOC. This is to provide a simpler mathematical definition to the algorithm.

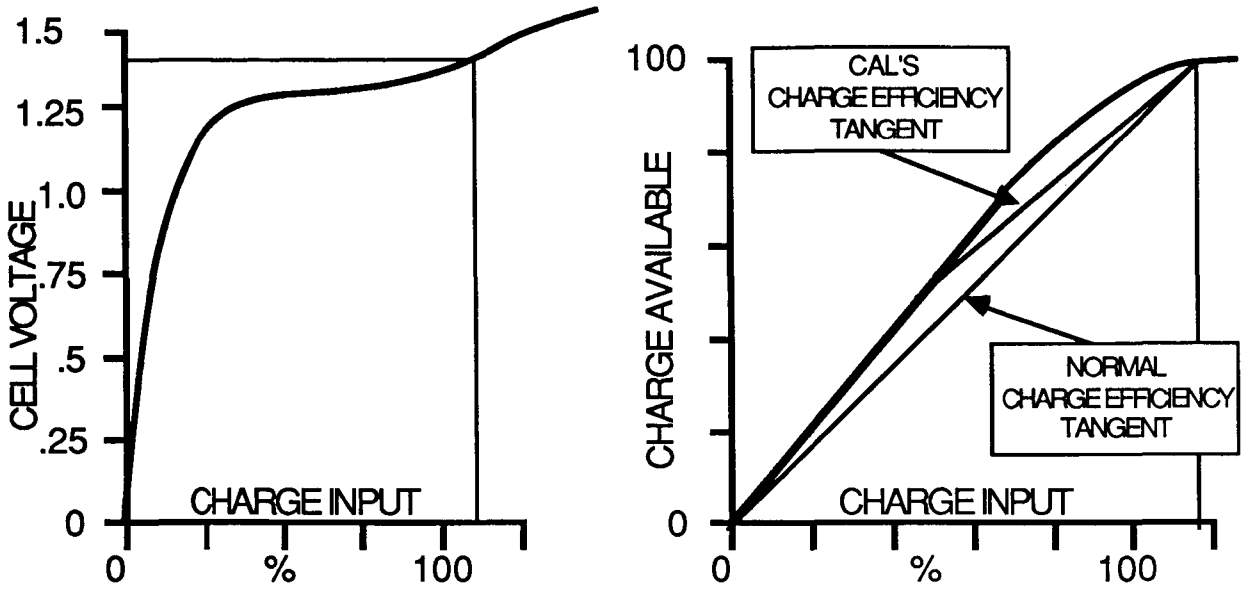

NB: All charge parameters expressed as a % of rated capacity

Figure 3. TYPICAL CELL CHARGING CURVES

An examination of the curves in Fig. 3 reveals that; with increasing charge input the cell voltage also increases, but that this is accompanied by a decrease in the numerical value of the ' charge efficiency', (i.e. the charge available divided by the charge input). If, then, a cell is charged to a predetermined terminal voltage, the charge necessary to do this can be compared to the charge previously removed, and the TOC terminal voltage can be adjusted, to change the 'charge efficiency' on the next cycle. This process may be better understood by examining the flow chart shown in Fig 4.

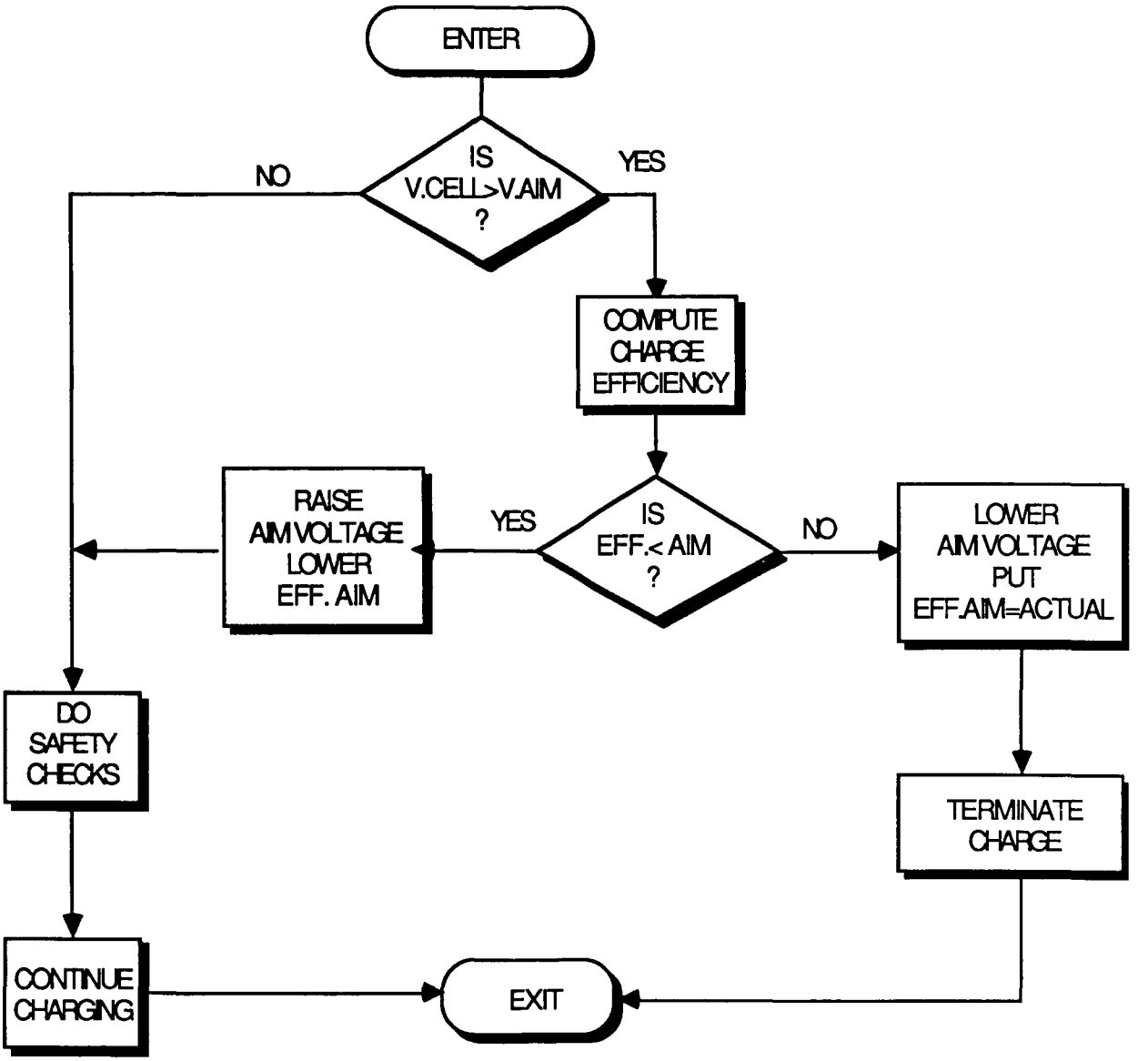

Figure 4. BASIC CELL MANAGEMENT ALGORITHM

The first decision is taken by examining the terminal voltage of the cell. This is always measured in the open circuit condition to eliminate the effects of different charge current and variations in cell internal impedance. If the cell has not reached the aim point then charging should continue, so, providing the voltage and temperature checks are satisfactory the charge is resumed.

If the cell has reached, or exceeds the aim point then the efficiency of the cell, in CAL'S terms,(i.e. the charge it has been necessary to return in order to replace the charge taken out), is compared to an aim efficiency. If the cell is showing greater efficiency than the aim,(i.e. numerically smaller), then the cell is operating in the more linear portion

of the "charge in / charge out" curve and can usefully accommodate more charge. Therefore the aim voltage is raised and the numerical value of the aim efficiency is lowered. This should result, the next time the measured cell voltage exceeds the aim voltage, in the computed efficiency being lower (i.e. numerically greater) than the aim. If this is not so the process repeats until that condition does occur. When the measured efficiency is found to be numerically greater than, or equal to, the aim, the aim efficiency is revised to be equal to this measured value, and the aim voltage is lowered a little. At this point the cell is said to be at top of charge, and it is switched to the maintaining mode.

It can be seen that the only way to terminate a charge is to have achieved a sufficient terminal voltage and to have absorbed enough energy to assure a full charge. The raising and lowering of the aim points is carried out using a number which is proportional to the difference between the measured and the aim value. This allows rapid 'zeroing in', without significant overshoot, although the values of proportionality must be carefully chosen to minimize oscillation.

Because this system is choosing the operating point for each cell, on the assumption that the cell is operating in a rational, or nominal, mode it is necessary to implement some traps and safeguards which will prevent attempts by the system to operate a faulty cell in a potentially hazardous or unknown operating area. For this purpose the aim voltage is not allowed to exceed 1.6 volts and the efficiency is not allowed to fall (numerically) below 110%. This should assure that the cell doesn't gas in overcharge and that a sufficient charge is always returned for the next discharge. There is no actual lower limit on the operating voltage of a cell except that in a discharge, if its voltage falls, and remains, below 0.5 volts, it is assumed to be drained, and is shorted out.

Recognizing the fact that there is also room for intuition and prediction in a good energy management system, the software also allows partial and total manually operated modes, wherein the aim points can be reset or locked to specific values, the factors of proportionality, governing the magnitude of changes in the aim points, can be changed, or the system can be placed in a passive (monitoring only) mode.

The system does contain one partially predictive algorithm in that, at the end of each discharge, the cell terminal voltage is checked and compared with the previous end of discharge. If the end of discharge voltage is found to be falling the top of charge aim voltage is increased by the same amount. This ensures that in a period of increasing usage, such as the first half of an eclipse season, maximum energy storage is

available, while in a stable or decreasing usage period, the cells are operated at their optimum point.

For the sake of clarity a number of refinements have not been mentioned, e.g. when 'aims' are to be revised the new computed value is 'averaged' with the existing value, before the new aim is set. This helps to prevent system noise, or spurious results, giving rise to significant changes in the operating mode. Additionally all cell voltage readings are scaled, according to the current cell temperature, to prevent cyclic, and long term, temperature effects from biasing the algorithm.

SYSTEM CONFIGURATION

As mentioned previously CAL implemented this system into hardware, some of its parts being developed to a level where they were demonstrated to pass qualification test for an STS launch, and GEO orbital environment. In order to provide the most representitive test bed for the management of a battery, the system was designed to emulate the power sub-system of an intermediate size communications spacecraft, say of the ANIK type. During the final testing of the system, the operation of the management system within a spacecraft in geostationarry orbit was simulated. The division of units into which the system was divided is illustrate in Fig 5 below.

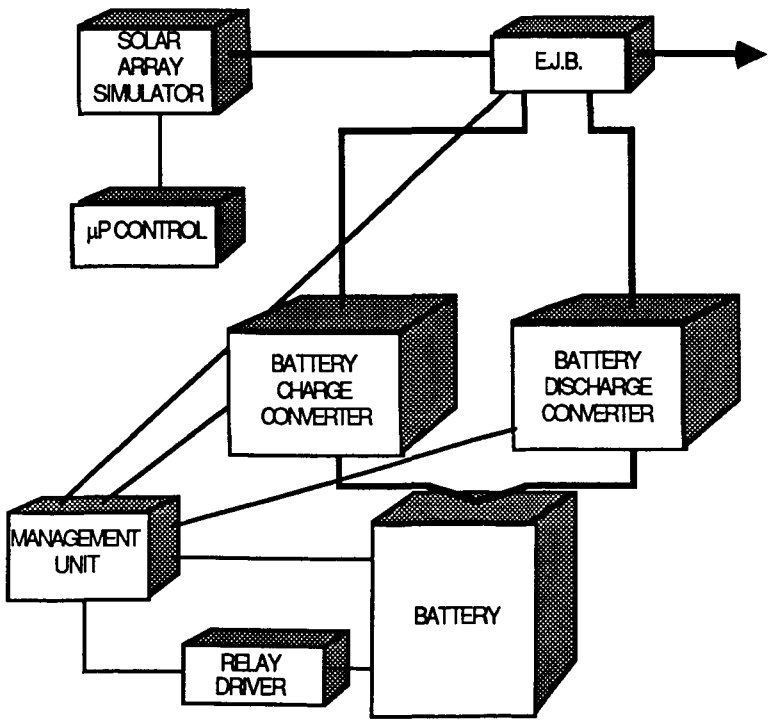

Figure 5. HIGH RELIABILITY BATTERY MANAGEMENT SYSTEM

The energy storage unit, or battery, consisted of three or four cell pack simulators and an optional eight cell pack of 37.5 AHr. GE, prismatic NiCd cells. The cell pack simulators were based on a string of 'D' cells, and their capacity was scaled to the desired level by the use of amplifiers and external power supplies. The use of these cell simulators had many advantages, not only in terms of their versatility, but also in terms of the safety advantage of not working with high energy storage cells while developing the system. In all cases the cell by-pass circuitry was housed within each cell pack, adjacent to the appropriate cell.

The solar array was simulated by a commercial power supply, controlled by a microprocessor to simulate eclipse entry and insolation.

Both the charge and discharge regulators use poly-phase, class 'D', switching techniques which give rise to excellent conversion efficiency, and in the case of the unique design for the discharge regulator,the ability to continue operation after the 'first failure'. The discharge regulator was developed to 'flight' hardware standard, and qualified. It was shown to supply 300 Watts at a conversion efficiency of 96.5%, and 600 Watts at a conversion efficiency of 95%, with a line regulation of less than 20mV.

The management unit was built in a breadboard format, but all the parts used were generic to space qualified equivalents. All the circuitry was redundant and dual such that continuous error checking in the management unit could be accomplished. The basic operating algorithm was 'burned' in a EPROM while all the operating variables were held in RAM. A set of start up parameters was also held in ROM. This allowed that the management unit could be completely powered down, but on reapplication of the power, the system would restart in a safe operating condition. The management unit also interfaced with a telemetry/telecommand port, formatting and sending housekeeping telemetry, and looking for commands which it interpreted and actioned, or passed on, as appropriate.

Other interfacing and interconnections were effected within the relay driver unit and the E.J.B. (electrical junction box).

CONCLUSION

Canadian Astronautics Ltd. has developed a microprocessor based system to autonomously manage batteries, particularly nickel cadmium batteries, on a cell by cell basis, which will enhance the life of the battery by ensuring that each cell is charged to its optimum level. The system uses an adaptive algorithm which accomodates changes in each cell's characteristics over life. The system also compensates for, and

protects against, the effects of individual cell failures.

The system was constructed to replicate the power sub-system of an intermediate size communications spacecraft, and a number of the individual units were developed to qualification status, including a 600 Watt poly-phase discharge converter.

ACKNOWLEDGMENT

The author wishes to recognize the skills and dedication of all those at CAL, and in the CRC, who made this project a success.

SESSION V

TOPIC: NICKEL-HYDROGEN TECHNOLOGY
Chairman: L. H. Thaller, NASA/LERC

RECENT ADVANCES IN Ni-H_2 TECHNOLOGY AT NASA LEWIS RESEARCH CENTER

Olga D. Gonzalez-Sanabria
Doris L. Britton
John J. Smithrick
Margaret A. Reid
Lewis Research Center
Cleveland, OH 44135

ABSTRACT

NASA Lewis Research Center has concentrated its efforts on advancing the Ni-H_2 system technology for low earth orbit applications. Component technology as well as the design principles have been studied in an effort to understand the system behavior and failure mechanisms in order to increase performance and extend cycle life. The design principles have been previously addressed (Ref. 1, 2). This paper will discuss the component development, in particular the separator and nickel electrode and how these efforts will advance the Ni-H_2 system technology.

INTRODUCTION

The Ni-H_2 technology group at NASA Lewis Research Center has been developing Ni-H_2 cells primarily for LEO applications. The overall objective is to improve the components, design and operating characteristics of Ni-H_2 cells and batteries. An active program to address the anticipated decay modes and failure mechanisms is underway both on contract as well as in-house.

The types of shortcomings that are associated with Ni-H_2 devices which are related to electrolyte management, oxygen management, electrode growth management and performance degradation can all be traced to problems associated with the nickel electrode and/or separator. Therefore, they are considered the critical components. The nickel electrode is the life limiting component while the separator is the critical risk component due to unavailability of asbestos and the electrolyte and oxygen management problems associated with Zircar.

The LeRC has concentrated its efforts in separator development and the understanding of the nickel electrode behavior in order to improve cycle life. The closer we get to understanding the nickel electrode the more able we will be to deal with the problems associated with it either by correcting the cause or by reducing its impact on cycle life. An attempt to reduce the impact of current shortcomings by modifying the design of Ni-H_2 cells is currently underway, but an in-depth understanding of the causes and effects is sought. This will ultimately allow us to understand the effect of uncontrolled changes on the system and will provide us the necessary tools to take

corrective measures so Ni-H_2 systems will be less affected by manufacturing and technology changes in the future.

The most recent advances in the nickel electrode and separator technology areas are expected to have a positive effect on life, weight, cost and performance. These include new separator materials, lightweight nickel electrodes and the understanding of the nickel electrode mechanism and structure.

SEPARATOR TECHNOLOGY

As part of the technology development at LeRC, a separator development program was designed to develop a separator that is resistant to penetration by oxygen and loose active material from the nickel electrode while retaining the required chemical and thermal stability, reservoir capability and high ionic conductivity. A close look at SOA separators, their properties and problem areas was undertaken to determine the necessary properties for a new improved separator. A set of standard properties were identified which would provide the necessary characteristics for short term performance while addressing the problems related to the long term performance of SOA separators.

Screening studies showed two laboratory separators which met the characteristic goals of electrolyte retention, bubble pressure, and conductivity, etc. These were 80% PKT-20% ZrO_2-10% EBL and PKT on ZrO_2 cloth where PKT is potassium titanate and EBL is emulsified butyl latex. These separators were incorporated into Ni-H_2 stacks and tested to examine their voltage characteristics and cell performance. The cells were submitted to the same characterization and testing as those with the baseline asbestos and Zircar separators. Cell characterization showed good cell voltage with mid-point and end of discharge voltages higher than either of the baseline separators (Ref. 3).

The results obtained from characterization and testing encouraged us to further pursue this effort. The process needed to be adapted and transferred from a laboratory operation to a manufacturing process since reproducibility and uniformity are important factors that will govern their future use and applications. The first step undertaken was to have the separators prepared by a commercial vendor (Quin-T) for further evaluation. The separators obtained lacked the necessary bubble pressure to prevent the oxygen produced at the nickel electrode from accessing the hydrogen electrode in a controlled fashion. This was due to small holes $\sim$50 μm in diameter apparently caused by localized swirls during the filtering step.

In order to overcome the manufacturing problems we started an effort with Miami University. Miami University has a Paper Science and Engineering Department well experienced in the paper making process and is equipped with a small pilot paper making machine. They also have handsheet molds and testing capabilities that will allow timely testing and modification of the production techniques to easily adapt to the new materials. The objective is to demonstrate the feasibility of manufacturing the new separator materials using

standard paper making techniques. This effort is intended to bridge the gap between the handsheet operation and the commercial processes and establish the potential of these separators for use in a variety of different applications. The one-year effort will reproduce the original handsheet material and will gradually adapt the fabrication from the handsheet techniques to the production techniques. It will study the effect of these changes on the separator properties and manufacturability and modify them to achieve a high performance separator that will be easily reproduced.

The final result is to be a separator which will be reproducible using standard paper making technology that will ensure uniformity, availability and lower costs. The technology will lead to a higher performance and extended life of the Ni-H_2 systems.

NICKEL ELECTRODE TECHNOLOGY

LIGHTWEIGHT NICKEL ELECTRODE

The second part of the technology development program focuses on the nickel electrode which, in addition to being identified as the critical component, has also been identified as the heaviest component of the Ni-H_2 battery system. The NASA Lewis Research Center is developing nickel electrodes for Ni-H_2 batteries which will be lighter in weight and have higher energy densities when cycled under a low earth orbit (LEO) regime at deep depths of discharge.

The weight of components in a typical 125 AH Ni-H_2 bipolar battery is shown in figure 1. A major weight reduction of as much as 14% can be accomplished by the use of lightweight electrodes.

Several commercially available materials or plaques other than sintered plaque have potential as a support for the active material. These plaques are lightweight and some of them have pore sizes comparable to a typical commercial sintered nickel plaque. These lightweight plaques are less conductive, but in a bipolar design the current flow is perpendicular to the electrode surface; hence the need for high lateral conductivity is eliminated (Ref. 4).

Plaques other than sintered nickel plaques that may be used to support the active material are the nickel plated plastic plaque developed here at NASA Lewis Research Center (Ref. 5, 6), commercially available Feltmetal (TM) and a needle punched web (80% Ni, 20% Cr) from Brunswick Technetics, graphite fiber mat manufactured by American Cyanamid and Fibrex (TM), a fiberous mat manufactured by National Standard Company. The lightweight plaques except for the Feltmetal are about 50 to 90% lighter than the standard sintered nickel plaque. The Feltmetal is about 5% lighter than the sintered nickel plaque.

Figure 2 shows the pore size distribution of the lightweight plaques as compared with the standard sintered plaque. Most of these plaques have larger pore radii than the sintered plaque. The Nichrome needle punched web and the Fibrex materials have about the same broad distribution at about 20 to 40 m.

The nickel plated plastic, the nickel plated graphite and the Feltmetal show peaks in the pore size distribution at 10 to 18 m. The standard sintered plaque has the lowest pore size distribution peak at 7 μm. Porosity and pore size distribution measurements were made by the mercury intrusion porosimeter method.

To evaluate the performance of the lightweight materials, the plaques were electrochemically impregnated in a saturated solution of nickel nitrate with cobalt nitrate using the Bell Telephone Laboratory method.[1] After washing the impregnated plaques, the electrodes were formed using the Eagle-Picher procedure which consists of eight cycles of 20 minutes charge and 20 minutes discharge at approximately the 3C rate. After formation, the electrodes were thoroughly rinsed in deionized water, dried and weighed. The theoretical C rate was determined from the weight of the active material in the electrode using the electrochemical equivalent of 0.289 AH/gram of nickel hydroxide. The electrochemical impregnation of these lightweight plaques using the aqueous bath yields loading levels comparable to commercial nickel electrodes.

The initial characterization screening testing of the electrodes is performed at five discharge levels, C/2, 1.0C, 1.37C, 2.0C and 2.74C rates. The voltage versus time and the capacities at each rate are recorded and compared with the sintered nickel electrode. After the initial characterization tests, the electrodes will be life cycle tested at a LEO regime to 80% depth of discharge. Capacities will be measured every 50 cycles during the duration of the test for the first 1000 cycles and every 500 cycles thereafter. The Feltmetal electrode has accumulated over 2000 cycles and is still being cycled.

A significant improvement in weight, thus an increase in energy density of the Ni-H_2 battery system can be achieved by the use of lightweight nickel electrodes using lightweight plaques. Life and performance are being investigated.

NICKEL ELECTRODE DEVELOPMENT - HUGHES CONTRACT

While the lightweight nickel electrode is under development, an effort is being made to improve the life of SOA nickel electrodes when cycled under a LEO regime at deep depths of discharge. For this reason a contract was awarded to Hughes Aircraft Company (Research Division) to develop a nickel electrode which will have a long cycle life when cycled to deep depths of discharge. The principal investigator for this contract is Dr. Hong Lim.

The approach taken was to investigate (1) the effect of electrode design parameters on cycle life of the nickel electrode, (2) the failure mechanism of the nickel electrode, (3) the effect of potassium hydroxide electrolyte concentration on performance and cycle life, and (4) the effect of electrolyte composition.

---

[1]T. D. O'Sullivan, Bell Laboratories, Personal Communications

The results from studying the effect of the design parameters on the cycle life of the nickel electrode were the following: (1) the plaque mechanical strength had no significant effect on cycle life over the range of values tested, (2) the pore diameter had a significant effect with the largest pore plaque (16 μm) resulting in the shortest cycle lives, the optimum pore size was 13 μm; (3) the active material loading level affected the cycle life the most with an optimum loading of 1.6 g/cc void volume. As a result of this effort a data base was established for optimum nickel electrode design parameters for maximum cycle life in Ni-H_2 cells.

A failure model of the nickel electrode based on the experimental data was advanced which suggests ways to further improve cycle life. Cell failure was due to loss of high rate capacity rather than an absolute loss in capacity. This could be explained by the active material expansion away from the current collecting nickel sinter due to cycling. This resulted in electrical isolation of active material and loss of high rate discharge capacity. Hence, control of active material expansion is the most important factor for increasing the cycle life.

It has been reported by others from work done in nickel cadmium cells that the nickel electrode growth was a function of the potassium hydroxide concentration. Another task was to investigate the effect of the KOH concentration (21, 26, 31, 36%) on the life of the nickel hydrogen cells. To date significant increases (greater than a factor of three) in cycle life of IPV Ni-H_2 cells have resulted from the reduction in KOH concentration from the traditional values of 31% to 26%. In this continuing test over 13,000 accelerated LEO cycles have been achieved thus far at 80% DOD. The significance of these results are the increased cycle life of Ni-H_2 cells; this will have a considerable effect on LEO applications in terms of life cost and enhanced performance.

The effect of alternate electrolyte compositions on the cycle life of the nickel electrode is scheduled to start in November 1985. It includes aqueous solutions of one or more of all alkali metal hydroxides and barium hydroxide with two level variation of the actual material loading of the nickel electrode. It is expected that with some electrolyte compositions, e.g. those containing LiOH, the active material expansion rate will be greatly reduced. The optimum loading level is expected to be higher than the 1.6 g/cc void found for the standard KOH electrolyte.

The overall results from this contract are an improved understanding of the various factors that effect cycle life of the nickel electrodes. The results provide an insight to the cycle life limitations and the failure mechanisms; they also indicate that control of the active material expansion is the most important factor for further improving cycle life in the Ni-H_2 systems.

NICKEL ELECTRODE STRUCTURE

Research is also being carried out, both in-house and through grants and contracts, to learn more about the structures of the active materials and the mechanisms of the electrode reactions. Dr. Bahne Cornilsen at Michigan

Technological University has been studying Laser Raman spectroscopy of nickel oxides prepared by chemical and electrochemical means, both oxidized and reduced. Each preparation method gives somewhat different spectral features. Some of the results of this study are presented on Figure 3. The most significant finding is that both chemically and electrochemically oxidized materials, as well as reduced electrodes that have been cycled, do not exhibit any bands in the 3500-3700 cm^{-1} range that can be attributed to an OH stretch of free water. In addition, electrodes that have been cycled exhibit similar spectra in both the oxidized and reduced states. The spectra of all these materials are distinctly different from that of the well-crystallized beta Ni $(OH)_2$.

The fact that no OH stretch is observed in most of these materials has led to a new interpretation of the structures of the various hydroxides in terms of a model which postulates a sizeable fraction of vacancies in the nickel lattice sites. These vacancies may be filled, either partially or completely, with hydrogen atoms or alkali metal ions. Additional hydrogen atoms can be accommodated in sites between the planes of oxygen atoms where they are hydrogen bonded between the layers. The symmetry of the crystal structure is such that the OH stretch modes are forbidden in the Raman spectra. General formulas for the oxidized and reduced forms are postulated.

$$(Ni_{1-x}V_x)_{1.0}(OOH)_{1.00} + (2x + 1)H^+$$

and

$$Ni_{1-x}(2H)_{x\ 1.0}\ (OOH)H_{\ 1.00}$$

where x represents the fraction of Ni lattice sites either vacant or occupied by H+ or M+ ions and can be up to about 0.27. V represents vacant Ni lattice sites. The protons can either occupy vacant lattice sites or bridge two adjacent oxygens. Alkali metal ions can also occupy lattice vacancies. Most of the postulated formulas in the literature fit into this scheme nicely. For example, Barnard's α-Ni $(OH)_2$ with an empirical formula of $0.25NiOOH \cdot 0.75Ni(OH)_2 \cdot 0.25H_2O$ with a Ni valence of 2.33 can be written as $Ni_{0.89}V_{0.11}(OOH_2)_{1.00}$. Barnard's β phases can be interpreted as having a vacancy ratio of about 0.11, while the γ phase, like the α phase, has about 0.25 Ni vacancies which in the case of γ are filled by alkali ions. Reinterpretation of the X-ray diffraction data is being carried out, and it appears that the data fit this scheme at least as well as the earlier structural formulations.

Other work in progress includes cyclic voltammetry studies, self-discharge measurements, and impedance studies of both planar and porous nickel electrodes. The data on the planar Ni electrodes is being interpreted as due to a variable resistance oxide film, with the resistance varying with both depth and potential, analogous to some studies of the passive film on Fe.

This research should lead to a better understanding of the nature of the active material which will assist in designing cells with improved life and performance.

CONCLUDING REMARKS

Improved performance and cycle life on the Ni-H_2 cells can be achieved by an understanding of the nickel electrode behavior and improved cell design and component technology development. Improving performance and cycle life as well as increasing the energy density of the system are the drivers of the technology development program at LeRC. Our means of achieving these goals are by developing lower cost, high performance separators and lightweight, longer life nickel electrodes. Our studies show that as much as a 14% system weight reduction and at least a three-fold increase in nickel electrode life can be achieved. These improvements have been possible through an improved understanding of the various factors affecting life and insights into cycle life limitations provided by the nickel electrode studies.

The most recent advances in the nickel electrode and the separator technology areas will have a positive effect in life, weight, cost and performance and will have a considerable effect on the use of Ni-H_2 systems for LEO applications.

REFERENCES

1. Thaller, L. H., Manzo, M. A., and Gonzalez-Sanabria, O. D.: Design Principles of Ni-H_2 Cells and Batteries. NASA TM 87037, Prepared for 20th IECEC Conference, August, 1985.

2. Smithrick, J. J. Manzo, M. A., and Gonzalez-Sanabria, O. D.: Advanced Design for IPV Ni-H_2 Cells. NASA TM 83643, Prepared for 19th IECEC Conference, August, 1984.

3. Gonzalez-Sanabria, O. D. and Manzo, M. A.: Separator Development and Testing Ni-H_2 Cells. NASA TM 83653, Prepared for 19th IECEC Conference, August, 1984.

4. Thaller, L. H.: Nickel Hydrogen Battery Systems. NASA TM 82946, NASA Lewis Research Center, 1982.

5. Reid, M. A., Post, R. E., and Soltis, D. G.: Method of Making a Lightweight Battery Plaque, U. S. Patent 4,439,465, March 27, 1984.

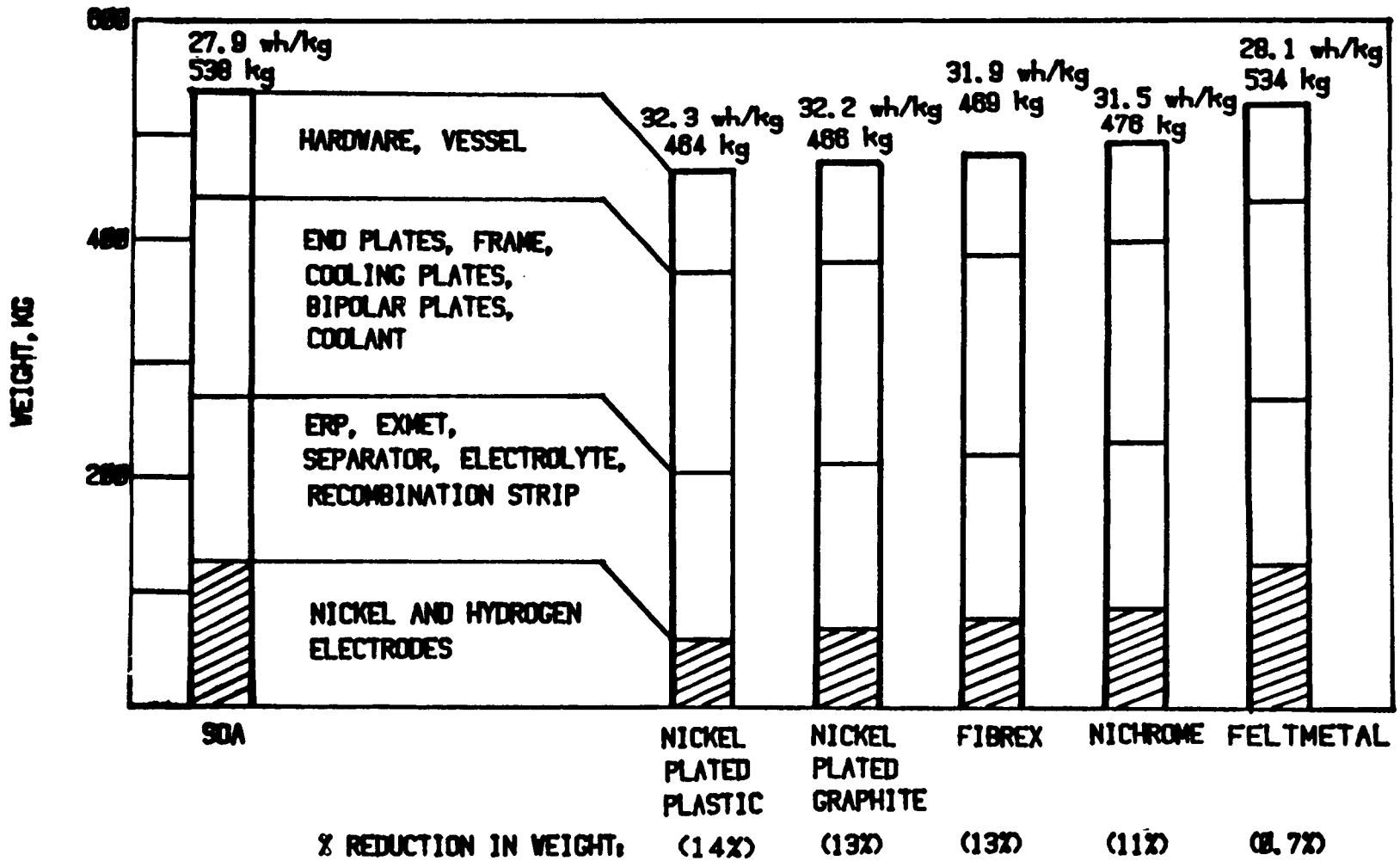

Figure 1. WEIGHT OF COMPONENTS IN A 125 Ah NiH_2 BIPOLAR BATTERY AND THE WEIGHT REDUCTION WITH LIGHTWEIGHT NICKEL ELECTRODES

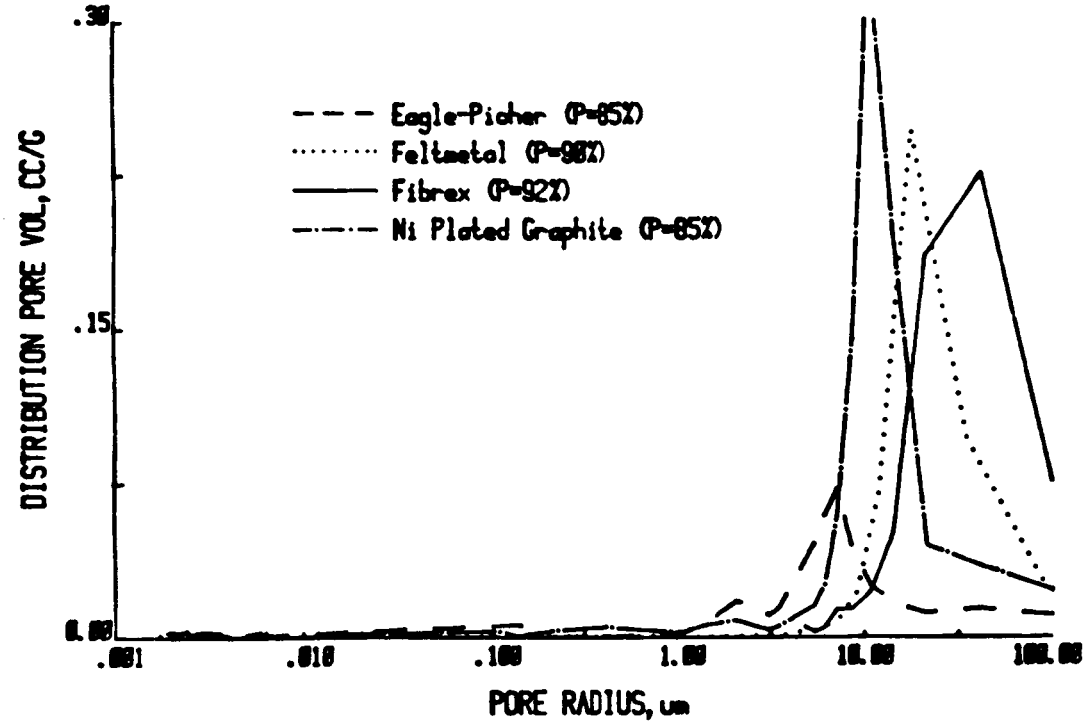

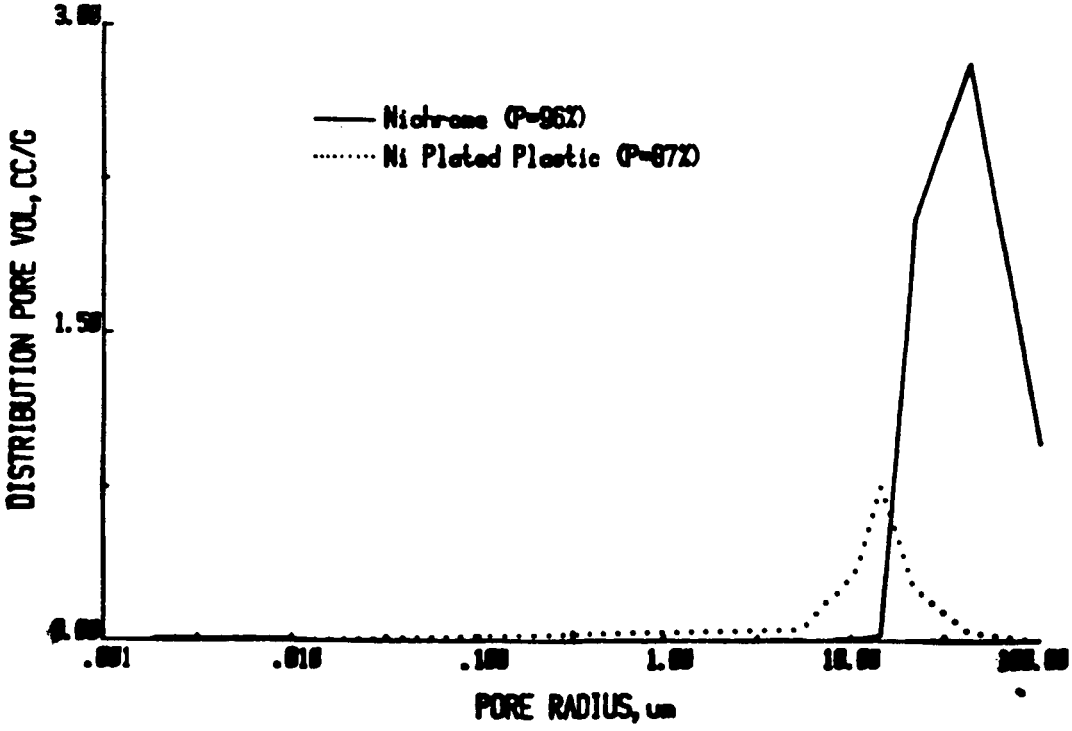

Figure 2. PORE SIZE DISTRIBUTION CURVES

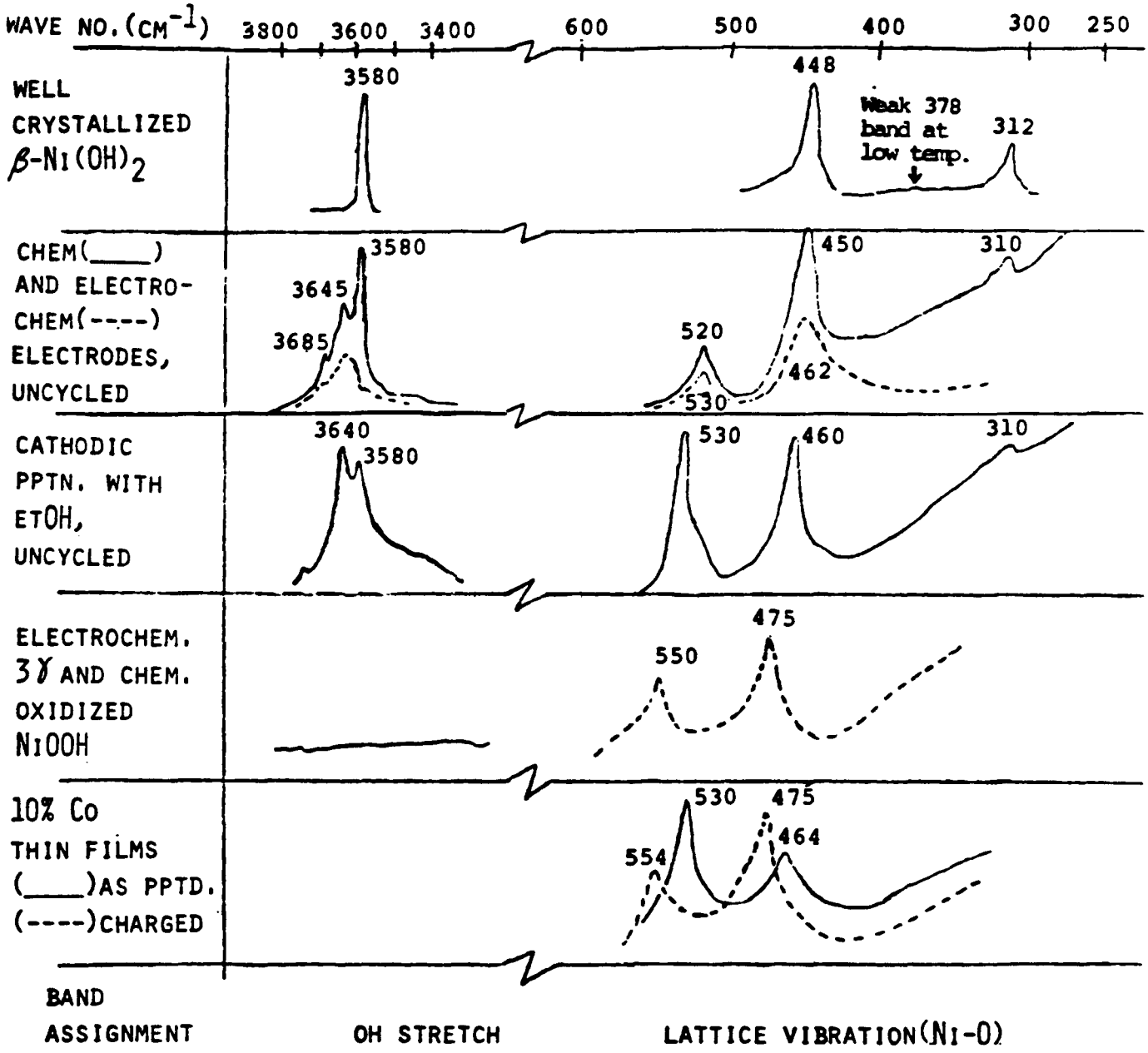

OH STRETCH BANDS DISAPPEAR ON CYCLING.

BACKGROUND BELOW 450 CM^{-1} RELATED TO PARTICLE SIZE EFFECTS, ALIGNMENT, AND SENSITIVITY.

DIFFERENT SPECTRA RUN WITH DIFFERENT SENSITIVITIES. RELATIVE INTENSITIES AND BACKGROUND MAY VARY SOMEWHAT.

WELL CYCLED ELECTRODES HAVE SPECTRA LIKE THE 10% Co THIN FILM-CHARGED.

Figure 3. RAMAN SPECTRA OF SELECTED NICKEL HYDROXIDES

LIGHTWEIGHT, DIRECT-RADIATING NICKEL HYDROGEN BATTERIES*

John R. Metcalfe
Canadian Astronautics Limited
Ottawa, Canada K2H 8K7

ABSTRACT

Two battery module configurations have been developed which, in addition to integrating cylindrical nickel hydrogen (NiH_2) cells into batteries, provide advances in the means of mounting, monitoring and thermal control of these cells. The main difference between the two modules is the physical arrangement of the cells: vertical versus horizontal. Direct thermal radiation to deep space is accomplished by substituting the battery structure for an exterior spacecraft panel. Unlike most conventional nickel-cadmium (NiCd) and NiH_2 batteries, the cells are not tightly packed together; therefore ancilliary heat conducting media to outside radiating areas, and spacecraft deck reinforcements for high mass concentration are not necessary.

Testing included electrical characterization and a comprehensive regime of environmental exposures. Despite significant structural differences, the test results were similar for the two modules. High energy density was attained without sacrificing structural rigidity. The results of computer structural analyses were confirmed by a series of vibration tests. Thermal excursions and gradients during geosynchronous orbit (GEO) eclipse day simulations in vacuum were within the nominal range for near optimum NiH_2 cell performance.

The designs are flexible with respect to quantity and type of cells, orbit altitude and period, power demand profile, and the extent of cell parameter monitoring.

This paper compares the characteristics of the two battery modules and summarizes their performance.

INTRODUCTION

The Space Systems Group at Canadian Astronautics Limited (CAL) has completed two programs for the design, fabrication and testing of nickel hydrogen batteries. These were respectively funded under:

1. Intelsat Contract-INTEL-151, entitled, "Qualification of an Advanced Nickel Hydrogen Battery"; for the R&D Department of the International Telecommunications Satellite Organization.

2. Supply and Services Canada contract file no.06ST.36001-3-2410, entitled, "The Enhancement of Advanced Nickel-Hydrogen Battery Technology"; for the Communications Research Centre of the Canadian Department of Communications (DOC).

* This paper is based on work performed, in part, under the sponsorship and technical direction of the International Telecommunications Satellite Organization (Intelsat). Any views expressed are not necessarily those of Intelsat, or of DOC.

The battery built under the first-mentioned contract is called "IBAT". Figure 1 is a photograph of its spacecraft interior side and Figure 2 is a photograph of its radiative side. This model employs a Crowned Sleeve and Flange cell mounting method, whereby the 24 cells pass through the panel with their longitudinal axes normal to the plane of the panel. This was one of the two optimum (energy density versus thermal performance and structure strength) concepts of the several candidate layouts analysed during the initial design phase of the Intelsat contract.

The alternate concept, named "LYBAT", because the cells "lie down" in the plane of the panel, was not originally chosen for development. This was due to the large radiating area needed to handle the peak dissipation of 24 cells on a single panel, in view of Intelsat's 80% depth-of-discharge (DOD)/1.2 hour eclipse requirement. The LYBAT concept was considered practical, however, for requirements of fewer cells per "pack" or for lower DODs. The major requirement of the second contract was the accommodation of nine (9) cells lying in the plane of the radiating support plate. Figure 3 is a photograph of the LYBAT prototype interior side and Figure 4 is a photograph of its radiative side.

CELLS

Both battery modules employ 3.5 inch diameter "Intelsat design" cells of 50 ampere-hour nameplate capacity (Yardney model YNH50-5). However, both designs can accommodate larger, longer and/or heavier individual pressure vessel (IPV) cells, including the new generations of very high energy 3.5 inch and 4.5 inch diameter cells. Both designs can be used in GEO and low earth orbit (LEO) applications. In addition, the LYBAT mounting system lends itself particularly well to common pressure vessel (CPV) cells of considerably greater length.

BATTERY CHARACTERISTICS

Table 1 compares the characteristics of the two units in summary form.

MECHANICAL AND THERMAL DESIGN

Both projects involved extensive use of stress analysis and thermal modelling to determine the optimum structure configurations and dimensions. Experiments were also carried out to evaluate materials and fastening/mounting techniques.

Panel Structures

IBAT - The IBAT was built employing a single hexagonal shaped sheet of 1.5 inch thick standard aerospace honeycomb panel to support the 24 cells and all of the associated hardware. Panel holes for components and fasteners were cut and later edge strengthened.

LYBAT - LYBAT employs a structure believed to be unique in the battery field. It is an "egg-crate" lattice of sheet aluminum web pieces, many as thin as 0.016 inch, which are dip-brazed to each other, to the cell support saddles and to the radiative face skin. Various forms of support brackets and strengthening techniques were utilized.

Cell Mounting

IBAT - The 24 IBAT cells are retained by through-plate mounts incorporating precision machined sleeves, flanges and crowns (Figure 5A). Each cell is bonded to the sleeve with a flexible, thermally conductive adhesive using special techniques to align the cell in its sleeve. A locking mechanism then assures a strong bond to the panel itself. Each cell assembly radiates directly to the external environment.

LYBAT - The nine LYBAT cells are seated in formed saddle sections which are recessed part way into the 2.5 inch deep support structure (Figure 5B). The cell covers are bolted to the panel via braces above and below the face skin, the cell having been bonded to the assembly in a manner similar to that of IBAT.

End-domes - Cell vessel end-domes for both batteries were fitted with thermal insulation prior to installation. This was to prevent excessive cooling of end-domes located on the "space" side of the panels.

Safety - For safety reasons, the cells for both batteries were conformally coated prior to installation. The thin layer of Urethane has negligible effect on heat transfer, but prevents accidental electrical contact from the cell vessel to other metal parts. Despite the relatively high impedance between a cell's case and its power path, it is known that a small intermittent contact point from a vessel to its mounting hardware (near negative battery terminal potential) can, with the battery fully charged, spark-erode an orifice through the Inconel wall of the pressure vessel, releasing hydrogen.

Temperature Gradients

A basic design goal was the minimization of intercell and internal cell temperature gradients, the former to within 5°C for prevention of temperature driven imbalances in cell capacities, and the latter to within 10°C (core to vessel) to prevent vapour transfer from the electrolyte to the inner wall of the cell vessel. Attention was paid to balancing the thermal conductivities of the cell mounting hardware. Transient thermal analyses were carried out to predict gradients from the effects of cell dissipations during an eclipse.

Cell Spacing/Surface Area - The distance between cell locations, which reflects directly upon volumetric energy density and occupied footprint area, was determined mainly by the panel area per cell required to augment the cell covers' ability to dissipate peak cell dissipation with acceptable temperature gradients. This was established by iterative analyses of the computer models. The practical constraints of structure/fastener interfacing also played a role.

If designed for the same dissipation levels, the IBAT technique is inherently smaller than the LYBAT in footprint area per cell. However, the IBAT was built for an approximately 60% higher peak cell dissipation. This resulted in the per cell footprint areas being nearly identical for the as-built models.

Thermal Aspects-LEO

The present limits of continuous discharge current, with respect to dissipation handling, are: LYBAT - 33.3 amperes for 36 minutes or 25 amperes for 72 minutes; IBAT - 36 amperes for 72 minutes.

The LYBAT thermal analysis was extrapolated for the higher current, shorter duration charge/discharge regime of a typical 110 minute orbit, LEO application. The main problem area is the high cell dissipation encountered at end of charge, just prior to eclipse commencement. If charge return ratios were balanced accordingly, and if cells with higher stack to shell thermal conductivity were employed, discharge rates of 50 to 60 amperes could be safely maintained during a 36 minute eclipse period with few design alterations. A similar prospect is foreseen for the IBAT design.

Electrical Design

Electrical Design made use of tolerance, stress and failure modes analyses, along with mass versus power loss tradeoff studies, to choose the methods and piece parts for the power paths, the main power connector interfaces, the cell bypass circuits and the sensor circuits for monitoring of temperatures, cell pressure and cell voltages.

Power Path - Both models employed special lightweight, low-loss cell interconnects, which proved to be superior to copper wire. Wiring was used to connect the ends of the series cell strings to the main power connectors and to connect the cell bypass circuits. The IBAT has a single main power connector. The LYBAT has two separate power connectors to facilitate series interconnection with identical modules on adjacent panels, to attain a battery with any multiple of nine cells.

Cell Bypass Circuits - The familiar method of open-circuit protection; three series diodes per cell for charge and one larger power diode per cell for discharge, was employed. These diodes were located to minimize thermal imbalance effects, should they become activated.

Because of the higher currents involved in a typical LEO application, the mass of the larger power rectifiers required, and their potentially high dissipations, would be prohibitive. High current aerospace relays are also relatively heavy. To increase battery energy density, special development of a low mass sense switch, designed for one closure operation across a failed cell, may be the solution for both GEO and LEO batteries.

Monitoring Circuits - Both batteries have isolated voltage sense lines from cell terminals to a monitoring harness connector. In addition, the LYBAT has four permanent temperature transducers (two on cells, two on panel structure) which are monitored via the same connector.

- Pressure Monitoring - The IBAT has a specially developed, on-board strain gauge processor (SGP), which selects the strain gauge bridge reading for the desired cell, amplifies it and transmits it to the ground station via spacecraft telemetry. The SGP entails a low-power module, containing two small circuit cards, on the spacecraft interior side of the battery panel (Figure 1). Integrated circuits were chosen on the basis of their availability in radiation hardened versions.

The SGP and strain gauge bridge wiring are relatively low in mass, as depicted by the proportion of monitoring circuits' mass in Figure 6, and they provide indication of state of charge.

Figure 7 illustrates the percentages of LYBAT's mass components. Figures 8 and 9 depict actual SGP cell pressure data and voltage of the same IBAT cell for a charge/discharge cycle at 10°C.

TESTING

The test results and other performance data, including projections for an advanced cell type, are summarized in Table 1. The test equipment used at CAL for electrical and thermal control (in air) of the batteries is shown in Figure 10.

CAPACITY

Battery capacities were determined from the time taken to reach an end of discharge voltage (EODV) equal to the number of cells times 1.00 volt, at a constant current of 25.0 amperes. Reference capacities were recorded during the last cycle of several overcharge/one hour stand/discharge sequences, at the reference temperature of 10 $\pm$3°C. Both batteries had typical capacities of 52 $\pm$1 AH.

ENERGY DENSITY

IBAT

The mass of the IBAT module is 40.0 Kg. After deducting the predetermined replaced structure allowance, the net mass is 37.3 Kg, for an energy density of 39.8 WH/kg, based on 51.5 AH capacity with a mid-discharge voltage of 28.8 volts.

LYBAT

The mass of the LYBAT module, not including 0.4 Kg of extra adhesives and brackets added to correct two minor problems (easily resolvable in a future model), is 14.8 Kg. After deducting the predetermined replaced structure allowance, the net mass is 13.3 Kg, for an energy density of 42.1 WH/Kg, based on 51.6 AH capacity with a mid-discharge voltage of 10.85 volts.

Comparisons

Figure 11 compares the energy densities of conventional "close-packed" 35 AH and 40 AH NiH_2 batteries with those of the IBAT and LYBAT, and with the projected energy densities for the as-built IBAT minus the mass of pressure monitoring apparatus, and for the IBAT and LYBAT concepts using 75 AH cells typical of those now nearing fully developed status.

Although the energy density of the LYBAT appears to be significantly greater than that of IBAT, the total weight per cell of the former is only 22 grams less. Additional mass saving measures are already assured for future models.

ELECTRICAL AND THERMAL CYCLING

IBAT - The IBAT successfully underwent a regime of extreme temperature excursions (in air) while electrically active at test temperatures ranging from -15°C to +40°C. In addition, reference cycling was done for capacity determination at 0°C, 10°C, 20°C and 30°C, and test stages were interspersed with capacity retention tests at 10°C to check for degradation.

LYBAT - LYBAT's testing in air was limited to characterization cycling at 10°C and a capacity determination at +25°C (46.6 AH). Power losses in the cell interconnects (bus bars) were measured to be only 3.3 Watts at 25 amperes.

VIBRATION TESTING

One-piece machined mounting fixtures were used to mount the batteries for vibration testing. The facilities of the David Florida Laboratory, located at the Communications Research Centre near Ottawa, were employed. An input spectrum, derived from a combination of available launch vehicle data (Delta/Shuttle/Ariane), was applied in the three orthogonal axes, in both random and swept sinusoidal modes.

The structures of both modules were successfully vibration tested to the limits specified for the cells. Force levels experienced by the cells were up to 13 g-rms in random mode, and 20 g-peak in sinusoidal mode. Panel resonances were slightly above the predicted frequencies, indicating that the intended stiffness had been achieved. The results supported the findings of the structural analyses, which predicted high stress capabilities at high confidence levels.

THERMAL VACUUM TESTING

Again at the David Florida Laboratory Space Simulation Facility, the batteries were tested in thermal vacuum at pressures less than 1×10^{-6} Torr. The set-ups involved enclosing the battery undersides and resistive heaters with insulating material to simulate the interior of the spacecraft. Thermocouples were placed at strategic locations. The chamber walls were cooled with liquid nitrogen to approximate deep space temperatures.

A GEO full-eclipse day simulation was run for each battery. Figure 12 illustrates the actual average cell temperature profiles through eclipse (discharging at 25A). Intercell temperature gradients were within the design maximum range, and internal cell gradients (stack to vessel differential) were determined, by analysis of measured versus predicted node temperatures, to be within the safe operational range.

CONCLUSION

Two lightweight support structures and cell mounting systems have been shown feasible for serious consideration in future spacecraft energy storage systems. Substitution of exterior, or space-viewing, panel sections not only saves the mass of the obviated panel, but liberates internal space for payload use. The layouts are adaptable to a variety of panel sizes and shapes, and to the voltage and power profile requirements of many communications, remote sensing and scientific satellites.

ACKNOWLEDGEMENTS

The author would like to express appreciation for the front-end design and organizational work by Mr. Malcolm H. Moody, of CAL.

These two projects have enabled CAL to establish a firm base in NiH_2 technology. We gratefully acknowledge the support and responsiveness of our customers' scientific authorities: Dr. John Stevenson of Intelsat and Mr. George Mackie and Dr. Don Edwards of Communications Canada.

TABLE 1

COMPARISON OF DIRECT-RADIATING NIH2 BATTERIES

MODEL	"LYBAT"	"IBAT"
STRUCTURE	DIP-BRAZED LATTICE	ALUM. HONEYCOMB
CELL MOUNTING	SADDLES IN PLANE OF PANEL	CROWNED SLEEVE AND FLANGE, THROUGH PANEL
CELL TYPE	50 AH NAMEPLATE "INTELSAT DESIGN"	50 AH NAMEPLATE "INTELSAT DESIGN"
CELL QUANTITY	9	24
PANEL SHAPE	RECTANGULAR	HEXAGONAL
FOOTPRINT AREA	2.635 FT^2/0.245 M^2 42.2 IN^2 PER CELL	7.079 FT^2/0.658 M^2 42.5 IN^2 PER CELL *
MASS	13.3 KG NET	37.3 KG NET
CAPACITY	51.6 AH (10°C)	51.5 AH (10°C)
ENERGY	560 WH (10.85V*)	1483 WH (28.8V*)
ENERGY DENSITY	42.1 WH/KG NET	39.8 WH/KG NET
PROJECTED E.D. 75 AH	46.5 WH/KG (SEE FIG. 6)	46.0 WH/KG (SEE FIG. 6)

TABLE 1 CONT'D

COMPARISON OF DIRECT-RADIATING NIH2 BATTERIES

	"LYBAT"	"IBAT"
VIBRATION TEST	SURVIVED SINE AND RANDOM TESTS (3 AXES)	SURVIVED SINE AND RANDOM TESTS (3 AXES)
STRUCTURE RESONANCES	>150 HZ	>85 HZ
DISCHARGE CURRENT RATINGS	25 A NOM. 36 A MAX 150 A SURGE	33.3 A NOM. 36 A MAX. 150 A SURGE
BUILT-IN MONITORING	TEMPERATURES, CELL VOLTAGES	CELL PRESSURES, CELL VOLTAGES
PROTECTION	REDUNDANT CONNECTIONS, DIODE BYPASSES	REDUNDANT CONNECTIONS, DIODE BYPASSES
HEAT OUTPUT	RADIATION TO SPACE	RADIATION TO SPACE
HEAT INPUT	ELECTRIC HEATERS DURING INSOLATION	ELECTRIC HEATERS DURING INSOLATION
EQUILIBRIUM TEMP.	$7 \pm 3°C$	$13 \pm 3°C$
THERMAL GRADIENTS	<6.5C° INTERCELL (<5° CAPABILITY) <10C° CELL INT.	<10C° INTERCELL (<4° CAPABILITY) <10C° CELL INT.

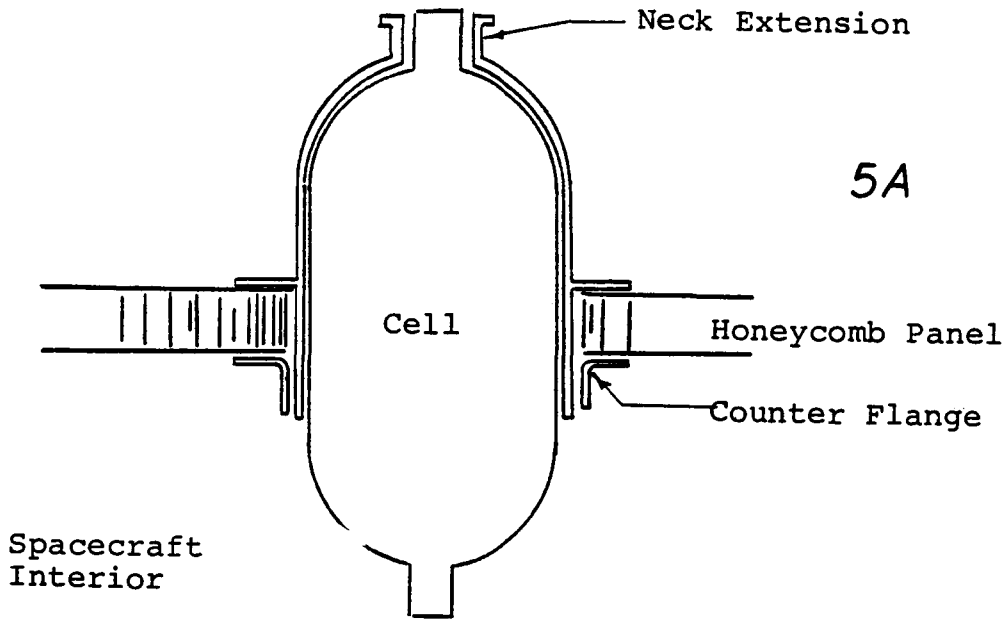
Neck Extension
5A
Cell
Honeycomb Panel
Counter Flange
Spacecraft
Interior

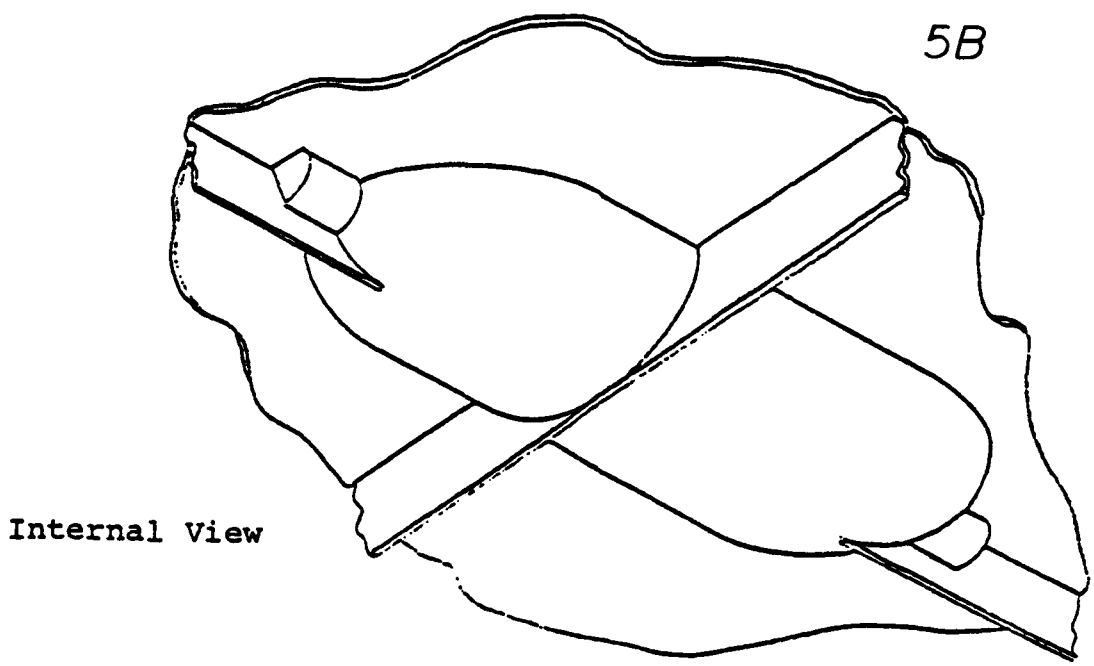
5B
Internal View

Figure 5.

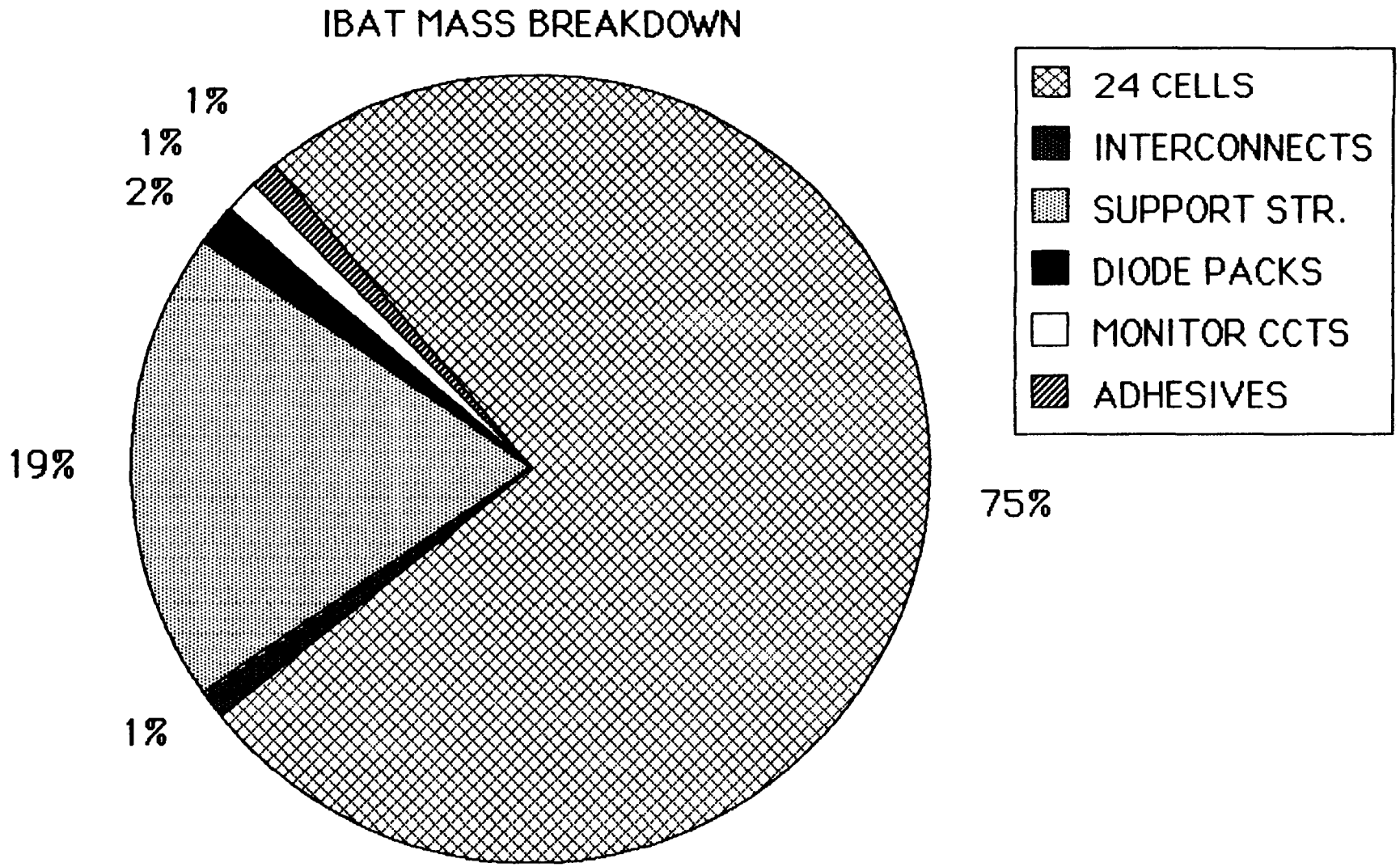
IBAT MASS BREAKDOWN
1%
1%
2%
19%
1%
75%
24 CELLS
INTERCONNECTS
SUPPORT STR.
DIODE PACKS
MONITOR CCTS
ADHESIVES

Figure 6.

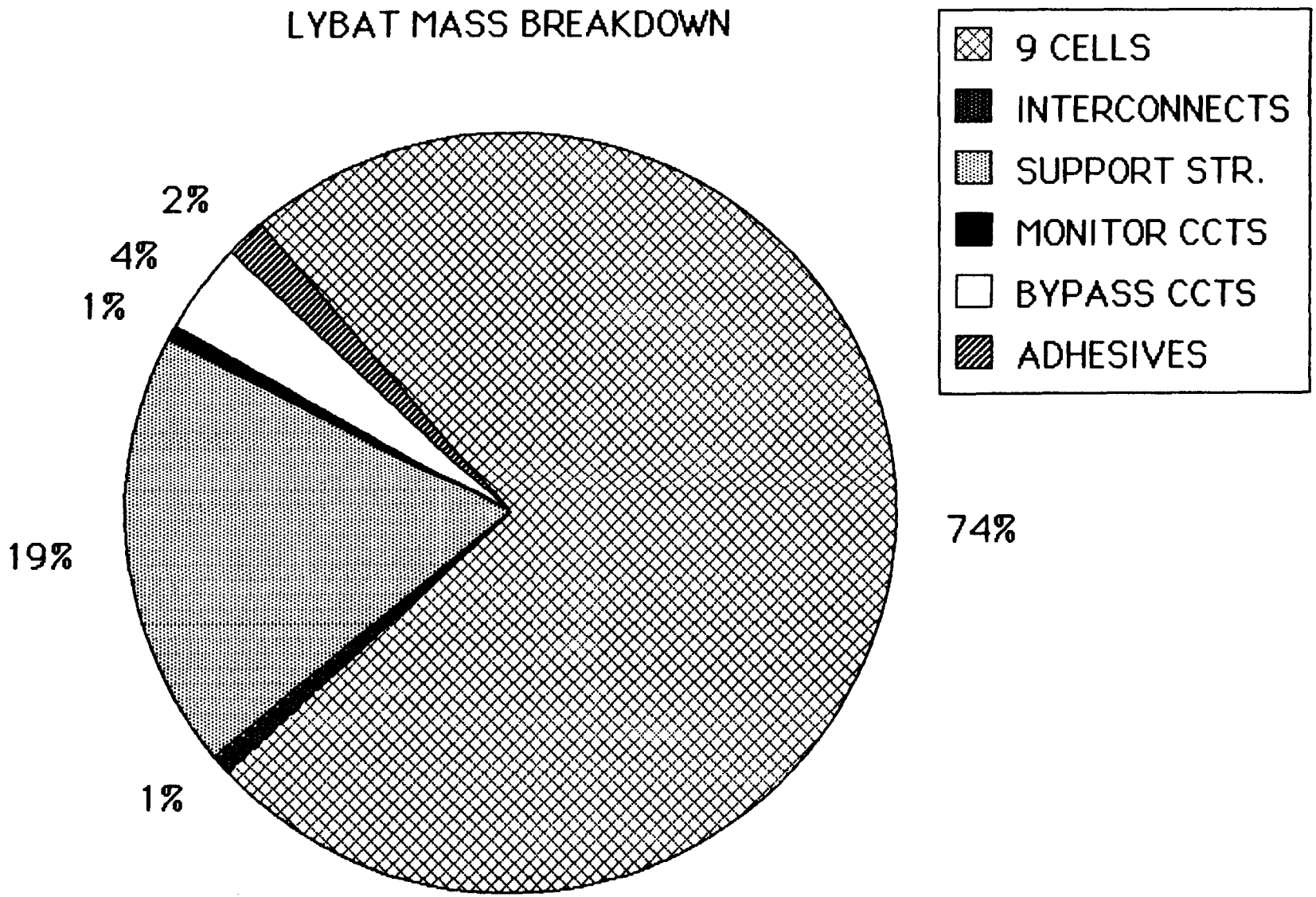
LYBAT MASS BREAKDOWN
9 CELLS
INTERCONNECTS
SUPPORT STR.
MONITOR CCTS
BYPASS CCTS
ADHESIVES
74%
19%
1%
1%
4%
2%

Figure 7.

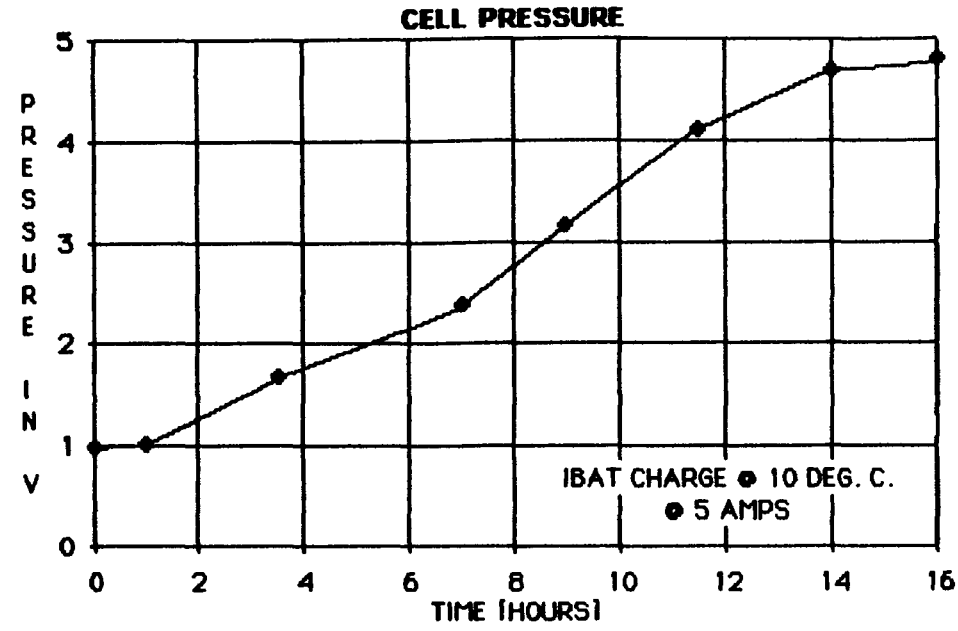
CELL PRESSURE
PRESSURE IN V
0
1
2
3
4
5
0
2
4
6
8
10
12
14
16
TIME (HOURS)
IBAT CHARGE @ 10 DEG. C.
@ 5 AMPS

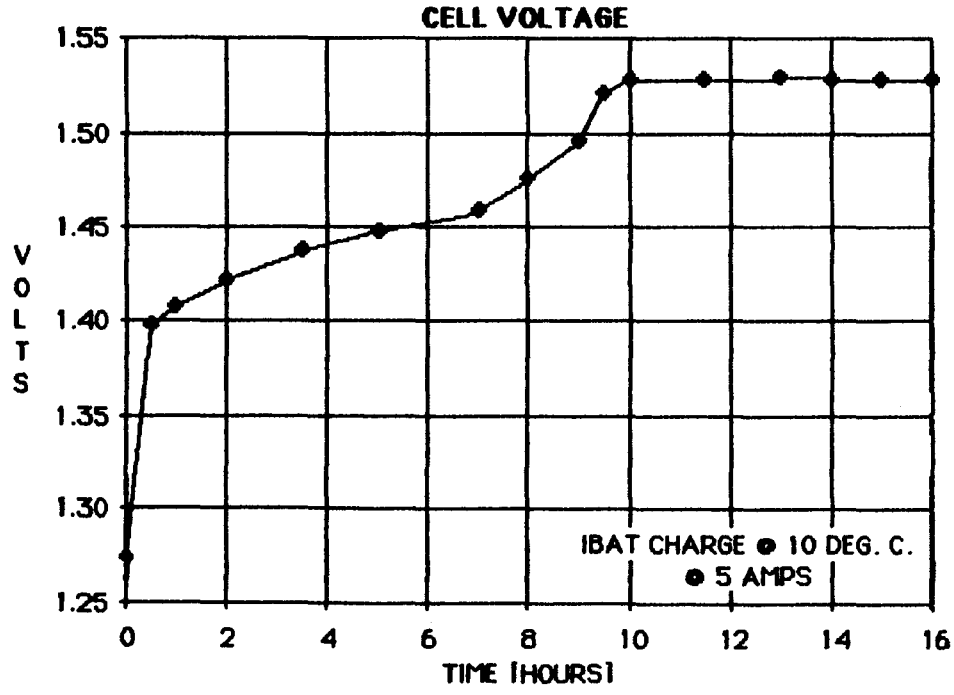
CELL VOLTAGE
VOLTS
1.25
1.30
1.35
1.40
1.45
1.50
1.55
0
2
4
6
8
10
12
14
16
TIME (HOURS)
IBAT CHARGE @ 10 DEG. C.
@ 5 AMPS

Figure 8.

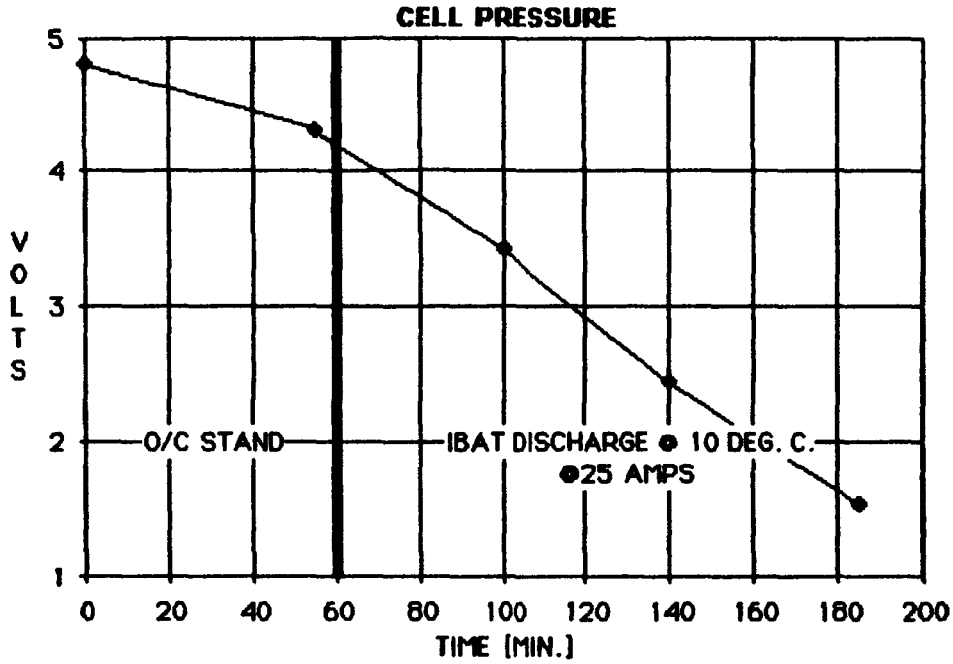
CELL PRESSURE
VOLTS
5
4
3
2
1
O/C STAND
IBAT DISCHARGE @ 10 DEG. C.
@25 AMPS
0
20
40
60
80
100
120
140
160
180
200
TIME [MIN.]

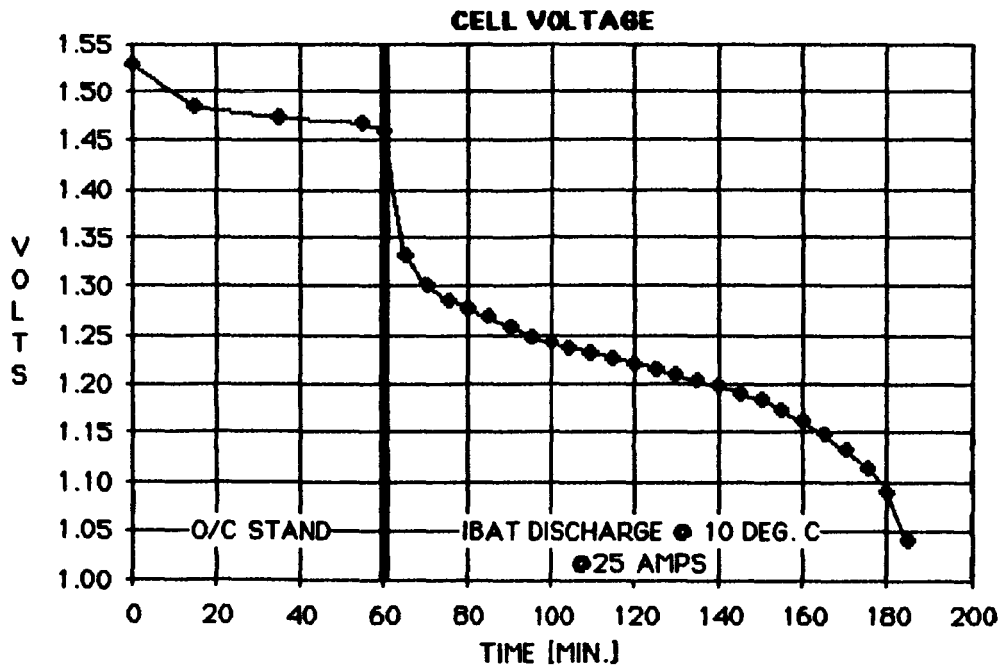
CELL VOLTAGE
VOLTS
1.55
1.50
1.45
1.40
1.35
1.30
1.25
1.20
1.15
1.10
1.05
1.00
O/C STAND
IBAT DISCHARGE @ 10 DEG. C
@25 AMPS
0
20
40
60
80
100
120
140
160
180
200
TIME [MIN.]

Figure 9.

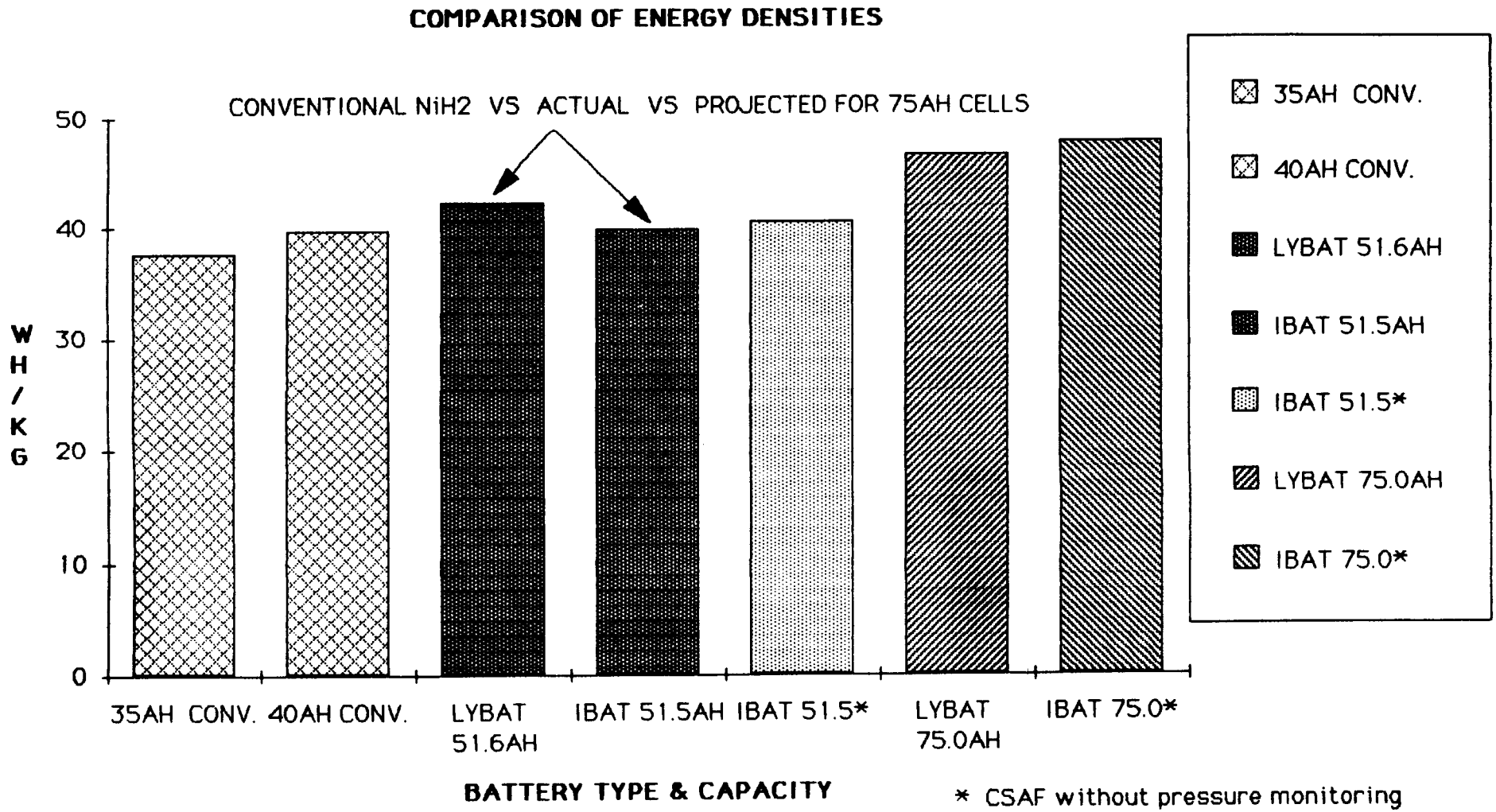
COMPARISON OF ENERGY DENSITIES
CONVENTIONAL NiH2 VS ACTUAL VS PROJECTED FOR 75AH CELLS
WH/KG
50
40
30
20
10
0
35AH CONV.
40AH CONV.
LYBAT 51.6AH
IBAT 51.5AH
IBAT 51.5*
LYBAT 75.0AH
IBAT 75.0*
35AH CONV.
40AH CONV.
LYBAT 51.6AH
IBAT 51.5AH
IBAT 51.5*
LYBAT 75.0AH
IBAT 75.0*
BATTERY TYPE & CAPACITY
* CSAF without pressure monitoring

Figure 11.

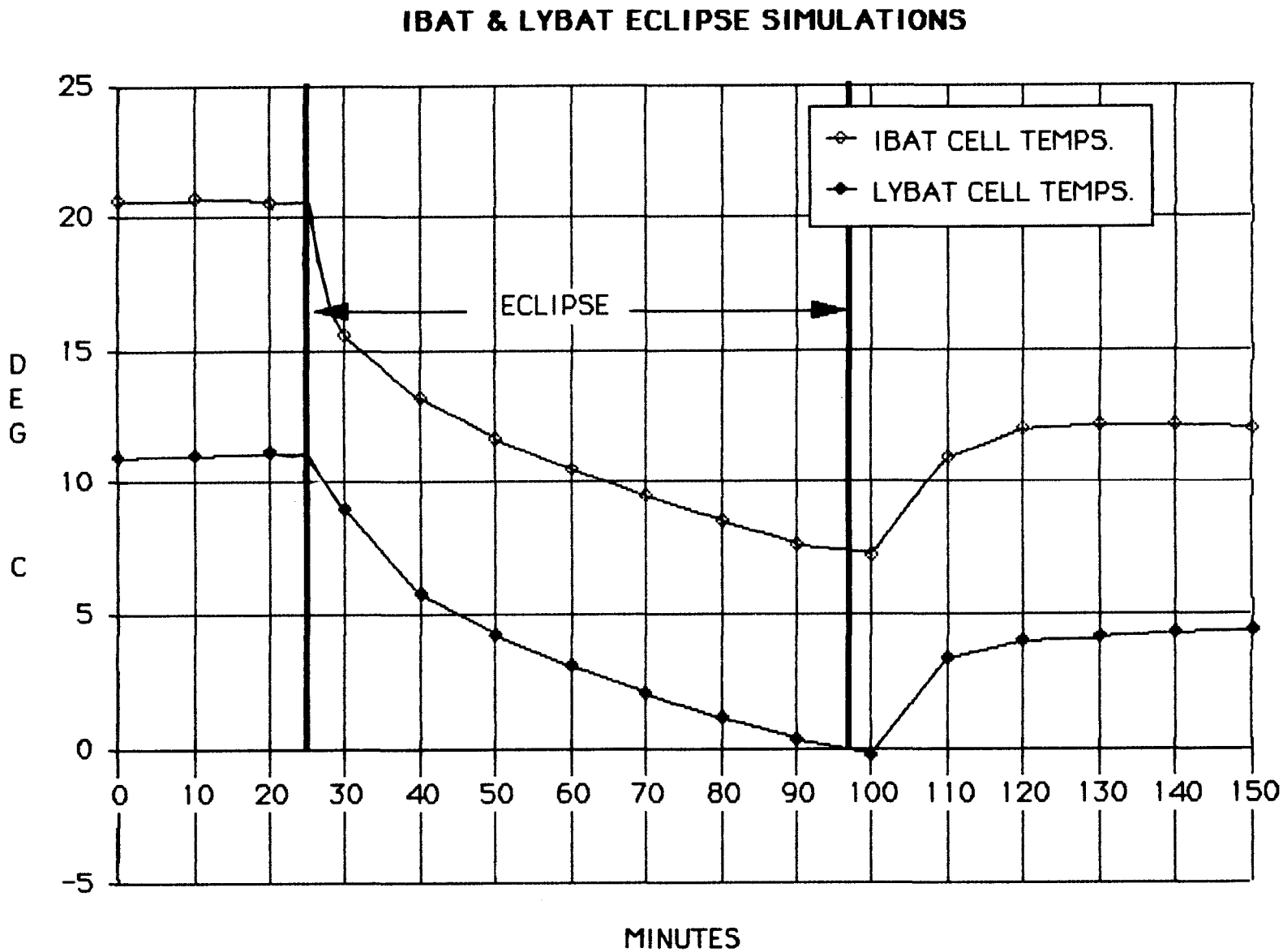
IBAT & LYBAT ECLIPSE SIMULATIONS
IBAT CELL TEMPS.
LYBAT CELL TEMPS.
ECLIPSE
DEG C
25
20
15
10
5
0
-5
0
10
20
30
40
50
60
70
80
90
100
110
120
130
140
150
MINUTES

Figure 12.

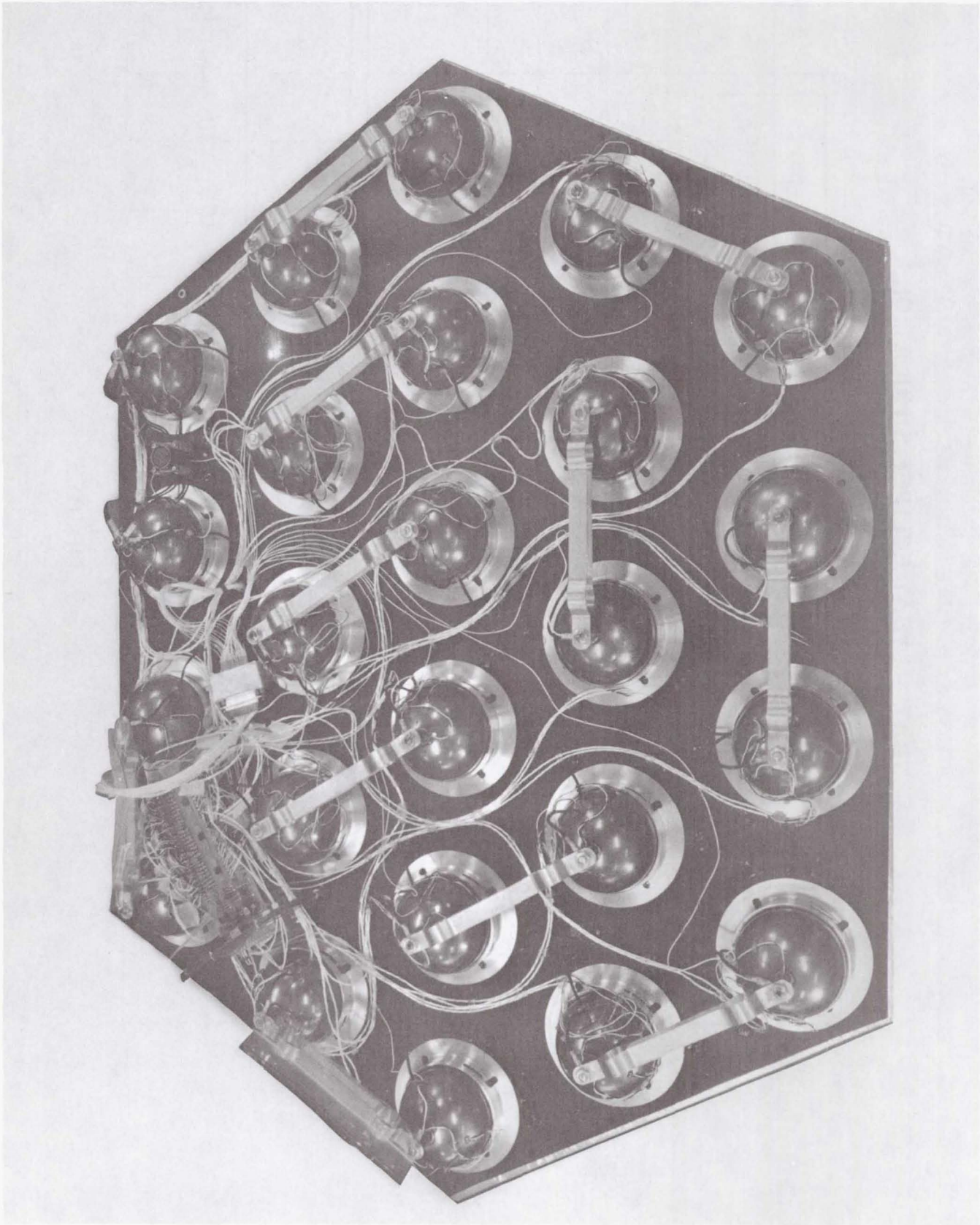

Figure 1. IBAT UNDERSIDE/MONITORING ELECTRONICS

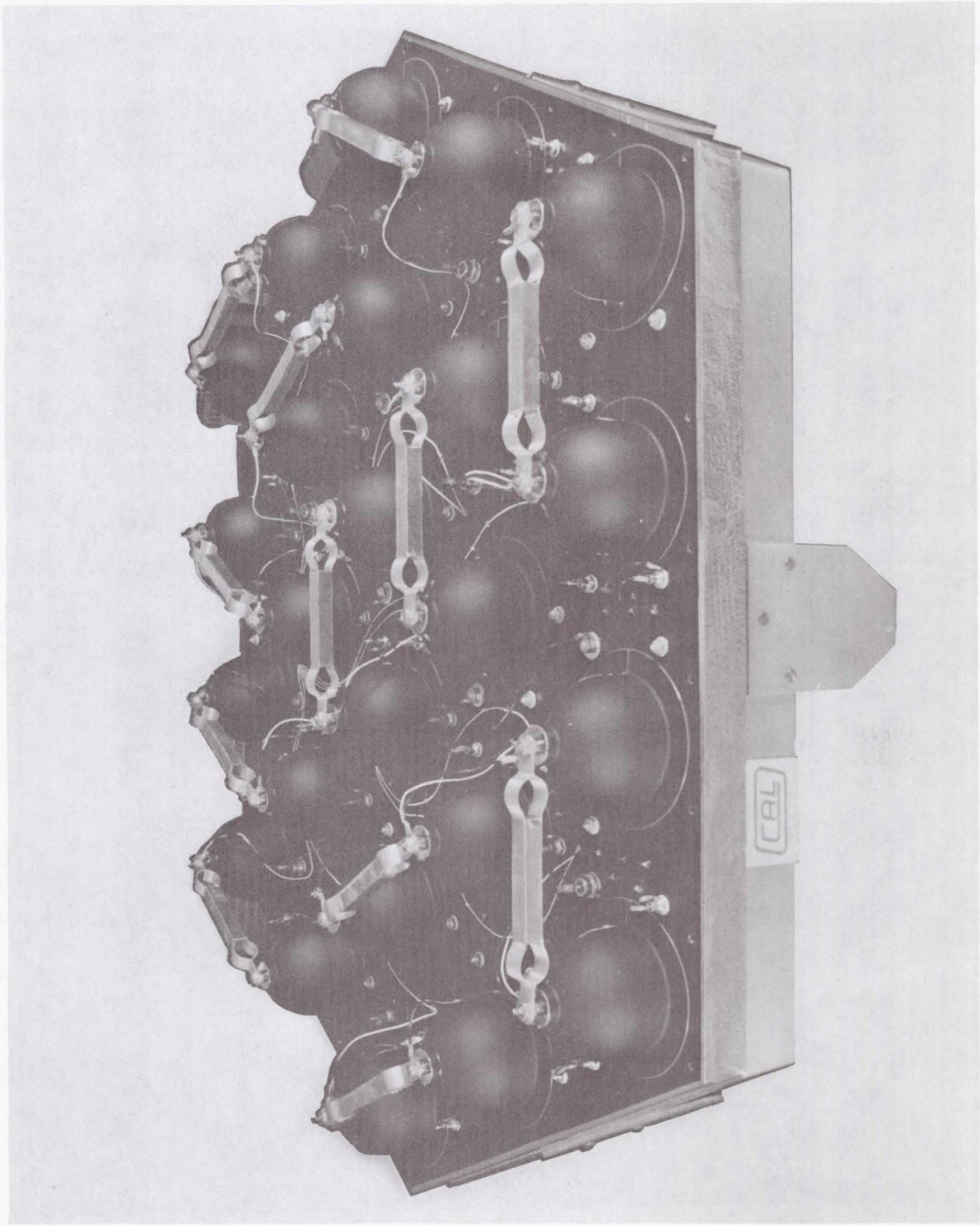

Figure 2. IBAT RADIATIVE SIDE

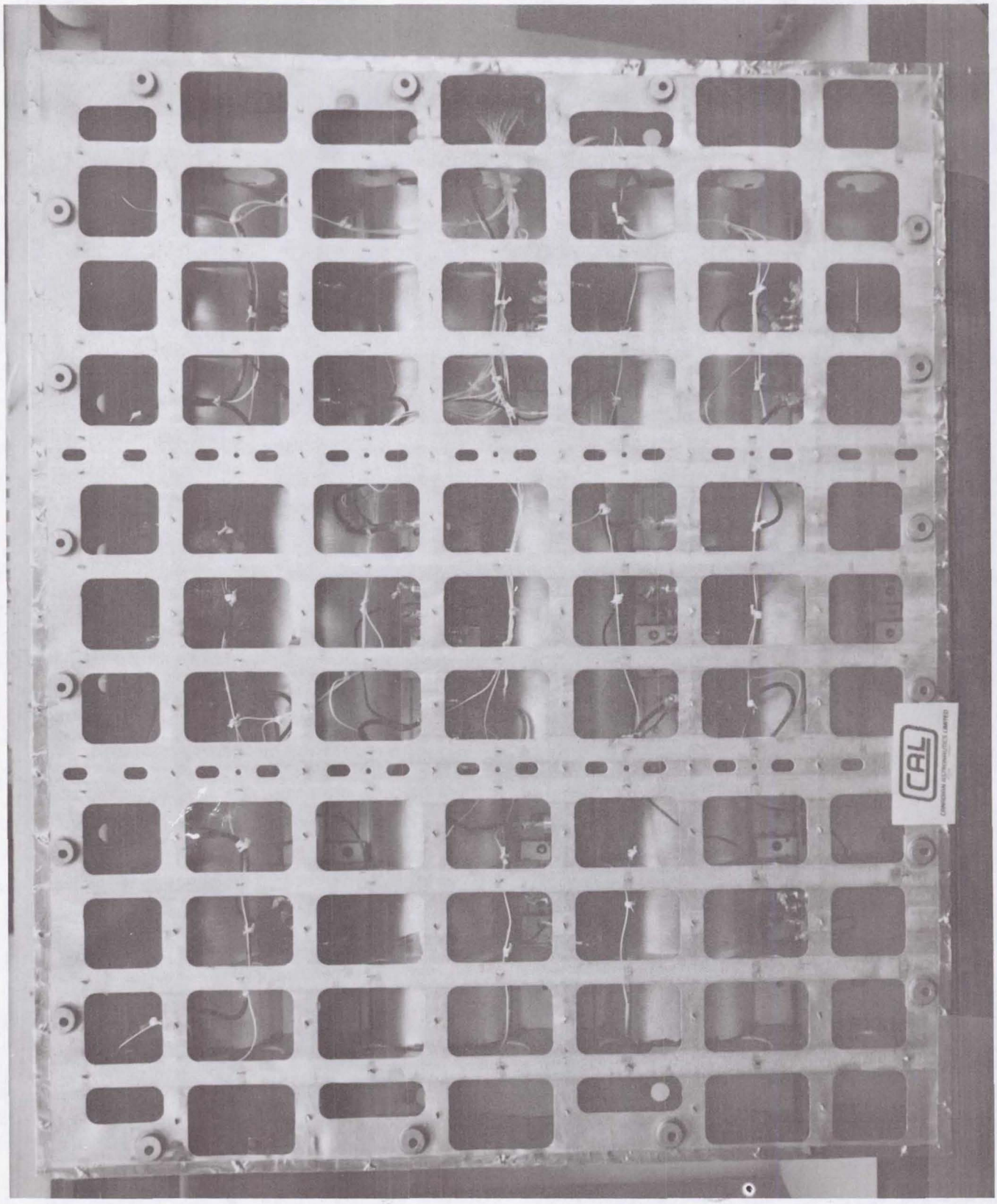

Figure 3. LYBAT UNDERSIDE

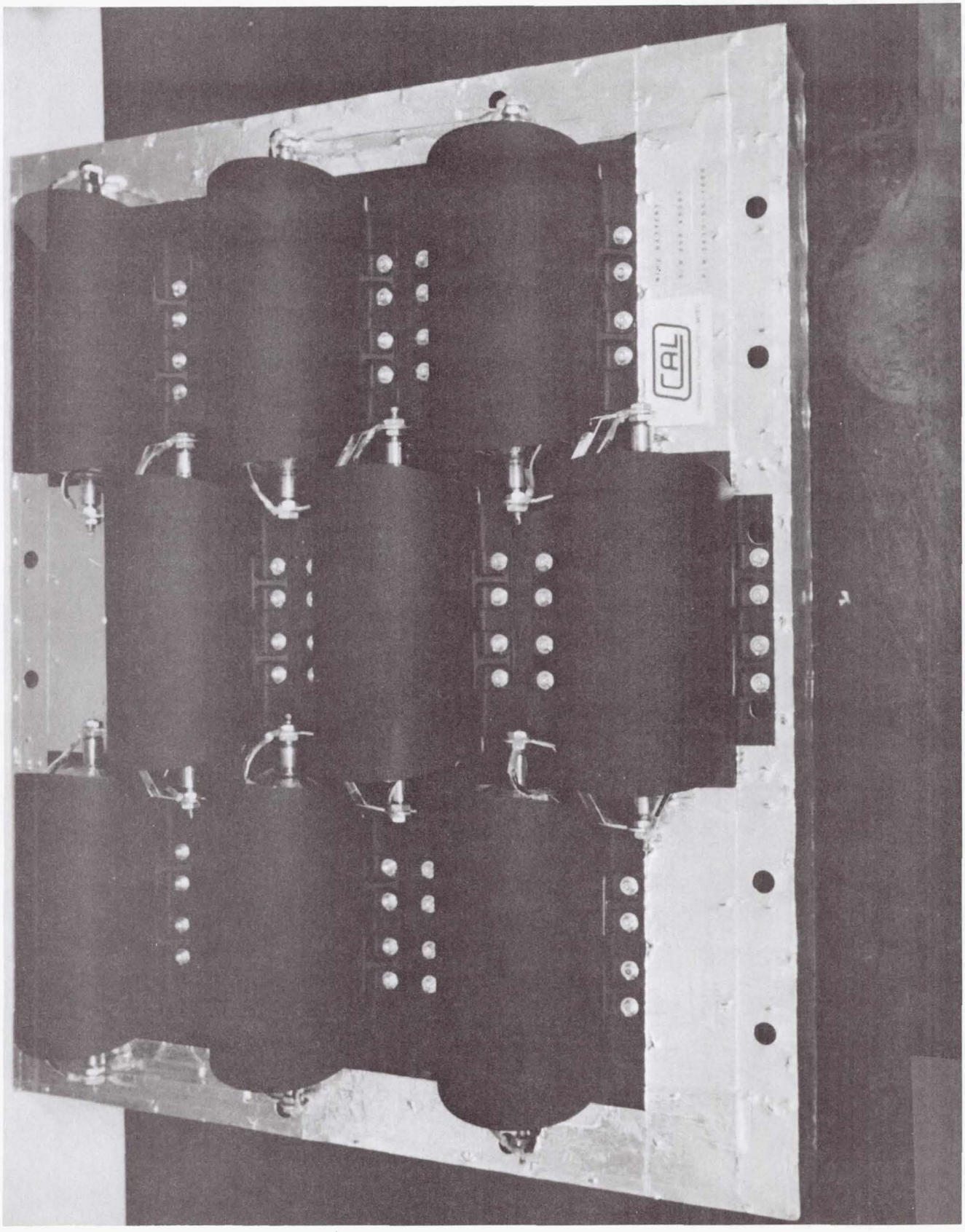

Figure 4. LYBAT RADIATIVE SIDE

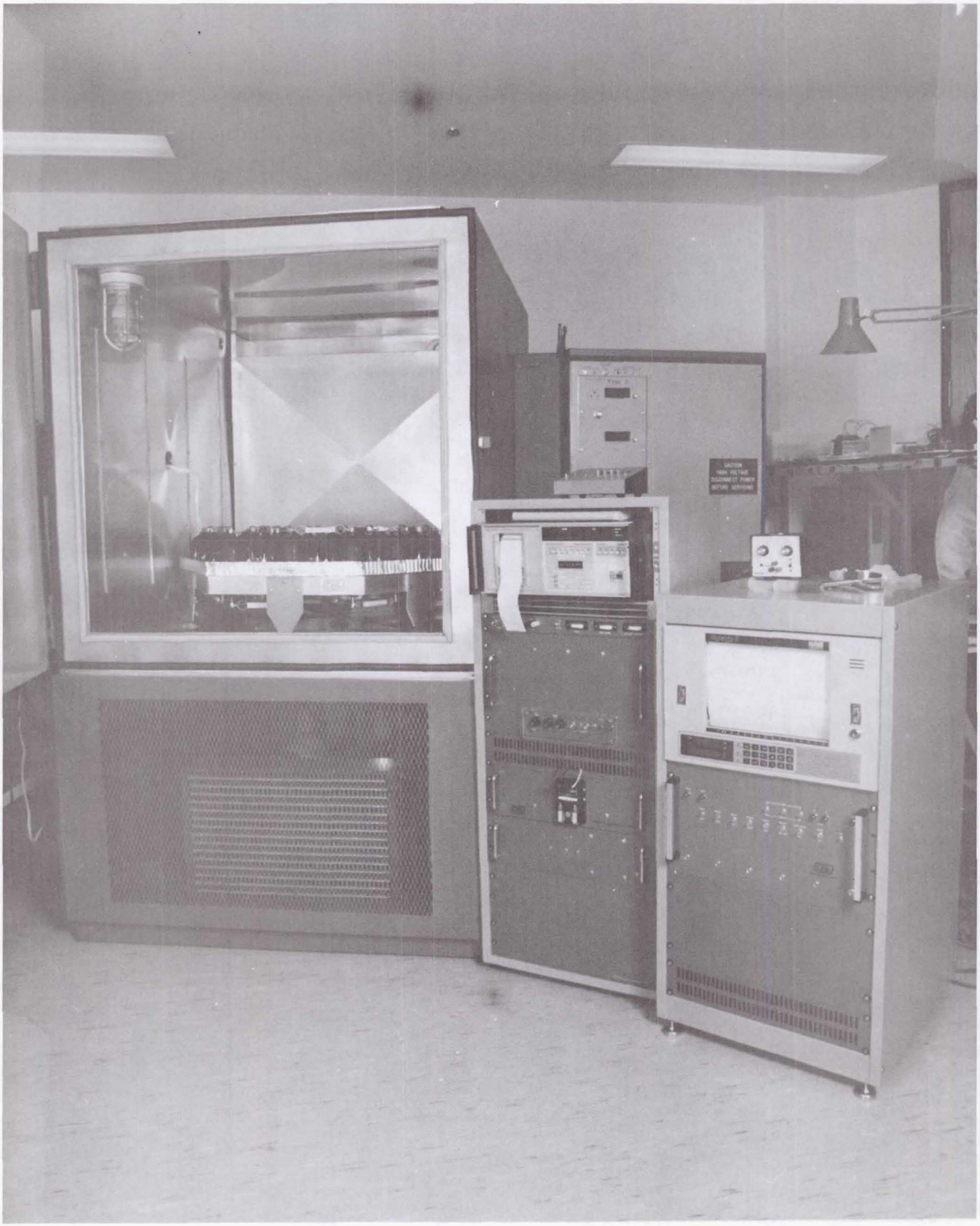

Figure 10. CAL's NiH_2 TEST FACILITY

1985 Goddard Space Flight Centre
Battery Workshop

Goddard Spaceflight Centre
Greenbelt, Maryland
Nov. 19-21, 1985

TITLE: Investigation of Nickel Hydrogen Battery Technology for the RADARSAT Spacecraft

D.A. McCoy
RADARSAT Spacecraft Engineer
Communications Research Centre
Dept. of Communications

J.L. Lackner
Energy Conversion
Systems Electrochemist
Defence Research
Establishment Ottawa
Dept. of National Defence

The Low Earth Orbit (LEO) operations of the RADARSAT spacecraft require high performance batteries to provide energy to the payload and platform during eclipse periods. Nickel Hydrogen cells are currently competing with the more traditional Nickel Cadmium cells for high performance spacecraft applications at GEO (Geostationary Earth Orbit) and LEO. Nickel Hydrogen cells appear better suited for high power applications where high currents and high Depths of Discharge are required. Although a number of GEO missions have flown with Nickel Hydrogen batteries it is not readily apparent that the LEO version of the Nickel Hydrogen cell is able to withstand the extended cycle lifetime (5 years) of the RADARSAT mission. The problems associated with Nickel Hydrogen cells are discussed in the context of the RADARSAT mission and a test program designed to characterize cell performance is presented.

Investigation of Nickel Hydrogen Battery Technology for the RADARSAT Spacecraft

The RADARSAT spacecraft is presently in the design definition phase of development for an expected launch in 1991 by the NASA Space Transportation System. The RADARSAT system will provide navigational information for marine operations in the Canadian Arctic, Atlantic and Pacific coastal regions as well as data on renewable and non-renewable resources over the Canadian land mass. The RADARSAT spacecraft will support four earth resources sensors in a sun synchronous polar orbit at an altitude of 1007 km. The sensor complement consists of a C-Band Synthetic Aperture Radar, a microwave Scatterometer and two optical imaging instruments. The on orbit configuration is depicted in Figure 1. The spacecraft is designed for five years of operations with an extension of the mission life to at least 8 years by on orbit servicing to upgrade equipment and instruments.

The RADARSAT mission requires the operation of sensors in sunlight and eclipse to provide the necessary coverage of the Canadian arctic and land mass. This requirement has influenced the design of the power supply system supporting the payload by requiring approximately 2 kW-hr of stored energy during eclipse. An example of a typical power consumption profile for the RADARSAT mission is shown in Figure 2.

A rough estimate of battery mass needed to supply this energy may be calculated by applying average power densities for battery systems as reported in the literature. Based on values of 40 W-Hr/kgm a Nickel Hydrogen battery system operating at 50% depth of discharge would have a mass of 75 kgm. while a Nickel Cadmium system would have a mass of 120 kgm. to supply the eclipse power requirement for RADARSAT. In the limited viewpoint of mass, Nickel Hydrogen batteries appear to be the best candidate for supplying the RADARSAT eclipse energy requirements. However, there are other factors of concern in comparing Nickel Hydrogen batteries to Nickel Cadmium batteries for the RADARSAT spacecraft. In particular, RADARSAT will have a design life of 5 years and will require a cycle lifetime of about 25,000 cycles. Based on data presently available it is not clear that Nickel Hydrogen cells are capable of providing the needs of RADARSAT for a 5 year mission while a data base for Nickel Cadmium cells in excess of the RADARSAT cycle life requirements does exist. Although the mass penalty associated with the use of Nickel Cadmium cells is undesirable to the RADARSAT spacecraft, the baseline design has adopted Nickel Cadmium over Nickel Hydrogen because of the issue of cycle lifetimes.

Notwithstanding the Nickel Cadmium baseline for the spacecraft a test program to evaluate Nickel Hydrogen battery technology has been initiated to develop a data base for a low earth orbit (LEO) RADARSAT type mission for future applications. The RADARSAT Nickel Hydrogen Battery Technology test program has been designed to address basic technology issues of concern to the project.

As mentioned previously, cycle lifetime is a prime concern in the use of Nickel Hydrogen cells. However, a number of other concerns are prominent and are often related to the cycle lifetime issue. The choice of separator material is an important decision that will affect the final performance of the cell as well as affecting a somewhat less observable phenomenon of electrolyte recirculation. This feature appears to be an important point in the higher current applications such as the RADARSAT mission and the test program will address the issue to some degree by comparison of cells with Asbestos separators to those with Zircar separators. Wicking has been incorporated in both types of cells to aid electrolyte recirculation. A schematic representation of the cell configuration for the RADARSAT NiH2 test cells is given in Figure 3 along with the general shape of the separator materials used.

The operational use of Nickel Hydrogen cells for a LEO regime raises questions concerning charge strategies since the exothermic charge regime produces high power dissipations that influence the design of thermal radiators. A representative analysis of this effect is depicted in Figure 4 which is based on a RADARSAT battery thermal analysis by British Aerospace. To address this issue, tests will be performed to study this characteristic and to try to reduce the heating effect by limiting charging in the highly exothermic region. Charge control methods considered are rate of change of temperature, as well as rate of change of pressure differentials and the standard voltage and capacity C/D measurement. The RADARSAT cells are fitted with pressure transducers and other sensing elements to investigate these control methods.

Self discharge is also of concern from an operational point of view and tests will be performed to characterize the phenomenon for the RADARSAT cells.

A flowchart of the testing plan for the RADARSAT NiH2 cells is shown in Figure 6. Two types of tests are identified in the charts, these being short term performance tests and long term life cycle tests.

The short term tests are performed in advance of cycle life tests to identify the performance characteristics of the NiH2 cells for comparison to other designs. The issues discussed above will be addressed via these tests in addition to standard issues such as the nature of cell capacities in relation to discharge current, which are important parameters to a spacecraft such as RADARSAT where discharge currents can approach C values.

Following tests to establish baseline performance of the cells, cycling tests will be performed with an attempt at following the expected operating profile of the RADARSAT spacecraft. The test format for the eight cells is shown in Figure 7.

Four cycling tests will run simultaneously on 2 cells each. The use of 2 cells permits a premature failure of one cell without a complete loss of data since one cell will continue to cycle. Two of each type of separators will experience cycling regimes resulting in a depth of discharge of about 50% rated capacity to about 80% rated capacity. This will permit an evaluation of each separator over a range of DOD. The higher depth of discharge rate may also permit an evaluation of accelerated life cycle testing wherein cycle life is related to depth of discharge.

Summary

The RADARSAT mission will require batteries capable of operating under extended cycle lifetimes on the order of 25,000 cycles to satisfy mission requirements. At the same time the batteries must satisfy constraints with respect to mass and volume as well as the interrelationship between current, amp hour capacity and depth of discharge. At present, the state-of-the-art in battery technology suggests Nickel Hydrogen cells are not proven for LEO operations and the diversity of design and opinion in the industry attests to the need for detailed study of the technology in advance of a commitment to fly. Although a decision to baseline Nickel Cadmium cells has recently been made, the RADARSAT program recognizes the value of Nickel Hydrogen systems for future applications and is proceeding with a test program to assess the technology. Future missions may then take advantage of the benefits accruing from Nickel Hydrogen systems without the risk of limited data.

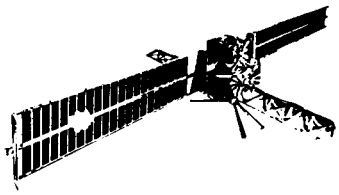

RADARSAT PROGRAM

MISSION OBJECTVES

- MONITOR ICE FORMATIONS IN CANADIAN COASTAL ZONES AND SHIPPING LANES, RENEWABLE LAND RESOURCES AND GEOLOGICAL EARTH FEATURES WITH C BAND SYNTHETIC APERATURE RADAR (SAR).
- OCEANS SEA STATE, WIND DIRECTION AND VELOCITY WITH A KU BAND SCATTEROMETER.
- REMOTE SENSING OF LAND MASSES FOR RENEWABLE AND NON-RENEWABLE RESOURCES, WITH OPTICAL SENSOR.

COVERAGE FOR SAR

- DAILY COVRAGE OF CANADIAN ARCTIC.
- 16 DAY WORLD REPEAT CYCLE.
- 3 DAY SUB CYCLE OVER CANADIAN LAND MASS.

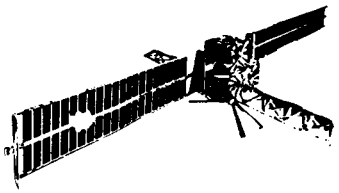

RADARSAT PROGRAM

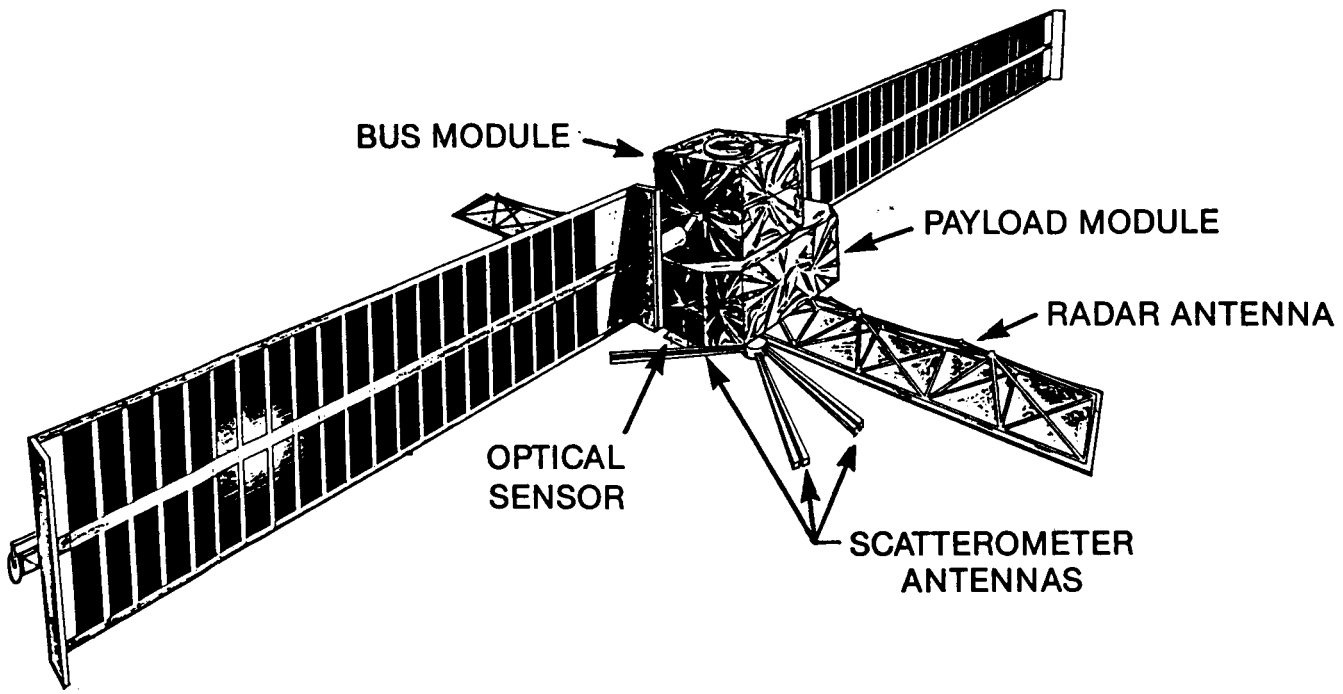

RADARSAT ON-ORBIT CONFIGURATION

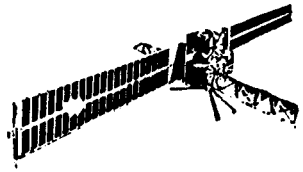

RADARSAT PROGRAM

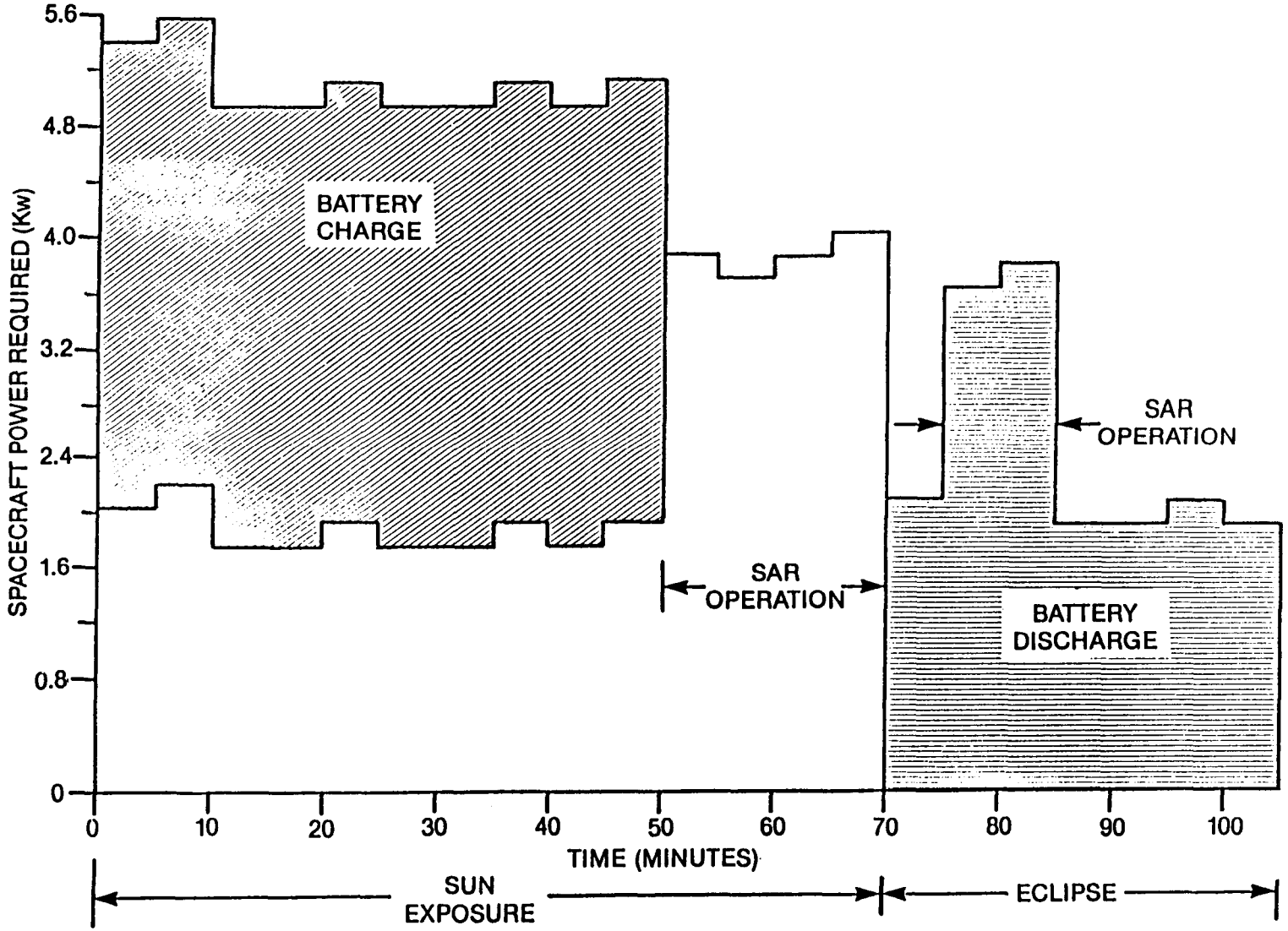

TYPICAL RADARSAT POWER TIMELINE (FOR DEMONSTRATION ONLY)

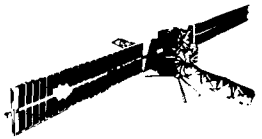

RADARSAT PROGRAM

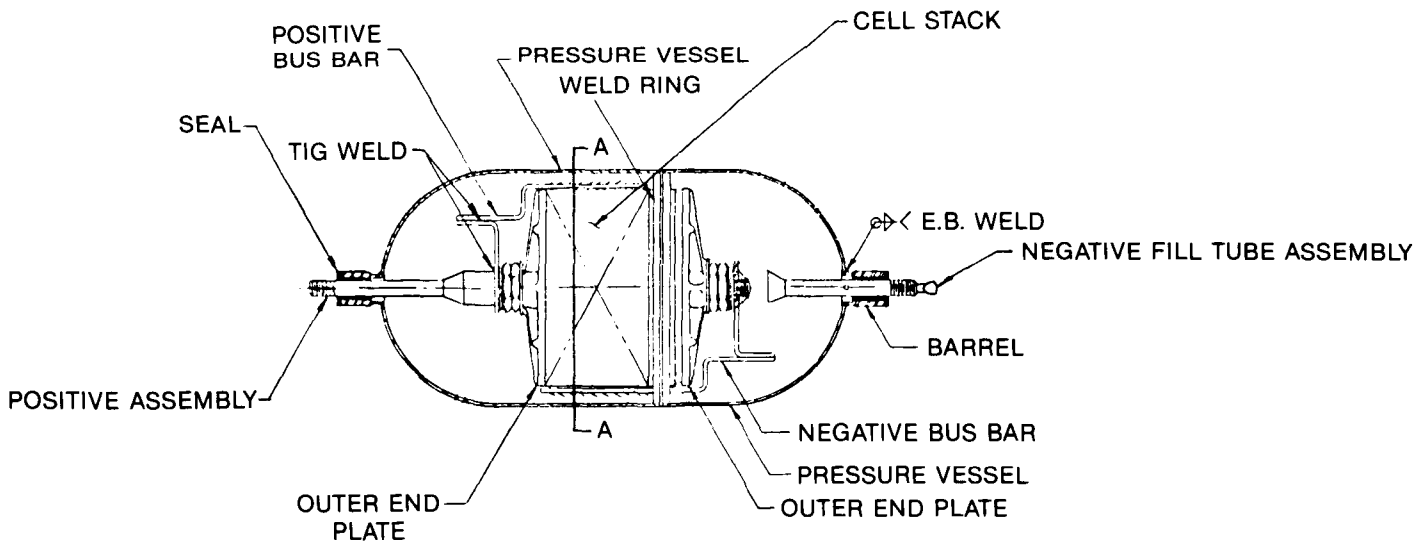

STANDARD INTELSAT CELL DESIGN

ASBESTOS SEPARATOR

ZIRCAR SEPARATOR

RADARSAT NICKEL HYDROGEN CELL CONFIGURATIONS

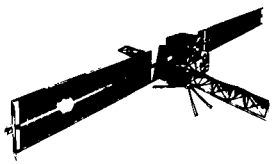

RADARSAT PROGRAM

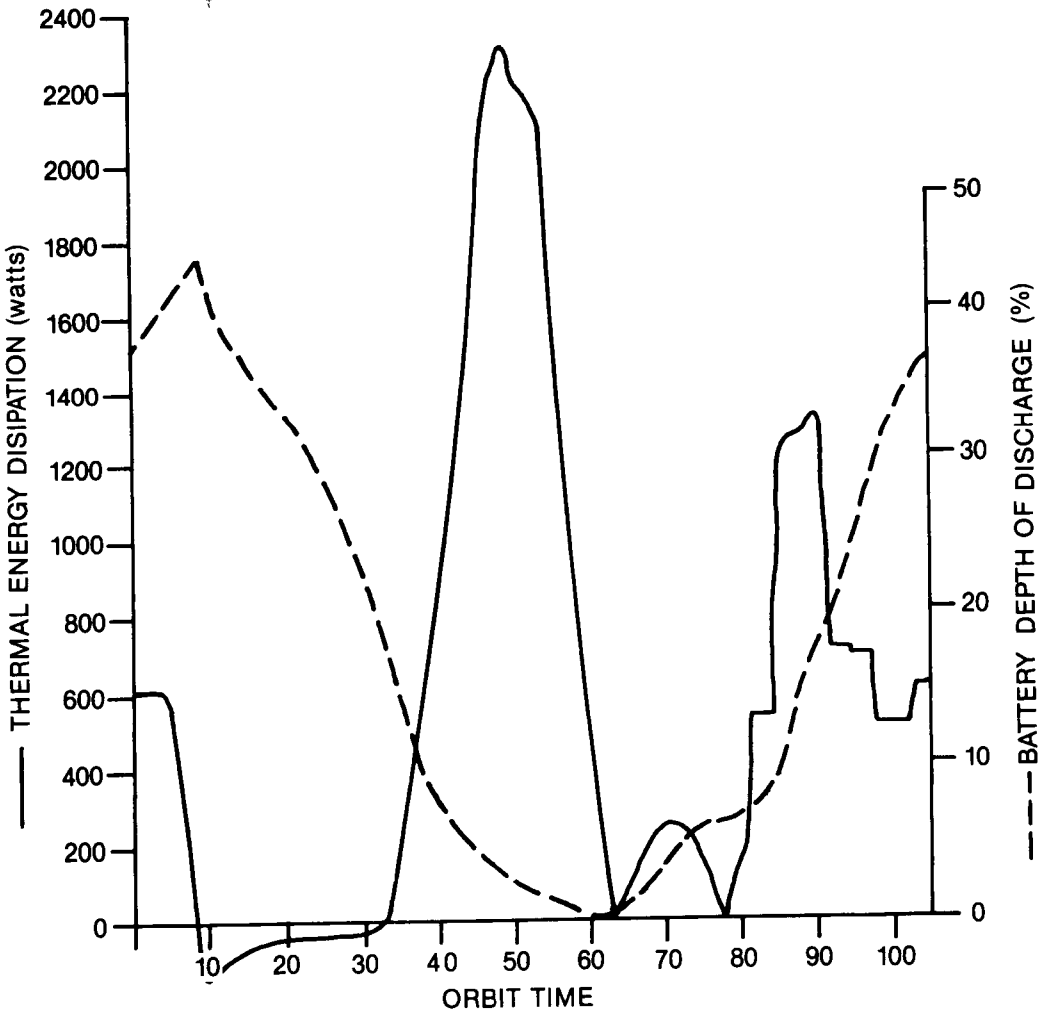

NICKEL HYDROGEN BATTERY THERMAL MODEL

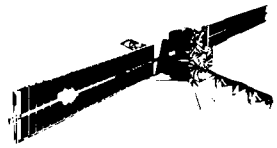

RADARSAT PROGRAM

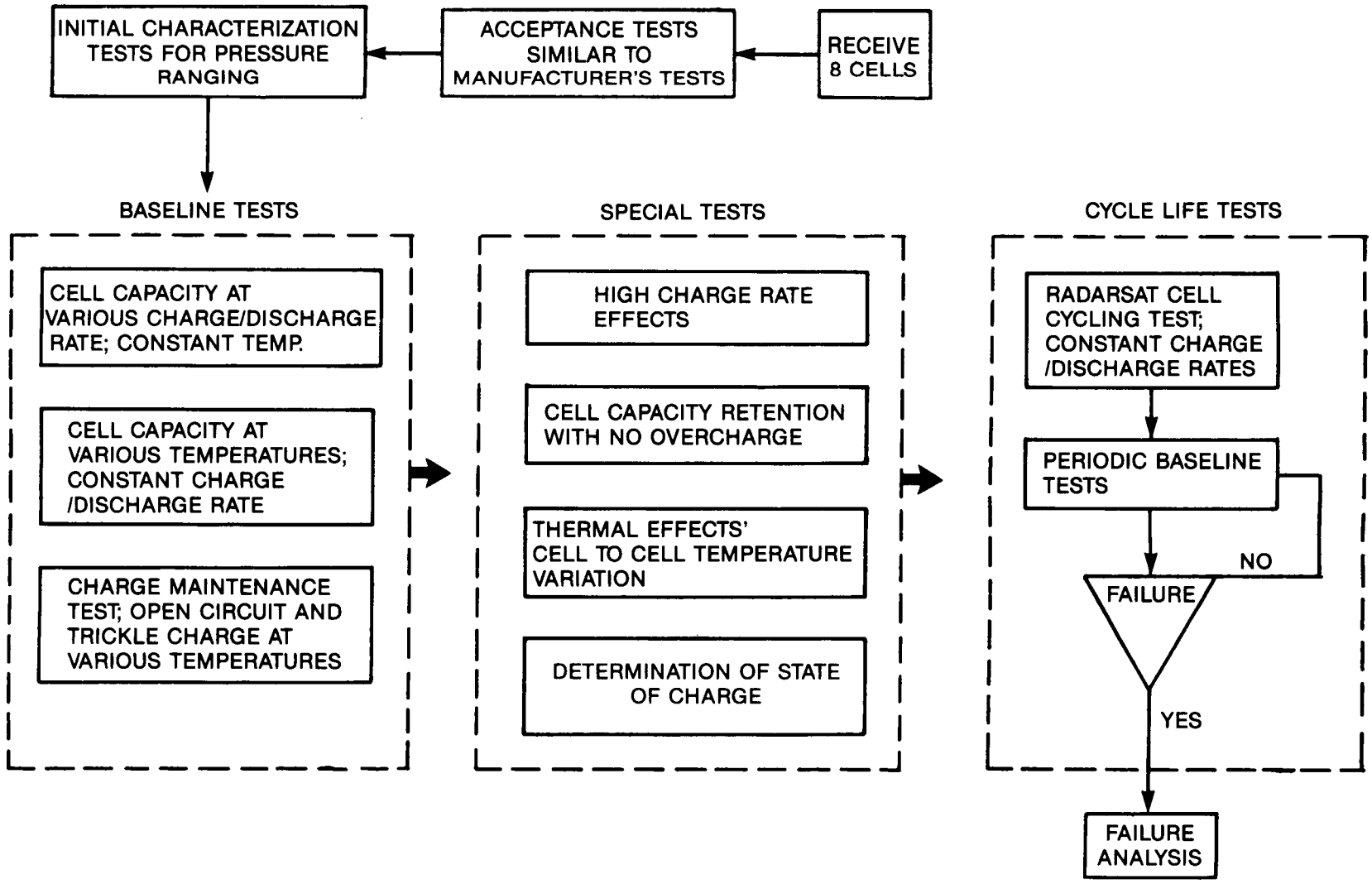

RADASAT NICKEL HYDROGEN CELL TEST PROGRAM FLOW CHART

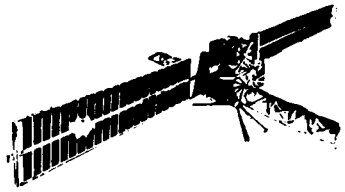

RADARSAT PROGRAM

	50% DOD	80% DOD	
50 AMP-HR CELLS WITH ASBESTOS SEPARATORS	2	2	ALL CELLS ON RADARSAT ORBIT TIMELINE
50 AMP-HR CELLS WITH ZIRCONIUM OXIDE SEPARATORS	2	2	

RADARSAT
NICKEL HYDROGEN CELL CYCLE TEST MATRIX

RADARSAT PROGRAM

SUMMARY

- THE RADARSAT SPACECRAFT IS CHALLENGING THE STATE-OF-THE-ART IN AEROSPACE BATTERY DESIGN.
- NICKEL HYDROGEN BATTERIES APPEAR TO BE THE BEST CHOICE BUT CYCLE LIFE IS UNKNOWN AT PRESENT.
- TESTS ARE UNDERWAY TO CHARACTERIZE NICKEL HYDROGEN CELLS FOR RADARSAT.
- PROBLEMS TO BE ADDRESSED BY THE RADARSAT NICKEL HYDROGEN CELL TEST PROGRAM ARE:
  - BASIC CELL CAPACITY AT VARIOUS CHARGE/DISCHARGE RATES AND VARIOUS TEMPERATURES.
  - CHARGE MAINTENANCE DURING CELL INACTIVE PERIODS.
  - STATE-OF-CHARGE MEASUREMENT METHODS AND OPERATIONS IN ENDOTHERMIC REGIME FOR THERMAL CONTROL.
  - CYCLE LIFE OF NICKEL HYDROGEN CELLS IN SIMULATED RADARSAT OPERATIONAL SCENARIO.
  - RELATIVE PERFORMANCE OF ZIRCAR AND ASBESTOS SEPARATORS.
- GENERATE CONFIDENCE IN BATTERY DESIGN FOR RADARSAT SPACECRAFT FOR 5 YEARS OF OPERATIONS IN LOW EARTH ORBIT

NICKEL-HYDROGEN LOW-EARTH-ORBIT TEST PROGRAM

Joseph K. McDermott
Martin Marietta Denver Aerospace
Denver, Colorado

ABSTRACT

The incorporation of nickel-hydrogen technology for low-earth-orbit (LEO) spacecraft applications require the establishment of a data base. An extensive test program has been established to provide this data base. This paper outlines the test program and presents preliminary test results.

INTRODUCTION

The vast majority of spacecraft secondary energy storage systems flown in the last two decades were nickel-cadmium batteries. Such applications took advantage of the inherently long cycle life, a good specific energy and high reliability. The hermetically-sealed nickel-cadmium system required a sophisticated charge control system, however, and as a result of temperature sensitivity required operation under close environmental control. Increasing spacecraft power requirements dictated the need toward a higher performance battery system capable of a 10 year mission life with deeper depths-of-discharge (DOD's) and variable load profiles. In the past, the extensive data base for nickel-cadmium systems had restrained aerospace contractors from investigating alternative energy storage systems. However, the limitations of nickel-cadmium batteries, particularly usable energy density, have provided strong economic incentives for a new system, and led to the recent development in nickel-hydrogen cell technology.

Nickel-hydrogen cell and battery technology has matured to the point where a viable choice now exists for current and future aerospace energy storage applications. The nickel-hydrogen system offers a true hermetically sealed design capable of thousands of maintenance free cycles without need for complex charge control circuitry or close environmental control. The real potential of nickel-hydrogen systems has aroused aerospace contractors to conduct in-house studies and investigate the feasibility of nickel-hydrogen implementation. Nickel-hydrogen cell technology represents the best engineering choice for numerous power storage systems, and with the

establishment and expansion in its data base, which is presently insufficient (ref. 1), the nickel-hydrogen system will become the practical choice.

Nickel-hydrogen battery cell technology has been successfully demonstrated for geosynchronous (GEO) orbit applications, both by ground testing and in-flight performance. The GEO data base cannot, however, be extrapolated to provide pertinent LEO data. Applications of nickel-hydrogen technology in LEO require the development of a cycle life data base with DOD's in the 40% to 60% range. A nickel-hydrogen test program was thus established to provide this LEO data base.

TEST PLAN

Table 1 identifies the suppliers and numbers of cells procured for nickel-hydrogen LEO testing. Eagle-Picher and General Electric were selected for the procurement of 36 Air Force designed nickel-hydrogen cells. Six (6) Yardney cells were also procured. Four cells from Eagle-Picher are identified on Table 1 as COMSAT designed cells. Eagle-Picher provided these cells to Martin Marietta for LEO testing. The general concensus by the aerospace industry is that the COMSAT cell is not adequately designed for LEO application. The addition of the four COMSAT cells to the test program will possibly provide evidence to either support or negate this assumption.

The matrix for the nickel-hydrogen testing is summarized in Table 2. The primary area of interest is 40% DOD. This would translate into appreciable weight savings when compared to nickel-cadmium systems (ref. 2). It is also assumed that 40% DOD is a conservative test parameter. The test temperature of 10°C is based on the present thermal design capabilities of typical spacecraft (ref. 3). Vendors predict that 20,000 cycles at 40% DOD and 10°C is attainable with their nickel-hydrogen cells. The 60% DOD test will serve two main purposes: first accelerate the testing and provide early failure rate data; and second, characterize cell performance at a higher DOD. The added temperature of 20°C is of interest because further weight and cost savings could be possible if the requirement for maintaining battery temperature was less stringent. All testing conducted under this matrix will be a 90 minute LEO regime consisting of a 55 minute charge and a 35 minute discharge. The 90 minute LEO is generic, and also accelerates testing to an extent. The charge control parameter was considered to be a significant factor with regard to LEO testing. Analysis of test equipment capabilites and the results of preliminary testing support charge control utilizing a current integrator. Charge control is therefore maintained by ending the charge and discharge phase after a predetermined capacity is achieved. A recharge fraction roughly between 1.05 and 1.10 (dependent upon test temperature and cell life) will be maintained for all testing.

TEST PROCEDURE

All the nickel-hydrogen cells subjected to Life Cycle Tests have aluminum collars. The collars provide cell support to the test fixture and aid in thermal management. All cells are tested in the horizontal position. Possible problems have been identified with testing in the vertical position, therefore the horizontal testing requirement was imposed. It is also the general concensus that testing the cells in the horizontal position will aid electrolyte distribution within the cell. The test fixture for mounting and thermal management consists of copper tubing pressure-fitted between two aluminum plates. Each test fixture has mounting provisions for four cells. The test fixtures are then mounted in an environmental test chamber. The test fixture temperature is controlled by a circulator bath. The chamber temperature is set to match the test fixture. Preliminary test data shown in Figure 1 indicates the delta temperature between cell case and test fixture is less than 5°C during LEO testing.

Nearly all the nickel-hydrogen cells tested have strain gages. The strain gages allow the cell pressure to be monitored during LEO testing. Possible charge control utilizing cell pressure data has been proposed for nickel-hydrogen cells, but for our test program the pressure data is for characterization purposes only. It has been shown that a direct relationship exists between the state-of-charge and the pressure of a nickel-hydrogen cell (ref. 4, 5).

Table 3 outlines the actual test parameters for nickel-hydrogen LEO testing. The discharge capacity for the 40% DOD testing is set at 20.0 ampere-hours. This translates into a discharge current of 34.4 amperes. The charge current for the 40% DOD testing is set between 22.9 amperes and 24 amperes. Depending upon cell test temperature and life, the recharge fraction is set between 1.05 and 1.10 by adjusting the charge current. The end of a discharge phase is when 20.0 ampere-hours has been removed. The end of a charge phase is when 21 to 22 ampere-hours (dependent upon test temperature and life) has been returned. The 60% DOD testing follows the same recharge fraction control scenario as the 40% DOD testing. The discharge current for 60% DOD testing is set at 51.5 amperes while the charge current is set between 34.3 amperes and 36.0 amperes.

For each test group, a representative cell will be temperature monitored to thermally characterize the cell and test fixture (equipment). The coolant plate will also contain thermocouple(s) to ensure test temperature is held as close to 10°C or 20°C as possible. Cell pressure will be monitored by strain gages. This data will be utilized for characterization purposes only and will be reported in the future. Due to safety concerns, all testing was conducted in an enclosed environmental chamber equipped with a nitrogen purge system.

The definition of a cell failure during life cycle tests is the inability of a cell to support an end-of-discharge voltage of 1.0 volt. At the discretion of the test engineer, an attempt may be made to recondition the cell. Cells which cannot support a 1.0 volt end-of-discharge voltage will be removed from the test group. Life cycling will then continue on the remaining cells. Analysis of the data from a failed cell will determine final cell disposition.

A capacity test will be conducted every 1,000 cycles starting with cycle 0. The capacity test will consist of a cell discharge to 1.0 volt, followed by a 16 hour charge at 5.0 amperes, followed by a 25.0 ampere discharge to 1.0 volt per cell. The objective of the capacity test is to characterize cell degradation in relationship to LEO cycling. The capacity check may also be in effect a reconditioning cycle, due to the fact the cell is fully recharged. The data from the capacity test may also indicate possible electrochemical changes within the cell associated with LEO cycling.

TEST RESULTS

Test results to date are primarily focused around the first delivery of 12 Air Force designed nickel-hydrogen cells and the four COMSAT cells. The Acceptance Test Procedure (ATP) conducted at the vendor on the twelve Air Force designed nickel-hydrogen cells during late May 1985 revealed a capacity range of 59.8 to 63.2 ampere-hours (10°C test, 34.4 ampere discharge to 1.0 volt per cell). Final ATP testing at the vendor was completed in June 1985. The cells were first tested in the Power Sources Laboratory in late July 1985. Initial capacity checks (five continuous cycles) consisting of a 5.0 ampere charge for 16 hours followed by a 25.0 ampere discharge to 1.0 volt per cell revealed a fourth cycle capacity range of 45.0 to 48.2 ampere-hours. Table 4 lists the capacities for both the vendor ATP data and the fourth cycle capacity check conducted in-house. The in-house capacity discharge was continued to an end-of-discharge voltage of 0.5 volt. Significant residual capacity was noted in the cells as shown in Table 4. A typical capacity discharge cycle is depicted in Figure 2. A second, distinct voltage plateau can be seen at 0.7 volt. All twelve nickel-hydrogen cells shared this second plateau characteristic.

The first twelve vendor cells were divided into two groups. The first test group consisted of eight series-connected cells tested at 10°C and 60% DOD. The initial capacity (25.0 A to 1.0 V/cell) of this cell/battery test group was 55.1 ampere-hours. Figure 3 depicts the end-of-discharge voltage and recharge fraction plots for this test to date. The remaining four cells were series-connected and placed on tests at 20°C and 60% DOD. The initial capacity of this cell/battery test group was 44.0 ampere-hours. Figure 4 depicts the end-of-discharge voltage and recharge fraction plots for this four cell test group to date.

The four COMSAT cells were series-connected and placed on tests at 10°C and 40% DOD. The initial capacity of this four-cell test group was 62.5 ampere-hours. Figure 5 depicts the end-of-discharge voltage and recharge fraction plots for this four-cell test group to date.

Testing has not been initiated to date on the 24 recently received vendor cells nor the 6 Yardney cells. LEO testing on these cells will be underway by December 1985. The addition of 36 more cells to the test program in 1986 will be the final group of cells procured for this test plan.

CONCLUSIONS

The significant loss of capacity observed in the first group of nickel-hydrogen cells from ATP testing to our initial capacity testing has several possible causes. The activation procedure for these cells followed Rev F of the "Product Specification Nickel-Hydrogen Battery Cell" (ref. 6). A hydrogen precharge of 40 psig is completed immediately prior to the conditioning cycles and ATP testing. The hydrogen precharge has recently been deleted from the specification, and nickel-hydrogen manufacturers have suggested that the hydrogen precharge of 40 psig may have caused the noted capacity degradation and resultant double-knee or second plateau discharge. The twelve cells were in a stored, shorted condition for approximately six weeks, and it has been postulated that during this period the hydrogen precharge reacted with and changed the positive plate. At the present time, extensive studies are underway by the vendor to characterize this positive plate change. It was decided that for the second cell build of 24 cells a revised cell activation procedure would be utilized. The 40 psig precharge was reduced to a one atmosphere precharge, or approximately 16 psig. Hopefully, this change will minimize the capacity loss observed on the first twelve cells. The twenty-four cells recently received will undergo the same receiving, inspection and initial capacity tests as the first twelve to ensure an accurate evaluation of the revised activation procedure. No other parameters in the manufacturing of the cell have been revised. Tests are scheduled for November 1985 on the second build of twenty-four cells.

Cells under LEO cycling have nearly 1000 cycles to date, therefore it is too early yet to draw any conclusions regarding nickel-hydrogen performance. Test control parameters were initially identified as major items for an accurate and reliable test program. Early tests have shown the most reliable method for charge control is ampere-hour integration. The coolant fixtures have been shown to provide excellent thermal conductivity for the removal of heat from the cells. Test control parameters have been optimized, and hopefully cells under the LEO test program will meet the goal of 20,000 cycles.

REFERENCES

1. "An Industry and Government Survey: A Nickel-Hydrogen Testing Data Base", Charles Badcock and Martin Milden, The 1984 Goddard Space Flight Center Battery Workshop, p. 583.

2. "Nickel-Hydrogen Spacecraft Module Configurations Study", William B. Collins, Joseph K. McDermott and Owen B. Smith, The 1984 Goddard Space Flight Center Battery Workshop, p. 459.

3. "In-Flight Performance of a Six Ampere-Hour Nickel-Cadmium Battery in Low-Earth-Orbit", Joseph K. McDermott, The 1983 Goddard Space Flight Center Battery Workshop, p. 325.

4. "The Open Circuit Stand Behavior INTELSAT VI Nickel-Hydrogen Batteries and Its Relationship to Charge Rates and Temperature", P. F. Ritterman and A. M. King, Proceedings of the 20th Intersociety Energy Conversion Engineering Conference, p. 1.176.

5. "The GSTAR and SPACENET Nickel-Hydrogen Batteries for Geosynchronous Orbit Applications", Stephen J. Gaston, Proceedings of the 19th Intersociety Energy Conversion Engineering Conference, p. 259.

6. "Product Specification Nickel-Hydrogen Battery Cell, PS 32014-031 Ref F", Hughes Aircraft Company, 23 June 1980.

C-5

TABLE 1. CELL SUPPLIERS FOR LEO TEST PROGRAM

CELL SUPPLIER	CELL TYPE	NUMBER OF CELLS PROCURED	STATUS
EAGLE-PICHER	AIR FORCE	36	12 CELLS RECEIVED 07/85 24 CELLS RECEIVED 10/85
EAGLE-PICHER	COMSAT	04	04 CELLS RECEIVED 08/85
GENERAL ELECTRIC	AIR FORCE	36	20 CELLS SCHEDULED FOR DELIVERY 01/86 16 CELLS SCHEDULED FOR DELIVERY 02/86
YARDNEY	MAN-TECH	06	06 CELLS RECEIVED 10/85

TABLE 2. NICKEL-HYDROGEN LEO TEST MATRIX

DEPTH-OF-DISCHARGE / TEST TEMPERATURE	40%	60%
10°C	16 EP CELLS 16 GE CELLS 6 YARDNEY CELLS 4 EP COMSAT CELLS	8 EP CELLS 8 GE CELLS
20°C	8 EP CELLS 8 GE CELLS	4 EP CELLS 4 GE CELLS

TABLE 3. NICKEL-HYDROGEN LEO TEST PARAMETERS

TEST TEMPERATURE	DOD	DISCHARGE RATE	CHARGE RATE	RECHARGE FRACTION
10°C	40%	34.3 A	22.9 A	1.05
	60%	51.5 A	34.3 A	1.05
20°C	40%	34.3 A	22.9-24.0 A	1.05 TO 1.10
	60%	51.5 A	34.3-36.0 A	1.05 TO 1.10

TABLE 4. EAGLE-PICHER ATP CAPACITY VERSUS IN-HOUSE CAPACITY TESTS

S/N	EAGLE-PICHER ATP CAPACITY (05/29/85) 34.3 A D/C TO 1.0 VOLT	MARTIN MARIETTA CAPACITY TEST (07/31/85) 25.0 A D/C TO	
		1.0 VOLT	0.5 VOLT
1	62.8 A-HR	46.9	55.6
2	63.2 A-HR	46.5	57.1
3	61.1 A-HR	48.2	57.7
4	64.5 A-HR	47.1	57.7
5	60.6 A-HR	46.9	55.8
6	62.9 A-HR	45.0	55.2
7	60.7 A-HR	47.3	57.1
8	59.9 A-HR	46.3	56.0
9	63.4 A-HR	48.0	57.3
10	60.3 A-HR	46.1	57.3
11	60.4 A-HR	46.3	57.1
12	59.8 A-HR	45.9	55.2

COLD PLATE TEMPERATURE AND CELL TEMPERATURE LEO CYCLING CONTROL

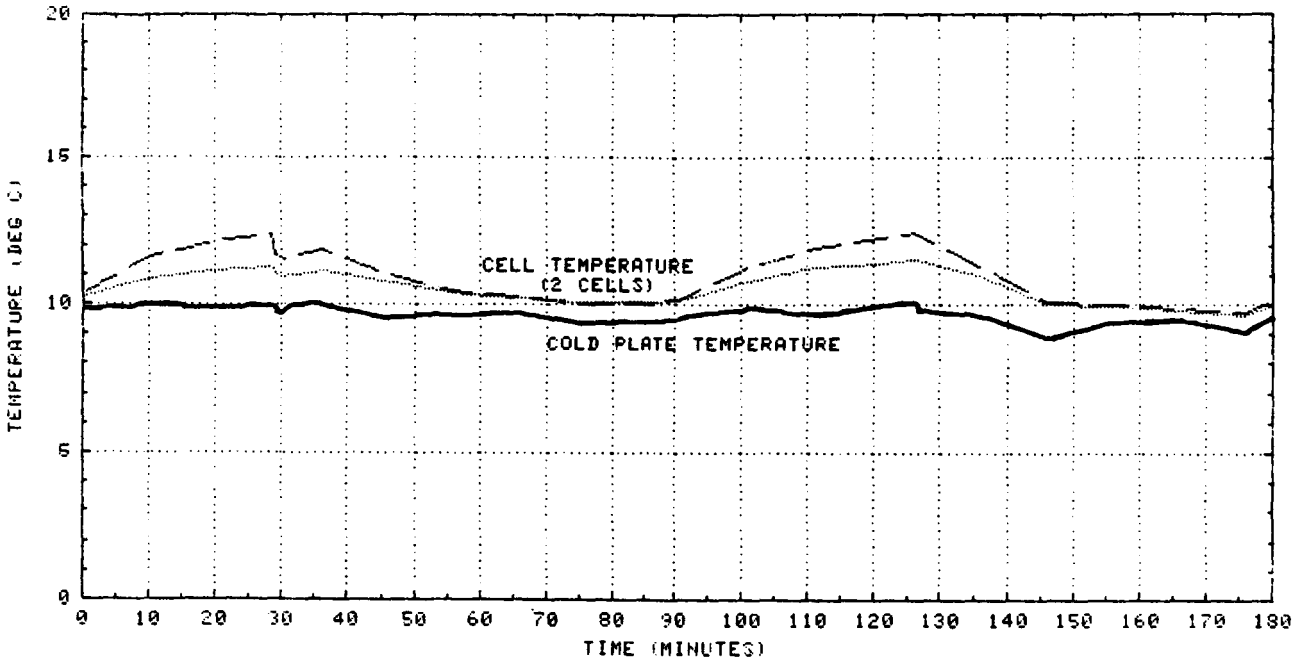

FIGURE 1

INITIAL CELL CAPACITY DISCHARGE CYCLE

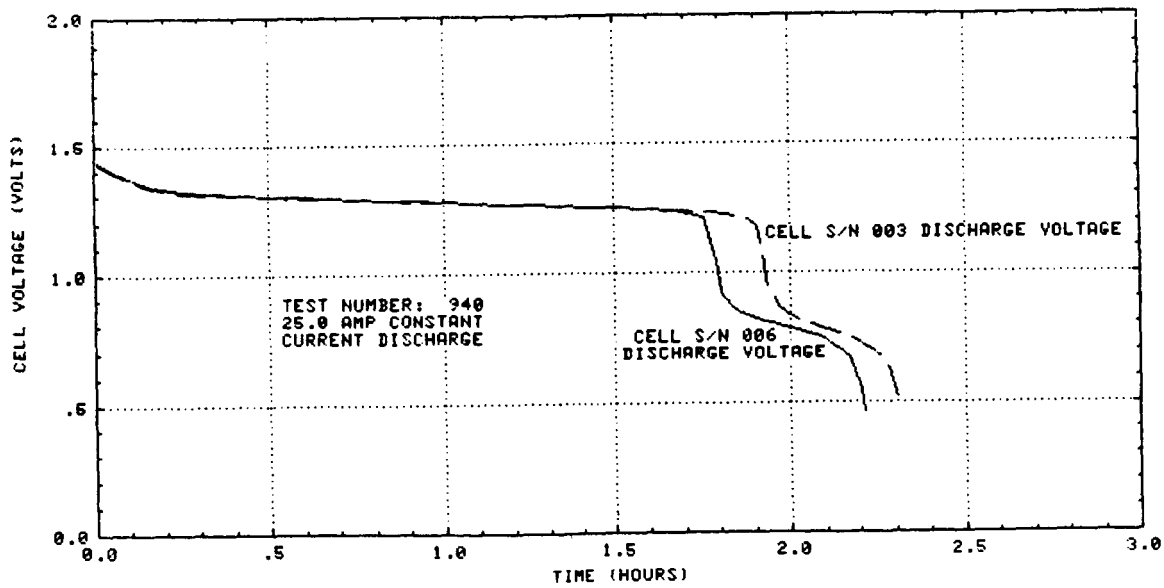

FIGURE 2

MARTIN MARIETTA

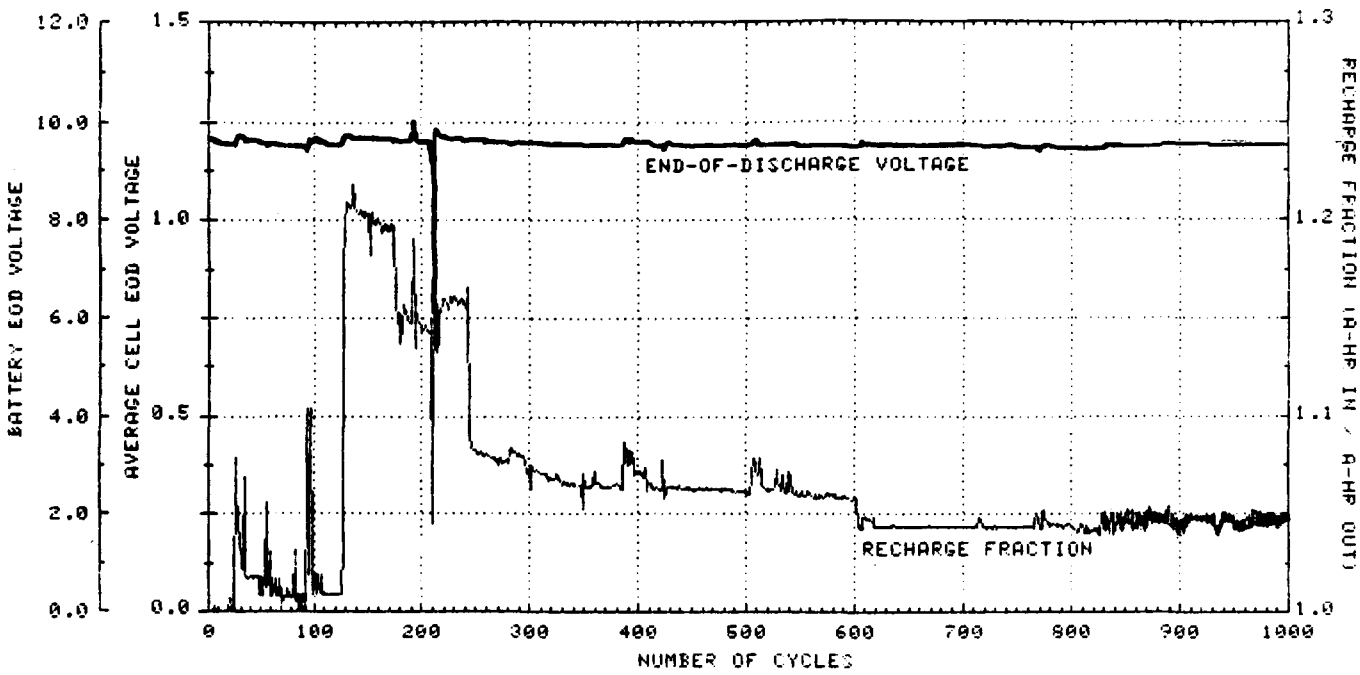

FIGURE 3

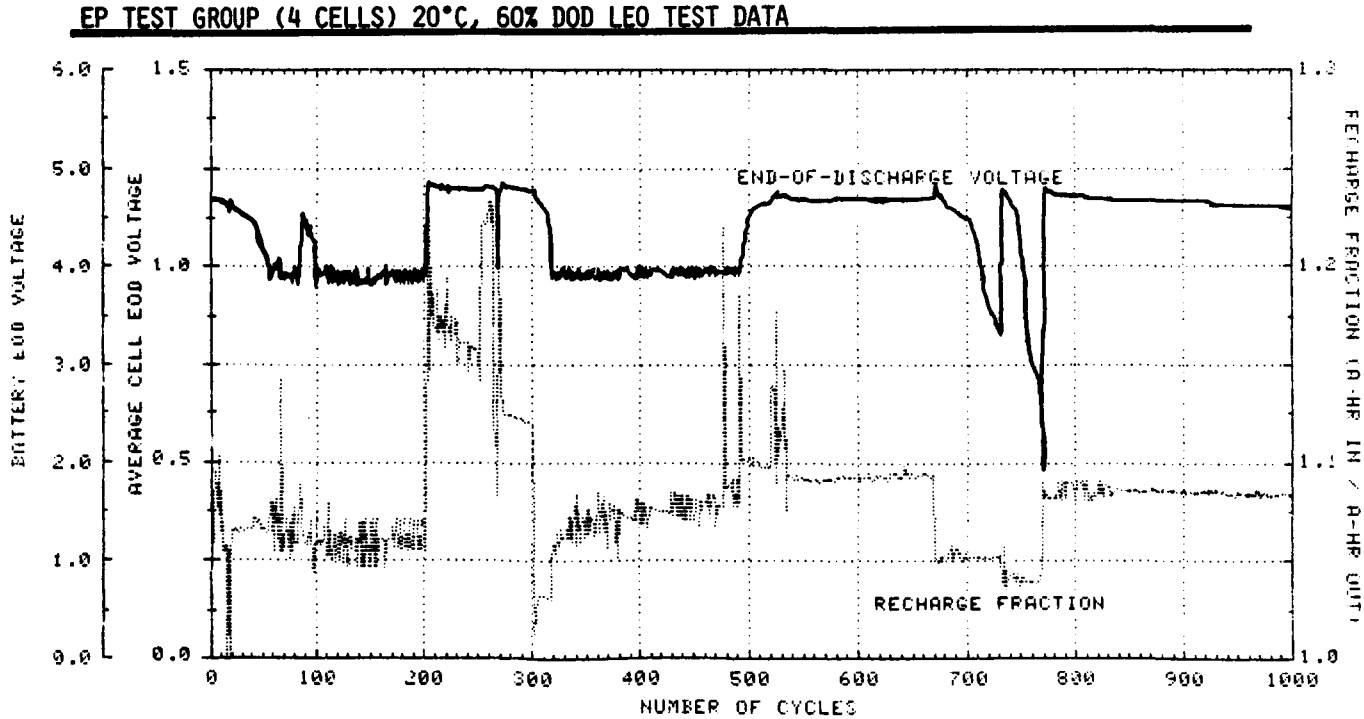

FIGURE 4

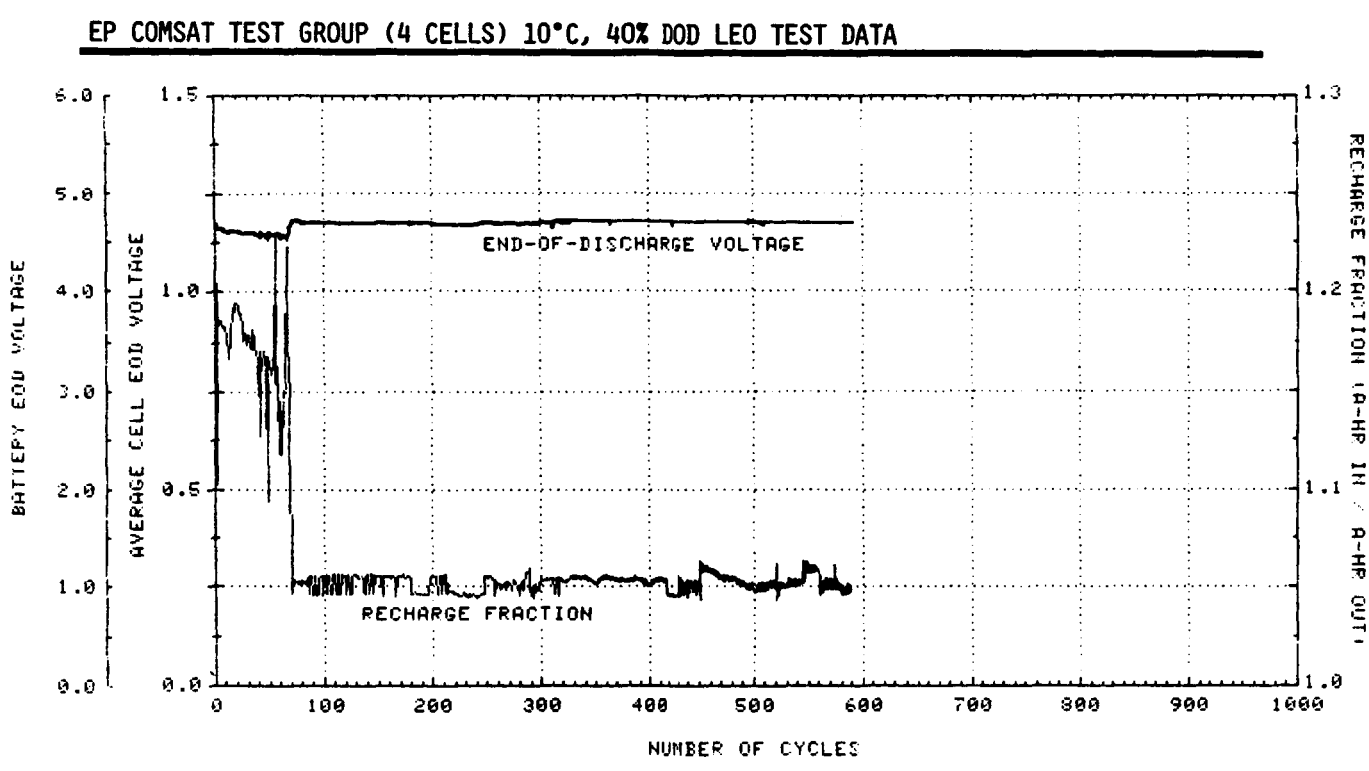

FIGURE 5

IMPACT OF SHUTTLE ENVIRONMENT ON PRELAUNCH HANDLING OF NICKEL-HYDROGEN BATTERIES

Robert S. Green
RCA Astro-Electronics Division
Princeton, New Jersey

ABSTRACT

Deployment of the ASC I spacecraft from the Space Shuttle Discovery in August 1985 set a new milestone in nickel-hydrogen battery technology. This communications satellite, built by RCA Astro-Electronics Division for the American Satellite Company, is equipped with two 35-Ah nickel-hydrogen batteries and is the first such satellite launched into orbit via the Space Shuttle.

The prelaunch activities, combined with the environmental constraints onboard the Shuttle, led to the development of a new battery handling procedure. An outline of the prelaunch activities, with particular attention to battery charging, is presented.

INTRODUCTION

On August 27, 1985, at 0702 hours EDT, the Space Shuttle Discovery lifted off from its launch pad at Cape Canaveral, carrying with it the ASC I* communications satellite built by RCA Astro-Electronics Division. ASC I is the first satellite launched into orbit via the Shuttle that is equipped with nickel-hydrogen batteries. While handling of nickel-hydrogen batteries during prelaunch activities was commonplace on the Ariane** launch vehicle, a more lengthy timeline needed to be evolved for NASA's prelaunch activities.

THE SATELLITE

ASC I is a communications satellite capable of transmitting via both C- and Ku-bands. Electrical power for satellite operation is normally supplied by solar arrays; however, two NiH_2 batteries are provided for eclipse operation and when power requirements exceed the solar array capacity during peak daytime loading. The NiH_2 batteries, having a 35-Ah nameplate capacity, are of similar design to those used on other RCA-built communications satellites.[1]

LAUNCH SITE TEST SEQUENCE

The batteries arrived at the Eastern Test Range already integrated with the satellite and in the electrically discharged condition. During the Spacecraft Electrical Performance and Evaluation Tests (SEPET), the batteries received a conditioning cycle. This included a complete charge, discharge, and electrical

* ASC I is owned and operated by the American Satellite Company.
** Ariane launch vehicle manufactured by Arianespace, launched from CSG, Kourou, French Guiana.

letdown, which served as a final conditioning cycle prior to launch and provided spacecraft-level performance data for comparison use during the prelaunch charge sequence.

The next major battery event occurred when the spacecraft was mated with the Shuttle, and prelaunch charging commenced. Between these two events, the batteries were generally kept in an electrically letdown condition, with the cell-level deep discharge resistors enabled. All active periods were kept brief, and all open-circuit stands (time periods) were minimized. This was done to facilitate safe handling of the spacecraft during other prelaunch operations. A typical ground operations flow is shown in Figure 1.

PRELAUNCH BATTERY CHARGING

When ASC I was mated with the Shuttle, the batteries were electrically drained and the deep discharge resistors enabled. Battery charging commenced with the closure of the cargo bay doors. The Shuttle environment was maintained in the 60° to 65°F (15.5° to 18.3°C) range during the first portion of the prelaunch charge to help maintain cooler batteries for a more efficient charge. This technique yielded battery temperatures similar to those experienced on Ariane-type launches. The maximum battery temperature limit of 30°C was never reached; and a successful, cool, prelaunch charge was accomplished.

The prelaunch handling goal was to maximize the battery's state of charge prior to launch. The general charge sequence is shown in Figure 2. Each battery was charged at a nominal C/20 rate (where C is its nameplate capacity) for a total input of 160% of rated capacity, then placed on C/60 (trickle) charge or C/120 (low rate trickle) charge until launch. The choice between charging at C/60 or C/120 depends upon the thermal conditions; the C/120 rate was capable of maintaining the battery's state of charge and prevented battery temperatures from rising above 30°C.

Telemetry was used to monitor battery voltage, charge current, temperatures, and sample cell pressures throughout the task. Battery temperatures throughout the C/20 charge portion were predominately in the 18° to 22°C range, with occasional brief excursions to approximately 28°C.

CONCLUSIONS

The prelaunch battery charging technique onboard the Shuttle was kept simple. A 32-hour charge portion at the C/20 rate in the 18° to 22°C range (with brief excursions to 28°C) was successfully used for the initial full charge for each battery. A low-rate trickle charge (C/120) was used to maintain the batteries in the fully charged condition until spacecraft launch from the Shuttle.

REFERENCES

1. S. J. Gaston, "The GSTAR and Spacenet Nickel-Hydrogen Batteries for Geosynchronous Orbit Applications," Proc. 19th Intersociety Energy Conversion Engineering Conference, 1984, pp. 257-263.

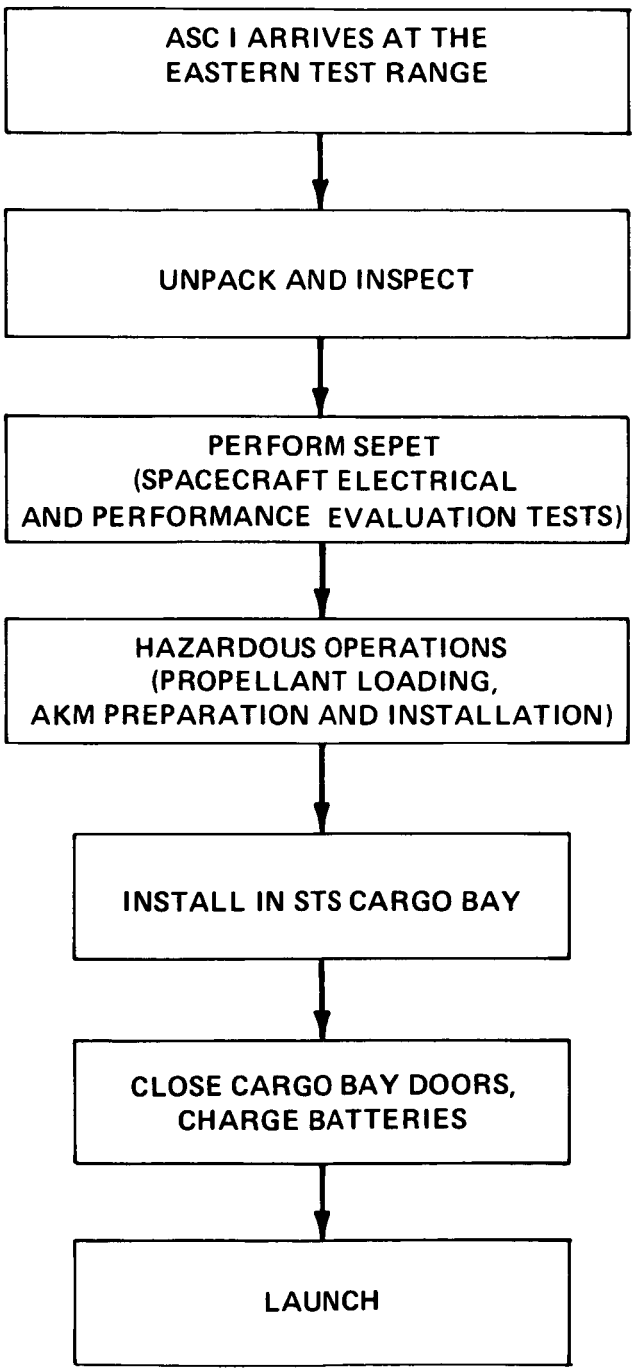

Figure 1. GENERAL KSC GROUND OPERATIONS FLOW

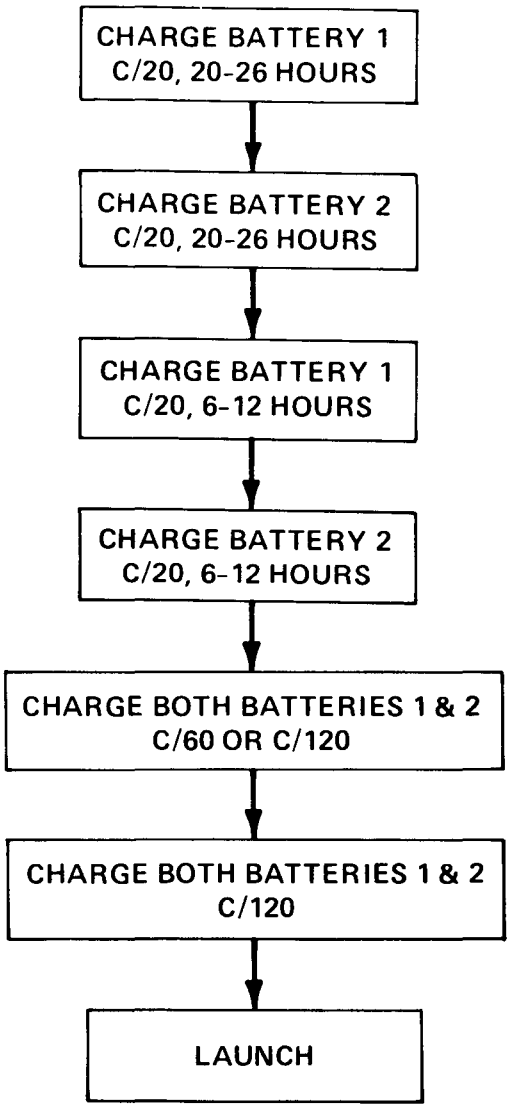

Figure 2. GENERAL PRELAUNCH CHARGE SEQUENCE

PARAMETRIC TESTS OF A 40-AH BIPOLAR NICKEL-HYDROGEN BATTERY

Robert L. Cataldo
National Aeronautics and Space Administration
Lewis Research Center
Cleveland, Ohio 44135

ABSTRACT

A series of tests were performed to characterize battery performance relating to certain operating parameters which included charge current, discharge current, temperature and pressure. The parameters were varied to confirm battery design concepts and to determine optimal operating conditions.

INTRODUCTION

Spacecraft power requirements are constantly increasing. Special spacecraft such as the Space Station and platforms will require energy storage systems of 130 kilowatt-hours and 25 kilowatt-hours, respectively. The complexity of these high power systems will demand high reliability, and reduced mass and volume. Candidate electrochemical systems are regenerative fuel cells, nickel-cadmium batteries and nickel-hydrogen batteries.

A system that uses batteries for storage will require a cell count in excess of 400 units. These cell units must then be assembled into several batteries with over 100 cells in a series connected string. In an attempt to simplify the construction of conventional cells and batteries, the NASA Lewis Research Center battery systems group initiated work on a nickel-hydrogen battery in a bipolar configuration in early 1981.

Features of the battery with this bipolar construction show promise in improving both volumetric and gravimetric energy densities as well as thermal management. Bipolar construction allows cooling in closer proximity to the cell components, thus heat removal can be accomplished at a higher rejection temperature than conventional cell designs. Also, higher discharge current densities are achievable because of low cell impedance. Lower cell impedance is achieved via current flow perpendicular to the electrode face, thus reducing voltage drops in the electrode grid and electrode terminal tabs.

BATTERY AND CELL DESIGN

The battery tested was a 12 volt (10 cell), 40 ampere-hour, bipolar battery. The battery was actively cooled with five inter-cell planar cooling plates. The cooling system was operated in the temperature range of 0 degrees centigrade to 40 degrees centigrade; allowing full thermal characterization and determination of appropriate operating temperature.

Accomodations were made for oxygen and electrolyte management. These two functions take place within an electrolyte reservoir plate that contains the oxygen recombination sites. Water, the product of recombination, equilibrates with the electrolyte of the nickel electrode. These functions and other design details are explained in greater depth in a previous paper (Ref. 1).

TEST PROCEDURES

Two initialization cycles were performed prior to characterization. The cycle regime was a C/10 (5.0A.), 13 hour charge and a C/4 (12A.) discharge terminated when the first cell reached 0.5 volts. A value of 50 A-hours was used for the capacity, C, which had been determined from previous tests results. The ampere-hours obtained on discharged the first cycle was 49, and 50 on the second cycle. The results proved that this new battery design could provide the predicted results.

Battery performance was characterized by carring out a series of parametric tests. Data was obtained at the following conditions: charge rates of C and C/2; discharge rates of 2C, C and C/4; temperatures of 0, 10, 20, 30 and 40 degrees centigrade; base pressures of 200 and 400 pounds per square inch.

Temperatures were maintained by circulating a non-conductive inert fluid through the five cooling plates of the battery. Temperatures were adjusted at static conditions and allowed to stabilize until the inlet and outlet coolant temperatures were equal. The coolant bath temperature was maintained to within 0.1 degrees centigrade by the chiller/heater unit.

The hydrogen pressure was also adjusted at the static discharged condition. The amount of hydrogen generated on charge was small compared to the free volume of the test chamber. Thus, the pressure increase from discharged to full charge was only about 25 pounds per square inch.

TEST RESULTS

Data taken for each charge/discharge cycle was as follows: individual cell voltages, temperatures, ampere-hours and watt-hours. Values were updated and integrated every 18 seconds with a digitizing voltmeter. Both charge and discharge current levels were held constant with power supplies and electronic discharge devices.

Table I and Table II display the test results of ampere-hours, watt-hours and end-of-discharge battery voltage. The remaining battery capacity was drained at the 12 ampere rate (C/4) when the discharge rate was greater than C/4. Charge input was 56 ampere-hours for each test matrix point. The data presented in Table II, 400 psi gas pressure, was a modified matrix where effects of hydrogen gas pressure could be observed at only those conditions

of greatest interest. Table III shows characterization data obtained at all pressure and temperature levels at the same charge rate of two hours and the same 50A (the C rate) discharge. The decision was made to increase the charge input to 65 ampere-hours for this series of tests for two reasons:

1) The C/4 drain resulted in total discharge capacities of 54 ampere-hours several times, thereby creating a situation of possible charge deficiency.

2) To minimize the influence of varying levels of charge acceptance of the nickel electrode at different temperatures.

Special tests were also conducted to determine battery performance beyond the normally expected range of conventional space power systems. High discharge rates and pulse discharge capabilities were tested because the bipolar battery has exhibited good performance in this area as previously reported (Ref. 2).

The battery was high rate discharged at both constant and pulsed currents for the 250A.(5C) and 500A.(10C) rates to a discharge cutoff voltage of 6.0 volts during the pulse. One additional pulse test was to discharge the battery at 1500A.(30C) for one second where a load voltage of 4.0 volts was established resulting in a 6 kilowatt pulse. This value was lower than expected from previous results (Ref. 2). This lower value of pulse power and the result of a dramatic increase in high rate capacity by pulsing compared to constant discharge level indicated that possibly the area for hydrogen gas access in the frames was not sufficient to support these high discharge rates. This problem was addressed by redesigning the gas access slots in future batteries for pulse applications.

Figure 1 shows plots of the data tabulated in Table 1 and results of the special pulse tests. Figure 1 displays battery voltage and discharge capacity as a function of discharge current at 20 degrees centigrade. The 12, 50 and 100 ampere discharge plots are characteristic of classical battery performance plots. However, the constant load discharge curves of 250 and 500 amperes do not have the standard platau and knee. This is because of the high rate discharge and possibly the decrease of hydrogen gas concentration at the electrode surface. These two tests were repeated by pulse discharging at a one second on, one second off duty cycle. The off, or relaxation time allows the gas concentration to increase in the gas cavity formed by the hydrogen electrode, gas screen and bipolar plate. The dashed curve in Figure 1 shows the increase in capacity discharged and the increase in watts and watt-hours. The greatest change is noticed of the 250 ampere level where the hydrogen gas concentration depletion is less than that of the 500 ampere rate. An increase in ratio of off to on time may have improved the pulsed performance, particularly at higher rates.

Figure 2 shows the relationship of energy delivered on discharge to battery temperature. The cooling configuration dictates that nickel electrode temperatures were equal over its entire area. A marked increase in energy delivered

and cyclic efficiency was observed at the 30 degree centigrade data point compared to both higher and lower temperatures. At temperatures lower than 30 degrees, battery voltage increases on charge and decreases on discharge causing a net decrease in efficiency. However, above 30 degrees, effects of nickel electrode charging efficiency was seen. These results indicate that a bipolar battery with intercell, planar cooling plates could operate at a higher thermal system temperature than conventional single cell designs that transmit heat in a radial direction via the vessel wall. Therefore, thermal system designs would need to consider the differences in battery design.

Figure 3 shows the battery voltage profile response to pulse discharges of 500 amperes. Only the first four cycles are shown here, although 155 pulses (21.5 ampere-hours) were discharged. The battery voltage drop during the pulse increased from 1.4 volts to 2.2 volts from beginning to end. This increase in voltage drop indicates that a 30 percent change in effective internal cell impedance occurred.

Figure 4 shows the voltage profile for a one pulse maximum power test. A 1500 ampere one second pulse was delivered. Battery voltage, measured at the external terminals of the vessel, was 4.0 volts resulting in a power level of six kilowatts. The instantaneous voltage drop was eight volts for the 1500 ampere pulse. Using these values, a cell resistance of about 0.5 milliohms was calculated.

CONCLUSIONS

The parametric tests conducted on the first actively cooled bipolar nickel-hydrogen battery demonstrates its feasibility. The results are comparable to previous NASA Lewis designs except for its high rate performance. The pulse tests conducted suggest an insufficient gas access to the hydrogen electrode which has resulted in increased polarization. This area has been addressed in other designs for high discharge rates.

The thermal aspects of this battery allow cooling system temperatures of about 30 degrees centigrade for maximum power efficiency. Battery operation in this temperature range of 30 degrees centigrade could have an impact on solar array and radiator sizing.

The NASA Lewis Research Center is working toward establishing a baseline design that would require only simple low cost modifications to the baseline design for integration into various applications. The successful application of active cooling is a major step in developing this baseline design.

REFERENCES

1. R. L. Cataldo, "Design of a 1-kWh Bipolar Nickel-Hydrogen Battery", NASA TM 83647, 1984

2. R. L. Cataldo, "Test Results of a Ten Cell Bipolar Nickel-Hydrogen Battery", NASA TM 83384, 1983

CR	DR	T	AH(OUT)	WH(IN)	WH(OUT)	EE	EODV
C	2C	0	42.4	879	468	53	9.3
C	C	0	44.4	882	533	60	10.4
C	C/4	0	49.3	883	629	71	10.8
C/2	2C	0	43.8	845	469	55	8.8
C/2	C	0	46	845	545	64	10.2
C/2	C/4	0	51.5	851	655	77	10.4
C	2C	10	43.6	856	497	58	9.5
C	C	10	46	860	557	65	9.8
C	C/4	10	51	856	648	75	10.1
C/2	2C	10	43.5	831	489	59	9.3
C/2	C	10	45	834	539	65	9.9
C/2	C/4	10	52	840	656	78	9.9
C	2C	20	45.5	843	529	63	9.5
C	C	20	47.5	842	582	69	10.1
C	C/4	20	51.5	818	652	80	8.4
C/2	2C	20	45	822	524	64	9.5
C/2	C	20	48	820	587	72	9.7
C/2	C/4	20	51.5	820	655	80	9.6
C	2C	30	43	834	505	60	10.1
C	C	30	46	834	560	67	10.5
C	C/4	30	50	832	639	77	9.5
C/2	2C	30	40	818	470	57	10.5
C/2	C	30	44	813	536	66	10.4
C/2	C/4	30	49	818	629	77	9.7
C	C	40	41.8	824	520	63	10.6
C/2	C	40	41.5	809	516	64	10.5

TABLE I Tabulated test matrix data at 200 psi where:

CR = Charge Rate DR = Discharge Rate T = Temperature
AH = Ampere-Hours WH = Watt-Hours EE = Energy Efficiency
EODV = End-Of-Discharge Battery Voltage

CR	DR	T	AH(OUT)	WH(IN)	WH(OUT)	EE	EODV
C	C	0	37	890	452	51	10.9
C/2	C	0	39	857	470	55	10.7
C	C	10	37.8	870	466	53.5	11.0
C/2	C	10	38.5	841	474	56	10.8
C	C	20	39.4	851	490	57	11.0
C/2	C	20	39.6	829	495	60	10.8
C	C	30	42.2	836	523	62.5	9.3
C/2	C	30	42.2	824	523	63.5	9.1
C	C	40	45.5	827	569	69	8.7
C/2	C	40	41.8	816	521	64	8.9

TABLE II Tabulated test matrix data at 400 psi where:

CR = Charge Rate DR = Discharge Rate T = Temperature
AH = Ampere-Hours WH = Watt-Hours EE = Energy Efficiency
EODV = End-Of-Discharge Battery Voltage

TEMPERATURE °C	PRESSURE (BASE)	AH(OUT)	WH(IN)	WH(OUT)	WATT-HR EFF.	EODV
0	400	44	1015	514	51	9.7
10	400	44	1000	524	52	9.9
20	400	46	978	554	56.5	9.0
30	400	48	967	575	60	8.9
40	400	45	980	553	56.5	8.9
0	200	43	1018	502	49	9.7
10	200	42	1007	502	50	10
20	200	42	975	506	52	10.3
30	200	44	970	532	55	9.8
40	200	42	957	510	53	8.6

TABLE III Characterization Test Matrix
(2 hr. 32.5 ampere charge; C rate (50A.) discharge)

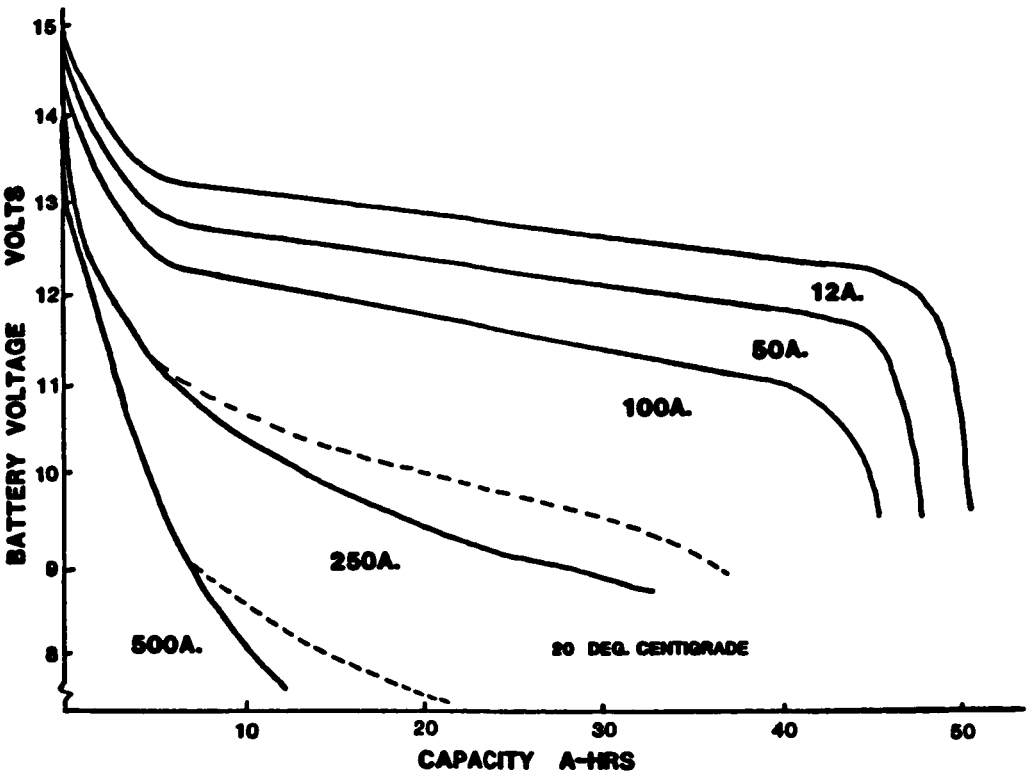

Figure 1. CAPACITY VS. DISCHARGE RATE

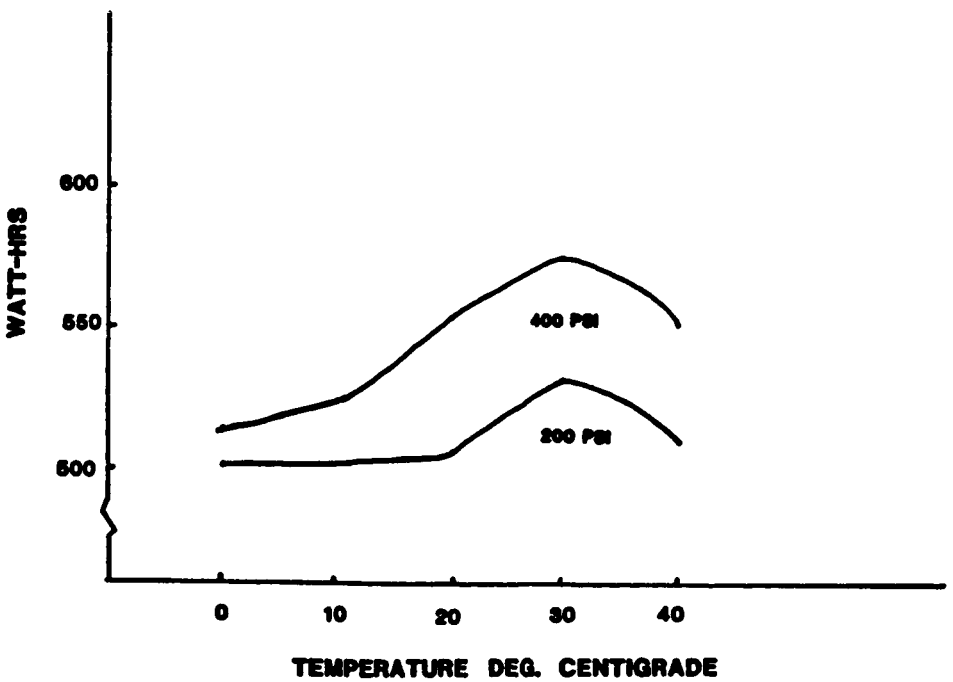

Figure 2. WATT-HRS. VS. TEMPERATURE

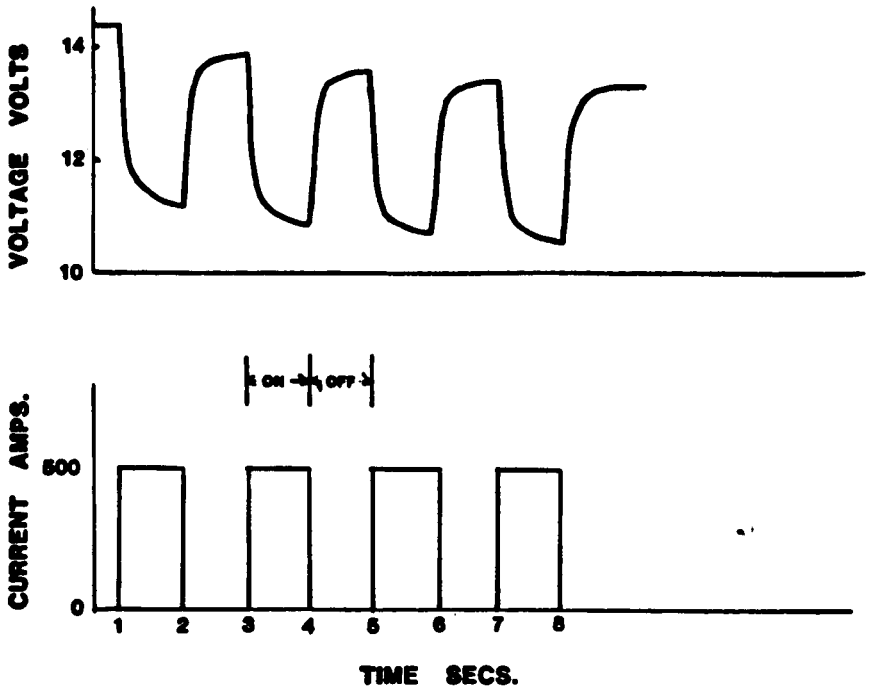

Figure 3. 500 AMPERE PULSE TEST

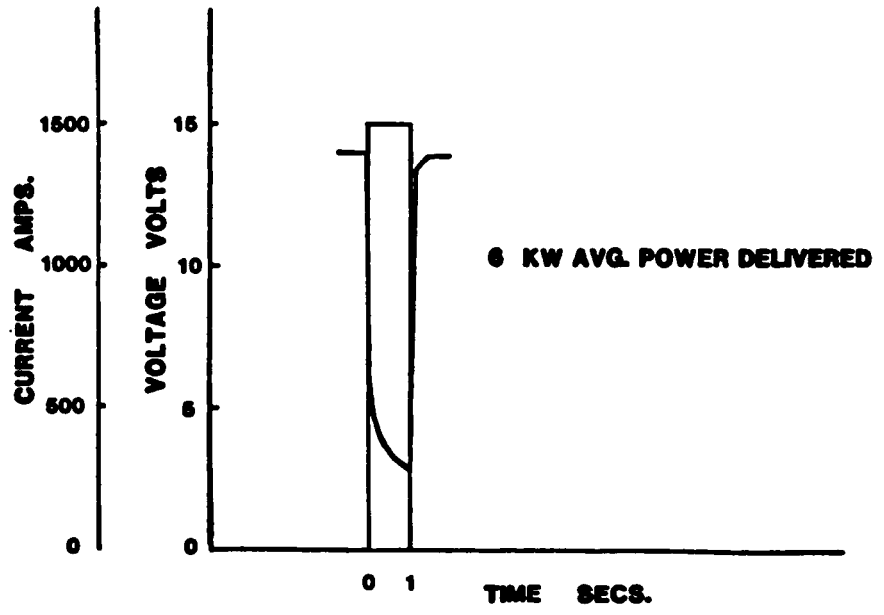

Figure 4. PEAK POWER TEST

NICKEL-HYDROGEN BATTERIES FROM INTELSAT V TO SPACE STATION

G. van Ommering and A.Z. Applewhite

Ford Aerospace & Communications Corporation
Palo Alto, California

INTRODUCTION

The Ni-H_2 battery system has been under development for about 14 years and has been flying on several geosynchronous orbit (GEO) spacecraft since 1983, in configurations such as the Intelsat V battery assembly shown in Figure 1. It has been qualified as well for low earth orbit (LEO) applications but is not as yet flying in LEO. An application now being studied in detail is the Space Station, which may require very large Ni-H_2 batteries to meet the 75 kW power requirement cost-effectively.

This paper discusses the heritage of Ni-H_2 technology that makes the Space Station application feasible. It also describes a design for a potential Space Station Ni-H_2 battery system. Specific design values presented here were developed by Ford Aerospace as part of the Rocketdyne team effort on the Phase B Definition and Preliminary Design of the Space Station Power System in support of NASA Lewis Research Center.

SPACE STATION Ni-H_2 BATTERY SYSTEM OVERVIEW

The Ni-H_2 battery system is a current option for the Space Station Initial Operating Capability (IOC). The system consists of four batteries of 105 individual pressure vessel (IPV) cells. Each cell has a nominal 275 Ah capacity. The four batteries each consist of five battery assemblies with 21 cells. The assemblies contain heat pipes for heat tranport to a fluid loop interface. The total system consists of 20 battery assemblies held in two racks, one in each Power System utility center. Design details will be provided following some background discussion.

CELL DESIGN HERITAGE

While Ni-H_2 cells are currently flying in GEO only, there is a large body of work and data that provides confidence in the readiness of the system for a large-scale LEO application in the early 1990s. The key features of the design of the 275 Ah Ni-H_2 cell required for the Space Station have already been individually demonstrated. Figure 2 illustrates some of these important efforts, some completed and some

still in process, along with their major background contribution to this program.

Intelsat V provides important background as the first and longest operational flight of Ni-H_2 batteries. Spacenet, G-Star, and Satcom K (RCA programs, not shown) demonstrate cell scale-up feasibility. The Air Force LEO cell and MANTECH programs provide LEO design and manufacturing data bases. The dual electrode stack design concept is being qualified on the MILSTAR program. While all these efforts involved 3.5-inch diameter cells, the 4.5-inch diameter required for high-capacity cells has been developed under Air Force sponsorship.

Component-level developments and life test programs are supporting these efforts. NASA-LeRC is funding electrode optimization studies for LEO, and has pursued other innovations such as vessel-wall-mounted oxygen recombination technology. The Air Force is initiating life tests at Naval Weapons Support Center in Crane, IN.

Ford Aerospace and Yardney are co-funding development of a 220 Ah Ni-H_2 cell which incorporates the necessary and best features of these other efforts. The cell is a 4.5-inch diameter, dual-stack LEO design, incorporating wall-mounted recombination sites, LEO-optimized components, and several new and upgraded features. Development of all components has been completed, and tests of the first cell will commence in December 1985. The cell is shown in Figure 3 next to a typical Intelsat V flight cell. This large-cell demonstration will establish readiness for future development of a specific Space Station size cell, in any capacity ranging up to 300 Ah. Current Space Station battery design calls for a 275 Ah cell, on which the discussion below is based.

CELL DESIGN

The 275 Ah Ni-H_2 cell is a 4.5-in diameter, tandem-stack LEO cell, based on a combination of proven features of already developed lower capacity cells.

The nickel electrode design for the 275-Ah LEO cell is based on design parameters developed by the space nickel battery industry over the last decade for long life electrodes, including sinter porosity, pore size distribution, and loading levels consistent with those derived in the NASA-LeRC funded research at Hughes Research Laboratories, as well as in U.S. Air Force development efforts. The hydrogen electrodes are based on a proven design that currently is flying on several spacecraft. The baseline separator system combines features of demonstrated separator materials to provide the necessary electrolyte reservoir and barrier characteristics.

The mechanical design of the cell is derived from the demonstrated Air Force 4.5-in cell technology. It also incorporates scaled-up features

developed under the Air Force/Yardney MANTECH program and additional improvements to provide more uniform stack support. The stack components are supported on a central core which attaches to the weld ring. Each stack is held between two support/end plates, one of which can move with respect to the core against a Belleville washer to maintain constant compressive force over the life of the cell. Electrode tabs are fed through the central core.

The pressure vessel is made of Inconel 718 with a 0.035-in design thickness. The two hydroformed and age hardened shells are joined by electron-beam welding to the Inconel 718 weld ring. The vessel has demonstrated a 3900 psi burst pressure. Maximum operating pressure is expected to be 1100-1200 psi. The electrical feedthroughs incorporate hydraulic cold-flow teflon seals.

Oxygen management is achieved by recombining oxygen generated on overcharge on the vessel wall which is coated with porous zirconia (wall wick), on which platinum catalyst is deposited based on a design pioneered by NASA-LeRC. Heat generated during overcharge thus is removed very effectively without thermal burden on the stack. The water formed is returned to the stack by the wall wick via separator edges in contact with it. The wall wick also serves as electrolyte concentration and inventory equilibrator, and as a reservoir.

BATTERY SYSTEM DESIGN DISCUSSION

Electrical Design

The 75-kW power requirement of the station, plus allocations for user converter inefficiency and PMAD processors, is provided by the battery through a 0.90 efficiency chain for a total battery system output of 95.8 kW (see Table 1). Power peaks are supported during sunlight periods by reducing the charge current if required and during eclipse by the battery at 125.8 kW. With 105 cells in series per battery and an average EOL discharge voltage per cell of 1.25 V, delivered capacity per cell is about 110 Ah for a typical eclipse. Table 2 provides additional electrical design data.

Nominal battery DOD is 40%, which assures the capability for contingency support following a peak eclipse, and is consistent with a 5-year life expectancy for the battery system. Cell capacity required to meet this requirement is 275 Ah, well within the estimated minimum 300-Ah capability of the tandem stack 4.5-in cell design. The 275 Ah capacity is achieved by adding six electrode modules to each of the two stacks of the 220-Ah cell discussed above.

Any non-wearout failures observed in Ni-H_2 cells have typically been short circuits. Because of this and the maintainability of the station hardware, no individual cell bypass hardware is included in the design. Outage of a single battery during maintenance or recondition-

ing represents a temporary increase in DOD to 53% for the remaining batteries, which represents no life risk.

Charge management involves microprocessor-based coulometry during charge and discharge. Charge current and time are determined based on a programmable recharge ratio and end-of-charge current taper profile.

Mechanical Design

The overall battery rack concept for one Utility Center is shown in Figure 4. It has space for 10 battery assemblies which slide into the rack. On one side cold plates are provided which interface with the heat exchanger of the corresponding battery assembly. Cable harnesses are incorporated in the rack with connectors at each battery shelf. Each battery assembly, as shown in Figure 5, contains 21 cells and is an independent unit interchangeable with any other. It consists of a graphite/epoxy honeycomb panel on which graphite/epoxy support beams are bonded that carry heat pipes on their top surface. Cells are contained in aluminum sleeves, which provide mechanical support and transport heat away from the cell as well. A resilient insulator layer electrically isolates the cell and sleeve and provides good thermal contact. Flanges on the sleeve are mounted to the heat pipe saddles forming both mechanical and thermal interfaces. The cell mounting design is shown in cross-section in Figure 6.

Battery physical data are shown in Table 3. Based on an individual battery assembly mass of 220 kg, and a rack mass of 75 kg, the total system mass is 4550 kg. This is not necessarily the lowest-mass battery design, but represents the overall most cost-effective approach.

Thermal Design

Battery thermal design relies on the cell sleeve, primary and secondary heat pipes, and the utility center coolant loop as major elements in the heat rejection path. The cell sleeve surrounds the cylindrical portion of the cell over the length of the cell stack and is insulated from it by a conductive layer. The sleeves conduct heat to two sets of flanges which contact the primary heat pipes as shown in Figures 5 and 6. The primary heat pipes carry heat to one side of the battery panel where their condensers interface with the evaporators of secondary heat pipes. The latter terminate on part of the long side of the panel where they form a heat exchanger which contacts a coolant loop cold plate. Instead of secondary heat pipes a simple coolant conduit fitted with quick-disconnect couplings can be used, into which an external coolant loop is plugged.

Average heat dissipations of each battery assembly during discharge and charge are 995 W and 270 W, respectively. Nominal temperatures are 10 to 20°C. The area requirement for an Al/NH_3 heat pipe radiator system to support the battery heat load would be 94 m^2, taking

advantage of heat load averaging by the battery heat capacity of 60 Wh/^{o}C per assembly.

Life and Reliability

Prediction of cycle life capability of Ni-H_2 batteries for LEO applications is more difficult than for Ni-Cd batteries. The latter have been tested extensively at Naval Weapons Support Center, Crane, IN (NWSC-Crane). A thorough analysis of this data base is represented by the model derived by McDermott and reported in various proceedings of the NASA Goddard Battery Workshop over the last four years.

Reported cycle capabilities for early developmental 50 Ah Ni-H_2 cells at 80% DOD equates to 33,000 to 40,000 cycles at 40% DOD, based on applying the McDermott Ni-Cd model, which should be conservative for the Ni-H_2 system. Sufficient progress has been made in Ni-H_2 cells since the mid-1970s, that a mean cycle life of 40,000 to 45,000 at 40% DOD in LEO appears to be a realistic projection for Ni-H_2 cells, particularly in view of the fact that even some Ni-Cd cells have achieved this (packs 1H, 1J, 8G at NWSC-Crane).

The large in-orbit data base shows that random failure probability for spacecraft batteries is extremely low on the many Ni-Cd and Ni-H_2 batteries that have been flown. Based on Ford Aerospace's in-orbit experience, Ni-Cd cells exceed 40,000,000 cell hours without random failures; industry-wide on Ni-H_2 the total is 7,000,000. Analysis yields an expected 0.6 random cell failures for the Space Station battery system over 5 years or an mean-time-to-failure of 68,000 hours.

Reliability analysis based on the Weibull distribution with a shape factor of 12 and a mean cycle life of 45,000 cycles was performed. The shape factor value is somewhat optimistic, but based on the smaller number of wearout mechanisms in Ni-H_2 cells compared to Ni-Cd (typical shape factor 8), and the tight control of operating conditions, not unrealistic. Table 4 shows the estimated system reliabilty based on these figures, an assumption that 3 shorted cell failures per battery string are allowed, and for shorted/open failure distributions of 98/2 and 80/20. Another variable is the possible presence of a spare assembly for every two batteries or 10 assemblies, which can be switched in on demand. Conclusions are:

- There is high probability (97%) that all four batteries in the system will be available for use at all times during a 5 year operational period
- Probability of uninterrupted power support for 5 years is 99.9%

- o A single spare battery assembly per set of two batteries provides sufficient open cell protection over a wide range of open cell failure possibilities

The reliability analysis results indicate that it may be not be necessary to plan for replacement of individual assemblies, but to replace instead the entire battery as a package upon wearout.

SUMMARY AND CONCLUSIONS

The heritage of space Ni-H_2 batteries from Intelsat V, through many LEO-oriented cell and component development efforts and culminating in the Ford Aerospace/Yardney development of a 220-Ah LEO cell, has prepared the technology to a point of readiness where application on the Space Station can be seriously considered. Practical battery system designs have been derived that are compatible with the requirements of the Station. While these designs do not necessarily have the lowest possible mass, they are configured to provide a 5-year battery system capability with maximal cost-effectiveness.

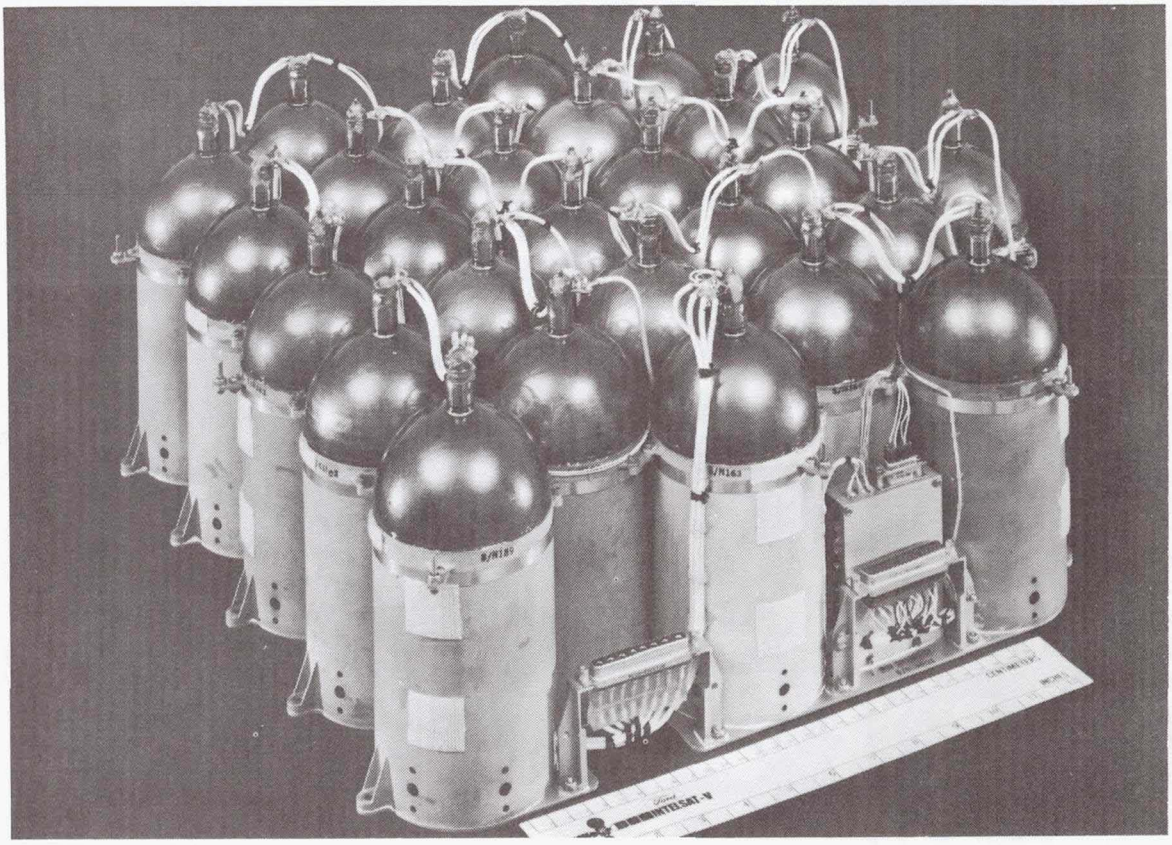

Figure 1. INTELSAT V NICKEL-HYDROGEN FLIGHT BATTERY

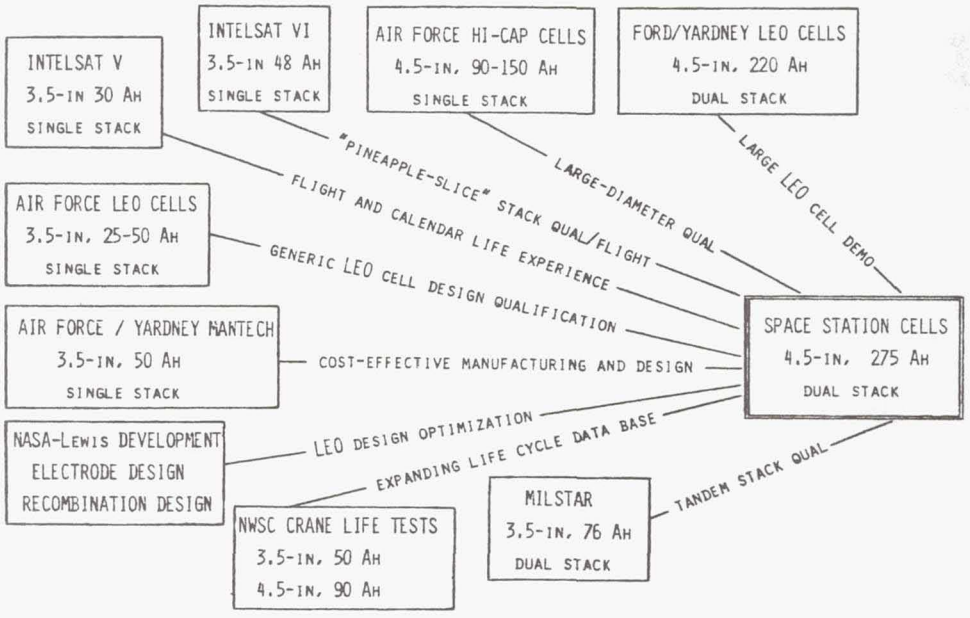

Figure 2. INTEGRATION OF DEMONSTRATED NICKEL-HYDROGEN TECHNOLOGIES FOR THE SPACE STATION

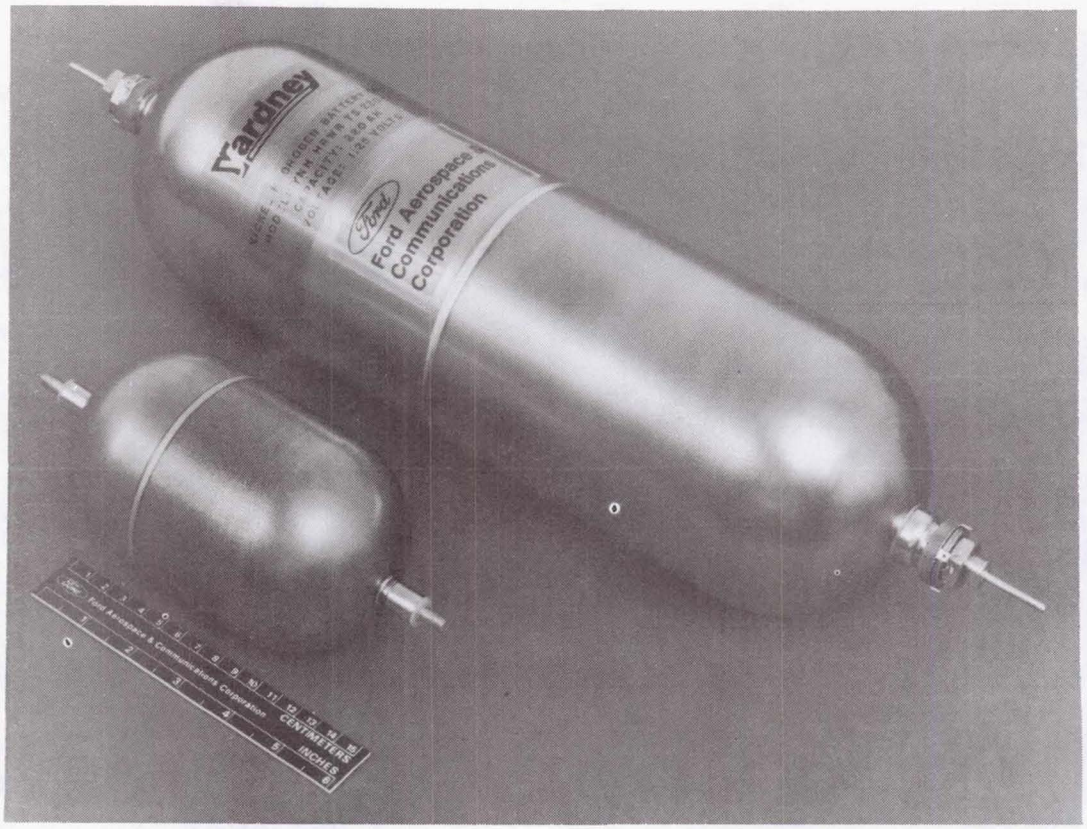

Figure 3. 220-Ah LEO NiH_2 CELL WITH 30 Ah GEO FLIGHT CELL

TABLE 1. SPACE STATION $Ni-H_2$ BATTERY SYSTEM OPERATING REQUIREMENTS

o NOMINAL DISCHARGE POWER	= 86.25 kW @ 0.90 EFF = 95.8 kW
o DISCHARGE DURATION	= 35.8 MIN
o PEAK POWER	= 113.25 kW @ 0.90 EFF = 125.8 kW
o PEAK DURATION	= 7.5 MIN
o RECHARGE DURATION - MAX	= 58 MIN
o DISCHARGE VOLTAGE	= COMPATIBLE WITH 160 V SOURCE BUS
o CHARGE VOLTAGE	= COMPATIBLE WITH 160 V SOURCE BUS
o CONTINGENCY CAPABILITY	= 50% OF LOAD FOR 1 ORBIT AFTER ECLIPSE

TABLE 2. SPACE STATION $Ni-H_2$ BATTERY SYSTEM DESIGN AND OPERATING CHARACTERISTICS

o NUMBER OF BATTERIES	4
o NUMBER OF IDENTICAL ASSEMBLIES PER BATTERY	5
o CAPACITY PER BATTERY	275 AH
o CELLS PER BATTERY	105
ECLIPSE	
o AVERAGE DISCHARGE VOLTAGE	131.3 V
o AVERAGE DISCHARGE CURRENT	182.5 A
o AVERAGE DEPTH OF DISCHARGE	39%
o PEAK ORBIT DOD	41.6%
o NON-PEAK ORBIT DOD	36.4%
o WORST-CASE CONTINGENCY DOD	97.9%
o AVERAGE HEAT DISSIPATION	19.9 KW
CHARGE	
o AVERAGE CHARGE VOLTAGE	154.4 V
o MAXIMUM CHARGE CURRENT	128.4 A
o AVERAGE HEAT DISSIPATION	5.4 KW

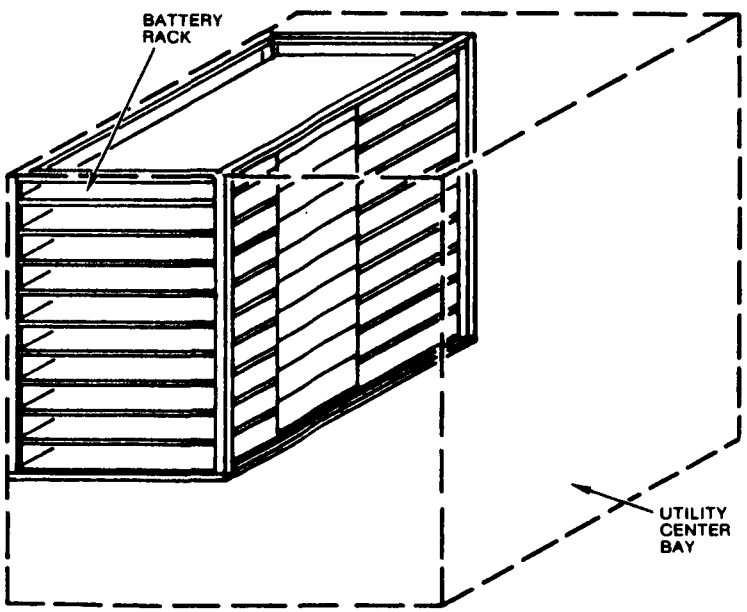

Figure 4. NiH_2 BATTERY RACK CONFIGURATION IN UTILITY CENTER BAY

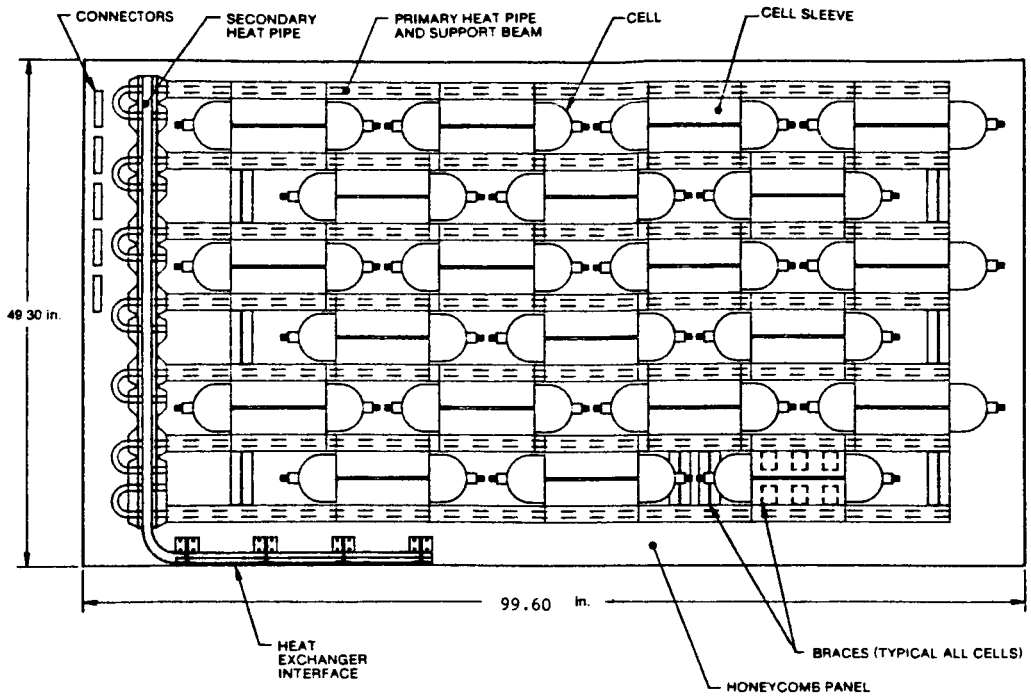

Figure 5. SPACE STATION NiH_2 BATTERY ASSEMBLY LAYOUT

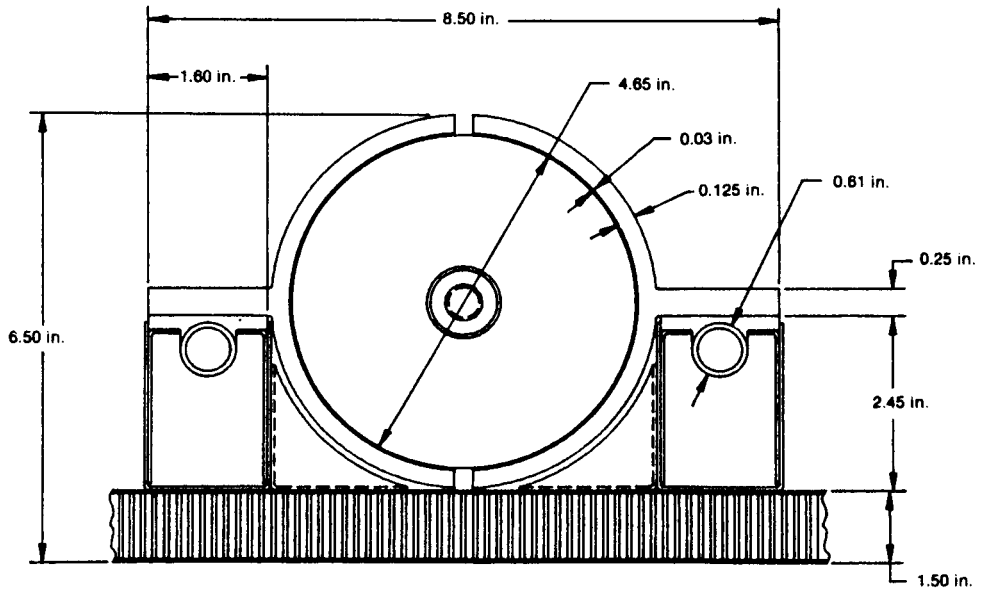

Figure 6. SPACE STATION NiH_2 CELL MOUNTING CONFIGURATION

TABLE 3. SPACE STATION $Ni-H_2$ BATTERY SYSTEM PHYSICAL CHARACTERISTICS

MASS PER CELL KG (LB)	6.99 (15.42)
MASS PER BATTERY ASSEMBLY KG (LB)	220 (485)
MASS PER BATTERY KG (LB)	1100 (2425)
TOTAL ESS MASS KG (LB)	4550 (10030)
CELL DIMENSIONS CM (IN)	55.1 x 11.8 DIA (21.7 x 4.65 DIA)
BATTERY ASSEMBLY DIMENSIONS M (FT)	2.52 x 1.25 x 0.17 (8.30 x 4.10 x 0.56)
BATTERY DIMENSIONS M (FT)	2.52 x 1.25 x 0.95 (8.30 x 4.10 x 3.12)
BATTERY SYSTEM DIMENSIONS (2 EA.) M (FT)	2.62 x 1.35 x 1.90 (8.60 x 4.43 x 6.23)
TOTAL BATTERY SYSTEM ENVELOPE VOLUME M^3 (FT^3)	13.4 (475)
THERMAL MASS $W_H/^oC$	1210

TABLE 4. SPACE STATION NI-H2 BATTERY RELIABILITY ESTIMATES

Mission Time (years)	98% Short/2% Open				80% Short/20% Open			
	Without Spare Assembly		With Spare Assemblies		Without Spare Assembly		With Spare Assemblies	
	4 Batteries	3 of 4 Batteries	4 Batteries	3 of 4 Batteries	4 Batteries	3 of 4 Batteries	4 Batteries	3 of 4 Batteries
1	>0.9999	>0.9999	>0.9999	>0.9999	>0.9999	>0.9999	>0.9999	>0.9999
2	>0.9999	>0.9999	>0.9999	>0.9999	>0.9999	>0.9999	>0.9999	>0.9999
3	>0.9999	>0.9999	>0.9999	>0.9999	0.9993	>0.9999	>0.9999	>0.9999
4	0.9979	>0.9999	>0.9999	>0.9999	0.9790	0.9998	0.9999	>0.9999
5	0.9674	0.9996	0.9974	>0.9999	0.7340	0.9699	0.9777	0.9998
6	0.0839	0.3721	0.1086	0.4310	0.0165	0.1347	0.0934	0.3955

NICKEL HYDROGEN LOW EARTH ORBIT LIFE TESTING

C.C. Badcock and R.L. Haag
The Aerospace Corporation Naval Weapons Support Center

ABSTRACT

A program to demonstrate the long term reliability of NiH_2 cells in low earth orbits (LEO) and support use in mid-altitude orbits (MAO) has been initiated. Both 3.5 and 4.5 inch diameter nickel hydrogen cells are included in the test plan. Cells from all U.S. vendors are to be tested. The tests will be performed at -5 and 10 deg. C at 40% and 60% DOD for LEO orbit and 10 deg. C and 80% DOD for MAO orbit simulations. The goals of the testing are 20,000 cycles at 60% DOD and 30,000 cycles at 40% DOD. Cells are presently undergoing acceptance and characterization testing at NWSC Crane. Funding has been provided by the AFSTC and two AF SPO's to initiate the testing, but additional funding must be acquired to complete the purchase of cells and to assure completion of the testing.

INTRODUCTION

The use of nickel hydrogen (NiH_2) batteries in high orbit applications is well established. Sufficient test data are available to make estimates of the actual reliabilities for both the COMSAT and the Air Force/Hughes designed cells. However, the application of properly designed NiH_2 cells to low earth orbits (LEO) has not been demonstrated. A program has been initiated by the USAF Space Technology Center to develop the necessary data base to support use of NiH_2 batteries in LEO at levels that would offer significant improvements in life and depth of discharge over present state-of-the-art nickel cadmium batteries. The program is to be performed at NWSC Crane using new test control facilities. The plans, requirements and status of the test program are presented.

BACKGROUND

In the Spring of 1984 a survey of life testing status and results for NiH_2 cells was performed (ref. 1). Data were found to either be available or would be available within the next two to three years to demonstrate reliability and confidence in the use of NiH_2 batteries in high orbits requiring up to 3000 cycles at maximum depths of discharge of up to 80%. Calendar life on orbit in excess of ten years was anticipated. It was suggested that optimum performance would be achieved when the temperature of operation was at less than 15 deg. C and the amount of overcharge should be minimized while maintaining an adequate state of charge.

The data available to support use of NiH_2 batteries in low earth orbits are deficient. The extant data base consists of mixtures of technologies and several generations of LEO cell designs. Cells have been tested under extreme conditions with less regard for the limitations of these cells than is normally applied to aerospace secondary cells. By the same token, testing

of the most recently built cells under severe conditions (90 min. cycle, 80% DOD, 1.4 C discharge, 0.8 C charge, 105% charge return ratio, 23±4 deg. C) has consistently given 10,000 cycles before failure (due to low voltage) occurred. This suggests that the cells have the capability to surpass the performance of present state-of-the-art NiCd cells in LEO applications. Presently, design variations among NiH_2 cells are beginning to stabilize and future changes are expected to be incremental. Testing to establish reliability and performance appears to be practical at this time.

NiH_2 cells must significantly outperform NiCd cells or they would be disadvantageous to use because of their greater specific volume, present higher unit cost, and the risks inherent in any new design. This increase in performance can be in life and/or usable energy density. Present NiCd batteries used under near-optimum conditions offer 14 - 18,000 cycles at 20 - 25% DOD and 25 - 30,000 cycles at 7 - 14% DOD with high reliability and confidence depending on the specific load profile, power system requirements, and environment. NiH_2 cells must demonstrate significant increases over these levels if they are to be the next generation of LEO batteries. This life test will demonstrate the performance capabilities of state-of- the-art NiH_2 cells in low earth orbit and will provide a database, when combined with other relevant life test data and with program specific testing, that will permit an estimate of reliability at an appropriate confidence level. State-of-the- art, individual pressure vessel-type cells of 3.5 and 4.5 in. diameter are to be tested.

OBJECTIVES

The test will be a predominantly LEO regime (90 min. orbit with 30 min. of eclipse and 60 minutes of sun) with some test packs tested in MAO-to-HEO conditions (400 to 500 cycles per year with a 4 to 12 hour orbit) if funding and schedule permit. The NiH_2 cell life test plan has the following objectives:

1. Demonstrate NiH_2 performance in LEO applications and support use in MAO at levels superior to current NiCd capabilities.
2. Develop a statistically significant NiH_2 battery cell database.
3. Disseminate the test data and results in a timely fashion.
4. Demostrate NiH_2 cell performance in pulse applications.
5. Demonstrate that the Manufacturing Technology Program (MANTECH) cells are capable of performing in high orbit as well as LEO.

STATISTICAL REQUIREMENTS

The statistical requirements for a test must be based on the largest homogeneous unit: single type of cell, same vendor, same test conditions. Analysis after testing has progressed may justify the combination of several of these units to increase the reliability and confidence level for a particular application. Generally tests performed under more severe conditions can support reliability assessments for applications at less

severe stress levels.

The two-parameter Weibull function (zero failure rate at the start of the test is assumed) will be used to estimate reliability. The expression for the reliability after integration of the probability density function is,

$$R(t) = \exp[-(t/\mu)\beta] \quad (1)$$

where β is the shape of the failure distribution parameter, μ is the scale parameter associated with the rate of failure and t is the test time (ref. 2). This is a general function that reduces to an exponential distribution function ($\beta = 1$) or closely approximates a normal distribution function ($\beta = 3.313$). The use of the function for evaluating NiCd test data has been demonstrated (ref. 3). When no failures occur in a test that has run for time t, the success-run theorem (Bayes' Formula),

$$R = (1 - C)^{1/(n+1)} \quad (2)$$

can give the relationship between confidence level C, the reliability at that confidence level R, and the sample size n.[2] Table I shows the relationship between sample size, test time, reliability, and confidence level for an assumed normal distribution ($\beta = 3.313$). Ten cell packs are chosen as the test unit because of the reliability and confidence levels attainable and because this sample size permits evaluation of the failure distribution function.

REPORTING

Reports will be issued when significant milestones are reached and at regular periods. Each major milestone, e.g. completion of acceptance testing, will result in a brief report. The progress of the test will be reported in an "Annual Report of Cycle Life Testing" and will, in addition, be summarized at least once a year and presented in an appropriate forum. The detailed data will remain available for access by qualified organizations.

COORDINATION WITH OTHER TESTING

In a separate, program-oriented test the Martin-Marietta Aerospace in Denver is performing similar life testing. Their test matrix has been coordinated with this matrix to assure proper distribution and adequate data at the key points; that is, at the center 10 deg. C test area. They are planning to test at 20 deg. C and accounts for that condition missing from this matrix. Any other testing data that becomes available and that is relevant will be incorporated into the growing database.

TEST ARTICLES

It is the intent to test cells from all viable vendors in sufficient numbers to provide a comparison and to establish a statistically significant

database with a sufficiently high confidence level. A minimum of 155 3.5 in diameter and 45 4.5 in diameter cells are included in the test plan. Additional cells will be added as the need is demonstrated. Insofar as schedule and funding permits, approximately equal numbers of cells from the four U.S. vendors (GEBBD, Eagle Picher, Yardney, and HAC) are to be tested. The initial test articles will be 3.5 in. diameter cells drawn from purchase orders previously placed with Yardney, Eagle Picher, and GEBBD by AFWAL/POOC and AFWAL/ML. It is hoped that part of the complement of 4.5 in. diameter cells will be drawn from orders already placed (CPV program) by AFWAL/POOC.

In the future cells will be purchased to a "Specification for Nickel Hydrogen Cells" that defines required performance in terms of voltage, capacity, weight, dimensions, and life. Presently used specifications will be covered by this specification because present versions specify additional details that are to be in the MCD or present test requirements are less severe. Each vendor's product will be procured to a designated part number with the details of construction contained in an associated, approved manufacturing control document (MCD). Stability, performance, and conformance to specification will be demonstrated at each vendor's facility. Formal acceptance testing is to be performed at the testing location (Naval Weapons Support Center (NWSC), Crane, IN).

All cells will be in flight configuration (no special test units) and of flight quality. The cells are to be hermetically sealed. Pressure monitoring will be by externally mounted strain gauges only.

TEST OUTLINE

The test consists of acceptance and characterization testing, life testing, and failure and end-of-test analyses.

PRE-LIFE TESTING

Acceptance testing will be conducted at the life test site. Tests include standard capacities at -5, 10, and 20 deg. C using rates appropriate to LEO applications (a rate of C is proposed because this approximates the conditions of the test), overcharge stability and reference capacities, and charged stand loss determinations. The ampere-hour and watt-hour capacities of the cells will be reported to 1.20, 1.15, 1.10, 1.05, 1.00, and 0.5 V. These data will provide reference data for system applications.

A 20% sample of the cells of each type (at least two cells) and from each vendor shall be subject to random vibration testing at levels 6 dB higher than the highest level anticipated in any application. The cells that are vibrated will be distributed throughout the test packs to determine any effects of vibration.

Characterization tests will be performed to determine the required charge characteristics. A group of 5 cells of each type and from each vendor will be tested to determine charge efficiencies at selected rates and temperatures. Watt-hour and ampere-hour efficiencies will be determined at four charge rates, 3 discharge rates, and at 4 temperatures.

The cells are to be assembled into test packs which contain cells from

only one vendor. Heat removal is by conduction through flanges attached to the cells onto thermally conductive plates. The flanges will be of a standard type similar to the units used on previous USAF/Hughes-type cells to provide for similar heat removal pathways and rates for all cells. Each pack will have at least one cell with a pressure transducer.

LIFE TESTING

The goals for these tests are to demonstrate at least 30,000 cycles at 40% DOD and at least 20,000 cycles at 60% DOD in LEO and at least 5000 cycles at 80% DOD in MAO or high orbit. The 40% DOD level is greater than present NiCd cells can expect to achieve at three years planned life. A small number of cells (5 from each vendor) will be tested at 25% DOD to provide correlation with present NiCd testing and life databases. Cells could fail to reach a desired goal, e.g. 60% DOD and 5 years, and still perform significantly better than present state-of-the-art NiCd cells.

A second goal is to establish a minimum reliability of 90% with a confidence level of at least 80% at the cycle lives stated above. This goal requires one additional year of testing beyond the life goals stated, but assumes that none of the groups of ten cells can be statistically combined.

The DOD is defined as the percent of the measured capacity to 1.00 V of the lowest capacity cell in the test pack under the most appropriate conditions in acceptance testing. This number may be higher or lower than the rated capacity used during acceptance testing.

Failure is defined as a voltage of less than 0.50 V at the end of the prescribed discharge or a voltage greater than 1.75 V during any portion of the charge. Data for other end-of-useful-life criteria will be available. Upon being declared a failure, the cell will be removed from the test pack and subjected to a repeat of at least part of the acceptance test within 180 days of failure. The cell shall then be dispositioned for failure analysis.

Data (current, voltage, pressure, and temperature) will be recorded for each test pack with sufficient frequency to assure that extrapolation between data points can be performed with adequate accuracy to detect any short term or long term trends. These data will be available for plotting or display and for the computation of watt-hour and ampere-hours input and output as well as charge returns. Periodically, e.g. every 2000 cycles, a complete plot of a charge/discharge cycle will be generated for each cell in test for comparison to detect trends.

The distribution of cells, the DOD's, and the temperatures are shown in Table II for the completely funded test and for the minimum test necessary to meet the primary goals. The LEO test will use 90 min. cycles with 30 min. discharges.

The charge procedure will consist of a high rate charge to return the bulk of the charge removed and a lower rate to complete the charge. This prevents subjecting the cells to high rate overcharge. The planned charge control method is ampere-hour integration (recharge fraction control). This method is flexible and particularly easy to integrate into a digital control system. Control shall be accomplished by changing the charge returned under a fixed depth of discharge until the following parameters are minimized:

1. The decrease in the end of discharge voltage
2. The increase in the end of charge voltage (high rate and trickle)
3. The recharge fraction (both watt-hour and ampere-hour)

These parameters will be adjusted during the test as performance dictates.

Reconditioning will not be performed on the cells in LEO testing. MAO testing may require reconditioning to maintain adequate efficiency. No capacity discharges shall be performed.

The test is scheduled over a seven year period as shown in Figure 1. To maximize the information and provide the best statistics, the test should continue until the majority of the cells in each pack have failed.

SPECIAL TESTING

The general test plan will use continuous constant current discharges. However, the applications requiring pulsed high rate discharge within the envelope of the planned DOD's are sufficiently prevalent to make the correlation of such results with the general life test important. A small group of cells will be placed on life test in a pulsed discharge regime at maximum rates of approximately 5C. The detailed test plan for this portion will conform to the overall test organization, but will be prepared separately. Cells will be acceptance tested at the testing organization and sent to The Aerospace Corporation Battery Evaluation Laboratory for this testing.

STATUS

In the Spring, 1985, two Air Force System Program Offices (SPO), AFWAL AeroPropulsion Laboratory (AFWAL/POOC), and the AF Space Technology Center (STC) completed a transition agreement that seeks to provide data needed to bring NiH_2 battery technology into general use in all intended applications. The two SPO's and the STC committed funds for the initiation of the testing. AFWAL/POOC agreed to provide NiH_2 cells from previous contracts for testing. The AFWAL Materials Laboratory agreed to commit the Manufacturing Technology Program (MANTECH) cells to the life test program. The numbers of 3.5 in. diameter cells committed to the test program and their expected availability dates are listed in table III.

Funding provided was sufficient to purchase test equipment, including a new computer facility for this test at NWSC Crane, and to proceed with the testing of the committed cells. This equipment will also serve as replacements for some of the outdated and less reliable equipment currently in use.

Test documentation including the life test plan, cell specification, and life testing procedure have been prepared and are currently undergoing review. Failure analysis documentation is yet to be prepared.

Cells have been received and are currently undergoing acceptance testing.

Additional funding is sought to complete the purchase of cells for the minimum test matrix shown in Table II and to assure the completion of the program.

SUMMARY

A program to demonstrate the long term reliability of NiH_2 cells in low earth orbits and support use in mid-altitude orbits has been initiated. Both 3.5 and 4.5 inch diameter nickel hydrogen cells are included in the test plan. Cells from all U.S. vendors are to be tested. The tests will be performed at -5 and 10 deg. C at 40% and 60% DOD for LEO orbit and 10 deg. C and 80% DOD for MAO orbit simulations. The goals of the testing are 20,000 cycles at 60% DOD and 30,000 cycles at 40% DOD. Cells are presently undergoing acceptance and characterization testing at NWSC Crane. Funding has been provided by the AFSTC and two AF SPO's to initiate the testing, but additional funding must be acquired to complete the purchase of cells and to assure completion of the testing.

REFERENCES

1. C.C. Badcock and M.J. Milden, "An Industry and Government Survey: Life Testing of Nickel Hydrogen Cells," Proceedings of the 1984 GSFC Battery Workshop, NASA Conf. Pub. 2382, 1985, p. 583.

2. Charles Lipson and Narendo J. Sheth, Statistical Design and Analysis of Engineering Experiments, McGraw-Hill, New York, 1973.

3 J.H. Matsumoto, G. Collins, and W.C. Hwang, "Applicability of Accelerated Test Data," Proceedings of the 19th Intersociety Energy Conversion Engineering Conference, Vol. 1, 303 (1984).

TABLE I. TEST TIME, RELIABILITY, AND CONFIDENCE LEVEL FOR A FIVE YEAR APPLICATION AS A FUNCTION OF THE SAMPLE SIZE

Sample Size Without Failures	Test Time (R=90%, C=69%)	Reliability (C=69%, t=5 yrs)	Confidence Level (R=90%, t=5 yrs)
1	8.36 yrs.	56.0%	19.0%
2	7.40	68.0	27.1
3	6.78	74.9	34.4
5	6.00	82.4	46.9
6	5.73	84.7	52.2
7	5.50	86.5	57.0
8	5.31	87.9	61.3
9	5.15	89.1	65.1
10	5.00	90.0	68.7
15	4.46	93.0	81.5
20	4.12	94.6	89.1

TABLE II. PLANNED NiH_2 LIFE TEST MATRIX

ORBIT	DOD	MFR	3.5" DIA. CELLS[1] TEMPERATURE[2] 10C	3.5" DIA. CELLS[1] TEMPERATURE[2] -5C	4.5" DIA. CELLS[1] TEMPERATURE[2] 10C	TOTAL CELLS 3.5"	TOTAL CELLS 4.5"
LEO	25%	YARD	5			5	
		EP	5			5	
		GEBBD	5			5	
		HAC	5			5	
	40%	YARD	10	10		20	
		EP	10		10	10	10
		GEBBD	10	10		20	
		HAC	10		10	10	10
	60%	YARD	10		10	10	10
		EP	10	10		20	
		GEBBD	10		10	10	10
		HAC	10	10		20	
MAO	80%	YARD	10 (5)		10 (0)	10 (5)	10 (0)
		EP	10 (0)		10 (0)	10 (0)	10 (0)
		GEBBD	10 (0)		10 (0)	10 (0)	10 (0)
		HAC	10 (0)		10 (0)	10 (0)	10 (0)
SPECIAL TESTS:							
		2 or 3 - 3.5 inch cells and 1+ - 4.5 inch cell from each vendor:				10	5
TOTAL CELLS:[3,4]						190 (155)	85 (45)

1. The complete test configuration is shown with the minimum credible test shown in () where the two differ.
2. The temperatures specified are to have tolerances of ±4 deg. C.
3. Strain gauge pressure monitors are required on at least 20% of the cells.
4. An additional set-aside of one each wet and dry cell of each size from each manufacturer is recommended (not in above totals).

Table III. 3.5 Inch Diameter NiH_2 Cells Committed to the Test

SOURCE	APPROXIMATE NUMBER[1]	DATE AVAILABLE
Yardney		
MANTECH	25 (ZA)	Winter 86
AFWAL	5 (ZA)	Winter 86
Eagle Picher		
Adv. Dev. Prog.	24 (A)	Spring 85
AFWAL	15 (Z)	Summer 85
HAC (for AFWAL)	18 (Z)	Spring 85
GE BBD		
AFWAL	15 (Z)	Winter 86

1. The letters indicate the type of separator: (A) asbestos, (Z) Zircar, and (ZA) MANTECH combination.

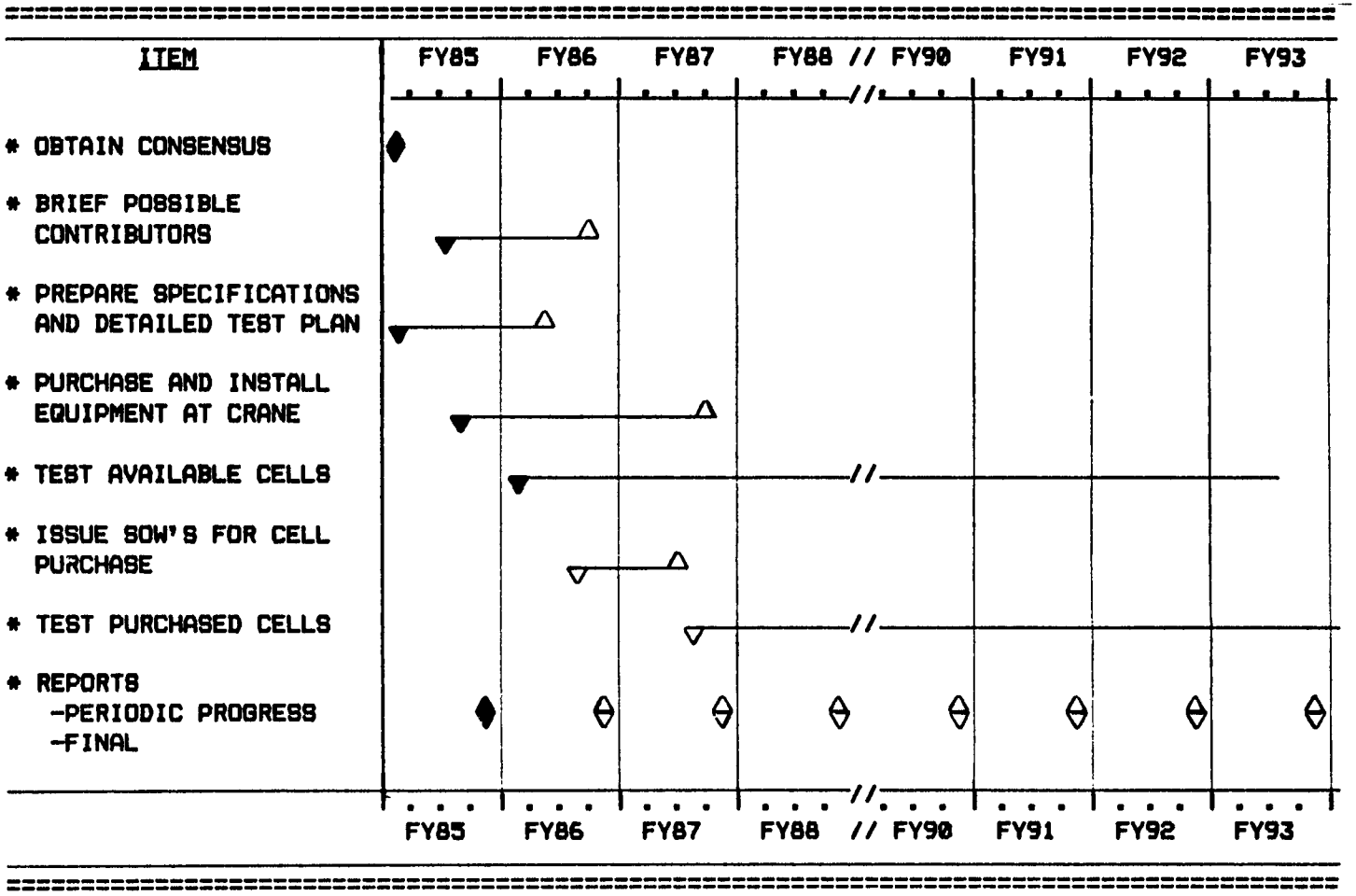

Figure 1. SCHEDULE FOR THE NiH_2 LIFE TEST FOR A MINIMUM OF 7 YEARS. OPEN TRIANGLES INDICATE THAT THE ACTIVITY HAS NOT STARTED OR IS NOT FINISHED. ARROWS INDICATE THE ACTIVITY MAY EXTEND LONGER THAN THE FIGURE SCALE.

N87-11103

4.5" DIAMETER IPV NI-H_2 CELL DEVELOPMENT PROGRAM

Lee Miller

Eagle-Picher Industries, Inc.

Introduction

Interest in larger capacity Ni-H_2 battery cells for space applications has resulted in the initiation of a development/qualification/production program. Cell component design has been completed and component hardware fabricated and/or delivered.

Finished cell design projections demonstrate favorable specific energies in the range of 70-75 Whr/Kg (32-34 Whr/Lb) for capacities of 100-250 AH.

It is further planned during this effort to evaluate the advanced cell design technology which has evolved from the work conducted at the NASA/ Lewis Research Center

Background

Cell pressure vessels (PV) of 8.89 cm (3.50 in) diameter have successfully accommodated cell capacities ranging from 30-90 AH. However, further growth in PV length imposes certain design and fabrication technology problems. PV's of approximately 11.43 cm (4.50 in) diameter are therefore of interest because similar diameter-to-length relationships are maintained while accommodating larger cell capacities.

Cell Designs

The photograph presented in Figure 1 displays two (2) PV designs to be evaluated under this program. They are primarily distinguished by the method used to effect the vessel girth or joining weld.

The design on the left accommodates an electron beam (EB) welding process. The vessel is of thin walled, uniform construction and the weld ring (not machined in this view) design facilitates the necessary back supported, vessel "butt" joint. This concept is often referred to as the "Intelsat" PV design.

The design on the right accommodates an automatic, tungsten-inert-gas (TIG) welding process. The vessel is of thin walled, multiple thickness (chem-milled) construction and the weld ring design facilitates an unsupported, vessel "butt" joint. This concept is often referred to as the "Air Force" PV design.

Production designs will accommodate either "compression seal" (Intelsat) or "hydraulic seal" (Air Force) terminal assemblies. In addition, both external/internal terminal mounting either axial or 45° off-set will be accommodated. An internal, 45° off-set terminal arrangement (3.5 in cell) is shown in the center of the above view.

Projected Cell Characteristics

The characteristics or design features for four (4) cell capacities (100, 200, 220 and 300 AH) have been projected with very favorable results.

The design features for a 100 AH cell are presented in Figure 2. It was noted several listed parameters are independent of cell capacity. In Figure 3 only the parameters which change are summarized for all four (4) cell capacities.

A review of these data reveal an inverse relationship between cell specific energy and cell capacity (see graph in Figure 4). This unusual relationship is primarily attributed to accelerated current conductor, cross-section growth with increased cell length.

Advanced Cell Design Technology

Advanced Ni-H_2 cell design technology has been reported by researchers at the NASA/Lewis Research Center. Technical details were most recently presented at the 1984 GSFC Battery Workshop [1] and the 20th Intersociety Energy Conversion Engineering Conference [2].

Portions of this technology will be evaluated under this program to assess their potential benefit. The enhanced thermal/oxygen/electrolyte management characteristics offered by the catalyzed wall wick/reservoir concept may be well suited to the larger diameter cell configuration particularly in LEO applications. Each of these parameters becomes more difficult to management as cell cross-section increases.

Conclusion

A development/qualification/production program is proceeding on schedule to introduce 4.5" diameter Ni-H_2 cell technology. Production tooling has been completed and cell hardware fabricated or delivered. Cell assembly will soon be initiated for design qualification and user industry evaluation.

Large capacity Ni-H_2 cell (100-250 AH) exhibiting specific energies of 70-75 Whr/Kg (32-34 Whr/Lb) and offering improved operational characteristics will be available for the most demanding space missions on a near term basis.

References

1. Thaller, L. H. (LRC), "Nickel-Hydrogen Technology", 1984 Goddard Space Flight Center Battery Workshop, Publication 2382, Greenbelt, Maryland, November 1984.

2. Thaller, L. H. & Assoc. (LRC), "Design Principles For Nickel-Hydrogen Cells and Batteries", Proc. 20th Intersociety Energy Conversion Engineering Conference, SAE P-164, Miami Beach, Florida, August 1985.

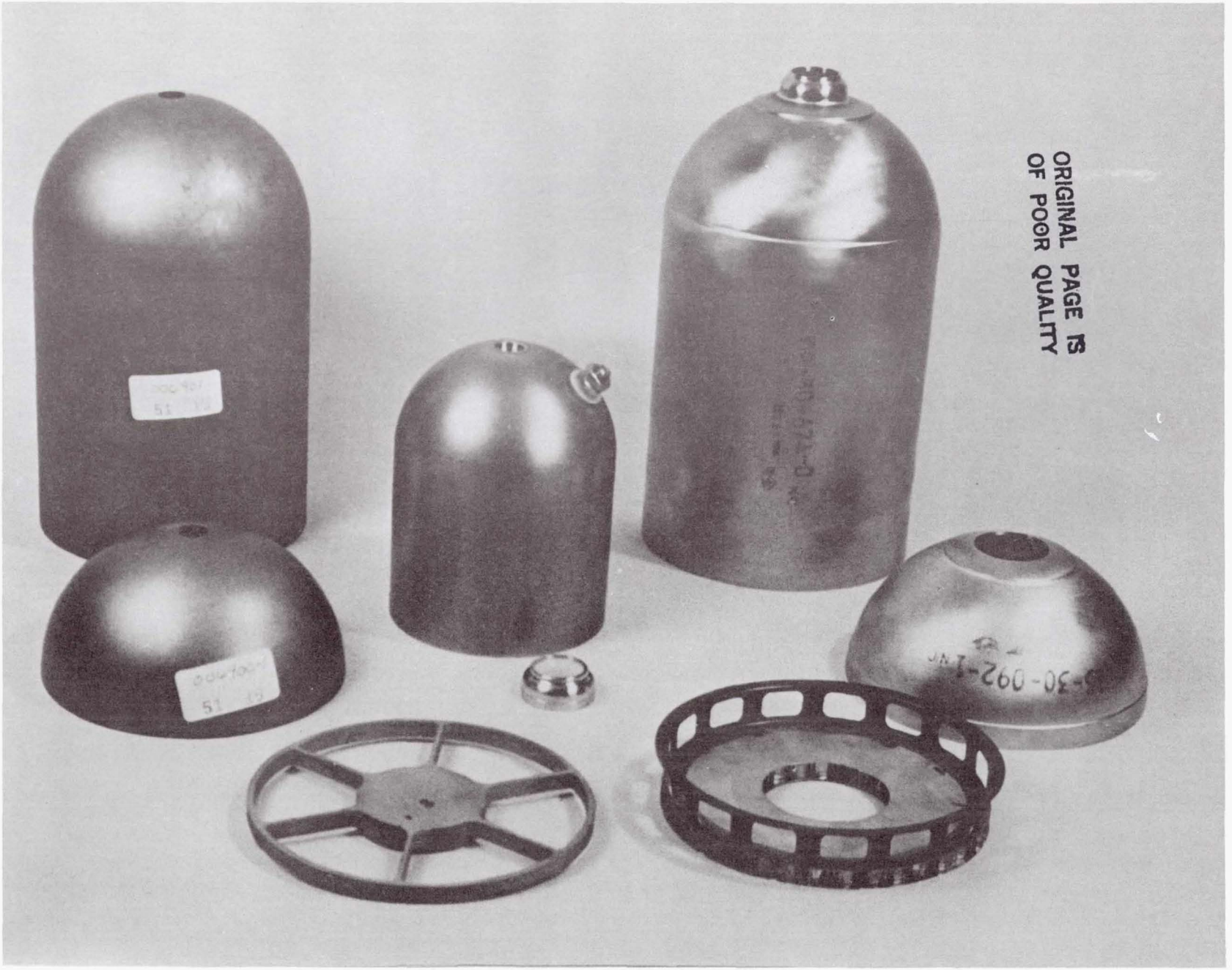

Figure 1.

100 AH 4.5" Dia NiH_2 CELL DESIGN FEATURES

NOMIMAL CAPACITY (to 1.00 V)	109 AH
DIAMETER	11.76 CM (4.63 IN)
LENGTH	18.29 CM (7.20 IN)
OPERATING PRESSURE	61 ATM (900 PSI)
SAFETY FACTOR	2.5 : 1
TERMINALS	INTERNAL, 45° OFF-SET
MASS	1783 GM (3.92 LB)
SPECIFIC ENERGY	74.6 WH/KG (33.9 WH/LB)

Figure 2.

EAGLE EPICHER

FEATURES	100 AH	200 AH	220 AH	300 AH
NOMIMAL CAP.(AH)	109	218	243	333
LENGTH (CM)	18.29	32.26	35.81	46.99
MASS (GM)	1783	3676	4164	6055
SPEC. EN. (WH/KG)	74.6	72.4	71.2	67.1

COMMON FEATURES

DIAMETER	11.76 CM (4.63 IN)
OPERATING PRESSURE	61 ATM (900 PSI)
SAFETY FACTOR	2.5 : 1
TERMINALS	INTERNAL, 45° OFF-SET

Figure 3. 4.5″ Dia. NiH_2 Cell Design Features

EAGLE PICHER

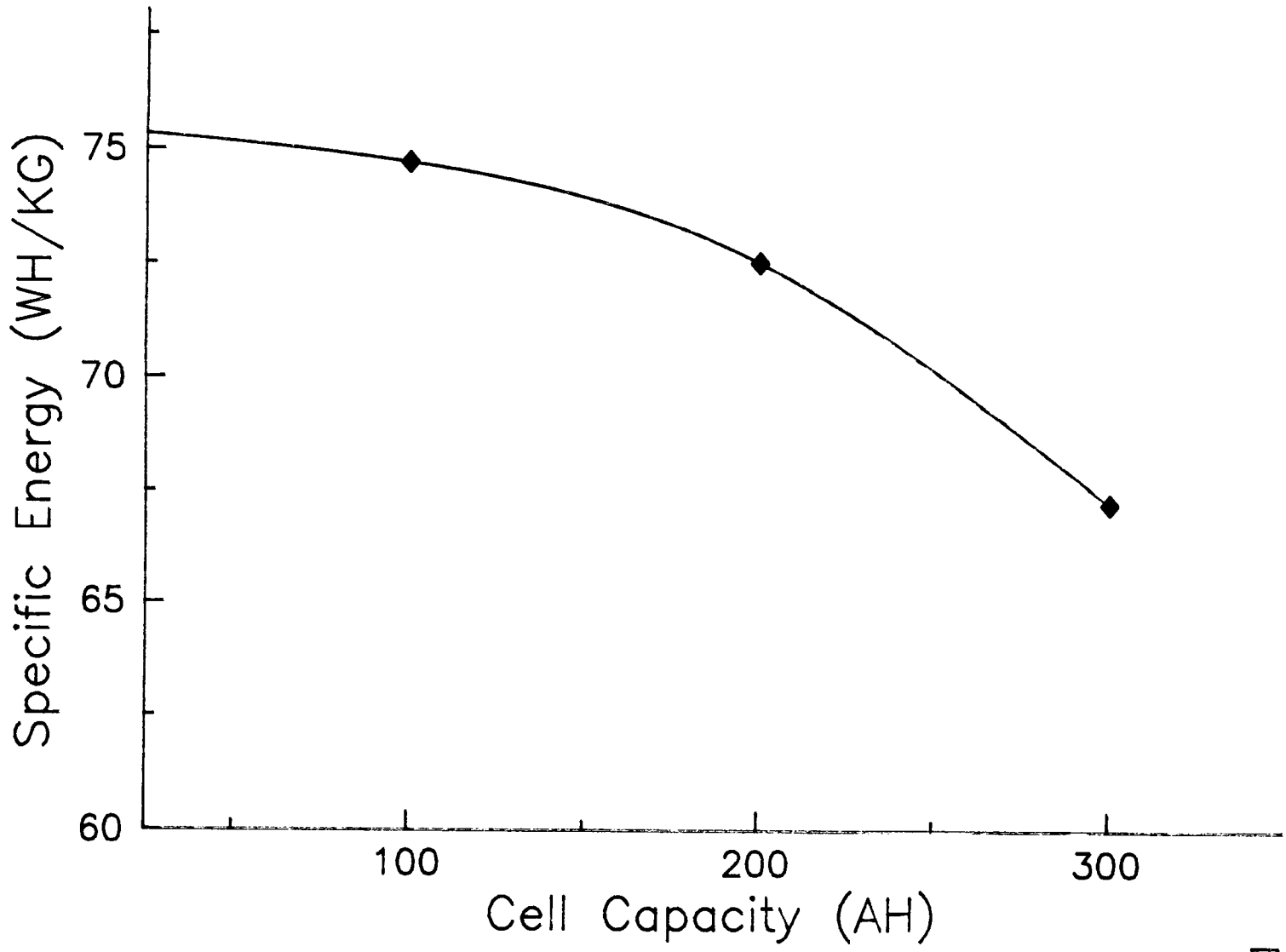

Figure 4. 4.5″ Dia. NiH_2 Cell Design Features

LIST OF PARTICIPANTS
1985 NASA/GSFC BATTERY WORKSHOP

Dr. K.M. Abraham
EIC Laboratories
111 Downey Street
Norwood, MA 02062
(617) 769-9450

Kerim A. Akel
USAF
SD/YDE Los Angeles AFS
Los Angeles, CA 90009
(213) 643-1327

Heidi Altherr
SAFT American Inc.
107 Beaver Court
Cockeysville, MD 21030
(301) 666-3200

J.J. Auborn
AT & T Bell Labs
Room GF-211
Murray Hill, NJ 07974
(201) 409-1590

Daniel Augenstene
DOJ
8199 Backlick Road
Lorton, VA 22079
(703) 550-7931

Charles Badcock
The Aerospace Corporation
P.O. Box 92957, MS M2/275
Los Angeles, CA 90009
(213) 648-5180

David Baer
Hughes Aircraft Company
Building S41
MS A315
P.O. Box 92919
LA Airport Station, CA 90009
(213) 648-3442

A. Stuart Baldwin
Johnson Control Inc.
1132 Langley Lane
McLean, VA 22101
(703) 790-9215

Robert Barnabei
Honeywell Power Sources Center
104 Rock Road
Horsham, PA 19044
(215) 674-3800

James A. Barnes
Naval Surface Weapons Center
Code R33
Silver Spring, MD 20903-5000
(202) 394-1299

Wilbert Barnes
Bendix Field Engineering
Naval Research Lab.
4555 Overlook Avenue S.W.
Washington, DC 20375
(202) 767-6517

C.W. Bennett
General Electric Co.
3198 Chestnut Street
Philadelphia, PA 19101
(215) 823-2183

Edwin R. Berry
Aerospace Corp.
M.S. M4/988
P.O. Box 92957
Los Angeles, CA 90009
(213) 648-6273

Samuel Birken
Aerospace Corp.
M.S. M4/986
P.O. Box 92957
Los Angeles, CA 90009
(213) 648-6080

R. F. Bis
Naval Surface Weapons Center
White Oak Labs
Silver Spring, MD 20903-5000
(202) 394-1299

Dr. G.D. Bizzell
Lockheed Missile Space Center
P.O. Box 3504
Sunnyvale, CA 94088-3504
(408) 742-2860

Carole Bleser
Eagle-Picher Industries
P.O. Box 5234
Colorado Springs, CO 80931
(303) 392-4266

Dick L. Bloomquist
David Taylor Naval Ship
Code 2752
Annapolis, MD 21402
(301) 267-3130

David P. Boden
Douglas Battery Manufacturing
500 Battery Drive
Winston-Salem, NC 27107
(919) 788-7561

John Boldt
Applied Physics Lab
Johns Hopkins Road
Laurel, MD 20707
(301) 953-5095/953-5000

Donald W. Bondeson
Martin Marietta Aerospace
P.O. Box 179
Denver, CO 80201
(303) 977-6066

Francis R. Boyce
RCA/PSEG
13305 Finsbury Court #1
Laurel, MD 20708
(301) 763-7577

William Boyd
Utah Research and DFW
P.O. Box 10
West Jordan, UT 84084
(801) 561-9385

Bob Bragg
NASA/JSC
MS, EP5
Houston, Texas 77058
(713) 483-4701

Dr. Klaus Brandt
Moli Energy Ltd.
3958 Myrtle Street
Burnaby, B.C. V5C 4G2
Canada
(604) 437-6927

Jack Brill
Eagle-Picher Industries
P.O. Box 47
Joplin, MO 64802
(417) 623-8000

Alfred O. Britting, Jr.
Aerospace Corp.
M.S. M4/986
P.O. Box 92957
Los Angeles, CA 90009
(213) 416-9253

Doris Britton
NASA/LRC
21000 Brookpark Road
Cleveland, OH 44135
(216) 433-5246

Dr. P. Bro
Southwest Electrochemical
209 Hyde Park Estates
Santa Fe, NM 87501
(505) 982-1286

Ralph Brodd
Amoco Corp.
P.O. Box 400
Naperville, IL 60566
(312) 961-7698

Richard Broderick
GTE Spacenet
1700 Old Meadow Road
McLean, VA 22102
(703) 790-7867

Ernest Busboso
NASA/GSFC
Code 743
Greenbelt, MD 20771
(301) 286-0285

Robert B. Byrnes
Dept of Army
Rt. 2, Box 595
Stafford, VA 22554
(202) 695-3516

Dr. Josip Caja
Precision Engineering
31 E. Tennessess Avenue
Oak Ridge, TN 37830
(617) 482-7200

Dr. Aaron Casperd
Fisher Aerospace
Space and Communications Division
Powers Subsystems Group
Argyle Way
Stevenage Herts, Code SG12AS
England
0438 736482

Bob Cataldo
NASA/Lewis
MS 309-1
21000 Brookpark Road
Cleveland, OH 44135
(216) 433-2185

Joseph E. Chilton
U.S. Bureau of Mines
P.O. Box 18070
Pittsburgh, PA 15236
(412) 675-6644

Roland Chireau
Yardney Corporation
82 Mechanic Street
Pawcatuck, CT 02891
(203) 599-1100

Professor Yong Cho
Department of Mech Engineering
Drexel University
Chestnut & 32nd Street
Philadelphia, PA 19104
(215) 895-2237

Leo Christensen
Pellon
20 Industrial Avenue
Chelmsford, MA 01824
(617) 256-6588

Dr. David Chua
Honeywell Power Sources Center
104 Rock Road
Horsham, PA 19044
(215) 674-3800

James J. Ciesla
Electrochem Industries
10000 Wehrle Drive
Clarence, NY 14031

Steven Cohen
RCA American Corp.
4 Research Way
M.S. 2-8
Princeton, NJ 08540
(609) 987-4118

Ernst M. Cohn
1138 Appian Way
Dothan, AL 36303

Dennis B. Cooper
INTERSAT
3400 International Drive
Washington, DC 20008-3098
(202) 944-7349

T. Counts
Eagle-Picher Industries
P.O. Box 47
Joplin, MO 64802
(417) 623-8000

John W. Cretzmeyer
Promeon
Medtronic Inc.
6700 Shingle Creek Parkway
Brooklyn Center, MN 55423
(612) 574-6388

Glenn F. Cruze
Duracell U.S.A.
Berkshire Industrial Park
Building 9
Bethel, CN 06801
(203) 796-4284

F. S. Cushing
Three E. Laboratories
840 Main Street
Lansdale, PA 19446
(215) 362-7012

Cheryl Danielson
Eagle-Picher Industries
P.O. Box 5234
Colorado Springs, CO 89031
(303) 392-4266

Ivan F. Danzig
U.S. Army
6812 Wild Rose Court
Springfield, VA 22152
(202) 695-3516

Gary Davis
Naval Ocean Systems Center
Code 712
San Diego, CA 91252
(619) 225-7711

Patrick Davis
Naval Surface Weapons Center
10901 New Hampshire Avenue
Silver Spring, MD 20903-5000
(303) 394-3588

Frank DeBold
Naval Surface Weapons Center
10901 New Hampshire Avenue
Silver Spring, MD 20903-5000
(301) 394-3588

Dr. Larry DeVries
Naval Surface Weapons Center
White Oak Laboratory
Code R-33
Silver Spring, MD 20903-5000
(202) 394-1302

S.W. Donley
Aerospace Corp.
P.O. Box 92957
M.S. M2-275
Los Angeles, CA 90009
(213) 615-4103

George Drengler
Union Carbide Corp.
P.O. Box 44135
Westlake, OH 44135
(216) 835-7616

Ross E. Dueber
Air Force
Wright Aeronautical Lab
P005-2 WPAFB
Dayton, OH 45433
(513) 255-6241

Orville Dunhem
National Standard
P.O. Box 1620
Corbin, KY 40701

Andrew F. Dunnet
INTELSAT
3400 International Drive
Washington, DC 20008
(202) 944-7245

A. D. Eales
British Aerospace Dynamics Group
Space & Communication Division
Argyle Way
Stevenage SG1 2AS
England
0438 736482

Martin W. Earls
COMSAT Labs.
22300 Comsat Drive
Clarksburg, MD 20906
(301) 428-4503

William Eppley
Honeywell Power Sources Center
104 Rock Road
Horsham, PA 19044
(215) 674-3800

Jack Faber
LASP
University of Colorado
Boulder, CO 80309
FTS 320-5333
(303) 492-8531

Rolan Farmer
Eagle-Picher Industries
P.O. Box 5234
Colorado Springs, CO 80931
(303) 392-4266

John Ferrell
U.S. Bureau of Mines
MS 4070
2401 E Street, NW
Washington, D.C. 20241
(202) 634-1177

Dr. Charles Fleischmann
Honeywell Power Sources Center
104 Rock Road
Horsham, PA 19044
(215) 674-3800

Robert W. Francis
Aerospace Corp.
M.S. M4-988
P.O. Box 92957
Los Angeles, CA 90009
(213) 648-6273

Harvey Frank
JPL
MS-198/220
4800 Oak Grove Drive
Pasadena, CA 91109
(818) 354-4157

Gary B. Freebern
McDonnell Aircraft
P.O. Box 516
Dept. 354, Bldg. 270E, Lev. 2, MS 416
St. Louis, MO 63166
(314) 232-1951

Steve Gaston
RCA Astro-Electronics Division
P.O. Box 800
Princeton, NJ 08540
(609) 426-2559

Paul Goldsmith
TRW
One Space Park
Redondo Beach, CA 90278
(213) 536-2754

Laura Goliaszewski
RCA Astro Electronics Division
410-2-C19
P.O. Box 800
Princeton, NJ 08540
(609) 426-3052

Lester Gordy
U.S. Army
8219 Running Creek Court
Springfield, VA 22153
(202) 695-3516

J. Goualard
SAFT
156 Avenue de Metz
Romainville, 93230
France
33(1)843-9361

H. R. Grady
Foote Mineral Co.
Route 100
Exton, PA 19341
(215) 363-6500

Gerald L. Griffin
Altus Corp.
1610 Crane Court
San Jose, CA 95112

Michael Groakanth
United Chem-Tech
P.O. Box 1067
Burlington, MA 01803

Robert S. Green
RCA Astro-Electronics Division
MS 4102/C19
P.O. Box 800
Princeton, NJ 08540
(609) 426-2045

Frank L. Gross
Martin Marietta Aerospace
P.O. Box 179
MS S0550
Denver, CO 80201
(303) 977-6067

S. Hafner
SAFT America Inc.
107 Beaver Court
Cockeysville, MD 21030
(301) 666-3200

Randy Haag
NWSC Crane
Code 30524 Bldg. 2949
Crane, IN 47522
(812) 854-1593

Norm Hagedorn
NASA/LRC
MS-301-3
21000 Brookpark Road
Cleveland, OH 44135
(216) 433-8601

Phil Hall
Motorola
8220 E. Roosevelt
Scottsdale, AZ 85252
(602) 990-5458

Steve Hall
NWSC Crane
Code 30524, Bldg. 2949
Crane, IN 47522
(812) 854-1593

Dr. Gerald Halpert
Jet Propulsion Laboratory
M.S. 277-102
4800 Oak Grove Drive
Pasadena, CA 91109
(818) 354-5474

Alan Harkness
Ballard Research Inc.
1164 15th Street W.
North Vancouver
BC, Canada V7P 1M9
(604) 986-4104

Albert F. Heller
Aerospace Corp.
M.S. M4-988
P.O. Box 92957
Los Angeles, CA 90009
(213) 648-6858

Ed Hendee
Telesat Canada
333 River Road
Ottawa, Ontario K1L 8B9
Canada
(613) 746-5920

Thomas J. Hennigan
T.J. Hennigan Associates
900 Fairoak Avenue
W. Hyattsville, MD 20783
(301) 559-0613

Duncan Henry
999 N. Sepulveda Blvd.
Suite 616
El Segundo, CA 90245

Gregg Herbert
Applied Physics Lab
Johns Hopkins Road
Laurel, MD 20707
(301) 953-5095/953-5000

George Higgins
Dow Chemical
Bldg. 566
Midland, MI 48640
(517) 636-6773

Jim Hill
Eagle-Picher Industries
P.O. Box 5234
Colorado Springs, CO 80931
(303) 392-4266

Mark A. Hoberecht
NASA/LRC
MS-301-3
21000 Brookpark Road
Cleveland, OH 44135
(716) 433-5362

Dr. Gerhard Holleck
EIC Laboratories
111 Downey Street
Norwood, MA 02062
(617) 769-9450

Franklin L. Hornbuckle
Fairchild Comm & Electron.
20301 Century Blvd.
Germantown, MD 20974
(301) 428-6221

Paul L. Howard
P. L. Howard Associates
P.O. Box K
Millington, MD 21651
(301) 928-5101

Daniel L. Hutchins
The Aerospace Corporation
Mail Station M4-988
P.O. Box 92957
Los Angeles, CA 90009
(213) 648-6273

W. C. Hwang
The Aerospace Corporation
MS M2-275
P.O. Box 92957
Los Angeles, CA 90009
(213) 615-4103

Jim Jagielski
NASA/GSFC
Code 711
Greenbelt, MD 20771
(301) 286-5964

D. H. Johnson
Union Carbide Corp.
Battery Products Division
P.O. Box 45035
Westlake, OH 44145
(216) 835-7619

Joseph Jolson
Catalyst Research
1421 Clarkview Road
Baltimore, MD 21209
(301) 296-7000

J. Karami
The Kendall Co.
95 West Street
Walpole, MA 02081
(617) 668-0175

John J. Kelley
Exide Corp.
19 W. College Avenue
Yardley, PA 19067
(215) 493-7203

James E. Kelly
Powell Corp.
Railroad Avenue
Andover, MA 01810
(617) 475-7500

Joseph Keogh
CIA
Washington, DC 20505
(703) 351-2066

R. C. Kientz
General Electric Battery Department
P.O. Box 114
Gainesville, FL 32602
(904) 462-3557

W. M. Kilroy
Naval Surface Weapons Center
Code R-33
Silver Spring, MD 20903-5000
(202) 394-1513

Michael Kimmey
Catalyst Research
1421 Clarkview Road
Baltimore, MD 21209
(301) 296-7000

Robert Kinday
Lockheed Missiles and Space Center
C/62-52, B156A
P.O. Box 3504
Sunnyvale, CA 94088-3504
(408) 742-3181

David Kirkpatrick
Lockheed Missiles and Space Center
Electrical Power Systems
D62-16
P.O. Box 3504
Sunnyvale, CA 94088-3504
(408) 742-5724

Paul W. Krehl
Electrochem Industries
10000 Wehrle Drive
Clarence, NY 14031
(716) 759-6901

Marvin Kronenberg
Duracell
37 A Street
Needham, MA 02194
(617) 449-7600 X414

J. L. Lackner
Defense Research Establish
3701 Carling Avenue
Ottawa, Ontario K2H 8S2
Canada
(613) 998-2360

Bob LaFrance
Aerospace Corp.
P.O. Box 92960
Los Angeles, CA 90009
(213) 643-1750

Dr. Anh H. Le
Naval Surface Weapons Center
White Oak Laboratory
Code R-33
Silver Spring, MD 20903-5000
(202) 394-1302

Keith Leavitt
USAF
P.O. Box 92960
Los Angeles, CA 90009
(213) 648-1750

I. Leavy
SAFT America Inc.
107 Beaver Court
Cockeysville, MD 21030
(301) 666-3200

Samuel Levy
Sandia National Laboratories
Division 2523
P.O. Box 5800
Albuquerque, NM 87185
(505) 844-8029

Hong S. Lim
Hughes Research Labs
MS RL70
3011 Malibu Canyon Road
Malibu, CA 90265
(213) 317-5379

David Linden
Duracel
78 Lovett Avenue
Little Silver, NJ 07739
(201) 741-2271

Chuck Lurie
TRW
One Space Park
Bldg R4/1028
Redondo Beach, CA 90278
(213) 536-3503

Gary Lyons
Howard Textile Mills
160 Great Neck Road
Great Neck, NY 11021
(516) 482-1880

Dr. Tyler X. Mahy
Central Intelligence Agency
c/o OTS
Washington, DC 20505
(703) 351-3912

Dr. Eugene L. Mainen
EIC Laboratories
111 Downey Street
Norwood, MA 02062
(617) 769-9450

B. Mani
Energy Conversion Devices
197 Meister Avenue
P.O. Box 5357
North Branch, NJ 08876
(201) 231-9069

Suzanne Maras
Ford Aerospace/SISD
Code 435.7
GSFC
Greenbelt, MD 20771
(301) 344-9384

Dr. Nehemiah Margalit
Tracor Battery Technology Center
3805 Mt. Vernon Avenue
Alexandria, VA 22305

Donald Maricle
International Fuel Cells, Inc.
P.O. Box 739
S. Windsor, CT 06074

Nikola Marincic
Battery Engineering, Inc.
1636 Hyde Park Avenue
Hyde Park, MA 02136
(617) 361-7555

Dean W. Maurer
AT & T Bell Labs
Murray Hill, NJ 07974
(201) 582-3237

J.H. McCann
RCA
9012 Stevens Lane
Lanham, MD 20706
(301) 763-7577

Joseph K. McDermott
Martin Marietta Aerospace
P.O. Box 179
M.S.-S0550
Denver, CO 80201
(303) 977-6601

Greg McDonald
Satellite Business Systems
P.O. Box 291
Clarksburg, MD 20871
(301) 428-3464

Dan McGuire
Martin Marietta Aerospace
9390 S. Warhawk
Conifer, CO 80433
(803) 977-9744

John R. Metcalfe
Canadian Astronautics Ltd
1050 Morrison Drive
Ottawa, Ontario K2H 8K7
(613) 820-8280

George Methlie
2120 Nathhoa Court
Falls Church, VA 22043
(703) 533-1499

Ronald P. Mikkelson
General Dynamics
Space Systems Division
Mail Zone 24-6390
P.O. Box 85990
San Diego, CA 92123
(619) 547-3706

Martin J. Milden
Aerospace Corp.
M5/720
P.O. Box 92957
Los Angeles, CA 90009
(213) 648-5225

Marvin Milewits
Flopetrol Johnston
P.O. Box 36369
Houston, TX 77036
(713) 240-7000

Lee Miller
Eagle-Picher Industries
P.O. Box 47
Joplin, MO 64802
(417) 623-8000

Ken Miyagi
Lockheed Missiles and Space Center
Electrical Power Systems
D62-16
P.O. Box 3504
Sunnyvale, CA 94088-3504
(408) 742-5724

Malcom Moody
Canadian Astronautics, Ltd
1050 Morrison Drive
Ottawa, Ontario K2H 8K7
Canada
(613) 820-8280

George W. Morrow
NASA/GSFC
Code 711
Greenbelt, MD 20771
(301) 286-6691

Dr. Carl E. Mueller
Naval Surface Weapons Center
White Oak Laboratory
Code R-33
Silver Spring, MD 20903-5000
(202) 394-2472

Buddy D. Murray
Martin Marietta Aerospace
P.O. Box 179, MS 4017
Denver, CO 80201
(303) 971-8075

David Namkoong
NASA/LeRC
MS 54-2
Cleveland, OH 44135
(216) 433-8208

Tim Ostwald
Ball Aerospace Systems Division
P.O. Box 1062
Boulder, CO 80306
(303) 939-4443

J. R. Ottenbacher
Martin Marietta Aerospace
P.O. Box 179, MS S0550
Denver, CO 80201
(303) 977-3481

Burton Otzinger
Rockwell International
SL-10/2600 Westminster Blvd.
P.O. Box 3644
Seal Beach, CA 90740-7644
(213) 594-3724

Boone B. Owens
Boone B. Owens, Inc.
P.O. Box 8205
St. Paul, MN 55108
(612) 645-2514

Charles Palendati
NASA/GSFC
Code 711
Greenbelt, MD 20771
(301) 286-6489

Paul Panneton
Applied Physics Lab
Johns Hopkins Road
Laurel, MD 20707
(301) 953-5095/953-5000

Andreas Papanicolasu
Naval Surface Weapons Center
Code R-33
Silver Spring, MD 20903-5000
(202) 394-2948

Robert E. Patterson
TRW
One Space Park
R4/1120
Redondo Beach, CA 90278
(213) 553-0723

Gene Pearlman
RCA Astro-Electronics Division
P.O. Box 800
Princeton, NJ 08540
(609) 426-3349

David Pickett
Hughes Aircraft
MS S12/V330
P.O. Box 92919
Los Angeles, CA 90009
(213) 648-2128

Philip R. Pierce
RCA Astro Electronics Division
410-2-C19
P.O. Box 800
Princeton, NJ 08540
(609) 426-3052

Patricia Plunket
U.S. Bureau of Mines
2401 E. Street, N.W.
MS 4050
Washington, DC 20241
(202) 634-1083

Henry J. Powell
Powell Corporation
Railroad Avenue
Andover, MA 01810
(617) 475-7500

William Price
FBI
8199 Backlick Road
Lorton, VA 22079
(703) 550-7931

Dalbir Rajoria
Energy Conversion Devices
P.O. Box 5357
North Branch, NJ 08876
(201) 231-9060

N. Raman
SAFT America Inc.
107 Beaver Court
Cockeysville, MD 21030
(301) 666-3200

Guy Rample
General Electric Co.
P.O. Box 114
Gainesville, FL 32602
(904) 462-3521

Dr. Benny Reichman
Ovonic Battery Co.
1826 Northwood
Troy, MI 48084
(313) 362-1750

Margaret Reid
NASA/LeRC
MS 309-1
21000 Brookpark Road
Cleveland, OH 44135
(716) 433-5253

R.N. Richards
Martin Marietta
P.O. Box 179
Denver, CO 80201
(303) 977-5517

Patrick Rissmiller
Catalyst Research
1421 Clarkview Road
Baltimore, MD 21209
(301) 296-7000

Paul Ritterman
COMSAT
2250 E. Imperial Highway
El Segundo, CA 90245
(213) 416-9106

G. Ernest Rodriquez
NASA/GSFC
Code 711
Greenbelt, MD 20771
(301) 286-6202

Mike Rose
Rose Development Associates, Inc.
2214 Country Club Dr., Suite A
Pittsburgh, PA 15241
(412) 835-6111

Gilbert Roth
NASA HQ
LB
Washington, DC 20546
(202) 453-8341

Ted Russell
Space Communications Company
1300 Quince Orchard Blvd.
Gaithersburg, MD 20878
(303) 258-6880

Chris J. Scharf
Martin Marietta Aerospace
P.O. Box 179
M.S.-S0550
Denver, CO 80201
(303) 977-6601

Steve Schiffer
RCA Astro-Electronics Division
MS111
P.O. Box 800
Princeton, NJ 08540
(609) 426-3277

Mark H. Schlam
Polytechnic Institute of New York
101 Hillside Road
Deer Park, NY 11729
(516) 242-9654

J. A. Schmidt
RCA AMERICOM
#2 Edsal Road
Sussex, NJ 07461
(201) 827-7900

A. Dan Schnyer
NASA HQ
Code R
Washington, DC 20546
(202) 453-2843

Willard R. Scott
TRW Inc.
R4-1120
One Space Park Drive
Redondo Beach, CA 90278
(213) 535-7790

Norman R. Schulze
NASA HQ
Code DE
Washington, DC 20546
(202) 453-1862

Ken Schwer
McDonnell Douglas Astro.
P.O. Box 516
St. Louis, MO 63166
(314) 839-7025

Charles Scuilla
U.S. Government
5501 Starboard Court
Fairfax, VA 22032
(703) 281-8440

Eddie Seo
Gates Corporation
P.O. Box 5887
Denver, CO 80215
(303) 744-4614

Christopher T. Shaper
Chemetals Sales
Empire Towers Building
7310 Ritchie Highway
Glen Burnie, MD 21061

David Shen
J.P.L.
MS 122-123
4800 Oak Grove Drive
Pasadena, CA 91109
(818) 354-2351

Dennis Sieminski
Electrochem Industries
10000 Wehrle Drive
Clarence, NY 14031
(716) 759-6901 ext. 528

David E. Simm
OAO Corp.
319 Lucust Thorn Court
Millersville, MD 21108
(301) 345-0750

Jack Sindorf
Johnson Controls
900 E. Keefe Avenue
Milwaukee, WI 53212
(414) 228-2719

Lu Slifer
7023 Dolphin Road
Lanham, MD 20706
(301) 552-1761

Dr. Patricia Smith
Naval Surface Weapons Center
Code R-33
Silver Spring, MD 20903-5000
(202) 394-2948

Rebecca A. Smith
Honeywell Power Sources Center
104 Rock Road
Horsham, PA 19044
(215) 674-3800

Robert Somoano
JPL
4800 Oak Grove Drive
Pasadena, CA 91109
(818) 354-2213

James Speirs
Honeywell Power Sources Center
104 Rock Road
Horsham, PA 19044
(215) 674-3800

William Spindler
Electric Power Research Institute
P.O. Box 10412
Palo Alto, CA 94303
(415) 855-2541

D. N. Srinivas
Comsat Corporation
950 L'Enfant Plaza
Washington, DC

Wayne T. Stafford
Aerospace Corporation
M6/202
P.O. Box 92957
Los Angeles, CA 90009
(213) 416-7302

P.H. Stakem
Interface Technology Inc.
P.O. Box 3040
Laurel, MD 20708
(301) 490-3608

Irv Stein
JPL
4800 Oak Grove Drive
M.S. 198-220
Pasadena, CA 91109
(818) 354-6048

Robert Stearns
General Electric Co.
1142 Plowshare Road
Blue Bell, PA 19422
(215) 354-1505

Joseph Stockel
Central Intelligence Agency
Washington, DC 20505
(703) 351-2065

Martin Sulkes
USAERADCOM
DELET-PC
Fort Monmouth, NJ 07703-5302
(201) 544-2458

Ralph M. Sullivan
Applied Physics Lab
Johns Hopkins Road
Laurel, MD 20707
(301) 953-5095/953-5000

David Surd
Catalyst Research
1421 Clarkview Road
Baltimore, MD 21209
(301) 296-7000

Rao Suroupundi
J.P.L.
MS 277-212
Pasadena, CA 91109
(818) 354-5974

William Swartz
Applied Physics Lab
Johns Hopkins Road
Laurel, MD 20707
(301) 593-5095/593-5000

Larry Swette
Giner Inc.
14 Spring Street
Waltham, MA 02254-9147
(617) 899-7270

Dr. Larry Thaller
NASA/LRC
MS-301-3
21000 Brookpark Road
Cleveland, OH 44135
(716) 433-2247

Helmut Thierfelder
General Electric Co.
P.O. Box 8555
Philadelphia, PA 19101
(215) 354-2027

M. Thomas
Naval Surface Weapons Center
White Oak Labs
Silver Spring, MD 20903-5000
(202) 394-1299

Paul J. Timmerman
Martin Marietta Aerospace
MS S-0550
P.O. Box 179
Denver, CO 80201
(303) 977-6130

Dr. Herman B. Urbach
David W. Taylor Naval Ship
Code 272T
Annapolis, MD 21402
(301) 267-2864

Hari Vaidyanathan
Comsat Labs
22300 Comsat Drive
Clarksburg, MD 20871
(301) 428-4507

Gert Van Ommering
3939 Fabian Way
MS G45
Palo Alto, CA 94303
(415) 494-7400

K. L. Vasanth
Naval Surface Weapons Center
R-32
10901 New Hampshire Avenue
Silver Spring, MD 20903
(202) 394-3549

Dan Verrier
Yardney
82 Mechanic Street
Pawcatuck, CT 02891
(203) 599-1100

Don R. Warnock
AFWAL/P005-2
WPAFB, OH 45433
(513) 255-6235

Thomas Watson
Catalyst Research
1421 Clarkview Road
Baltimore, MD 21020
(301) 296-7000

Don Webb
McDonnell Douglas Astro.
P.O. Box 516
St. Louis, MO 63166
(314) 839-7025

Max M. Wertheim
Grumman Corp
Aircraft Systems Division
E03-31T
Bethpage, NY 11743
(516) 575-2869

Turner White
LTV Aerospace Defense
MS TH-42
P.O. Box 225907
Dallas, TX 75265

Alvin H. Willis
Boeing Aerospace Co.
P.O. Box 1770, MS/JA-72
Huntsville, AL 35807
(205) 895-7423

Thomas Willis
AT & T Bell Labs
600 Mountain Avenue
Murray Hill, NJ 07974
(201) 582-3545

Richard M. Wilson
SOHIO
Midland Bldg 3 (808 HB)
Cleveland, OH 44115
(216) 575-8346

Roger A. Wood
US Air Force
FLTSATCOM
1860 W. 181 St
Torrance, CA 90504
(213) 643-2181

Edward L. Woodbury
COMSAT General
950 L'Enfant Plaza, S.W.
Washington, DC 20024
(202) 863-7477

Will J. Worley
University of Illinois
216 Talbot Lab
104 South Wright
Urbana, IL 61801-2983
(217) 333-1607

David I. Yalom
Consultant
10813 E. Nolcrest Drive
Silver Spring, MD 20903
(301) 593-1973

Dave Yedwab
ARDC
Building 354
Dover, NJ 07814-5001
(201) 724-3058

Thomas Y. Yi
NASA/GSFC
Code 711
Greenbelt, MD 20771
(301) 286-3051

W. Zajac
Naval Surface Weapons Center
White Oak Labs
Silver Spring, MD 20903-5000
(202) 394-1299

BIBLIOGRAPHIC DATA SHEET

1. Report No.	2. Government Accession No.	3. Recipient's Catalog No.
NASA CP-2434		

4. Title and Subtitle	5. Report Date
THE 1985 GODDARD SPACE FLIGHT CENTER BATTERY WORKSHOP	September 1986
	6. Performing Organization Code: 711
7. Author(s): G. MORROW, EDITOR	8. Performing Organization Report No.: 86B0366
9. Performing Organization Name and Address: GODDARD SPACE FLIGHT CENTER, GREENBELT, MARYLAND 20771	10. Work Unit No.
	11. Contract or Grant No.
	13. Type of Report and Period Covered: CONFERENCE PUBLICATION
12. Sponsoring Agency Name and Address: NATIONAL AERONAUTICS AND SPACE ADMINISTRATION, WASHINGTON, D.C. 20546	14. Sponsoring Agency Code

15. Supplementary Notes

16. Abstract

This document contains the proceedings of the 18th Annual Battery Workshop held at Goddard Space Flight Center, Greenbelt, Maryland on November 19-21, 1985. The workshop attendees included manufacturers, users, and government representatives interested in the latest developments in battery technology as they relate to high reliability operations and aerospace use. The subjects covered included advanced energy storage, lithium cell technology, nickel-cadmium design evaluation and component testing, simulated orbital cycling and flight experience, and nickel-hydrogen technology.

17. Key Words (Selected by Author(s))	18. Distribution Statement
BATTERIES, ELECTRO-CHEMICAL, NICKEL-CADMIUM, NICKEL-HYDROGEN, LITHIUM	UNCLASSIFIED-UNLIMITED SUBJECT CATEGORY 33

19. Security Classif. (of this report)	20. Security Classif. (of this page)	21. No. of Pages	22. Price*
UNCLASSIFIED	UNCLASSIFIED	446	A19

*For sale by the National Technical Information Service, Springfield, Virginia

22161

GSFC 25-44 (10/77)

*U.S. GOVERNMENT PRINTING OFFICE:1986-625-014:40012